New Routes to Chiral-at-Metal

Organometallic Complexes

and their Application

in Asymmetric Synthesis

December 2021

UNIVERSITY OF HULL

By Stephanie Shroot

Abstract

This project develops new organometallic frameworks, to target the asymmetric transfer hydrogenation and hydrosilylation of ketones, aiming for enhanced activity and substrate scope relative to current state-of-the-art. The anticancer activity of some of the complexes were assessed against a human colorectal adenocarcinoma cell line. The first chapter of this work discusses relevant research published, identifying key areas that possess limitations.

Chapter 2 describes the synthesis of tethered ruthenium(II) half-sandwich complexes, constructing structures bearing chirality within the tether; a prospect not yet explored. The key to this design is the stereocentre, situated at the benzylic position. A bulky substituent, methyl, isopropyl or *t*-butyl, emanates hoping to control the tether coordination. The tether was designed to influence the metal-centred configuration and thus the configuration of the ATH product. Although configurational exchange was seen over time, the complexes yielded products in modest ee.

Chapter 3 describes the synthesis of manganese(I) half-sandwich frameworks, aiming to incorporate a stereocentre into the tether so the approach of the substrate to the complex during hydrosilylation would be influenced by the steric bulk of the tether. Irradiation of the achiral tethered complexes outlined in this chapter showed great promise, hence if the reaction conditions can be tuned accordingly, the frameworks can still be considered as good target complexes to be used in hydrosilylation.

Chapter 4 describes exploration towards the synthesis of a polymer-supported ruthenium(II) half-sandwich complex, analogous to those developed in Chapter 2, anticipated to be capable of the asymmetric transfer hydrogenation of ketones. Frameworks in the literature incorporate supports through amino, sulfonamide or phenyl groups within the ligand, allowing for cheaper and less toxic reaction conditions, and advantageous recyclability, without loss of enantioselectivity. The anticipated immobilisation during this project was via the stereocentre on the tether, but due to time limitations immobilisation was not performed.

Acknowledgements

Thank you to Dr Kevin Welham and Dean Moore for MS data collection on all of the synthesised products; Carol Kennedy for elemental analysis of the final complexes; and Dr Tim Prior for X-ray diffraction of both intermediate compounds and final complexes, in addition to the help and support received towards other aspects of my PhD.

I would also like to thank Dr Charlotte Wiles for her copiousness amount of time, encouragement and advice that has allowed me to persevere to this stage of my PhD. I would also like to thank Dr Nigel Young who has always given me positive guidance and made the lab a fun place to work.

I would like to mention my supervisor, Dr Ben Murray, for his continued support and guidance. I truly appreciate all the time he has dedicated towards me and I have thoroughly enjoyed working alongside him every day. Dr Murray's hard-working nature and enthusiasm towards this field of chemistry has inspired me to become the researcher I am today.

Finally, and most importantly, to my mum. Your abundance of love and support throughout this challenging period will never be forgotten. Thank you for always being my shoulder to cry on and forever showing willingness to try to understand my work; this thesis is dedicated to you!

Publication

The work from Chapter 2 has been published in the Journal of Organometallic Chemistry: Tethered ruthenium(II) η^6-arene complexes: assessing the potential of benzylic substituents to control metal-centred chirality, and applications in asymmetric transfer hydrogenations of ketones. DOI: https://doi.org/10.1016/j.jorganchem.2021.122232

List of abbreviations

AH	Asymmetric hydrogenation
Ar	Aromatic ring
ATH	Asymmetric transfer hydrogenation
A2780	Human Ovarian Carcinoma cell line
BINAP	2,2'-bis(diphenylphosphino)-1,1'-binaphthyl
Boc	*Tert*-butyloxycarbonyl protecting group
BsDPEN	*p*-Benzenesulfonyl-1,2-diphenylethylenediamine
*c*Hex	Cyclohexane
C=O or CO	Carbonyl group
COSY	COrrelation SpectroscopY
Cp	Cyclopentadienyl
Cy	Cyclohexyl
DCM	Dichloromethane
DEPT	Distortionless Enhancement by Polarization Transfer
DIPEA	Diisopropylethylamine
DMAP	4-Dimethylaminopyridine
DMF	Dimethylformamide
DMSO	Dimethyl sulfoxide
DNA	Deoxyribonucleic acid
DPEN	1,2-Diphenyl-1,2-ethylenediamine
ee	Enantiomeric excess
ESI	Electrospray ionisation
EtOAc	Ethyl acetate

EtOH	Ethanol
FA/TEA	Formic acid/Triethylamine
FID	Flame ionisation detector
Fmoc	Fluorenylmethoxycarbonyl protecting group
GC	Gas Chromatography
GI_{50}	The concentration which inhibits cell growth by 50 %.
HMBC	Heteronuclear Multiple Bond Correlation
HOBt	Hydroxybenzotriazole
HPLC	High Performance Liquid Chromatography
HT-29	Human Colorectal Adenocarcinoma Cell Line
IC_{50}	The half maximal inhibitory concentration is a measure of the potency of a substance in inhibiting a specific biological or biochemical function.
*i*Pr	Isopropyl
IR	Infrared radiation
KCN	Potassium cyanide
KHMDS	Potassium bis(trimethylsilyl)amide
KO*t*Bu	Potassium *tert*-butoxide
Me	Methyl
MeCN	Acetonitrile
MeOH	Methanol
Mes	Mesityl
Ms	Methanesulfonyl
MS	Mass spectrometry (LR: low resolution, HR: high resolution)
MsCl	Methanesulfonyl chloride
Mts	2,4,6-trimethylphenylsulfonyl

MTT	3-(4,5-dimethylthiazol-2-yl)-2,5-diphenyltetrazolium bromide
NAD^+	Nicotinamide adenine dinucleotide (oxidised)
NADH	Nicotinamide adenine dinucleotide (reduced)
NCI-60	NCI-60 Human Tumour Cell Lines Screen (a range of 60 cell lines on which chemotherapeutics are screened)
NHC	N-Heterocyclic Carbene
NMR	Nuclear magnetic resonance
OMe	Methoxy
PEG	Polyethylene glycol
Ph	Phenyl group
PTsDPEN	PEG-supported TsDPEN catalyst
R enantiomer	Rectus enantiomer
R_f	Retention factor
Ru-H	Ruthenium hydride
S/C	Substrate to catalyst molar ratio
S enantiomer	Sinister enantiomer
S_N2	Bimolecular nucleophilic substitution
TBTU	O-(Benzotriazol-1-yl)-N,N,N',N'-tetramethyluronium tetrafluoroborate
*t*Bu	*Tert*-butyl
TEA	Triethylamine
TFA	Trifluoroacetic acid
TH	Transfer hydrogenation
THF	Tetrahydrofuran
TLC	Thin Layer Chromatography
Tris	2,4,6-triisopropylphenylsulfonyl

TS	Transition state
Ts	Toluenesulfonyl (Tosyl)
TsDPEN	Tosyl-(1,2-diphenyl-1,2-ethylenediamine)
TsDENEB®	[Ru(II)-(N-[2-(4-methylbenzyloxy)ethyl]-N'-(*p*-toulenesulfonyl)-1,2-diphenylethylenediamine)Cl]
UV	Ultraviolet
XRD	X-ray diffraction
2C	2-Carbon
3C	3-Carbon
4C	4-Carbon
5C	5-Carbon

List of figures

List of schemes

List of Tables

Contents Page

Chapter 1

Introduction and literature review

To date, chiral-at-metal complexes have found a myriad of applications in various fields within chemistry, namely in asymmetric synthesis in addition to their use in the bioinorganic research fields.[1–25]

The most popular examples in bioinorganic chemistry are enzyme inhibitors that target protein kinases (Figure 1), whereby the aim is to design structures that mimic biological compounds and complement the shape of their active sites.[1–3,5,9–22,24–27]

R$_1$ = H, OH, Cl or Br
R$_2$ = H, F, CF$_3$, CH$_2$OH, CH$_3$, N(CH$_3$)$_2$, OCH$_3$ or CO$_2$H
R$_3$ = H, Cl, Br or CH$_2$OH
R$_4$ = H or Br
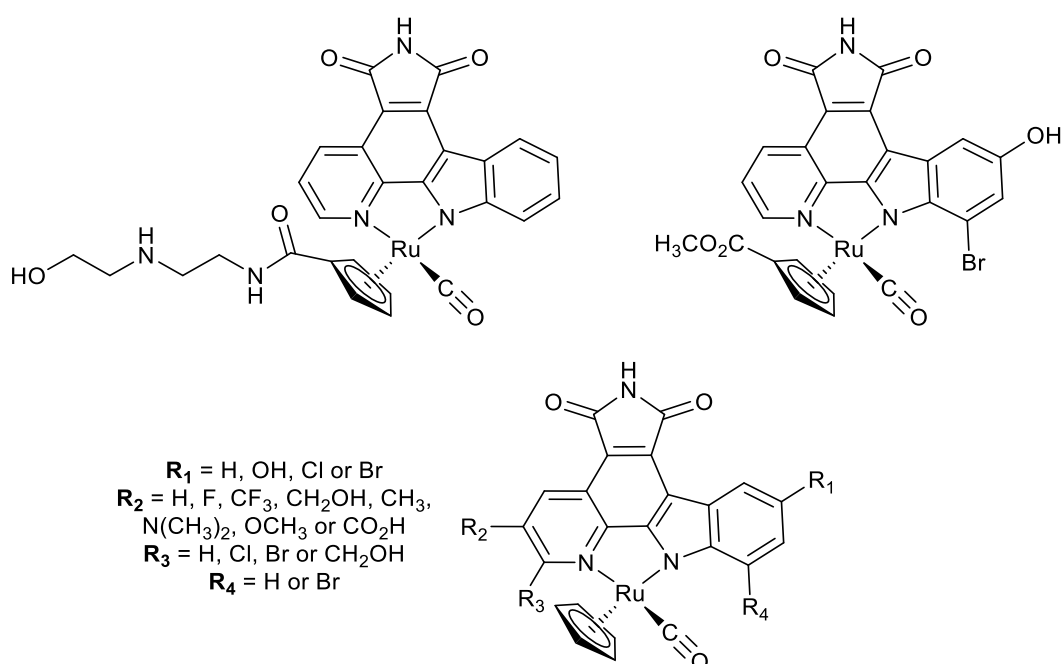
Figure 1. Examples of enzyme inhibitors that target protein kinases.[18,25]

The purpose of the chiral metal centre is to orientate the surrounding ligands to match that found within the target protein. As the metal itself is not directly part of the interactions that take place, this highlights that the relative position of the ligands and their functionality, as determined by the stereochemical configuration within the complex, is of great importance.[1,2,5,7,9,11–13,15–19,21,22] Researchers focus upon manipulating rigid three-dimensional metal complexes to occupy particular geometries in the hope to "increase structural diversity"[6], whilst achieving specificity and kinetic stability, and proving kinetically inert too.[1,2,4,6,8,10–13,15–22,24,25]

Within asymmetric synthesis, chiral-at-metal catalysts have transferred chiral information, enantioselectively catalysing various reactions, for example, aldol-type alkylations, esterifications, Diels-Alder cycloadditions, 1,3-dipolar cycloadditions, asymmetric cyclopropanation, olefin metathesis, ring closing alkene metathesis, kinetic resolution of alcohols, asymmetric hydrogenation and asymmetric transfer hydrogenation. A plethora of catalysts follow the piano stool framework; reported structures include achiral ligands, chiral monodentate ligands and chiral bidentate ligands. To achieve the greatest stereocontrol over the metal centre, researchers have favoured chiral bidentate ligands, achieving high enantiocontrol during asymmetric reductions, due to an increase in stability of the complex, reducing inversion of configuration at the metal during catalysis.[28–30]

Chiral-at-metal catalysts can be found as octahedral or half-sandwich frameworks[16,30], whereby the chirality of the metal can be induced in two ways. The first is the attachment of achiral ligands to a metal centre, resulting in metal-centred chirality due to the enantiomers formed; this is most prominent in octahedral catalysts.[10,27,31–34] Alternatively, chirality can be induced to the metal via the complexation of chiral ligands, either monodentate or bidentate, to prevent the challenge of separating the isomers at the end of the synthetic route, assuming that a single isomer has formed as opposed to a pair of diastereoisomers[30]. This idea is more applicable for half-sandwich complexes, leaving room for fine-tuning and modification of chiral ligands by their steric and electronic properties.[23,28,30,34–38] Multiple studies have encountered difficulties when trying to synthesise piano stool complexes without chiral bidentate ligands. One example is the inversion of configuration at the metal centre during catalysis, which prevents high enantioselectivity being achieved during asymmetric transformations.[39] Unfortunately, research thus far has therefore relied upon the use of chiral bidentate ligands to control the chirality at the metal centre, which limits the variations of novel chiral-at-metal complexes synthesised. Hence, if chiral ligands were no longer a requirement to synthesise a chiral-at-metal framework, then the possible structural designs can be seen to have limitless potential.[16,20,22,23,31]

1.1 Asymmetric catalysis

Stereochemically pure compounds can be difficult to synthesise but are hugely important in a variety of sectors; namely fine chemicals, pharmaceuticals and agrochemicals.[12,15,36,40–67] Prior to recent advances in synthesis, agrochemicals and medicines were often brought to the market as mixtures of isomers, with each having different biological effects.[41,68–71] To be

specific, a review in 2006 stated that 56 % of pharmaceutical drugs were chiral and of those, 88 % were marketed as racemates containing both isomers.[72] From 2007 onwards, approximately 43 % of agrochemicals were chiral, with 47 % being marketed as racemic.[69]

The importance of the synthesis of enantiomerically pure products is most clearly illustrated in the pharmaceutical industry. One example was the tragic case of thalidomide, a drug introduced in 1957, which treated morning sickness during pregnancies. One isomer induced sedative effects, whilst the other caused birth defects.[70,73] Another example is formoterol, a chiral drug utilised in the therapy of asthma and chronic bronchitis. This therapeutic alcohol comprises of two stereocentres, hence giving rise to four stereoisomers, each with very different toxicities and effects. Of these, (*S,S*)-formoterol has been found to have a toxic effect that would be harmful to the patient, compared with (*R,R*)-formoterol that has shown the most promise in terms of clinical benefit.[71,74,75] To avoid such dangers, modern drug discovery focuses on separating isomers before their use in medicines.[76]

Since only one isomer is often useful, 50 % of the yield of racemic processes is wasteful. Primarily, the rotation of plane-polarised light, in equal but opposite directions, is the physical property that allows enantiomers to be differentiated between.[77] Nowadays, simpler modern chromatographic methods are typically used to separate racemic mixtures, into the (*R)* and (*S)* enantiomers, based upon their retention time on the chiral stationary phase.[34,41,52,78,79] For example, (*S*)-finerenone, a receptor antagonist for the treatment of chronic kidney disease, is synthesised as its racemic form followed by separation from the (*R*)-isomer via chiral column chromatography.[80] Due to their identical physical and chemical properties, enantiomer separation can be challenging and costly.[41,52,67,76,80] An alternative approach is to develop reactions, like in nature, that produce only one isomer.[45,81]

Asymmetric synthesis is one example that represents an umbrella of reactions that aim to create chiral products. Two popular methods of asymmetric synthesis include asymmetric hydrogenation (AH) and asymmetric transfer hydrogenation (ATH). Asymmetric hydrogenation has eco-friendly characteristics, based on the abundance and low cost of hydrogen as a clean proton donor.[60,82–86] Comparatively, asymmetric transfer hydrogenation uses alternative hydrogen donors, for example isopropanol, formic acid/triethylamine azeotropes and water/sodium formate mixtures. These safer reaction conditions generate smaller amounts of hazardous by-products and allow the catalyst to be recycled.[41,42,45,48,55,58,83,85–101] Further, ATH does not require a large amount of catalyst to perform the reduction; "typically less than 1 mol %"[98].

ATH is a versatile method that includes the addition of hydrogen, from a non-H_2 source, to ketones and imines by a catalyst, to create enantiomerically enriched chiral alcohols and amines.[43,45,46,48,53,54,59,81,92,97,102–110] Explained further, ATH uses a catalyst to transfer configurational bias to the product and therefore controls the relative ratio of the enantiomers produced.[81,110] The enantiopurity of the reduction product is usually denoted as the enantiomeric excess and is given as a percentage. It defines the extent to which the major enantiomer is in excess of the minor enantiomer or in other words, the "percentage excess of the enantiomer over the racemate"[78].

In Scheme 1, the goal of the catalyst is to reduce the carbonyl bond selectively to produce only one isomer, regardless of the difference in substituents on the substrate.
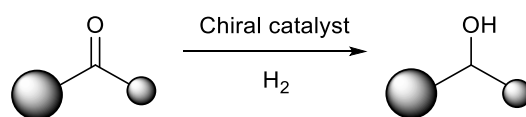
Scheme 1. Generic scheme showing the ATH of ketones by a chiral catalyst.[111]

The larger ball signifies a group comprising of high electron density, for example an aryl or alkyne moiety, and the smaller ball signifies a group comprising of low electron density, for example an alkyl moiety.[111] This is a typical example of how ruthenium-based half-sandwich ATH catalysts asymmetrically reduce achiral ketones.

ATH reactions are focused upon in ongoing research and ruthenium is a popular transition metal investigated due to its formation of relatively kinetically stable complexes and economic advantages over alternative transition metals.[112] As a result of poor enantioselectivity with a range of substrate classes, the usage of homogeneous catalysts in asymmetric catalysis is used less frequently on industrial scales than researchers would like.[52,81,88,93,113] Similar ruthenium structures are being extensively explored in the development of anticancer compounds, allowing dual-propertied ruthenium(II) complexes to become more common.[114] Further research has also focused upon alternative asymmetric synthetic processes, for example, hydrosilylation of ketones to create chiral products[115] because the process is much simpler and allows for milder conditions to be employed, enhancing green chemistry aspects of the catalysis.[115–118] The majority of studies have utilised rhenium, ruthenium and iridium complexes, but more sustainable projects have concentrated on iron, zinc and copper catalysts.[31,115,117,118]

1.1.1 Noyori's catalysts

Noyori made several breakthroughs in the field of ATH in the mid-1990s, which later led to his share in the 2001 Nobel Prize award for "the ability to control stereoselectivity via catalysis"[37,47,93,119]. Noyori's half-sandwich ruthenium-based catalysts[27,39,41,43,46,48,49,53,58,67,81,86,89,96,97,99,100,106,107,110,120–122], based upon monotosylated diamines[27,39,46,47,60,64,65,86,89,90,100,105,110,112,123,124] (Table **1**), inspire the majority of ruthenium half-sandwich ATH catalysts designed nowadays[39,40,81,88,92,97,106,107,110,125], often being referred to as the 1st generation[93].

Table 1. Noyori's catalysts.[67]
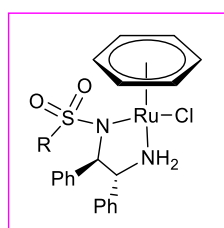
Catalyst	η^6-arene ligand	R	N-sulfonyldiamine
C1	Benzene	$4\text{-}CH_3\text{-}C_6H_4$	Ts-DPEN
C2	*p*-cymene	$4\text{-}CH_3\text{-}C_6H_4$	Ts-DPEN
C3	Mesitylene	$4\text{-}CH_3\text{-}C_6H_4$	Ts-DPEN
C4	Hexamethylbenzene	$4\text{-}CH_3\text{-}C_6H_4$	Ts-DPEN
C5	Benzene	1-naphthyl	Nps-DPEN
C6	*p*-cymene	$2,4,6\text{-}(CH_3)_3\text{-}C_6H_2$	Mesitylsulfonyl-DPEN

Chiral diamine ligands possess greater stability in air than their phosphine analogues, in addition to their ease of tunability and readily available nature.[47,65,126] Further, the success of these catalysts, as a result of their flexible structure, allows easy modification to tune the substrate scope, increasing the activity and selectivity of the catalyst.[37,41,45,46,53,65]

Within Noyori's framework it is the stereochemical configurations at the carbon atoms bearing the phenyl substituents that dictate the stereochemistry of the TsDPEN ligand to be either (*R,R*) or (*S,S*). It is important to note that the (*R,R*)-TsDPEN and (*S,S*)-TsDPEN ligands confer opposite stereochemical configuration at the metal centre and therefore influence the chirality of the alcohol product too.[39,46,81] The (*S,S*)-ligand yields a complex where the configuration at the metal centre is (*R*)-absolute and the (*R,R*)-ligand determines the stereochemistry at the metal centre to be (*S*)-absolute (Figure 2).[39,67,127]

(S,S)-**C1** (R,R)-**C1**
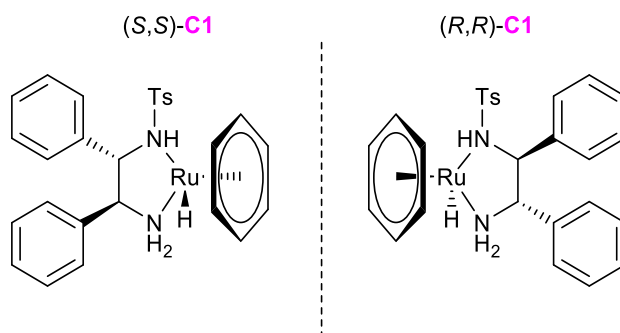
Figure 2. Noyori's catalysts bearing (S,S) and (R,R)-TsDPEN ligands.[128]

A favoured diastereoisomer is then able to form (Figure 3), where there is attractive CH-π interactions between hydrogens on the arene ring of the catalyst and the phenyl ring of the substrate.[46,59,64,67,81,86,127,129–131] Though this concept is generally accepted, it is important to highlight this transition state is only one explanation for the enantioselectivity during ATH.

Favourable "edge-face" π-interaction
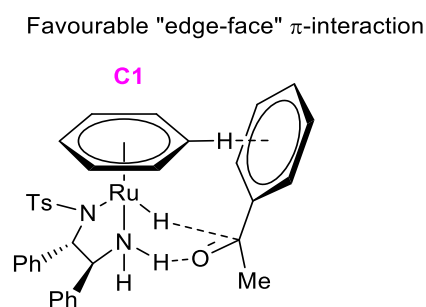
Figure 3. Noyori's favoured diastereoisomer.[127,132]

Interestingly, one research group[133] investigated whether it was the *anti*-arrangement of substituents or the 1,2-disubstitution of the phenyl groups within the TsDPEN ligand that controlled the activity and selectivity of the ligand during ATH by removing one of the phenyl groups and reversing the ligand to a *syn*-arrangement (Figure 4).[46,107,131,133]

(R,R)-**L1** (S)-**L2** (R)-**L3** $(1S,2R)$-**L4**
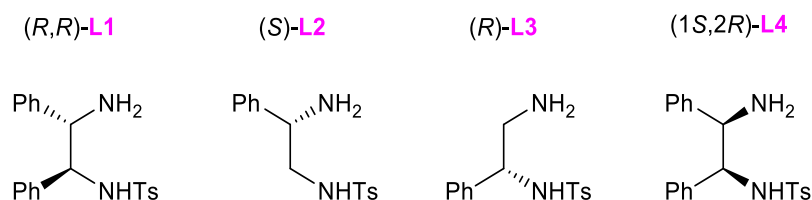
Figure 4. TsDPEN and variations of the ligand to investigate their influence on ATH.[46,133]

For **L2** and **L3**, the configuration of the alcohol was identical to the stereochemistry of the chiral centre on the ligand. It has been postulated that ligands **L2** and **L3** allowed for more

flexibility in the catalyst due to only one phenyl group being present, which resulted in lower conversion rates and extended periods of time for the reduction. For **L1** and **L4**, the configuration of the alcohol matched the stereochemistry of the chiral centre attached to the tosylated amine. Based on the results in Table **2**, both phenyl groups were favourable to be present (**L1** and **L4**) to achieve high enantioselectivity. When the ligand comprised of stereogenic centres of opposite stereochemistry (**L4**), the lowest amount of conversion was achieved, in addition to the longest reaction time being required. In comparison, **L1** that comprised of identical stereochemistry at the stereogenic centres, obtained the highest activity and selectivity during ATH, in turn shortening reaction times.[27,45,46,86,107,131,133]

Table 2. ATH of acetophenone by ligands shown in Figure 4.[46,133]

Ligand	Time	Conversion (%)	ee (%)	Chirality
L1	22 hours	100	98	*(R)*
L2	48 hours	95	69	*(S)*
L3	13 days	46	33	*(R)*
L4	220 hours	32	70	*(S)*

Once the ligand has coordinated to the metal centre, the two possible complexes formed with each enantiomer of the TsDPEN ligand exist as diastereoisomers (Figure 5).[39]
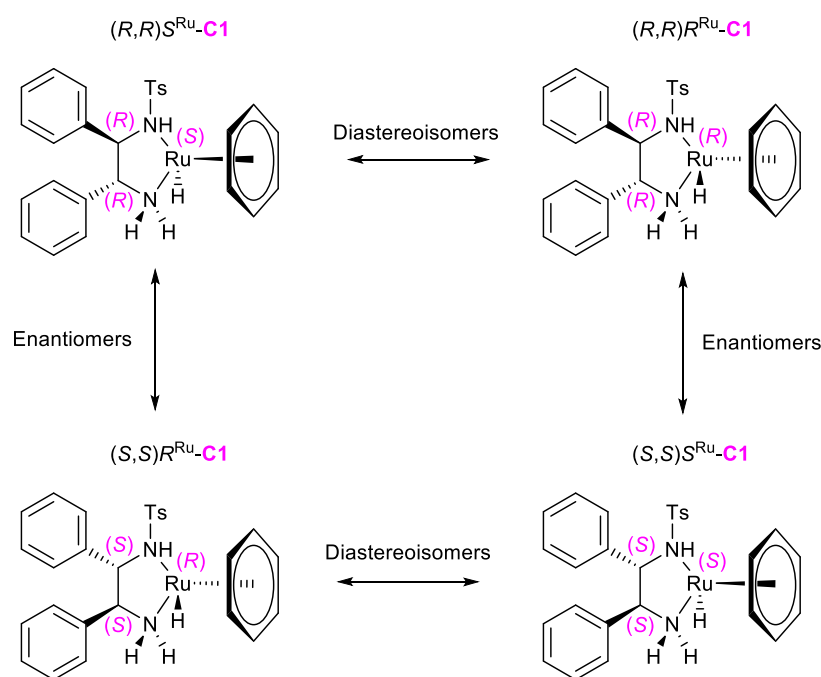
Figure 5. The four diastereoisomers of [(η^6-benzene)RuH(TsDPEN)].[39]

Of most significance is that the configuration of ligands around the metal centre influences the chirality of the metal centre, which in turn induces chirality to the alcohol products during ATH (assuming the standard mechanism applies - see section 1.1.4). It has been experimentally determined that although both diastereoisomers may exist during catalysis (due to configurational isomerism at the metal centre), one isomer is significantly more active than the other, hence is responsible for the major product (enantiomeric excess). Computational studies of catalysts comprising the (*R,R*)-TsDPEN ligand, shown in Figure 6, confirm the more active diastereoisomer in ATH comprises (*S*) chirality at the metal centre.[39]
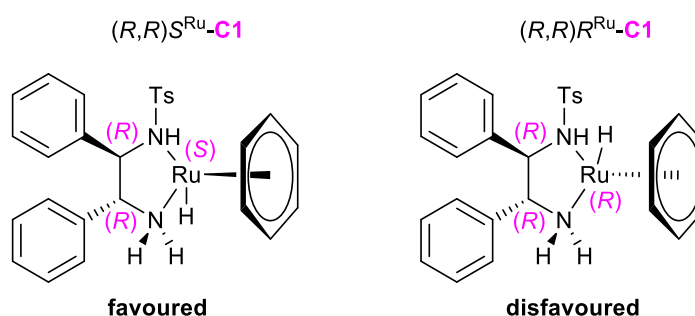
Figure 6. Favoured diastereoisomer as a result of the location of the hydrogen.[39]

One significant ATH method includes **C2** (Table **1**) in a 5:2 ratio of formic acid/triethylamine (FA/TEA) azeotrope, which acts as a source of hydrogen to be transferred from the catalyst to the substrate, regenerating the catalyst during the cycle (see section 1.1.4 for the mechanism). The low catalyst loading required for this method is advantageous because the reaction can be carried out cheaply.[27,44–46,48,53,56,58,85,90,106,126,134–137]

Other novel ruthenium AH catalysts have been discovered by Noyori and coworkers, for example [RuCl$_2$(diphosphine)(diamine)], whereby the diphosphine[86,116,138] and diamine[37,49,86,90,139–141] both possessed chirality (Figure 7) producing a fast, stereoselective route to reducing simple ketones.[70,83,86,90,139]
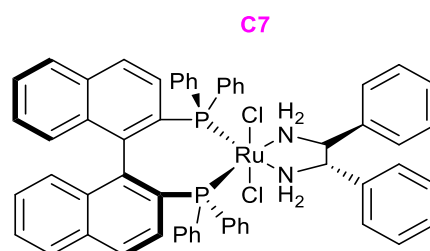
Figure 7. Catalyst whereby the ligands are chiral but the metal centre is not.[37]

To achieve this effective transfer of hydrogen during the ATH transition state, the larger group within unsymmetrical ketones is orientated away from the phosphorus ligands to prevent steric clash as a result of their bulky nature. Moreover, research has suggested that there is a stabilising interaction between the aryl ring of the substrate with the diamine ligands. This therefore leads to a favourable and unfavourable approach of the ketone towards the catalyst during ATH and both have been depicted in Figure 8.[142]
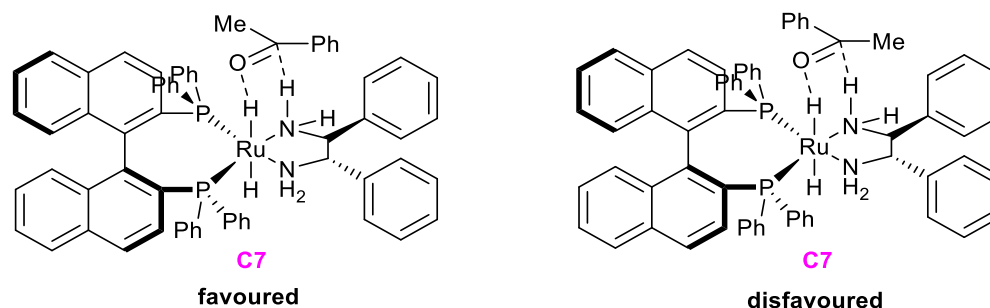
Figure 8. Favoured and disfavoured interaction of **C7** with acetophenone.[142]

Incorporating BINAP into octahedral metal frameworks allows for the use of monodentate, bidentate or tridentate ligands to contribute to inducing asymmetric catalysis (Figure 9).[142]
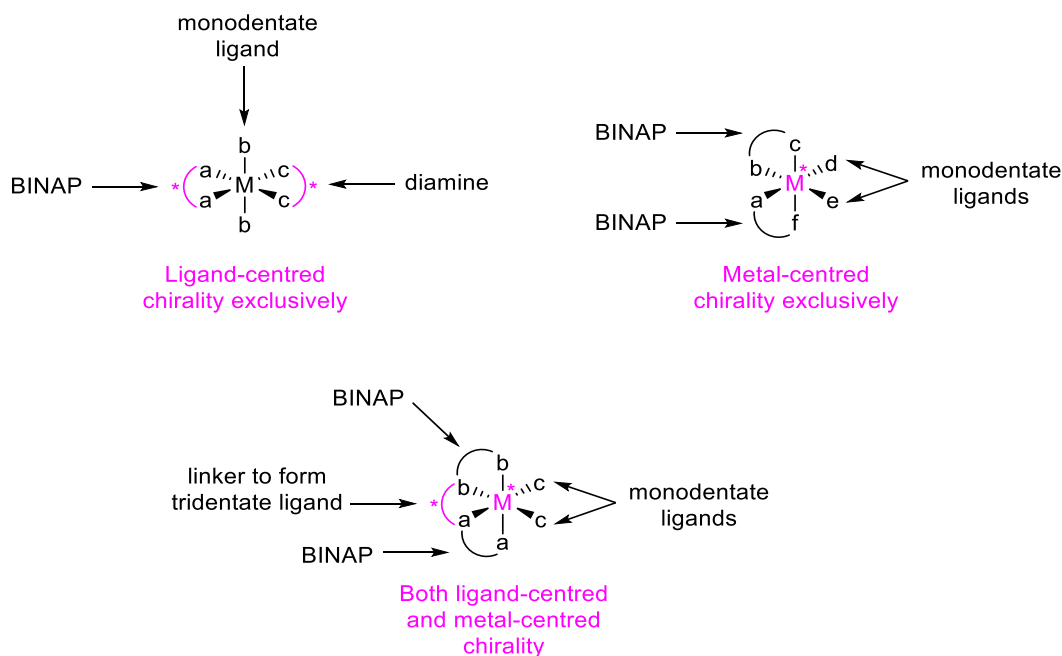
Figure 9. Octahedral metal complex frameworks used in asymmetric catalysis, showing the effects that chiral and achiral ligands can exert on the chirality of the metal. The pink colour defines the ligand or metal to be chiral.[37]

As shown in Figure 8, the two chiral ligands, BINAP and the diamine, were capable of transferring chirality to the substrates via ligand-centred chirality as represented by the octahedral framework on the top left of Figure 9.[37] Within other catalyst frameworks BINAP can render the metal centre chiral by placing the two BINAP ligands adjacent to one another (Figure 9 – metal-centred chirality). If the two BINAP ligands are linked to form a tridentate ligand, the complex becomes chiral both at the metal centre and within the ligand sphere (Figure 9 – ligand-centred and metal-centred chirality).[37]

BINAP has been key in creating (-)-menthol and selectively hydrogenating α-(acylamino)-acrylic acids and esters, α,β- and β,γ-unsaturated carboxylic acids, allylic and homoallylic alcohols, β-Keto esters[70,90] and α-chlorinated acetophenones[105].

1.1.2 Wills' catalysts

Originally inspired by Noyori's catalyst (Table **1** – **C2**), Wills incorporated a tether in order to increase the stability of the catalyst[39,42,46,57,81,88,90,92,93,107,122,125,143,144] (Figure 10 - **C8**).
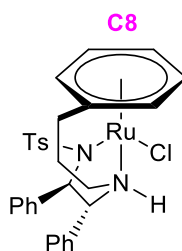
Figure 10. Most widely utilised tethered ruthenium catalyst created by Wills et al.[81]

The arene was initially linked through the sulfonamide group (Figure 11 - 2nd generation of catalysts), and then later to the diamine (Figure 11 - 3rd generation of catalysts). Interestingly, the 3rd generation possesses higher activities than the 2nd generation.[93,144,145] When more heavily substituted arene ligands were used, the rotation of the arene relative to the remaining ligands was restricted, preventing dissociation of the arene ligand.[39,46,90,131,146,147]

2nd generation

alkyl-tethered

C9 R = H, n = 1
C10 R = H, n = 2
C11 R = Me, n = 2
C12 R = H, n = 3
C13 R = Me, n = 3
C14 R = *i*-Pr, n = 3
C15 R = OMe, n = 2

3rd generation

alkyl-reverse-tethered

C8 R = H, n = 0, Ar = toluene
C17 R = H, n = 0, Ar = NMe$_2$
C18 R = H, n = 0, Ar = piperidine
C19 R = Me, n = 0, Ar = piperidine
C20 R = *i*-Pr, n = 0, Ar = piperidine
C21 R = H, n = 1, Ar = NMe$_2$
C22 R = H, n = 1, Ar = piperidine
C23 R = H, n = 2, Ar = toluene

2nd generation

alkyl-tethered

C16
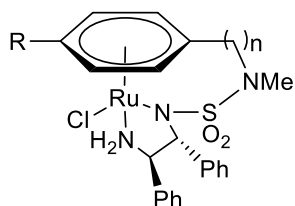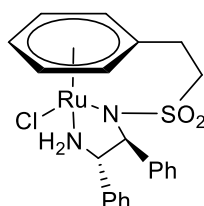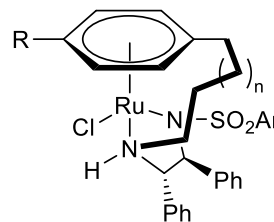
3rd generation

oxo-tethered

C24 R = Ts
C25 R = Ms
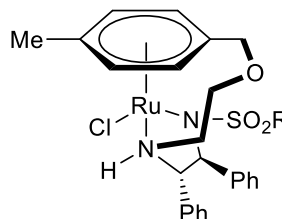
Figure 11. Tethered ATH catalysts by Wills, Ikariya and Mohar.[57,58,81,145,147,148]

Inclusion of a tether allows for lower catalyst loading and increased temperatures, which are essential in reducing challenging substrates[42,81], thereby amplifying the activity[57,92,143] and speed of the ATH in comparison to untethered analogues[90] (see Table 3). Moreover, varying the tether length, in addition to the inclusion of different groups to the tether, for example, a benzene ring[132] or sulfonamide groups[46,146], provided interesting results for Wills et al. and hence by discovering a successful catalyst structure, Wills et al. have defined a clear template by which most research now follows.

Table 3. Comparison of the reduction of various substrates (under identical conditions) by Noyori's untethered catalyst against a few examples of Wills' catalysts to show that the inclusion of a tether increased activity of the catalyst.[81,123,146,149–151]
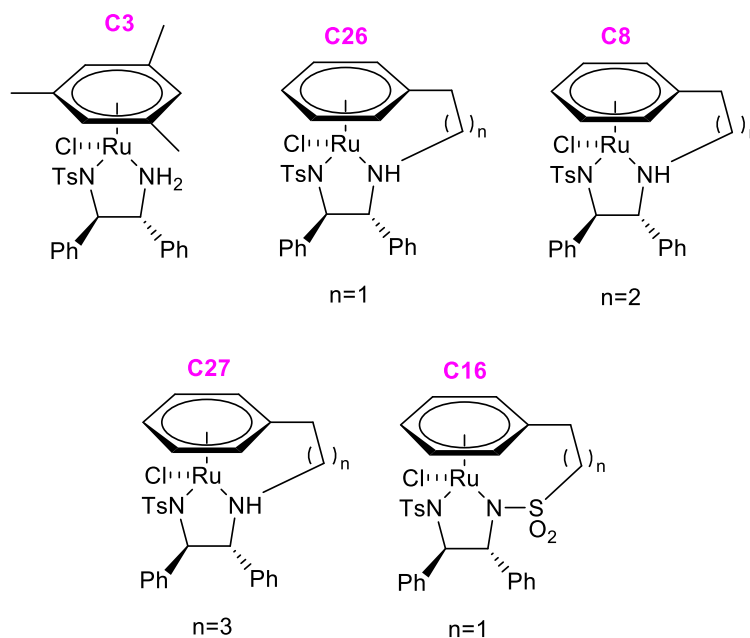
Substrate	Catalyst	Temp (ºC)	Time (h)	Conversion (%)	ee (%)
acetophenone	C3	28	20	>99	98
acetophenone	C26	40	15	19	92
acetophenone	C8	28	3	100	96
acetophenone	C8	40	2	100	96
acetophenone	C27	40	1.25	100	96
acetophenone	C16	28	21	>99	96
1-tetralone	C3	28	48	>99	99
1-tetralone	C3	40	3	97	94
1-tetralone	C8	40	5	100	99.8
1-tetralone	C27	40	5	100	>95
1-tetralone	C16	28	18	>99	98

p-chloro-acetophenone	**C3**	28	24	>99	95
p-chloro-acetophenone	**C3**	40	2	>99	91
p-chloro-acetophenone	**C8**	40	5	100	91
p-chloro-acetophenone	**C27**	28	3	100	91
p-chloro-acetophenone	**C27**	40	5	100	93
p-chloro-acetophenone	**C16**	28	12	>99	92
p-methoxy-acetophenone	**C3**	28	60	99	97
p-methoxy-acetophenone	**C8**	40	1.67	100	94
p-methoxy-acetophenone	**C27**	28	18	100	94
p-methoxy-acetophenone	**C16**	28	44	98	90

Wills et al. also investigated the attachment of the tether to the chelating ligand in place of the phenyl groups usually present (Figure 12). The idea was that the catalyst would favour one diastereoisomer to form during the ATH catalytic cycle. Unfortunately, long reaction times were required and low enantioselectivity was observed.[131]
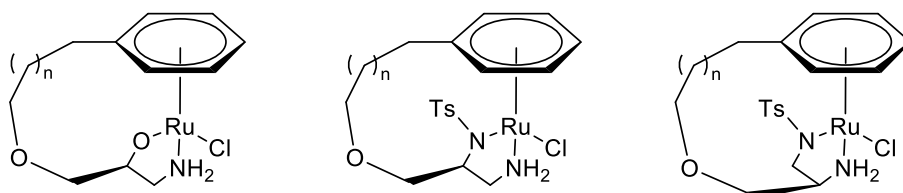
Figure 12. Ether tethered catalysts by Wills et al., whereby n = 1 or 2.[131]

By modifying aspects of the framework, the hope is to tune the catalyst more precisely[144] because the larger the range of ketone substrates that can be reduced by a single catalyst, the more useful the catalyst will be within industry on a larger scale. In fact, to be utilised for multiple purposes within industrial research, catalysts ideally possess a wide substrate scope and are also highly active.[45] ATH can therefore be used as a fundamental intermediate step during the synthesis of various compounds useful in the medicinal industry, for example, cyclic hydrazines[152] or aromatic epoxides[45,58,83,85,105,144,153–155].

C8 (Figure 10)[81,92] was employed by Synthon BV to create montelukast, an anti-asthmatic drug,[81,156] and later by Archimica GMBH to reduce cyclic ketones to prepare

eslicarbazepine, an antiepileptic drug.[81,157] Following these successes, AstraZeneca also used this same catalyst to design an enantioselective and chemoselective pathway towards anti-asthmatic bronchodilator drugs.[81,158] Alternative tethered catalysts synthesised by Wills have been successfully used by pharmaceutical companies worldwide.[92,159] A couple of examples include to obtain chemokine inhibitors via reductive routes in Germany[160] and to prepare intermediates for non-steroidal selective oestrogen receptor modulators in Slovenia[161]. The success of Wills' tethered catalysts also inspired Takasago International Corp. to synthesise Ts-DENEB® (**C24**) which was applicable in many industrial uses.[81,93]

1.1.3 Reaction conditions

Ruthenium catalysts with differing chiral ligands, comprising of diamine, amino alcohol or phosphine moieties, have been developed to be used in the asymmetric transfer hydrogenation of ketones and imines with 2-propanol or formic acid as the hydrogen donors.[27,39,44–46,48–51,54–56,58,59,65,81,85,88–90,97,105–108,110,122,124,126,131,137,139,141,143,144,147,162–170]

Formic acid is the preferred solvent as reactions are more likely to proceed to completion, evolving CO_2 as a byproduct[39,45,46,53,67,105,164,169], as opposed to 2-propanol which allows for reversibility of the reaction as a result of its oxidation to acetone.[44,45,55,59,67,83,88,89,105,112,123,164] As the reaction proceeds, the reverse reaction becomes more predominant, encouraging racemisation of the chiral product, hence the acetone can be distilled off during the reaction to prevent this from occurring.[46,67] Another advantage of the FA/TEA azeotropic mix is that the formic acid is consumed during the reaction and therefore the triethylamine can buffer the pH to create optimum conditions.[45] In fact, by changing the ratio of formic acid to triethylamine, Zhou et al. showed how the azeotropic mixture could affect the asymmetric transfer hydrogenation of ketones. Utilising a lower formic acid:triethylamine ratio (>2.5:1), and therefore neutral conditions, proved to be much more efficient. With an optimum FA:TEA ratio of 0.2:1, increased rates and enantioselectivities were achieved. At higher ratios (from 4.6:1 to 3.1:1), with acidic conditions, the metal hydride and TsDPEN ligands were protonated causing the catalyst to become less active and less enantioselective.[45,171]

Despite this, amino alcohol ligands are not compatible with formic acid/triethylamine[46,90,112,129] and decreased enantioselectivities have been reported after an extended period of time[89]. This has led to the more recent discovery of the metal-ligand bifunctional mechanism to which these reactions follow.[130,139]

1.1.4 The metal-ligand bifunctional mechanism

The metal-ligand bifunctional mechanism for the reduction of ketones by ruthenium catalysts is carbonyl-selective, "tolerating a plethora of functional group substituents"[140] and occurs by concerted proton-hydride transfer. This mechanism is advantageous because the ketone converts into the alcohol directly without the formation of metal alkoxide. Furthermore, the metal-ligand bifunctional mechanism first proved the pathway for octahedral catalysts before later being applied to half-sandwich Ru-TsDPEN catalysts too. The cycle (Figure 13) begins once the ketone substrate interacts via hydrogen bonding to the basic ligand on the active bifunctional catalyst.[27,39,41,45–48,54,56,58,59,61,64,67,81,83,88,105,130,140–142,165,172–180]
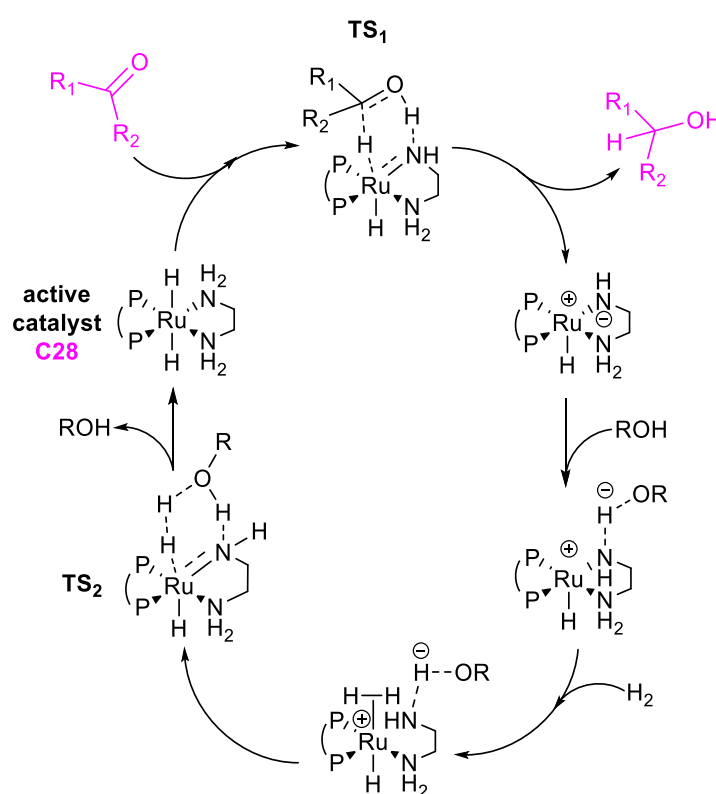
Figure 13. The metal-ligand bifunctional mechanism shown as a catalytic cycle.[142,173]

This forms a six-membered pericyclic transition state (TS$_1$), ensuring the ketone is present in the immediate vicinity of the metal centre. The principle of the metal-ligand bifunctional mechanism is the hydrogen bonding between the carbonyl group of the ketone and the NH functionality of the ligand, which stabilises the transition state and hence encourages a low energy enantio-determining reduction step to occur. In fact, the acidity and polarity of the N-H bond is rendered significantly larger when incorporated into a ruthenium catalyst, allowing the hydrogen bonding to occur with more ease, known as the NH effect. Unusually, there is

no interaction between the metal centre and carbonyl oxygen, highlighting the importance of the NH moiety further.[27,39,41,45–48,54,56,58,59,61,64,67,81,83,88,105,130,140–142,165,172–180]

The NH moiety protonates the oxygen of the ketone concurrently to the hydrogenation of the carbonyl carbon by the Ru-H moiety, directly giving the alcohol product and a zwitterionic complex. Due to the selective simultaneous transfer of hydrogen to the ketone substrate, it is only possible to transfer NH protons in the axial position to the ketone's oxygen, to prevent steric repulsion between the substrate and the ligands on the catalyst.[27,41,45,54,105,130,140,173,178] Next, a solvent molecule protonates the zwitterionic ruthenium complex. As a result, the ruthenium centre becomes more electropositive, and hence has a greater affinity for the dihydrogen. The labile 16-electron complex encourages interaction between the dihydrogen and the alkoxide to form a six-membered cyclic transition state (TS$_2$). The heterolytic splitting of H$_2$ by the alkoxide base regenerates the active catalyst, allowing the catalytic cycle to repeat.[54,82,138,140,173,181]

The main role of the ruthenium, which remains in its +2 oxidation state throughout the cycle, is to activate the dihydrogen and support the hydride before it is transferred. For this mechanism to be successful, the hydride and two nitrogens must be in a *fac*-position within the octahedral complex (Figure 14).[59,82,138,140,173,181]
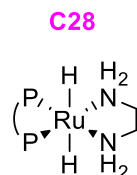
Figure 14. Octahedral complex with the hydride and two nitogens in a *fac*-position.[12]

The real success of this hydrogenation mechanism lies within the H-Ru-N-H conformation (Figure 15).[39,56,67,82,140,144,173,181]
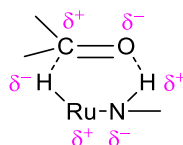
Figure 15. Conformation adopted by the H-Ru-N-H moiety to successfully activate the carbonyl substrate through hydrogen bonding.[82,140,181]

Research suggests that the closer the torsion angle of the H-Ru-N-H is to zero, the more active the catalyst is.[140,144] This six-membered configuration encourages the metal hydride and the proton on the amine to recognise the polar carbonyl double bond selectively.[90,116] The activation of the carbonyl substrate is facilitated by the nucleophilic nature of the Ru-H moiety and the strongly dipolar nature of the H-Ru-N-H functionality, and in turn these features help to stabilise TS_1.[56,67,82,144,173,181]

For half-sandwich ruthenium(II) catalysts, studies suggest that by utilising isopropanol or formic acid as the hydrogen donor, the catalytic cycle can be illustrated as shown in Figure 16.[53,81,83,141,182]
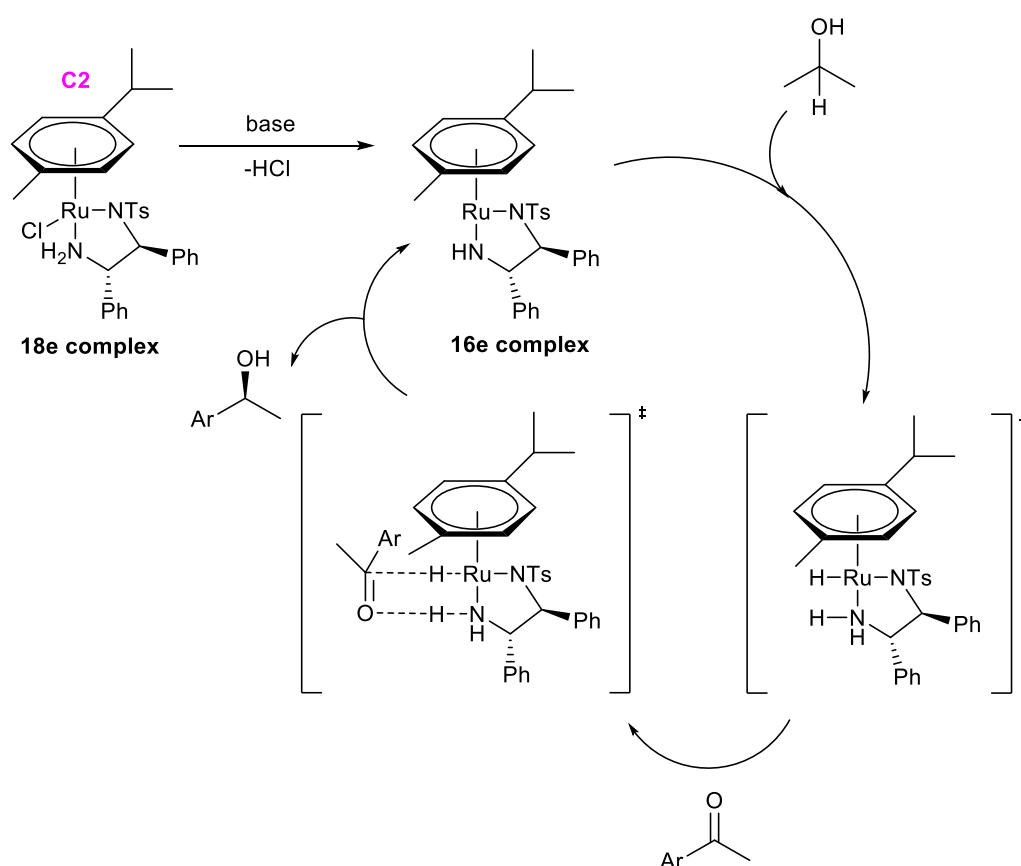
Figure 16. The mechanism for the ATH by half-sandwich Ru(II) catalysts.[83,130,182]

The mechanism follows a cycle of three steps; first the active catalyst is generated by elimination of HCl, next the transfer of hydrogen from the hydrogen donor to the catalyst and subsequently to the substrate, and finally the active catalyst is regenerated by the hydrogen source.[39,47,53,58,81,98–100,106,131,141,169,170,172,177] As further proof, all intermediates were isolated and characterised except for the transition state.[53,81,83,130,177,182–184]

A high linearity between conversion (%) and time was established by Wills et al.[132], utilising the inclusion of a cyclohexyldiamine ligand to replace the TsDPEN ligand (Figure 17), suggesting the beginning of the reduction to be of zero-order.
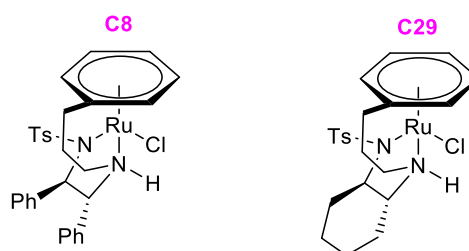
Figure 17. Substitution of Noyori's TsDPEN ligand for a 1,2-cyclohexanediamine ligand.[132]

This emphasised that the concentration of the ketone did not majorly affect the rate and therefore it has been presumed that the rate determining step within the catalytic cycle does not depend on the rate of hydrogen transfer to the substrate, but in fact relies upon the regeneration of the metal hydride.[132,170]

^{1}H-NMR and chiral GC was used to kinetically deduce how the rate was directly affected by this mechanism (shown in Figure 18), utilising tethered catalysts comprising of the TsDPEN ligands (shown in Table **4**). Assumptions were made that the ketone reduction followed a second-order pathway, and that the hydride was regenerated by the formic acid in first-order fashion. Conclusions were made that the rate of Ru-H regeneration limited the overall reduction rate of the tethered catalysts until the concentration of ketone was low.[150,170]
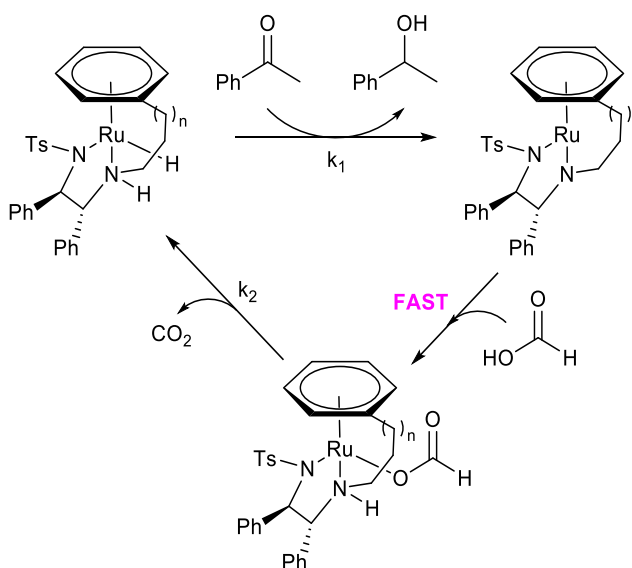
Figure 18. Kinetic model for the ATH of acetophenone by Ru(II) catalysts. The rate constants have been shown in Table 4.[170]

Table 4. Table to show the structure of Ru(II) catalysts with their rate constants included for the reduction of acetophenone. Substrate loading: 0.5 mol %, temperature: 40 °C and 5:2 FA/TEA azeotrope.[170]

Catalyst		Tether length	k_1/M^{-1} min^{-1}	k_2/min^{-1}
n=1	C26	2C	0.5	0.034
n=2	C8	3C	10	3.7
n=3	C27	4C	11	9.3
n=4	C23	5C	3.0	0.25
	C1	Untethered	0.75	1.0
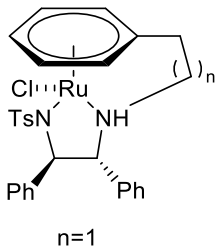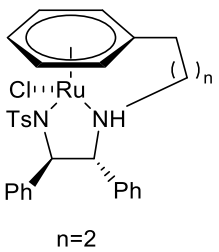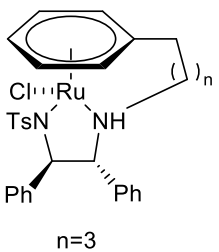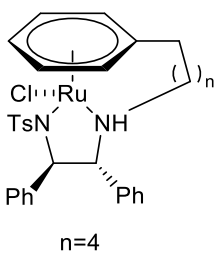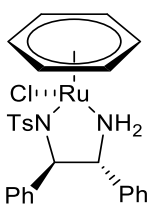
In fact, the 4C-tethered catalyst **C27** in particular gave an increased regeneration of the hydride in comparison to similar analogues, and hence a faster rate of ketone reduction was observed.[150,170] Wills et al. proposed the idea that the tether and ligands were positioned in such a way to allow for the most efficient transfer of hydrogen.[144] This was confirmed by a study that calculated the torsion angles of the Cl-Ru-N-H moieties for catalysts **C8** and **C27**, which were 4.59/4.14 (two complexes in the asymmetric unit) and 3.04 respectively. The smaller the torsion angle was in magnitude, the more efficiently the hydrogen transfer to the substrate was.[170] In fact, the torsion angle of the Cl-Ru-N-H moiety in **C2** was calculated to be -18.31, which gave further support that the incorporation of a tether of three carbon atoms in length increases the activity of the complex.[162]

The NH moiety attached to the ruthenium(II) centre, that takes part in the pericyclic six-membered transition state by "acting as the proton donor"[141], has been concluded to "selectively recognise substrates"[141] by forming a hydrogen bond between the NH moiety and the oxygen of the substrate (Figure 15), hence "encouraging favourable orientations in close proximity to the ruthenium(II) metal centre"[141] if the distance between the NH moiety and metal centre was optimum (Figure 19).[141]
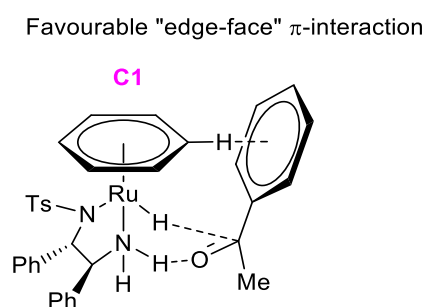
Figure 19. Noyori's catalyst in the transition state during ATH.[86]

1.1.5 Approach of the substrate to the ATH catalyst

When asymmetric ketones are used, whereby only one of the ketone substituents is aryl, one orientation of the ketone towards the catalyst is favoured, thereby controlling the absolute stereochemistry of the reduction product.[27,39,46,58,64,67,81,90,97,100,102,107,125,130–132,137,144,169,172,178,185] To adopt this favoured configuration, catalysts must be able to discriminate between the two enantiofaces on the ketone substrate[39,59,67,81,90,107,131,168,169,181], hence dialkyl ketones and benzophenones are often reduced with less selectivity as a result of the lack of discrimination[39,45,67,81,90,92,98,102,106,107,131,137,168,169,172,184].

Aromatic ketones are attractive substrates because of the CH-π interaction, which further stabilises the six-membered transition state (TS_1) during the hydrogen transfer.[27,39,46,58,64,67,81,90,97,100,102,107,125,130–132,137,144,169,172,178,185] The combination of stabilising attractive electrostatic CH-π interactions and destabilising SO_2-arene interactions, as a result of the moieties lone pair, dictates the enantioselectivity of the reduction.[39,42,97,125,184,186] If the attractive CH-π interactions outweigh the repulsive SO_2-arene interactions, the major enantiomer forms (Figure 20 - left). However, if the SO_2-arene interactions dominate, the minor enantiomer is formed (Figure 20 - right).[39,97,186]
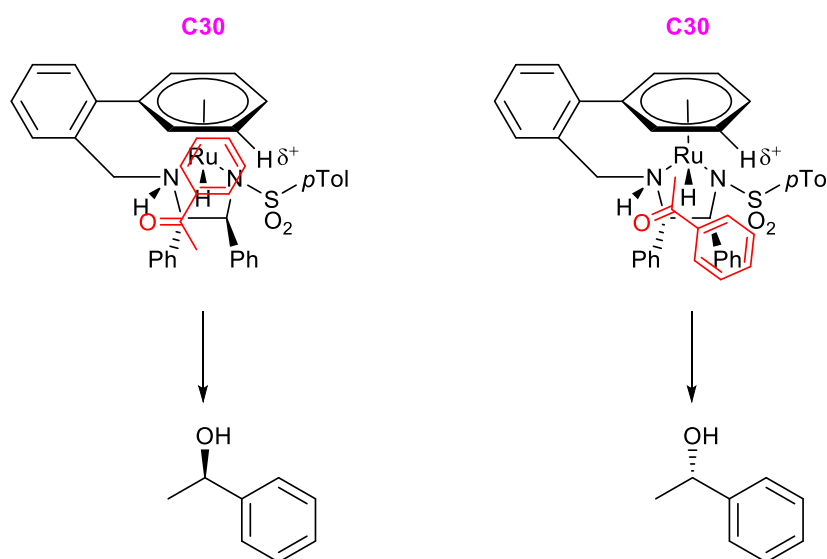
Figure 20. Interactions between acetophenone and a benzyl-tethered catalyst to give the major (*R*)-enantiomer (left) and minor (*S*)-enantiomer (right).[186]

Alternatively, if the ring of the substrate is saturated, the major and minor enantiomers are opposite to Figure 20 (see Figure 21). The catalyst is unable to discriminate the enantiofaces of the substrate via electrostatic interactions, therefore the TS is stabilised via discrimination of the enantiofaces by the attraction between the SO_2 lone pair on the catalyst and the C-H groups on the ketone.[42,67,125,186]
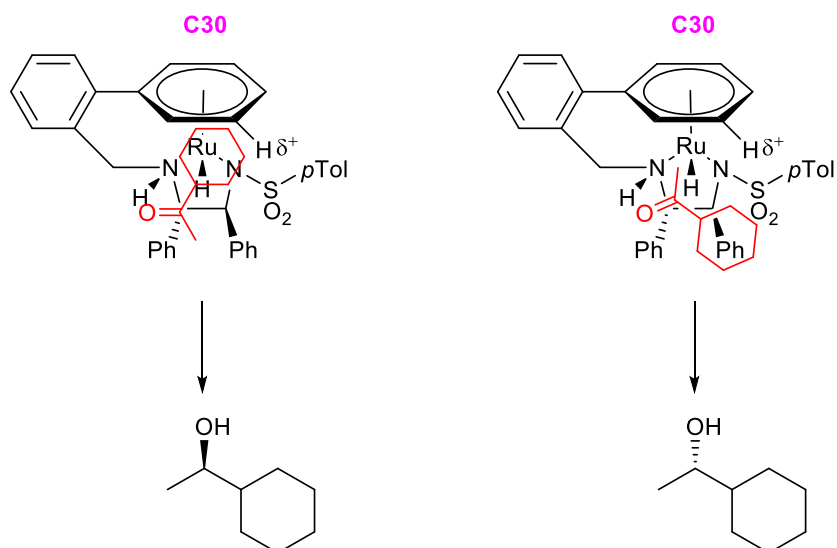
Figure 21. Interactions between 1-cyclohexylethanone and a benzyl-tethered catalyst to give the minor (*R*)-enantiomer (left) and major (*S*)-enantiomer (right).[186]

Research conducted by Wills et al. supports this idea. Their results concluded that when using the (*R*,*R*)-catalyst **C8**, all ketones (Figure 22) reduced gave the (*R*)-enantiomer except 1-cyclohexylethan-1-one which gave the (*S*)-enantiomer (Figure 23).[27,67,123,144]

acetophenone   propiophenone   2-methyl-1-
phenylpropan-1-one

2,2-dimethyl-1-   cyclohexyl(phenyl)
phenylpropan-1-one   methanone
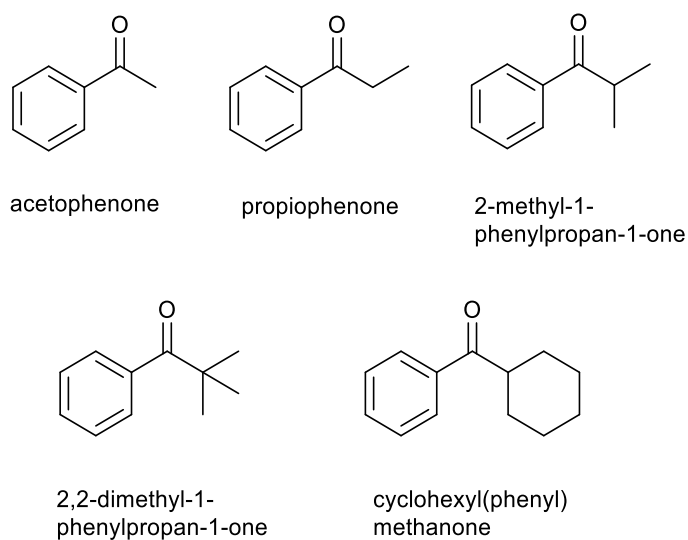
Figure 22. Ketones reduced by **C8**.[123]
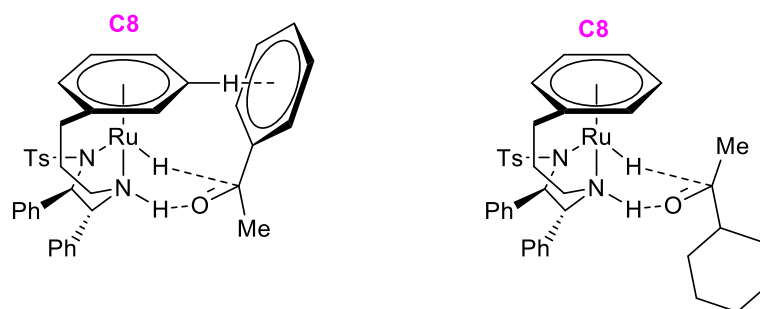
Figure 23. The influence of electrostatic interactions on the position of the substrate adopted during ATH.[123]

This indicates that the favoured configuration, comprising of the aromatic group occupying the site adjacent to the η^6-arene ligand, is adopted primarily but if the π-aryl-η^6-arene interaction is not present, then in some instances the spatial orientation of the substrate in the transition state may be reversed (Figure 23)[67,81,123,144,169], with the larger alkyl moiety facing away from the arene ligand as a result of steric hindrance, hence delivery of the hydrogen occurs from the opposite face[123,168,187]. Though this is clear evidence that steric effects contribute to the enantioselectivity induced during ATH, research suggests that these forces are too weak to induce high enantioselectivity towards dialkyl ketones alone.[169]

A similar substrate-catalyst interaction can be formed by the electrostatic or dispersion forces dominating. For example, addition of methyl groups to the arene ring (Figure 24 - C31).[150,169] The CH-π interaction was "extended through the methyl group on the arene ring"[169], forming a stabilising interaction with the electron rich ketone group.[42,46]
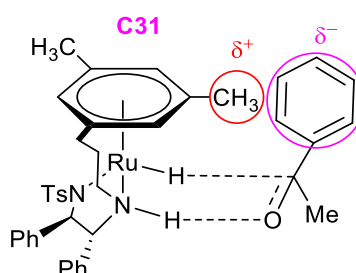
Figure 24. Conformation adopted during ATH, directed by electronic effects.[150]

Another example of this alternative substrate-catalyst interaction being adopted was when the CF_3 group in 1,1,1-trifluoroacetophenone took priority and competed with the phenyl group to occupy the site adjacent to the η^6-arene ligand in the TS during the reduction (Figure 25), which resulted in low enantioselectivities (Table 5).[81,151,188]

C32, C8, C33, C34
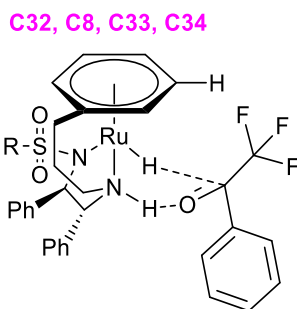
Figure 25. Competition between CF_3 and Ph groups of the substrate to occupy the space adjacent to the arene ring of the Ru(II) catalysts.[151,188]

Table 5. Catalysts investigated by Hodgkinson et al., alongside their enantioselectivity obtained for the reduction of 1,1,1-trifluoroacetophenone.[151]
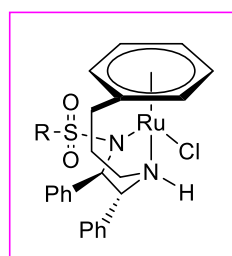
Catalyst	R		ee (%)
C32	Ms		22
C8	Ts		45
C33	Mesitylene		17
C34	1,3,5-triisopropylbenzene		1

If a ketone comprised of two aromatic rings, an out-of-plane orientation was observed when the aromatic ring with lower electron density or higher steric demand faced

away from the arene ring.[81,147,168] The greater the difference in electron density or steric demand between the rings, the easier it was for the catalyst to discriminate between the two groups on the substrate.[147]

Further, research showed that when a ketone comprised of both a hindered aromatic ring with a substituent at the *ortho* position and a *ortho*-hydroxyphenyl group, very high selectivity was obtained (Figure 26). This was because the bulky aromatic ring was forced out-of-plane during the reduction, whilst the *ortho*-hydroxyphenyl group remained in-plane with the catalyst, dictating the enantiomer formed as a result of this appended directing effect. Moreover, the –OH was suspected to form a hydrogen bond to the carbonyl group within the ketone whilst in the transition state, which encouraged the favoured interaction between the aryl ring on the catalyst and the aryl ring on the substrate to occur.[189]
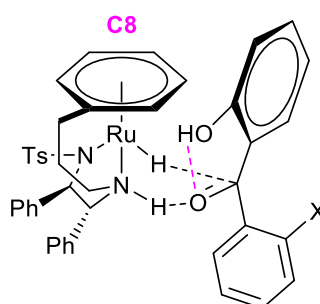
Figure 26. In-plane and out-of-plane interaction between **C8** and a diaryl ketone, whereby X = OCH_3, Cl or Br.[189]

1.1.6 Types of substrates

The size of the scope of substrates successfully reduced is one important factor to be considered when creating a catalyst to be used in ATH. A large range of substrate classes have been reduced by various successful catalysts including benzophenones, benzaldehydes, benzoylacetate esters, β-keto esters, benzils, unsymmetrically substituted 1,2-diketones, 1,3-diketones, α-substituted acetophenones, α,α-disubtituted ketones, sulphur- or oxygen-containing ketones, α,β-unsaturated ketones, α,β-acetylenic ketones, α-alkynyl ketones, diynones, propargylic ketones, heteroarenes, pyridones, amides and imines.[27,45,47,81,83,88,90,97,98,102,105,106,108,126,135,141,144,162,168,172,176,190–202]

Most catalysts, as a result of stability and electron density or their compatibility with ketones containing certain substituents, can only reduce a small selection of substrates. The most difficult substrates to reduce are alkynyl ketones, α-chloroketones and 2-ketopyridines, due to their susceptibility to side reactions leading to deactivation of the catalyst, and

hindered dialkyl ketones, due to their nearly identical steric and electronic nature, making discrimination of the groups challenging.[45,81,92,97,106,107,137,151,159,172,184,189,192,194]

Activity and enantioselectivity achieved during ATH can depend upon the position and type of substituent on the aromatic ring of the substrate.[89] It has been shown that *para*- and *meta*-substituted aryl ketones produce alcohols with greater ee values than *ortho*-substituted ketones due to steric hindrance.[106,144,148,203] Other highly hindered substrates like ᵗBuCOPh (Figure 27) have been reported to be difficult to reduce via ATH reactions[89,123,144], with a reduction of enantioselectivity observed as the size of the aliphatic group on the ketone increases[144]. Incorporating a tether to the catalyst framework saw an increase in activity, reducing ᵗBuCOPh in 95 % using FA/TEA, in addition to an ee of 77%.[123] Comparatively, **C3** (Table **1**) reduced ᵗBuCOPh in >1 % conversion using FA/TEA.[128]
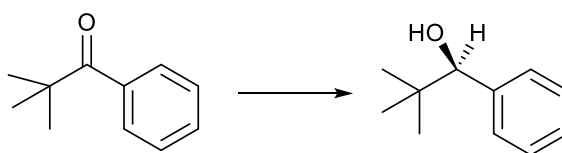
Figure 27. Reduction of hindered substrate tBuCOPh.[81]

Soni et al. focused upon the reduction of electron-rich hydroxyl- and methoxy-substituted ketones. *Ortho*-methoxyacetophenone (Figure 28) was reduced with high conversion rates and ee values of up to 96%. A majority of this class of ketone was more soluble in FA/TEA, hence improved results determined that FA/TEA was more favourable as the solvent for the ATH, as opposed to water.[87]
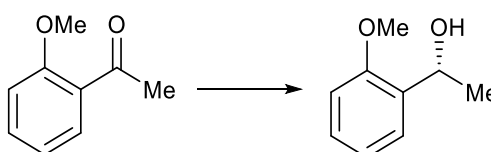
Figure 28. Reduction of *ortho*-methoxy acetophenone.[87]

Para-methoxyacetophenone was reduced by all catalysts studied at a slower rate than *para*-chloroacetophenone (Figure 29), but with higher enantioselectivity due to the electron-donating nature of the methoxy-substituent and electron-withdrawing nature of the chlorine substituent. 3,5-dimethylacetophenone was reduced with high ee, whereas 3,5-bis-trifluoromethylacetophenone was reduced with 18 % ee, proving that enantioselectivity can be affected by electron-withdrawing/-donating substituents on the substrate.[45,81,151]
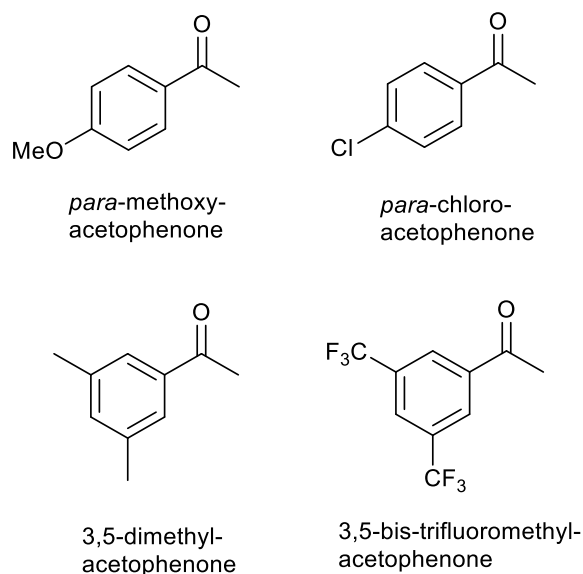
Figure 29.Ketones reduced by Wills et al.[151].

Another investigation by Wills et al. identified that **C8** (Figure 30), reduced 2-acetylpyridine (Figure 31) with 94 % ee. Further studies revealed that this catalyst was also compatible with some ketones comprising of α-substituents or heterocyclic moieties.[81,100]
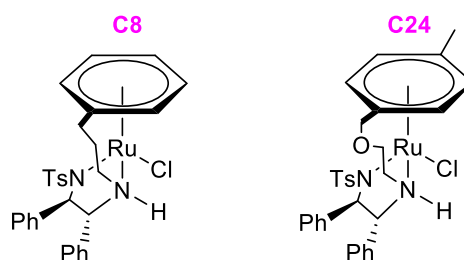
Figure 30. Will's catalysts: 3C-tethered (left) and Ts-DENEB® (right).[81,100]
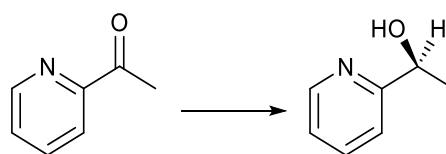
Figure 31. Reduction of 2-acetylpyridine.[81]

Conversely, 2-acetylpyridine inhibited the reduction by Ts-DENEB® (Figure 30 – **C24**).[81,100] This was due to hydrogen bonding between the protonated substrate and the catalyst (Figure 32), stabilising the transition state to such an extent that the "product was not released"[100].
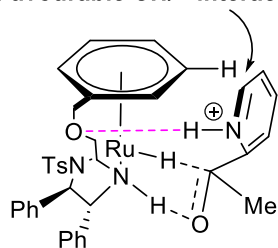
Figure 32. Additional interaction between the tether of Ts-DENEB® and 2-acetylpyridine.[100]

Mohar's catalysts (Figure 33) are unique from Wills' catalysts in two possible ways. The first is by incorporating an amide within the tether (C10), and the second is either an increase in tether length, a change of the R group to an alkyl substituent, or modification of the Ar group to an amine functionality (C17-C23).

C17 R = H, n = 1, Ar = NMe$_2$
C18 R = H, n = 1, Ar = piperidine
C19 R = Me, n = 1, Ar = piperidine
C20 R = *i*-Pr, n = 1, Ar = piperidine
C21 R = H, n = 2, Ar = NMe$_2$
C22 R = H, n = 2, Ar = piperidine
C23 R = H, n = 3, Ar = toluene
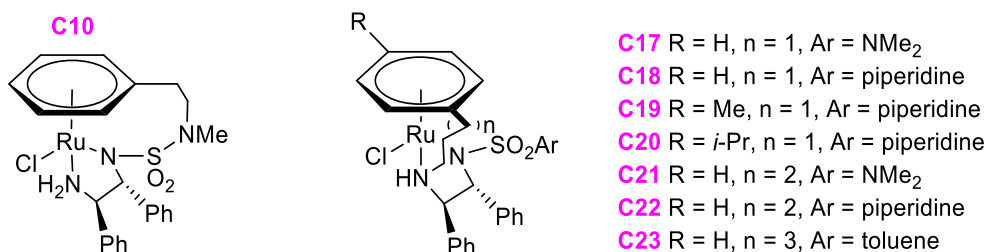
Figure 33. (*S*,*S*)-Mohar's catalysts.[81]

Mohar's catalysts reduce 1-naphthyl ketones[81,204] the most efficiently. There has been a further increase in conversion efficiency reported for the tethered catalysts in comparison to the untethered analogues.[81] Despite this, 1'-acetonaphthone comprising of a 2'-OMe group (Figure 34) was inert to reduction[81] because the acetyl group was orientated in a different plane to the flat aromatic rings of the substrate, preventing conjugation between the acetyl group and the naphthalene moiety, hence hindering interaction with the catalyst.[204]

1-(naphthalen-2-yl)ethan-1-one

Reduced with 96 % ee

1-(2-methoxynaphthalen-1-yl)-
ethan-1-one
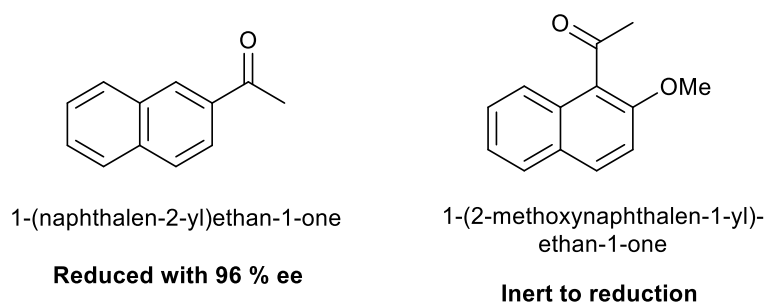
Inert to reduction

Figure 34. 1-naphthyl ketones subjected to reduction by Mohar catalysts.[81]

1.2 Design factors that can be manipulated within the structures of ruthenium(II) catalysts

1.2.1 The half-sandwich framework

The features (Figure 35) that can be explored in order to determine their significant effect on the reactivity and enantioselectivity on a range of substrates for ATH.
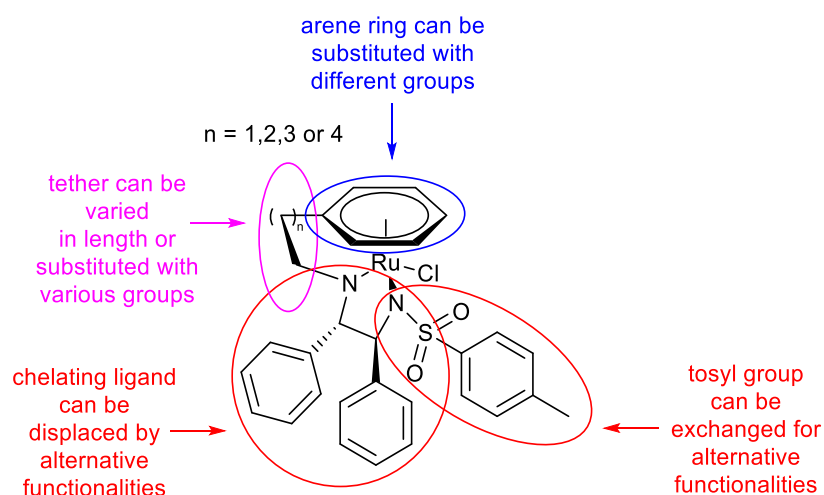
Figure 35. Diagram showing the distinct parts of the catalyst that can be tuned.[41]

The monodentate chloride ligand has been substituted for alternative functionalities, for example an iodide ligand, however, the complexes comprising of the chloride ligands portray higher activity due to reduced stability and hence ease of substitution of the chloride ligand to form the hydride intermediate for the catalytic cycle during ATH.[99,205–208]

1.2.2 Chiral-at-metal catalyst

The induction of chirality at the metal centre, by inclusion of chiral ligands or the organisation of achiral ligands around the metal centre, is key to creating enantioselective half-sandwich catalysts. This is because the bidentate ligand dictates the configuration at the metal, and, in conjunction with stabilising interactions, namely the favourable CH-π interactions, between the catalyst and the substrate, this ultimately determines the enantioface of the ketone to which hydrogen will be transferred.[27,32,33,35–37,172]

1.2.3 Varying the chelating ligand within the ruthenium catalyst

Modifying ligands holds the key to enhanced catalytic performance because the chirality of the ligand dictates the chirality of the metal centre, which in turn determines the chirality of

the reduction product. To attain high catalytic activity and selectivity, the optimum steric and electronic properties of the overall catalyst can be manipulated through variation of the ligand's steric hindrance and electron density (Figure 36).[15,23,37,38,45–47,58,59,66,90,105,141]

Figure 36. Examples of chelating ligands in half-sandwich Ru(II) ATH catalysts.[45]

1.2.3.1 Functionalisation of the basic amine of the TsDPEN ligand

The introduction of groups to the basic nitrogen atom allows linkage to molecules with varying uses, for example, "secondary catalysts, fluorescent tags or polymeric supports"[100,209,210], plus modification of the amine does not affect the stabilising hydrogen bonding between the proton on the amine of the ligand with the oxygen on the carbonyl of the ketone substrate during ATH.[27,98,100] Incorporating a diverse range of functionalities (Figure 37) can improve the activity of the catalyst, alongside lower temperatures and catalyst loading to be employed for ATH. For example, a catalyst including an N-PEG chain was more soluble in aqueous conditions, and hence was more successful reducing ketones in water.[209]

Figure 37. Examples of N-alkylated catalysts.[103,209,211]

1.2.3.2 Functionalisation of the sulfonamide group of the TsDPEN ligand

The reactivity and enantioselectivity of catalysts has been affected by the steric hindrance and electron-withdrawing property of the sulfonamide group within the TsDPEN ligand (Figure 38).[58,124,126,151,212] Electron-withdrawing groups rendered the -NH group more acidic and the adjacent -NH$_2$ less basic, positively influencing the enantioselectivity of the catalyst.[46,59,124,126] Further, incorporation of a sulfonyl group was crucial in "lowering the pK$_a$ of the amine to permit the formation of an ionic bond between the ligand and the metal centre"[45,126], confirming that sulfonylated diamines accelerated hydride transfer[59].

Figure 38. Differing groups attached to sulfonamide moieties within chelating ligands.[126]

Hodgkinson et al. expanded the family of 3C-tethered and 4C-tethered ruthenium catalysts (Table **6**) by increasing the steric bulk of the R group attached to the sulfonamide moiety; the four ligands explored were TsDPEN, MsDPEN, MtsDPEN and TrisDPEN.[81,151]

Table 6. Ru(II)-TsDPEN tethered catalysts with alternative sulfonamide groups.[151]
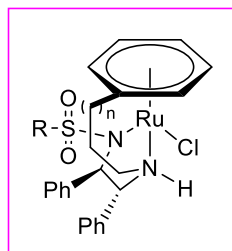
Catalyst	R		Tether length
C32	Ms (MsDPEN)		3C, n = 1
C8	Ts (TsDPEN)		3C, n = 1
C33	Mesitylene (MtsDPEN)		3C, n = 1

C34	1,3,5-triisopropylbenzene (TrisDPEN)		3C, n = 1
C35	Ms (MsDPEN)		4C, n = 2
C27	Ts (TsDPEN)		4C, n = 2
C36	Mesitylene (MtsDPEN)		4C, n = 2
C37	1,3,5-triisopropylbenzene (TrisDPEN)		4C, n = 2
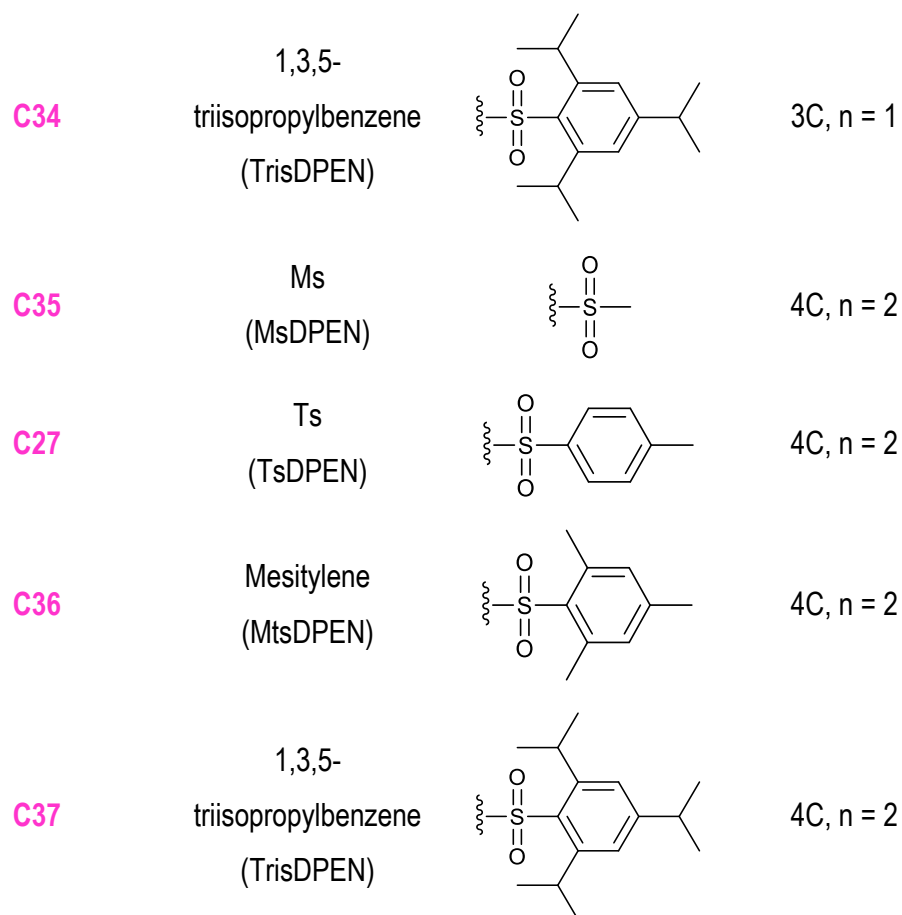
At 40 °C, a majority of substrates, including acetophenone, α-tetralone and *meta*-methoxyacetophenone (Figure 39), were reduced in high enantioselectivity with very minimal difference observed by the change in sulfonamide functionality.[151]

acetophenone

α-tetralone

ortho-chloro-acetophenone

ortho-methoxy-acetophenone

meta-methoxy-acetophenone

para-methoxy-acetophenone
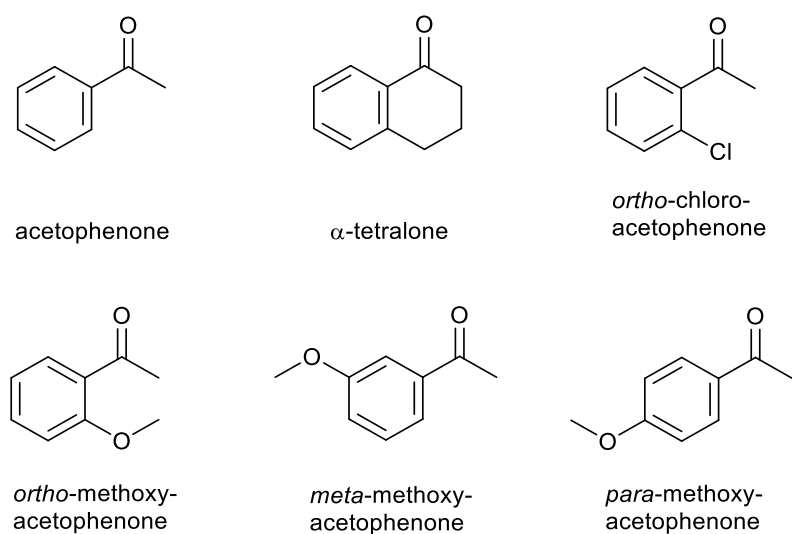
Figure 39. Substrates reduced by catalysts comprising of the ligands: TsDPEN, MsDPEN, MtsDPEN and TrisDPEN.[151]

However, two substrates in particular, *ortho*-methoxyacetophenone and *ortho*-chloroacetophenone (Figure 39), showed a drastic decline in enantioselectivity on increase of steric bulk on the sulfonamide moiety, with the electron-donating methoxy substituent being reduced with ee values as low as 22 %, in comparison to the electron-withdrawing chloride substituent reduced with only 35 % ee.[151]

Conversion rates appeared to be more tolerant of change to the sulfonamide group, with most substrates being reduced near to or at 100 %. Despite this, some substrates showed a drop in conversion when the MtsDPEN (**C33** and **C36**) or TrisDPEN (**C34** and **C37**) ligands were employed. In some cases this was a subtle decrease, for example with α-tetralone, which was reduced by the 3C-tethered catalysts containing the MsDPEN (**C31**) and TsDPEN (**C8**) ligands by 95 % and 100 % respectively, but only by 82 % by the two bulkier catalysts (**C33** and **C34**). A greater difference in conversion was spotted for *para*-methoxyacetophenone (Figure 39), which was reduced fully by the two least bulky catalysts (**C32** and **C8**), but only 69 % and 37 % conversion was achieved by the catalysts comprising of the MtsDPEN (**C33**) and TrisDPEN (**C34**) ligands respectively. Overall, the TsDPEN ligand showed the most promise with regards to conversion rates and enantioselectivity for all substrates tested, and hence was determined to be the most effective catalyst (**C8**).[151]

Another study modified the sulfonamide group with various alkyl groups (Table 7), determining the ligand comprising of the smallest substituent to be the most active.[48]

Table 7. Chiral ligands whereby the modification occurred on the sulfonamide group.[48]

	R		R
L5	Me	**L9**	Me
L6	-(CH$_2$)$_5$-	**L10**	-(CH$_2$)$_5$-
L7	*c*Hex	**L11**	*c*Hex
L8	*i*Pr	**L12**	*i*Pr

This does not allow for a trend to be spotted, therefore it has been concluded that the influence of altering the sulfonamide moiety depends upon the nature of the substrate itself, in particular its electronic and steric properties.[58,59,151]

1.2.3.3 Changing the length of the spacer on the TsDPEN ligand

The size of the chelating ligand affects the stability, reactivity, and selectivity of catalysts. One way that this was investigated was by changing the length of the spacer within the diamine ligand (Figure 40). The effect was suspected to be as a result of a change to the bite angle, affecting flexibility of the ligand and in turn the strength of coordination to the metal centre.[58]
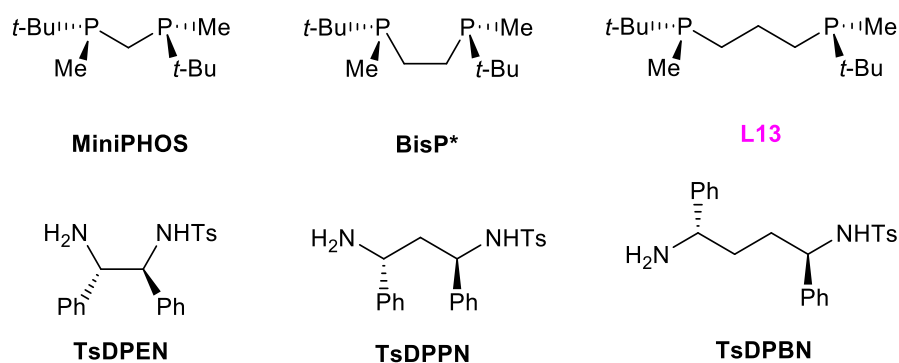
Figure 40. Chelating ligands with varying spacer lengths.[58]

1.2.4 The incorporation of a tether

Tethered catalysts, whereby the tether is linked from the η^6-arene ring to either the basic amine moiety or the sulfonamide moiety (Figure 41), are significantly more stable than non-tethered catalysts and catalyse ATH reactions at a much faster rate, showing their capability to reduce electron-rich ketones, consisting of alkoxy and amine substituents, despite these substrates reluctance to be reduced.[58,81,144,150]

2nd generation

alkyl-tethered

C9 R = H, n = 1
C10 R = H, n = 2
C11 R = Me, n = 2
C12 R = H, n = 3
C13 R = Me, n = 3
C14 R = i-Pr, n = 3
C15 R = OMe, n = 2

3rd generation

alkyl-reverse-tethered

C8 R = H, n = 0, Ar = toluene
C17 R = H, n = 0, Ar = NMe$_2$
C18 R = H, n = 0, Ar = piperidine
C19 R = Me, n = 0, Ar = piperidine
C20 R = i-Pr, n = 0, Ar = piperidine
C21 R = H, n = 1, Ar = NMe$_2$
C22 R = H, n = 1, Ar = piperidine
C23 R = H, n = 2, Ar = toluene

2nd generation

alkyl-tethered

C16
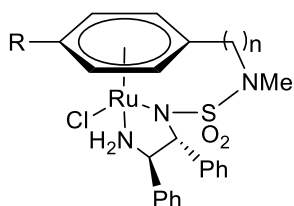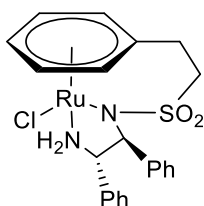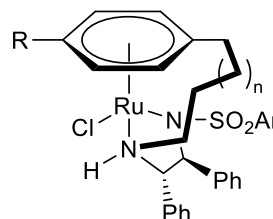
3rd generation

oxo-tethered

C24 R = Ts
C25 R = Ms
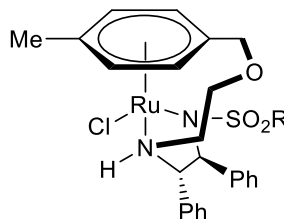
Figure 41. Tethered ATH catalysts by Wills, Ikariya and Mohar.[57,58,81,145,147,148]

Tethered complexes have shown such increased activity that one study showed ^{t}BuCOPh, a highly hindered substrate, was reduced successfully even though it was usually resistant to reduction by the untethered analogue. Often the untethered catalyst degrades or its ligands dissociate in low pH, but incorporating a tether improves both activity and stability and the catalyst continues to be active for a greater number of catalytic cycles as compared to the untethered analogues.[81] Interestingly, the most active catalyst had a tether of four carbon atoms in length, although the tethers of three and five carbon atoms in length also produced chiral products with high ee values.[58,81,150]

The increased activity of the various tethered [Ru(II)(TsDPEN)(η^6-arene)] catalysts allowed lower temperatures to be employed during the reduction, with the most successful catalyst linking the η^6-arene to the diamine via the basic N substituent (Figure 42).[81]
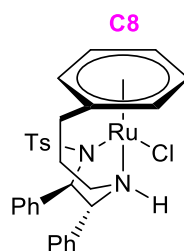
Figure 42. Modification of Noyori's Ru(II) complex by incorporation of a tether.[132]

The potential increase in stability was suspected to be from the 'three-point' attachment between the ligand and metal centre.[46,129,144] This tethered complex (C8) showed that incorporation of the tether reduced the reduction time of acetophenone by 21 hours, in turn allowing reduced catalyst loading.[81] Moreover, (*S*)-1-cyclohexylethan-1-one, a dialkyl ketone difficult to reduce enantioselectively, was reduced in 69 % ee after two hours[107,123,144], comparable to an untethered catalyst, [((1*R*,2*S*)-ephedrine)Ru(*p*-cymene)Cl], that reduced the dialkyl ketone in only 6 % ee under identical reaction conditions.[107]

Analysis of the x-ray crystallographic structure concluded the tether was orientated away from the location where the ketone approached during ATH.[144] Repulsive forces induce steric control from the tether to the substrate, whereby the larger group on an alkyl/alkyl substrate occupies the area further from the arene ring and the tether (Figure 43).[97,107,144]

**Favoured
conformation**   **Disfavoured
conformation**
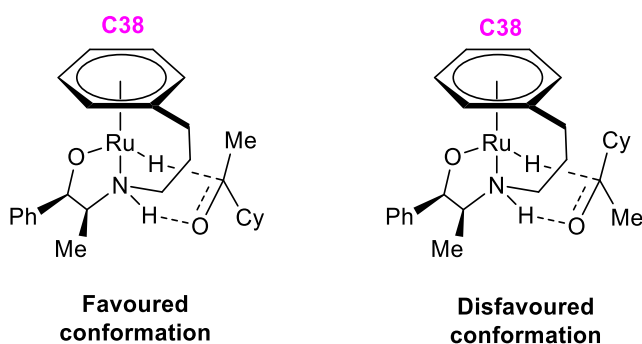
Figure 43. The effect of the tether on the conformation adopted during the ATH of 1-cyclohexylethanone.[107]

This was also the case for pentafluoroacetophenone but not for acetophenone because the CH-π interactions dominated over steric repulsion induced by the tether.[97,188]

An alternative version of tethered catalysts includes an oxygen atom incorporated into the tether (Figure 41), increasing the electron density within the tether and in turn the catalytic activity of the complexes.[57,81] Two variations were synthesised, whereby the group on the sulfonyl moiety was either a tosylate or mesylate. Both showed high activity and

selectivity towards a range of ketones, including 1-indanone, 1-tetralone and diarylmethanols, despite the longer reaction times required.[57,81,147] For example, acetophenone was reduced with a S/C = 1000 and temperature of 60 ˚C within 3 hours to an extent of 97 % ee for the tosylate oxo-tethered catalyst (C24), with only a 2 % drop in ee for the mesylate analogue (C25). The tosylate oxo-tethered catalyst was superior, maintaining stability and activity for 4 days of ATH in one experiment. Additionally, this catalyst matched the high enantioselectivity achieved at S/C = 1000 even at S/C = 30,000, and portrayed increased activity when compared to Wills' 4C-tethered catalyst (C27).[57,81]

Research investigated Noyori's catalyst by altering the sulfonamide group in the tether to develop new catalysts (Figure 41) capable of higher conversions as a result of their higher stability, and were found to be particularly successful in the reduction of 1-naphthyl ketones, except acetonaphthone which proved to be inactive due to the 2'-OMe group.[81] Further investigation varied both tether length and the substituents at the *para* position of the arene ring to create a rigid catalyst structure. Enantioselectivity increased marginally with an increase of steric bulk of the *para* substituent on the arene ring, however, the reaction rate decreased, requiring an increased reaction duration for complete conversion of acetophenone. Catalyst C18 was the most efficient catalyst, reducing acetophenone at S/C = 1000 and a temperature of 60 ºC within 3.5 hours to an extent of 94.5 % ee. This result matched the activity observed by Wills' 3C-tethered catalyst C8 and Ikaryia's Ts-DENEB® C24, plus the catalyst portrayed an increase in activity in comparison to 2nd generation catalysts C13 and C14. Moreover, the absence of a *para* substituent on the arene ring encouraged higher activities towards 2-acetylfurans and 2-acetylthiophenes. Overall, a broad range of ketones were reduced with excellent enantioselectivities including indanones and α-tetralones.[145]

1.2.5 Bulky substituent on the benzylic carbon

One example was the incorporation of a benzyl tethering group (C30) to replace the aliphatic tether usually present (Figure 44), which proved higher enantioselectivity and conversion rates than the first 3C-tethered catalyst (C8) synthesised.[125,132,168]
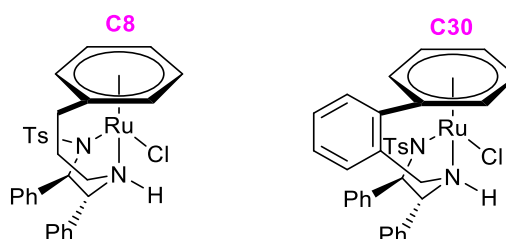
Figure 44. Modification of Wills' tethered catalyst framework to incorporate a bulkier benzylic tether.[132]

Acetophenone derivatives with chloro-substituents were reduced at 28 °C, producing high ee values.[132] Additionally, smaller aliphatic substituents on substrates gave more selective ATH, plus aromatic ketones were reduced with higher enantioselectivity than alkyl ketones due to the presence of strong interactions between the aryl ring and the catalyst.[125,168] However, most ketone substrates were reduced at a decreased rate to other tethered catalysts due to the increased bulky nature of the benzylic tether.[132] Studies found that it was possible to maintain enantiocontrol whilst increasing the reaction temperature to 40 °C.[123,125]

1.2.6 η^6-arene substitution

Of particular interest was a catalyst proposed by Wills et al. that introduced a *tert*-butyl group onto the arene ring (Figure 45) in the hope to encourage the larger substituent on a ketone substrate away from the arene ring and hence render hydrogen delivery only possible towards one face of the substrate, in turn portraying high enantioselectivity.
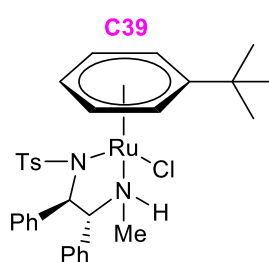
Figure 45. Catalyst created to promote stereocontrol via steric forces in place of electronic forces.[169]

Unfortunately, the research suggested that this framework would be difficult to create as fixing the *tert*-butyl group in one position would be challenging "due to the flexibility of the arene ligand"[169]. Instead, the group decided to incorporate a tether to "restrict the possible conformations of the arene ligand"[169], which has been discussed in section 1.2.4.

Despite this, one study successfully substituted the arene ring with two methyl groups (Figure 46).[81,150]
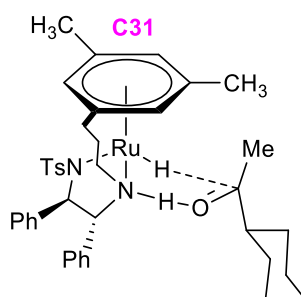
Figure 46. Substitution of the arene ring with methyl groups.[150]

Their results show there was significant steric hindrance which forced the large substituent of the ketone away from the methyl groups, indicating that steric factors outweighed electronic ones. Therefore, substrates like acetyl cyclohexanone were reduced with higher ee values, in comparison to the tethered analogue without a substituted arene ring.[81,150]

Interestingly, Nedden et al. pointed out that when two methoxy groups were substituted onto the arene ring of the ruthenium catalyst (Figure 47), reduction of aromatic ketones occurred with lower enantioselectivity.[81,168]
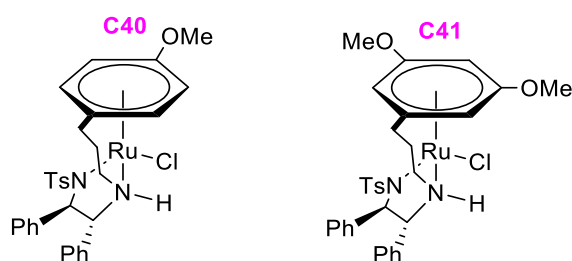
Figure 47. Comparison of 4-methoxy and 3,5-dimethoxy Ru(II) catalysts.[81]

Competing effects were observed as the methoxy group acted as a π-donor, via the oxygen lone pair, which donated electron density into the π-system of the ring, but these groups were inductively electron-withdrawing due to the electronegativity of the oxygen. When a single methoxy group was present, it lay *para* to the tether, hence the ring had an increase in electron-rich properties. The second complex contained two methoxy groups, that lay *meta* to the tether, rendering the complex more unstable as the ring was less electron rich, which decreased the CH-π interactions between the catalyst and the substrate during ATH.[81]

The arene ring can also be substituted for bulkier alternatives, however, research shows that the enantioselectivity of ATH reactions decrease with the increase of the size of the ligand. For example, the catalysts bearing a η^6-benzene ligand was more reactive than those with *p*-cymene, mesitylene or hexamethylbenzene ligands (Figure 48).[81,105,106]
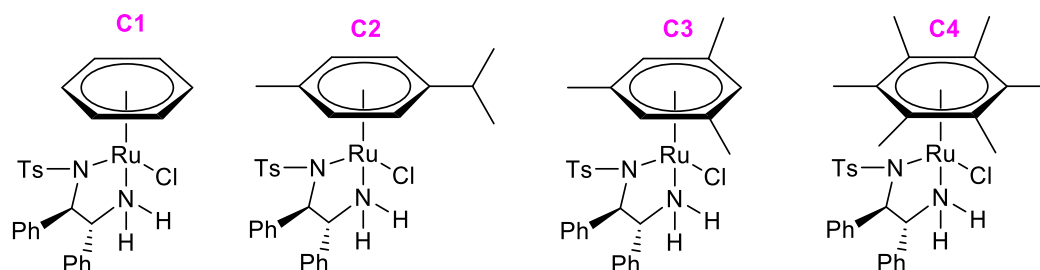
Figure 48. Substitution of the arene ring by Wills et al.[103,176]

Additionally, a report by Ikariya et al. altered one of the substituents on the arene ring to investigate its effect on the activity of the non-tethered catalysts (Figure 49).[57]
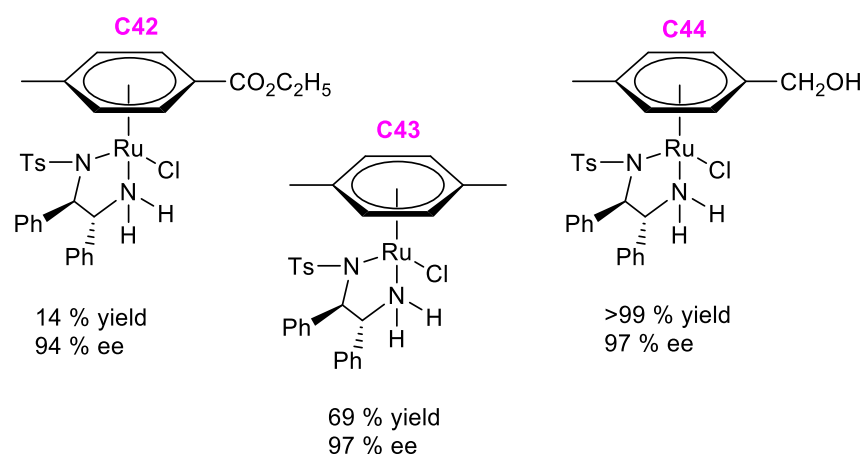
Figure 49. Non-tethered catalysts comprising of varying substituted arenes, alongside the yields and enantioselectivities for the reduction of acetophenone.[57]

When electron-donating *p*-xylene was incorporated, an increase in activity was observed in comparison to an electron-withdrawing ester group. Further, when the arene ring was substituted with an alcohol group, full conversion and high enantioselectivity was achieved.[57] Conclusions were made that the addition of electron-donating groups on the arene ring was beneficial for activity of the catalyst, whereas electron-withdrawing groups encouraged a large drop in ATH reactivity[124,145], particularly if the arene ring was substituted in positions 3

and 5 as opposed to position 4.[81] It is therefore of great importance to finely tune the arene ring, as the CH-π interaction is often responsible for the degree of enantioselectivity.[41,46]

For more improved results, the choice of solvents, temperature and the hydrogen donor employed can be adjusted to suit the substrate specifically,[41,46,53,59,81,106,140] plus tether type and length can be manipulated to tune the electronic and steric catalyst properties and target specific molecules more effectively.[15,46,53,81,107,144] Additionally, by incorporating the tether, the arene ring is locked into place and hence directing groups can be added at precise points (on the arene ring or on the tether) to finely tune the resulting catalyst.[15,81,129,144]

1.3 Anticancer activity

The design of organometallic complexes has a large impact on their ability to become successful anticancer drugs.[17,206,208] The oxidation state of the metal and the properties of the ligands define the biological activity of the complex.[3,17,208,213–215] Ruthenium compounds, NAMI-A and KP1019 in particular, have shown great medicinal progress within this field, passing Phase 1 and Phase 2 clinical trials.[205,215,216] Following this, half-sandwich ruthenium(II) complexes were found to have applications as anticancer agents in addition to their ATH activity.[26,205,207,208,214–217] The importance of this research stems from the idea to introduce less toxic metallodrugs in place of well-known platinum anticancer complexes. The hope is also to circumvent cisplatin resistance which currently limits clinical research.[218]

Water soluble TH catalysts, in particular those with a framework based on **C1**[96] (Figure 50), can reduce the coenzyme NAD^+ to NADH using sodium formate as the hydrogen donor (Figure 51).[114,206,217–221] However, the hydrophobic phenyl groups on the diamine ligand have been suggested to render the complex less soluble in water and hence minimise the activity of the complex towards the reduction of NAD^+ in biological conditions, hence the phenyl groups were removed from the half-sandwich Ru(II) frameworks.[96]
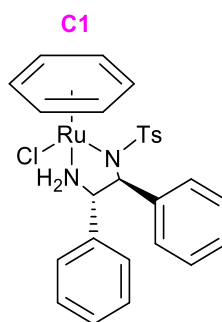
Figure 50. Noyori's catalyst.[96]
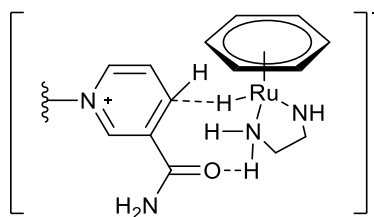
Figure 51. Proposed transition state for the ATH of NAD+.[220]

The mode of action inhibited the functioning of the mitochondria, which in turn killed the cancerous cells due to the decrease in NAD+ concentration.[206,219,220] The observed cytotoxicity by these complexes was greater by fifty times magnitude, due to the presence of sodium formate.[96,206]

Incorporating sulfonamide groups into the diamine chelating ligand and tuning of the arene ligand has been confirmed to improve the efficiency of the complex.[114,220–222] Studies confirmed that hydride transfer between sodium formate and NAD+ was facilitated with greater effectiveness by an increased electron-withdrawing nature of the sulfonamide moiety.[114,218–220] Moreover, the favourable increase in hydrophobicity of the arene ligand has been postulated to be as a result of the increase in lipophilicity, which influenced the uptake of the complex by the cell, increasing the anticancer activity.[219–221] A representative range of complexes that have been investigated for their catalytic activity towards the reduction of NAD+ in the presence of formate has been shown in Table **8**.

Table 8. Complexes investigated for their ATH activity towards NAD$^+$.[96,218,220]
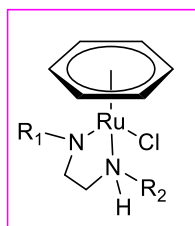
Arene		R$_1$	R$_2$
p-cymene, hexamethylbenzene, biphenyl or benzene	Ms		H
p-cymene, hexamethylbenzene, biphenyl or benzene	Ts		H
p-cymene, hexamethylbenzene, biphenyl or benzene	Tf		H
p-cymene	Nb		H
p-cymene	Ts		Me
p-cymene	Ts		Et
p-cymene	Ts		
p-cymene	Ts		
p-cymene	Ts		

Chirality is important in the recognition of substrates, therefore by comparing the anticancer activity exhibited by each enantiomer, research may be able to conclude the exact role that chirality plays in the mechanisms of action by these complexes.[14] In this context, chiral-at-metal complexes are of significant interest due to the potential to tune interactions between biomacromolecules and metal configurations.

One literature precedent has reported a family of chiral tethered Ru(II) catalysts (Figure 52), which have been proven to possess dual properties, acting as effective ATH catalysts and as catalysts inside cells to produce cytotoxic agents.[114,217]
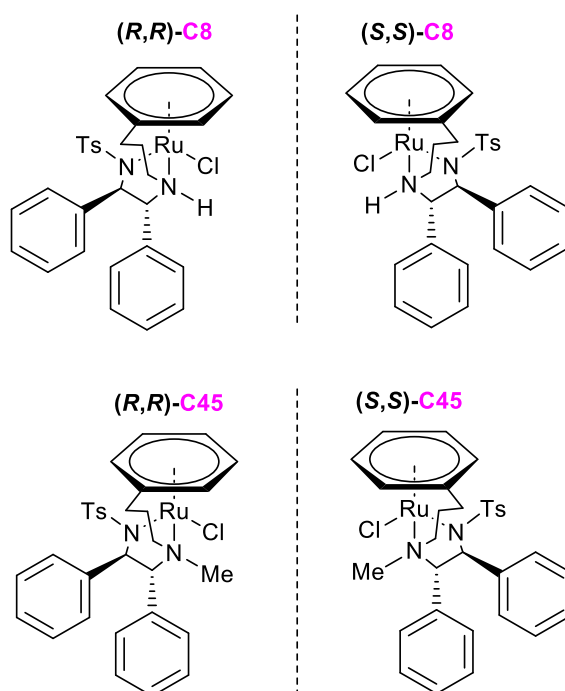
Figure 52. Chiral tethered Ru(II)-TsDPEN enantiomers.[114,217]

They portrayed antiproliferative activity against NCI-60 cancer cell lines, including towards A2780 human ovarian cancer cells, with a further potency of 25 % when sodium formate was incubated alongside the catalyst.[114,217] Upon replacing the NH moiety of the chelating ligand with a N-CH$_3$ moiety, the complexes became more efficient in their cytostatic activity, but their cytotoxic activity decreased. Complexes (Figure 52) comprising of the (*R,R*)-ligand showed increased activity compared to complexes with the (*S,S*)-ligand (Table 9).[217]

Table 9. Anticancer activity of catalysts C8 and C45 (Figure 52) towards the proliferation of A2780 human ovarian carcinoma cells.[217]

Catalyst	Ligand chirality	Metal chirality	GI_{50} (µM)	IC_{50} (µM)
C8	(R,R)	(S)	5.5 ± 0.5	1.1 ± 0.1
C8	(S,S)	(R)	13.7 ± 0.4	1.5 ± 0.2
C45	(R,R)	(R)	1.2 ± 0.3	17 ± 3
C45	(S,S)	(S)	1.8 ± 0.2	25 ± 3

"GI_{50}: the concentration which inhibits cell growth by 50 %"[217]

"IC_{50}: the concentration which kills 50 % of the original cells"[217]

Sadler et al. also confirmed a faster reaction rate for tethered complexes, in comparison to non-tethered analogues, as the catalyst was able to interact more tightly with the substrate NAD^+ during the transfer hydrogenation catalytic cycle.[114,217,219,220] Their research altered the sulfonyl group of the chelating ligand, also discovering that the more electron withdrawing groups increased the rate of hydride transfer from the formate to the NAD+.[114]

Overall, this NAD^+ reduction via ATH by these half-sandwich Ru(II) complexes has shown good success thus far, allowing an alternative mechanism to be employed to the DNA attack observed for cisplatin drugs currently.[96]

1.4 Hydrosilylation of ketones

Despite their success, ruthenium catalysts have their drawbacks, namely cost and toxicity.[115] Less toxic alternatives are now emerging based on first-row transition metals, including iron and manganese[31,35,223,224], with activity and selectivity that matches or even exceeds precious metal catalysts[225], more readily available and at a lower cost too.[31,35,115,117,224] Researchers nowadays hope to develop catalysts, based on these more environmentally friendly metals, to facilitate the selective transfer of chiral information to prochiral substrates producing desired intermediates fundamental in the agrochemical, pharmaceutical and fine chemical industries. Despite the success of ATH, research is now switching some attention towards the activity of catalysts towards the hydrosilylation of ketones to their corresponding silyl ethers, which are subjected to hydrolysis to produce chiral alcohols (Scheme 2 - The larger ball signifies a group comprising of high electron density, for example an aryl or alkyne

moiety, and the smaller ball signifies a group comprising of low electron density, for example an alkyl moiety.[111]).[115,226]
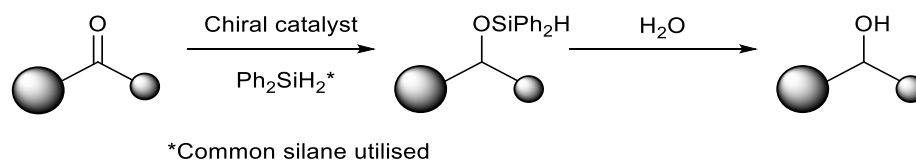
Scheme 2. Generic scheme showing the asymmetric hydrosilylation of ketones by a chiral catalyst.[226]

1.4.1 Iron catalysts

Half-sandwich iron catalysts (Figure 53) relevant to this project were devised by two main research groups; first Royo and then Darcel and Sortais.[227]
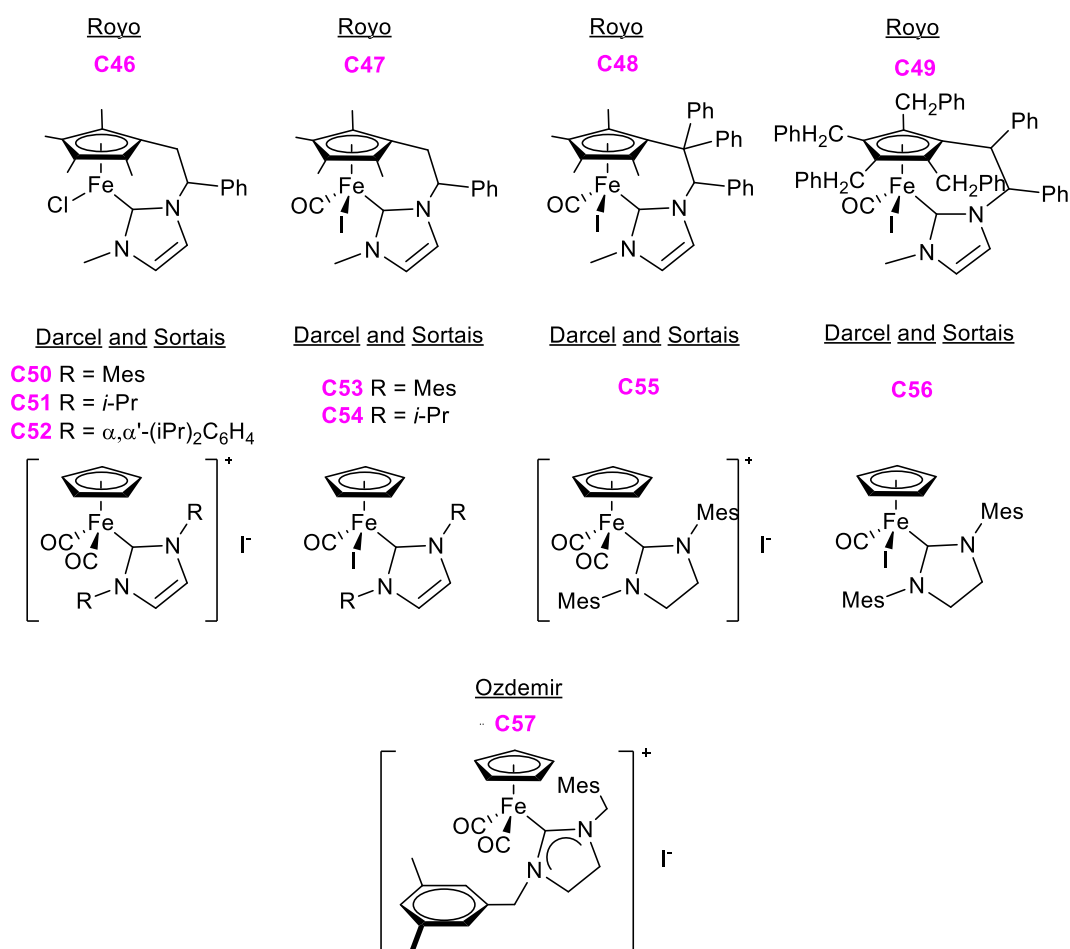
Figure 53. Royo, Darcel/Sortais and Özdemir's half-sandwich iron catalysts.[228–230]

Royo and coworkers created tethered half-sandwich Cp-NHC iron(II) complexes, efficient and selective in producing enantiomerically enriched products via both transfer hydrogenation and hydrosilylation, making them novel in current literature as a result of their duel usage.[230–232] Darcel and Sortais developed piano-stool Cp-NHC iron(II) catalysts of similar structure to Royo et al. but without the tether.[228,231,233] These frameworks (**C50** and **C53**) were originally prepared by Guerchais[234], but had not been tested for their activity. Another research group led by Özdemir reported a family of piano-stool complexes capable of reducing carbonyl compounds, but they required high temperatures of 100 °C.[229,235]

1.4.2 Manganese catalysts

The research on iron catalysts by Darcel and Sortais consequently stimulated interest into the creation of isostructural half-sandwich Cp-NHC manganese(I) catalysts (Figure 54).[236,237]

C58 R_1 = Me, R_2 = Me
C59 R_1 = *i*-Pr, R_2 = *i*-Pr
C60 R_1 = Cy, R_2 = Cy
C61 R_1 = Mes, R_2 = Me
C62 R_1 = Mes, R_2 = Mes
C63 R_1 = Dipp, R_2 = Dipp
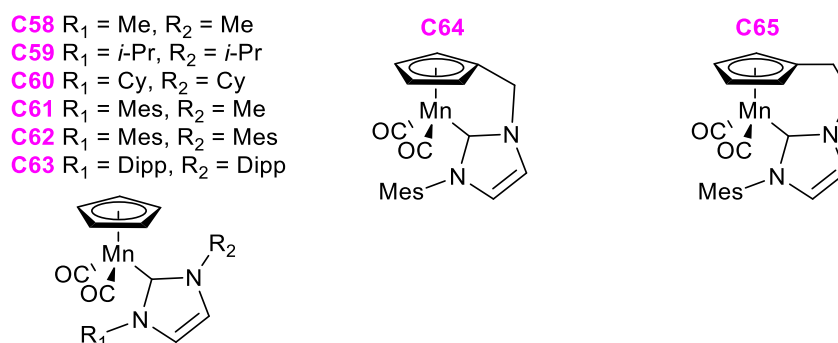
Figure 54. Half-sandwich manganese catalysts by Darcel/Sortais et al.[236,237]

The synthesis began with cymantrene, due to its commercial availability and low cost, and simply displaced a carbonyl ligand directly with the NHC ligand via irradiation with UV light >250 nm. The untethered catalysts **C58-C63** were created in yields of 46-80 %, and were active towards a range of substrates, aldehydes and ketones, with differing functional groups.[237] The success of this project inspired the development of tethered analogues. The most active catalyst was **C62**, whereby both R groups were 2,4,6-trimethylphenyl-substituents, hence it can be presumed this was the reason for the incorporation of this particular NHC into the tethered catalysts. The hope was that increased stability of the catalyst, by tethering the Cp ring to the NHC ligand, would boost the catalytic activity observed during hydrosilylation. The catalysts had varying tether length; one carbon atom (**C64**) and two carbon atoms (**C65**). Direct comparison shows that the untethered catalysts were more active towards 2-acetonaphthone than the tethered catalysts. Interestingly, the catalyst **C65**, comprising of a longer tether length, was more active than the catalyst **C64**.[236]

Alberto et al. targeted half-sandwich manganese complexes (Figure 55).[238]

Figure 55. Half-sandwich manganese catalysts by Alberto et al.[238].

The complexes were novel as a result of their stereocentres. **C66** had the stereocentre next to the Cp ring, whereas **C67** had the stereocentre next to the functional groups. Though similar to the frameworks targeted during this project, neither **C66** nor **C67** comprised of enantiopure ligands, hence these compounds were not suitable for asymmetric synthesis.[238]

1.4.3 Reaction conditions

The hydrosilylation of carbonyl compounds depends upon the following: reaction time, temperature, solvent, silane and amount of catalyst loaded. When a new catalyst is synthesised by a research group and is ready for activity testing, conditions have to be re-established due to vast differences in catalyst solubility.[239] To date, long reaction times and high temperatures are required, hence further research needs to be carried out to optimise the structure of the catalyst, which in turn will influence more desirable reaction conditions.

For the hydrosilylation of manganese untethered catalysts **C58-C63** (Figure 54), a universal method was employed for both aldehydes and ketones. This protocol comprised of 1 mol % catalyst loading, 1.50 equivalents of diphenylsilane, 350 nm UV light, toluene solvent and a temperature of 25 ºC. Tuning the amount of catalyst loaded had a major impact on the selectivity of the reduction, whereas lowering the amount of silane introduced (to one equivalent) had no effect on the conversion. The typical reaction length for aldehydes was an hour, but in some cases an increase to eight hours total was required. Similarly, ketone reduction duration was four hours, but for certain substrates had to be lengthened to twenty-four hours. For tethered catalysts **C64** and **C65**, the hydrosilylation method was identical to that described above for the untethered analogues. In spite of this, higher yields for the reduction of 2-acetonaphthone were achieved by increasing the reaction duration from two to twenty-four hours, in conjunction with reduction of the catalyst loading to 0.50 mol %.[236]

It is important to note that there was an improvement of protocol for the reduction of ketones by manganese catalysts from that employed for the iron catalyst analogues. To be specific, catalyst loading was reduced from 2 mol % to 1 mol %, the temperature of the

reaction was reduced from 50-70 ºC to 25 ºC, and finally a reduction in the duration of the hydrosilylation was observed from sixteen hours to only four hours.[237]

1.4.4 Mechanism

A mechanism for the hydrosilylation of carbonyl compounds by manganese catalysts has been proposed by Lugan et al. (Figure 56), including the substitution of the carbonyl ligand for diphenylsilane in the presence of photochemical light. Following this oxidative addition of the Si-H bond occurs, then photochemical dissociation of the carbonyl ligand. Next, the carbonyl compound coordinates to the metal, followed by insertion of the carbonyl into the metal-Si bond, then finally the silyl ether product is released by reductive elimination.[226,236]
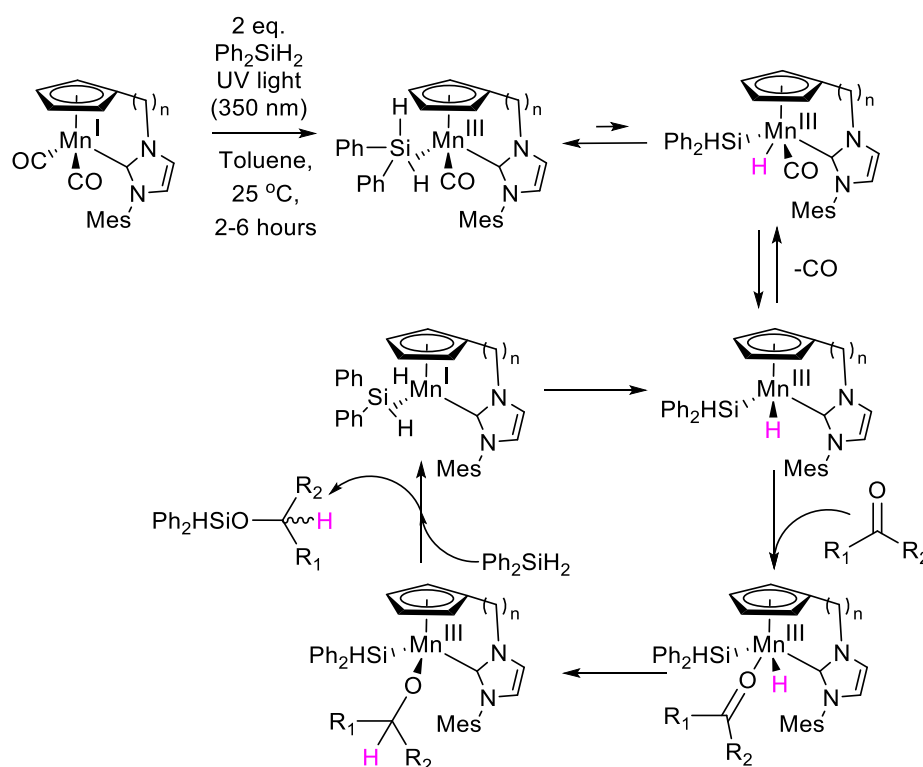
Figure 56. Catalytic cycle for the ketone hydrosilylation catalysed by Mn(I) NHC complexes, whereby n = 1 or 2.[236]

1.4.5 Types of substrates

Preliminary testing of the activity of catalysts **C58-C63** (Figure 54) focused on the reduction of acetophenone only. All catalysts reduced acetophenone in two hours, but only **C61** and **C62** achieved >97 %; all other catalysts converted the substrate in low to moderate yields.

After optimisation of the reaction conditions, both aldehydes and ketones were utilised in the hydrosilylation reductions. One successful example showed that >97 % of

benzaldehyde was reduced to its corresponding alcohol by C62 within 30 minutes. Further, aldehydes bearing *para*-substituents, irrelevant of their electron-withdrawing or electron-donating nature, were reduced by >97 % within an hour. *Meta*-fluorobenzaldehyde was converted by 92 %, notwithstanding a longer reaction time of eight hours was required. The most important case to note was that of 2-formylpyridine. Catalyst C62 reduced this aldehyde by >97 % in one hour at 25 °C, in comparison to its iron analogue [Cp(CO)$_2$Fe(IMes)]I which required just under sixteen hours to convert the substrate by 88 % at 70 °C. Additionally, both aromatic and aliphatic ketones were subjected to hydrosilylation by C62. Most substrates were converted efficiently, however, some required a duration of twenty-four hours; namely *ortho*-methylacetophenone, acetylferrocene, undecan-2-one and 3,4-dihydronaphthalen-1(2*H*)-one. Unfortunately, no conversion was observed for 4'-chloroacetophenone and 4'-bromoacetophenone, suspected to be as a result of photochemical decomposition of the catalyst during the reduction.[237] Catalysts C64 and C65 were only tested for their activity against 2-acetonaphthone. This benchmark substrate allowed for unambiguous comparisons to be made between the untethered and tethered catalysts. At the optimum catalyst loading of 0.50 mol %, 2-acetonaphthone was reduced in 98 %, 92 % and 98 % yields respectively for catalysts C62, C64 and C65.[236]

1.5 Immobilisation to solid supports

The production of chiral alcohols and amines by ATH is well established, with a vast range of catalysts capable of obtaining high conversion rates coupled with favourable enantiocontrol. The most popular catalysts are based upon the chiral (1*R*, 2*R*)- or (1*S*,2*S*)-N-(*p*-tolylsulfonyl)-1,2-diphenylethylenediamine ligands that are capable of achieving up to 99 % enantioselectivity when reducing aryl ketones, alkynyl ketones and imines during ATH.[43,46,60,63,64,67,90,91,102,162,240–245] However, the chiral ligands are expensive or require a difficult and lengthy synthesis,[38,52,65,91,95,116,125,241] whilst the transition metal is toxic and expensive too[65,90,91,95,116,136,241,246].

Due to the difficulty and time-consuming nature of separating enantiomers, research considers immobilising the catalyst to a solid support to promote easier catalyst separation[52], focusing upon attaching these successful catalysts to solid phase supports in order to minimise metal leaching[62,242,247] (and hence contamination of the chiral product with toxic metals[45,67]) and make the separation of the catalyst from the reduction product easier[43,45,51,52,62,64,67,88,90,91,95,136,155,185,240–243,245,246,248,249], allowing them to be reused[43,45,52,64,83,88,90,91,241,243,246,247,249,250] by extraction into an organic solvent[45,52],

filtration[52,65,67,91,241,249,251,252], precipitation in organic solvent[45,46,65,67,91,249,253,254] or centrifugation[176], thereby ensuring no work-up or column is required to remove the catalyst.

The most significant framework, Noyori's Ru(II)-TsDPEN[43,46,60,63,241,244,249,255,256] (**C2**), has been anchored to solid supports in various locations (Figure 57) by derivatisation through covalent bonding to soluble supports (e.g. PEG chains[45,46,65,67,90,91,176,240,246,249,253–255,257–261], polymers comprising of methacrylate units linked through a triazole ring[176,262], polystyrene[43,48,67,83,91,176,240,241,244,249,252,255,256,263], dendrimers[45,46,65,67,91,249–251], silica or mesopores[45,62,67,90,242,249,264–267]), by entrapment within the support (e.g. silica or mesopores[67,266,268–270]) or modified into a structure that can be removed from catalysis (e.g. surfactants or ionic liquids)[50,51,85,90,91,94,137,155,185,243,247,262,271].
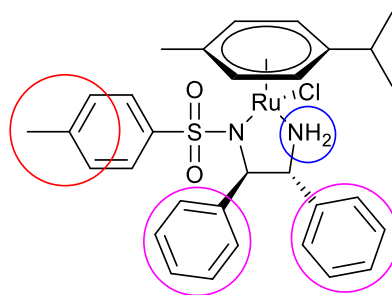
Figure 57. Noyori's Ru(II)-TsDPEN with the sites of possible attachment circled to represent where the solid support could be anchored to.

These ATH catalysts have portrayed higher activity and enantioselectivity than their unsupported analogues.[60,90,94,248,261,272] Further, a favourable reduction of costs due to the reductions in temperatures and lower substrate to catalyst ratios[62,149,253,254], in addition to the recovery and recycling of these chiral catalysts[155,240,241,256,261,264,272], has proven the importance of these immobilised frameworks as environmentally benign alternatives.

1.5.1 Reaction conditions

Current research is searching for cleaner approaches to creating ATH catalysts, by switching the reaction solvent to water as one key feature, to match the conditions utilised by enzymes in nature.[44,45,51,67,90,137] Creating analogues of previously successful ATH catalysts with increased solubility is challenging[46,51,52,90], but allows for a greener ATH process when operated at industrial levels. This is because water is a safer and eco-friendlier option than the FA/TEA azeotrope and organic solvents utilised by unmodified catalysts during the reduction.[44,50,51,53,60,63,64,67,85,88,90,94,124,130,137,155,185,243,247,272–277]

Research has shown that the use of water has promoted mechanistic advantages, in particular, in aiding the decarboxylation during the catalytic cycle and hence has formed the hydride rapidly.[67] It has also been postulated that water can help to conduct the proton transfer during ATH by acting as a proton donor or alternatively by forming hydrogen bonds with the lone pair on the oxygen of the ketone to stabilise it.[44,53,67,175] This hydrogen bonding reduces the energy barrier of the proton transfer and renders it a stepwise mechanism.[53,67,90] The use of water has often been coupled with sodium formate as the hydrogen donor (Figure 58), leading to fast reaction times and a longer lifetime of the catalyst.[50,51,53,67,90,124,185,275–277] However, it must be considered that the vast changes in reduction time could be as a result of the solubility of the catalyst in the ketone as opposed to in the water.[67,276]
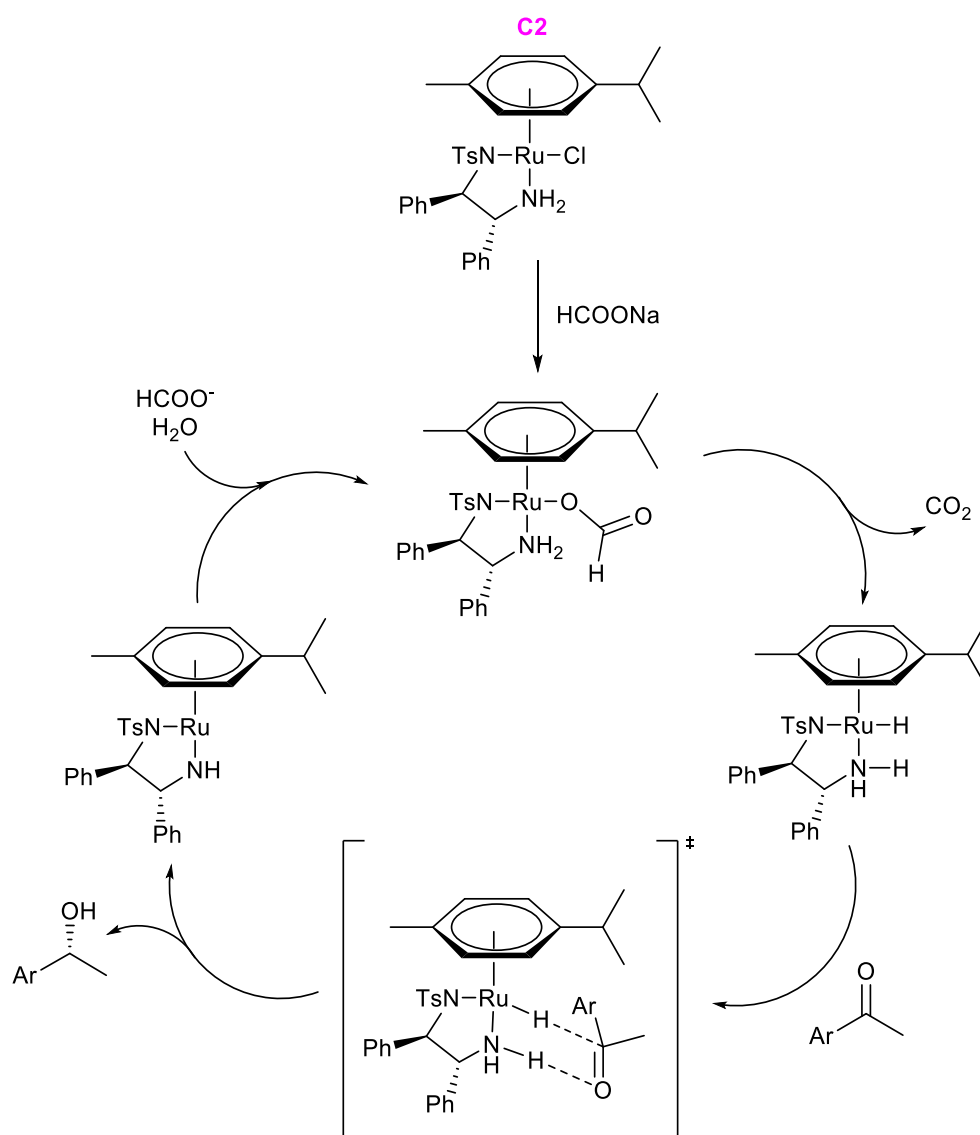
Figure 58. Proposed ATH mechanism in water with sodium formate.[276]

Unfortunately, biphasic catalysis has also been observed due to the catalyst, and their substrates, being insoluble in water[45,46,51,53,63,67,90,137,155,273,275,276], hence new methodology is required to overcome this limitation[63,67,137,247,273]. The hydrophilic/hydrophobic nature of a catalyst depends upon the nature of the ligands surrounding the metal centre, and therefore attaching a hydrophilic ligand has been proposed to increase solubility.[67,137,275] Other solutions include the addition of surfactants as cosolvents during ATH to help solubilise the catalyst[44,46,51,53,90,137,155,243,247,273,275,277]. In particular, PEG can act as both a support or a cosolvent.[65,90,261] The idea behind the use of surfactants lies with their ability to form micelles in water, whereby the ketone substrates can be solubilised within the micelles and the sodium formate resides outside the micelle. The cationic charge on the surfactant micelles attracts the HCOO- ions from the sodium formate hydrogen source. This therefore facilitates the transfer of hydrogen between the water-soluble catalyst and the hydrophobic ketones[53,137,273,274], driving the transfer hydrogenation, and in turn increasing the rate of reaction[44,50,53,67,137,155,272].

Despite this, some research still utilises the FA/TEA azeotrope in water.[45,67,124,164,272] ATH in water is pH dependent[53,67,90,185,272,275]. When the pH is above 4[45,90,272], more precisely between 5 and 8[46,67,272], the catalyst becomes most active, likely as a result of an increased concentration of HCOO$^-$. This pH range matches the pKa of aqueous formic acid (pK$_a$ = 3.6) closely. Further, the CO_2 evolved in aqueous reaction conditions may form bicarbonate, which could lead to a shift in pH of the reaction as a function of time, as the bicarbonate concentration increases, in turn controlling the rate of reaction.[45,53,90,185,268,272] However, if reaction conditions are acidic, the TsDPEN ligand can partially dissociate due to protonation of the sulfonamide nitrogen, reducing the activity and selectivity of the ATH.[67,81,90]

1.5.2 Attachment to polymer supports

1.5.2.1 Immobilisation through the phenyl groups

One key example is the immobilisation of TsDPEN with two PEG-2000 chains at the *meta*-position of the phenyl groups to create the PTsDPEN ligand (Figure 59).[67,246,253,259] Direct comparisons have been made between Ru-PTsDPEN **C68** (Table 10) and its unsupported analogue (

Table 11).[149,254,276]
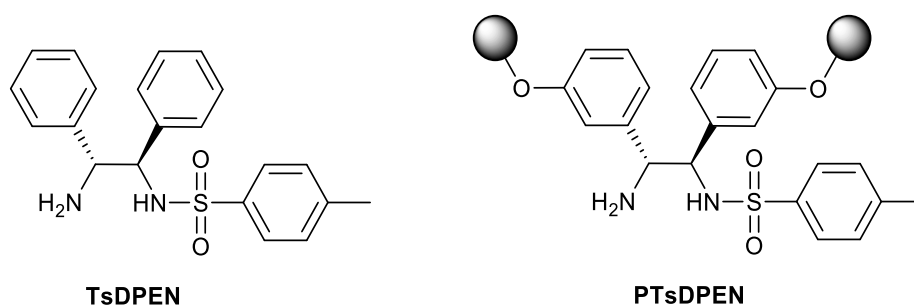
Figure 59. Chiral diamine ligands based on TsDPEN; the ligand on the right is supported by PEG chains through the phenyl rings.[253]

Table 10. The catalytic performances of Ru-PTsDPEN (C68).[149,254,276]
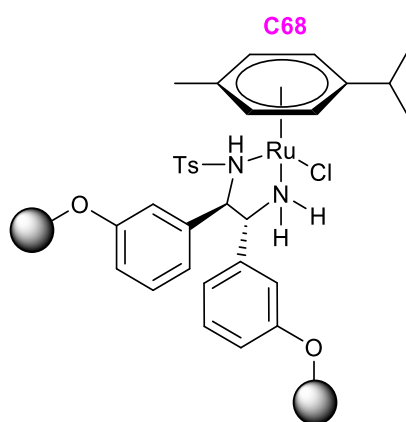
Substrate	Temp (ºC)	Time (h)	Conversion (%)	ee (%)
acetophenone	22	8	>99	93
acetophenone	40	1	99	92
1-indanone	22	18	>99	93
1-indanone	40	3	100	92
1-tetralone	22	18	>99	94
1-tetralone	40	3	98	92
p-chloroacetophenone	22	13	>99	90
p-chloroacetophenone	40	1.5	100	85
p-methylacetophenone	22	18	>99	86

Conditions: H_2O, 5 eq. HCOONa, S/C = 100.[149,254,276]

Table 11. The catalytic performances of Ru-TsDPEN (**C2**).[149,254,276]
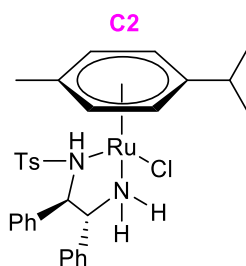
Substrate	Conditions	Time (h)	Conversion (%)	ee (%)
acetophenone	A	20	>99	98
acetophenone	B	2	>99	94
1-indanone	A	48	>99	99
1-indanone	B	2	93	95
1-tetralone	A	48	>99	99
1-tetralone	B	3	97	94
p-chloroacetophenone	A	24	>99	95
p-chloroacetophenone	B	2	>99	91
p-methylacetophenone	B	2	98	90

Conditions A: Neat FA/TEA, S/C = 200, 28 ºC;

Conditions B: H_2O, 5 eq. HCOONa, S/C = 100, 40 ºC.[149,254,276]

The results indicate that the Ru-PTsDPEN catalyst showed enhanced activity towards 1-indanone and 1-tetralone, with a reduced reaction time in water at 22 °C (18 hours for both substrates) compared to the unsupported Ru-TsDPEN catalyst in FA/TEA at 28 °C (48 hours for both substrates). Alternatively, if both catalysts were investigated in water, although Ru-PTsDPEN required a longer period of time (18 hours) for the reduction than the unsupported Ru-TsDPEN catalyst (3 hours), a much lower temperature of 22 °C could be employed instead of 40 °C, which supports the idea that using an eco-friendly solvent can match the activity obtained in the more popular azeotrope, in addition to other advantages like a reduction in temperature and cheaper reaction media.

A similar trend, in the vast reduction of ATH duration and catalyst loading with retention of enantioselectivity, was seen for acetophenone, *p*-chloroacetophenone and *p*-methylacetophenone too (compare TsDPEN ligand in FA/TEA to PTsDPEN ligand in water),

as a result of immobilising the catalyst. Further, if the duration of the reduction was increased, the temperature of the ATH in water could be reduced by nearly half for some of the substrates. In general, the catalyst showed a preference for electron-withdrawing substrates, but unfortunately the catalyst was less selective towards substrates with bulky or electron-donating substituents in the *ortho*-position. This was in agreement with the trend observed towards substrates reduced by **C2**.[46,124,149,253,254,276]

Overall, this catalyst was created to enable its separation from the reduction product and was successfully recovered fourteen times. During the repeat three runs of the reduction of acetophenone in water using sodium formate as the hydrogen source, only 0.4 mol % of ruthenium leached into the organic phase[90,254]. This low degree of leaching suggest that the catalyst may be suitable for applications in the synthesis of pharmaceutical products[246] as guidelines allow a maximum daily intake level of 10 ppm of ruthenium[278]. However, in FA/TEA, the catalyst decomposed and could not be recycled.[90,253,254] Moreover, the research suggests that discrimination of the enantiofaces of the ketone substrate by the catalyst remains unaffected when the support is immobilised through the phenyl groups.[253]

1.5.2.2 Immobilisation through the sulfonamide moiety

The Ru-PEG-BsDPEN catalyst **C69** comprised of the PEG-BsDPEN ligand (Figure 60) that was immobilised to a single PEG-750 chain at the *para*-position of the arene substituent of the sulfonamide functional group through an oxygen atom.[67,259]

PEG-BsDPEN
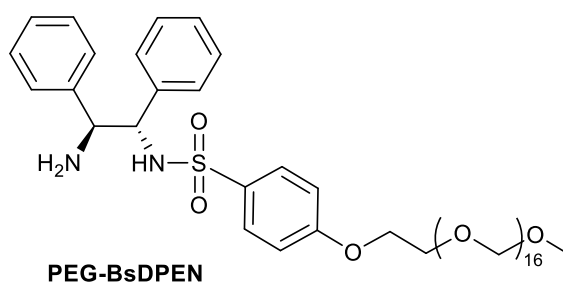
Figure 60. Chiral ligand based on TsDPEN; derivatised through the sulfonamide moiety.[259]

The catalyst was both active and selective (Table **12**)[149,259,276], reducing electron-withdrawing *para*-substituted acetophenones with higher enantioselectivities than those with electron-donating substituents. In fact, 4'-fluoroacetophenone was reduced with 99 % ee, the highest in the whole experiment.[259]

Table 12. The catalytic performances of Ru-PEG-BsDPEN (**C69**). [259]

Conditions: H$_2$O, 5 eq. HCOONa, S/C = 100.[259]
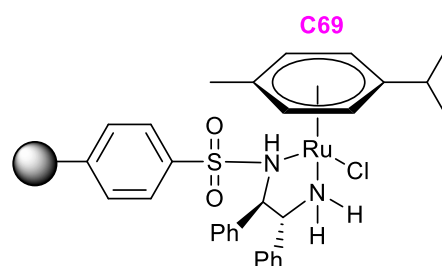
Substrate	Temp (°C)	Time (h)	Conversion (%)	ee (%)
acetophenone	22	2	99	96
1-indanone	22	2	99	95
1-tetralone	22	2	99	96
p-chloroacetophenone	22	2	99	97
p-methylacetophenone	22	2	99	92

Observations can be made that the Ru-PEG-BsDPEN catalyst (**C69**) ensures accelerated ATH activity in water, with the key fact being that it can be recovered and reused eight times whilst retaining its increased activity and selectivity, with no mention of leaching of the metal, in environmentally benign conditions. Interestingly, **C69** reduced all substrates in two hours, compared with Ru-PTsDPEN (Table 10 - **C68**) that reduced a majority of substrates between eight to thirty-six hours, when employing identical reaction conditions.[259]

1.5.2.3 Immobilisation through the amino moiety

The N-PEG-TsDPEN catalysts comprised of ligands (Figure 61) that had different PEG chain lengths and substituents on the amino group.[260]
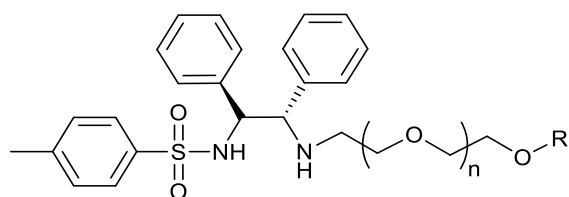
N-PEG-TsDPEN

PEG = 200, 300, 400, 750, 1000 or 2000

R = H or CH$_3$

Figure 61. Chiral ligand based on TsDPEN; derivatised through the amino moiety.[260]

In particular, increased activity and selectivity was portrayed towards 1-indanone and 1-tetralone when utilising the N-PEG750-TsDPEN catalyst (**C70**) (Table 13).[149,260,276]

Table 13. The catalytic performances of Ru-N-PEG-TsDPEN (**C70**).[260]
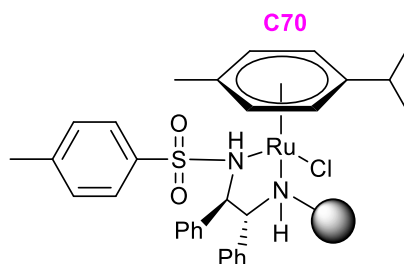
Substrate	Temp (°C)	Time (h)	Conversion (%)	ee (%)
acetophenone	22	<15	>99	94
1-indanone	22	<15	97	99
1-tetralone	22	<15	98	99
p-chloroacetophenone	22	<15	>99	89
p-methylacetophenone	22	<15	>99	99

Conditions: H$_2$O, 5 eq. HCOONa, S/C = 100.[260]

The catalyst was highly favourable for substrates like 2,3-dihydro-1H-inden-1-ol, which acts as an intermediate for various drugs, including neuroprotective and anti-AChE agents Rasagiline and Ladostigil, demonstrating a clear path towards industrial level research.[260] Also, the catalyst reduced electron-donating *para*-substituted acetophenones with higher enantioselectivities than those with electron-withdrawing substituents, which was opposite

to the results found for **C69** (Table **12**). **C70** showed preference for acetophenone substrates with electron-donating substituents instead.[259,260]

Increasing the length of the PEG chain had negligible influence on conversion rates and enantioselectivity.[65,260] Despite this, a longer PEG chain was associated with greater ease of reuse, with the PEG-2000 ligand being reused eight times with retention of high conversion, in comparison to the PEG-750 ligand that was recycled five times and the PEG-200 ligand only three times, with no discussion of leaching of the metal.[260]

1.6 Summary

ATH is an established approach to producing chiral compounds with enriched enantioselectivity, allowing the difficulty and cost of separating isomers to be avoided.[41,67,81] Noyori developed ruthenium(II)-based half-sandwich catalysts that were efficient in catalysing ATH reductions.[121,139] Since then, there has been continual development within this field, which has led to excellent progress. Of great importance was incorporation of a tether to increase stability of Noyori's [Ru(II)(*p*-cymene)-TsDPEN] catalyst (**C2**). This led to enhanced activity towards a larger group of substrates.[81,90,122] Manipulating the catalyst framework further to achieve higher activity, selectivity and compatibility towards substrates is an ongoing investigation. Continuing progress focuses on linkage of the basic amine to diversify the catalyst's applications[209], addition of steric bulk to the benzylic carbon allowing for greater selectivity[183], and tuning of steric hindrance and the electron-withdrawing nature of the sulfonyl group to affect the catalyst's reactivity and enantioselectivity, showing bulkier electron donating ligands to be less preferable.[105,124,151]

Despite this, severe limitations persist, notably the activity of these current chiral catalysts lags behind that of achiral catalysts[279,280] and the range of substrates reduced is lacking, rendering ATH to be infrequently used on industrial scales.[88] Most frequently, aryl ketones are focused upon and it has been found that due to their steric hindrance, *para-* and *meta*-substituted aryl ketones produce alcohols with greater ee values than *ortho*-substituted ketones.[46,148,203] So far, the stereochemistry of chiral ligands[121,123,147] has dictated the enantioselectivity within existing catalysts, but only a limited range of chiral ligands are commercially available, restricting the ability to tune electronic and steric properties at the metal centre, which is responsible for the catalytic activity observed.[90]

More recent research has proven ruthenium catalysts to be capable of both ATH and anticancer activity. Moreover, complexes were able to reduce the coenzyme NAD$^+$ using sodium formate.[114,217–221] The research thus far shows great promise, but this niche area is

lacking support, still searching for highly active catalytic metallodrugs to be administered in a low dose, capable of overcoming platinum-drug resistance in cells.[213,219]

Research has also turned its attention towards cheaper and less toxic alternatives to Ru-based ATH catalysts, primarily first row transition metal half-sandwich catalysts to reduce aldehydes and ketones. In particular, iron has received the greatest amount of focus, but manganese also offers cheaper and safer advantages over ruthenium, due to the mild reaction conditions employed during hydrosilylation.[237] Current catalysts require long reaction times, high temperatures and high catalyst loading, therefore greater efficiency towards hydrosilylation is desirable.

To provide a cheaper and more environmentally friendly route to chiral alcohols, ruthenium ATH catalysts have been immobilised onto solid supports to allow for their recovery and reuse.[62,64,83,90,241,256] The most significant examples are based upon Noyori's chiral TsDPEN ligand, differing in location of the linkage; phenyl groups, sulfonamide group or amino group.[259,260] These catalysts act as phase-transfer catalysts between the water and substrates, explaining the high conversion rates and enantioselectivities observed.[253,254] Overall, high recovery rates have been possible but leaching, as a result of the dissociation of the metal from the ligand, is common[62,176], minimising the amount of catalyst that can be recycled. To date, limitations in the diverse functionalities on the polymer chain end has been proven to be undesirable,[255] plus immobilisation through the sulfonamide or amine group prevents further tuning of the bidentate ligand to be carried out.[259]

In short, there is demand for more selective catalysts towards a larger substrate scope including challenging substrates, for example, dialkyl ketones, α-chloroketones and alkynyl ketones[45,47,83,106,151,189] in ATH and *ortho*-substituted aldehydes, diaryl ketones and α,β-unsaturated ketones[90,228] in hydrosilylation. The following work produces novel catalysts with the hope to exert increased stability, activity and selectivity towards substrates, offering a reduction in costs, safety and toxicity. For even more improved results, the tether, chelating ligand and immobilisation will be manipulated to target specific substrates more effectively.

Chapter 2

Novel ruthenium(II) chiral-at-metal tethered half-sandwich complexes

2.1 Background

As the safety of drugs increases in importance, the pharmaceutical industry continues to invest significantly in the research and development of active pharmaceutical ingredients and the processes needed to manufacture them.[76] Whilst nature is adept at performing reactions with a high degree of atom efficiency and enantio-control, synthetic chemistry has until recently found this challenging[67,281]; traditionally relying on the chiral resolution of racemic mixtures by chromatography[34,41,79] or fractional crystallisation techniques.

A very successful approach to the preparation of chiral alcohols is asymmetric transfer hydrogenation (Scheme 3), whereby a chiral catalyst transfers hydrogen to a once optically inactive reagent to produce an enantiomerically pure product.[41,42,45,77,112]
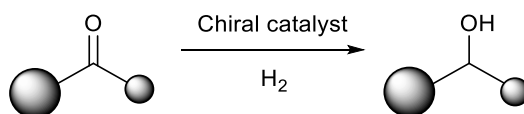
Scheme 3. Generic scheme showing the asymmetric transfer hydrogenation of ketones by a chiral catalyst. The larger ball signifies a group comprising of high electron density, for example an aryl or alkyne moiety, and the smaller ball signifies a group comprising of low electron density, for example an alkyl moiety.[111]

The key aspect of this chemoselective and reproducible reaction is the ability of the catalyst to chirally discriminate between the groups on the substrate to allow for the transfer of hydrogen enantioselectivity. ATH is a fundamental reaction for modern synthetic chemistry, with high atom economy and efficiency, allowing reduced costs and simplified methodology for industrial syntheses.[62,64,98,165,282,67,84,88,90,92,93,95,96] This vital reaction supports high conversion rates, hence has been a successful route to reducing prochiral ketones for many years.[62,64,67,84,88,90,92,98,150,282]

The separation of drugs to their enantiomerically pure products is important within the pharmaceutical industry to prevent the implicit dangers racemic drugs have on the body. Since the risk to a patient is high because of the large differences in biological activity and

therapeutic effect exhibited by isomers, researchers target enantio-control via catalyst or ligand selection.[41,76,77] For example, **C3** (Figure 62) selectively obtained the building blocks for the popular drugs MK-0417 ("a carbonic anhydrase inhibitor to treat glaucoma"[58]) and L-699,392 ("an LTD$_4$ antagonist"[58]) as their alcohols with 98 % and 92 % ee respectively.[27,58,59,128]
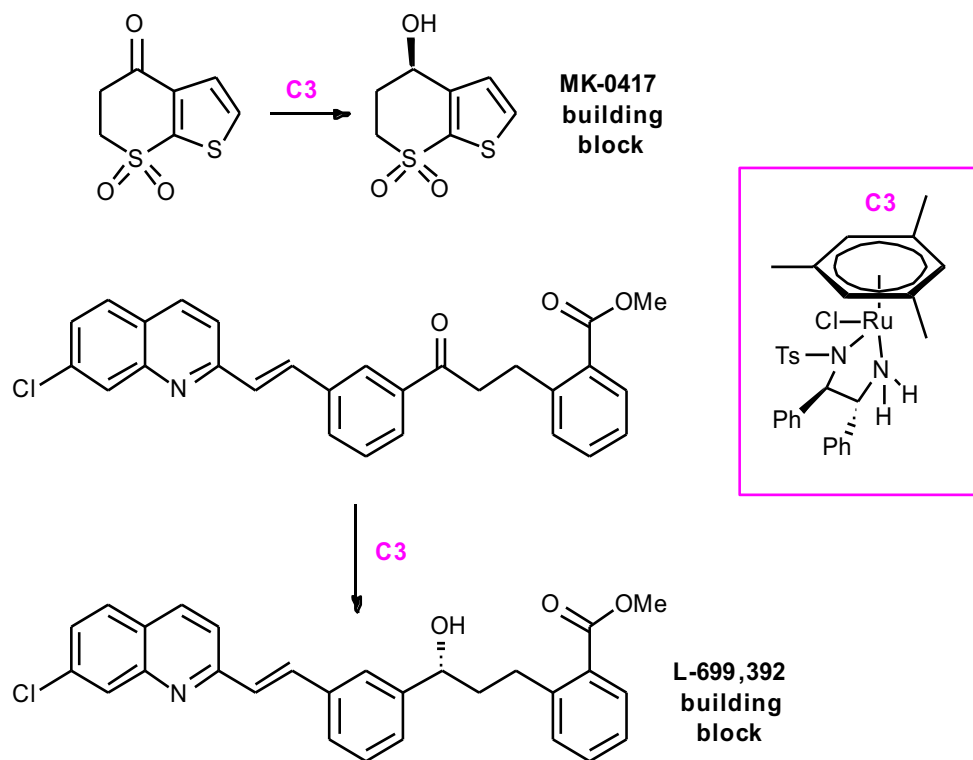
Figure 62. Noyori's (*R,R*)-catalyst responsible for reducing key intermediates highly selectively for the pharmaceutical industry.[128,283,284]

Following this, **C8** (Figure 63)[81,92] was proven to be a huge success within the pharmaceutical industry, taken advantage of for its high activity, enantioselectivity and chemoselectivity when reducing ketones to their corresponding alcohols.[58,81,92,93]
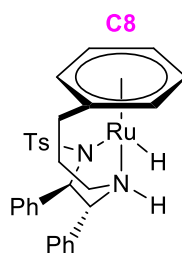
Figure 63. Tethered ruthenium catalysts created by Wills et al.[81,93]

The synthesis of chiral alcohols via asymmetric transfer hydrogenation is also fundamental in the agrochemical industry. These enantiomerically pure building blocks are significant intermediates to produce pesticides and fungicides.[91,285] Unfortunately, there is a huge lack of research towards the production of chiral agrochemicals in comparison to the development of chiral drugs within the pharmaceutical area. The agrochemical industry still requires more environmentally safe and economic prospects.[69,76]

A majority of research never reaches industrial markets due to the difficult nature to scale up the processes, whilst ensuring high enantiomeric excess and conversion rates and preventing potential side reactions. A successful example within the agrochemical industry is the manufacture of (*S*)-MA20565 by Mitsubishi Chemical. The ATH (Scheme **4**) in an equimolar mixture of formic acid to triethylamine produced this agricultural fungicide.[45,88,286]
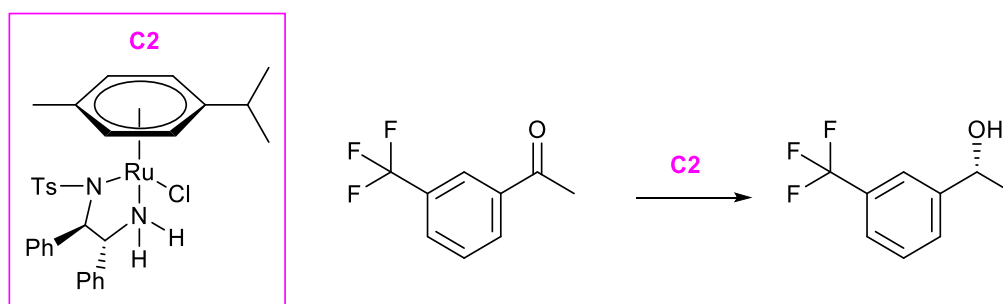
Scheme 4. ATH to produce (*S*)-1-(3-trifluoromethylphenyl)ethanol by Noyori's chiral Ru(II)-(*S*,*S*)-TsDPEN complex.[45,88,286]

The use of the azeotrope in a small excess to the ketone led to completion of the reaction with the ability of recycling the triethylamine if employed at an industrial scale. The reaction was scaled up to 100 kg through pilot plant testing and an increase in the rate of the reaction was observed due to the evolution of CO_2 as a by-product.[45,88,286] Nevertheless, researchers focusing on the agrochemical industry continue to search for novel and innovative chiral intermediates with the hope to produce more enantiomerically pure agrochemicals.[69]

Homogeneous asymmetric catalysis is infrequently used at an industrial-scale due to low catalytic activity and minimal substrate scope.[45,82,88] The structural differences of substrates elucidates that no single catalyst can be utilised universally; hence ligand tuning is necessary to create highly selective and specific catalysts with broader scope.[37,38,41,45,46,56,67,82,105]

The widely investigated field of piano-stool ruthenium(II) catalysts began with the design of Noyori's catalysts[41,120] (Figure 64), which forms the basic framework of new transition metal ATH catalysts developed today.[40,88]
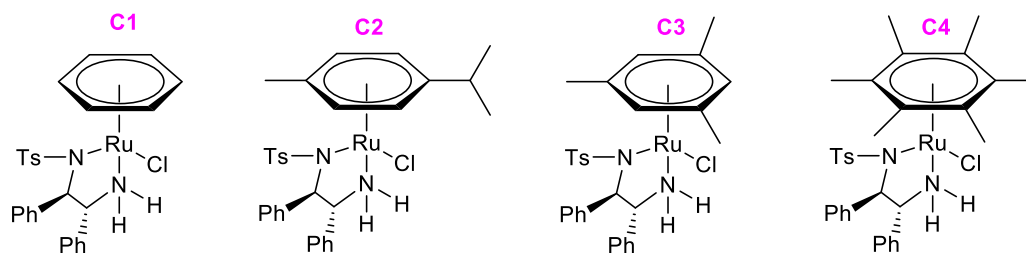
Figure 64. Ru(II)-TsDPEN catalysts with different substitutions of the arene ligand.[81]

The most promising piano-stool structure for ATH was devised by Wills (Figure 65), whereby a tether was incorporated to increase the activity and stability of Noyori's framework.[121]
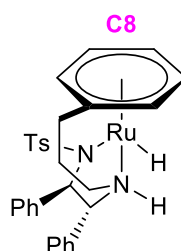
Figure 65. Structure of Wills' half-sandwich piano stool catalyst.[121]

The success of Noyori's prototypical catalyst, and the tethered analogue by Wills, inspired other research groups to create similar frameworks (Figure 66).[93]
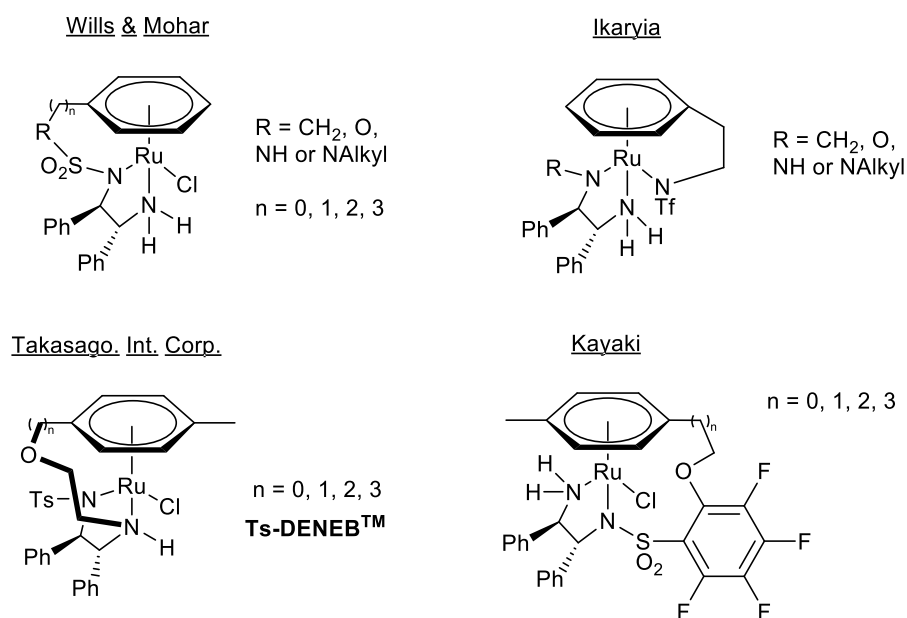
Figure 66. Tethered catalyst variations by different research groups.[93]

Within these frameworks, the chelating ligand is responsible for determining the stereochemistry at the metal.[39,67,86,121] In turn, the stereochemical configuration at the metal centre of the catalyst, coupled with substrate-ligand interactions, is what determines the

stereochemistry within the alcohol product and hence it is important to influence control over the absolute configuration at the metal.[15,37,38,67,150]

Discrimination of the enantiofaces of prochiral ketones is what allows chiral catalysts to yield chiral alcohols of specific configuration. The stabilising CH-π interaction between the catalyst and the substrate[39,81] that result in the positioning of the ketone, with the phenyl group of the substrate occupying the site adjacent to the arene ligand, into the favoured orientation (Figure 67) is vital[150].

Favourable "edge-face" π-interaction
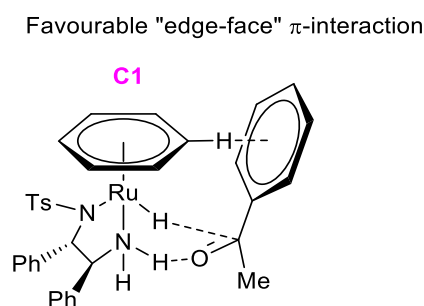
Figure 67. The most sterically favoured diastereoisomer.[150]

In addition to studies looking at the utility of these novel catalysts in ATH, similar ruthenium structures are reported as novel anticancer compounds, so called dual-propertied. More recently, transfer hydrogenations in cellular systems by half-sandwich ruthenium catalysts have been reported. In particular, the *in vitro* reduction of the coenzyme NAD$^+$ to NADH has been of great focus, utilising non-toxic concentrations[218] of sodium formate as the hydride donor.[96,114,217–221,287] The complexes target cancerous cells by reducing the concentration of NAD$^+$ in the cells to cause apoptosis, leaving the normal cells unaffected.[220,287]

Taking all of the above into consideration forms the basis of this chapter of the research project. The interest is to design novel catalytic compounds, aiming to impact this area through the development of fundamental understanding of the structure-activity relationship for ruthenium-based transfer hydrogenation catalysts and therefore this research builds on seminal work by Noyori and Wills. An overlap between ATH and anticancer activity is clear and if tuned precisely, creation of dual-propertied ruthenium(II) complexes would have a massive impact on current research and industry.

2.2 Ligand and complex design

The approach taken to design the chiral-at-metal ruthenium(II) complexes in this project was based around a scaffold previously utilised by a myriad of research groups. The piano-stool structure has portrayed success in both ATH and anticancer fields; however, the major difference incorporated into the catalyst framework presented here is the introduction of a bulky substituent at the benzylic carbon of the arene ligand (Figure 68 - group R_1). A range of complexes were proposed, where the benzylic substituent ranged from a methyl group to an isopropyl and *tert*-butyl group and even further to a mesityl group.
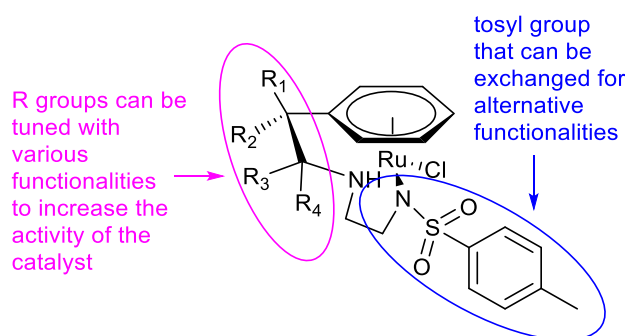
Figure 68. Various moieties that can be manipulated in the proposed catalyst framework.

The inclusion of a bulky functionality at the benzylic position was postulated to be able to dictate the manner by which the tether ligates to the metal centre, and hence promoting a single stereochemical configuration at the metal centre. The modulation of steric bulk at the benzylic carbon was identified as a major factor that could potentially influence the absolute configuration at the metal centre. Which diastereoisomer forms depends on how the ligands bind to the metal centre, determining metal-centred chirality. As discussed earlier, different stereoisomers of each compound are likely to interact and bind differently with biomacromolecular targets so investigating both isomers of a catalyst separately is of great importance.[14] Moreover, research has suggested that the addition of a bulky group to the arene ring would limit the number of possible conformations of the arene ligand, which would force the ketone substrate into one diastereoisomer predominantly during ATH.[169]

During interactions, for example with unsymmetrical diaryl ketones, the increased bulk of the substituent was hypothesized to better discriminate between the substituents of the aryl groups due to steric interactions, allowing substrates to approach the catalyst from only one face during ATH reactions, increasing enantioselectivity of the alcohol product.

Literature confirms a tethered complex gives a more stable catalyst and increased activities in comparison to untethered analogues.[81] Research has focused mainly on tethers of three, four or five carbon atoms in length, with a lack of investigation towards tethers of two carbon atoms in length. In this project, initial complexes comprise of tethers of two carbon atoms in length. It was hoped that the tether incorporation would promote locking of the bulky substituent above the plane of the arene ligand[46] (Figure 69), preventing free rotation[46,146] and resulting in a single stereochemical configuration at the metal centre on ligation of the tether nitrogen atoms.
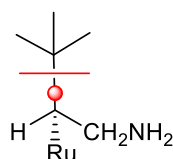
Figure 69. The postulated lowest energy conformation for the proposed new framework; with the red line acting as the arene ligand and the red circle indicating the stereocentre.

This project primarily aimed to investigate whether stereochemistry of the metal could be controlled by a single stereocentre on the tether as an alternative to the chiral phenyl groups that control stereochemical configuration at the metal in established catalysts. Though catalysts comprising of these phenyl groups have shown great ATH and anticancer activity, research has shown that their hydrophobicity prevent complexes from performing efficient transfer hydrogenation of NAD$^+$.[96] Wills et al. have created one ruthenium(II) complex without the phenyl groups, but described the synthesis to be challenging.[109]

Further, if successful, this project was interested in investigating if this novel induction of stereochemistry could effect conversion and enantioselectivity of ketones during ATH. The project also intended to determine which length of tether was optimal, and hence whether the tether was influential towards the conversion and enantioselectivity obtained. The final aim was to conclude whether the bulky group and tether influenced ATH activity simultaneously or mutually exclusively. Overall, the hope was that the library of complexes developed during this project would be assessed for their ability to act as ATH catalysts against a range of substrates. The choice of ketone was led by literature precedents to allow the activity and enantioselectivity to be benchmarked against reported structures. Utilising techniques like NMR and x-ray diffraction enabled the research here to be further understood in terms of conformations and stability. The initial Ru(II) complexes would also be tested for their anticancer activity.

2.3 Ligand and complex synthesis

It is worth noting that the stereochemistry's for the final chiral complexes have been drawn to reflect the major diastereosiomer (see section 2.4.2).

2.3.1 Synthesis of complex 6a
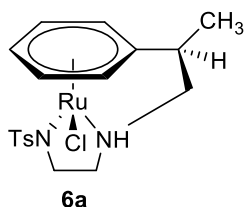
Figure 70. Structure of **6a**.

Development of a synthetic route to produce the first chiral-at-metal ruthenium framework, given as an overview in Scheme 5, was inspired by Wills et al.[109].
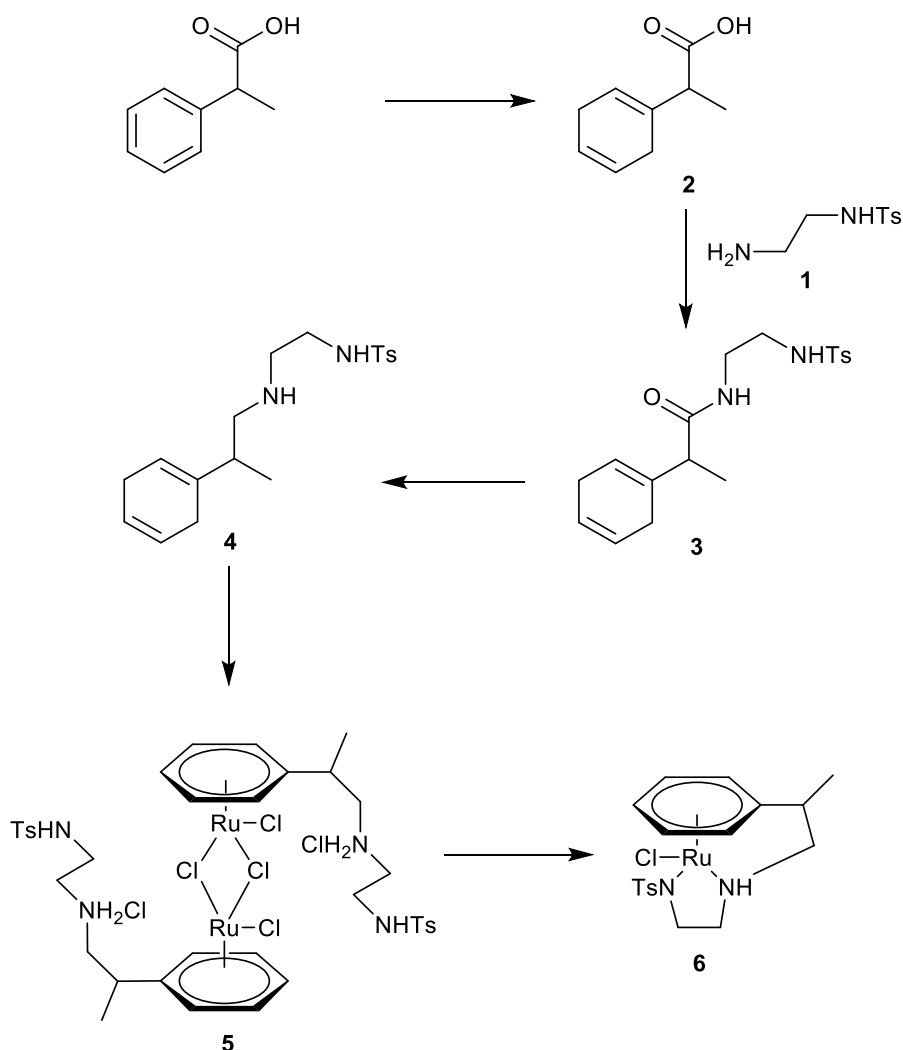
Scheme 5. Global synthetic scheme to show the successful synthesis of **6a** and **6b**.

1 was prepared as a fine white powder in a suitable yield of 89 % via a substitution reaction of ethylenediamine, in a vast 10 fold excess, with *p*-toluenesulfonylchloride (Scheme 6), following the procedure reported by Pedrosa et al.[288].
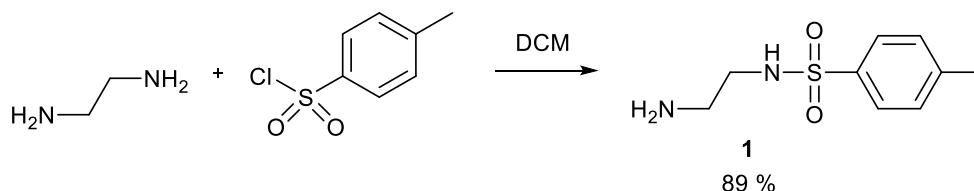
Scheme 6. Synthesis of *N*-(2-aminoethyl)-4-methylbenzenesulfonamide.[288]

Electrospray ionisation mass spectrometry verified the product by showing a molecular ion peak of 215.0 m/z, equivalent to the $[M + H]^+$ ion. The peak was also observed by Hou et al.[289]. Further, the ^{1}H-NMR spectrum produced with peaks correctly corresponding to each proton environment, with identical chemical shifts to that found by Pedrosa et al.[288]. Furthermore, all seven distinctive carbon environments were accounted for with ease in the ^{13}C-NMR, which were in agreement with that reported in the literature[290].

Concurrently, **2a** was synthesised via the Birch reduction of (*R*)-2-phenyl-propionic acid (Scheme 7), giving a yield of 92 %.
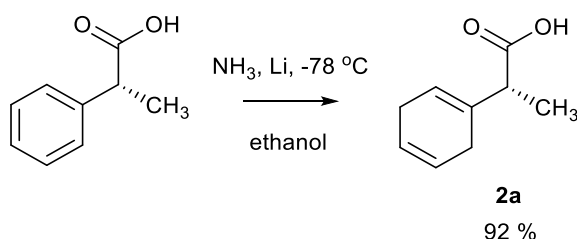
Scheme 7. Synthesis of (*R*)-2-(cyclohexa-1,4-dien-1-yl)propanoic acid.

The first attempt at this reaction used nine equivalents of Li but non-reduced aromatic was still present after work-up and hence subsequent attempts at this reaction were monitored by ^{1}H-NMR to ensure the amount of non-reduced aromatic was minimised. Repetition of the reaction added 31 equivalents of Li and still approximately 3 % of non-reduced material was observed in the ^{1}H-NMR, however, this was not significant enough to impact the remainder of the synthetic route. Inspection of the ^{1}H-NMR spectrum proved the reaction to be successful due to the appearance of signals from the alkenyl ring protons at δ = 5.62-5.73 ppm and loss of signals in the aromatic region at δ = 7.23-7.25 ppm. The diene environments were also observed in the ^{13}C-NMR at δ = 124.1, 123.9 and 121.9 ppm, with the CH_2 groups

from the ring appearing at δ = 27.1 and 26.9 ppm. Further, the CH$_2$ groups from the diene ring were found at δ = 2.61-2.79 ppm in the ^{1}H-NMR and at δ = 26.9 ppm and δ = 27.1 ppm in the ^{13}C-NMR. The CH$_2$ environments were not identical as a result of the 3D nature and twisting of the diene ring, hence two carbon environments were observed, but these couldn't unambiguously be assigned. On analysis by electron impact ionisation mass spectrometry the predicted fragmentation pathway was seen with the loss of the -COOH at 107.3 m/z. Additionally, analysis by high resolution ESI in negative mode gave a peak at 151.0764 m/z responsible for the [M - H]$^-$ ion.

Following this, **2a** was coupled to **1** using TBTU and HOBt in a solvent mixture of DCM and DMF (Scheme 8).
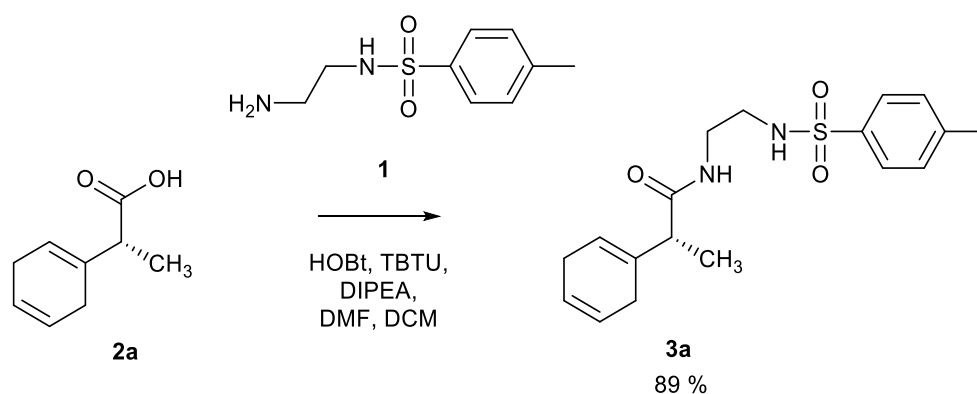
Scheme 8. Synthesis of (*R*)-2-(cyclohexa-1,4-dien-1-yl)-*N*-(2-((4-methylphenyl)sulfonamido)ethyl)propenamide.

The combination of TBTU and HOBt and were utilised to reduce racemisation[291,292] and retain the stereochemical purity of the starting material. The product **3a** was obtained, following purification, in 85 % yield as a white solid. The ^{1}H-NMR and ^{13}C-NMR spectra of **3a** were recorded in CDCl$_3$ to confirm the bonding of the acid to the sulfonamide. In the ^{13}C-NMR spectrum, the carbonyl resonance was shifted upfield relative to the starting material, now being observed at δ = 175.4 ppm. This was in agreement with the CH$_2$ groups of the amine which also shifted downfield, to δ = 39.4 ppm and δ = 43.5 ppm, after coupling to the acid. A clear indication of this coupling was also seen in the appearance of the broad peak at δ = 6.26 ppm in the ^{1}H-NMR signifying the NH environment adjacent to the carbonyl moiety, confirmed by a COSY experiment. Furthermore, the CH$_2$ protons from *N*-(2-aminoethyl)-4-methylbenzenesulfonamide became further deshielded and shifted downfield upon coupling due to the change in environment, including the interaction with the

stereocentre and the electronegativity of the carbonyl moiety nearby. From the integrals of the phenyl protons to the alkene protons, a 4:3 ratio was observed proving that the components had reacted in a stoichiometric 1:1 ratio with no major excess of reagents in the isolated sample or formation of by-products. Only minor impurities were seen along the baseline of the spectrum, which was suspected to be unreacted starting material. Further confirmation of the desired product was granted via ESI mass spectrometry in positive mode with a peak at 349.1584 m/z corresponding to the [M+H]$^+$ ion in high resolution.

　　　　Next, the amide **3a** was reduced to its corresponding amine by LiAlH$_4$ (Scheme 9), producing **4a** in 82 % yield. The reflux temperature was required to push the reaction to completion, indicating that the reaction had a high energy barrier.
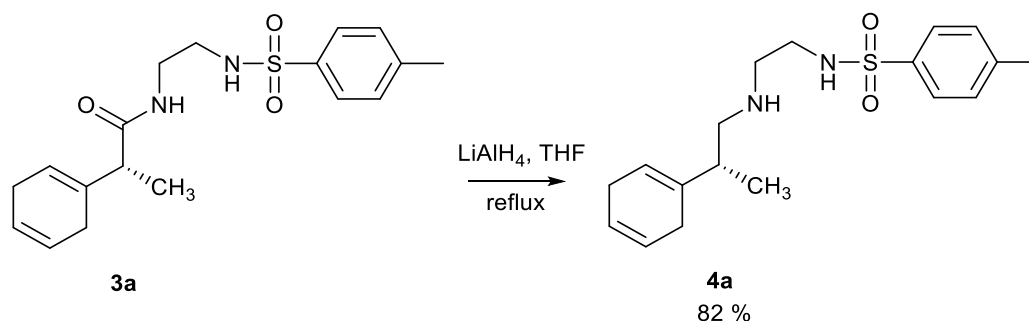
Scheme 9. Synthesis of (*R*)-*N*-(2-((2-(cyclohexa-1,4-dien-1-yl)propyl)amino)ethyl)-4-methylbenzenesulfonamide.

Confirmation of completion of the reaction was by TLC analysis and the use of ninhydrin staining. Clear indications towards product formation were seen by the appearance of the CH$_2$ protons in the alkyl region of the ^{1}H-NMR, at δ = 2.26-2.33 ppm and δ = 2.41-2.44 ppm, and the disappearance of the C=O peak in the ^{13}C-NMR at δ = 175.4 ppm. Additionally, in comparison to the starting material **3a**, the protons observed in the alkyl region of the product amine shifted upfield slightly and showed a more complex splitting pattern due to the interaction of the CH$_2$ protons with the stereocentre. This was made possible by the loss of the rigid carbonyl group, which allowed for greater bond rotation within the amine. Multiple impurities were seen along the baseline, suspected to be present as a result of the harsh forcing conditions by LiAlH$_4$. In the future, the use of a milder reducing agent may give a cleaner spectrum. Finally, analysis using high resolution ESI gave a peak at 335.1799 m/z, which proved to be the [M+H]$^+$ ion, further confirming the formation of **4a**.

The penultimate step was complexation of the ligand **4a** to form the ruthenium-based dimer (Scheme 10). A fairly low yield of **5a** was obtained in two batches as a brown solid; 23 % and 21 %.
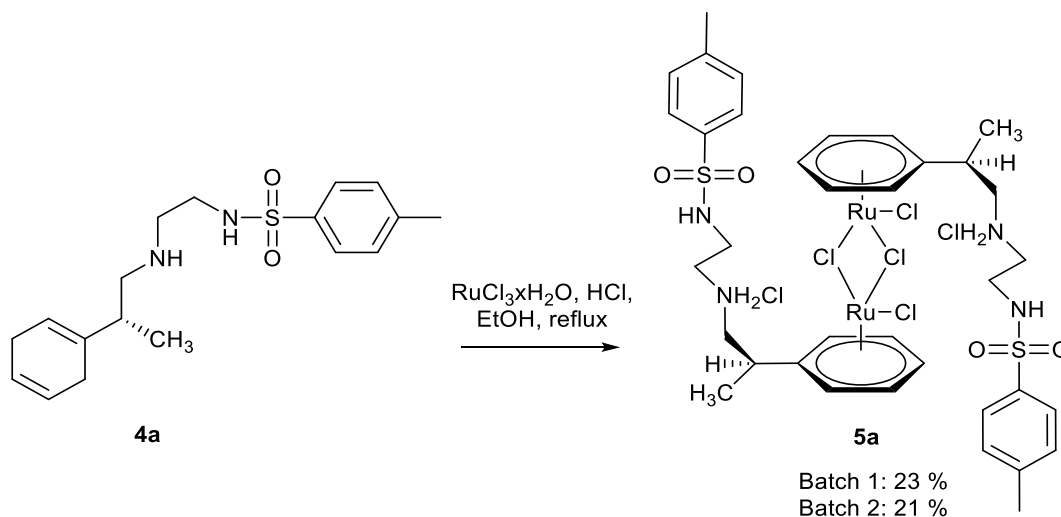
Scheme 10. Synthesis of [Ru(η^6-(*R*)-4-methyl-*N*-(2-((2-phenylpropyl)amino)ethyl)benzenesulfonamide)Cl$_2$]$_2$.2HCl.

The change in shift of the alkene protons originally seen as two environments, at δ = 5.45 ppm and δ = 5.69 ppm, to a single environment, at δ = 5.97-6.03 ppm (a typical chemical shift of Ru-coordinated arene protons), confirmed the capping of the two ruthenium centres by the arene rings. This slight shifting downfield compared to the original ligand before coupling to the ruthenium suggested deshielding of the protons due to their coordination to the ruthenium. Further, a drastic change in the chemical shift of the arene environments in the ^{13}C-NMR was noted, previously seen at δ = 119.8 ppm, δ = 124.2 ppm and δ = 124.5 ppm as alkene environments in the ligand, with the quaternary carbon at δ = 136.8 ppm. Now, five peaks were observed between δ = 85.3-88.3 ppm and a single peak at δ = 103.6 ppm for the quaternary carbon. It was postulated that there was limited rotation either around the Ru-arene bond or by the tether at the arene-benzyl bond, or both, which rendered the arene environments non-equivalent and hence five peaks were observed.

The final step of this synthesis was to cleave the dimer **5a** and isolate the ruthenium complex **6a** by treatment with a base (Scheme 11). The light brown solid was obtained in 86 % yield from the purification step by column chromatography.
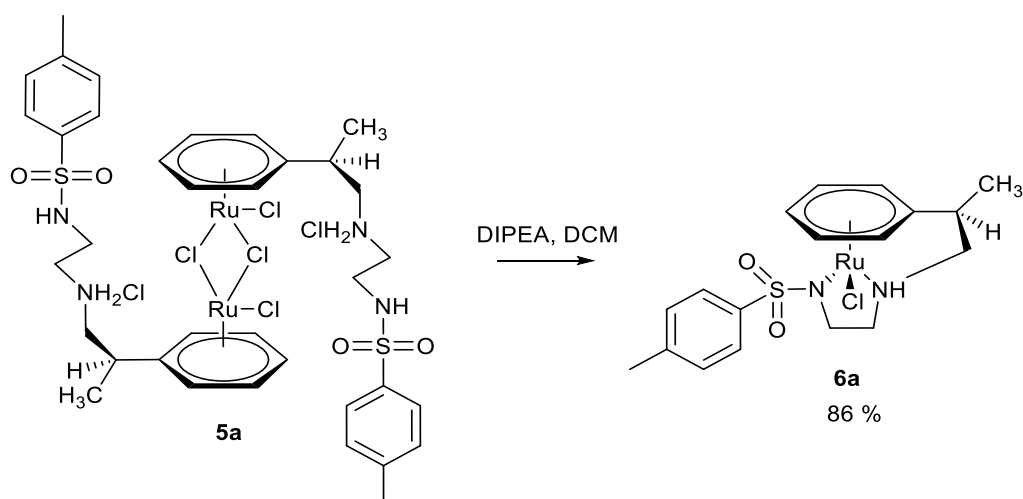
Scheme 11. Synthesis of final complex **6a**.

In the ^{1}H-NMR spectrum, ten arene signals were observed, indicating that on coordination of the tether to the metal centre, the arene rotation was now restricted, rendering each arene proton environment non-equivalent. As **6a** only contains five arene protons, the presence of ten arene resonances indicated the presence of two isomers, in a relative abundance of 35 % and 65 % respectively. The isomers have been attributed to the formation of two configurational isomers, whereby the tether wrapped around the metal centre in two different directions (Figure 71), imparting opposing chirality to the metal centre, whilst the carbon stereocentre remained the same chirality.
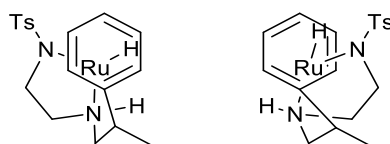
Figure 71. Possible two configurational isomers formed as a result of the second N-atom on the chelating ligand changing coordination site on the complex, with the first N-atom remaining in the same position.[150]

The fact that one conformer was in excess of the other suggested that one was of greater stability, hence was the kinetic product of the tethering process, and therefore had a larger probability of being adopted.

Further evidence of two diastereoisomers residing in the solution was found in the ^{13}C-NMR as two distinct peaks were assigned to each environment on the complex. Initially the assignments were challenging, however, collecting 2D NMR allowed for greater confidence. For example, the DEPT spectrum confirmed the CH_2 groups to be of shifts δ =

49.9 ppm, δ = 51.2 ppm, δ = 56.1 ppm, δ = 56.5 ppm, δ = 67.9 ppm and δ = 69.8 ppm. Additionally, the HMBC spectrum displayed correlation between the CH_3 adjacent to the stereocentre (δ = 1.43-1.48 ppm) to the stereocentre (δ = 41.6 ppm), CH_2 next to the stereocentre (δ = 67.9 ppm) and the quaternary carbon on the arene ring (δ = 104.6 ppm and δ = 104.7 ppm). Moreover, the high resolution ESI spectrum collected showed an envelope of peaks at 433.0534 m/z, corresponding to the [M - Cl]$^+$ ion of the complex **6a**, displaying the characteristic ruthenium isotopic pattern. All data obtained for this compound (^{1}H-NMR, ^{13}C-NMR and MS) was in close agreement to a similar analogue synthesised by Wills et al.[150] (Figure 72 – **C26**).
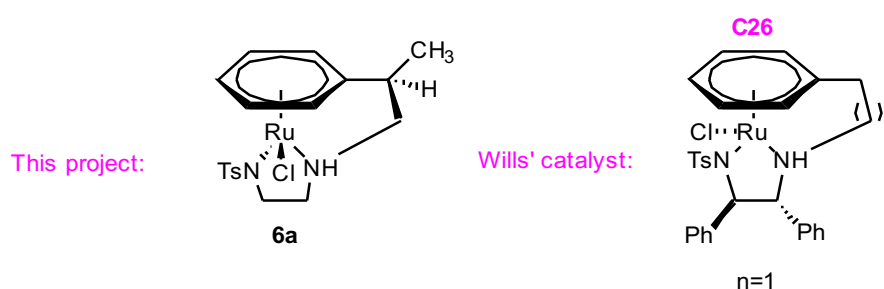
Figure 72. Comparison of **6a** to one of Wills' catalysts with the same tether length.[150]

Elemental analysis was collected and the results indicated the complex was pure when solvent of crystallisation was accounted for. Studying the ^{1}H-NMR, it was clear that DCM was contaminating the product, hence integration of the solvent peak against product peaks allowed conclusions to be drawn as to how many equivalents of solvent were present. This was close enough to the elemental data to proceed with catalysis at a later point.

2.3.2 Synthesis of complex 6b
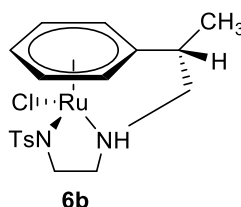
Figure 73. Structure of **6b**.

The stereochemical purity of the complex is of great importance in effecting enantioselectivity during ATH of ketones to produce one predominant alcohol in high enantiomeric excess. As discussed previously, **6a** was synthesised, and hence to allow for direct comparisons during ATH reactions, an identical synthetic route was repeated for the (*S*)-analogue (Scheme 5).

The analysis (^{1}H-NMR, ^{13}C-NMR, and MS) was compared to that obtained for the (R)-analogue at every step and has been included in the experimental section but will not be discussed in depth here due to the identical nature of them all. The synthetic route to **6b** began with a Birch reduction of the commercially bought (S)-2-phenyl-propionic acid, using liquid ammonia and lithium wire in ethanol to form the corresponding diene **2b** in 92 % yield. A large excess of Li (34 equivalents) was required to push the Birch reduction to completion. Chiral HPLC was performed on both the non-Birch reduced (Figure 74) and the Birch reduced product (Figure 75). The (S)-2-phenyl-propionic acid was utilised as a comparison for **2b**, to allow for proof of retention of stereochemistry, alongside the alternate isomers; (R)-2-phenyl-propionic acid and **2a**. Unfortunately, the spectrum in Figure 75 shows that **2a** didn't experience full reduction of the aromatic ring due to the small peak observed at 8.51.
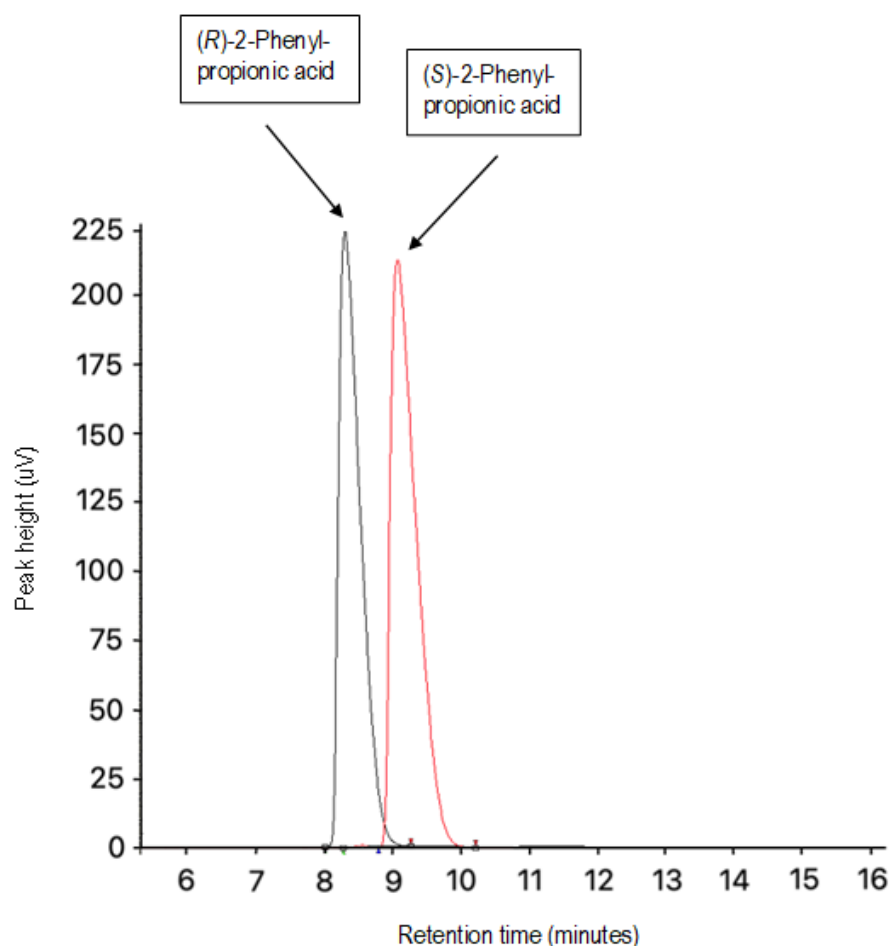
Figure 74. Overlay of the chromatograms of (R)- and (S)-2-phenyl-propionic acid (both isomers were purchased with 98 % enantiopurity) obtained using chiral HPLC. The black peak at 8 minutes corresponds to (R)-2-phenyl-propionic acid and the red peak at 9 minutes corresponds to (S)-2-phenyl-propionic acid.
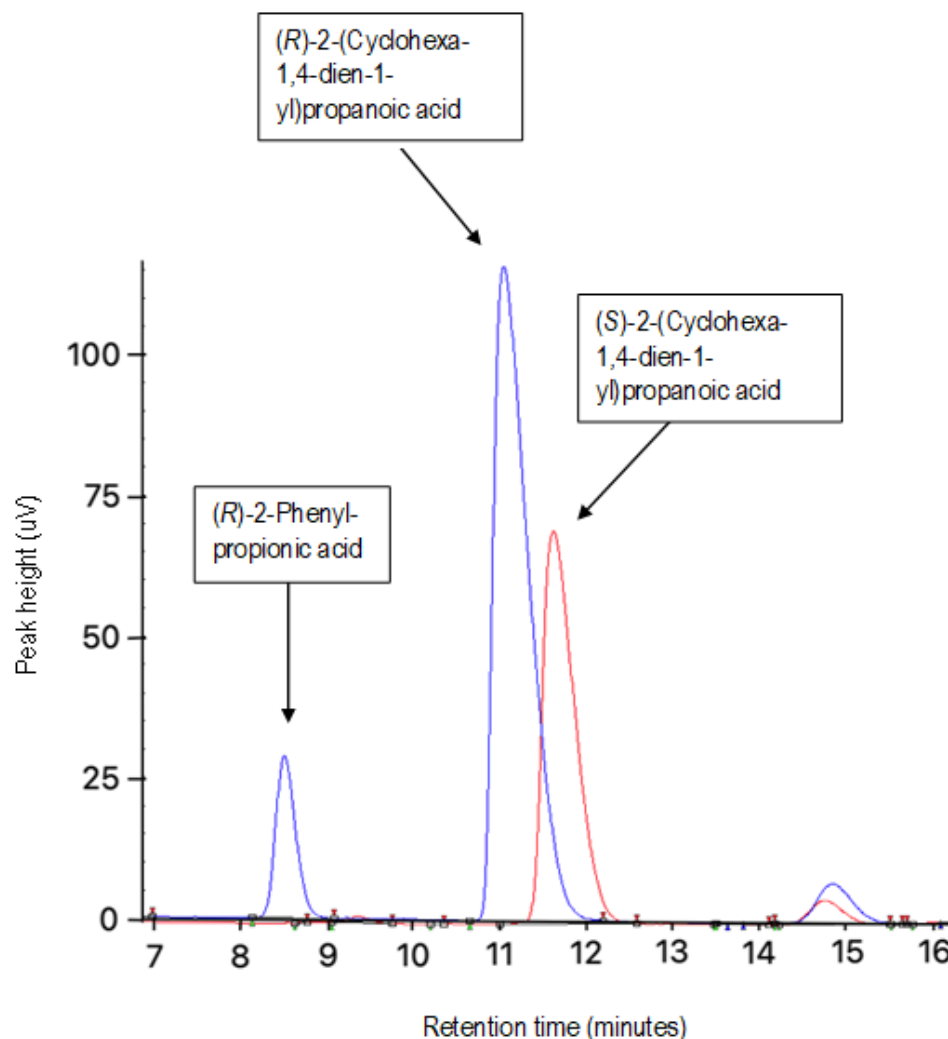
Figure 75. Overlay of the chromatograms of (*R*)- and (*S*)-2-(cyclohexa-1,4-dien-1-yl)propanoic acid obtained using chiral HPLC, whereby the two peaks overlayed relate to the two isomers of **2a** and **2b**. The blue peak at 11 minutes corresponds to **2a** and the red peak at 12 minutes corresponds to **2b**. The additional peaks at 8 and 9 minutes represent residual non-Birch reduced starting material (also confirmed by ^{1}H-NMR) and the additional peaks at 15 minutes represent unidentified impurities from the Birch reduction.

Next, the amide was prepared by attachment of the diene **2b** to the diamine precursor **1** in the presence of HOBt and TBTU to prevent racemisation[291,292]. Further purification by column chromatography produced the amide **3b** as a white solid in a high yield of 79 %. The enantiopurity of **3b** was confirmed via chiral HPLC, with comparison to the alternate isomer **3a** (Figure 173).

The amide was subsequently reduced by LiAlH$_4$ to form the final amine ligand **4b** in 89 % yield. The enantiopurity of **4b** was confirmed via chiral HPLC, with comparison to the alternate isomer **4a** (Figure 174).

Following this, the isolated ligand was reacted with RuCl$_3$xH$_2$O to form the dimer **5b** as an orange solid in 22 % yield, which was then converted to the final complex **6b** by treatment with DIPEA. The resulting orange solid was obtained in 96 % yield. The ^{1}H-NMR spectrum of the final complex successfully confirmed full coordination of the ligand to the ruthenium centre with subsequent cleaving of the dimer and was in agreement with the spectra assigned to **6a** and also to a similar catalyst by Wills et al.[109]. As with **6a**, two configurational isomers were observed in the ^{1}H-NMR and the relative proportion of each was calculated from the ratio of arene peaks, indicating that a minor isomer was present in 30 % and the major isomer was present in 70 %. The presence of two diastereoisomers formed upon synthesis of complex **6b** was further confirmed by ^{13}C-NMR, due to two peaks per distinct environment. Mass spectrometry (ESI) of the product revealed an envelope of peaks characteristic of the ruthenium isotope pattern. Elemental analysis was obtained and determination of the number of equivalents of DCM present was calculated from the ^{1}H-NMR. The theoretical elemental compositions were in close enough agreement (± 0.3 %) to utilise this complex as a catalyst in the ATH experiments for this project.

2.3.3 Synthesis of complex 7
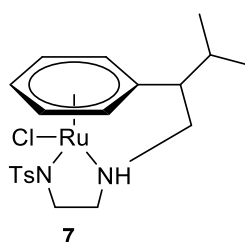
Figure 76. Structure of **7**.

The racemic dimer bearing an isopropyl group was synthesised by Dr Murray's research group. The dimer was treated with base, followed by purification on silica (Scheme 12) to form the mononuclear complex.
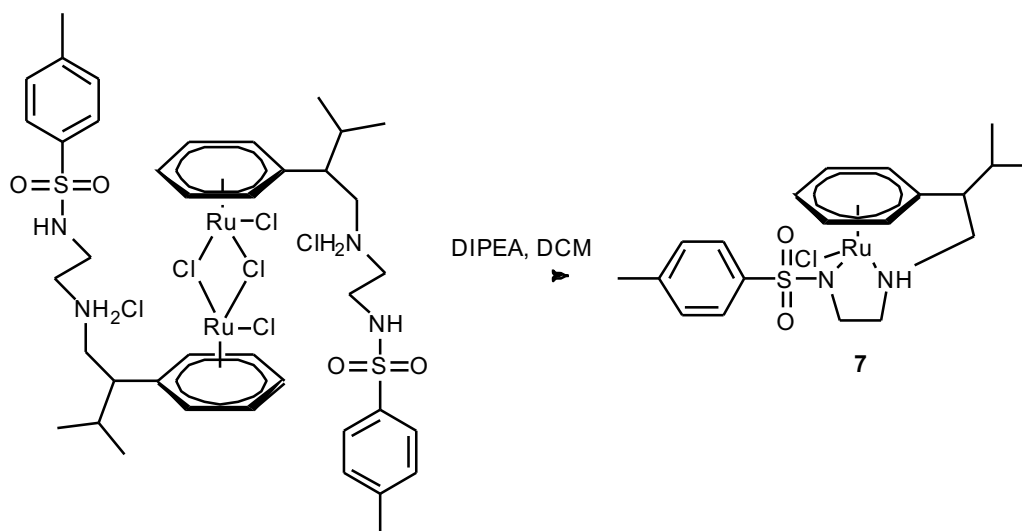
Scheme 12. Synthesis of final complex **7**.

Complex **7** was obtained in 95 % yield as an orange crystalline solid, which was fully characterised by ^{1}H-NMR, ^{13}C-NMR, ESI and elemental analysis. The ^{1}H-NMR of the complex revealed multiple different Ru-arene environments, indicating the presence, like for the methyl analogues **6a** and **6b**, of configurational isomers. Significant peaks in the ^{1}H-NMR include those attributed to the arene ring, found as doublets and triplets in the region δ = 4.87-6.70 ppm, the two CH$_3$ groups of the isopropyl moiety were seen separately at δ = 1.01-1.03 ppm and δ = 1.10-1.13 ppm, and the CH on the isopropyl group at δ = 1.98-2.08 ppm. The ^{13}C-NMR spectrum indicated the presence of two diastereosiomers, for example the stereocentre was confirmed at δ = 54.7 ppm and δ = 57.0 ppm, whilst the ^{1}H-NMR spectrum indicated a third diastereoisomer of relatively lower intensity to the other two. The relative abundance of each isomer was calculated from the arene peaks in the ^{1}H-NMR. The increased steric bulk of the substituent to an isopropyl group dictated the relative proportions of the isomers to a different extent to that of the methyl substituent; a 20 %:80 % ratio was observed for **7** in comparison to 35 %:65 % for **6a**. The use of the 2D NMR data collected allowed for ambiguous assignments of all environments in the complex, bar the three CH$_2$ groups that could not be distinguished between. Further confirmation of the complex formation was by high resolution ESI, whereby the [(M - Cl)]$^+$ ion was found at 461.0843 m/z as an envelope of peaks characteristic of the ruthenium isotope pattern. Additionally, the complex was recrystallised using ethanol to isolate one of the diastereosiomers, observed in the ^{1}H-NMR, in >94 % excess, which was then analysed by x-ray diffraction (see section 2.1.3.2). Elemental analysis confirmed the purity of the complex **7**.

2.3.4 Synthesis of complex 14a
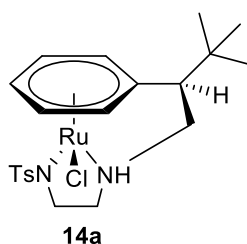
Figure 77. Structure of **14a**.

Promising initial results achieved with complexes **6a**, **6b** and **7** prompted the idea of increasing the bulky substituent even further to a *tert*-butyl group. Initially, the route attempted arene exchange as an alternative approach to the Birch reduction due to the hazardous reaction conditions of the Birch reduction, plus arene exchange would reduce the number of steps required to form the complex, which in turn would hopefully have improved the yield obtained. Explained simply, arene exchange is the substitution of an electron-poor η^6-arene by an electron rich one, whereby the desired tethered ligand displaces the arene ligands coordinated to ruthenium in a dimer such as [Ru(C$_6$H$_5$CO$_2$Et)Cl$_2$]$_2$ (Scheme **13**).
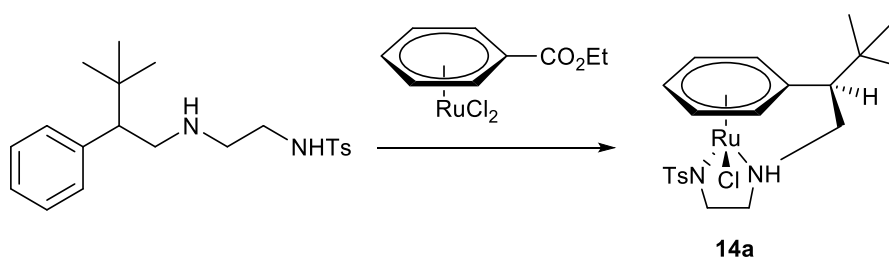
Scheme 13. The arene exchange step attempted to form **14a**.

The arene exchange was attempted as both a reflux and in a microwave, following methods employed by a literature precedent[122], and full experimental procedures can be found in the experimental chapter. Neither methods isolated **14a** and therefore the Birch reduction route was focused upon instead. The synthetic route followed that shown in Scheme 14.
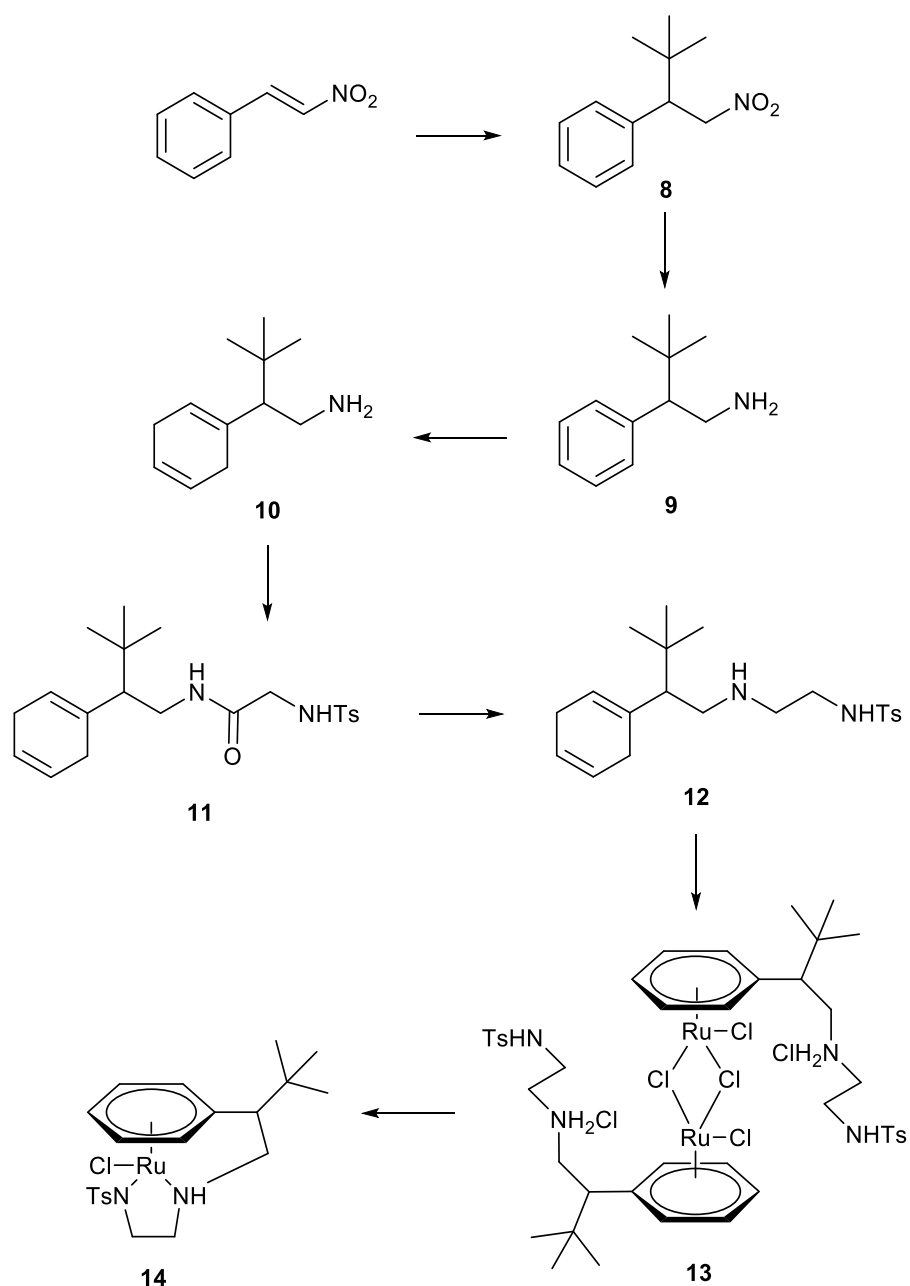
Scheme 14. Global synthetic scheme to show the successful synthesis of **14a** and **14b**. **14a** is suspected to be of (*R*) stereochemistry at the benzylic stereocentre and **14b** is suspected to be of (*S*) stereochemistry at the benzylic stereocentre (for full discussion see section 2.4.3.2).

The starting material was achiral with the idea to introduce stereochemistry and then to separate the isomers in the subsequent steps. β-nitrostyrene was subjected to Michael-type nucleophilic addition with *tert*-butylmagnesium chloride at -20 ºC (Scheme 15) and later treated with 5 % HCl before the rest of the workup steps. It was important to note that the weak concentration of acid was important in obtaining the nitro moiety. Multiple trial and error

reactions were required otherwise the functional group comprised of an "NO" moiety attached to the carbon adjacent to the stereocentre via a triple bond (see Scheme 15).
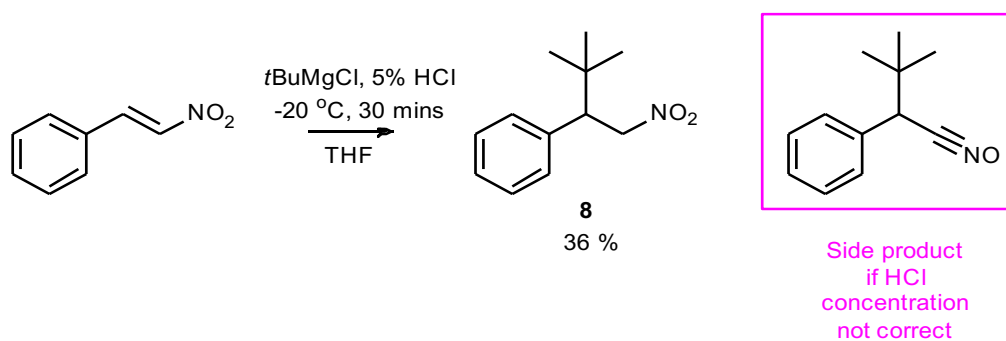
Scheme 15. Synthesis of (3,3-dimethyl-1-nitrobutan-2-yl)benzene.

Purification by column chromatography yielded the racemic compound **8** as a red/orange solid with a yield of 36 % with full characterisation by IR, ^{1}H-NMR, ^{13}C-NMR and MS. The IR spectrum gave rise to the expected bands corresponding to the nitro compound, in particular the N-O stretching mode (1546.19 cm^{-1}), which was in similar agreement to the IR spectrum produced by Bandichhor et al.[293] who synthesised the identical nitro compound. The lack of IR stretching or bending modes associated with alkene C=C moieties proved the completion of the reaction and hence disappearance of β-nitrostyrene. The creation of the stereocentre was clearly shown in the ^{1}H-NMR as a double doublet at δ = 3.35 ppm, and the appearance of the CH$_2$ protons at δ = 4.76-4.87 ppm also proved the reaction to be successful. Moreover, the CH$_2$ environment was observed as the furthest shifted peak in the ^{13}C-NMR at δ = 137.6 ppm due to the electron withdrawing nature of the NO$_2$ group. Additionally, low resolution ESI found the [M + Na]$^+$ peak at 230.1 m/z. Overall, all data collected (IR, ^{1}H-NMR, ^{13}C-NMR and MS) was in agreement with that found in the literature[294].

Subsequent treatment of **8** with iron powder at 70 ºC for one hour afforded, after extractions and pH adjustments, the corresponding amine **9** in 99 % yield (Scheme 16).
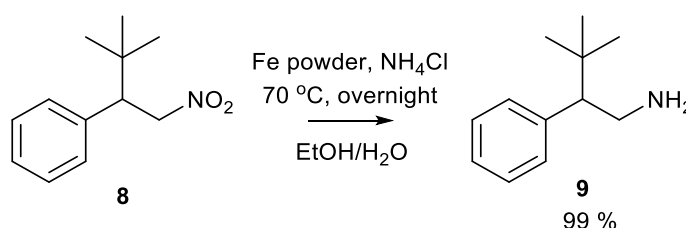
Scheme 16. Synthesis of 3,3-dimethyl-2-phenylbutan-1-amine.[295]

Confirmation of the amine was by ^{1}H-NMR, whereby the amine protons showed as a broad peak at δ = 1.38 ppm. The ^{13}C-NMR showed that the carbon environments belonging to the stereocentre and the CH$_2$ moiety shifted upfield in comparison to the starting material due to the less withdrawing nature of the NH$_2$ group and hence the reduced shielding. Additionally, low resolution ESI found the [M + H]$^+$ peak at 178.2 m/z, and further confirmation of the amine was achieved by TLC analysis using ninhydrin staining. Moreover, all data collected (^{1}H-NMR, ^{13}C-NMR and MS) was in agreement with that found in the literature[295].

To separate out the isomers, (*S*)-mandelic acid and **9** were combined to create diastereoisomeric pairs (Scheme 17), followed by separation via fractional crystallisation.
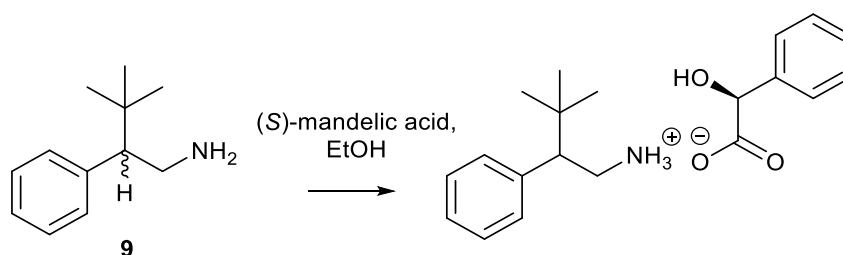
Scheme 17. Synthesis of the acid-base pair formed between (*S*)-mandelic acid and racemic 3,3-dimethyl-2-phenylbutan-1-amine **9**.

Proof of the structure of these acid-base pairs was seen by the growth of clear single crystal needles, analysed by x-ray diffraction (Figure 78).
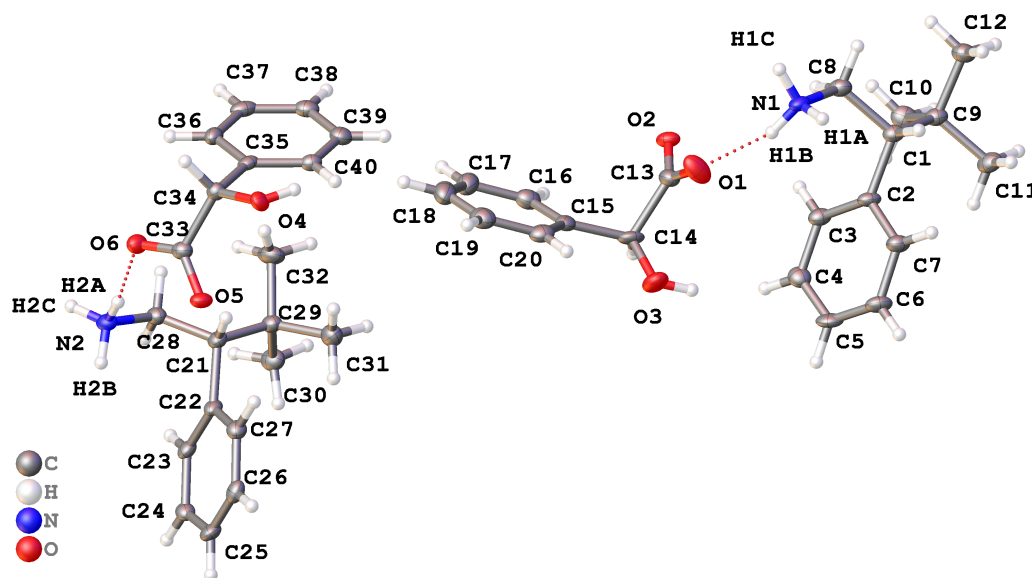
Figure 78. Structures of the acid-base pair formed between (*S*)-mandelic acid and **9**.

The structure was solved by setting the mandelic acid chiral centre to be of (*S*) stereochemistry. The data confirmed the (*S*) configuration for the two acids and revealed each of the bases to be of (*R*) configuration. Two slightly different conformations were seen for the (*S*)-mandelic acid, with a similar angle at the chiral centre of 107.96 and 111.35 for C13-C14-C15 and C33-C34-C35 respectively. The two amines had different conformations, in particular relating to the orientation of the aromatic ring and the *tert*-butyl group, confirmed by a difference in torsion angles of 176.71 and 165.83 for C8-C1-C9-C11 and C28-C29-C31 respectively. An overlay of the two acids and two bases can be seen in Figure 79.
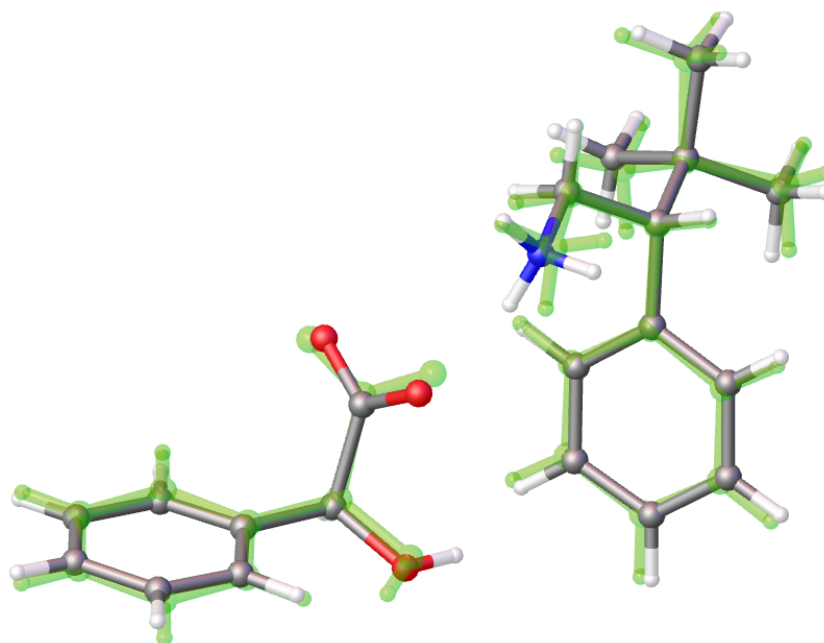
Figure 79. An overlay of the two acid-base pairs found during x-ray diffraction analysis. The grey structures represent the acid with O3 and the amine with N1 from Figure 78. The green structures represent the acid with O4 and the amine with N2 from Figure 78.

Continuous recrystallisations were carried out in the hope to achieve >95 % enantiopurity. Chiral HPLC analysis showed that the starting material was in an isomeric ratio of 47 % (*R*) isomer:53 % (*S*) isomer (Figure 80). The commercially purchased (**R**)- and (*S*)-2-phenyl-propionic acid for the synthetic routes followed for **6a** and **6b** were run on the same chiral HPLC column, along with the subsequent steps, which indicated that the (*R*) isomer interacted with the column for a shorter length of time than the (*S*) isomer. Due to this consistency and therefore on the basis of the columns selectivity, it was suspected that the isomers of **9** were retained in the order (*R*) then (*S*). Furthermore, the crystals obtained during the recrystallisations, with confirmed stereochemistry by x-ray diffraction as seen in

Figure 78 and Figure 79, was also analysed by chiral HPLC displaying the peaks in a ratio of 84 %: 16% (Figure 175) and hence was further proof that the (*S*) isomer retained on the column for longer.
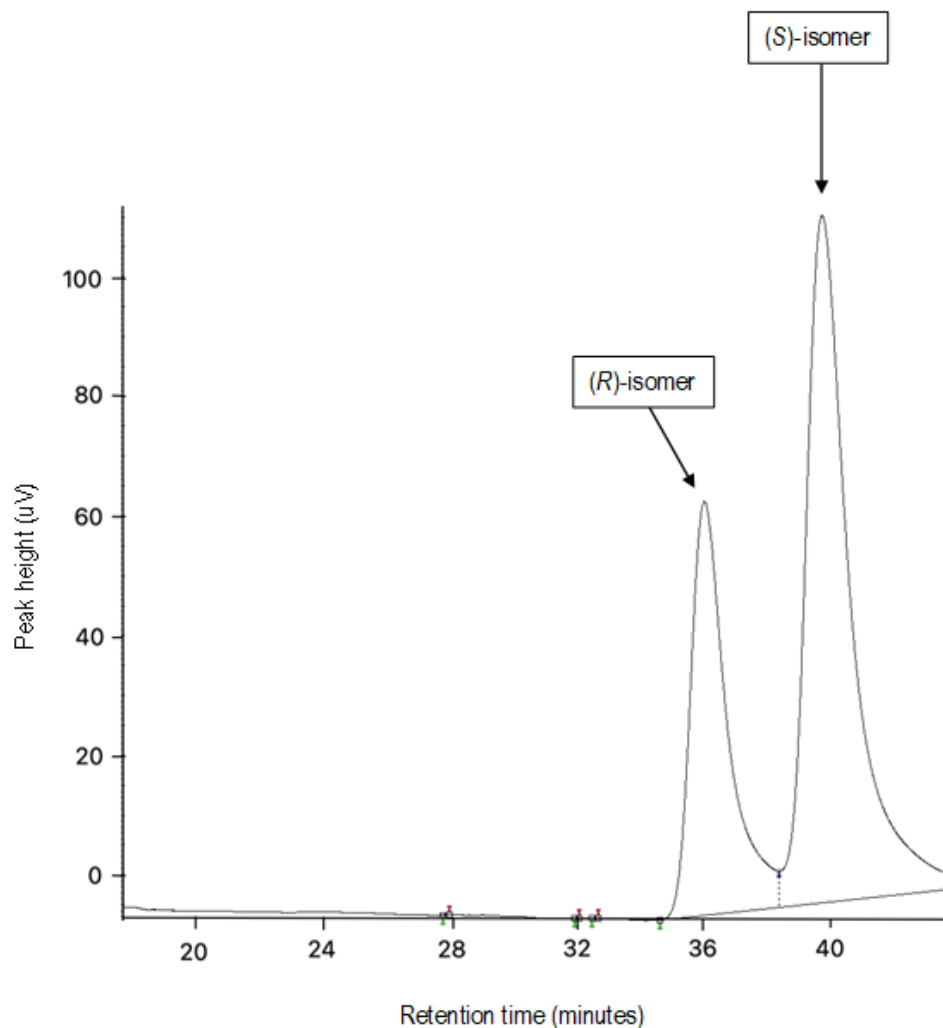
Figure 80. Chromatogram obtained using chiral HPLC, whereby the ratio of peaks relates to the percentage of isomers in the starting amine **9**.

Multiple solvents were screened and it was concluded that the salt was very soluble in methanol, fairly soluble in ethanol and sparingly soluble in isopropanol. Confirmation of the ratio of isomers at each stage was by chiral HPLC. Figure 81 and Figure 82 show the enhancement of enantioselectivity after the first recrystallisation in ethanol.
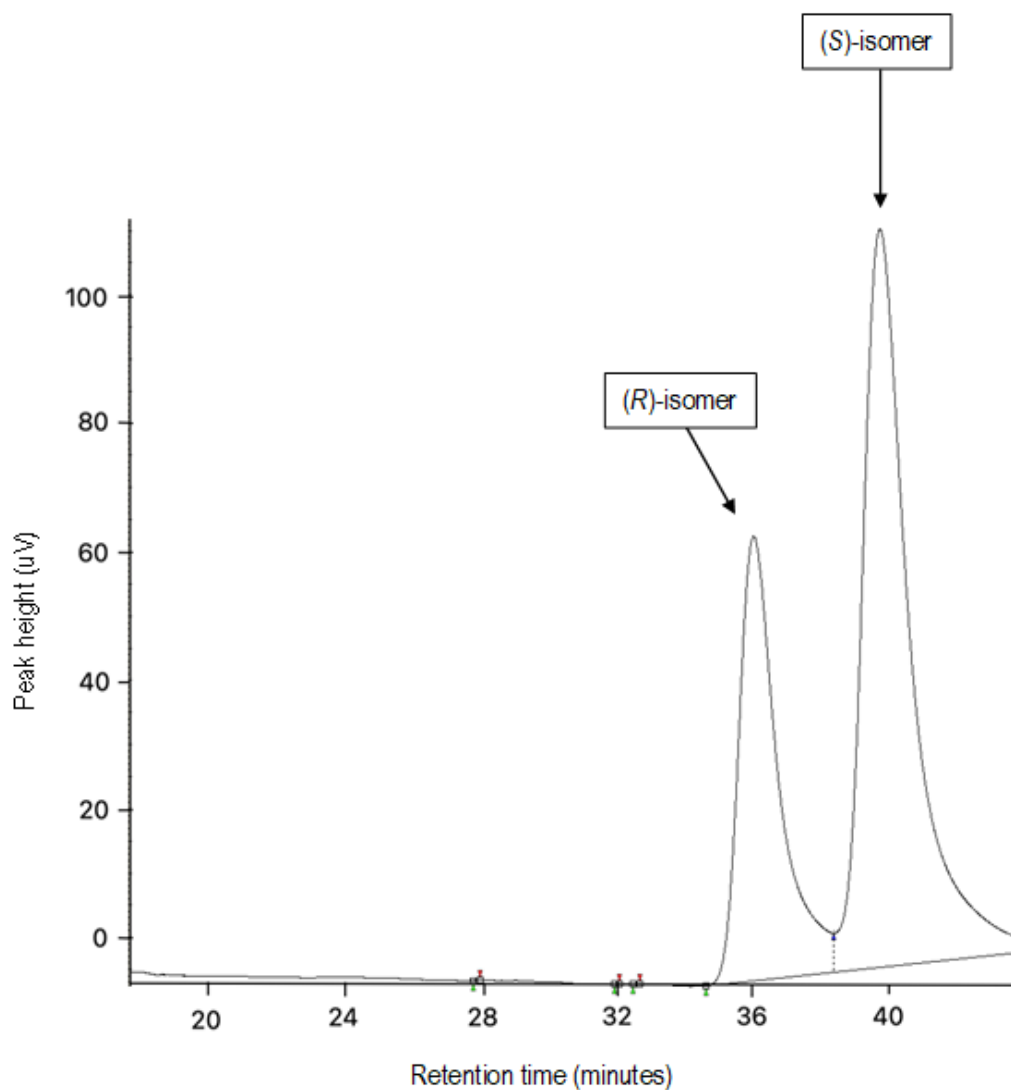
Figure 81. Chromatogram obtained using chiral HPLC, whereby the ratio of peaks relates to the percentage of isomers after the first recrystallisation, representing the solid precipitate (33 %:67 %). The peak at 36 minutes is suspected to be of (R) stereochemistry and the peak at 40 minutes is suspected to be of (S) stereochemistry (for full discussion see section 2.4.3.2).
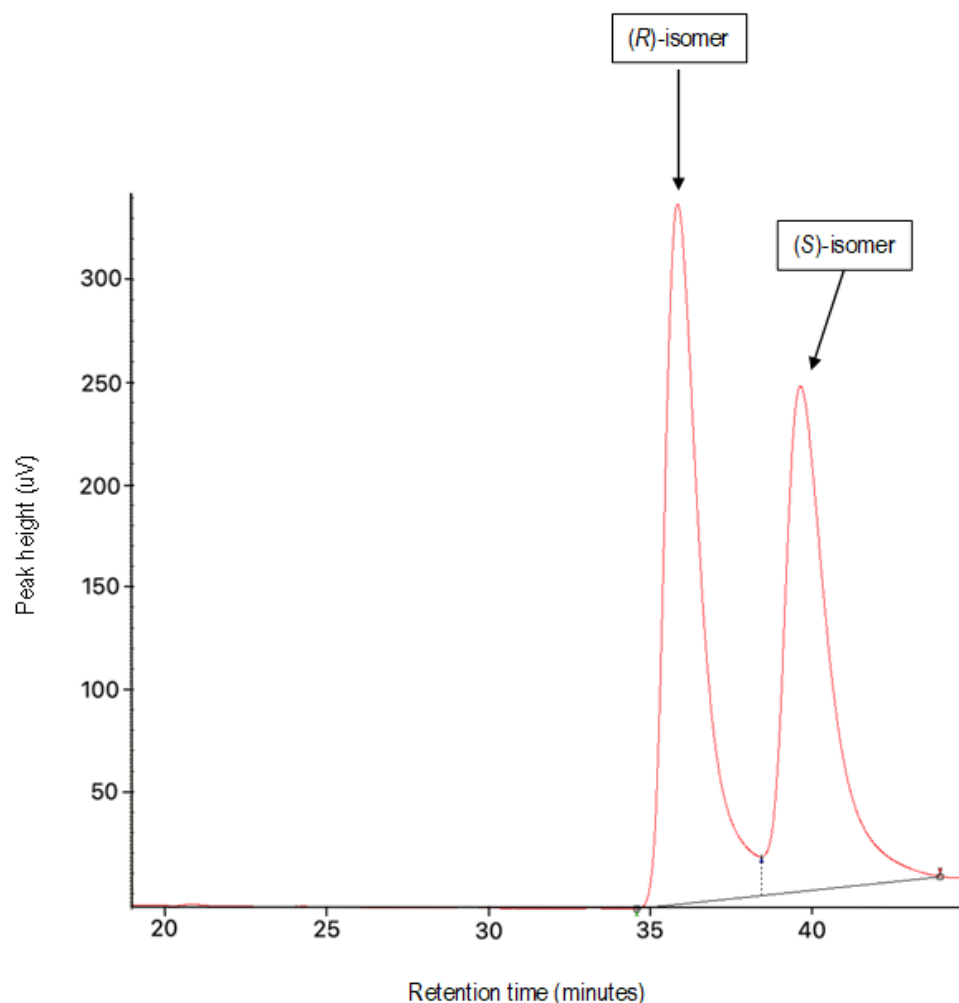
Figure 82. Chromatograms obtained using chiral HPLC, whereby the ratio of peaks relates to the percentage of isomers after the first recrystallisation, representing the supernatant (53 %:47 %). The peak at 36 minutes is suspected to be of (*R*) stereochemistry and the peak at 40 minutes is suspected to be of (*S*) stereochemistry (for full discussion see section 2.4.3.2).

The hot recrystallisations in these alcohols could not exceed ratios of 70 %:30 % and 20 %:80 %. This method was both time consuming and also resulted in large losses of product.

Subsequently, ether on its own, mixtures of ether/hexane and DCM alone were investigated as alternative recrystallisation solvents, whereby the salt was stirred at room temperature with the respective solvent, followed by separation of the solid and liquid phase, whereby the solvent was removed in vacuo from the liquid phase. Extractions were carried out to liberate the amine from the diastereoisomeric pair. In the later stages, hexane was utilised to encourage precipitation as ether alone only achieved ~80 %:20 %. After a total of 78 recrystallisations, 1.04 g of **9b** (91 % ee *S*), 0.41 g of **9b** (80 % ee *S*) and 0.71 g of **9a**

(72 % ee *R*) were obtained. Due to the lower yield of 0.41 g, which still required extraction to remove the mandelic acid, **9b** (80 % ee) was utilised to investigate the proposed route on a test scale. The route was determined successful and hence was applied to the other two amines yielded from the recrystallisations.

Following the synthetic scheme shown in Scheme 14, the next step was the Birch reduction of **9a,** taken from the crystallisation that yielded **9a** in 72 % ee, which was produced in 53 % yield (Scheme 18). The amine **9a** showed good solubility during the Birch reduction, requiring only ten equivalents to reduce the aromatic ring. Despite this, the low yield obtained was suspected to be as a result of solubility issues, whereby too large a volume of solvent was utilised during workup, solubilising the amine into both the organic and aqueous phases.
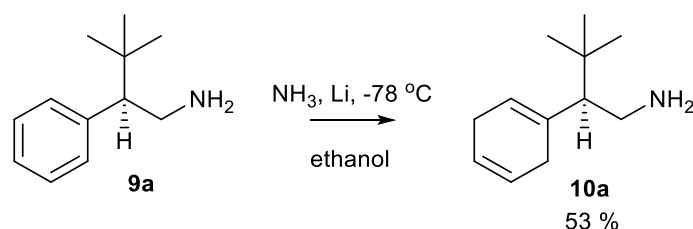
Scheme 18. Synthesis of (*R**)-2-(cyclohexa-1,4-dien-1-yl)-3,3-dimethylbutan-1-amine.

Confirmation of the reduction of the aromatic ring was by ^{1}H-NMR where there was a loss of the peaks at δ = 7.18-7.33 ppm, which instead appeared simultaneously as diene protons at δ = 5.45-5.50 ppm and δ = 5.64-5.70 ppm, and two CH_2 groups observed at δ = 2.53-2.81 ppm. No non-reduced starting material was observed in the ^{1}H-NMR even at a baseline level and hence the reaction was confirmed as complete. Unfortunately, another product was formed during the reduction and was of similar structure to **10a** but was not identified. Using 2D NMR, the diene carbon environments of **10a** were confirmed in the ^{13}C-NMR at δ = 124.1, 123.9 and 122.1 ppm, which were slightly upfield in comparison to the carbon environments in the ^{13}C-NMR of the starting material. Further confirmation of the successful formation of **10a** was by high resolution ESI, whereby the [M + H]$^+$ peak was found at 180.1747 m/z.

Next, **10a** was coupled to (*p*-toluenesulfonyl)glycine in the presence of TBTU, to prevent racemisation[291,292], in a mixture of DMF and DCM (Scheme 19). Following work-up and purification by column chromatography, **11a** was obtained as a white solid in 67 % yield.
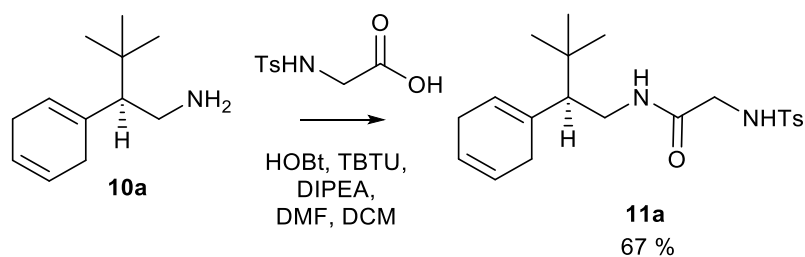
Scheme 19. Synthesis of (*R**)-*N*-(2-(cyclohexa-1,4-dien-1-yl)-3,3-dimethylbutyl)-2-((4-methylphenyl)sulfonamido)acetamide.

Analysis of the ^{1}H-NMR saw a change in chemical shift of the CH_2 adjacent to the NH_2 in the starting material amine from δ = 1.50-1.73 ppm to δ = 1.77-2.12 ppm as a result of its change in environment. Furthermore, evidence showed the shift of the carbon environment associated with this CH_2 group from δ = 60.7 ppm to δ = 56.6 ppm, due to the electron withdrawing nature of the carbonyl group, which in turn shielded the nucleus of the CH_2 carbon environment. The amide **11a** was also successfully confirmed by high resolution ESI in the positive mode as a peak at 413.1868 m/z, associated to the [M + Na]$^+$ ion.

The unknown side product formed in the previous step appeared to be substituted at this step and remained present in the NMR spectra, with similar structure to the anticipated product. The stereocentre coupled with the bulky *tert*-butyl group and conformational flexibility of the cyclohexadiene ring led to two or more different chemical environments for some protons. This resulted in multiple peaks in the ^{1}H-NMR spectrum that integrated to non-integer values, which were situated at unusual chemical shifts from what would initially have been expected. A prime example was the two diene CH_2 groups found at δ = 1.77-2.12 ppm and δ = 2.55-2.78 ppm.

Reduction of **11a** using LiAlH$_4$ in anhydrous THF yielded **12a** (Scheme 20) in 73 %.
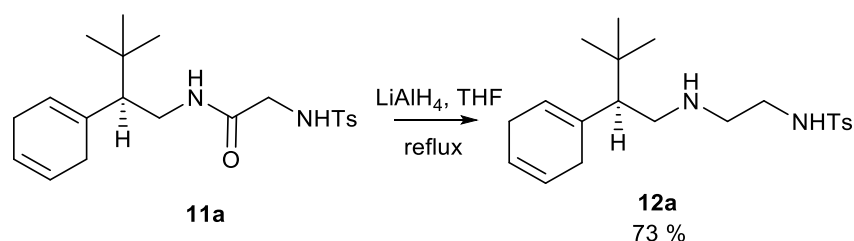
Scheme 20. Synthesis of (*R**)-*N*-(2-((2-(cyclohexa-1,4-dien-1-yl)-3,3-dimethylbutyl)amino)ethyl)-4-methylbenzenesulfonamide.

Successful confirmation of the reduction was found in the ^{1}H-NMR, whereby the new CH_2 group appeared at either δ = 2.38-2.86 ppm or δ = 2.91-2.95 ppm, as it could not unambiguously be assigned, and the carbonyl peak originally found in the ^{13}C-NMR at δ = 167.9 ppm was no longer observed. Upon reduction of the carbonyl bond, the splitting of the peak attributed to the *tert*-butyl group became more complex in the ^{1}H-NMR. Plus, high resolution ESI confirmed the product as the [M + H]$^+$ ion at 377.2265 m/z.

Complexation of the chiral ligand **12a** with RuCl$_3$xH$_2$O allowed formation of the anticipated ruthenium dimer **13a** (Scheme 21) in 39 % yield as a brown solid. This was carried forward to the next step without full characterisation.
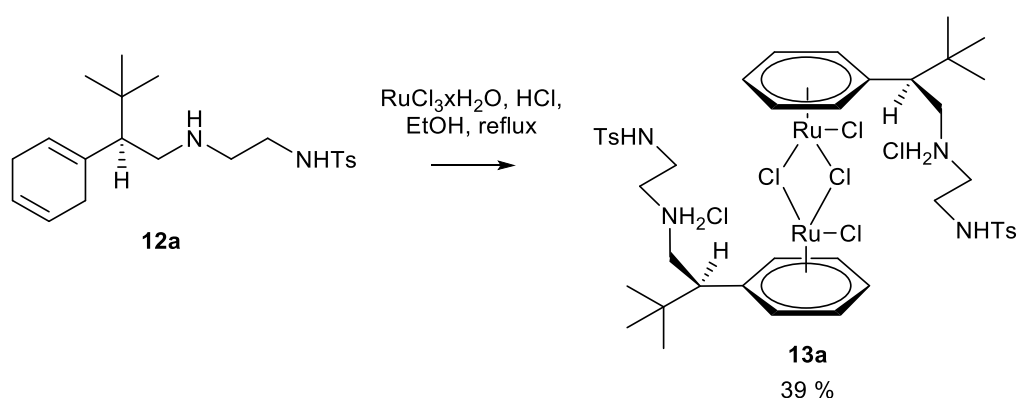
Scheme 21. Synthesis of [Ru(η^6-(*R**)-*N*-(2-((2-(cyclohexa-1,4-dien-1-yl)-3,3-dimethylbutyl)amino)ethyl)-4-methylbenzenesulfonamide)Cl$_2$]$_2$.2HCl.

Finally, **13a** was subjected to cleavage, induced by the addition of DIPEA, to form the target complex **14a** (Scheme 22) in 17 % yield. The product was obtained in low yield and contaminated with DIPEA even after purification, therefore due to the assumption that DIPEA wouldn't affect the ATH results, the contaminated product was carried forwards.
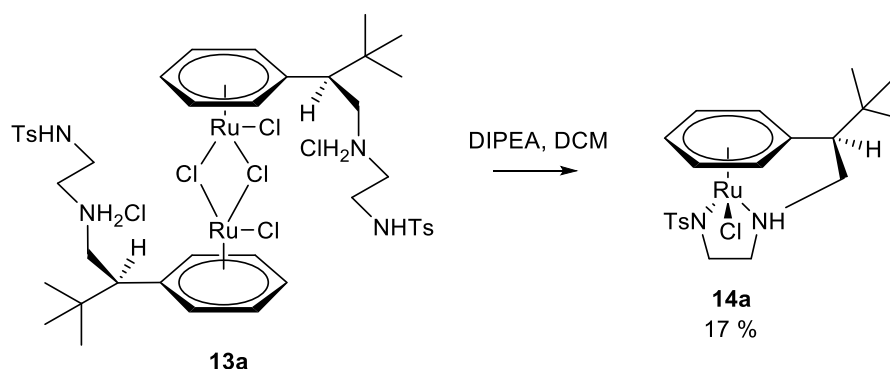
Scheme 22. Synthesis of final complex **14a**.

The ^{1}H-NMR spectrum of **14a** revealed the presence of two diastereoisomers, present in an abundance of 30 % for the minor conformer and 70 % for the major conformer. The arene protons were displayed as three triplets, one doublet and three multiplets in the region of δ = 4.93-6.67 ppm. Further, the high resolution ESI spectrum found the [M - Cl]$^+$ peak at 475.0998 m/z as an envelope of peaks characteristic of the ruthenium isotopic pattern.

2.3.5 Synthesis of complex 14b
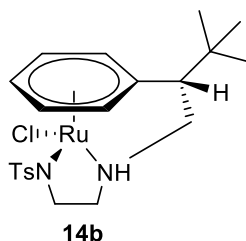
Figure 83. Structure of **14b**.

Concurrently, the other isomer hypothesised to be (*S*), separated during the recrystallisations earlier, followed the synthetic pathway shown in Scheme 14. The starting amine **9**, from the recrystallisation that yielded **9b** in 91 % ee, was Birch reduced to **10b** in 47 % yield. The Birch reduction was monitored by ^{1}H-NMR to ensure sufficient Li was added, concluded to be ten equivalents. Non-reduced starting material was observed at a baseline level in the ^{1}H-NMR and the same side product formed as found for **10a**. **10b** was then coupled to (*p*-toluenesulfonyl)glycine in the presence of TBTU, to prevent racemisation[291,292], and was obtained in 63 % yield as a white solid after purification by column chromatography. Then **11b** was reduced to **12b** in 95 % yield, which was refluxed with RuCl$_3$xH$_2$O to form **13b** in 16 % yield as an intermediate step to the final complex **14b**, which was obtained in 76 % yield. All ^{1}H-NMR, ^{13}C-NMR and high resolution MS was in agreement with that found for the alternate isomer and can be found in Chapter 5. Two diastereoisomers were observed in the ^{1}H-NMR, whereby the minor and major isomers were found in 35 % and 65 % abundance, which was marginally different to that found for **14a**, hence the complex appeared to be flexible due to the variation in the ratio of conformers formed, suggesting that the ratio of isomers can be influenced by experimental conditions, in particular the concentration of the catalyst in NMR solvent and the temperature surrounding the sample, which is in accordance with the NMR studies carried out for **6a** and **7** in section 2.4.1. that discusses the exchange/interconversion between isomers at room temperature.

2.3.6 Synthesis of complex 14
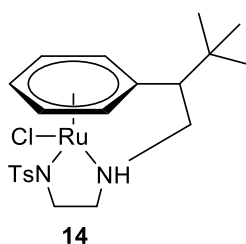
Figure 84. Structure of **14**.

For comparison, and to later be used in the ATH NMR time course studies, the racemic analogue **14** was synthesised but only obtained in 5 mg yield. The route employed was identical to that shown in Scheme 14. The data collected for the complex (^{1}H-NMR, ^{13}C-NMR and high resolution ESI) matched that found for **14a** and **14b**, with the two diastereoisomers found in solution in a relative abundance of 35 % and 65 % for the minor and major conformers respectively in the ^{1}H-NMR spectrum, calculated by determining the ratio of the arene peaks of the respective isomers.

2.3.7 Synthesis of complex 19

Due to the successful synthesis of **6a**, **6b**, **7**, **14a** and **14b**, a further branch of this project focused on increasing the tether length by one carbon length to give rise to **19** (Figure 85).
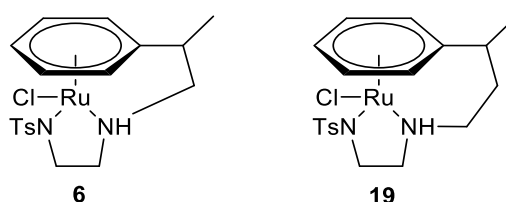
Figure 85. 2C- and 3C- tethered Ru(II) complexes synthesised in this project.

The rationale was that a longer tether would reduce the amount of strain within the catalyst, hence reducing conformational restraints, allowing for greater activity towards ketone substrates. Catalysts with tethers of three carbon atoms in length are the most active.[150]

3-Phenylbutyric acid was purchased as its racemate to purely test the activity of the catalyst with a longer tether without focusing on the enantioselectivity. To investigate whether the shorter length of tether affected the failure of the arene exchange, this attempt utilised racemic 3-phenylbutyric acid to create a tethered ligand, comprising of a longer tether of three carbon atoms in length, which was refluxed with [Ru(C$_6$H$_5$CO$_2$Et)Cl$_2$]$_2$ (Scheme **23**).
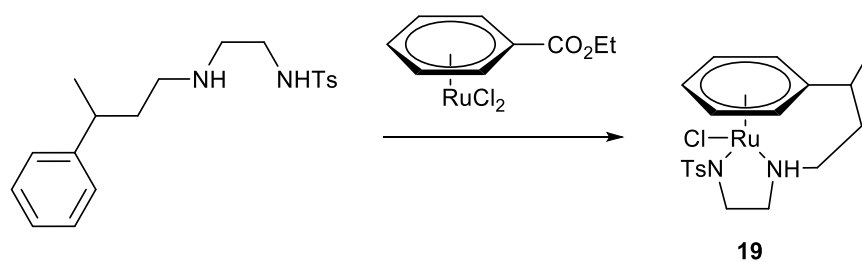
Scheme 23. The arene exchange step attempted to form **19**.

The method employed followed a literature precedent[122] and has been fully described in the experimental chapter. Unfortunately, **19** was not detected and therefore the Birch reduction route was employed. Therefore, to produce the fourth chiral-at-metal ruthenium catalyst framework in this project, the route followed that shown in Scheme 24.
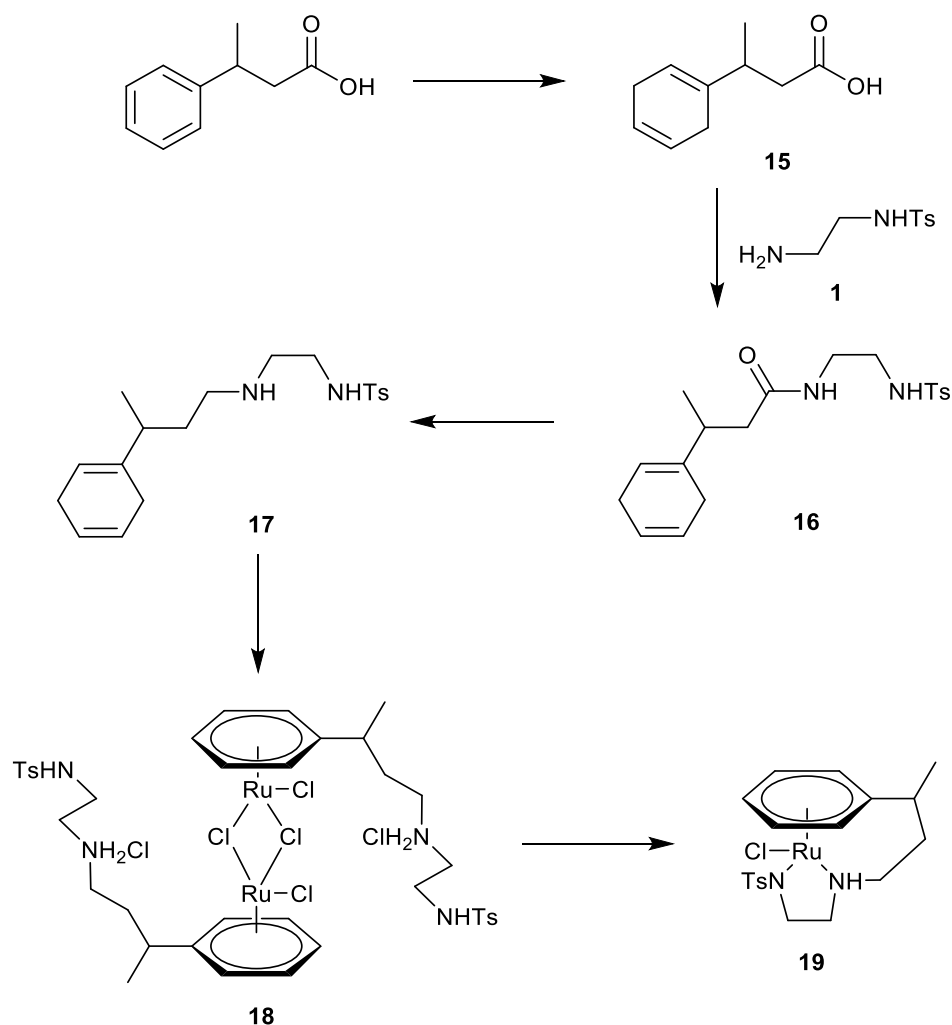
Scheme 24. Global synthetic scheme to show the successful synthesis of **19**.

The synthetic route followed was based entirely on that described previously for **6a** and **6b**, commencing with a Birch reduction to form the diene **15** in 84 % yield (Scheme 25).
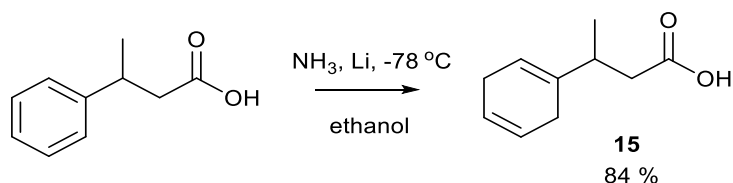
Scheme 25. Synthesis of 3-(cyclohexa-1,4-dien-1-yl)butanoic acid.

An excess of 19 equivalents of Li was required to push the reaction towards completion. Minimal non-reduced starting material was observed in the ^{1}H-NMR spectrum. The Birch reduction was confirmed by the appearance of the diene ring protons at δ = 5.50-5.50 ppm and δ = 5.65-5.75 ppm in the ^{1}H-NMR, and δ = 118.3, 124.3 and 124.3 ppm in the ^{13}C-NMR.

Coupling of **15** to the tosylated amine precursor **1** (Scheme 26), which was purified by column chromatography, yielded 72 % of the pure amide **16** as a white solid.
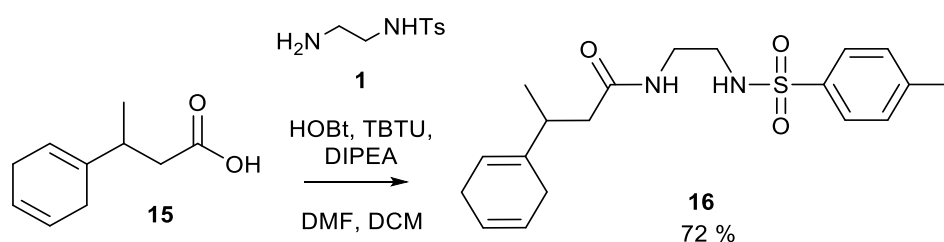
Scheme 26. Synthesis of 3-(cyclohexa-1,4-dien-1-yl)-*N*-(2-((4-methylphenyl)sulfonamido)ethyl)butanamide.

Evidence for the success of this reaction was found by the shielding of the CH$_2$ group adjacent to the carbonyl group from δ = 2.28-2.34 ppm and δ = 2.48-2.54 ppm to δ = 2.05-2.15 ppm and δ = 2.26-2.34 ppm in the ^{1}H-NMR. Baseline impurities were also present, possibly attributed to unreacted starting material. A shift of the carbonyl group in the ^{13}C-NMR was observed from δ = 179.4 ppm for the acid to δ = 173.4 ppm for the amide. Furthermore, high resolution ESI found the [M + Na]$^+$ peak at 385.1556 m/z.

16 was treated with LiAlH$_4$ at reflux overnight to obtain 91 % of **17** (Scheme 27).
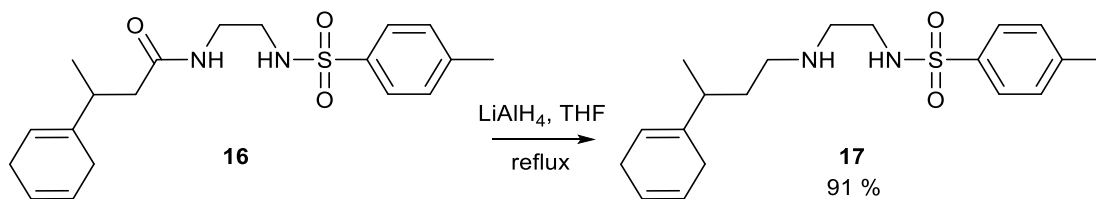
Scheme 27. Synthesis of *N*-(2-((3-(cyclohexa-1,4-dien-1-yl)butyl)amino)ethyl)-4-methylbenzenesulfonamide.

Completion of the reaction was confirmed by TLC analysis and ninhydrin staining. Success of this reduction was observed by the disappearance of the C=O peak in the ^{13}C-NMR, plus the protons of the CH$_2$ group appeared at δ = 2.37-2.41 ppm in the ^{1}H-NMR. Additional support was found by the ESI spectrum, whereby 349.1944 m/z confirmed the [M + H]$^+$ ion.

Following this, the ligand **17** was reacted with RuCl$_3$xH$_2$O to form the dimer **18** in 44 % yield (Scheme 28) as a light brown/orange solid.
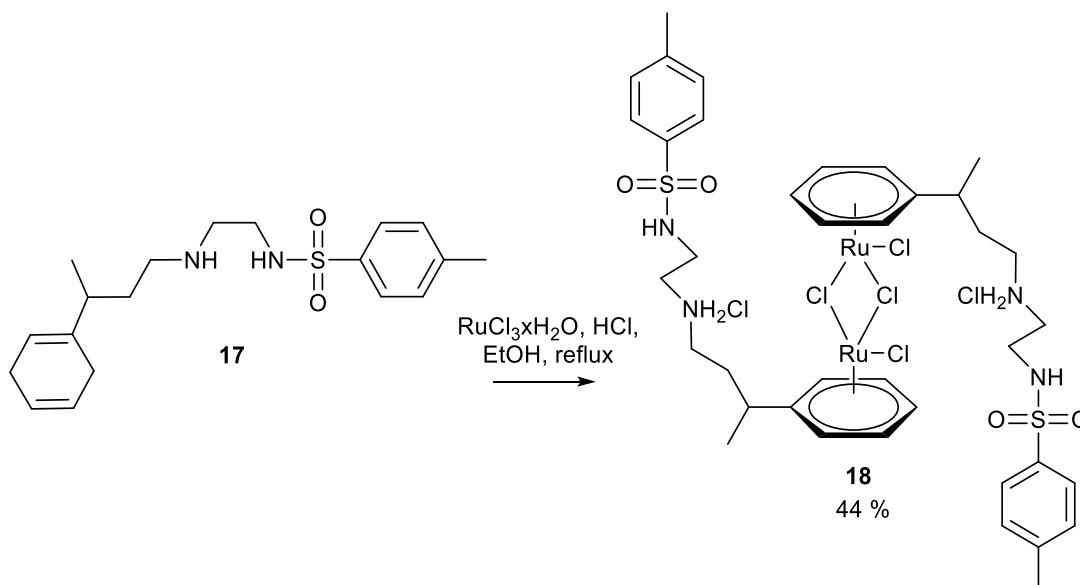
Scheme 28. Synthesis of [Ru(η^6-*N*-(2-((3-(cyclohexa-1,4-dien-1-yl)butyl)amino)ethyl)-4-methylbenzenesulfonamide)Cl$_2$]$_2$.2HCl.

Unfortunately, the dimer was not pure and from the ^{1}H-NMR it appeared that a small amount of chelation may have occurred. Despite this, distinctive arene protons were observed at δ = 5.19-6.45 ppm, indicative of the different environments of the arene ring on the dimer. The ^{13}C-NMR was successfully assigned utilising the assignments made for **6a** and **6b** coupled with 2D NMR experiments that were also run.

18 was treated with DIPEA to create the final complex **19** (Scheme 29), obtained as a light brown solid in 62 % yield from the purification step by column chromatography.
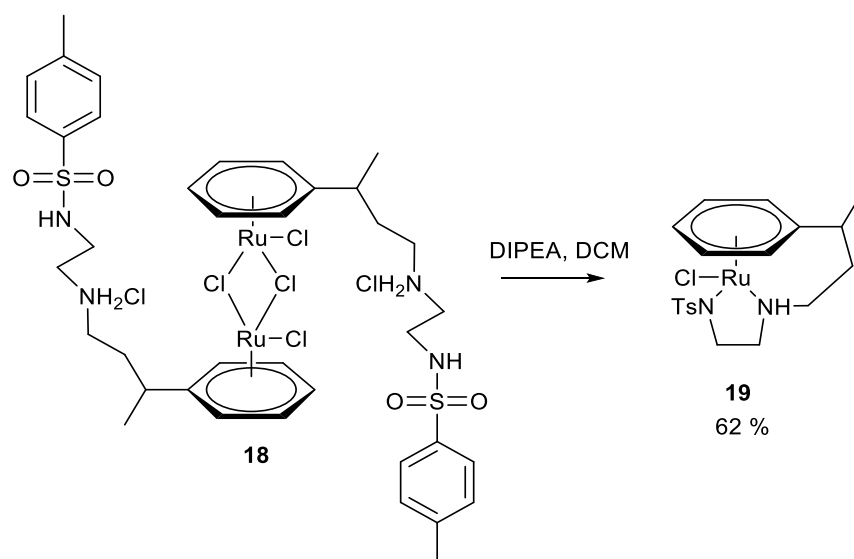
Scheme 29. Synthesis of final complex **19**.

The arene protons in the ^{1}H-NMR were observed as seven arene environments with the integrations adding to ten protons, indicating that two configurational isomers were present in solution in equal abundance. These two configurational isomers were suspected to be as a result of the differing stereochemistry surrounding the metal centre, likely as a result of the tether chelating around the metal centre in both possible senses. This idea was further supported by the ^{13}C-NMR, which displayed two peaks per distinct carbon environment. Further evidence for the formation of complex **19** was found by collecting high resolution ESI, whereby the [M - Cl]$^+$ ion was observed at 447.0686 m/z as an envelope of peaks displaying the characteristic ruthenium isotope pattern. The data found for this compound was closely supported by two complexes of similar structure previously synthesised in the literature.[109,123] Elemental analysis was collected but the expected and found values did not match within the acceptable margin error of ± 0.3 %. Trying to fit solvent or known impurities did not solve the problem, however, vanadium pentoxide was not utilised (as it was for the majority of the other analyses presented in this thesis) and therefore incomplete combustion of the sample is the most likely source of the deviation.

2.3.8 Synthesis of complex 19a
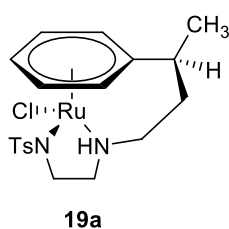
Figure 86. Structure of **19a**.

Due to the success of this route, the synthetic pathway was repeated with an enantiopure starting material (Scheme 30).
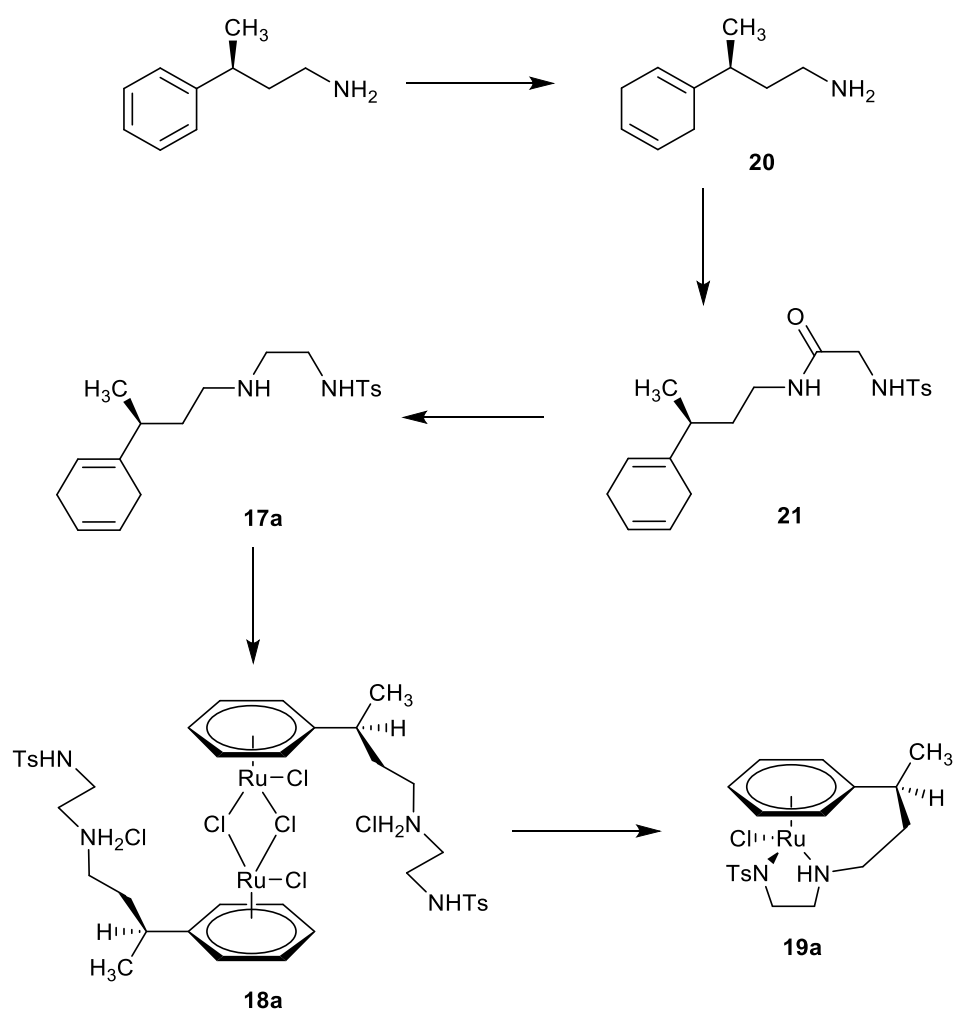
Scheme 30. Global synthetic scheme to show the successful synthesis of **19a**.

The first step (Scheme 31) comprised of the Birch reduction of the enantiopure amine, previously synthesised by Dr Murray's research group, to produce **20** in 79 % yield.
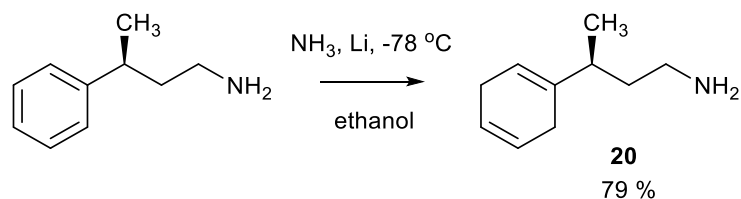
Scheme 31. Synthesis of (*S*)-3-(cyclohexa-1,4-dien-1-yl)butan-1-amine.

Due to greater solubility, only seven equivalents of Li were required to reduce the aromatic ring. The ^{1}H-NMR proved the reaction to be complete due to the appearance of signals from the alkenyl ring protons at δ = 5.37-5.44 ppm and δ = 5.63-5.72 ppm and lack of signals in the aromatic region. The carbon peaks relating to the diene environments were observed at δ = 118.1 and 124.4 ppm and the CH_2 groups of the ring were found at δ = 25.5 ppm and δ = 26.8 ppm, further confirming the successful production of the Birch reduced amine. Moreover, high resolution ESI showed the [M + H]$^+$ ion at 152.1436 m/z.

Following this, **20** was coupled with (*p*-toluenesulfonyl)glycine (Scheme 32) in a mixture of DMF and DCM. In addition to its use as a coupling agent, TBTU helped to prevent racemisation[291,292].
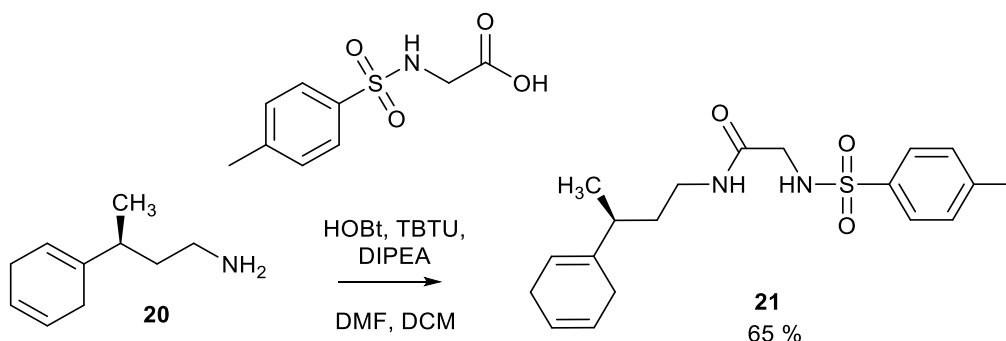
Scheme 32. Synthesis of (*S*)-*N*-(3-(cyclohexa-1,4-dien-1-yl)butyl)-2-((4-methylphenyl)sulfonamido)acetamide.

21 was purified by column chromatography in 65 % yield. The ^{1}H-NMR confirmed a 1:1 reaction between the amine and acid due to the integration of 3:4 of the diene to aromatic protons. The NH_2 peak was no longer observed, but instead a new resonance appeared, which integrated to one proton, corresponding to the newly formed amide NH. Furthermore, the CH_2 protons immediately adjacent to the NH_2 moiety shifted from δ = 2.46-2.68 ppm to δ = 3.04-3.21 ppm upon coupling to the acid, and the carbon environment from δ = 40.5 ppm

to δ = 38.4 ppm as a result of deshielding due to interaction with the nearby electronegative carbonyl group. Additionally, high resolution ESI found the [M + H]⁺ ion at 363.1732 m/z.

21 was reduced to **17a** in 19 % yield using LiAlH$_4$ (Scheme 33). The low yield may be due to loss of product during work-up steps, e.g. extraction, or formation of side products.
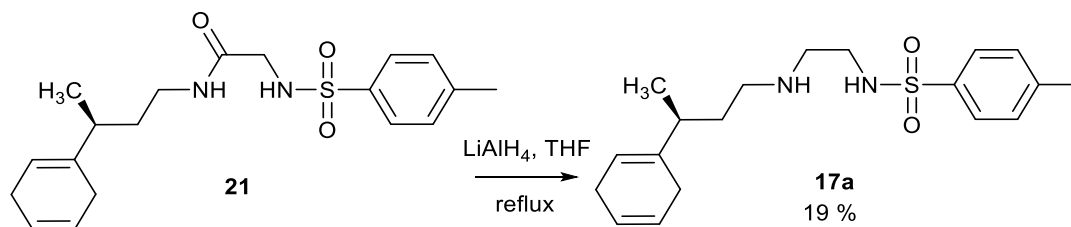
Scheme 33. Synthesis of (*S*)-*N*-(2-((3-(cyclohexa-1,4-dien-1-yl)butyl)amino)ethyl)-4-methylbenzenesulfonamide.

Confirmation of the reaction was by TLC analysis and ninhydrin staining. Moreover, the appearance of the CH$_2$ protons at δ = 2.22-2.35 ppm in the ¹H-NMR and the disappearance of the carbonyl environment at δ = 167.9 ppm in the ¹³C-NMR validated the reduction. The new CH$_2$ environment appeared at δ = 48.0 ppm, distinctive of an aliphatic moiety. Also, the [M + H]⁺ ion was observed at 349.1952 m/z in the high resolution ESI.

Sequentially, **17a** was refluxed with RuCl$_3$xH$_2$O (Scheme 34) to obtain **18a** in 52 % yield as a brown solid, but was carried forwards to the next step without full characterisation.
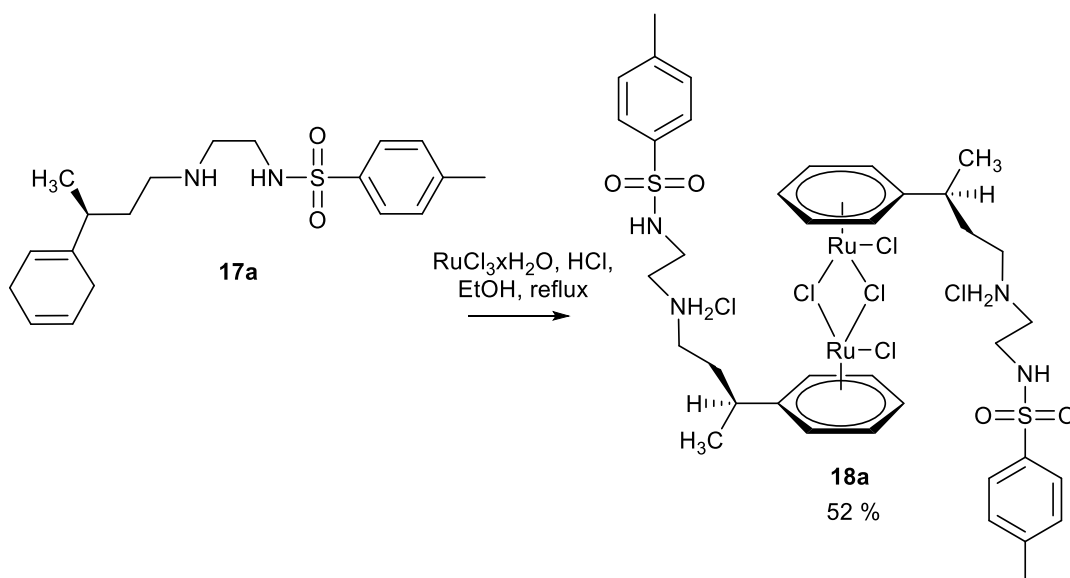
Scheme 34. Synthesis of [Ru(η⁶-(*S*)-*N*-(2-((3-(cyclohexa-1,4-dien-1-yl)butyl)amino)ethyl)-4-methylbenzenesulfonamide)Cl$_2$]$_2$.2HCl.

The final step of this reaction pathway required cleavage of the chloride ligands in **18a** (Scheme 35), which was successful in obtaining **19a** in 33 % yield as a brown oil. The product was unfortunately contaminated with DIPEA even after purification was attempted. Therefore due to the low quantity of product obtained, coupled with the assumption that DIPEA wouldn't affect the ATH results, the contaminated product was carried forwards.
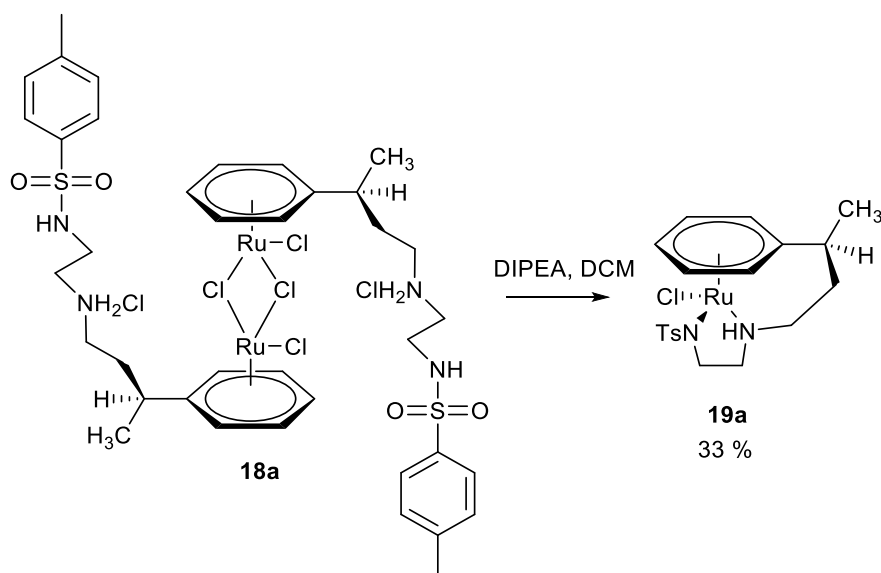
Scheme 35. Synthesis of final complex **19a**.

Analysis by ^{1}H-NMR and ^{13}C-NMR confirmed the production of the complex **19a**. Unfortunately, the integrals of the aliphatic protons did not perfectly match the arene protons (or simply were not observed) due to the contaminating DIPEA, however, the chemical shifts of identified signals did match that of the racemic analogue **19**. Further, important peaks corresponding to the arene ring were observed in the ^{1}H-NMR at δ = 4.92-6.58 ppm. There appeared to be two diastereoisomers present in equal abundance. The ^{13}C-NMR displayed the same issues found in the ^{1}H-NMR, namely contamination by DIPEA and poor signal to noise ratio, providing small or absent peaks. Though the complex could not be unambiguously assigned, peaks were able to be picked out based on the ^{13}C-NMR data collected for the racemic analogue **19**. Most importantly, two diastereoisomers were observed due to two peaks of similar shift per each distinct carbon environment, for example, δ = 20.5 ppm and δ = 20.6 ppm, responsible for the CH$_3$ group adjacent to the stereocentre. Further evidence for the formation of the complex was observed in the high resolution ESI spectrum at 447.0688 m/z, consistent with the predicted peak for the [M - Cl]$^+$ ion, observed as an envelope of peaks displaying the characteristic ruthenium isotope pattern.

2.3.9 Synthesis of complex 24
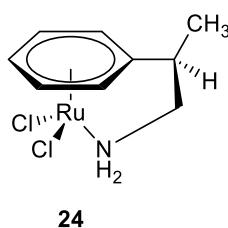
Figure 87. Structure of **24**.

To investigate the stereochemical control and stability of this family of complexes further, a route to produce a monodentate complex was followed as shown in Scheme 36.
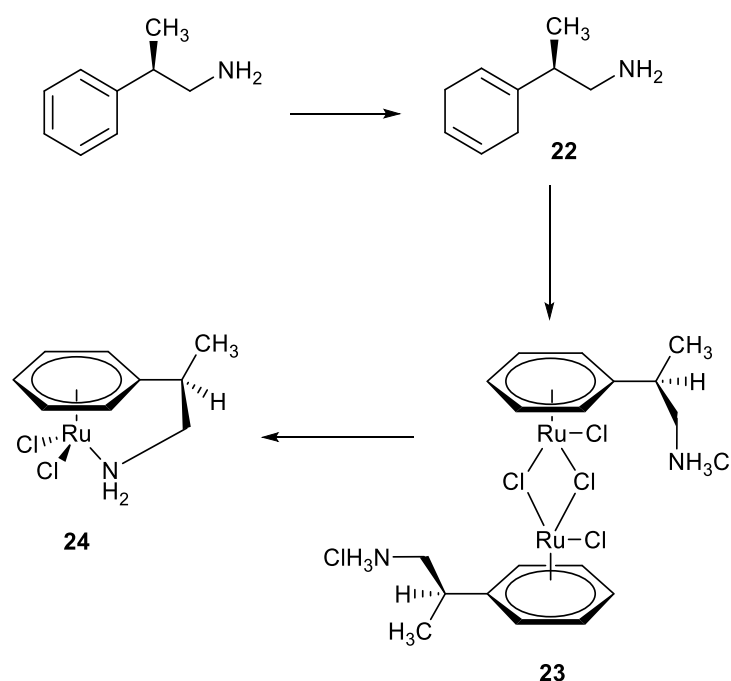
Scheme 36. Global synthetic scheme to show the successful synthesis of **24**.

The complex would confirm if the two diastereoisomers, observed in solution by ^{1}H-NMR for all previous complexes discussed in this chapter, were as a result of the tethered section between the benzylic carbon and chelating moiety or the chelating moiety alone. The synthesis of **24** would also allow comparison for characterisation purposes. Furthermore, the results from the ATH would highlight the importance of the incorporation of the chelating section within the ligands of the original family of complexes synthesised in this project.

The starting material was commercially purchased with 99 % enantiopurity of (*R*)-stereochemistry and the synthetic pathway begun with the Birch reduction of this amine to produce **22** (Scheme 37) in 88 % yield.
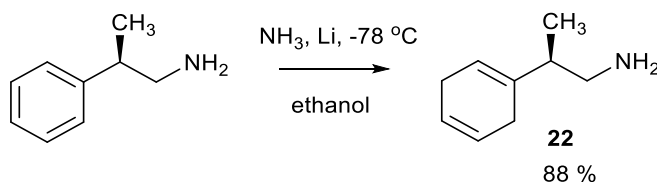
Scheme 37. Synthesis of (*R*)-2-(cyclohexa-1,4-dien-1-yl)propan-1-amine.

Particularly good solubility was observed for the starting material, hence only 3.60 equivalents of Li were used to reduce the aromatic ring. Three protons were seen at δ = 5.47 ppm and δ = 5.65-5.72 ppm in the ^{1}H-NMR, which was a clear indication of the success of the reduction of the aromatic ring, coupled with the absence of aromatic protons. The arene environments were observed in the ^{13}C-NMR at δ = 119.8, 124.3 and 124.4 ppm. Further, the [M + H]$^+$ peak was found in the high resolution ESI spectrum at 138.1277 m/z.

Consequently, the chiral ligand **22** was refluxed with $RuCl_3xH_2O$ to obtain the dimer **23** (Scheme 38) in 9 % yield as an orange solid.
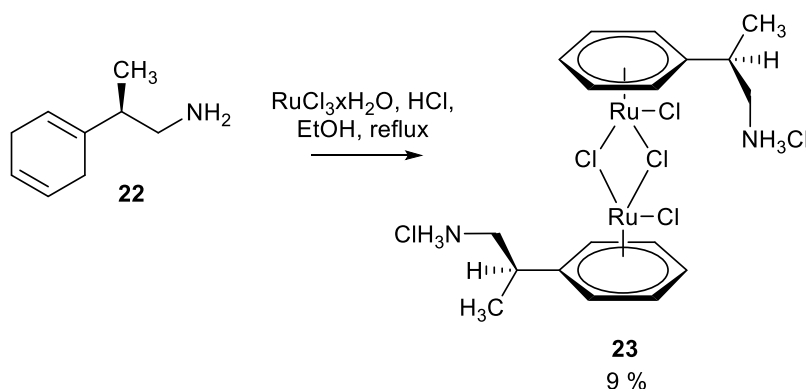
Scheme 38. Synthesis of [Ru(η^6-(*R*)-2-(cyclohexa-1,4-dien-1-yl)propan-1-amine)Cl$_2$]$_2$.2HCl.

The dimer was fully characterised by ^{1}H-NMR and ^{13}C-NMR. Of particular interest was the change of the diene ring in the starting material, found at δ = 5.47-5.72 ppm, to the arene ring in the dimer **23**, found at δ = 5.97-6.02 ppm. Additionally, the stereocentre shifted from δ = 2.05-2.13 ppm in the starting material to δ = 3.21-3.29 ppm in the product, whereby the stereocentre in the dimer experienced deshielding as a result of decreased electron density at the nucleus, which caused a downfield shift in the ^{1}H-NMR, suggesting that the arene ring was more electron withdrawing than the diene ring. Unfortunately, the spectrum was contaminated with an impurity, likely to be the arene analogue of the diene ligand.

Fortunately, this impurity would be removed at the next step by purification on silica. Utilising 2D NMR data, the ^{13}C-NMR was successfully assigned.

Finally, the dimer **23** was subjected to deprotonation by DIPEA (Scheme 39), which simultaneously caused cleavage of the chloride ligands. The resulting complex **24** was purified by column chromatography to obtain the orange sold in 95 % yield.
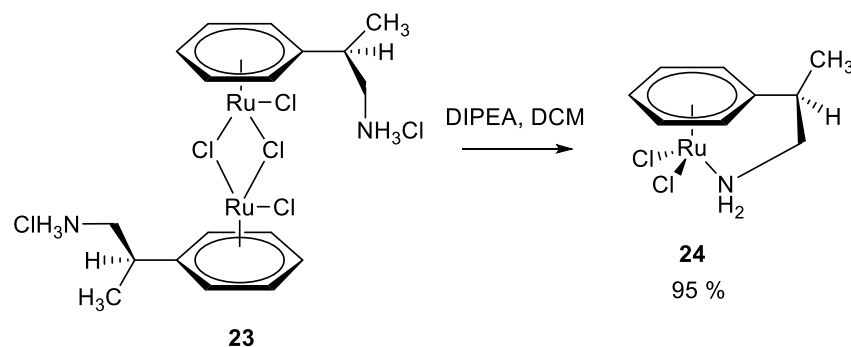
Scheme 39. Synthesis of final complex **24**.

The complex was fully characterised by ^{1}H-NMR, ^{13}C-NMR, ESI and elemental analysis. The ^{1}H-NMR displayed the arene ring as three triplets and two doublets in the region δ = 5.25-5.94 ppm, characteristic of arene ring protons and indicating that the arene protons were in non-equivalent environments, and the stereocentre proton was observed at δ = 3.15-3.24 ppm, which therefore had experienced further deshielding than that seen for the dimer. From analysis of the 2D NMR, each distinctive carbon environment of the complex **24** was assigned to the nine peaks found in the ^{13}C-NMR, with a particularly large shifts for the stereocentre from δ = 34.6 ppm in the dimer **23** to δ = 43.0 ppm in the complex **24** and for the CH$_2$ from δ = 43.3 ppm in the dimer **23** to δ = 62.8 ppm in the complex **24**, indicating a significant change in environments upon complexation. A single enantiomer was found as the starting ligand used was enantiopure. As the metal centre remained achiral, diastereoisomers were not possible. This suggested that the chelating section of the tether was responsible for the diastereoisomers found in the ^{1}H-NMR, ^{13}C-NMR and x-ray diffraction of complexes **6a**, **6b**, **7**, **14a**, **14b**, **19** and **19a**. High resolution ESI confirmed the [M - Cl]$^+$ peak of **24** at 271.9781 m/z as an envelope of peaks, characteristic of the ruthenium isotope pattern. Unfortunately, the identity of the complex was not confirmed by elemental analysis due to the expected and found values not matching within the acceptable margin error of ± 0.3 %. The deviation was determined to be as a result of the lack of vanadium pentoxide, which was used during elemental analysis for the majority of the other compounds

analysed during this project. This piece of evidence does not hold too much significance as compound **24** was synthesised to allow for comparison to all other complexes made in this project and further to confirm that the chelating ligand was a requirement for achieving good activity during ATH.

2.4 Further investigative analysis of final complexes

2.4.1 NMR studies

To investigate the idea of the possibility of interchange between the configurational isomers formed further, ^{1}H-NMR studies were performed (Figure 88) in DMSO-d_6 at varying temperatures (25 ºC, 40 ºC, 60 ºC, 80 ºC and 100 ºC).
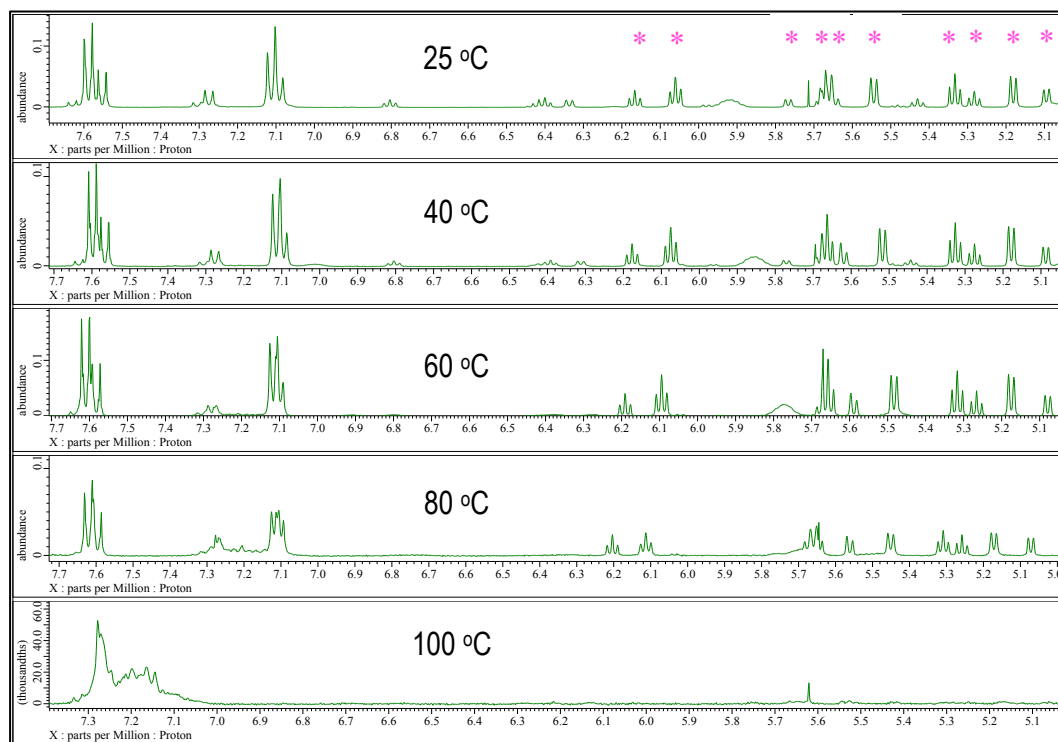
Figure 88. Stacked NMR showing the arene and aromatic regions from a temperature variation experiment carried out on **6b** to monitor configurational isomerism. Pink asterisks denote the ten peaks associate with two configurational isomers initially observed for **6b**.

Conclusions were drawn from observations of changes to the two triplets at δ = 6.00-6.20 ppm that correspond to protons within the arene ligands of the two configurational isomers. Upon increasing the temperature from 25 ºC to 80 ºC, a change in the ratio of peaks was noted from 1.00:2.31 (6.20 ppm:6.00 ppm) to 1.00:1.55 (6.20 ppm:6.00 ppm). At 80 ºC, the signals corresponding to the ten arene proton resonances of the two configurational isomers

were observed to have reduced in intensity. At 100 ºC, free arene ligand was observed in the spectrum, however, no peaks corresponding to arene ligands coordinated to ruthenium were seen and hence the assumption was that the complex had decomposed. To confirm this, the NMR sample was rerun at 25 ºC and the lack of peaks observed in the spectrum proved decomposition had occurred. Additionally, a fresh sample was made, and the NMR run three times; first at 25 ºC, then at 60 ºC and finally again at 25 ºC. At 25 ºC, the two triplets focused upon were in the ratio of 1.00:2.12 (6.20 ppm:6.00 ppm). At 60 ºC, the two triplets focused upon were in the ratio of 1.00:2.21 (6.20 ppm:6.00 ppm). Upon returning the temperature to 25 ºC, the two triplets focused upon were in the ratio of 1.00:2.14 (6.20 ppm:6.00 ppm). This confirmed that the minimal interconversion observed reverted upon cooling, plus the majority of interconversion occurred between 60 ºC to 80 ºC.

In summary, the change of temperature allowed slow interconversion between the two configurational isomers. The peaks did not converge into one isomer, suggesting that interchange between the two configurational isomers was sufficiently slow at the temperatures the experiments were ran at. This further confirmed that the arene peaks were in different chemical environments to one another, although the results overall remain inconclusive as to which diastereoisomer species were in fact observed in solution. Additional species were observed in DMSO-d_6, which were not observed in CDCl$_3$-d, possibly as a result of the DMSO displacing the chloride ligand, arene ligand or tethered ligand and coordinating to the metal centre of **6a**. This postulated complex was rendered unstable due to the disappearance of these additional resonances at higher temperatures. DMSO-d_6 was chosen as the initial solvent for studying configurational isomers at elevated temperatures due to the lower boiling point of CDCl$_3$-d. Nevertheless, upon noticing decomposition above 60 ºC, it was of interest to repeat the NMR study in CDCl$_3$-d.

^{1}H-NMR studies were performed in CDCl$_3$-d, whereby two diastereoisomers were observed (Figure 89).
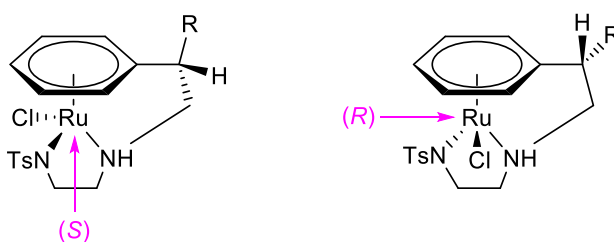
Figure 89. Two diastereoisomers proposed to be present in the NMR spectra of **6a** and **7**.

Complex **6a** was dissolved in CDCl$_3$-d and left to stand at 25 ºC. Slow exchange of the two isomers were observed with an equilibrium being reached after 60 hours, portraying the two diastereoisomers in a 1:1 ratio (Figure 90). Upon further heating at 40 ºC for 24 hours, no further change in the ratio of isomers was observed.
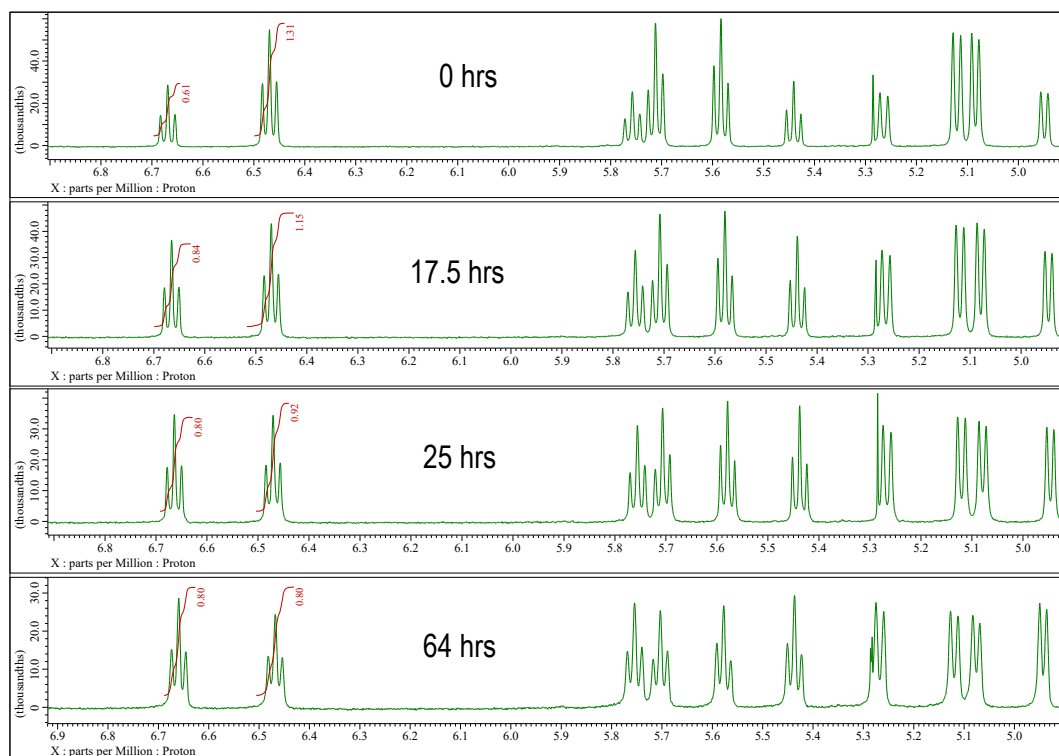
Figure 90. Stacked NMR showing the ten arene peaks from the time variation experiment carried out on **6a** at 25 °C to monitor conformer % change.

Comparatively, **7** was dissolved in CDCl$_3$-d and left to stand at 25 ºC. This sample never reached equilibrium, even after seven days, and showed the diastereoisomers in a ratio of 0.35:1.00. Further analysis confirmed a third isomer in the spectra for both **6a** and **7**, however this project was not able to identify the nature of this species.

Overall, it was postulated that the ^{1}H-NMR arene protons were influenced by the positioning of tether, which was predicted to be controlled by the bulky substituent at the carbon stereocentre and the amount of strain exerted within the complex. As a result, one diastereoisomer was initially formed preferentially (shown by one diastereoisomer being present in excess in the ^{1}H-NMR spectra), due to the bulky substituent residing at a perpendicular angle to the arene ligand (see section 2.4.2), giving a less strained complex.

For final confirmation, it would have been useful to have carried out ^{1}H-NMR studies of the catalysts in the FA/TEA azeotrope, utilised during the ATH studies, at 40 ºC to confirm the relative abundance of each diastereoisomer under these conditions.

2.4.2. X-ray diffraction

Single orange crystals for complexes **6a**, **6b**, **7**, **19** and **24**, suitable for single crystal X-ray diffraction, were obtained via slow evaporation of a solution of the complex in ethanol.

The crystal structure of **7** was utilised to determine the major diastereoisomer observed in the ^{1}H-NMR spectra for all complexes. This was possible because the complex was recrystallised to obtain one diastereosiomer in >94 % excess. Although the complex synthesised was racemic, hence both enantiomers were present, only one diastereoisomer was observed in the solid state and has been shown in Figure 91, whereby the benzylic stereocentre was of (*S*) configuration and the metal centre was of (*R*) configuration[296].
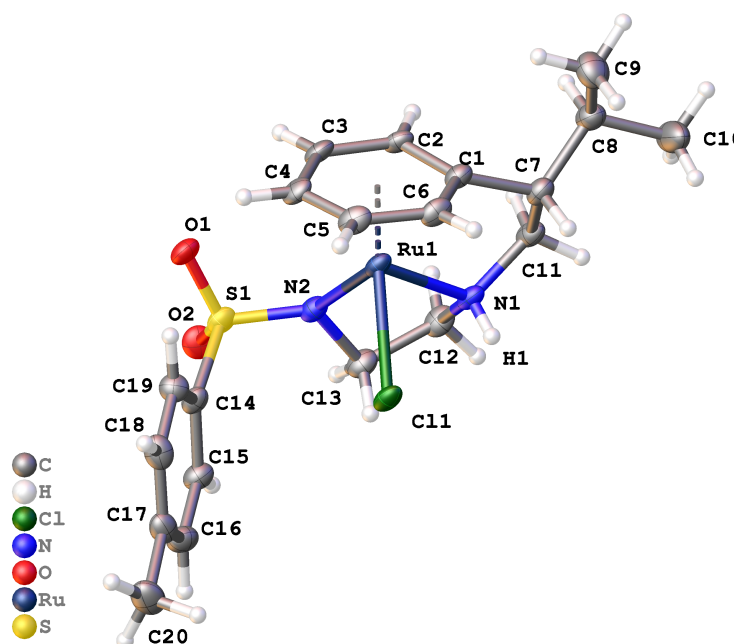
Figure 91. Structure showing how complex **7** crystallised.

The chirality at the metal centre was determined by utilising a literature precedent that set the arene ligand as the first priority group as a result of "summing the atomic weights of all the atoms bonded to the metal centre"[217,296]. There was observable bending of the tether to position the benzylic carbon below the plane of the arene ligand, whilst the *iso*-propyl group was orientated above the plane of the arene ligand, at an approximately perpendicular angle. It was determined that this was the major diastereosiomer observed in the ^{1}H-NMR.

Structural data for **6a** showed two diastereoisomers (Figure 92), whereby the complex on the left had the CH$_3$ group orientated above the plane of the arene ligand, approximately at a perpendicular angle, displaying (*S*) stereochemistry at the carbon stereocentre and (*R*) stereochemistry at the metal centre[217,296].
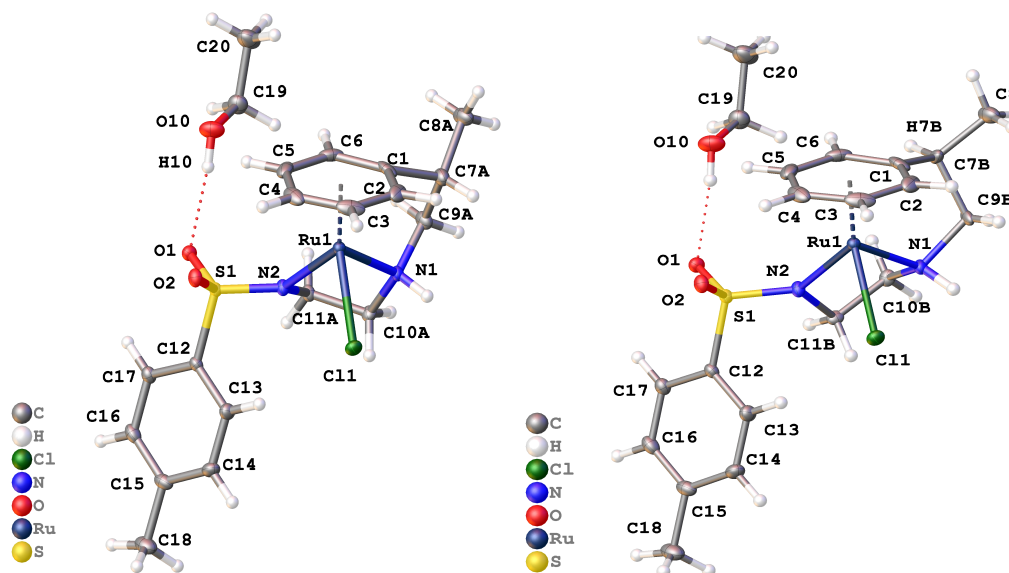
Figure 92. Structures of the two diastereoisomers observed for the complex **6a**.

The alternate diastereoisomer (Figure 92 - right) comprised of (*R*) stereochemistry at the carbon stereocentre, as anticipated from the starting material **2a**, and (*S*) stereochemistry at the metal centre[217,296] and was predicted to be the major diastereoisomer observed in the ¹H-NMR spectrum.

In addition, both enantiomers of each diastereoisomer was observed in structural data. The mixture of stereoisomers in the crystal analysed was apparent from the disorder seen in the resulting structures in the region of the tether, resulting from complexes with the same metal-centred configuration but differing configurations at the benzylic position. If both orientations of the molecule were overlayed, a clustered structure was observed (Figure 93).
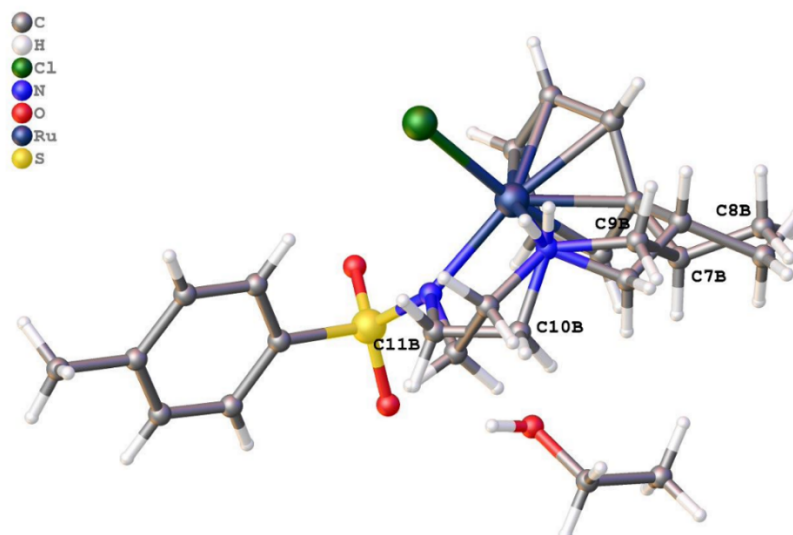
Figure 93. Overlay of two structures showing how the complex **6a** crystallised.

This data confirms that both configurations at the ruthenium ion and both configurations at the stereogenic centre C7 were observed, giving rise to a total of four stereoisomers of the complex within this crystal sample.

Although both possible stereochemical configurations at the benzylic stereocentre were observed in the crystals of **6a**, HPLC analysis showed that the bulk ligand **4a** was enantiomerically pure, so by extension the ligand component of **6a** had not racemised. Therefore, it was possible that the recrystallisation managed to co-crystallise the 2 % of the isomer comprising of (*S*) stereochemistry at C7a (Figure 92), alongside the anticipated complex with (*R*) stereochemistry at C7a, suggesting that the presence of the enantiomeric complex in the x-ray sample was due to the commercially available starting material being purchased at only 98 % enantiomeric excess.

Structural data for **6b** portrayed a centrosymmetric and enantiomerically pure structure, whereby a single configuration at the carbon stereocentre was seen. Despite this, two different modes of tether binding at the metal centre was observed, indicating that two diastereoisomers were present in the solid state, with the two diastereosiomers assembling into centrosymmetric dimers via hydrogen bonds as shown in Figure 94.
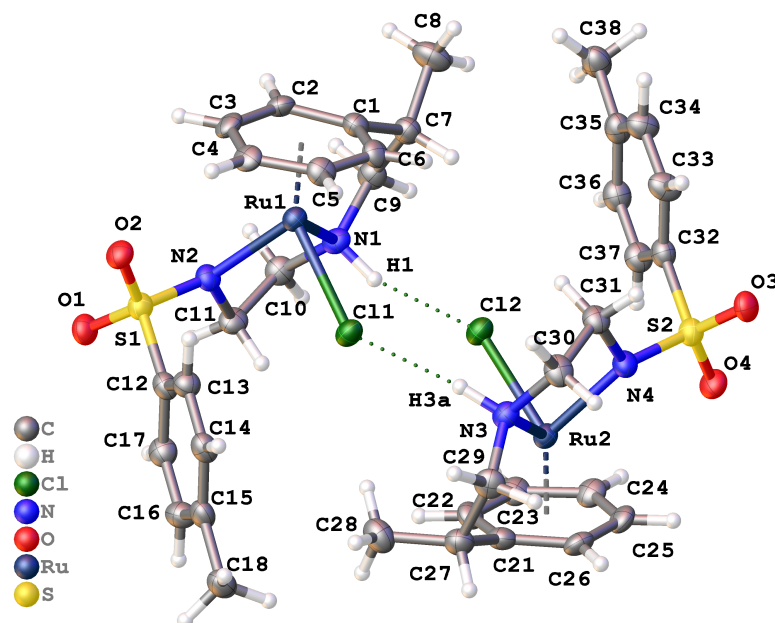
Figure 94. Structure showing how the complex **6b** crystallised.

The two diastereoisomers have been depicted in Figure 95.
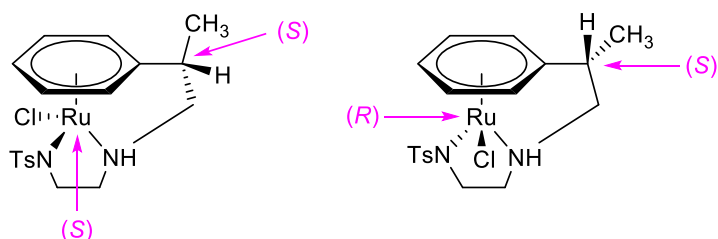
Figure 95. Proposed diastereoisomers present in the crystal structure of **6b** from the binding of the bidentate chelating section of the tether to the metal centre in two different geometries; observed tether wraps behind the metal centre (left) and infront of the metal centre (right).

When the benzylic carbon was orientated perpendicular to the CH_3 group, the complex had (*S*) stereochemistry at the carbon stereocentre and (*R*) stereochemistry at the metal centre[217,296], identical to Figure 92. Alternatively, the other diastereoisomer had the benzylic carbon in the same plane as the arene ligand, which orientated the CH_3 group slightly below the plane of the arene ligand and found the amine group of the tether directly below the arene carbon from which the tether emanates. This was representative of the complex that had (*S*) stereochemistry at both the carbon stereocentre and the metal centre[217,296].

Interestingly, the tether of **19** was only observed to orientate in one direction in the solid state, indicating that only one diastereoisomer was present (shown in Figure 96).
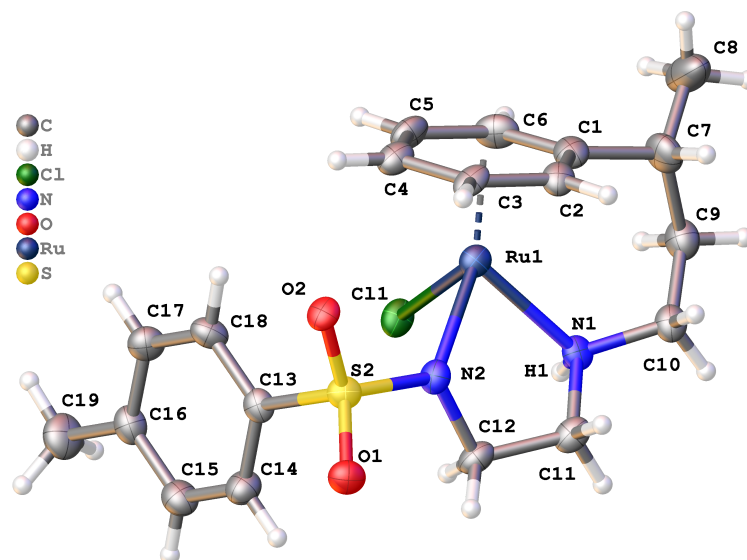
Figure 96. Structure showing how the complex **19** crystallised.

In fact, the tether was observed in the opposite direction to that observed for the 2C-tethered analogues **6a**, **6b** and **7** (Figure 92, Figure 94 and Figure 91). For the single diastereoisomer observed for **19**, the benzylic stereocentre was bearing (*R*) chirality and the metal centre was bearing (*S*) chirality[217,296]. In this configuration, the CH_3 group was perpendicular to the arene ligand, orientating above the plane of the arene ligand. As a result of reduced strain, this longer chained complex saw the benzylic carbon align in the same plane as the arene ligand, which was opposite to the shorter tethered complexes that portrayed the benzylic carbon below the plane of the arene ligand.

Although each complex was chiral, the centre of symmetry meant that the crystal analysed was a racemic mixture; the solid contained both enantiomers (Figure 97) in an ordered arrangement because of the presence of the inversion centre at C7. This was expected as the reaction pathway stemmed from a racemic starting material.
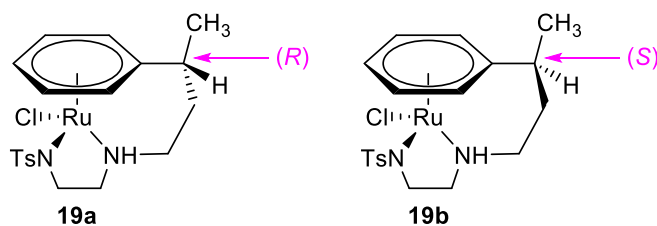
Figure 97. The two diastereoisomers of complex **19**, whereby both comprised of (*S*)-stereochemistry at the metal centre[217,296], observed in the x-ray diffraction data and suspected to be present in the NMR solution too.

Pairs of enantiomers were assembled into centrosymmetric dimers by hydrogen bonds as shown in Figure 98.
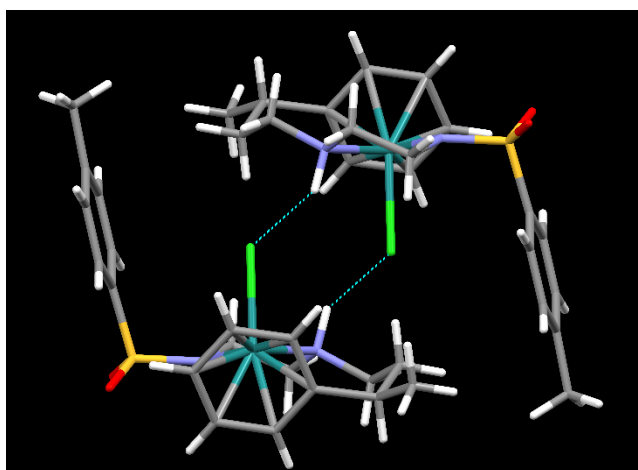
Figure 98. Packing of the complexes **19a** and **19b** within the crystals grown.

The two enantiomers were seen as a result of the difference in stereochemistry at the benzylic carbon C7, which in turn also affected the stereochemistry of the ruthenium centre and NH moiety. Confirmation of two diastereoisomers was concluded by the ^{1}H-NMR due to two sets of arene peaks being observed in a 1:1 ratio. Therefore overall, it was concluded that the full tether was able to coordinate to the metal centre in both senses, giving rise to a total of four stereoisomers.

24 (Figure 99) possessed (*R*) chirality at the stereocentre on the tether, as anticipated from the (*R*) chirality of the starting ligand, but the metal centre was confirmed as non-chiral due to the complex comprising of two chloride ligands.
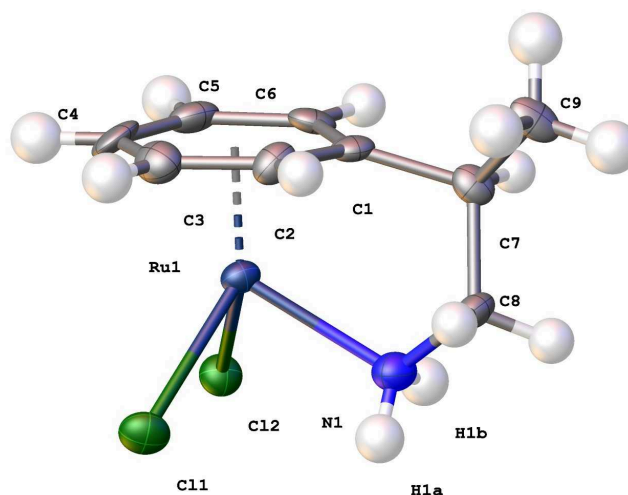
Figure 99. Structure showing how the complex **24** crystallised.

The data showed four independent ruthenium units in the asymmetric unit, whereby one asymmetric unit is shown in Figure 99 as a representative. The CH_3 group was found perpendicular to the plane of the arene ligand, with bending of the arene-benzylic carbon due to the benzylic carbon present below the plane of the arene ligand, creating strain within the complex. Three out of the four units were identical configurations, however, the bulky CH_3 group of one unit was fixed at a different angle to the other units. An overlay of the centres of mass for the four units can be seen in Figure 100 and shows down the Ru-N bond.
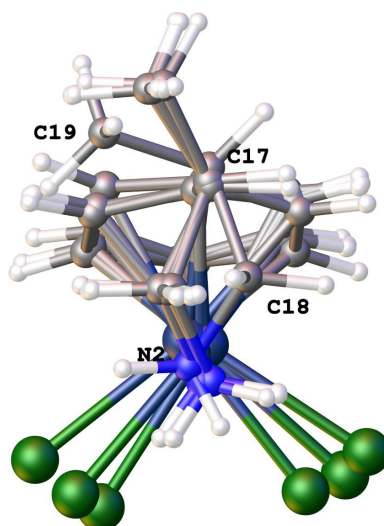
Figure 100. An overlap of the four independent ruthenium units observed in the asymmetric unit of the single crystal of complex **24**.

Comparisons of torsion angles (Table 14) further confirms that the four molecules were identical but that the conformation of the unit comprising Ru2 was different to the other three units (Figure 101).

Table 14. Comparison of torsion angles for the four ruthenium units observed in the asymmetric unit of the single crystal of complex **24**.

Metal centre notation	Atoms in torsion angle	Torsion angle value
Ru1	N1 - C8 - C7 - C9	167(1)
Ru2	N2 - C18 - C17 - C19	80.0(12)
Ru3	N3 - C28 - C27 - C29	173.9(10)
Ru4	N4 - C38 - C37 - C39	169.7(10)
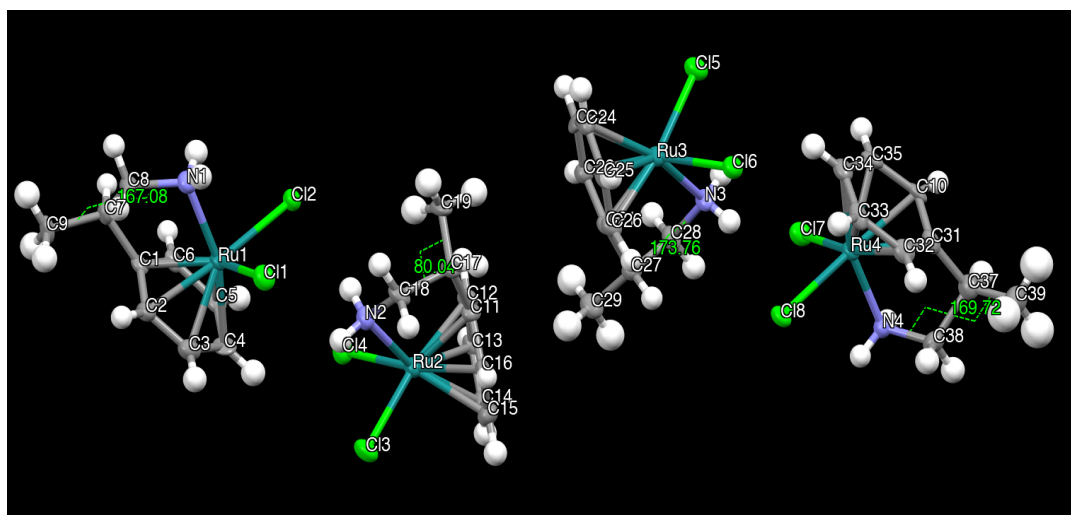
Figure 101. The four ruthenium units observed in the asymmetric unit of the single crystal of complex **24**.

2.4.3 Asymmetric Transfer Hydrogenation

To measure the activity of these complexes, ATH reactions were performed to evaluate the extent to which the complexes could reduce various substrates to their corresponding alcohols. In this study, FA/TEA was employed as the solvent to allow for completion of the reaction, if possible, and a greater comparison to literature precedents[123,150]. The azeotrope was bought in commercially and checked for the correct 5:2 ratio by ^{1}H-NMR before commencing ATH reactions. Further, a S/C (S/C is the substrate to catalyst molar ratio[297]) loading of 0.50 mol %, i.e. 200 equivalents of substrate to catalyst, was chosen due to

success in previous literature[123,150], hence consolidating the possibility of direct comparison. The overall method employed here was followed from a literature precedent[150] but instead the substrates were added directly by syringe to the reaction mixture during this project, whereas the research group added their substrate solubilised in DCM to the reaction mixture. Purification of the reduction products in order to remove excess catalyst followed methodology by Wills et al.[123]. A blank reaction was run without any complex present (i.e. azeotrope and substrate only), which showed no conversion of acetophenone by ^{1}H-NMR. This confirmed that any activity seen in future reactions would solely be attributed to the complex itself.

2.4.3.1. Acetophenone

Acetophenone is the most widely studied substrate within ATH, granting a benchmark for direct comparison of all catalysts synthesised and tested for their activity by ATH. In fact, a majority of successful catalysts reduce acetophenone in 100 % conversion with enantioselectivity >90 %[107,123,150], allowing the focus of researchers to shift onto tuning reaction conditions in the hope to reduce reaction times and catalyst loading.

Preliminary experiments were carried out at 28 ºC for 24 hours with acetophenone, to ensure enough time to allow for full conversion, and the lower temperature investigated the extent of activity of the catalyst. The quick screen was carried out against **C2**, used as a control, and **7** (Figure 102).
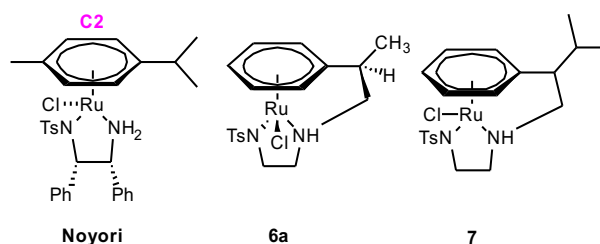
Figure 102. Noyori's catalyst[81] and Ru(II) complexes synthesised in this project; **6a** and **7**.

The results showed poor conversion rates for **6a** and **7**, especially in comparison to **C2**. Due to this lack of conversion (>10 %) initially observed at 28 ºC, the subsequent ATH reactions were carried out at 40 ºC for 24 hours with the hope to improve conversion rates. This increase of temperature to 40 ºC has been described in numerous papers[123,144,150]. Comparing the two preliminary experiments at 28 ºC and 40 ºC, it can be noted that an increase in temperature made a drastic improvement in the conversion of acetophenone to

by all three complexes. In particular, the complexes synthesised in this project became more active by 4-fold.

Once the temperature for the reactions had been decided upon, an investigation into whether the inclusion of an induction period to activate the complex was beneficial in order to improve results. The reason for this suggested induction period was to encourage formation of the hydride (Scheme 40), which was therefore ready to perform reduction on the substrate immediately as it was added.
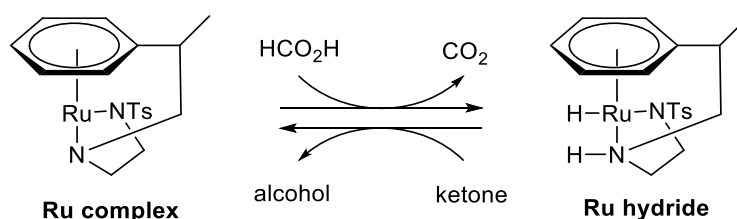
Scheme 40. Formation of the hydride during the induction period.[150]

As seen in Table 15, the presence of an induction period did make a substantial difference to the conversion. The longer the reaction was left for, the more significant the induction period was. On the other hand, the induction period had absolutely no impact on the enantioselectivity of the reaction after the 72 hours. From these conclusions, it was decided that an induction period would be included in all ATH reactions run from this point on.

Table 15. Comparison of experiments run with and without a 30 minute stirring induction period of the complex and azeotrope before addition of the substrate. ATH of acetophenone by **6b** (0.5 mol % loading, 40 °C, 24 hours, 3 repeats).
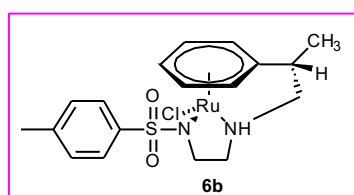
Time (hours)	Conversion (%)	
	No induction period	Induction period
24	14 ± 0	18 ± 1
48	33 ± 0	46 ± 4
72	59 ± 4	74 ± 5

The results for the conversion and enantioselectivity for the reduction of acetophenone at 40 °C for 24 hours in FA/TEA can be seen in Figure 103.
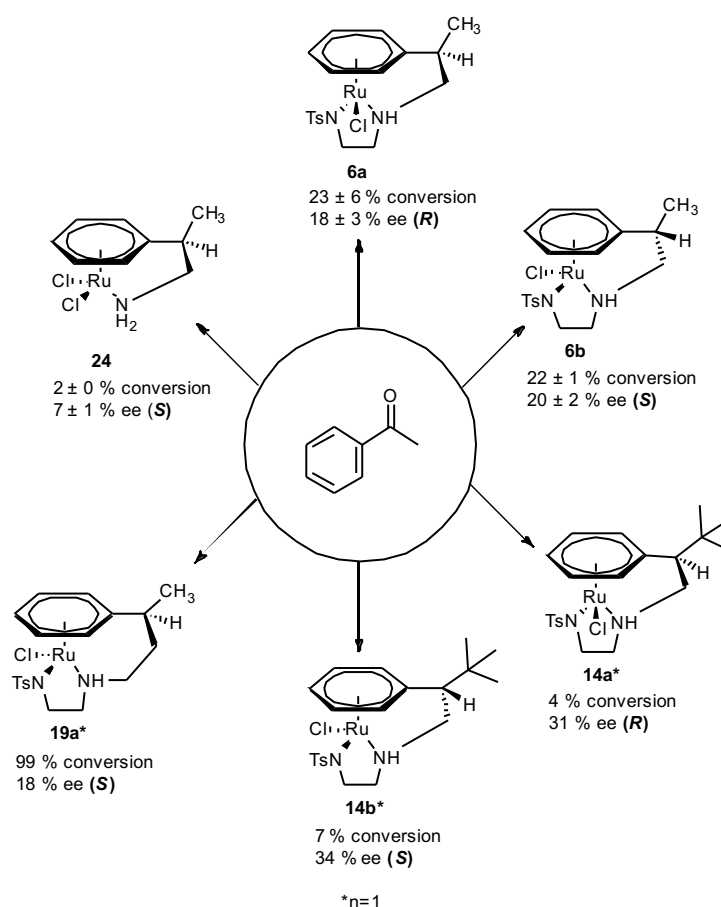
Figure 103. ATH of acetophenone catalysed by various complexes synthesised within this project. Substrate loading: 0.5 mol %, temperature: 40 °C and reduction duration: 24 hours. Reaction set up in oil bath followed by workup and purification by column (see experimental section). The conversion rates and enantioselectivities are averages of the three replicas of each substrate experiment. Conversion rates for **6a**, **6b** and **24** were calculated from the ^{1}H-NMR (CDCl$_3$) after workup. Conversion rates for **14a**, **14b** and **19a** were calculated from the ^{1}H-NMR (no solvent) before workup. All enantioselectivities were obtained after purification by column.

6a, comprising of (*S*)-stereochemistry at the metal stereocentre, produced (*R*)-1-phenylethanol in excess, whereas **6b**, comprising of (*R*)-stereochemistry at the metal stereocentre, produced (*S*)-phenylethanol in excess, confirming that the metal stereocentre transferred chirality to the alcohol product as supported by previous literature[39]. The degree of enantioselectivity was equal for **6a** and **6b**, therefore the chirality at the carbon

stereocentre was influential towards which isomer was produced predominantly during ATH; however, it did not determine the extent of enantiomeric excess achieved.

Interestingly, the conversion of acetophenone decreases from **6a** / **6b** to **14a** / **14b**, suggesting that the increase of bulk at the stereocentre was influential to the activity of the complex. On the other hand, the increase of the tether, from two carbon atoms to three carbon atoms in length, drastically increased the conversion. Overall, this indicated that conversion of the ketone to the alcohol was significantly influenced by the length of the tether, with a smaller effect observed from changing the bulk of the group at the stereocentre.

Unfortunately, the chirality at the carbon stereocentre of **14a** and **14b** was not unambiguously confirmed during this project, but techniques like XRD could have been useful to determine this. Regrettably, crystals of **14a** and **14b** were not obtained during this project. Although the chirality at the stereocentre could not be determined conclusively, the enantioselectivity of the alcohol products along with the selectivity of the chiral HPLC column (for full discussion see section 2.4.3.2) were utilised as an indication that the complexes formed the same diastereoisomer as **6a** and **6b** due to the identical tether length. As a result of the which isomer was formed in excess matching respectively (**6a** with **14a** and **6b** with **14b**), it was postulated that major diastereoisomer of **14a** was of (*R*)-configuration at the carbon stereocentre and (*S*)-configuration at the metal stereocentre, whilst **14b** was of (*S*)-configuration at the carbon stereocentre and (*R*)-configuration at the metal stereocentre. Moreover, the fact that acetophenone was reduced by **14a** and **14b** with opposing enantioselectivity (Figure 104) was confirmation that enantiopure complexes were synthesised, as literature has predicted that "inverting the stereochemistry of the metal centre leads to alcohol products of opposite stereochemistry"[39].
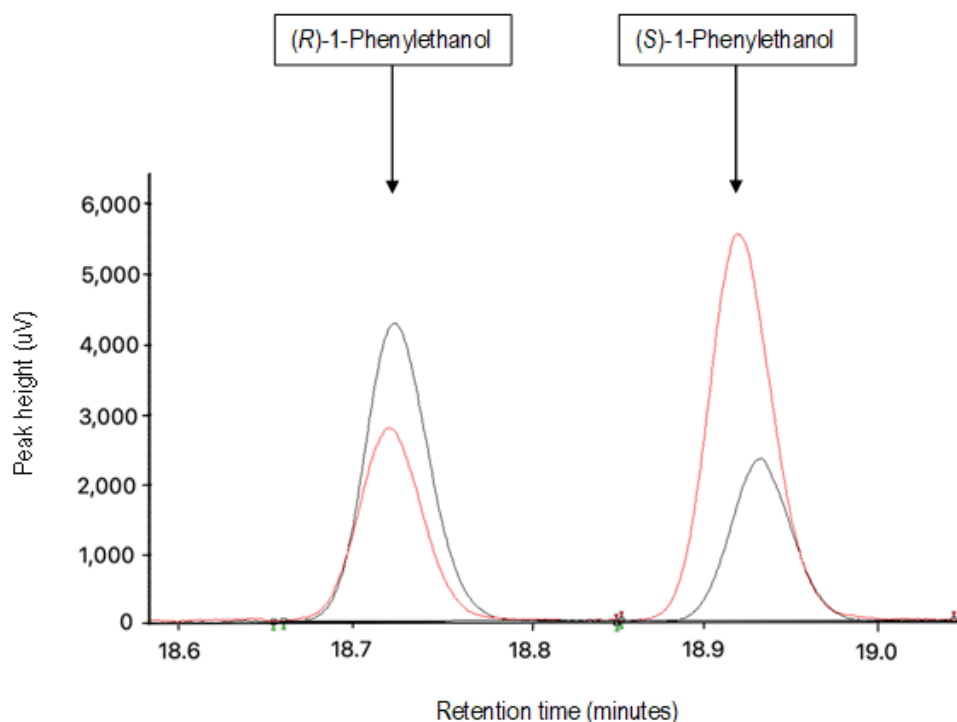
Figure 104. Representative chiral GC chromatogram of the 1-phenylethanol enantiomers obtained from the reduction of acetophenone by **14a** (black) and **14b** (red).

A trend was observed in the increase of enantioselectivity as the group at the carbon stereocentre increased in size, suggesting that the bulkier substituents were the reason for promoting higher enantioselectivity during ATH. This is supported by literature that discusses a catalyst (**C31**) with methyl groups attached to the arene ring, which lengthen the CH-π interaction and therefore attracted the electron rich ring of acetophenone (Figure **24**). It may therefore be possible that the alkyl substituents on the tethers in this project's frameworks adopt this CH-π interaction extension too, explaining the increase in enantioselectivity.[42,46,150,169] Further, the enantioselectivity obtained by **6a** and **19a** matched identically, proposing that the length of the tether had no influence on the enantioselectivity of the ATH of acetophenone, but in fact that it was the size of the group at the carbon stereocentre solely responsible. Despite this observable trend from the results presented here, the caveat was that only one repeat was performed for **14a** and **14b**, therefore further experiments would be required to confirm the postulation here.

On the other hand, the results suggest that tether length influenced the enantiomer produced in excess, likely to be as a result of the configuration adopted during ATH. **19a**, which possessed (*R*)-stereochemistry at the metal stereocentre, produced (*S*)-1-phenylethanol in excess. This was opposite to **6a**, which comprised of (*S*)-stereochemistry

at the metal stereocentre but produced (*R*)-1-phenylethanol in excess. Both product enantiomers produced in excess matched that predicted to be formed by the hydride derivative of the major diastereosiomer observed during the NMR studies, assuming the mode of action was the same as that reported for tethered TsDPEN catalysts previously.[150] Interestingly, despite displaying a 1:1 ratio of diastereosiomers during the NMR studies, **19** did produce an isomer in enantiomeric excess, which suggests that the catalyst with (*R*)-stereochemistry at the metal stereocentre is dominant/possesses greatest activity under the ATH reaction conditions.

As a result of two diastereoisomers being observed in the ^{1}H-NMR and x-ray diffraction studies, two hypotheses were proposed. The first was that the diastereoisomer in excess in the ^{1}H-NMR remained in excess during ATH, therefore producing one alcohol in excess. The second was that both diastereoisomers catalysed the ATH, producing alcohols of opposite chiralities, however, the diastereosiomer in excess in the ^{1}H-NMR possessed greater activity than the minor diastereoisomer, which induced the enantioselective excess during the ATH. Research carried out prior to this project also observed two diastereoisomers of the active hydride complex and the ratios of each did not vary much during ATH. Researchers confirmed the diastereoisomers were vastly different in activity with one diastereoisomer much more active than the other towards the acetophenone reduction due to the large enantiomeric excess observed.[39,170] They explained that if the diastereosiomers were equally active, the "maximum ee would be 50 %"[170].

The increase of tether length by one carbon length drastically increased the extent of conversion of acetophenone by ATH. This was further highlighted by the NMR studies described below.

NMR time course studies were performed to compare the activity of **6b**, **7**, **14** and **19** to further conclude the influence that both tether length and bulk of the substituent at the stereocentre had on the conversion of acetophenone over time.

Full conversion of acetophenone by **19** was observed during the NMR studies and hence a separate graph had to be plotted for this set of data (Figure 105).

● Racemic ruthenium 3C-methyl bidentate mononuclear complex (19)
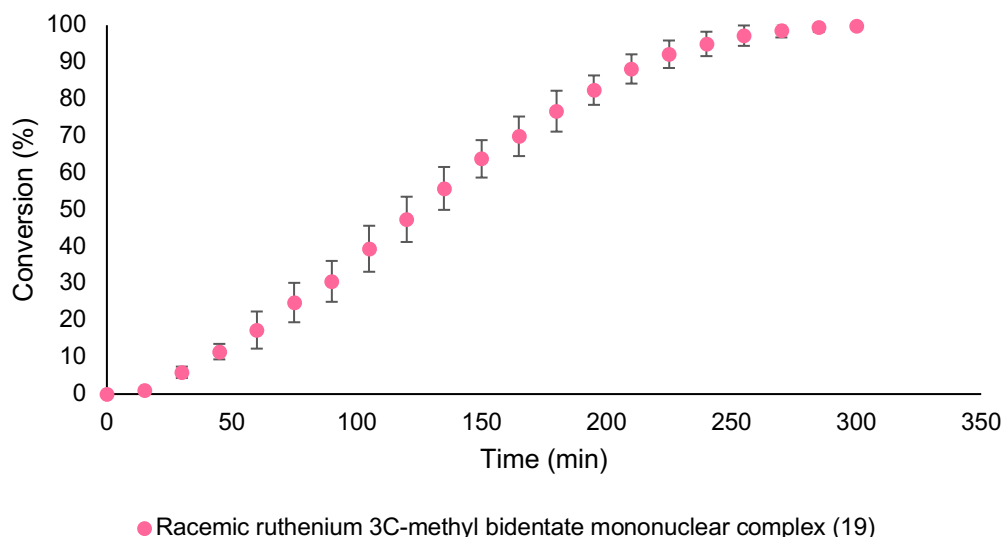
Figure 105. Conversion of acetophenone by **19** at 40 ºC over 5 hours; n=3.

The conversion reached 100 % after five hours, which was drastically faster than all other complexes in this project, therefore it was deduced that an increase in tether length encouraged a more active catalyst. The shape of the curve displayed an increase of conversion over time, with an induction period showing slow initiation at the beginning and once 100 % conversion was achieved, the graph levelled off. These trends were also observed by Wills et al.[102,144], except the non-tethered analogue (**C2**) was slower to convert acetophenone than **19** and inclusion of phenyl groups to the chelating ligand of the tethered analogue (**C8**) decreased reaction time (Figure 106). This suggested that the removal of the phenyl groups from the complexes in this project may have been one factor as to why reduced activity was observed, although further studies would be required to confirm this.
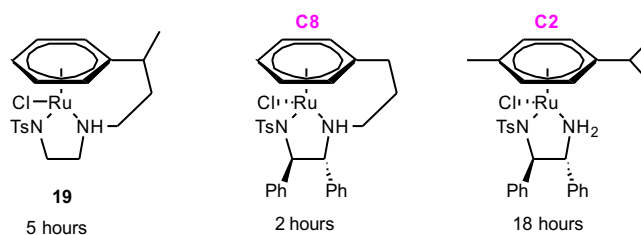
Figure 106. Time required to achieve 100 % conversion of acetophenone (FA/TEA (5:2), 40 °C, 0.5 mol % loading) alongside the corresponding complex framework.[144]

The ATH reactions for **6b**, **7** and **14** were performed over 24 hours with data collected every thirty minutes, allowing a scatter graph to be plotted (Figure 107) to observe the shape of the curves, reflective of the activity of the complexes.
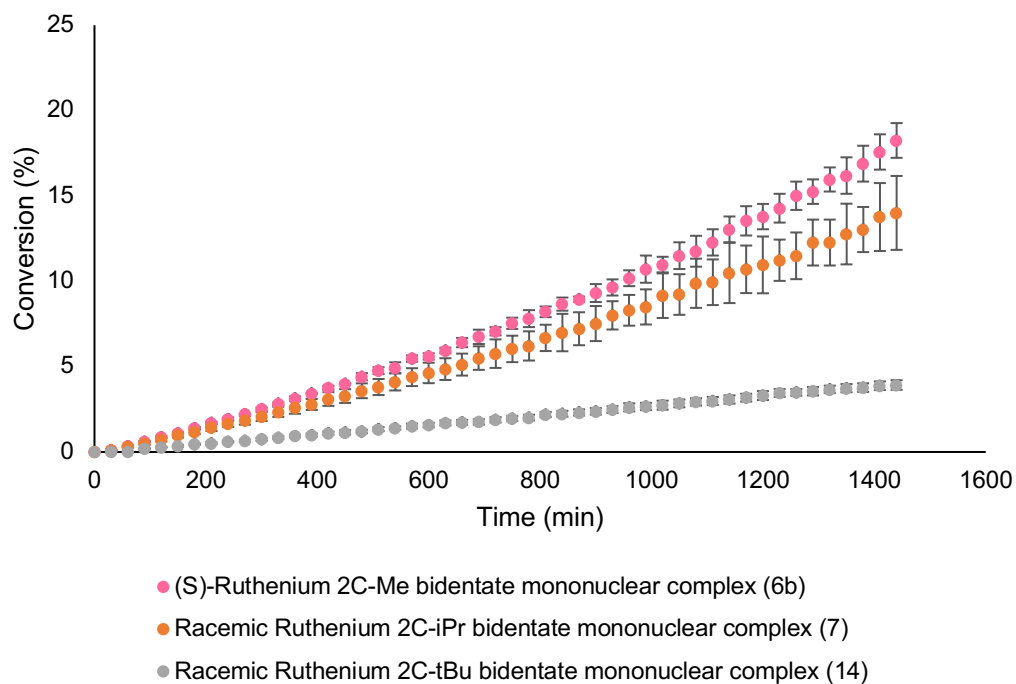
Figure 107. Conversion of acetophenone by **6b**, **7** and **14** at 40 ºC over 24 hours; n=3.

The shapes of the curves agreed with that found by Wills et al.[102,144], however, due to the lag in activity by **6b**, **7** and **14**, only the first section of the full trend was observed. The trend seen from this graph was that the increase of the size of the group at the stereocentre (Me < *i*Pr < *t*Bu) displayed a decrease in conversion, attributed to the bulk of the group making it more challenging for the substrate to approach and interact with the complex.

Due to the slow conversion observed, the reaction time was extended to 72 hours to see how far the reaction went. A time point at 48 hours was also included. The conversions at 24 hours, 48 hours and 72 hours for **6b**, **7** and **14** can be seen in Figure 108. The bar graph shows that with an increase in time, the conversion of acetophenone by all three complexes increased.
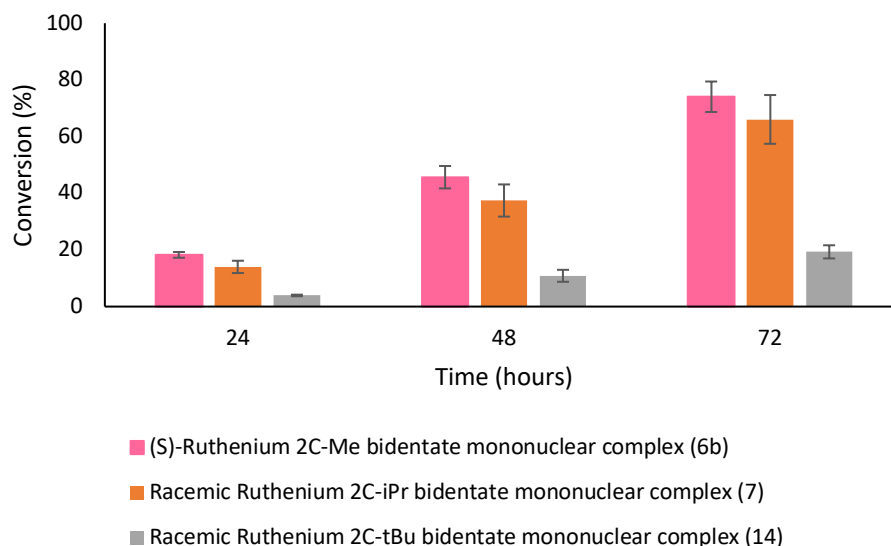
Figure 108. Conversion of acetophenone by **6b**, **7** and **14** at 40 ºC at 24, 48 and 72 hours; n=3.

In this NMR study only **6b** was an enantiopure complex, hence after the 72 hour experiment the reaction was worked up and purified by column to analyse the sample by chiral GC. This allowed direct comparison to the results obtained at 24 hours (Figure 109).
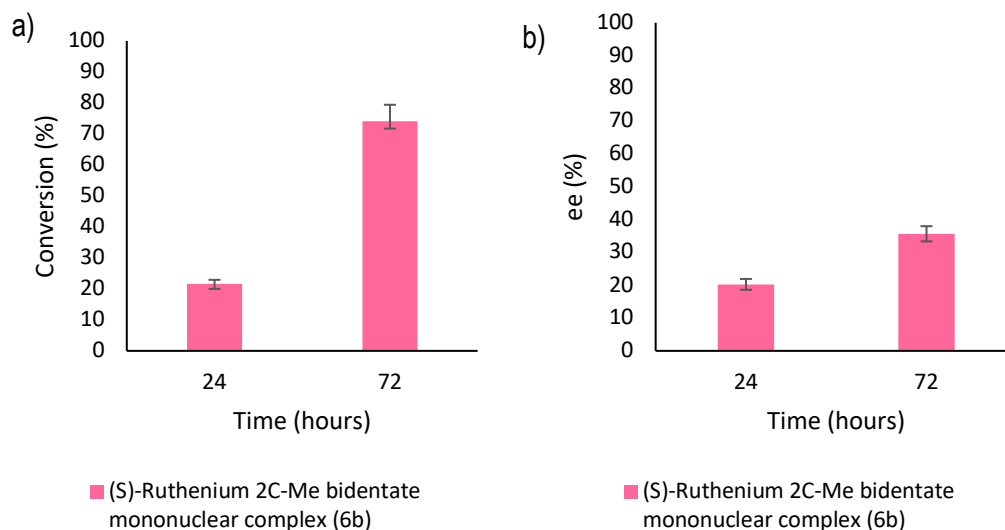
Figure 109. Graphs to show a) conversion (%) and b) ee (%) for the ATH of acetophenone at 40 ºC by **6b** at 24 and 72 hours; n=3.

The data showed that no loss of enantioselectivity was observed with an extended reaction time. In fact, both conversion and ee increased with time, suggesting that these complexes were simply slow to portray sufficient activity and selectivity.

Evaluation of the conversion and enantioselectivity rates obtained in this project were comparable (Table 16) to those achieved by a collection of Wills' catalysts (Figure 110).

Table 16. Comparison of the ATH of acetophenone catalysed by ruthenium(II) complexes in this project against ruthenium(II) catalysts in the literature.[150]
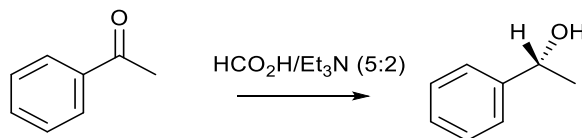
Catalyst	Tether length	Loading (mol %)	Temp (ºC)	Time (h)	Conversion (%)[a]	ee (%)[b]
Wills (*R,R*)[150] **C26**	2C	0.50	40	15	19	92 (*R*)
6b	2C	0.50	40	24	22 ± 1	20 ± 2 (*S*)
6b	2C	0.50	40	72	74 ± 5	36 ± 2 (*S*)
7	2C	0.50	40	24	14 ± 2	-*
7	2C	0.50	40	72	66 ± 9	-*
14a	2C	0.50	40	24	4**	31 (*R*)**
14	2C	0.50	40	72	19 ± 2	-*
Wills (*S,S*)[150] **C8**	3C	0.50	40	2	100	96 (*S*)
19a	3C	0.50	40	24	99**	18 (*S*)**
19	3C	0.50	40	5	100	-*
Wills (*R,R*)[150] **C27**	4C	0.50	40	1.25	100	96 (*R*)
Wills (*R,R*)[150] **C23**	5C	0.50	40	6	38	94 (*R*)

*Racemic catalyst therefore ee not collected.

**No uncertainty, n=1.

[a]Determined by ^{1}H-NMR.

[b]Determined by chiral GC.
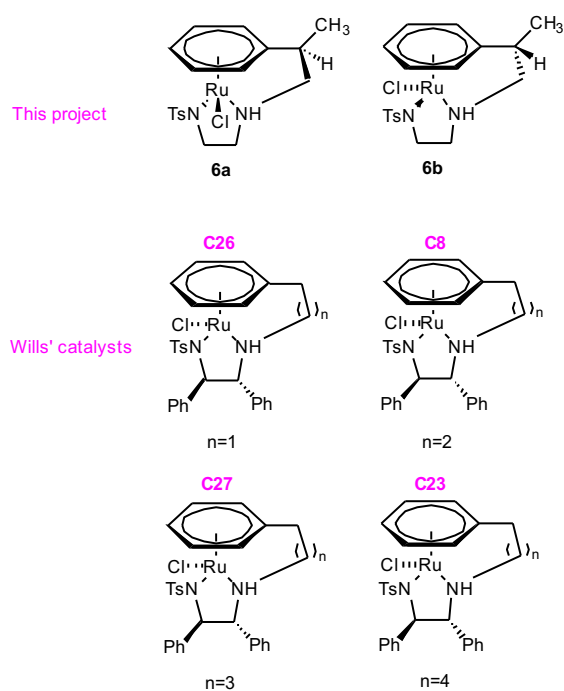
Figure 110. Comparison of **6a** and **6b** to a collection of Wills' catalysts with tether lengths varying between two and five carbons.[150]

From the data obtained from the literature, there was a clear increase in activity of the catalyst on expansion of the tether from two to three to four carbon atoms in length, with a dip in activity upon reaching five carbon lengths, hence the optimum tether appeared to be four carbon atoms in length.[150] Comparison of the **C26** against **6a**, which both comprised of a tether with two carbon atoms in length, showed that this new framework achieves a similar degree of conversion of acetophenone, but over a longer period of time. Furthermore, it proved that the removal of the phenyl groups on the diamine moiety did not have a negative impact on the results obtained thus far. However, **C26** was able to obtain ATH with much greater selectivity than that observed for **6a**.[150]

Full conversion of acetophenone was achieved by the **C8**, **19** and **19a**, all comprising of a tether with three carbon atoms in length. Although, the rate of reaction was slower for **19**, which required five hours, whereas **C8** performed the reduction in two hours, indicating that **19** was less active than **C8**. There was also a significant difference in enantioselectivity between **C8** and **19a**.[150]

Overall, the conversions in this project were supported by literature precedents, but Wills' et al.[150] achieved the conversions in faster times, coupled with vast improvements in enantioselectivities, suggesting that the bulky substituent on the tether was one factor influencing the reduced activities and selectivity's within this project. The more likely

explanation is the absence of phenyl groups on the chelating ligand, hence further studies would be required to investigate this. Despite this, one literature precedent synthesised a catalyst comprising of a benzyl tether and the diamine component without the phenyl substituents. **C72** (Figure 111) converted acetophenone by 100 % at 28 °C within 24.5 hours[186], which indicated that the complexes synthesised during this project were inferior to **C72** in both activity and selectivity, however the results may not be due to the hypotheses suggested above; presence of the bulky substituent on the tether or absence of phenyl groups on the chelating ligand. Further experiments with varying reaction conditions may aid the resolution to the question that asks why the complexes during this project were minimally active and selective towards acetophenone.
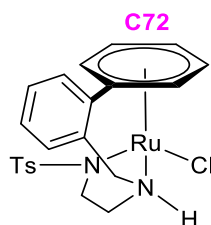
Figure 111. Benzyl-tethered Ru(II) catalyst.[186]

2.4.3.2. Other substrates

As discussed earlier, preliminary experiments were carried out to establish whether the complexes from this project were efficient in ATH. Following this, further testing in replicas of three were performed on a range of substrates at the more profitable reaction temperature of 40 °C, as previously determined. Nine substrates were focused upon, with each being selected carefully for a particular reason. Results including conversion rates and enantioselectivity can be seen for all chosen substrates in Figure 112 and Figure 113. Unfortunately, not all chiral commercial standards were available in the lab and so the Restek certificate of analysis, which accompanied the chiral GC column and showed the retention times of the test mix and alcohols of similar structure, was utilised to base the chirality assignments on, which indicated that (*R*)-1-phenylethanol interacted with the chiral GC column for a shorter length of time than (*S*)-1-phenylethanol. This pattern was consistent with other alcohols on the certificate of analysis, therefore on the basis of the columns selectivity, it was suspected that the isomers of all other alcohol ATH products were retained in the order (*R*) then (*S*). For the substrates that were subjected to ATH using both **6a** and **6b**, similar conversions were observed by both complexes and the enantioselectivities of the

complexes matched closely but comprised of opposite configuration. For example, **6a** produced (*R*)-1-phenylethanol in excess and **6b** produced (*S*)-1-phenylethanol in excess. This confirmed that the chirality of the alcohol products were induced via the chirality at the metal stereocentre of the complex.
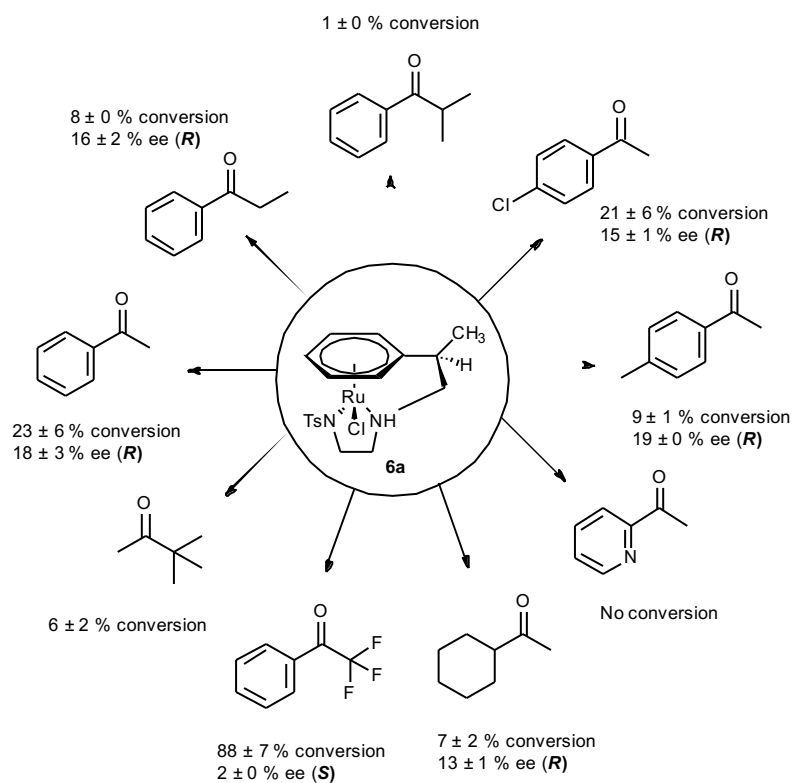
Figure 112. ATH of ketones catalysed by **6a**. Substrate loading: 0.5 mol %, temperature: 40 °C and reduction duration: 24 hours. The conversion rates and enantioselectivities are averages of the three replicas of each substrate experiment. Enantioselectivities were only calculated if sufficient conversion yield was obtained, with the chirality of the alcohol in ee defined by the assumption that the (*S*)-isomers interacted for longer on the chiral column.

22 ± 1 % conversion
20 ± 2 % ee (*S*)

11 ± 2 % conversion
18 ± 0 % ee (*S*)

7 ± 2 % conversion

78 ± 4 % conversion
1 ± 0 % ee (*R*)
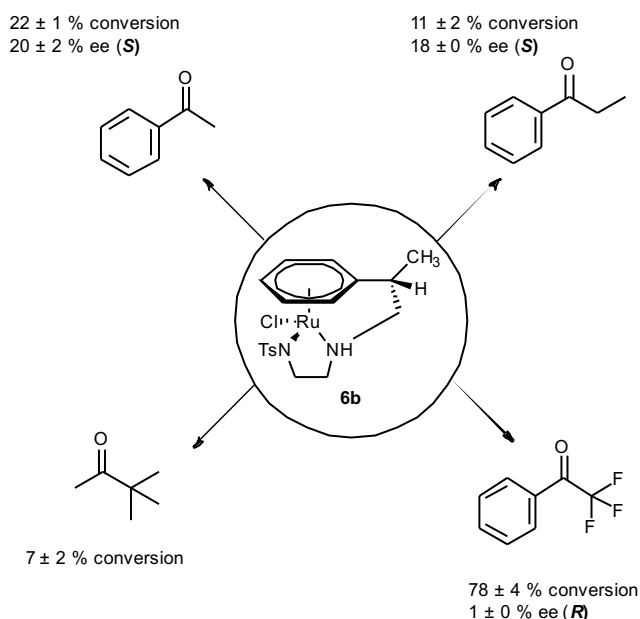
Figure 113. ATH of ketones catalysed by **6b**. Substrate loading: 0.5 mol %, temperature: 40 °C and reduction duration: 24 hours. The conversion rates and enantioselectivities are averages of the three replicas of each substrate experiment. Enantioselectivities were only calculated if sufficient conversion yield was obtained, with the chirality of the alcohol in ee defined by the assumption that the (*S*)-isomers interacted for longer on the chiral column.

The first trend to be focused upon was to investigate whether increasing the steric bulk of the alkane substituent on the substrate had an effect on the activity of the complex. For this, acetophenone, propiophenone and isobutyrophenone were studied. A similar study had been carried out before by both tethered and untethered catalysts, which confirmed that increasing the hindrance of the substrates decreased reactivity, owing to longer reaction times and in the case of the untethered catalyst, a large reduction in both yield and enantioselectivity.[46,81,84,100,144] It may be postulated that the reduction in activity may be due to the steric bulk preventing the favoured diastereosiomer from being adopted, with the steric factors taking precedence (Figure **46**). Results obtained here confirmed that the increase of steric hindrance around the ketone decreased the amount of ketone converted, with isobutyrophenone being reduced with such low conversion (1 ± 0 %) that analysis by chiral GC to determine the enantioselectivity of the reaction was not possible. Despite this, 1-phenylethanol and 1-phenylpropanol were successfully resolved into their respective isomers using chiral GC and the chromatograms can be seen in Figure 114 and Figure 115.
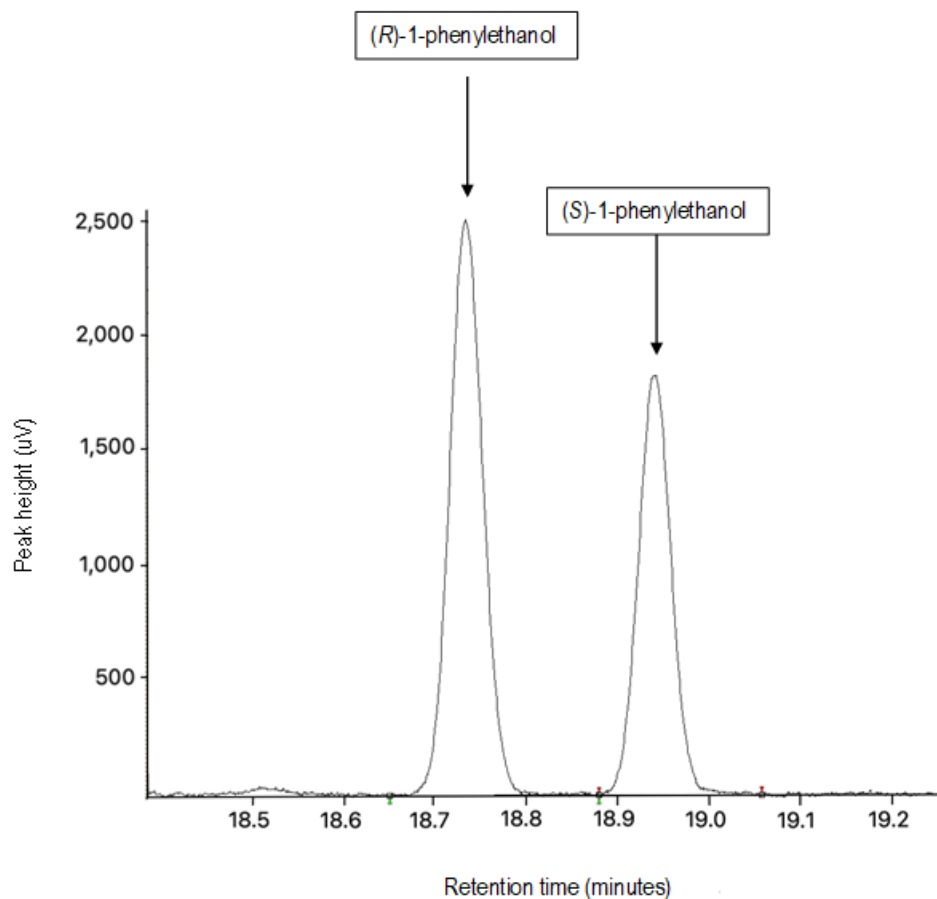
Figure 114. Representative chiral GC chromatogram of the 1-phenylethanol enantiomers obtained from the reduction of acetophenone by **6a**.
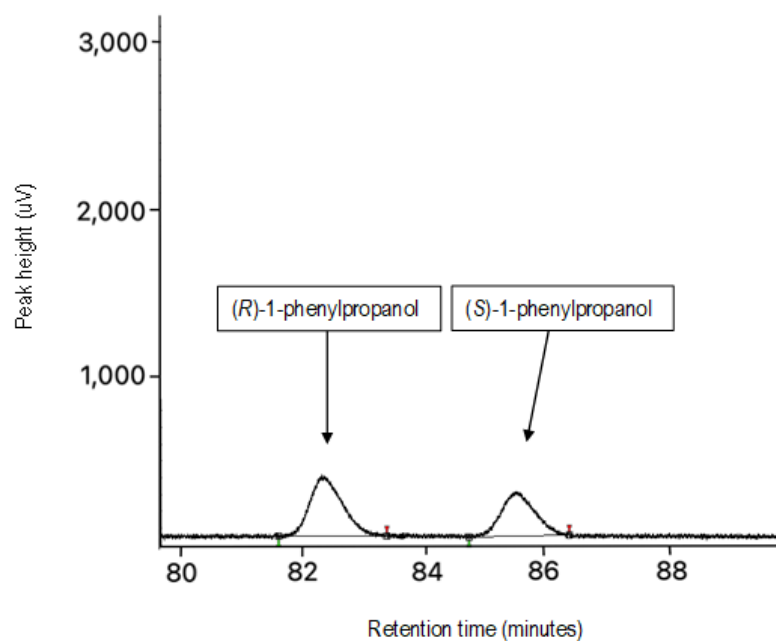
Figure 115. Representative chiral GC chromatogram of the 1-phenylpropanol enantiomers obtained from the reduction of propiophenone by **6a**.

The reduction of propiophenone could be compared to Wills et al.[186] (Figure 116) who achieved 99 % conversion and enantioselectivity of 94 % (*R*) in 26 hours.
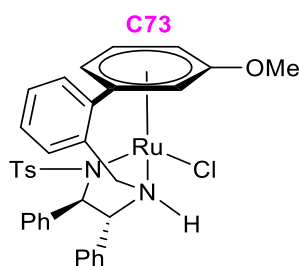
Figure 116. Wills' catalyst used for the comparison of the reduction of propiophenone.[186]

However, it must be taken into account that their project loaded half the amount of substrate, giving a lower ratio of S/C = 100, in comparison to this project which employed S/C = 200.

The second trend to be tested was the effect of electron withdrawing or donating groups on the aromatic ring of the substrate with one of each class chosen; 4'-chloroacetophenone and 4'-methylacetophenone. Research suggests that electron withdrawing groups on the substrate encourage a decrease in enantioselectivity.[45,46,59,184] This is because the withdrawing nature of the groups render the aromatic ring of the substrate less electron rich, which results in minimal difference in electron density between the arene ring of the catalyst and the aromatic ring of the substrate, therefore weak CH-π interactions are observed.[42,46,150,169] A larger conversion rate of 21 ± 6 % was seen for 4'-chloroacetophenone compared to 9 ± 1 % for 4'-methylacetophenone, suggesting that it was more favourable to reduce a substrate comprising of an electron-withdrawing group. Nevertheless, 4'-chloroacetophenone was reduced marginally less than the benchmark acetophenone, therefore it was decided that this complex was not significantly active towards this class of substrate. Previous studies by other research groups confirm this, showing 100 % conversion within three hours[150]. **6a** showed a slight preference towards 4'-methylacetophenone, as opposed to 4'-chloroacetophenone, in terms of selectivity (Figure 117 and Figure 118), however, the enantioselectivity was minimal in comparison to a similar catalyst (Figure 119 - C27) which portrayed an enantioselectivity of 91 % (*R*)[150,186].
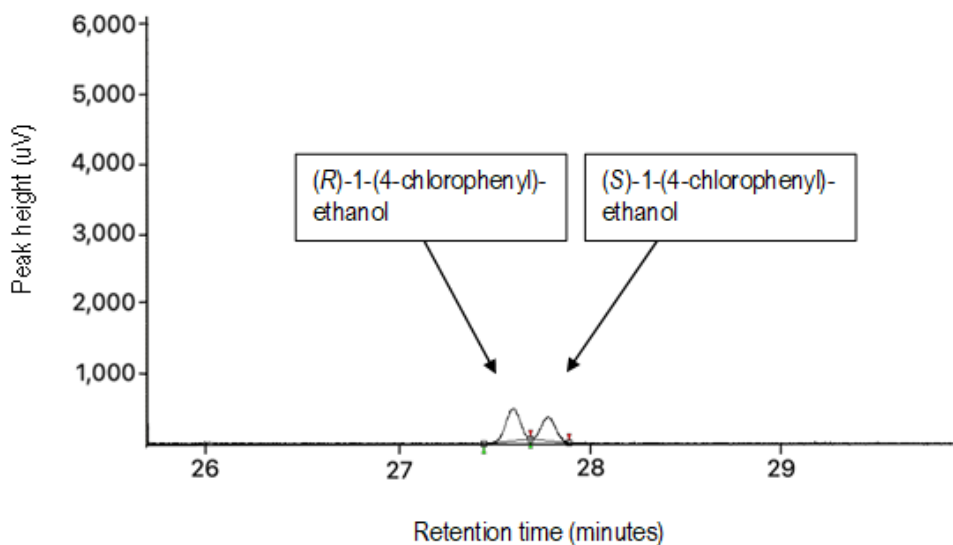
Figure 117. Representative chiral GC chromatogram of the 1-(4-chlorophenyl)-ethanol enantiomers obtained from the reduction of 4'-chloroacetophenone by **6a**.
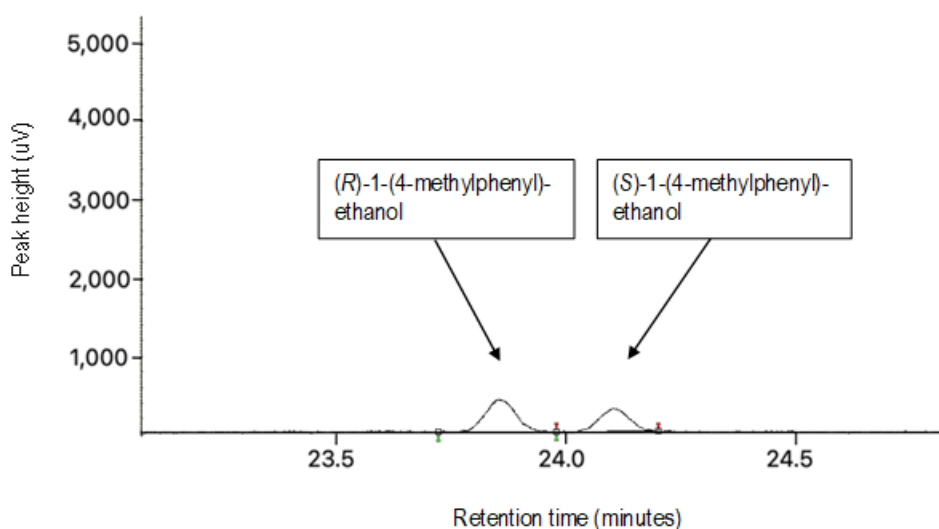
Figure 118. Representative chiral GC chromatogram of the 1-(4-methylphenyl)-ethanol enantiomers obtained from the reduction of 4'-methylacetophenone by **6a**.
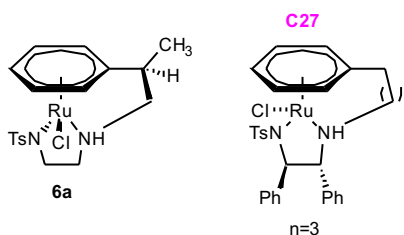
Figure 119. Complex synthesised during this project adjacent to one of Wills' catalysts.[150]

Unfortunately, **6a** was unsuccessful at reducing 2-acetylpyridine which was in agreement with the results found by Wills et al.[81] who confirmed that 2-acetylpyridine inhibited their catalyst (Ts-DENEB® - **C24**) during ATH potentially due to hydrogen bonding between the catalyst and protonated substrate. Despite this, Wills' 4C-tethered catalyst (**C27**) reduced 2-acetylpyridine fully in two hours with a high ee value of 91 % (*R*).[150]

The substrate cyclohexylmethyl ketone has been utilised by many researchers to prove the importance of the stabilising CH-π interactions and destabilising SO_2-arene interactions between the substrate and the catalyst. Literature states that the opposing enantiomer forms when reducing cyclohexylmethyl ketone.[97,144,186] Discrimination between the substituents on the substrate no longer occurs by CH-π interactions, instead, the transition state is stabilised by the attraction between the SO_2 lone pair and the CH groups of the cyclohexane ring on the ketone.[97,186] In this project, cyclohexylmethyl ketone was reduced by **6a** (Figure 120) in low yield and the enantioselectivity suggested the opposing (*S*)-enantiomer was formed in excess (Figure 121), by comparison of the stereochemistry of the acetophenone reduction.
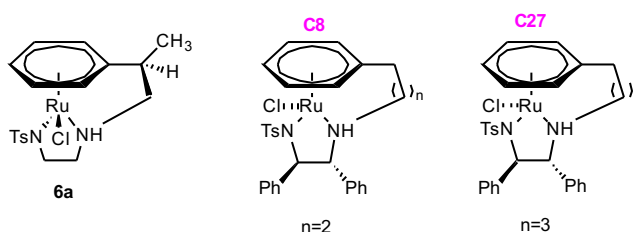
Figure 120. **6a** synthesised during this project, alongside Wills' 3C-tethered (**C8**) and 4C-tethered (**C27**) catalysts.[123,150]
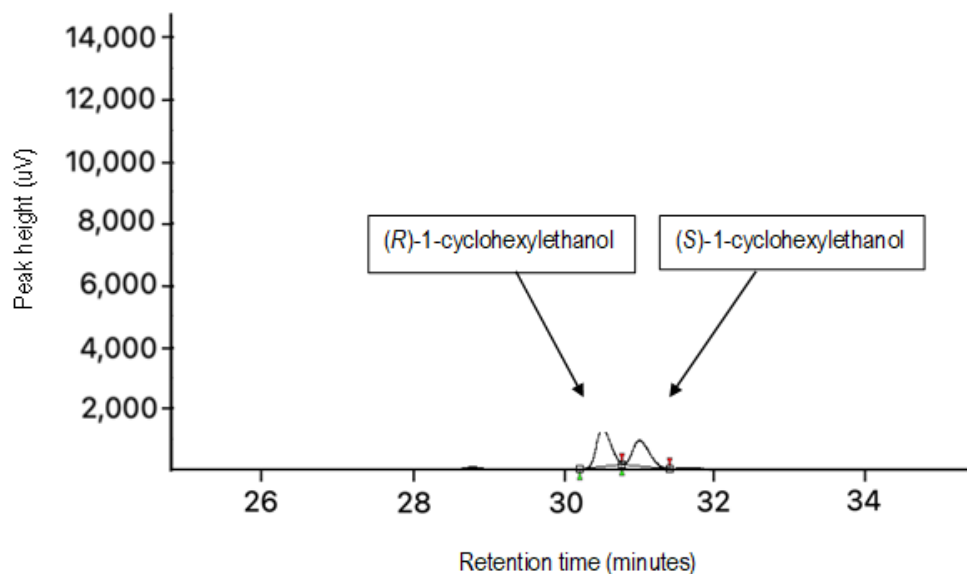
Figure 121. Representative chiral GC chromatogram of the 1-cyclohexylethanol enantiomers obtained from the reduction of cyclohexylmethyl ketone by **6a**.

Other research achieved 100 % conversion of this substrate at 28 °C, with an enantioselectivity of 69 % (*S*) for the 3C-catalyst (Figure 120 – **C8**) and 66 % (*S*) for the 4C-catalyst (Figure 120 - **C27**) respectively[123,150,186]. It is noteworthy that longer reaction times of 41 hours[186] or overnight[150] were employed by others, likely to be as a result of the lower temperature employed.

α,α,α-trifluoroacetophenone is another substrate that has previously been seen to reverse the conformation taken up during ATH, allowing the CF_3 group to take priority and occupy the space alongside the arene ligand within the transition state. A study testing the activity of catalysts with varying sulfonamide groups achieved 100 % conversion of α,α,α-trifluoroacetophenone in all reductions performed, although enantioselectivity was comparatively low with one catalyst only obtaining 56 % ee. However, results were consistent in obtaining the predicted major isomer, which would be formed as a result of the competition between the CF_3 and phenyl groups for the position adjacent to the arene protons in the transition state.[151] In this project, α,α,α-trifluoroacetophenone displayed a low enantioselectivity of 2 ± 0 % with a slight preference for the (*S*)-isomer (Figure 122), opposite to the reduction of acetophenone that gave the (*R*)-isomer, which was expected from carrying out the ATH with the **6a**, hence supporting the evidence of chirality reversal found in the literature.
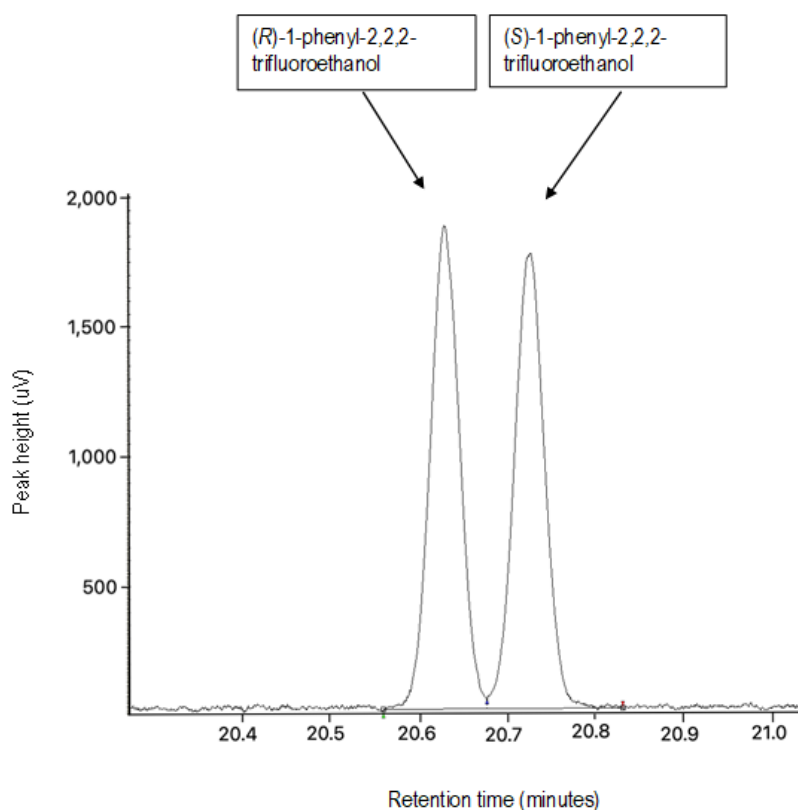
Figure 122. Representative chiral GC chromatogram of the 1-phenyl-2,2,2-trifluoroethanol enantiomers obtained from the reduction of α,α,α-trifluoroacetophenone ketone by **6a**.

Additionally, **6b** reduced acetophenone to (*S*)-1-phenylethanol and α,α,α-trifluoroacetophenone to (*R*)-1-phenyl-2,2,2-trifluoroethanol, displaying that the reversed conformation was also adopted here too. The ee's obtained were disappointing but were counteracted by the highest conversion rate of 79 ± 3 % seen within this project.

Dialkyl ketones are a difficult class of substrate to reduce as a result of their lack of stabilising CH-π interactions, due to the absence of an aromatic ring on one face.[45,92,123,137,184] Pinacolone was reduced in low yield during this project so calculation of enantioselectivity was unsuccessful. Research[123,144] reported a successful reduction of pinacolone, however, the substrate failed to be reduced enantioselectively, as a result of the steric interactions between the methyl groups on the ketone and the tether on the catalyst.[144]

Direct comparison for all substrates (other than acetophenone) focused upon in this project is not possible because all tethered catalysts synthesised by other groups incorporate a tether larger than two carbon atoms in length. Conclusions were made that **6a** and **6b** showed minimal activity towards this range of substrates, likely to be as a result of the shorter tether of two carbon atoms in length. This hypothesis was investigated further by searching

the literature for ideas that might explain the trends observed during this project and hence been included in section 2.4.3.3.

2.4.3.3. ATH conclusions

To summarise, two main trends were spotted from the data in this project collectively.

The first trend seen was that the increase of the size of the group at the carbon stereocentre (Me < *i*Pr < *t*Bu) displayed a decrease in conversion. It was anticipated that this may have been as a result of steric hindrance between the bulky substituent at the carbon stereocentre with the substrate in the transition state adopted during ATH, preventing or minimising the favourable CH-π interaction[81,150] and making it more challenging for the substrate to approach and interact with the complex. Despite this, the larger the group at the carbon stereocentre was, the more selective the complex was, suggesting enantioselectivity was influenced primarily by the bulky substituent at the stereocentre.

The second trend was that the tether length influences the degree of conversion of acetophenone, with the longer tether of three carbon atoms in length obtaining full conversion and the complexes with shorter tethers of two carbon atoms in length showing decreased activity. Therefore, it could be inferred that the increased tether length encouraged the substrate to approach with the aromatic ring pointing upwards, to allow for CH-π interaction which stabilises the six-membered transition state (TS_1) during the hydrogen transfer[46,58,132,137,144,178,185,64,67,81,90,102,107,125,130], hence explaining the high activity and selectivity observed. In comparison, it could be postulated that the 2C-diastereoisomer had the phenyl group of the acetophenone facing away from the arene ligand, indicating that no CH-π interaction could take place and therefore delivery of the hydrogen occurred via the opposite face, in turn inverting the enantioselectivity of the alcohol product[67,81,123,144,187]. This would explain the slow activity, low conversion and minimal ee observed for the shorter tethered complexes.

Alternatively, as a result of the increase of tether length, the more likely explanation suggests that the more favourable dihedral angle was responsible for the enhanced hydrogen transfer to the substrate during catalysis, influencing different geometric constraints to those imposed by the shorter tether of two carbon atoms in length. This hypothesis was supported by literature, whereby the closer the torsion angle was to zero for the H-Ru-N-H moiety, the higher the activity observed for the catalyst was, as a result of favoured pre-organisation of the diastereoisomer adopted during ATH.[39,144,170] In other

words, when the torsion angle was close to zero, the ketone approached the catalyst with the most preferable orientation, encouraging hydride transfer with greatest ease.[170]

From the x-ray diffraction data obtained from the growth of crystals for **6b**, **7** and **19**, utilised in the ATH experiments performed during this project, a trend was observed in the size of the torsion angle for the Cl-Ru-N-H moiety. Though this angle was not directly equivalent to the H-Ru-N-H angle discussed within the literature, calculating the estimate value for this similar torsion angle using the chloride ligand was still comparable to understand the effect these angles had over activity. Plus, it was comparable to one study by Wills et al.[170] (Table 17).

Table 17. Comparison of the dihedral angles of the Cl-Ru-N-H moiety ruthenium(II) complexes in this project against ruthenium(II) catalysts in the literature (Figure 123).[162,170]

Catalyst	Tether length	Dihedral angle (º)
6b	2C	-17.11
7	2C	-19.49
19	3C	12.70
C8	3C	4.59/4.14*
C27	4C	3.04
C71	3C	14.25
C2	0C	-18.31

*Two complexes found in the asymmetric unit.
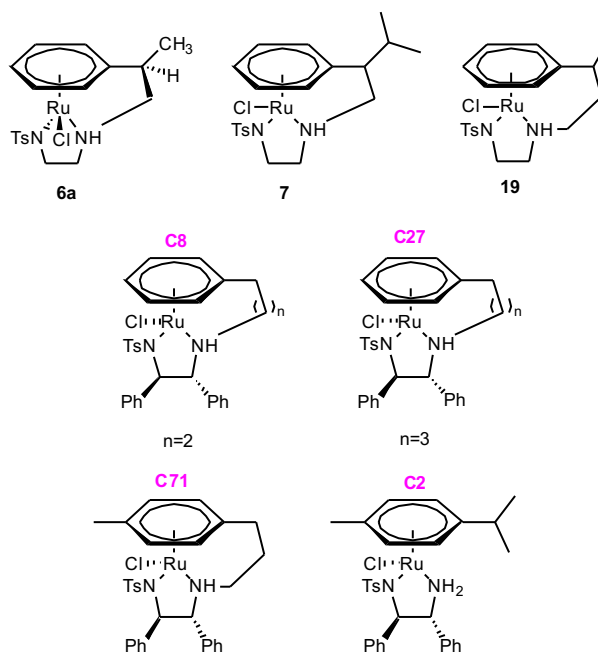
Figure 123. **6a**, **7** and **19** synthesised during this project alongside Wills' 3C-tethered (**C8** and **C71**) and 4C-tethered (**C27**) catalysts and Noyori's untethered (**C2**) catalyst.[123,150,162,170]

The values of Wills' torsion angles are significantly closer to zero, explaining that a longer tether length creates catalysts with less strain and a preferrable conformation, which allowed for higher activities to be observed. Further, Wills' et al. measured the angle of **C71**, which was in similar magnitude to **19** from this project. It could be postulated that the inclusion of additional alkyl substituents to the complex framework creates greater steric strain, enforcing a larger torsion angle, therefore decreasing the activity of the complex.[170] The torsion angle of the Cl-Ru-N-H moiety in **C2** further confirmed that a tether of three carbon atoms in length increases the activity of the complex.[162]

The x-ray diffraction data from this project predicted **19** would have the highest activity, due to the torsion angle being closest to zero, and that **6b** would convert acetophenone to a greater extent than **7**, which was exactly what was found within this project. Overall, both the tether length and size of the group at the carbon stereocentre had an effect on the torsion angle of the Cl-Ru-N-H moiety, which influenced the activity of the complex during ATH.

2.4.4 Anticancer studies

Preliminary experiments using a human colorectal adenocarcinoma cell line were performed to identify any activity of **6a** and **6b** as anticancer compounds (Figure 124-Figure 127). At

the highest concentration of 500 µM, the results showed similar values of cell survival for both sets of studies indicating that the toxicity was not isomer specific.
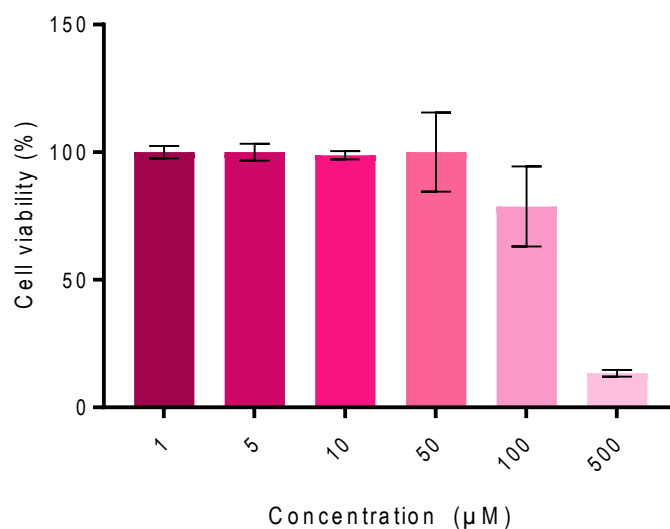
Figure 124. Cytotoxicity of **6a** (shown in Figure 70) over HT-29 cells after 72 hours of incubation. Error bars represent $\overline{x} \pm$ sd (where n=5).
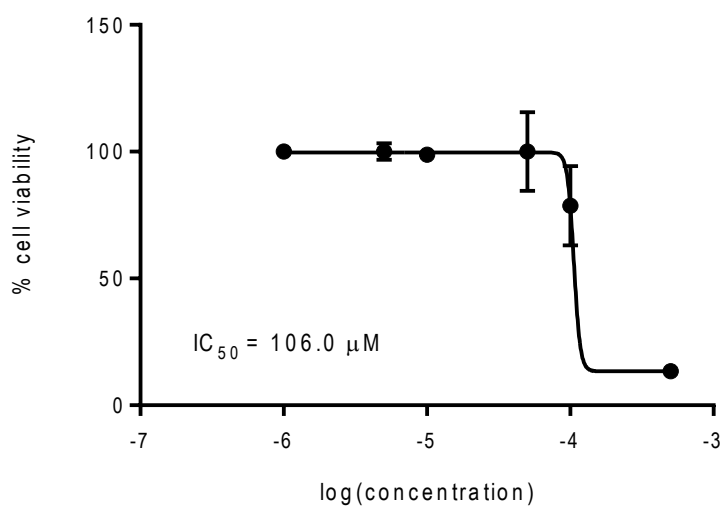
Figure 125. Graph showing the dose-response plot of the cytotoxicity test of **6a** (shown in Figure 70) and hence a calculation of the IC_{50} value. Error bars calculated using n=5.
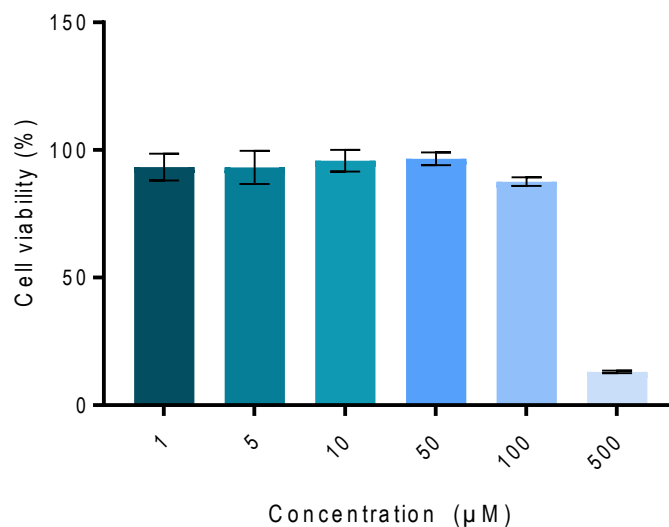
Figure 126. Cytotoxicity of **6b** (shown in Figure 70) over HT-29 cells after 72 hours of incubation. Error bars represent $\overline{x} \pm$ sd (where n=5).
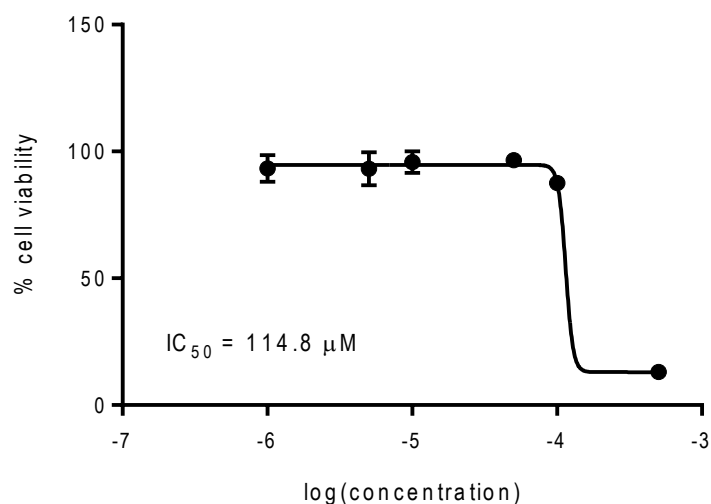
Figure 127. Graph showing the dose-response plot of the cytotoxicity test of **6b** (shown in Figure 70) and hence a calculation of the IC_{50} value. Error bars calculated using n=5.

Experimental design dictated that high concentrations of DMSO were required to fully solubilise the complex, hence the concentration of the catalyst was limited.[206] It can be seen that the high DMSO concentrations required resulted in significant cell death, and the results reported are those corrected for the impact of DMSO, but the fact that DMSO caused high cell death was a limitation to gauging the full impact of metallodrug biological activity. It was concluded that the low cytotoxicity observed for these complexes may be useful for work similar to literature precedents that focused on reducing the coenzyme NAD^+ to NADH using

sodium formate as the hydrogen donor[96,114,206,217–221], where cytotoxicity would be activated in the presence of the hydrogen donor, whilst inactive without. Future work would aim to produce a more water-soluble analogue to modulate biological activity that would allow for tuning of intracellular localisation by investigating the change in hydrophobicity and in turn the change of cytotoxicity.

2.5 Conclusions

This chapter describes the synthesis of novel tethered-Ru(II) complexes, with variation to the bulky substituent on the benzylic carbon and the length of the tether, inspired by influential work by Noyori and Wills. The data for this full family of complexes supported one another and was backed up by literature precedents too.[109,123,150] The main disadvantage was that complexes were isolated as a mixture of diastereoisomers, confirmed by NMR and x-ray diffraction, due the second N-atom on the chelating ligand changing coordination site (Figure 128), thereby inducing two different configurations at the metal centre.
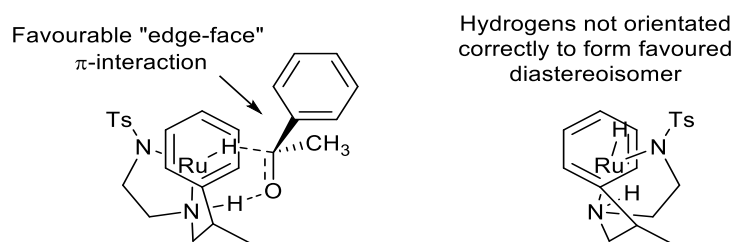
Figure 128. The two configurational isomers predicted to be present for **6a**.[150]

The relative abundance of the two configurational isomers initially isolated were calculated, confirming that one was formed in excess of the other, except in the case of **19**. From these results, coupled with literature[39,170], two ideas have been postulated. The first suggests the diastereoisomer obtained in excess remained in excess during ATH, reducing the substrate with an excess towards one isomer. The second suggests both diastereoisomers are reducing the substrate simultaneously but that one diastereoisomer was more active, hence the enantiomeric excess towards one isomer.

ATH studies revealed that the complexes were able to portray activity towards a large percentage of the substrates, however, they were not very selective with regards to which enantiomer was produced in excess. In summary, two main trends were spotted. The first was that an increase of steric bulk at the benzylic carbon limited the amount of acetophenone converted, but the selectivity transferred to the alcohol product was greater.

The second was that an increase in the length of tether portrayed a vast improvement in the conversion of acetophenone, but the enantioselectivity remained on par with the 2C-analogues, suggesting that the enantioselectivity was influenced by the bulky substituent on the tether.

The complexes showed a preference for ketones with aromatic rings, in support of the stabilising CH-π interactions established during the transition state, formed by the favoured diastereoisomer being adopted. Differences in chirality transferred from the metal centre to the alcohol product were observed between the 2C- and 3C-tethered complexes, which agrees with previous discussions in literature.[39] This suggested an alternative configuration of the favoured diastereoisomer was adopted during ATH, encouraging approach by the substrate in an opposite manners for the 2C- and 3C-tethered analogues. This hypothesis was supported by x-ray diffraction data, whereby upon lengthening the tether, much less strain was observed, and the complex comprised of opposite chirality due to the tether coordinating to the metal centre in the opposing sense. Two explanations are proposed based on ideas in the literature: the size of the dihedral angle and the orientation of the tether with regards to substrate approach.

Literature explains the favoured diastereoisomer is adopted when the dihedral angle is favourable; the closer the angle to zero, the more active the catalyst.[144,170] The H-Ru-N-H angle was not calculated, but a similar angle of Cl-Ru-N-H was calculated and was comparable to, and in accordance with, literature.[170] Conclusions suggest a larger substituent at the carbon stereocentre resulted in a larger dihedral angle, inducing greater strain, hence the catalyst displayed decreased activity. The longer tether length gave a smaller dihedral angle, presenting less strain and a more active catalyst.

Research has previously explained that high activity was observed when the tether of a complex was orientated away from the approach of the ketone. Due to two configurational isomers being observed in solution during this project, it was postulated that one of the diastereoisomers, likely the major isomer, did not follow this ideal, inducing repulsive forces towards the substrate from the tether. Though the explanation is not conclusive, it suggests that the larger group on the ketone was orientated away from the tether, either not promoting the attractive CH-π interactions, or just minimising the degree of CH-π interactions present.[107,144] We suggest that the first idea of the influence of the size of the dihedral angle is a much more likely explanation for the minimal ATH activity observed during this project.

In addition to the investigation of their ATH activity, **6a** and **6b** were tested for their anticancer activity. Cytotoxicity studies proved the complexes to only be cytotoxic at high concentrations. Future work has been suggested to modulate biological activity via tuning of the solubility of these complexes.

In conclusion, it was determined that tether length influenced the extent of conversion, whilst the size of the bulky substituent at the carbon stereocentre was responsible for the enantioselectivity. The initial aims of this project anticipated a bulky substituent at the carbon stereocentre would encourage the chiral ligand to coordinate to the metal centre in a strong enough fashion to obtain a single stereochemical configuration at the metal centre. Although the design didn't allow for complete stereocontrol at the metal centre, these complexes provided an alternative route towards enforcing chirality at the metal centre. Improvements have been proposed to reduce the flexibility of the tether, to encourage only one configurational isomer to form, which would allow for the single diastereoisomer to enhance our knowledge towards the asymmetric synthesis and biological fields. Lastly, this project investigated whether removal of the phenyl groups from the chelating ligand was detrimental to results achieved during ATH. Conclusions suggest their removal did have a negative impact on the activity and selectivity of the complexes, however, we suspect that once the remainder of the framework has been tuned, namely the length of the tether, this novel incorporation of a stereocentre at the benzylic carbon will override the need for the phenyl groups within the chelating ligand. This would be advantageous due to the limited solubility observed for half-sandwich Ru(II) complexes comprising of phenyl groups on the diamine ligand under biological conditions for the reduction of NAD^+ by ATH.[96]

2.6 Future work

First and foremost, repetition of the synthesis of **14a** and **14b** on a larger scale would influence higher yields and therefore allow for numerous ATH repeats on a larger variety of substrates to be conducted. This could be extended to **6a** and **6b**, which was synthesised in good yield, however there was not enough time during this project to run ATH on a greater scale of substrates. Additionally, confirmation of **14a** and **14b** by passing elemental analysis or the growth of crystals to allow analysis by x-ray diffraction would be useful to further prove that the activity seen during ATH is in fact due to the complex itself, plus determination of chirality would be helpful.

Secondly, as a result of time restraints and resources, only one temperature and time duration were carried out for the ATH in this project. Therefore, by extending the length

of time for the ATH reaction to run, varying the reaction temperatures, and adjusting substrate/catalyst loading ratios, a larger pool of results would be obtained and would allow for optimum reaction conditions to be chosen for testing the impact of the activity of the complex whilst also encouraging direct comparisons to literature results. Further, it would be good practice to repeat all ATH experiments on both isomers of complexes to prove that the complexes can reduce the substrates in equal but opposite enantioselectivity. By testing more unusual substrates, surprising results may be found in the form of conversion rates or enantioselectivity because research has confirmed that each individual complex interacts differently with substrates, rendering the results of ATH to be substrate dependent.[58,59,151]

Thirdly, repetition of the synthesis of the enantiopure analogues of **19** so that ATH reactions can be carried out to obtain full conversion in shorter time frames, but prevent diminishing of enantioselectivity due to prolonged exposure with the catalyst and azeotrope at high temperatures. The graphs obtained confirmed full conversion of acetophenone in five hours, the fastest experiment in this project. Despite this, **19** and **19a** were not subjected to any other substrates and hence this would be of interest to explore.

Increasing the time of the NMR time course experiments for catalysts **6a**, **6b** and **7** to obtain the full curve would allow calculation of the time required to achieve full conversion of acetophenone. It is expected that this would require a time frame in the magnitude of days not hours, with **7** requiring longer than **6a** and **6b**. Comparison to the graph plotted for catalyst **19** would show if the complexes react in a similar fashion by the shape of the curve.

During the project, results indicated that incorporation of a bulky group was beneficial towards the enantioselectivity obtained during ATH. To investigate the effects of incorporating a planar bulky group, a suggestion of a mesityl group at the benzylic carbon was raised. Devising a synthetic route for the mesityl analogue was time consuming and difficult. Various routes were investigated, but the route to this target complex was terminated due to the success of the methyl, *iso*-propyl and *tert*-butyl complexes. As this route remains incomplete, it may be of interest to repeat the pathway to the final complex to investigate the influence that this varying substituent may have on the results yielded from ATH studies.

Evidence points towards utilising a tether of greater length to achieve full conversion. The length of the tether in Wills' catalysts[150] has previously been investigated and a longer tether is more likely to prevent strain and bending of bonds to give a more stable catalyst. Abundant research has been performed in the literature on various tether lengths, with a tether of three or four carbon atoms in length appearing the most effective.[150] It would be of interest to investigate a tether of three and four carbon atoms in length, with a bulky

substituent attached, allowing for more direct comparisons to Wills' catalysts. Including a methyl group would allow for greater conversion, although the tether length should dominate this, whilst improved enantioselectivity should be observed with the *tert*-butyl group attached following trends found during this project. Though a framework hasn't been chosen, synthesis of the four suggested frameworks (Figure 129) would allow for trends to be found, with anticipation of increased activity and selectivity by at least one of the complexes.

Figure 129. Suggested frameworks for future work based upon the results found in this project; a 3C-tether would have n=1, a 4C-tether would have n=2.

Following this, it would be of interest to modify the framework even further. Removing the tosyl group of the most active catalyst of the four (Figure 129), this could be substituted by alternative functionalities, for example, P or N chelates[113,166,280,298,299], Schiff base scaffolds[300,301], heteroaromatic compounds[65] and N-heterocyclic carbenes[180,302,303]. If these frameworks show promise, further substituents could be introduced to the arene ligand too. This hopefully would affect the steric interactions with the substrate during ATH and would help tune the electronic properties of the complex.

Lastly, it may be beneficial to carry out *in vitro* testing using cell cultures in replicas to investigate the selectivity and cytotoxicity of all pure complexes synthesised irrelevant of their ATH activity. This would allow for more reliable results than that given in this report currently. In fact, it may even be possible to carry out an investigation on the catalytic activity within cells alike Wills et al. or show antiproliferative activity as opposed to cytotoxicity.[114]

Overall, there is scope for development to further tune the properties of the complexes designed during this project to allow for better ATH results and more selectivity towards targeting cancerous cells.

Chapter 3

Novel manganese(I) cyclopentadienyl complexes comprising of a chiral tether

3.1 Background

Chiral alcohols and amines are of great importance in the construction of fine chemicals, pharmaceuticals and agrochemicals.[46,82,118] ATH is a major route to prepare these stereochemically pure products due to high atom economy and efficiency. However, the asymmetric hydrosilylation of prochiral ketones (Scheme 41) is becoming an increasingly popular two step alternative due to its simplicity and mild conditions.[115,118]
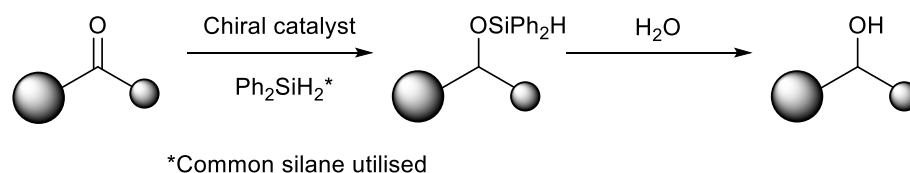
Scheme 41. Generic scheme showing the asymmetric hydrosilylation of ketones by a chiral catalyst.[226] The larger ball signifies a group comprising of high electron density, for example an aryl or alkyne moiety, the smaller ball signifies a group of low electron density, for example and alkyl moiety.[111]

Second and third row transition metals, including rhenium, ruthenium and iridium, have already been extensively explored in the reduction of ketones via hydrosilylation.[115,118] Researchers have focused on routes to recover and recycle the catalyst[304] but unfortunately, on repeated cycles of use, catalyst degradation results in decreasing activity and selectivity of the reaction.[304] Therefore, work has been performed with eco-friendly catalysts, in particular those base on iron, zinc and copper, to reduce the cost and toxicity, which is detrimental to both our welfare and the environment[281], when performing hydrosilylation of aldehydes and ketones with noble metals.[115,117] Despite the impact already made by first row transition metal catalysts for the hydrosilylation of aldehydes and ketones, there is still a large gap pending within this field of research with the need for a catalyst capable of reducing a broader range of ketones, in particular dialkyl ketones, by cheaper silanes[226] with lower temperatures and shorter reaction times, whilst ensuring high yield and enantioselectivity.[115]

Half-sandwich manganese(I)-NHC catalysts (Figure 130) capable of the hydrosilylation of ketones, as cheaper and less toxic alternatives to second-row transition metal complexes, have been synthesised from commercially available cymantrene due to its low cost.[236]
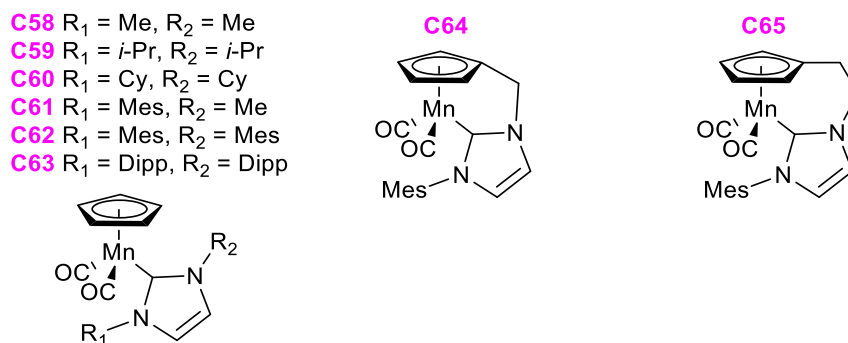
Figure 130. Half-sandwich manganese catalysts by Darcel/Sortais et al.[236].

The untethered catalysts showed good functional group tolerance reducing aldehydes and ketones with "mild conditions (1 mol % catalyst loading, 1.5 equivalents of diphenylsilane, 350 nm UV light, toluene solvent, 25 ºC and a maximum of 24 hours)"[237]. This research inspired a subsequent project, whereby two catalysts were synthesised with variant tether lengths; one carbon (C64) and two carbons (C65). The idea of tethering the Cp ring to the NHC ligand was to increase the catalysts' stability and activity. The method of reduction was identical to that utilised to investigate the untethered analogues and it was found that both tethered catalysts were capable of reducing 2-acetonaphthone. Interestingly, the longer tether length of two carbons was more active than the catalyst comprising of a one carbon tether. Direct comparison showed that the untethered equivalents were more active, however, higher yields were exhibited upon lengthening of the reaction time from two to twenty-four hours whilst also reducing the catalyst loading to 0.5 mol %.[236]

Similar frameworks to those targeted during this project, whereby one manganese complex comprised of a stereocentre adjacent to the Cp ring (Figure 131 - left), whilst the other included the stereocentre adjacent to the functional groups (Figure 131 - right).[238]

Figure 131. Half-sandwich manganese catalysts by Alberto et al.[238].

Both complexes contained carboxylic acid and amine functional moieties that allowed for further derivatisation if necessary. Unfortunately, none of the target complexes were tested for their activity in hydrosilylation reactions as enantiopure ligands were not utilised.[238]

To date, there are limited enantiopure Cp-tethered complexes in the literature.[305] The majority of hydrosilylation is performed by achiral catalysts to produce racemic primary and secondary alcohols, therefore it is of interest to synthesise a chiral catalyst to produce hydrosilylation products with enriched enantioselectivity suitable as intermediates on industrial scales in the fine chemical, pharmaceutical or agrochemical sector.[82,91]

This project focuses on the catalyst framework shown in Figure 132, whereby the moieties that could be modified have been circled including tether length and functional groups labelled R_1 and R_2. The rationale, based upon literature precedents, has been described in section 3.1.1.
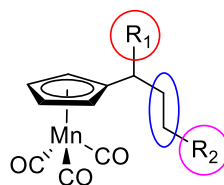
Figure 132. Proposed framework of the manganese complexes bearing Cp tethered ligands to be synthesised in this project.

3.1.1 The approach to creating novel half-sandwich manganese(I) catalysts

The investigation into iron half-sandwich catalysts has received a greater amount of popularity than manganese piano-stool frameworks to date.[306] However, manganese catalysts offer the same advantages, in comparison to noble transition metals alternatives, particularly lower cost and toxicity, hence manganese will be focused upon in this project.[237] The half-sandwich framework encourages a versatile range of ligands to be incorporated, in order to determine their significant effect on activity and enantioselectivity towards substrates during asymmetric hydrosilylation.[307] Metal-carbonyl complexes are key examples as the loss of a carbonyl ligand is promoted by exposure to UV light.[308]

3.1.1.1 A framework based on cymantrene

Cymantrene is a useful manganese framework that can be easily derivatised, to allow for promising performance in multiple fields; "fuel additives, photochromic materials, polymerisation catalysts and for the treatment of cancer, malaria and bacterial infections"[309].

In fact, both cymantrene and its methylated derivative are advantageous due to their cheap cost and high quality, synthesised by industry.

3.1.1.2 Varying the chelating ligand, with preference for NHCs

Phosphine-based ligands were the first chiral ligands incorporated into catalysts capable of performing hydrosilylation.[226] Unfortunately, research found phosphine ligands to be sensitive to oxygen, alongside the dangers they exerted whilst being synthesised and during catalysis.[179,180,310–312] Although phosphines are attractive ligands, N-heterocyclic carbenes (NHCs) have shown equal strength, possessing advantageous steric and electronic properties.[179,310–312] In fact, NHCs are more basic than phosphines, allowing activation of the C-H bond to occur with more efficiency, forming a more stable complex.[313] Bulky chiral NHCs have risen in popularity in recent years due to their stabilising nature as strong σ-donor ligands and weak π-acids, which allows them to form strong bonds with electron-rich metals of choice, creating highly covalent M-C_{NHC} bonds.[34,179,213,311,314–317] This strong bond formation between the NHC and the metal ensures that the catalyst stays active, preventing dissociation of the NHC ligand[316] and increasing stability of the complex.[312,318]

3.1.1.3 Incorporation of a tether

To further increase the stability of these half-sandwich complexes, it has been postulated that tethering the Cp ring to the NHC ligand provides significant support and rigidity, influencing the catalytic activity of the complex.[230,236,305,319] The idea stemmed from the limitations observed towards half-sandwich complexes, shown on the left of Figure **133**, where only a single coordination site was left vacant. By tethering the NHC ligand to the Cp ligand, the framework freed up a second coordination site as seen on the right of Figure 133.[307]
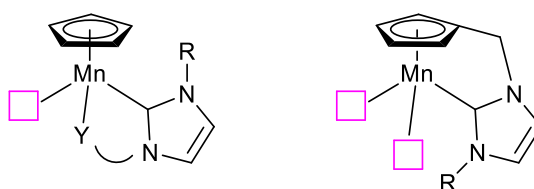
Figure 133. Frameworks with the NHC as a chelating ligand or linked through a tether.[307]

Overall, it has been confirmed by numerous research groups that an increase in performance towards catalysis, coupled with greater stability, has been as a result of the introduction of a tether between the Cp ring and NHC.[305,307]

3.2 Ligand and complex design

Manganese catalysts[306], a cheap and safe alternative, for the asymmetric hydrosilylation of ketones[237,306] remain underexplored, hence this chapter aims to contribute to bridging this gap. The aim of this work was to develop new tethered half-sandwich manganese complexes to be utilised for the asymmetric hydrosilylation of ketones, whereby the chirality of the tether, induced by incorporating a stereocentre adjacent to the Cp ligand (Figure 134), would be the origin of selectivity, transferring chirality to the substrates. Previous work outlined in Chapter 2 inspired the design and synthesis of the following novel manganese(I) complexes.
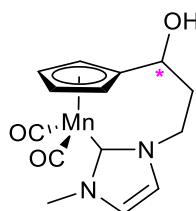
Figure 134. Example of one final manganese(I) complex targeted during this project.

The half-sandwich piano-stool framework was a key feature to retain when developing the catalysts. The insertion of a single stereocentre to control the stereochemistry of the complex is the defining feature of the proposed catalyst. By tuning aspects of the framework, in particular the ligands and tether, this project will investigate the influence that the individual components of the complex exert on the activity and stereochemical control of the complex towards the hydrosilylation of ketones.[311,312] With this catalyst design, on irradiation, a carbonyl ligand would be replaced by the coordinating functionality present on the tether, yielding an intramolecular tethered species (Scheme 42).
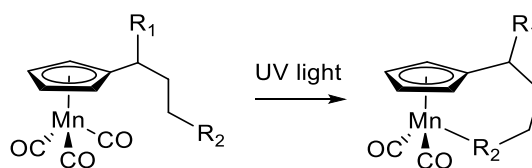
Scheme 42. Representative complexation step showing the pendant tether on the left and the final complex on the right.

It is postulated that the tether stereocentre, and the control this has on the position of the tether, could, due to steric interactions, potentially restrict substrate approach to the complex to be limited to a defined segment of the metal coordination sphere during hydrosilylation, enhancing stability and catalytic activity and allowing for a greater degree of selectivity.[319]

3.3 Ligand and complex synthesis

Multiple routes were employed to target an Mn-NHC complex suitable for hydrosilylation. All routes were based on literature precedents that "anchor the imidazolium moiety to the cyclopentadienyl ring, followed by complexation to the manganese metal"[236], though alternative ligands to imidazolium based ligands were investigated first in this project.

The first route aimed to anchor ligand **34** onto complex **35** (Scheme 43).
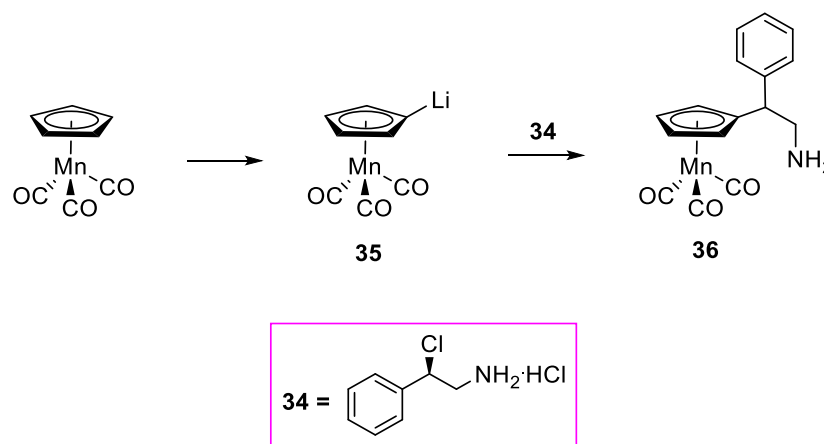
Scheme 43. Global scheme to show the route employed to synthesise **36**.

The ligand was synthesised by addition of SOCl$_2$ in anhydrous toluene to (*R*)-2-amino-1-phenylethanol-1-ol (Scheme 44), obtaining **34** as a crude product in 90 % yield.
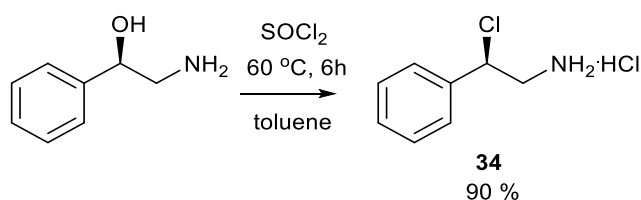
Scheme 44. Synthesis of (*R*)-2-amino-1-phenylethan-1-ol hydrochloride.

Confirmation of the formation of the desired product was observed by the shift of the stereocentre from δ = 4.43 ppm to δ = 5.46 ppm in the ¹H-NMR from the starting material to the product **34**. This accounts for the substitution of the more electron-withdrawing chlorine due to the deshielding effect seen towards the stereocentre. Further, the protons from the NH$_2$ moiety were seen as a broad singlet at δ = 8.62 ppm. Unfortunately, baseline impurities were found to be contaminating the ¹H-NMR and ¹³C-NMR, however, both were assigned successfully. Despite this, the CH and CH$_2$ environments could not be distinguished between

in the ^{13}C-NMR. This could have been solved by running 2D NMR experiments. Additional analysis by mass spectrometry gave a peak at 156.9 m/z representing the [M - Cl]$^+$ ion, with the isotopic pattern for chlorine also observed in the spectrum.

Utilising the successful design of Mn(I) tethered complexes by Lugan et al.[236] as a template, the next route (Scheme 45) achieved "selective deprotonation of the Cp ring of [CpMn(CO)$_3$] using *n*-BuLi in THF at -80 °C"[236] to produce the organolithium compound **35**. Following this, sequential attachment of the amine hydrochloride **34** was attempted, with the hope that leaving the amine free would allow for multiple derivatisations of the final complex.
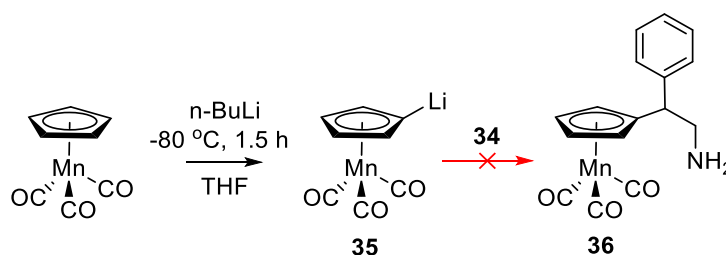
Scheme 45. Synthesis of [(η^5-C$_5$H$_4$CH(C$_6$H$_6$)CH$_2$NH$_2$)Mn(CO)$_3$].

Upon analysis, the chemical shifts for the CH$_2$ and CH moieties in **36** were not found in their expected regions in the ^{1}H-NMR, but impurities were found between δ = 1.29 ppm and δ = 3.27 ppm. This was not consistent with shifts found for the starting material **34**, in fact, there were no peaks present that indicated excess starting material **34**. Despite this, five protons, corresponding to the phenyl ring, were found at δ = 7.14-7.29 ppm. Further, the Cp protons were observed as a singlet at δ = 5.01 ppm consistent with that seen in the ^{1}H-NMR of the starting material cymantrene with an integration of eight protons, consistent with the 2:1 ratio of **35**:**34**, suggesting that the lithium species had been quenched to reform the starting cymantrene product. It was expected that the singlet would have split into more than one peak upon creation of the mono-substituted Cp ring as seen by Lugan et al.[236] upon attachment of their ligand to the organolithium complex **35**. This was all evidence for the failure of this reaction, rendering this route unsuccessful. The main suspicion for the failure of the reaction pathway was the choice of ligand, perhaps due to the bulky phenyl group, therefore an alternate route would be attempted with a different group substituted onto the cymantrene Cp ring.

The synthesis described in Scheme 46 originated from ruthenium-based research by Wills et al.[186], due to the success of Chapter 2, where the Cp ligand was acetylated in the presence of aluminium chloride and benzene (Scheme 47)[320].
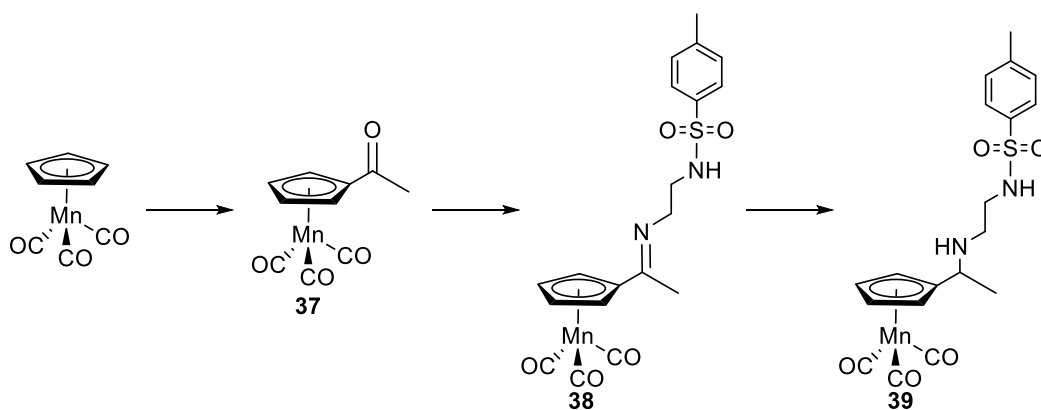
Scheme 46. Scheme showing the overall route employed to synthesise **39**.
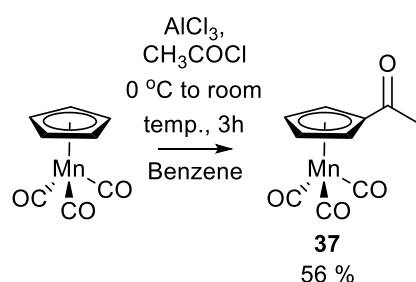
Scheme 47. Synthesis of acetylcymantrene.[321]

Purification of the reaction product by column chromatography yielded three products; the starting material cymantrene, acetophenone as the side product and the target product **37**, initially seen in the ^{1}H-NMR of the crude product in a ratio of approximately 0.30:1.70:1.00. Optimisation and refinement of the method was investigated via use of an alternative choice of solvent (DCM) and a reduced number of equivalents of aluminium chloride and acetyl chloride, with an extension of reaction time, which resulted in **37** as a single spot on the TLC plate. The primary evidence for the success of the reaction was from the ^{1}H-NMR. Upon formation of the ketone, the single peak at $\delta = 5.04$ ppm representing all five protons in the Cp ring of [CpMn(CO)$_3$] split into two distinctive triplet environments representing two sets of two protons at $\delta = 5.22$ ppm and $\delta = 5.80$ ppm. Further proof of acetylation of the Cp ring was confirmed by the non-equivalence of the carbon environments of the cyclopentadienyl ring in the ^{13}C-NMR at $\delta = 85.3$ ppm, $\delta = 87.9$ ppm and $\delta = 92.3$ ppm, plus the appearance of the C=O environment from the acetyl chloride moiety was observed at $\delta = 195.4$ ppm. Moreover, high resolution MS found the [M + Na]$^+$ ion at 268.9612 m/z.

This route incorporated compound **1**, previously discussed in Chapter 2, to form the imine tethered complex **38** in the presence of a few drops of acetic acid followed by partial reduction of the imine using NaBH₄ to **39** (Scheme 48).
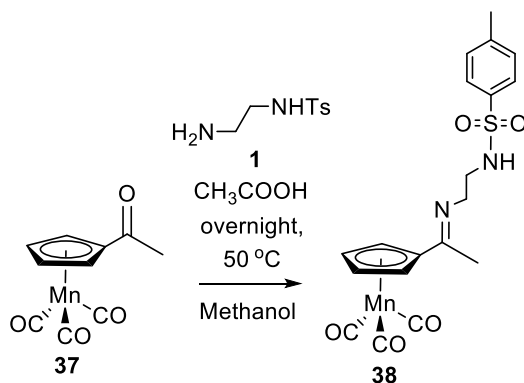
Scheme 48. Synthesis of [(η⁵-C₅H₄CH(CH₃)NHCH₂CH₂NHTs)Mn(CO)₃].

The formation of the imine was monitored by ¹H-NMR via integration of the starting material protons to the product protons. Both the Cp ring protons and the CH₃ protons experienced an upfield shift when the imine was formed. Upon addition of two equivalents of the linker, the peaks corresponding to the starting material decreased in intensity whilst the product signals, that were found further upfield, increased in intensity. Completion of the reaction was not reached entirely despite a further addition of one equivalent of linker **1** and heating to 50 °C overnight, plus the separation of excess linker from the imine product was difficult, therefore a new route would be employed. Although the formation of **37** was successful, the attachment of the ligand was still unfavourable.

Therefore, the third route (Scheme 49) aimed to derivatise the functional group once the ligand was anchored to the Cp ring as opposed to the addition of a pre-derivatised ligand to the Cp ring. This route followed a literature precedent[320], transforming the previously synthesised **37** (Scheme 47) to a complex comprising a longer tether.
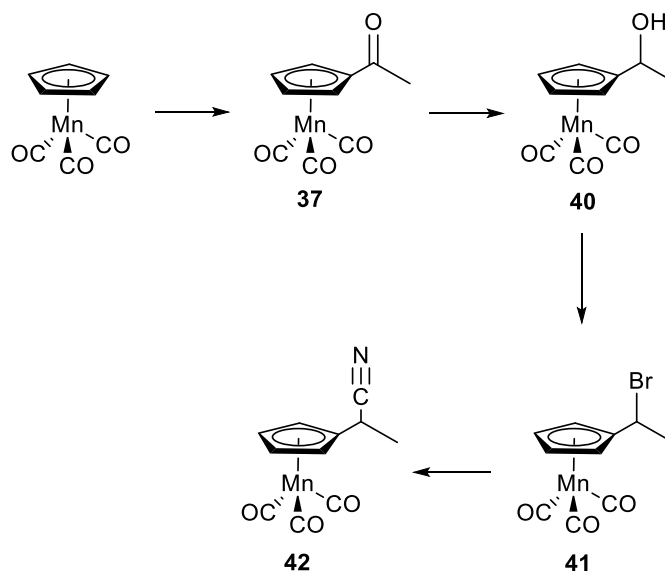
Scheme 49. Global scheme to show the route employed to synthesise **42**.

Subsequent treatment of **37** with NaBH$_4$ in methanol afforded the corresponding alcohol **40** (Scheme 50) in 90 % yield.
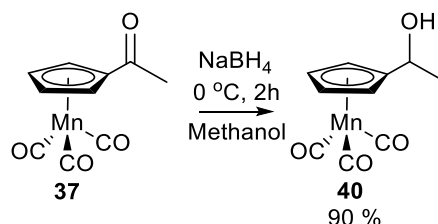
Scheme 50. Synthesis of 1-cymantrenylethanol.[309,322]

Confirmation of the product was primarily by the appearance of the stereocentre in the ^{1}H-NMR at δ = 4.36-4.42 ppm and by a D$_2$O shake with the peak farthest downfield at δ = 5.26 ppm disappearing to prove the presence of the OH moiety. The ^{13}C-NMR, which was in agreement with Potkin et al.[309], showed the disappearance of the C=O carbon environment at δ = 195.4 ppm and the appearance of the stereocentre environment at δ = 61.9 ppm. Furthermore, high resolution ESI found the [M + Na]$^+$ ion at 270.9770 m/z.

Under anhydrous conditions, **40** was reacted with PBr$_3$ (Scheme 51), however, the reaction did not reach completion despite stirring for four hours with the brominating agent in excess of nine equivalents.
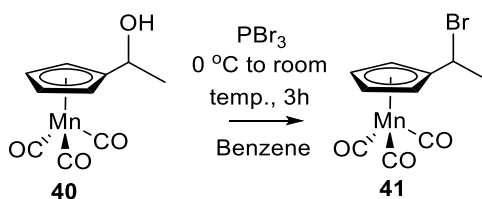
Scheme 51. Synthesis of $[(\eta^5\text{-}C_5H_4CH(CH_3)Br)Mn(CO)_3]$.[322]

Evidence of the conversion from alcohol to bromide was seen in the ^{1}H-NMR, whereby the stereocentre proton shifted from $\delta = 4.36\text{-}4.42$ ppm to $\delta = 5.13\text{-}5.20$ ppm. Baseline impurities were observed in both the ^{1}H-NMR and ^{13}C-NMR, in addition to a mixture of starting material **40** and anticipated product **41**. For example, two peaks were observed at $\delta = 61.9$ ppm and $\delta = 66.4$ ppm corresponding to the stereocentre carbons in the ^{13}C-NMR of starting material **40** and anticipated product **41**, and approximately twelve or more peaks in the region of $\delta = 81.0\text{-}83.2$ ppm, typical of Cp ring environments. Even though a yield of 0.80 g of crude product was obtained, the reaction produced approximately a 1:1 ratio of starting material to product, which was used without further purification in the next step.

The corresponding crude bromide **41** was treated with KCN in anhydrous DMF (Scheme 52) in the hope to increase the length of the linker by one carbon length.
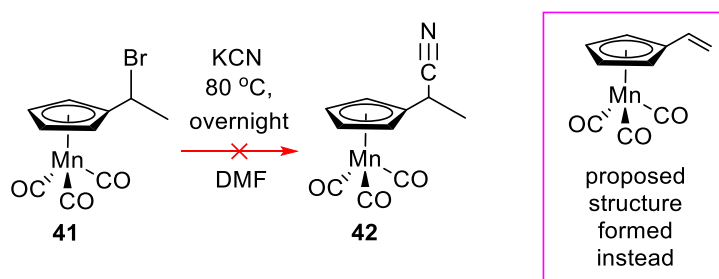
Scheme 52. Synthesis of $[(\eta^5\text{-}C_5H_4CH(CH_3)CN)Mn(CO)_3]$.

The product was confirmed by ^{1}H-NMR to in fact be an alkene, as opposed to the expected nitrile. It appeared that an elimination took place, showing the disappearance of the CH$_3$ protons in the spectrum and the appearance of three distinct environments each accounting for one proton within the alkene moiety. The ^{13}C-NMR was in agreement, showing five carbon environments; three corresponding to the Cp ring and the furthest two shifted environments characteristic of the two alkene carbons at $\delta = 115.8$ ppm and $\delta = 129.1$ ppm. Moreover, the high resolution ESI found the [M + H]$^+$ ion at 230.9851 m/z.

The anticipated route would have converted the nitrile to its corresponding carboxylic acid, followed by reduction to the alcohol and conversion to the bromide. The final steps would have attached **43**, then coordinated the tether to the manganese metal centre. Due to the unsuccessful nature of the nitrile step, this route was terminated.

The next route (Scheme 53) originates from the success in the first few steps of route three. All steps were identical to produce **41** (Scheme 47, Scheme 50 and Scheme 51), but instead of conversion to **42**, **43** was reacted directly with **41** in DMF in the presence of NaH, taking inspiration from Loim et al.[322].
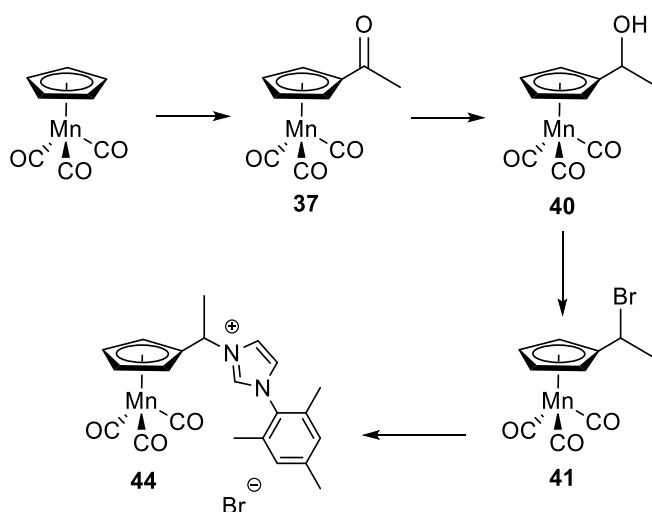
Scheme 53. Global scheme to show the route employed to synthesise **44**.

43 was synthesised (Scheme 54) in a fair yield of 50 %, with confirmation of the product by ^{1}H-NMR, ^{13}C-NMR and MS, in agreement with a literature precedent[323].
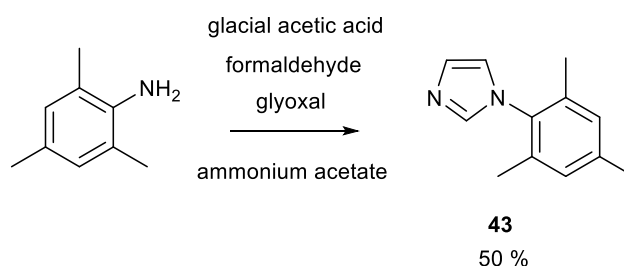
Scheme 54. Synthesis of 1-mesitylimidazole.[323]

Further, crystals of **43** were grown and analysed by x-ray diffraction to produce a unit cell with values a: 10.38 Å, b: 9.25 Å, c: 10.82 Å, which closely match the unit cell found by J. Brannon et al.[324].

The anticipated reaction of **41** with **43** can be seen in Scheme 55.
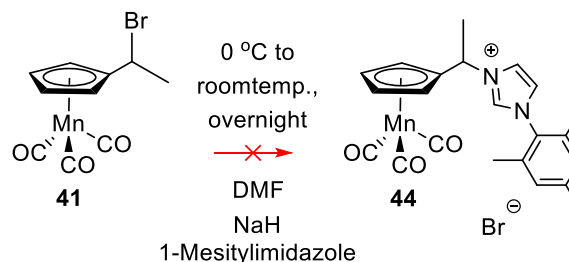
Scheme 55. Synthesis of $[(\eta^5\text{-}C_5H_4CH(CH_3)NHC^{Mes})Mn(CO)_3]Br$.

Initially, the expected reaction appeared successful with a shift of the imidazole proton, the proton that resided between the two nitrogen atoms, to δ = 7.95 ppm and the stereocentre from δ = 5.13-5.20 ppm in **41** to δ = 4.36-4.42 ppm for the product obtained. The hope for this reaction was that **43** would be deprotonated at the carbon present between the two nitrogens, allowing for attachment to the metal centre by displacement of a carbonyl ligand, followed by N-alkylation to replace the bromine with the nitrogen on **43** to result in formation of the intramolecular tether. Unfortunately, upon looking closer, the stereocentre proton signal was identical to that found for **40**, and further inspection indicated that all shifts found for the product matched that for the alcohol synthesised two steps prior, with multiple Cp resonances present that indicated more than one product. Further, no other peaks corresponding to **43** shifted in the ^{1}H-NMR. A likely explanation was the reduced number of 0.4 equivalents of **43** added. This was supposed to be one equivalent but calculations in the lab were carried out incorrectly, hence a mixture of Cp resonances were observed indicating that some product may have formed, but an excess of starting material or side products, all comprising Cp rings, were present. Moreover, the stability of **41** was already questioned in the step before, hence conversion back to the alcohol was not surprising. Analysis by ^{1}H-NMR proved the reaction to be unsuccessful, with **43** being clearly present but not coordinated to **40**.

The subsequent route (Scheme 56) was inspired by the original literature precedent discussed by Lugan et al.[236].
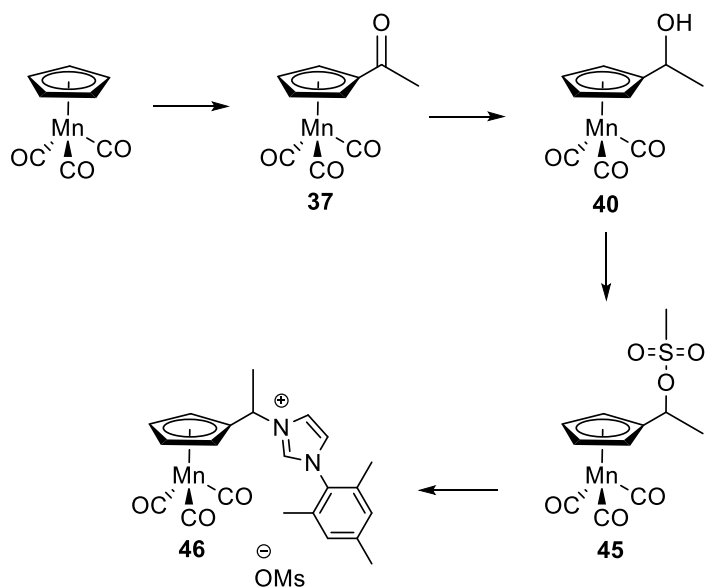
Scheme 56. Global scheme to show the route employed to synthesise **46**.

This method also follows route three (Scheme 49), but instead treats **40** with MsCl in the presence of TEA and DMAP (Scheme 57).
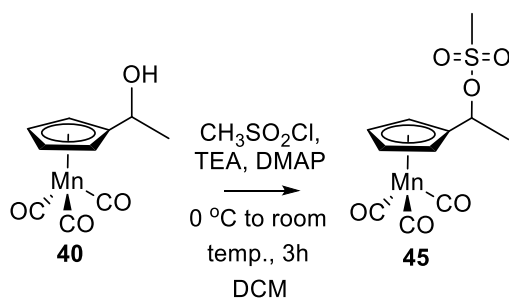
Scheme 57. Synthesis of 1-cymantrenylethyl methanesulfonate.

Due to the shift of the stereocentre from δ = 4.36-4.42 ppm to δ = 4.78 ppm coupled with TLC analysis, it was clear that the reaction had worked successfully. Plus, observation of the CH_3 from the mesylate at δ = 1.25 ppm gave further certainty. The mesylate was carried forwards as an intermediate to the next step without isolation and full characterisation.

45 was treated insitu with **43**, in the presence of NaH, but was proved unsuccessful by ^{1}H-NMR. This route was repeated, but as an alternative, **43** was added directly to **45** (Scheme 58) without deprotonation by NaH, allowing for nucleophilic substitution **43**.
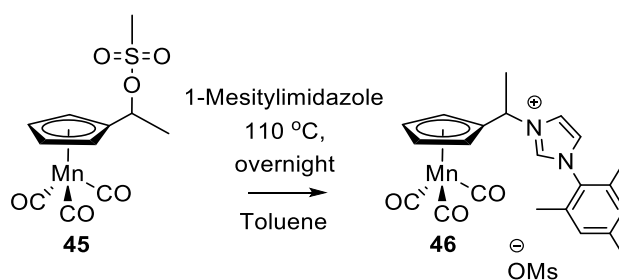
Scheme 58. Synthesis of [(η^5-C$_5$H$_4$CH(CH$_3$)NHC^{Mes})Mn(CO)$_3$]OMs.

The resulting product was filtered through celite and treated with ether to induce precipitation of impurities. A second purification through silica, using toluene/hexane then DCM/MeOH, obtained a brown oil, suggesting that the product was not completely dry. All chemical shifts in the ^{1}H-NMR were in fair agreement with the results found in the paper by Lugan et al.[236], which influenced this method. The protons from the imidazole ring shifted drastically upfield upon coupling to the manganese complex from δ = 7.11-7.63 ppm to δ = 5.16-6.25 ppm. Further, the stereocentre proton shifted from δ = 4.78 ppm to δ = 3.14 ppm. However, on comparison to the ^{1}H-NMR obtained for **[(44)Br]**, the peaks for the imidazole, mesityl and stereocentre were found to be significantly different shifts to that found for this compound. Unfortunately, the integrals did not portray the correct ratios, with the NHC and stereocentre environments comprising of integrals slightly too high and the Cp environments displaying integrals too low. Further purification may have solved this; however, the yield was already low, and it was suspected that the bulk of the NHC may have contributed to the issues occurring, therefore two amines of smaller size would be investigated in the pursuing routes.

Due to the success of steps in the previous routes three to five, the penultimate route (Scheme 59) followed that employed previously, whereby cymantrene was acetylated to form **37**, followed by reduction to **40** (Scheme 49).
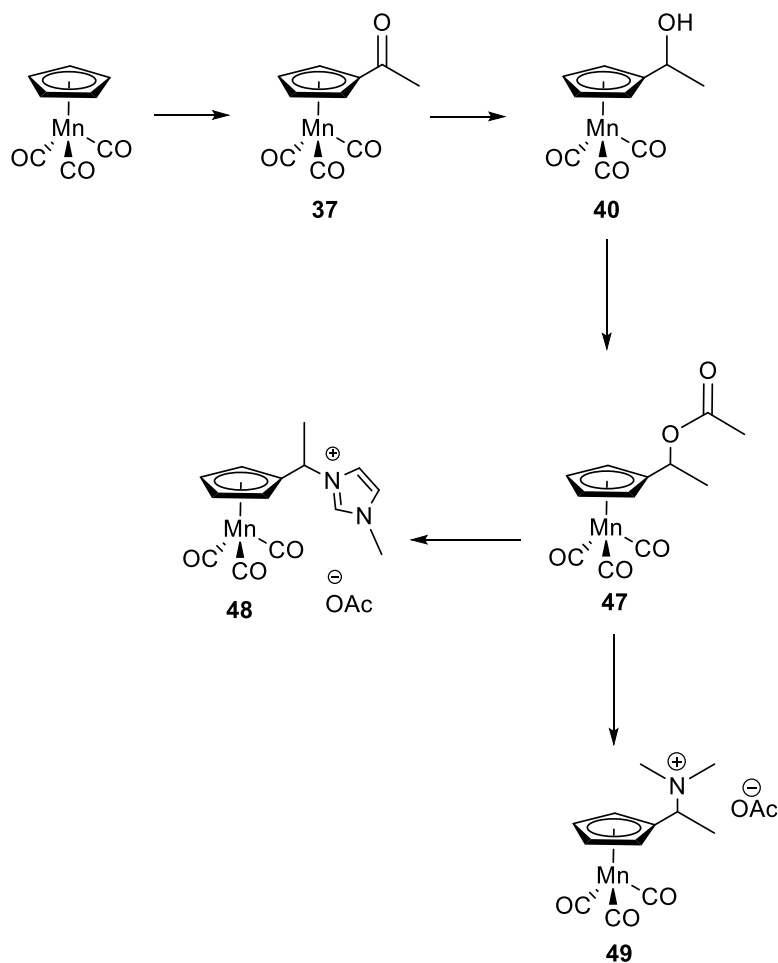
Scheme 59. Global scheme to show the route employed to synthesise **48** and **49**.

From here, the alcohol was reacted with acetic anhydride to form the ester **47** (Scheme 60) as a yellow oil in 49 % yield as a crude product.
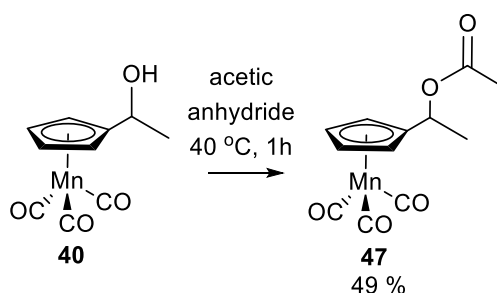
Scheme 60. Synthesis of 1-cymantrenylethyl acetate.

Interestingly, the ^{1}H-NMR showed a significant shift of the stereocentre to δ = 5.55 ppm, originally observed at δ = 4.36-4.42 ppm in the ^{1}H-NMR of **40**. Also, the disappearance of the OH peak at δ = 5.26 ppm indicated completion of the reaction. Moreover, the appearance

of the second CH_3 group, adjacent to the carbonyl carbon, was at δ = 2.03 ppm, found as a singlet. In the ^{13}C-NMR, the carbonyl peak appeared at δ = 169.5 ppm and the quaternary carbon of the Cp ring shifted from δ = 112.3 ppm to δ = 104.6 ppm.

We decided to attempt displacement of the ester group with two different ligands to investigate their differing properties towards substrates once the catalyst was formed. The first ligand used was 1-methylimidazole with two solvent conditions investigated simultaneously: acetic acid and a mixture of MeCN/H_2O (Scheme 61).
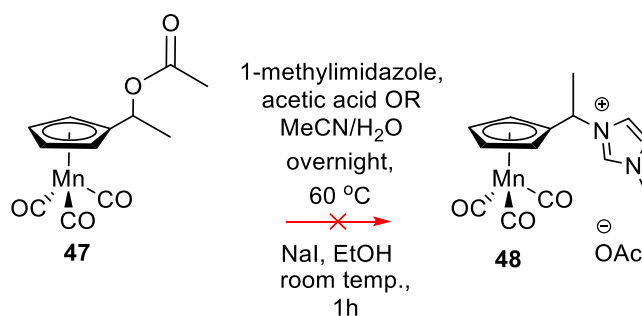
Scheme 61. Synthesis of [(η^5-$C_5H_4CH(CH_3)CH_3C_3H_3N_2$)Mn(CO)$_3$]OAc.

Both routes failed, with only **47** observed in the ^{1}H-NMR, regardless of the solvent was used. It was unclear why the amine ligand failed to displace the ester moiety of **47**.

The second ligand used was dimethylamine (Scheme 62). The inspiration stemmed from a literature precedent that substituted the dimethylamine moiety with the desired imidazole.[325]
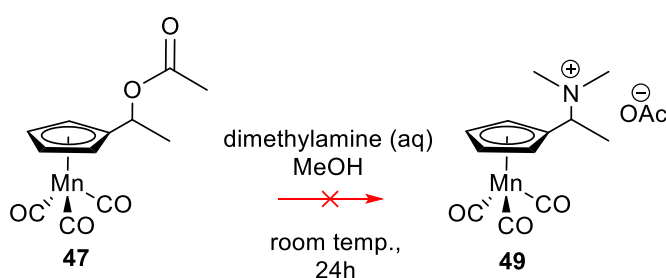
Scheme 62. Synthesis of [(η^5-$C_5H_4CH(N(CH_3)_2)CH_3$)Mn(CO)$_3$]OAc.

This reaction was unsuccessful, producing an ^{1}H-NMR spectrum identical to **40**, indicating the alcohol reformed due to hydrolysis by the water present in the dimethylamine reagent. A D_2O shake confirmed this as the peak at δ = 5.24-5.25 ppm disappeared. It was suspected that the reaction conditions employed were too harsh, displacing the ester moiety of **47**.

Due to the failure of both ligands, an entirely new route (Scheme 63) was proposed, following a literature precedent that substituted nucleobases onto **50**.[326]
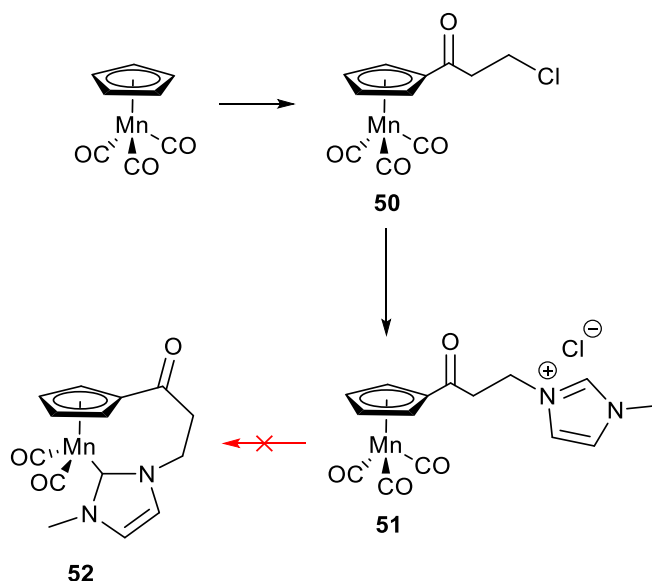
Scheme 63. Global scheme to show the route employed to synthesise **52**.

The final route began with substitution of 3-chloropropionyl chloride onto the Cp ring of cymantrene in the presence of AlCl$_3$ in DCM (Scheme 64).
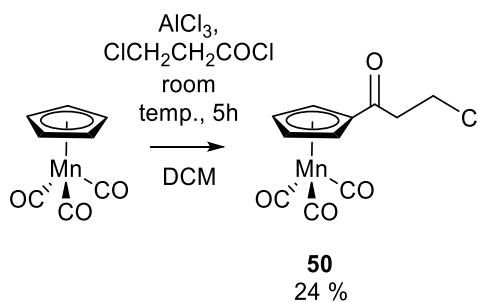
Scheme 64. Synthesis of chloropropionylcymantrene.[326]

Purification through silica using Hexane/EtOAc as the eluent produced the acid chloride derivative **50** as a yellow oil in 24 % yield. This suggests that the product may not have been completely dry as the literature reports a yellow solid, however, in the literature the solid was then crystallised from dichloromethane/*n*-pentane at -78 °C to yield yellow crystals.[326] The product was obtained and matched the data reported in the literature.[326] Further, high resolution MS confirmed the product as the [M + Na]$^+$ ion at 316.9391 m/z.

The second step substituted 1-methylimidazole onto the tether of the Mn complex utilising TEA as the base and DMF as the solvent (Scheme 65). **[(51)Cl]** was obtained as a dark brown solid in 97 % yield.
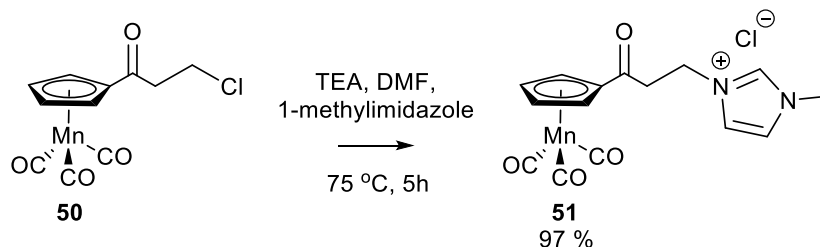
Scheme 65. Synthesis of $[(\eta^5\text{-}C_5H_4COCH_2CH_2(NHC\text{-}CH_3))Mn(CO)_3]Cl$.

Analysis by ^{1}H-NMR confirmed all environments. In particular, one of the CH_2 environments shifted to $\delta = 4.46$ ppm from either $\delta = 3.84$ ppm or $\delta = 3.16$ ppm in the ^{1}H-NMR of the starting material. 2D NMR would have been useful to distinguish between the two CH_2 environments, however, the experiments were unsuccessful, likely due to concentration issues or decomposition on prolonged exposure to DMSO. Furthermore, the ^{1}H-NMR spectrum was missing a CH_2 environment, suspected to be hidden under the H_2O peak due to comparison to literature precedents[326]. COSY and HMBC would have been particularly useful to allow for correlations to be observed. The ^{13}C-NMR, comprising of eleven peaks, was easy to assign with shifts associated to each distinct environment in their anticipated regions. High resolution MS confirmed the product as the [M - Cl]$^+$ ion at 341.0331 m/z.

Following this, the final complex was anticipated to be made by deprotonation of the imidazole ring and irradiation by UV light to displace one of the carbonyl ligands attached to the metal centre (Scheme 66). The methods attempted here were inspired by Lugan et al.[236].
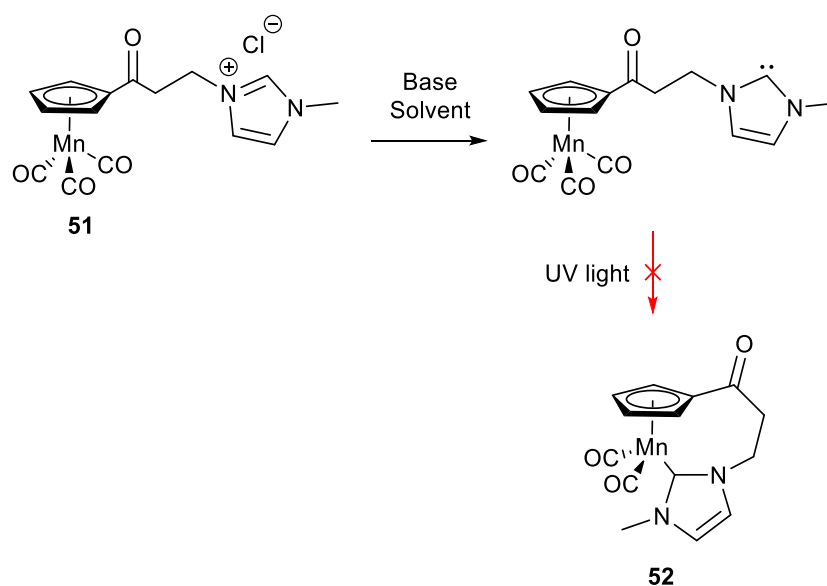
Scheme 66. Synthesis of (η^5-C$_5$H$_4$COCH$_2$CH$_2$(NHC-CH$_3$))Mn(CO)$_2$.

An initial experiment using cymantrene was carried out to see if the equipment in the lab was capable of removing a carbonyl ligand to allow for complexation later on. The cymantrene was dissolved in anhydrous THF to give a yellow solution. Upon irradiation with UV light on the long wavelength setting of the lamp, a colour change to a cloudy orange suspension was observed. TLC analysis on silica with EtOAc/Hexane (5 % EtOAc) confirmed the starting material spot was still present at R_f = 0.70, with an additional new intense yellow spot at R_f = 0.95. This gave confidence to pursue further irradiation studies with complex **[(51)Cl]**.

Two bases were tested during this project, KHMDS and KOtBu. Intially, KHMDS in anhydrous toluene was investigated. After 45 minutes of irradiation, a new spot was observed on the alumina TLC plate at R_f = 0.57, utilising a solvent system of EtOAc/Hexane (20 % EtOAc). However, after one hour, the eluted spot went brown, indicating that decomposition had occurred. As a direct comparison, the alternative choice of base, KOtBu, was employed with anhydrous toluene, but the reaction route was terminated due to insolubility issues. This led to the investigation of KOtBu in THF, despite the literature precedent utilising toluene[236]. Though **[(51)Cl]** was of similar structure to the Mn complexes described by Lugan et al.[236], the complex in this project comprised of a less bulky NHC and the carbonyl bond adjacent to the Cp ring affected the acidity surrounding this environment, which let us anticipate a difference in solubility.

The respective base was added in various amounts ranging from 0.30 to two equivalents. Experiments began utilising the larger number of equivalents to ensure deprotonation was occurring, however, it was later suspected that excess of base was

causing the site adjacent to the carbonyl moiety to be deprotonated simultaneously, therefore an experiment was conducted whereby base was added in 0.10 equivalents and analysed by ^{1}H-NMR until the imidazole proton peak disappeared at δ = 9.12 ppm. The minimum amount of base required to therefore deprotonate the NHC was 0.30 equivalents, indicating that impurities were present in the crude complex.

^{1}H-NMR was run immediately after addition of base before irradiation began to confirm deprotonation of the NHC. Initial experimentation ran the ^{1}H-NMR and TLC at time points 15, 30, 45 and 60 minutes of irradiation, however, a dark brown colour change was observed after 30 minutes, followed by a precipitate formation after 45 minutes, both of which were suspected to be as a result of decomposition. Alongside this experiment, an experiment of identical conditions, but utilising KHMDS in THF, was run but the red/brown colour change occurred faster, coupled with the formation of the dark brown precipitate, after just 5 minutes of irradiation. This indicated that the weaker base KOtBu was more suitable for **[(51)Cl]** and hence the reaction utilising KOtBu in THF would be repeated. The reaction time was reduced to a total of 15 minutes, with time intervals of 5, 10 and 15 minutes to run the analysis. The initial NMR before irradiation showed the Cp resonances at δ = 5.27 ppm and δ = 5.94 ppm, both which were shifted slightly downfield upon addition of base. This suggested that the CH$_2$ adjacent to the carbonyl may have been deprotonated despite a reduction in the number of equivalents of base, hence suggesting that the base was still too strong. After 5 minutes, a colour change to red/brown colour was observed, from an initially light brown sample, and the TLC analysis showed three new faint spots of R$_f$ values 0.66, 0.88 and 0.95. Plus, multiple peaks in the region of δ = 4.00-6.00 ppm were observed, indicating that more than one species was being formed, which was in agreement with the TLC analysis. However, after 10 minutes of irradiation, the peaks disappeared, therefore it was inferred that decomposition had taken place. In conclusion, it was suggested that the base employed was still too strong and therefore a weaker choice of base coupled with a solvent that offered increased solubility from that observed during this project would be preferable.

Overall, four manganese precursors were targeted. Complexes comprising of a CH$_3$ at the carbon stereocentre adjacent to the Cp ring showed greater progress than the initial bulkier phenyl group investigated, hence investigation into the size of the bulk at the stereocentre, dictating the stability of the final complex, was terminated. However, the complexes comprising of a CH$_3$ group emanating from the stereocentre had to be modified due to a lack of success, despite multiple routes being attempted.

Instead, a carbonyl moiety replaced the CH$_3$ group. A literature precedent[236] led the synthesis towards the proposed final framework. **[(51)Cl]** was successfully synthesised and subjected to deprotonation and irradiation in the hope to obtain the final complex. Following complexation, it was anticipated that the carbonyl moiety would be reduced to its corresponding alcohol, to create a stereocentre, following a method found in another research article[326]. From there, simple derivatisations could be carried out to modify the framework further with various functional groups or even attachment to solid supports (see Chapter 4) in order to encourage recyclability of the catalyst. Unfortunately, the reaction conditions employed here were not successful, leaving room for improvement in future work. With regret, there was not enough time during this project to tune irradiation conditions, reduce the carbonyl bond or modify the stereocentre.

3.4 Conclusions

The aim of this chapter was to produce novel tethered manganese complexes for the asymmetric hydrosilylation of ketones due to the current gaps in research within this field of work. To date, all frameworks reported are racemic, which is unfavourable within the agrochemical, pharmaceutical and fine chemical industries.[115] This work followed on from Chapter 2, whereby enantiopure complexes were created, with control over the metal centre and alcohol product during ATH via the insertion of a stereocentre adjacent to the arene ring. Therefore, within this chapter, the idea initially was to incorporate a stereocentre adjacent to the Cp ring in order to render the complex chiral and to influence its interactions with substrates. The synthesis was performed to yield racemic products, with the hope to later separate the isomers by chromatography.[319]

The synthesis of four manganese precursors was attempted, with only one of these showing promise at the final synthetic step. Data obtained during the irradiation of **[(51)Cl]** showed great promise and therefore there is confidence in forming the final complex if the reaction conditions can be tuned correctly, allowing for multiple analogues of these manganese complexes to be targeted in the future. Further, no hydrosilylation reactions were performed since no final complexes were obtained, therefore conclusions as to whether the insertion of a chiral stereocentre adjacent to the Cp ring could not be made. Due to this idea being completely novel and showing success in alternative fields of work, namely ruthenium(II) piano-stool frameworks, it is expected that this work will be pursued by other researchers.

3.5 Future work

The tethered Mn complexes outlined in this chapter can still be considered as good target complexes to be used in hydrosilylation. Although the partial insolubility in various solvents observed during this project proved problematic and consequently precluded detailed analysis after subsequent irradiation with UV light. Future work may focus upon tuning of the reaction conditions when attempting to deprotonate the NHC and simultaneously encouraging displacement of one of the carbonyl ligands. Namely, the solvent in which the deprotonation and irradiation is carried out in could be investigated. Interestingly, the Mn complex **[(51)Cl]** was very soluble in MeOH, however, it was anticipated that MeOH would quench the base, or in other words, the chosen base would deprotonate the MeOH instead of the target site on the Mn complex, and hence the deprotonated MeOH could coordinate to the metal centre. Though it was considered to use MeOH as a dual solvent and base, it was suspected that the strength of methoxide as a base may not have been great enough to deprotonate the NHC. Despite this, the doubts here are merely postulated, thus differing solvent studies would be of interest in an attempt to achieve the desired Mn complexes.

An extension of the tuning of the deprotonation and irradiation reaction conditions includes investigation of different bases, for example utilising a weaker base. The reason for the use of a weaker base arises from the current failure whilst using KOtBu and KHMDS in this project. Though the ^{1}H-NMR indicated successful deprotonation of the imidazole ring, it was unclear as to whether the base was also deprotonating the CH_2 adjacent to the carbonyl moiety on the tether. The protons on this CH_2 group were very acidic protons and suspected to be of similar pK_a to the proton on the NHC, susceptible to deprotonation by addition of base, therefore a weaker base is less likely to induce these same problems. The addition of K_2CO_3, which has been utilised previously in literature[327], would not lead to immediate and quantitative deprotonation of the imidazole in the same way that addition of KOtBu and KHMDS did due to its weaker properties. However, addition of K_2CO_3 followed by immediate irradiation of the sample is suspected to lead to the formation of the target Mn-NHC complex **52**. This is because there is a vacant coordination site at the metal centre, from loss of one carbonyl ligands during irradiation, and the weaker base is present to remove the proton from the imidazole ring of the activated intermediate complex. To summarise, KOtBu and KHMDS were both utilised during this project but were suspected to be too strong, therefore weaker alternatives of methoxide or K_2CO_3 could be investigated. The order of strength for

these four bases are as follows: KHMDS, KO*t*Bu, methoxide, K_2CO_3, with KHMDS being the strongest and K_2CO_3 being the weakest.

Alternatively, to combat the deprotonation of these acidic protons adjacent to the carbonyl moiety, reduction of the carbonyl bond to its corresponding alcohol, as discussed by Kowalski et al.[326], would render these protons less acidic and hence less susceptible to deprotonation. It is important that the choice of base to aid coordination of the tether to the metal centre must be strong enough to deprotonate the NHC, but not too strong that the alcohol would be deprotonated.

Furthermore, it may be of interest to modify the Mn framework to comprise of alternative ligands, for example phosphine-based. Current projects being pursued in Dr Murray's research lab include the addition of 2-(diphenylphosphino)ethylamine to acetylcymantrene **37**, followed by reduction of the imine bond before irradiation and complexation (Scheme 67).
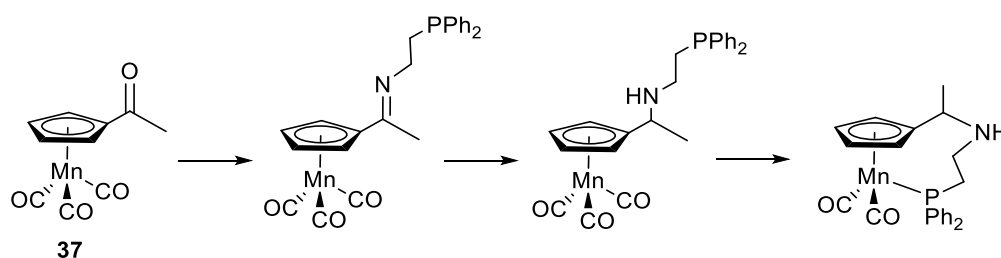
Scheme 67. Synthesis of $[\eta^5\text{-}C_5H_4CH(CH_3)NHCH_2CH_2PPh_2Mn(CO)_2]$.

This alternative ligand does not require a base for deprotonation, instead the phosphine lone pair forms a dative bond with the metal centre once the complex is irradiated and a carbonyl ligand lost. Current literature reports poor phosphine-based half-sandwich manganese complexes[237]; therefore we hope that this new framework will portray improved activity during hydrosilylation due to the inclusion of the tether to increase the stability of the complex.

The work during this project and proposed for future work therefore indicates that the Mn frameworks targeted here show promise as appropriate candidates for hydrosilylation catalysts. As suggested above, there are new avenues that can be pursued to achieve these target complexes, and hopefully bring success to this underdeveloped field of work.

Chapter 4

Novel polymer-supported ruthenium(II) chiral-at-metal tethered half-sandwich complexes

4.1 Background

The immobilisation of ATH catalysts to polymer supports allows for cheaper and more environmentally friendly reaction conditions.[60,64,95,256,261] In light of the discussion in Chapter 1, the approach in this chapter aims to investigate and evaluate whether the tethered catalysts developed in Chapter 2 are able to be readily immobilised to a solid support. Polymer beads have been chosen as a result of their commercially available nature, and hence cost effectiveness, and the tunability of functional groups on the polymer bead enabling easy attachment of the bead to the catalyst.[328] These advantages are also supported by the high yields and enantioselectivities observed in literature precedents discussed in Chapter 1.[60,241,249,253,254,259,260] Further, polymer supports are partially soluble and hence allow for homogeneous ATH, overcoming solubility and kinetic problems often observed with insoluble supports.[328]

Thus far, research of PEG-supported catalysts in water has successfully shown high enantioselectivity and recycling of the catalyst. As described earlier, ATH is a significant method towards the preparation of key drug intermediates. For example, production of (*R,R*)-formoterol and (*R*)-salmeterol was possible with a catalyst comprising of the ligand PEG-BsDPEN (Figure 135) with molecular weights of 2000 and 800 g/mol respectively.[58,67,74,85,329]
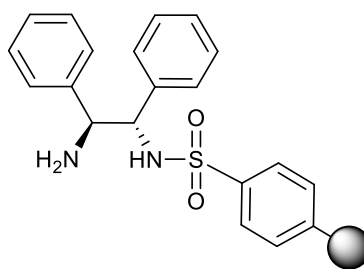
Figure 135. PEG-BsDPEN ligand.[259]

Further, the ATH of ketones to produce enantiomerically enriched alcohols, as intermediates for the synthesis of the antidepressant (*S*)-fluoxetine, has been successfully carried out by immobilising the chiral DPEN ligand onto aminomethylated polystyrene polymer beads. This

research was environmentally green and supported the recovery and reuse of the catalyst, minimising toxic contamination by the ruthenium metal.[58,67,241] Despite these advantages, immobilisation to solid supports has disadvantages too, namely the complex synthetic pathways necessary to create these catalysts[241], incompatibility with solvents which hinders access to active sites and difficulty in calculating the ratio of catalyst loaded onto the polymer bead[249]. It is for this reason that the following catalyst design was prepared very carefully.

4.2 Ligand and complex design

To date, researchers have immobilised ruthenium(II) half-sandwich catalysts at various locations on the framework (Figure **136**).
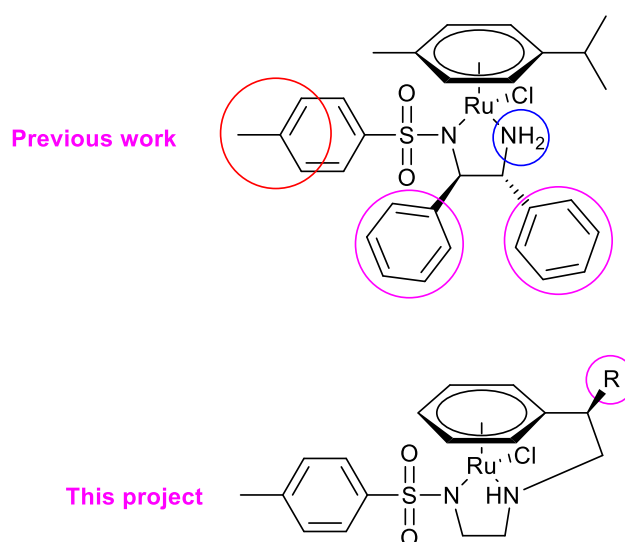
Figure 136. Various locations that have been attached to solid supports in literature precedents[253,254,259,260], alongside where the framework will be immobilised during this project.

The location of the attachment of the support in this project is novel, with current work linking the support through the phenyl groups, the amino moiety or the sulfonamide moiety.[253,254,259,260] This is advantageous as the remaining framework can be tuned to heighten activity observed during ATH.[253] Important research suggests the reactive Ru-Cl and NH_2 of the TsDPEN must be left unoccupied due to their essential roles during ATH.[67] Therefore, introducing reactive functionality at the benzylic position provides a route by which the catalysts could be attached to a solid support without the inhibition of ATH activity.[253] Another advantage of using this position is that the support would be attached to the catalyst without unduly interfering with the rest of the catalyst, as compared to the non-supported

catalyst. The attachment can be done with or without the addition of a linker between the catalyst and the solid support because immobilisation by this method allows the catalyst to be hanging pendant from the support. The inclusion of a linker also allows for "sufficient distance between the polymeric support and the catalytic centre"[253,257,259] during ATH, allowing for easier approach of the substrate.[328]

Furthermore, all solid supported catalysts synthesised to date focus upon the untethered Noyori ligand.[240,251,262,264–266,268,281,304,253–260] However, it has been concluded that the incorporation of a tether to Noyori's framework has increased stability and enantioface discrimination, therefore enhancing activity of the unsupported catalyst during ATH.[81,257] As discussed earlier, two carbon tethers have been minimally researched, hence the design of novel complexes for this project follows on from Chapter 2.

The functional group stemming from the carbon stereocentre differs here to allow for easier attachment of the support. The methyl group from Chapter 2 was replaced with an NH$_2$ moiety (Figure 137), which has been shown to be a desirable functional group to immobilise solid supports onto as a result of its nucleophilic nature, meaning that it can be alkylated or used in amide bond formation.[141] This NH$_2$ moiety required protection during the route and Boc was chosen due to the milder conditions required to remove the protecting group in comparison to Fmoc for example.
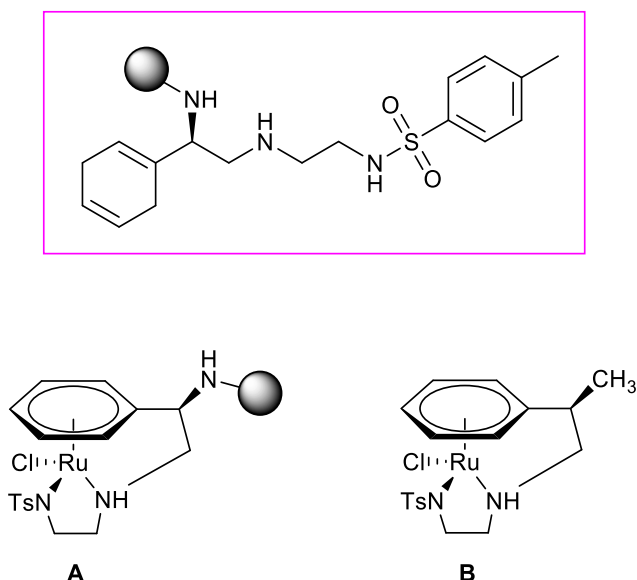
Figure 137. Structures of the final immobilised chiral ligand above (**A**) the immobilised chiral catalyst to be targeted during this chapter and (**B**) the 2C-tethered complex **6a** synthesised in Chapter 2.

This research inspired us to design a solid supported ruthenium(II) catalyst both tethered and controlled in its stereochemistry. Previous studies have focused on attaching a ligand to a solid support, followed by subsequent formation of the metal complex.[330] The alternative route of directly attaching the complex to the solid support has been investigated to a lesser extent. The direction taken in this chapter follows the former route route, aiming to anchor the chiral chelating ligand to the polymer bead prior to reaction with ruthenium as it has been postulated that the free amine at the stereocentre could coordinate to the ruthenium metal centre in place of the anticipated amines on the chiral ligand.

4.3 Ligand and complex synthesis

The first route proposed follows that displayed in (Scheme 68) and began with the Birch reduction of (*R*)-2-amino-2-phenylacetic acid hydrochloride (Scheme 69).
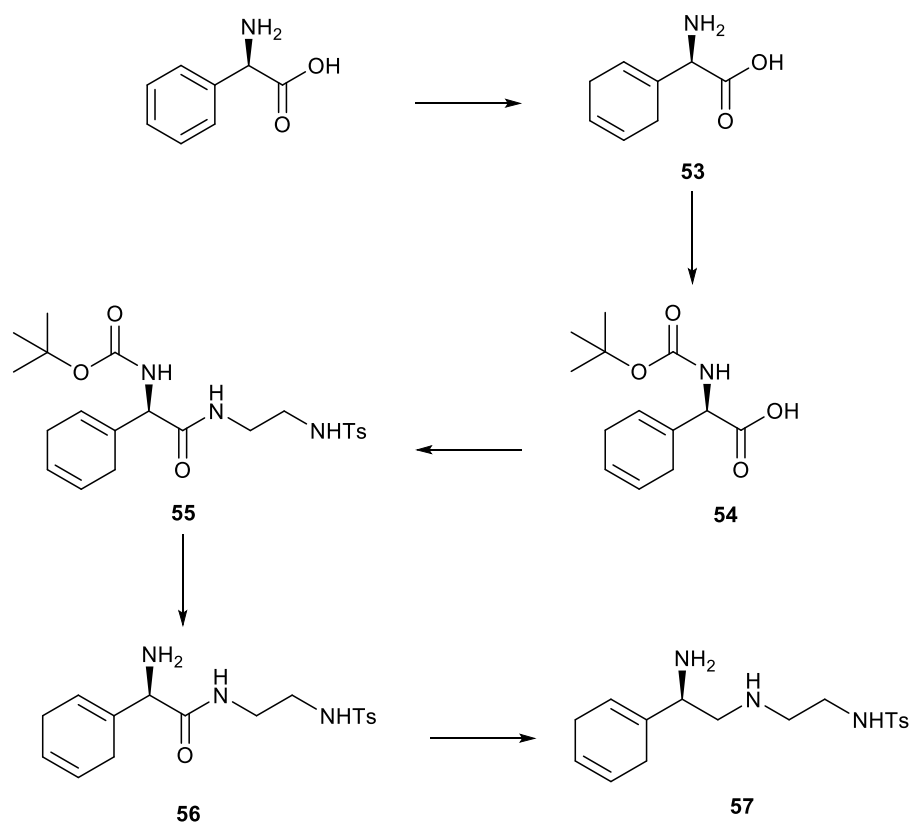
Scheme 68. Global scheme of the first solid supported route proposed.
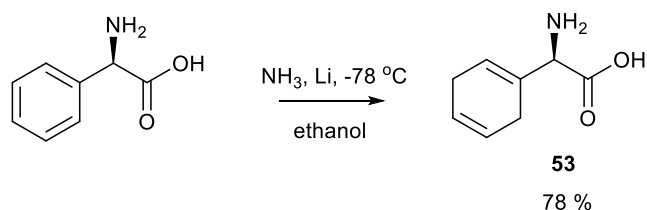
Scheme 69. Synthesis of (*R*)-2-amino-2-(cyclohexa-1,4-dien-1-yl)acetic acid.

53 was obtained in 78 % yield as a pearlescent white solid with confirmation by ^{1}H-NMR, whereby the disappearance of peaks at δ = 7.10-7.38 ppm was accompanied by the appearance of peaks at δ = 5.69 ppm and δ = 6.01 ppm, indicating that the aromatic ring had been successfully reduced. Furthermore, the two CH$_2$ groups of the diene ring were observed at δ = 2.50-2.74 ppm. From this, 2D NMR was utilised to assign the peaks in the ^{13}C-NMR spectrum with all eight peaks being accounted for. Of note were the alkenyl carbon environments of the diene ring, at δ = 122.8 ppm, δ = 123.7 ppm and δ = 126.0 ppm, and the CH$_2$ groups of the diene ring, at δ = 24.6 ppm and δ = 26.2 ppm. Furthermore, high resolution MS run in negative mode confirmed the [M - H]$^-$ peak at 152.0717 m/z. Though the compound had been previously synthesised, it had not been characterised.[331]

Next, **53** was protected with Boc (Scheme 70), producing **54** as a white honeycomb solid in 55 % yield.
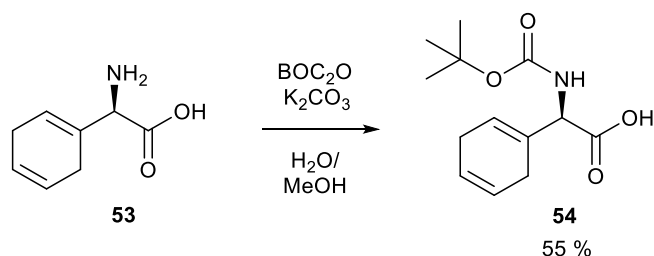
Scheme 70. Synthesis of (*R*)-2-((*tert*-butoxycarbonyl)amino)-2-(cyclohexa-1,4-dien-1-yl)acetic acid.

The three CH$_3$ groups from the Boc group were observed in the ^{1}H-NMR spectrum at δ = 1.42-1.44 ppm and in the ^{13}C-NMR spectrum at δ = 28.3 ppm. Moreover, the quaternary carbon and the carbonyl moiety of the Boc group were seen in the ^{13}C-NMR at δ = 81.6 ppm and δ = 157.2 ppm respectively, assigned with help from the 2D NMR experiments. Unfortunately, the ^{13}C-NMR spectrum appeared to be contaminated with a minor impurity, suspected to be excess starting material. Low resolution MS confirmed the product as the

[M + Na]$^+$ ion at 276.1 m/z. Both NMR and MS analysis were in agreement with that found in the literature.[332]

Following this, **54** was coupled to **1** in the presence of TBTU to prevent racemisation[291,292] (Scheme 71). After purification by column chromatography on silica, **55** was obtained as a white honeycomb solid in 70 % yield.
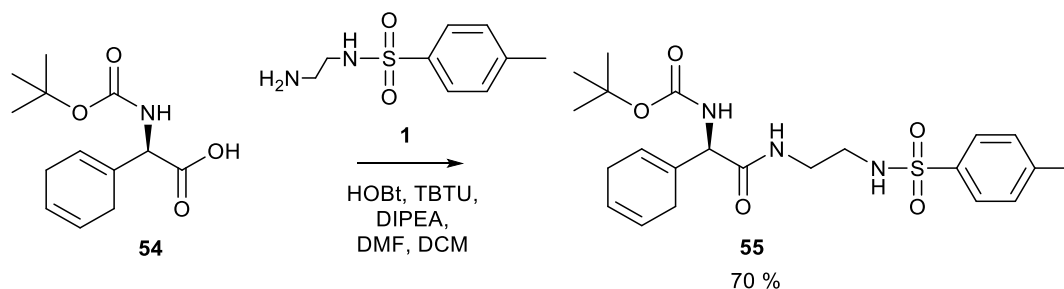
Scheme 71. Synthesis of (*R*)-*tert*-butyl (1-(cyclohexa-1,4-dien-1-yl)-2-((2-((4-methylphenyl)sulfonamido)ethyl)amino)-2-oxoethyl)carbamate.

Success of the reaction was observed by the 3:4 ratio of diene protons (at δ = 5.58-5.79 ppm) to aromatic protons (at δ = 7.69 ppm and δ = 7.26 ppm). Moreover, **55** was now soluble in CDCl$_3$ unlike the starting material **54**. Confirmation of the product was found in the high resolution MS, whereby the [M + Na]$^+$ ion was observed at 472.1879 m/z.

The penultimate step to synthesise the target ligand required removal of the Boc group (Scheme 72) from **55**. This was essential before the LiAlH$_4$ reduction as the Boc carbonyl group could also be reduced under these conditions.
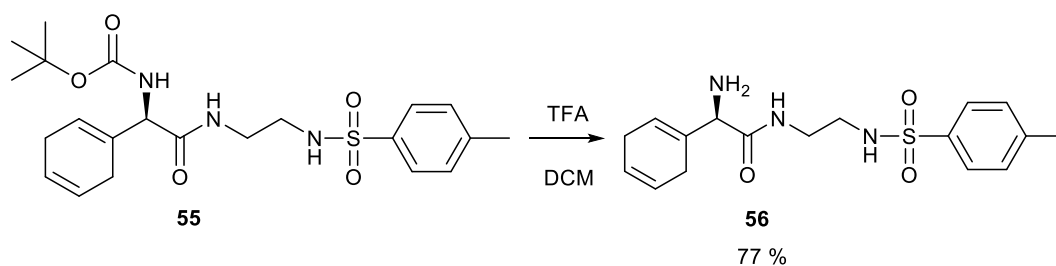
Scheme 72. Synthesis of (*R*)-2-amino-2-(cyclohexa-1,4-dien-1-yl)-N-(2-((4-methylphenyl)sulfonamido)ethyl)acetamide.

56 was produced in 77 % yield. Upon analysing the ^{1}H-NMR spectrum, the disappearance of the three CH$_3$ groups of the Boc group at δ = 1.39 ppm replaced with a broad singlet at δ = 1.68 ppm, responsible for the NH$_3$$^+$, confirmed successful removal of the Boc group by

TFA. The most significant shift was observed for the stereocentre from δ = 4.54-4.56 ppm in the starting material **55** to δ = 3.89 ppm in the product **56**. Furthermore, the peaks representing the three different carbon environments of the Boc group at δ = 155.5 ppm, δ = 80.0 ppm and δ = 28.4 ppm were no longer present in the ^{13}C-NMR spectrum. Additonally, ^{19}F-NMR was run and displayed a single peak at δ = -75.5 ppm, which represented the CF_3COO^- counterion. The peak for the [M + H]$^+$ ion was observed at 350.1533 m/z in the high resolution mass spectrum.

The final step aimed to reduce the amide **56** to amine **57** using LiAlH$_4$ (Scheme 73).
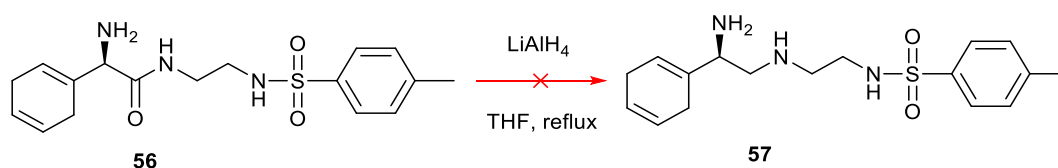
Scheme 73. Synthesis of (*R*)-*N*-(2-((2-amino-2-(cyclohexa-1,4-dien-1-yl)ethyl)amino)ethyl)-4-methylbenzenesulfonamide.

Despite manipulation of the conditions, including an increase of the reaction length at room temperature to 96 hours and then an increase of reaction temperature to 60 °C overnight, the reaction was unsuccessful. Starting material was observed in the ^{1}H-NMR and ^{13}C-NMR spectra, alongside multiple impurities, and analysis by TLC confirmed purification would be too challenging. This route was terminated and another route proposed instead (Scheme 74).
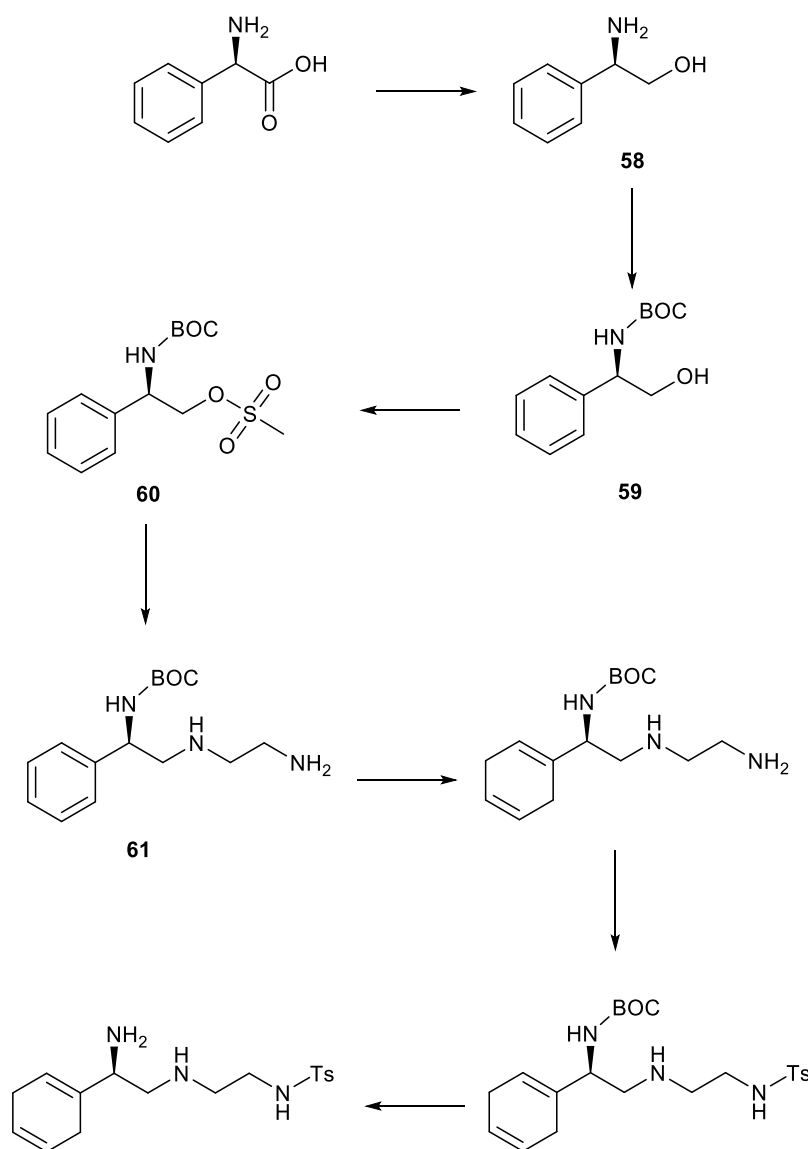
Scheme 74. Global scheme of the second solid supported route proposed.

The second route begun with the reduction of the carbonyl bond of (*R*)-2-amino-2-phenylacetic acid hydrochloride by LiAlH$_4$ (Scheme 75).
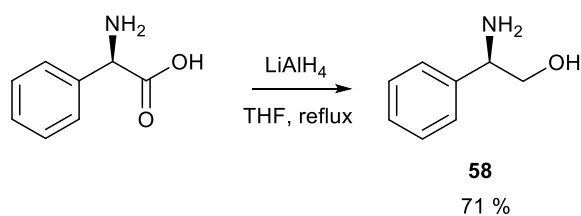
Scheme 75. Synthesis of (*R*)-2-amino-2-phenylethan-1-ol.

58 was obtained in 71 % yield with the diastereotopic CH_2 protons observed at δ = 3.72-3.75 ppm and δ = 3.54-3.58 ppm in the ^{1}H-NMR spectrum. Furthermore, the CH_2 environment was observed in the ^{13}C-NMR spectrum at δ = 68.0 ppm, with no peaks seen in the expected carbonyl region of the spectrum. Low resolution MS confirmed the product as the [M + H]$^+$ ion at 138.1 m/z. The data obtained for this compound matched that reported in the literature.[333]

Subsequently, **58** was protected with a Boc group (Scheme 76), acquiring **59** in quantitative yield.
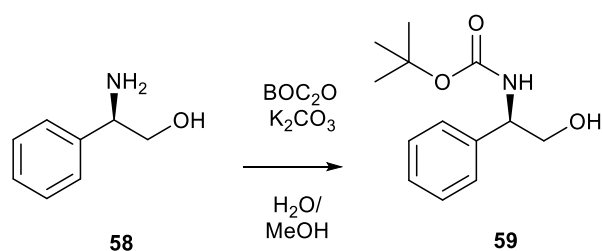
Scheme 76. Synthesis of (*R*)-*tert*-butyl (2-hydroxy-1-phenylethyl)carbamate.

The stereocentre proton was found to shift upon addition of the Boc group from δ = 4.03-4.06 ppm in the starting material **58** to δ = 4.78 ppm in the product **59**. The broad singlet representative of the NH_2 group was no longer seen in the ^{1}H-NMR spectrum at δ = 2.49 ppm, instead the NH moiety from the amide was found at δ = 2.37 ppm and the three CH_3 groups of the Boc group at δ = 1.44 ppm. By inspecting the ^{13}C-NMR spectrum, the CH_3 groups, quaternary carbon and carbonyl moiety of the Boc group were seen at δ = 28.4 ppm, δ = 80.0 ppm and δ = 156.3 ppm respectively. Low resolution MS confirmed the product as the [M + Na]$^+$ ion at 260.1 m/z. The data here was in agreement with that found previously in the literature.[334]

Next, **59** was converted to a mesylate via reaction with methanesulfonyl chloride (Scheme 77), obtaining **60** in 87 % yield.

59 → **60**

87 %
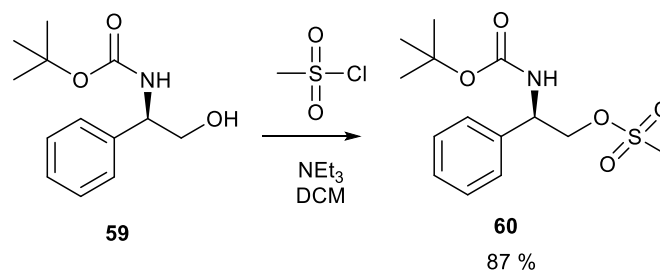
Scheme 77. Synthesis of (*R*)-2-((*tert*-butoxycarbonyl)amino)-2-phenylethyl methanesulfonate.

In the ^{1}H-NMR spectrum, the CH_3 of the mesylate was present at δ = 2.86 ppm and was also found in the ^{13}C-NMR spectrum at δ = 37.5 ppm. The CH_2 group adjacent to the mesylate moiety became less shielded, shifting from δ = 3.84 ppm to δ = 4.37-4.47 ppm in the ^{1}H-NMR specta and from δ = 66.6 ppm to δ = 71.4 ppm in the ^{13}C-NMR spectra. Low resolution MS found the [M + Na]$^+$ ion of **60** at 338.1 m/z. Data obtained for this compound matched that reported in the literature.[335]

The subsequent step attempted to convert **60** to **61** (Scheme 78).

60 → **61**
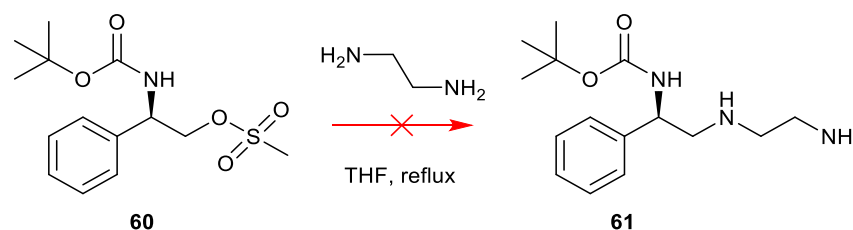
Scheme 78. Synthesis of (*R*)-*tert*-butyl-(2-((2-aminoethyl)amino)-1-phenylethyl)carbamate.

It was challenging to confirm whether the reaction had been successful in the crude ^{1}H-NMR spectrum but the Boc group was still present at δ = 1.43 ppm, which seemed promising. Also, two triplets were observed at δ = 2.63 ppm and δ = 2.73 ppm, however, it was unclear as to whether these were corresponding to ethylenediamine or anticipated product **61**. With regret, the product decomposed during purification on alumina. The route was therefore terminated, and a third route proposed (Scheme 79).
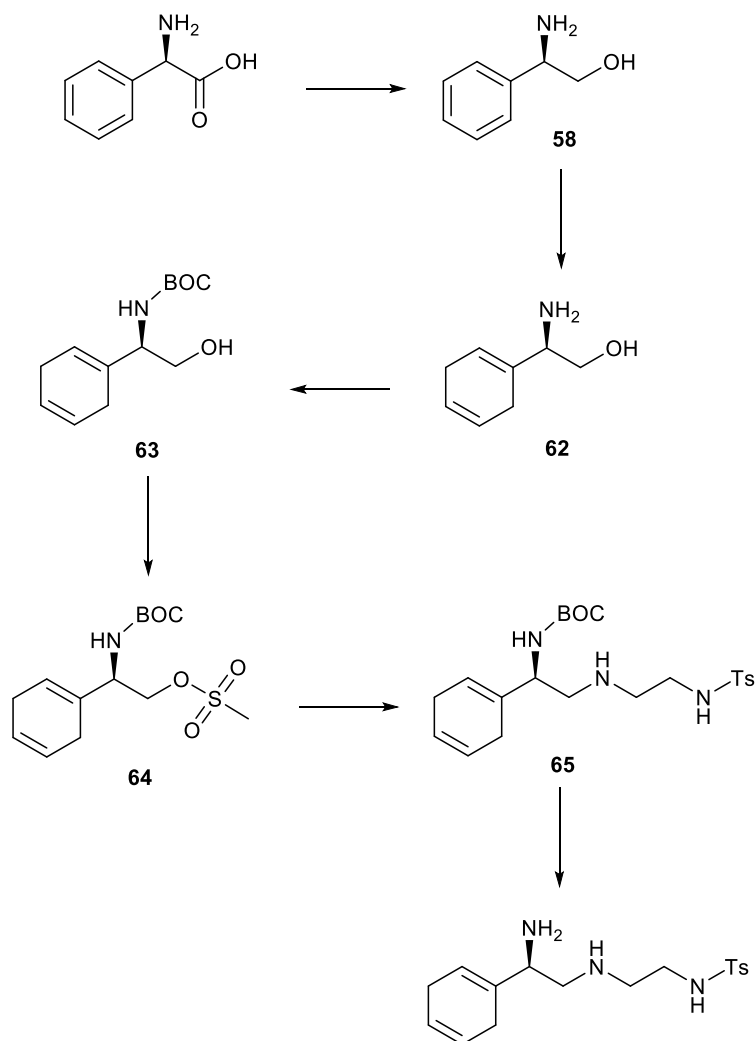
Scheme 79. Global scheme of the third solid supported route proposed.

To begin with, (*R*)-2-amino-2-phenylacetic acid hydrochloride was reduced using LiAlH$_4$ to yield **58**. The ^{1}H-NMR spectrum matched the data obtained earlier, which was in agreement with literature[333], and therefore further analysis was unnecessary.

Next, **58** was subjected to a Birch reduction to produce **62** in 74 % (Scheme 80).
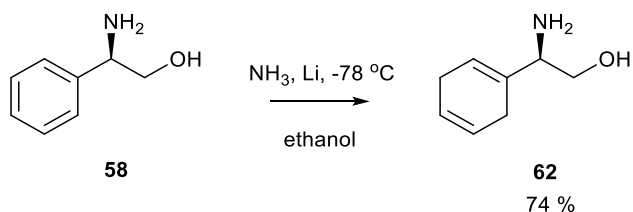
Scheme 80. Synthesis of (*R*)-2-amino-2-(cyclohexa-1,4-dien-1-yl)ethan-1-ol.

The diene ring was observed in the ^{1}H-NMR spectrum with the two CH_2 groups at δ = 2.53-2.75 ppm and the diene protons at δ = 5.68-5.74 ppm, which were also found in the ^{13}C-NMR spectrum at δ = 26.4 ppm and δ = 26.6 ppm for the CH_2 groups, and at δ = 120.1 ppm, δ = 124.0 ppm and δ = 124.3 ppm for the diene moieties. The loss of the aromatic protons at δ = 7.26-7.38 ppm in the ^{1}H-NMR spectrum and δ = 128.7 ppm in the ^{13}C-NMR spectrum was evidence of complete reduction of the aromatic ring. Additionally, in the ^{13}C-NMR spectrum the quaternary carbon of the ring shifted from δ = 142.6 ppm in the starting material **58** to δ = 135.8 ppm in the product **62**. Low resolution MS confirmed the product as the [M + H]$^+$ ion at 140.1 m/z. All data collected was in agreement with that found in the literature.[336]

Subsequent protection of **62** with Boc produced **63** in 47 % yield (Scheme 81).
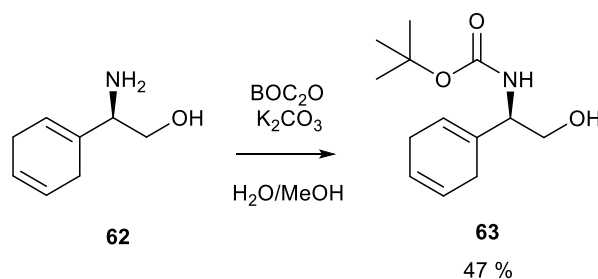
Scheme 81. Synthesis of (*R*)-*tert*-butyl (1-(cyclohexa-1,4-dien-1-yl)-2-hydroxyethyl)carbamate.

The stereocentre proton shifted from δ = 3.32-3.35 ppm to δ = 4.06 ppm in the ^{1}H-NMR spectra. A singlet for the Boc protons was seen at δ = 1.45 ppm, with the carbon environment corresponding to these three CH_3 environments at δ = 28.5 ppm in the ^{13}C-NMR spectrum. The quaternary carbon of the Boc group was at δ = 79.9 ppm and the carbonyl moiety at δ = 156.3 ppm. The [M + Na]$^+$ ion was found in the high resolution MS at 262.1414 m/z.

63 was reacted with methanesulfonyl chloride to form **64** in 97 % yield (Scheme 82).
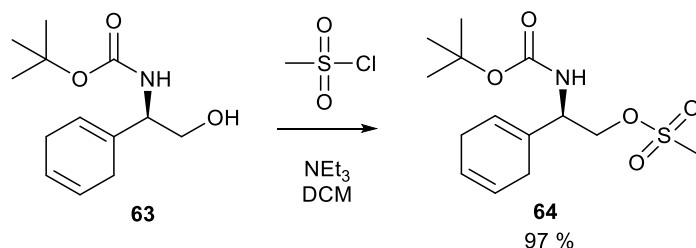
Scheme 82. Synthesis of (*R*)-2-((*tert*-butoxycarbonyl)amino)-2-(cyclohexa-1,4-dien-1-yl)ethyl methanesulfonate.

Evidence of the success of this reaction was seen by the disappearance of the OH peak in the ^{1}H-NMR spectrum at δ = 4.97-4.99 ppm, in addition to the appearance of the mesylate CH$_3$ at δ = 2.99-3.03 ppm in the ^{1}H-NMR spectrum and at δ = 37.7 ppm in the ^{13}C-NMR spectrum. Furthermore, a shift downfield was observed for both the stereocentre, from δ = 4.06 ppm to δ = 4.88 ppm, and the CH$_2$ adjacent to the stereocentre, from δ = 3.69-3.70 ppm to δ = 4.29-4.31 ppm, as a result of deshielding. Described further, this was due to the decrease in electron density at the nuclei because of the larger electron withdrawing nature of the mesylate moiety in comparison to the alcohol moiety in the starting material. Finally, the [M + Na]$^+$ ion was observed at 340.1192 m/z in the high resolution mass spectrum.

64 was then reacted with linker **1** in the hope to obtain **65** (Scheme 83).
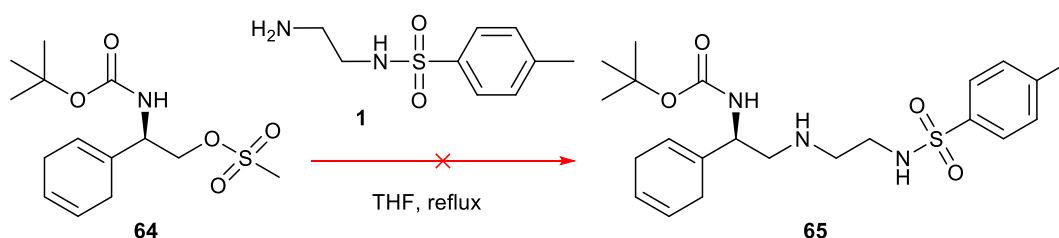
Scheme 83. Synthesis of (*R*)-*tert*-butyl (1-(cyclohexa-1,4-dien-1-yl)-2-((2-((4-methylphenyl)sulfonamido)ethyl)amino)ethyl)carbamate.

Unfortunately, the reaction proved stubborn requiring multiple attempts with varying conditions: anhydrous THF at 50 °C, ethanol at 50 °C, ethanol at room temperature and DCM at room temperature. Despite attempting differing conditions, all methods gave the same product, which was not the anticipated one. After purification by column chromatography to remove excess linker, the ^{1}H-NMR spectrum indicated two products were present: a cyclic carbamate and a ditosylated linker (Figure 138).
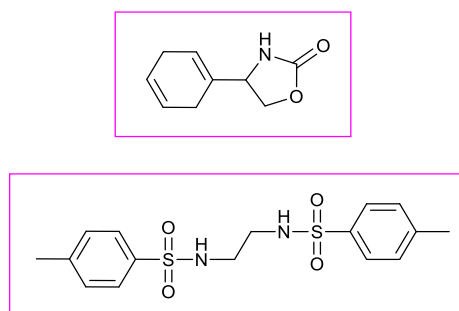
Figure 138. Structures of the products suspected to have formed for the reaction of **64** and **1**.

Utilising 2D NMR experiments allowed for complete assignments of both the ^{1}H-NMR and ^{13}C-NMR spectra for both the Birch reduced cyclic carbamate and the ditosylated linker. The cyclic carbamate and ditosylated linker appeared to be present in a ratio of 2:1, with the ditosylated linker environments overlapping due to the symmetry of the molecule. The ditosylated linker had similar shifts to linker **1**, but only showed one CH_2 environment which confirmed ditosylation had occurred during the reaction. Further, the ^{1}H-NMR and ^{13}C-NMR spectra for the ditosylated linker matched that found in the literature.[337] It was suspected that intramolecular cyclisation occurred due to the oxygen from the Boc group acting as a nucleophile. From this, it can be explained that the Boc group was no longer present, which was confirmed by the NMR spectra, x-ray diffraction data and MS. The distinctive environments of the stereocentre and CH_2 group of the cyclic carbamate were found at δ = 4.11-4.14 ppm, δ = 4.34-4.38 ppm and δ = 4.49-4.53 ppm. This was in agreement with a literature precedent.[338] Interestingly, the cyclic carbamate was present with the Birch reduced ring still intact, with the diene protons found at δ = 5.67-5.76 ppm in the ^{1}H-NMR spectrum. Crystals grew from the NMR sample and hence were analysed by x-ray diffraction. Two structures were obtained and have been shown in Figure 139.
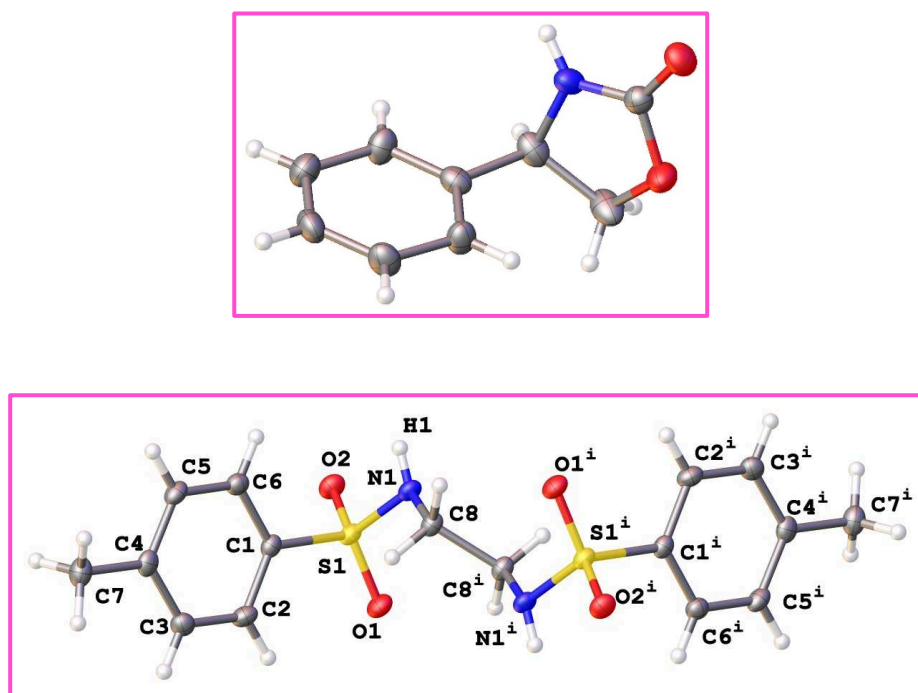
Figure 139. Structures obtained upon crystallising the NMR sample from the reaction between **64** and **1**.

Oddly, the diene had converted to the aromatic analogue upon crystallisation. It remains inconclusive as to why this occurred. Despite this, low resolution MS showed the [M + Na]⁺ ion for both the Birch reduced cyclic carbamate and the ditosylated linker at 188.1 and 391.1 m/z respectively.

Due to time restraints, the final two routes were carried out simultaneously on test scales, meaning that only raw data was collected. The idea was to approach **67** from two different angles in order to increase the chances of reaching the final target ligand. **67** would then be coupled to a linker, which would be attached to a solid support and then reacted with ruthenium to create a metal complex comprising of a bidentate chelating ligand.

One route (Scheme 84) followed the reaction pathway that utilised the azide ion to create a reactive intermediate **66** that could then be reduced to the corresponding amine **67**.
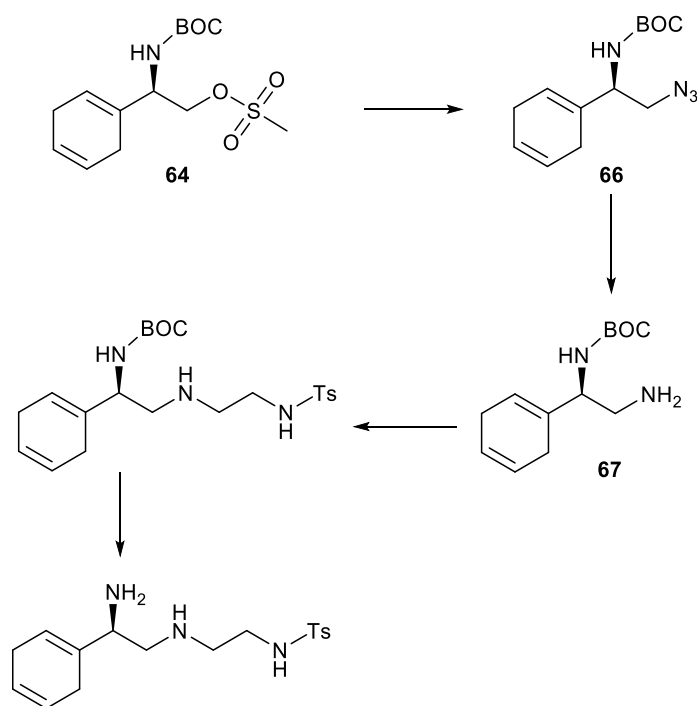
Scheme 84. Global scheme of the fourth solid supported route proposed.

Conversion of **64** (synthesised in previous route – Scheme **82**) to **66** (Scheme 85) required only a short heating period in DMF, with the azide being confirmed by ¹H-NMR, ¹³C-NMR, IR and high resolution MS. This reaction was carried out on a test scale with no further purification or calculation of yield due to the preliminary experimental nature of this route.
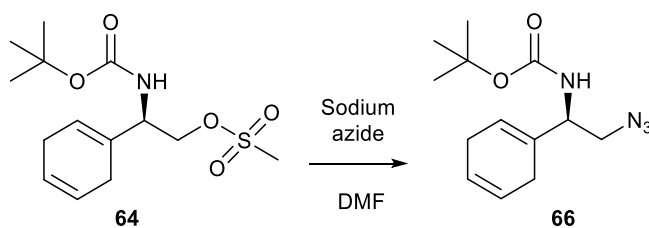
Scheme 85. Synthesis of (*R*)-*tert*-butyl (2-azido-1-(cyclohexa-1,4-dien-1-yl)ethyl)carbamate.

The ^{1}H-NMR spectrum showed the loss of the mesylate CH_3 peak at δ = 2.99-3.03 ppm and at δ = 37.7 ppm in the ^{13}C-NMR spectrum. The stereocentre shifted from δ = 4.88 ppm to δ = 4.11-5.10 ppm, plus the CH_2 shifted from δ = 4.29-4.31 ppm to δ = 3.42-3.51 ppm. Despite this, the integration of the Boc group decreased to 7H, suggesting slight removal or decomposition of the Boc group under the conditions of this reaction. The ^{13}C-NMR spectrum allowed for assignments to each differing environment, however, peaks were also observed of identical chemical shifts to that found in the ^{13}C-NMR spectrum of the starting mesylate, in particular that of the Birch reduced ring, suggesting unreacted starting material. Of particular interest was the shift of the CH_2 adjacent to the functional group moiety, from δ = 69.6 ppm in the starting material **64** to δ = 53.2 ppm in the product **66**. IR indicated successful installation of the azide moiety due to the appearance of a band at 2099.02 cm^{-1} that was not present in the IR spectrum of **64**. To confirm that the band observed was not residual NaN_3, the IR sample of the azide product was spiked with NaN_3 and two overlapping bands were observed; 2099.02 cm^{-1} for **66** and 2040.29 cm^{-1} for NaN_3. Finally, **66** was found as the [M + Na]$^+$ ion at 287.1499 m/z in both the low and high resolution spectra. A fragment in the low resolution spectrum at 188.1 m/z was consistent with the loss of the C_4H_9O fragment of the Boc group, confirming the loss of Boc can occur with ease.

Following this, **66** was reduced using LiAlH$_4$ to obtain **67** (Scheme 86).
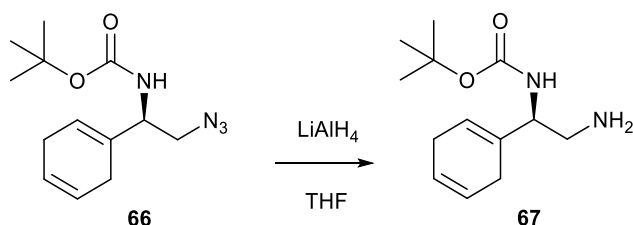
Scheme 86. Synthesis of (*R*)-*tert*-butyl (2-amino-1-(cyclohexa-1,4-dien-1-yl)ethyl)carbamate.

Purification by column chromatography was attempted and although improved purity was observed by TLC, minimal difference was observed in the ^{1}H-NMR spectrum. **67** eluted in DCM/MeOH (1 % MeOH) gave an R_f = 0.11, coupled with slight staining by ninhydrin. Other impurities were also seen on the TLC plate and would need to be removed by an additional column if this route was chosen to be pursued and repeated. Due to the route being preliminary, a yield was not calculated. The ^{1}H-NMR spectrum was complex and though rough assignments could be made, the data obtained in the ^{13}C-NMR and 2D NMR spectra provided peaks for all environments except for the Boc group. Impurities were also observed in the aromatic region of the ^{1}H-NMR spectrum, which could not be attributed to the desired product, instead it may have been as a result of rearomatisation of the diene ring. Of particular interest was the shift of the CH_2 group adjacent to the amine moiety in the ^{13}C-NMR spectrum from δ = 53.2 ppm in the starting material **66** to δ = 69.0 ppm in the product **67**. Though it was possible that the peak attributed to the Boc group may have been present in the ^{1}H-NMR spectrum, with significant further decrease of integration to 2H under the impurity at δ = 1.36-1.51 ppm, the most likely explanation was complete loss of the Boc group. Further support of this was the appearance of the free amine protons at δ = 3.78 ppm and δ = 3.63 ppm and the absence of the Boc group in the ^{13}C-NMR spectrum. This matched the evidence found in the low resolution MS, whereby the peak of highest abundance at 188.1 m/z corresponded to loss of part of the Boc group (C_4H_9O). Moreover, low resolution MS confirmed **67** both as the [M + Na]$^+$ ion at 262.2 m/z and as the [M + H]$^+$ ion at 239.2 m/z, with high resolution observing the [M + H]$^+$ ion at 239.1753 m/z too. IR data collected indicated that the reaction to form **67** was complete due to the loss of the band at 2099.02 cm^{-1} observed in the IR spectrum of **66**. Therefore, it appeared that although the LiAlH$_4$ successfully reduced the azide group, this reagent was too strong a reducing agent for the Boc group to withstand, hence this route was terminated.

The alternative route (Scheme 87) of this project mimics the Gabriel synthesis, whereby a primary alkyl halide is transformed into a primary amine using potassium phthalimide followed by hydrazine hydrate. Instead, in this pathway, the transformation would occur from **64** (synthesised previously – see Scheme 82).
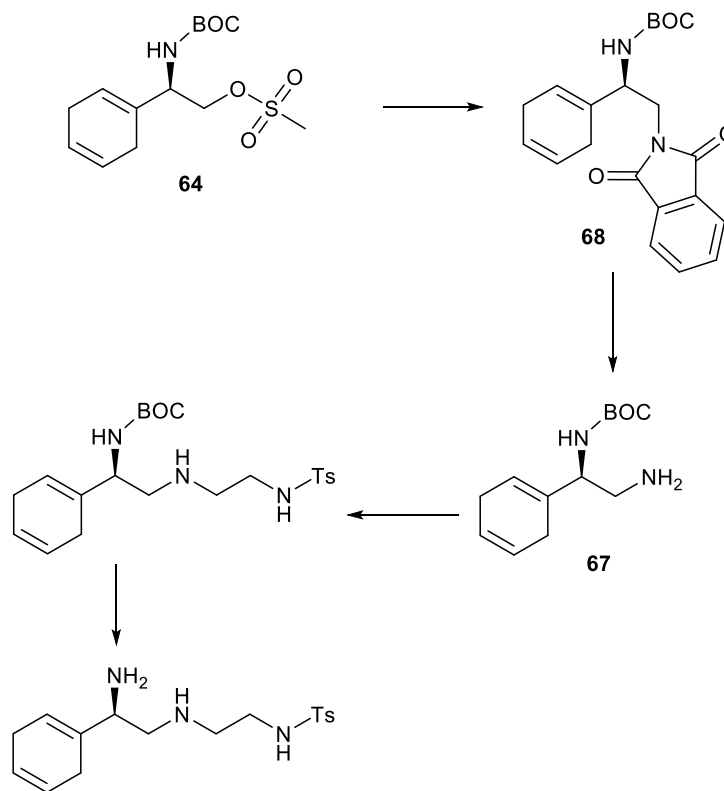
Scheme 87. Global scheme of the fifth solid supported route proposed.

This route was chosen as a result of the milder conditions it would employ in comparison to the previous route that used LiAlH$_4$, which caused drastic reduction of the Boc group. The first step (Scheme 88) successfully produced the phthalimide derivative **68**. This reaction was carried out on a test scale with no further purification or calculation of yield due to the preliminary experimental nature of this route.
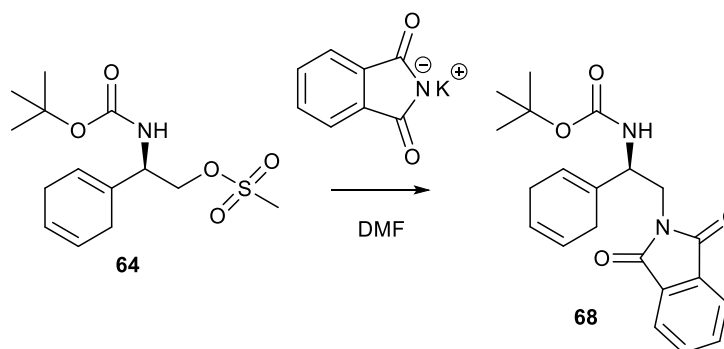
Scheme 88. Synthesis of (*R*)-*tert*-butyl-(1-(cyclohexa-1,4-dien-1-yl)-2-(1,3-dioxoisoindolin-2-yl)ethyl)carbamate.

The ^{1}H-NMR spectrum showed the presence of the phthalimide group, but not with a 3:4 ratio of diene protons to aromatic protons from the phthalimide ring, suggesting incomplete addition of the phthalimide group. The integration of the Boc group decreased to 5H, suggesting slight removal or decomposition of the Boc group under the conditions included in this reaction. Despite this, the stereocentre shifted from δ = 4.88 ppm in the starting material **64** and the CH$_2$ group adjacent to the stereocentre shifted from δ = 4.29-4.31 ppm in the starting material **64** to overlap with one another at δ = 3.70-4.53 ppm in the product **68**. The ^{13}C-NMR spectrum was difficult to assign with the 2D NMR experiments presenting unsuccessful bar the DEPT experiment which was very useful. Therefore most assignments were based on previous analogues, whilst the phthalimide moiety was compared to the ^{1}H-NMR and ^{13}C-NMR spectra of phthalimide in a literature precedent.[339] The product was confirmed as the [M + Na]$^+$ ion at 391.1633 m/z in both the low and high resolution MS. In addition to the anticipated product, a side product (Figure 140) formed by loss of the Boc group followed by cyclisation.
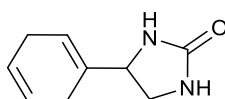
Figure 140. Structure of the side product suspected to be present during the formation of

68.

The side product was only detected in the low resolution MS, therefore it is inconclusive as to whether the mechanism occurred during the reaction or just during MS analysis.

The second step (Scheme 89) of the Gabriel synthesis yielded **67**. This reaction was carried out on a test scale with no further purification or calculation of yield due to the preliminary experimental nature of this route.
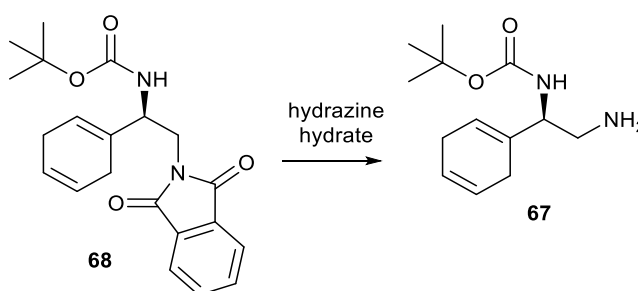
Scheme 89. Synthesis of (*R*)-*tert*-butyl (2-amino-1-(cyclohexa-1,4-dien-1-yl)ethyl)carbamate.

Analysis by TLC showed **67** at R_f = 0.11 when eluted in DCM/MeOH (1 % MeOH), with strong staining by ninhydrin confirming the primary amine was present. Additional impurities were also observed by TLC, which would require removal by column chromatography if this route was chosen to be pursued and repeated.

The peak corresponding to the Boc group integrated to 12H in the ^{1}H-NMR spectrum, which suggested that there were two different species present in this reaction sample due to the spectrum of the previous step displaying an integration of 7H. The anticipated product **67** displayed the stereocentre and CH_2 group at δ = 3.88-5.07 ppm in the ^{1}H-NMR spectrum, which overlapped with the side product obtained from this reaction. In addition to the main product, the side product was also observed in the ^{13}C-NMR spectrum, whereby the two species were observed with similar shifts for each individual environment, and in the low resolution MS, whereby a peak was found at 185.1 m/z predicted to be the sodium adduct of the cyclised side product, suggesting the mechanism was occurring during the reaction as opposed to in the analysis stages. The side product was the same cyclised compound observed for the previous step (Figure 140), which closely matched the data found for the cyclic carbamate formed when attempting the synthesis of **65** (Scheme **83**). Following on from this, it would have been of interest to separate the desired product from the cyclised side product by column chromatography. Unfortunately time limitations prevented purification from being carried out.

All shifts matched **67** previously synthesised (Scheme **86**), with the presence of the Boc group for this attempt, suggesting that this methodology was more effective in obtaining **67** provided further purification was successful. Confirmation that the Boc group was still attached was the absence of free amine protons that were found for the previous route to obtain **67**. Moreover, the [M + H]$^+$ was observed in both the low and high resolution MS at 239.1758 m/z, indicating that the Boc group remained attached during analysis.

The final two routes; via the azide and via the phthalimide, successfully produced **67**. However, both routes encountered problems respectively and hence the pros and cons would require weighing up before choosing to repeat one of the routes on a larger scale.

The azide route (Scheme 84) produced **66** and **67** successfully with full characterisation. Unfortunately, during the LiAlH$_4$ reduction, the Boc protecting group was completely cleaved off due to the harsh forcing conditions. Overall, it was therefore possible that the reaction conditions were not optimum and therefore a milder reducing step should be employed if this route was repeated. The route would also be hazardous to scale and thermally unstable.

The Gabriel synthesis (Scheme 87) offered milder conditions to form **67**, displacing **64** with a phthalimide protecting group as an intermediate step. This phthalimide route was successful, however, it was suspected that the reactions did not reach completion and hence excess starting material remained. Moreover, a cyclised side product formed simultaneously during the reaction. To combat these issues, the reactions could either be left for longer, the temperature could be increased or separation by column chromatography would allow for pure product to be obtained. The scale up of this route seems more viable in producing the pure desired product **67**, including the fact that the phthalimide is less polar and so would extract better into the organic layer during work-up. All data obtained for **67** pointed towards success, despite a side product forming too.

4.2 Conclusions

In conclusion, the two final routes proposed simultaneously showed great promise. Preliminary experiments on test scales meant that no final yields were obtained and data collected was raw, purely to indicate whether the reactions showed promise. After attempting both routes, comparison of the data for **67** was carried out to gain more confidence in the success of synthesising the desired amine. Overall, the TLC evidence for the amine matched in both routes, as did the ^{1}H-NMR, ^{13}C-NMR and MS analysis. The only minor difference was the degree of the loss of the Boc group, which would be removed in the later stages of the reaction pathway anyway. It can therefore be concluded that both routes would allow the target amine **67** to be reached.

Overall, multiple synthetic pathways were attempted to anchor a chiral ligand onto a solid support. Regrettably, aims of this chapter remain unmet, with no immobilisation attempted. Further work to achieve the aims set out at the beginning of this chapter was not able to be performed due to the time period of the project ending. Despite this, two routes employed during this project showed great promise, hence allowing for the desired ligand to be achieved prior to immobilisation, and therefore have been discussed in section 4.3.

4.3 Future work

If the project comprised of more time, it would have been of interest to repeat the phthalimide route. The subsequent steps following the formation of **67** have been performed previously on very similar analogues by Dr Murray's research group, in particular the route towards the complex **7** in Chapter 2, therefore there is confidence in the final chelating ligand being successfully targeted. A change in the choice of protecting group may be of interest as it

remains possible that intramolecular cyclisation was occurring with the Boc protecting group. As an alternative, the use of the protecting group benzyloxycarbonyl (Cbz) may be wise as this group would not fragment via formation of the relatively stable ^{t}Bu carbocation, preventing cyclisation from occurring. It may also be interesting to repeat the azide route but to pursue the route with an alternative protecting group due to that being the reason for the failure of the current attempt. One example would be to use Fmoc[340] as the removal by 20 % piperidine[341] provides milder conditions, avoiding the use of TFA, which was anticipated to cause issues with the diene ring and amine moieties of the target chelating ligand.

Unfortunately, no final target chiral ligand was reached and hence none of the anticipated solid supports were attached. In turn, this meant that no ATH was performed and so it remains unclear as to whether the inclusion of a solid support to these catalyst frameworks would have heightened activity or selectivity. If the final catalyst is therefore synthesised, ATH could be run in both FA/TEA azeotrope, to allow for direct comparison to untethered analogues described in Chapter 2, and in water to investigate the more sustainable and recyclable approach anticipated for solid supported catalysts[44,45,51,67,90,137]. By using water as the solvent, the ATH could be performed with FA/TEA in addition[45,67,124,164,272] to help solubilise the catalyst and act as the hydrogen source, or with sodium formate as the hydrogen donor due to its success in increasing the rate of reaction[44,50,53,67,137,155,272].

Although no investigations towards the ATH of acetophenone were carried out, this project was productive in taking great strides towards accessing new structures that could be explored as tools to identify targets of chiral organometallic frameworks. The idea would be that the chiral complexes could be tethered to solid supports before being exposed to cell lysate. The biomacromolecules which bind could then be eluted with a suitable buffer and analysed by mass spectrometry, in particular fragmentation studies. This would identify the targets of the complex, inclusive of binding sites, and may even allow for the development of metal-based chemotherapeutics to target specific protein or DNA/RNA targets. Particularly of interest would be the impact of metal-centred chirality on this process. Furthermore, target selectivity could be probed via this methodology.

Overall, there is still potential for advances to be made in this area of chemistry and this project has enabled confidence in new routes to create novel chiral solid supported catalysts. With additional research, there is promise that the target complexes anticipated here can be obtained and tested for their ATH activity and selectivity, in addition to their biological activity within cells.

Chapter 5

Experimental

5.1 Materials and methods

All commercially purchased materials were used as received. It was assumed that all solvents were not anhydrous and all analysis conducted at room temperature (21 °C), unless stated otherwise. Schlenk-lines were used under a nitrogen atmosphere for reactions that required anhydrous conditions, plus glassware was oven-dried. Liquids greater than 20 mL were added or moved by cannula transfer.

^1H and ^{13}C-NMR spectra were recorded on a JEOL ECZ 400S spectrometer (^1H at 400.2 MHz, ^{13}C at 100.6 MHz) at 295 K unless stated otherwise. Spectra are referenced internally relative to the solvent used (D_2O: ^1H δ 4.79 ppm, ^{13}C δ unreferenced; DMSO-d^6: ^1H δ = 2.50 ppm, ^{13}C δ = 39.52 ppm; CDCl$_3$: ^1H δ = 7.26 ppm, ^{13}C δ = 77.16 ppm).

Mass spectra were recorded at the University of Hull using a Bruker Maxis Impact QqTOF MSMS. Calibration of the instrument against sodium formate over the range 90 to 1550 Da was conducted before mass measurement. Resolution used was typically 45000. Unless stated otherwise, samples were prepared as solutions in methanol (10^{-5} M), these were injected into the solvent stream from a syringe pump at 3 µL min^{-1} via a 5 µL loop injector. The data was then internally mass measured against an internal calibrant peak from hexakis(1H,1H,4H-hexafluorobutyloxy)phosphazine (CAS No. 186406-47-2) $C_{24}H_{18}O_6N_3P_3F_{36}$ m/z 1220.99064. An average result from 3-5 separate injections is quoted. The mass was measured and calculated using Bruker DataAnalysis 4.2 software.

HPLC analysis was performed with a Varian Prostar gradient high performance/pressure liquid chromatography system, comprised of two reservoirs, two pumps (Varian Prostar, 10 mL pump head), a two-position rheodyne valve, an autosampler (model 410), a chromatography column and an ultra-violet/visible detector (Varian Prostar with deuterium lamp). HPLC chiral column: Phenomenex Lux 3 µm AMP, 150 mm x 4.6 mm. Method A: flow rate = 1 mL/min, wavelength (λ) = 230 nm, injection volume = 20 µL, isocratic gradient = 50 %: 50 % (aqueous ammonium formate pH 3.20:methanol). Method B: flow rate = 1 mL/min, wavelength (λ) = 230 nm, injection volume = 20 µL, isocratic gradient = 60 %: 40 % (aqueous ammonium bicarbonate pH 10.50:acetonitrile). Method C: flow rate = 0.2 mL/min, wavelength (λ) = 210 nm, injection volume = 10 µL, isocratic gradient = 35 %: 65 % (aqueous ammonium bicarbonate pH 11:methanol).

GC analysis was recorded with a Varian 430 GC-FID system, comprising of an autosampler, column oven and flame ionisation detector. GC chiral column: Restek RT-βDEXsm, 30 m x 0.25 mm x 0.25 μm. Method D: flow rate = 2.0 mL/min, start temperature = 60 °C, end temperature = 177 °C, rate of temperature ramp = 5 °C/min. Method E: flow rate = 2.0 mL/min, start temperature = 100 °C, end temperature = 100 °C, rate of temperature ramp = 0 °C/min.

Experimental X-ray single crystal diffraction data were collected using a Stoe IPDS2 image plate diffractometer operating with Mo radiation. Crystals were covered in a thin film of perfluoropolyether oil and mounted on a Mitogen© loop and held at 150 K using an Oxford Cryosystems nitrogen gas cryostream. Data were scaled and merged and treated for the effects of absorption using standard methods. Crystal structures were solved using dual space methods implemented within SHELXT. and refined using SHELXL-2018/3 implemented with Olex2. Non-hydrogen atoms were located using difference Fourier methods and refined using anisotropic displacement parameters. Hydrogen atoms were placed at geometrically calculated positions using a riding model.

5.2 Synthetic procedures

N-(2-Aminoethyl)-4-methylbenzenesulfonamide[289,290,342] **(1)**
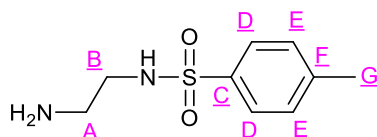
p-Toluenesulfonylchloride (6.00 g, 0.03 mol, 1 eq.) in DCM (75 mL) was added dropwise to a stirred solution of ethylenediamine (20 mL, 0.30 mol, 10 eq.) in DCM (75 mL) at 0 °C under N_2. During addition, white clouds formed and a brown oil-like precipitate was observed. The resulting mixture was stirred for a further 30 minutes before washing with H_2O (2 x 30 mL). The organic layer was dried with Na_2SO_4, then filtered. The solvent was removed under reduced pressure and the product dried further on a vacuum line to afford a white solid (5.74 g, 26.79 mmol, 89 %). ^{1}H-NMR (CDCl$_3$, 400 MHz): δ = 7.74 (d, 2H, *J* = 8.25 Hz, H$_D$) , 7.30 (d, 2H, *J* = 8.48 Hz, H$_E$), 2.95 (t, 2H, *J* = 5.62 Hz, H$_B$), 2.78 (t, 2H, *J* = 5.62 Hz, H$_A$), 2.41 (s, 3H, H$_G$); ^{13}C{^{1}H}-NMR (CDCl$_3$, 400 MHz): δ = 143.4 (1C, C$_C$), 137.0 (1C, C$_F$), 130.0 (2C, C$_E$), 127.1 (2C, C$_D$), 45.4 (1C, C$_B$), 41.0 (1C, C$_A$), 21.6 (1C, C$_G$) ppm; LRMS (ESI$^+$): m/z found 215.0 [M + H]$^+$; C$_9$H$_{15}$N$_2$O$_2$S [M + H]$^+$ requires 215.3 m/z; **1** (C$_9$H$_{14}$N$_2$O$_2$S; 214.3 g/mol).

(*R*)-2-(Cyclohexa-1,4-dien-1-yl)propanoic acid (2a)
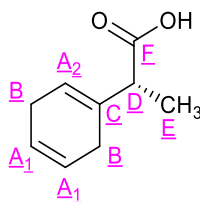
A solution of (*R*)-2-phenylpropanoic acid (4.50 g, 29.97 mmol, 1 eq.) in ethanol (50 mL) was added to liquid NH_3 (1 L) at -77 °C. Lithium wire (6.52 g, 0.94 mol, 31 eq.) was washed in hexane before addition in 0.50 g portions until a dark blue colour persisted. The reaction was left to stand overnight to leave a white solid. H_2O (1 L) was added whilst stirring at 0 °C, followed by addition of $HCl_{(aq)}$ (12 M, 78 mL) to acidify the solution. The cloudy suspension was extracted with Et_2O (3 x 100 mL), the organic layers combined, dried with Na_2SO_4 and then filtered. The solvent was removed under reduced pressure and the product was dried further on a vacuum line as a yellow oil (4.21 g, 27.66 mmol, 92 %). ^{1}H-NMR ($CDCl_3$, 400 MHz): δ = 5.62-5.73 (m, 3H, H_{A1} + H_{A2}), 3.06-3.14 (m, 1H, H_D), 2.61-2.79 (m, 4H, H_B), 1.29 (d, 3H, *J* = 7.11 Hz, H_E) ppm; ^{13}C{^{1}H}-NMR ($CDCl_3$, 400 MHz): δ = 181.3 (1C, C_F), 133.2 (1C, C_C), 124.1 (1C, C_{A1}), 123.9 (1C, C_{A1}), 121.9 (1C, C_{A2}), 46.6 (1C, C_D), 27.1 (1C, C_B), 26.9 (1C, C_B), 15.3 (1C, C_E) ppm; HRMS (ESI$^-$) m/z found 151.0764 [M - H]$^-$; $C_9H_{11}O_2$ [M - H]$^-$ requires 151.0765; LRMS (EI$^+$): m/z found 153.3 [M + H]$^+$ (5 %), 152.3 [M]$^+$ (25 %), 107.3 [M - CHO_2]$^+$ (100 %); $C_9H_{13}O_2$ [M + H]$^+$ requires 153.2; **2a** ($C_9H_{12}O_2$; 152.1904 g/mol); Enantiopurity confirmed by chiral HPLC using method A.

(*R*)-2-(Cyclohexa-1,4-dien-1-yl)-*N*-(2-((4-methylphenyl)sulfonamido)ethyl)propenamide (3a)
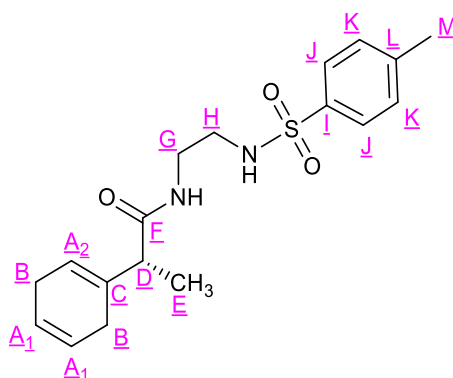
(*R*)-2-(Cyclohexa-1,4-dien-1-yl)propanoic acid (2.22 g, 14.59 mmol, 1 eq.), HOBt.xH$_2$O (1.97 g, 14.59 mmol, 1 eq.) and TBTU (5.63 g, 17.50 mmol, 1.2 eq.) were dissolved in DMF (20 mL), DCM (20 mL) and DIPEA (5.10 mL, 29.30 mmol, 2 eq.). The solution was left to stir for 10 minutes before *N*-(2-aminoethyl)-4-methylbenzenesulfonamide (3.18 g, 14.59 mmol, 1 eq.) was added and the resulting yellow solution was left to stir overnight. Following this, the product solution was pipetted into a separating funnel containing HCl$_{(aq)}$ (1 M, 100 mL) and extracted with DCM (3 x 50 mL). The organic layers were combined and washed with H$_2$O (100 mL). The organic layer was dried with Na$_2$SO$_4$ and filtered, then the solvent was removed under reduced pressure. The yellow/orange oil was dissolved in Et$_2$O (50 mL) and washed with H$_2$O (8 x 50 mL) to remove DMF residues. The organic layer was dried with Na$_2$SO$_4$, filtered and the solvent removed under reduced pressure to yield an orange oil. The oil was purified by column chromatography on silica gel with a solvent system of DCM/MeOH (0-3 % MeOH) to yield the product as a white solid (4.33 g, 12.43 mmol, 85 %). ^{1}H-NMR (CDCl$_3$, 400 MHz): δ = 7.72 (d, 2 H, *J* = 8.46 Hz, H$_J$), 7.30 (d, 2H, *J* = 8.23 Hz, H$_K$), 6.26 (br. s, 1H, <u>NH</u>-C=O), 5.69 (s, 2H, H$_{A1}$), 5.65 (s, 1H, H$_{A2}$), 3.26-3.40 (m, 2H, H$_G$), 3.04 (t, 2H, *J* = 5.61 Hz, H$_H$), 2.92 (q, 1H, *J* = 7.32 Hz, H$_D$), 2.44-2.76 (m, 4H, H$_B$), 2.42 (s, 3H, H$_M$), 1.24 (d, 3H, *J* = 7.32 Hz, H$_E$) ppm; ^{13}C{^{1}H}-NMR (CDCl$_3$, 400 MHz): δ = 175.4 (1C, C$_F$), 143.6 (1C, C$_I$), 136.8 (1C, C$_L$), 134.8 (1C, C$_C$), 129.9 (2C, C$_K$), 127.1 (2C, C$_J$), 124.1 (1C, C$_{A1}$), 124.0 (1C, C$_{A1}$), 122.2 (1C, C$_{A2}$), 48.3 (1C, C$_D$), 43.5 (1C, C$_H$), 39.4 (1C, C$_G$), 26.9 (2C, C$_B$), 21.7 (1C, C$_M$), 15.1 (1C, C$_E$) ppm; HRMS (ESI$^+$) m/z found 349.1584 [M + H]$^+$; C$_{18}$H$_{25}$N$_2$O$_3$S [M + H]$^+$ requires 349.1580; **3a** (C$_{18}$H$_{24}$N$_2$O$_3$S; 348.4598 g/mol); Enantiopurity confirmed by chiral HPLC using method B.

(*R*)-*N*-(2-((2-(Cyclohexa-1,4-dien-1-yl)propyl)amino)ethyl)-4-methylbenzenesulfonamide (4a)
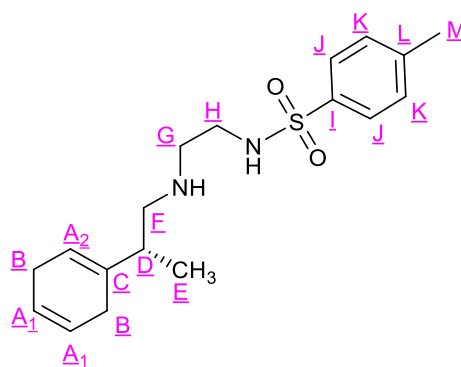
(*R*)-2-(Cyclohexa-1,4-dien-1-yl)-*N*-(2-((4-methylphenyl)sulfonamido)ethyl)propanamide (4.20 g, 12.05 mmol) was dissolved in anhydrous THF (50 mL) and added dropwise to a suspension of $LiAlH_4$ (0.95 g, 30.13 mmol, 2.50 eq.) in anhydrous THF (50 mL) under N_2. The reaction was heated at reflux overnight. The reaction was allowed to cool to room temperature, quenched with $NaHCO_3$ (50 mL), to give a biphasic mixture, which was then filtered. The sticky solid left behind in the flask was washed with Et_2O (40 mL). The combined organic phases were concentrated under reduced pressure to a volume of approximately 20 mL. Et_2O (40 mL) was added and the organic solution was extracted with H_2O (10 mL). The aqueous layer was washed with Et_2O (2 x 30 mL) and the organic layers combined, dried with Na_2SO_4 then filtered. The solvent was removed under reduced pressure to obtain an orange oil. To remove any residual THF, the oil was dissolved in DCM (5 mL) then the solvent was removed under reduced pressure. This process was repeated twice. The product was dried further on a vacuum line to yield a yellow oil (3.31 g, 9.90 mmol, 82 %). ^{1}H-NMR ($CDCl_3$, 400 MHz): δ = 7.74 (d, 2H, *J* = 8.46 Hz H_J), 7.30 (d, 2H, *J* = 8.0 Hz, H_K), 5.69 (s, 2H, H_{A1}), 5.45 (s, 1H, H_{A2}), 2.95 (t, 2H, *J* = 5.72 Hz, H_G), 2.65-2.70 (m, 2H, H_H), 2.45-2.71 (m, 4H, H_B), 2.41-2.44 (m, 1H, H_F), 2.42 (m, 3H, H_M), 2.26-2.33 (m, 1H, H_F), 2.15-2.24 (m, 1H, H_D), 0.95 (d, 3H, *J* = 6.86 Hz, H_E) ppm; ^{13}C{^{1}H}-NMR ($CDCl_3$, 400 MHz): δ = 143.4 (1C, C_I), 136.8 (1C, C_L), 136.8 (1C, C_C), 129.7 (2C, C_K), 127.2 (2C, C_J), 124.5 (1C, C_{A1}), 124.2 (1C, C_{A1}), 119.8 (1C, C_{A2}), 52.5 (1C, C_F), 47.7 (1C, C_H), 42.2 (1C, C_G), 41.0 (1C, C_D), 26.8 (1C, C_B), 25.5 (1C, C_B), 21.6 (1C, C_M), 17.3 (1C, C_E) ppm; HRMS (ESI$^+$) m/z found 335.1799 [M + H]$^+$; $C_{18}H_{27}N_2O_2S$ [M + H]$^+$ requires 335.1788; **4a** ($C_{18}H_{26}N_2O_2S$; 334.4762 g/mol); Enantiopurity confirmed by chiral HPLC using method B.

[Ru(η⁶-(*R*)-4-methyl-*N*-(2-((2-phenylpropyl)amino)ethyl)benzenesulfonamide)Cl₂]₂.2HCl (5a)
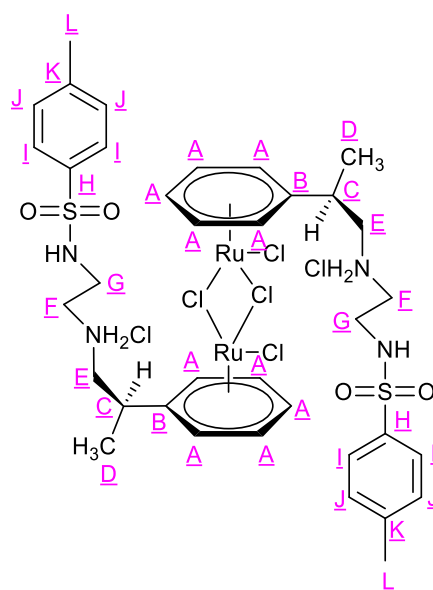
HCl$_{(aq)}$ (12 M, 0.99 mL, 12.02 mmol, 2 eq.) was added to (*R*)-*N*-(2-((2-(cyclohexa-1,4-dien-1-yl)propyl)amino)ethyl)-4-methylbenzenesulfonamide (2.01 g, 6.01 mmol) dissolved in ethanol (32 mL). The solution was stirred for 5-10 minutes and then RuCl₃xH₂O (0.31 g, 1.50 mmol, 0.25 eq.) was added to the stirring solution. The reaction was heated at reflux overnight to yield a red solution. The reaction was allowed to cool to room temperature then approximately half of the solvent was removed under reduced pressure. The solution was then stored in the freezer (-18 °C) for two hours before the solid, which precipitated, was separated from the solution by centrifugation at 10,000 rpm for ten minutes. The solid was washed with Et₂O (15 mL) and separated again by centrifugation before being dried on a vacuum line to yield a brown solid (0.38 g, 0.35 mmol, 23 %). The supernatant contained unreacted diene ligand so was heated at reflux overnight with additional RuCl₃xH₂O (0.31 g, 1.50 mmol, 0.25 eq.). The work up procedure was repeated as per the first batch to yield a brown solid (0.35 g, 0.32 mmol, 21 %). <u>Note:</u> Number of moles and % yields were calculated assuming zero equivalents of H₂O for RuCl₃xH₂O as the extent of hydration was not calculated. ¹H-NMR (DMSO, 400 MHz): δ = 9.28 (br. s, 2H, NH₂Cl), 8.85 (br. s, 2H, NH₂Cl), 8.03 (t, 2H, *J* = 5.50 Hz, 2 x NH), 7.72 (d, 4H, *J* = 8.25 Hz, H$_I$), 7.42 (d, 4H, *J* = 8.02 Hz, H$_J$), 5.97-6.03 (m, 10H, H$_A$), 3.00-3.27 (m, 14H, H$_C$ + H$_E$ + H$_F$ + H$_G$), 2.39 (s, 6H, H$_L$), 1.36 (d, 6H, *J* = 5.73 Hz, H$_D$) ppm; ¹³C{¹H}-NMR (DMSO, 400 MHz): δ = 143.1 (2C, C$_H$), 136.8 (2C, C$_K$), 129.8 (4C, C$_J$), 126.7 (4C, C$_I$), 103.6 (2C, C$_B$), 88.3 (2C, C$_A$), 87.9 (2C, C$_A$), 86.7 (2C, C$_A$),

85.8 (2C, C_A), 85.3 (2C, C_A), 51.6 (2C, C_E), 47.0 (2C, C_G), 38.5 (2C, C_F), 33.6 (2C, C_C), 21.0 (2C, C_L), 17.0 (2C, C_D) ppm; **5a** ($C_{36}H_{50}Cl_6N_4O_4Ru_2S_2$; 1081.7946 g/mol).

Final complex (6a)

[Ru(η^6-(*R*)-4-methyl-*N*-(2-((2-phenylpropyl)amino)ethyl)benzenesulfonamide)Cl$_2$]$_2$.2HCl (0.50 g, 0.46 mmol, 1 eq.) was suspended in DCM (100 mL) then DIPEA (0.32 mL, 1.84 mmol, 4 eq.) was added and the suspension was stirred under N_2. After 1.5 hours, the dark brown solution was reduced to a quarter of its volume under reduced pressure and then purified by column chromatography on silica gel with a solvent system of DCM/MeOH (0-1 % MeOH). Fractions containing the product, which were intensely yellow in colour, were combined. The solvent was removed under reduced pressure and the product was dried further on a vacuum line to afford a light brown solid (0.37 g, 0.79 mmol, 86 %). ^{1}H-NMR (CDCl$_3$, 400 MHz): δ = 7.71-7.76 (m, 4H, H_D), 7.13-7.16 (m, 4H, H_C), 6.69 (t, 1H, *J* = 5.62 Hz, H_L), 6.49 (t, 1H, *J* = 5.50 Hz, H_L), 5.78 (t, 1H, *J* = 5.73 Hz, H_L), 5.73 (t, 1H, *J* = 5.62 Hz, H_L), 5.60 (t, 1H, *J* = 5.62 Hz, H_L), 5.46 (t, 1H, *J* = 5.62 Hz, H_L), 5.28-5.30 (m, 1H, H_L), 5.10-5.14 (m, 2H, H_L), 4.97 (d, 1H, *J* = 5.50 Hz, H_L), 4.51 (br. s, 2H, NH), 3.55-4.00 (m, 4H, H_H), 3.13-3.31 (m, 4H, H_I + $H_{F/G}$), 2.79-2.86 (m, 2H, $H_{F/G}$), 2.47-2.67 (m, 2H, $H_{F/G}$), 2.32-2.33 (m, 6H, H_A), 2.16-2.40 (m, 2H, $H_{F/G}$), 1.43-1.48 (m, 6H, H_J) ppm. <u>Note:</u> ^{1}H-NMR assigned to show the 2 diastereoisomers present in the sample, however, the signals overlap directly due to identical properties; ^{13}C{^{1}H}-NMR (CDCl$_3$, 400 MHz): δ = 140.7 (1C, C_E), 140.5 (1C, C_E), 140.3 (1C, C_B), 140.2 (1C, C_B), 128.9 (1C, C_C), 128.7 (1C, C_C), 127.6 (1C, C_D), 127.4 (1C, C_D), 104.7 (1C, C_K), 104.6 (1C, C_K), 95.1 (1C, C_L), 94.3 (1C, C_L), 93.6 (1C, C_L), 92.9 (1C, C_L), 78.7 (1C, C_L), 75.3 (1C, C_L), 75.1 (1C, C_L), 74.6 (1C, C_L), 72.8 (1C, C_L), 70.8 (1C, C_L), 69.8 (1C, C_H), 67.9 (1C, C_H), 56.5 (1C, $C_{F/G}$), 56.1 (1C, $C_{F/G}$), 51.2 (1C, $C_{F/G}$), 49.9 (1C, $C_{F/G}$), 44.1 (1C, C_I), 41.6 (1C, C_I), 21.5 (2C, C_A), 15.8 (1C, C_J), 15.3 (1C, C_J) ppm; HRMS (ESI$^+$) m/z found 433.0534 [M - Cl]$^+$; $C_{18}H_{23}N_2O_2RuS$ [M - Cl]$^+$ requires 433.0522; **6a** ($C_{18}H_{23}ClN_2O_2RuS$; 467.9754 g/mol); Found (%): C, 45.28; H, 5.12; N, 6.02; S, 6.60. Calculated [M + 0.20 eq DCM] (%): C, 45.07; H, 4.86; N, 5.78; S, 6.61. Expected (%): C,

46.20; H, 4.95; N, 5.99; S, 6.85; Single orange crystals were grown in EtOH (5 mL), unit cell: a = 7.8771(17) Å, b = 11.646(3) Å, c = 13.554(4) Å. α = 113.68(2)°, β = 100.79(2)°, γ = 97.053(18)°.

(*S*)-2-(Cyclohexa-1,4-dien-1-yl)propanoic acid (2b)
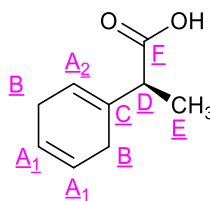
A solution of (*S*)-2-phenylpropanoic acid (4.02 g, 26.77 mmol) in ethanol (50 mL) was added to liquid NH_3 (1 L) at -77 °C. Lithium wire (6.33 g, 0.91 mol, 34 eq.) was washed in hexane before addition in 0.5 g portions until a dark blue colour persisted. The reaction was left to stand overnight to leave a white solid. H_2O (1 L) was added whilst stirring at 0 °C, followed by addition of $HCl_{(aq)}$ (12 M, 86 mL) to acidify the solution. The cloudy solution was extracted with Et_2O (3 x 100 mL), the organic layers combined, dried with Na_2SO_4 and the solution was filtered. The solvent was removed under reduced pressure and the product was dried further on a vacuum line to yield the acid as a yellow oil (3.75 g, 24.64 mmol, 92 %). ^{1}H-NMR (CDCl$_3$, 400 MHz): δ = 5.62-5.73 (m, 3H, H_{A1} + H_{A2}), 3.06-3.14 (m, 1H, H_D), 2.62-2.80 (m, 4H, H_B), 1.29 (d, 3H, *J* = 7.11 Hz, H_E) ppm; ^{13}C{^{1}H}-NMR (CDCl$_3$, 400 MHz): δ = 181.2 (1C, C_F), 133.2 (1C, C_C), 124.1 (1C, C_{A1}), 123.9 (1C, C_{A1}), 121.9 (1C, C_{A2}), 46.6 (1C, C_D), 27.1 (1C, C_B), 26.9 (1C, C_B), 15.3 (1C, C_E) ppm; HRMS (ESI$^-$) m/z found 151.0769 [M - H]$^-$; $C_9H_{11}O_2$ [M - H]$^-$ requires 151.0765; LRMS (EI$^+$): m/z found 153.1 [M + H]$^+$ (6 %), 152.1 [M]$^+$ (49 %), 107.1 [M - CHO$_2$]$^+$ (100 %); $C_9H_{13}O_2$ [M + H]$^+$ requires 153.2; **2b** ($C_9H_{12}O_2$; 152.1904 g/mol); Enantiopurity confirmed by chiral HPLC using method A.

(*S*)-2-(Cyclohexa-1,4-dien-1-yl)-*N*-(2-((4-methylphenyl)sulfonamido)ethyl)propenamide (3b)
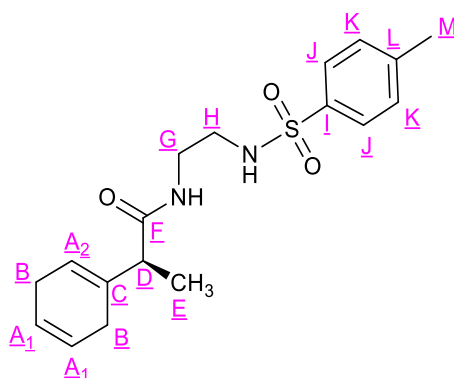
(*S*)-2-(Cyclohexa-1,4-dien-1-yl)propanoic acid (2.22 g, 14.59 mmol), HOBt.xH$_2$O (1.97 g, 14.59 mmol, 1 eq.) and TBTU (5.63 g, 17.50 mmol, 1.20 eq.) were dissolved in DMF (20 mL), DCM (20 mL) and DIPEA (5.10 mL, 29.30 mmol, 2 eq.). The solution was left to stir for 10 minutes before *N*-(2-aminoethyl)-4-methylbenzenesulfonamide (3.18 g, 14.59 mmol, 1 eq.) was added and the resulting yellow solution was left to stir overnight. Following this, the product solution was pipetted into a separating funnel containing HCl$_{(aq)}$ (1 M, 100 mL) and extracted with DCM (3 x 50 mL). The organic layers were combined and washed with H$_2$O (100 mL). The organic layer was dried with Na$_2$SO$_4$, filtered and the solvent was removed under reduced pressure. The orange oil was dissolved in Et$_2$O (50 mL) and washed with H$_2$O (8 x 50 mL) to remove DMF residues. The organic layer was dried with Na$_2$SO$_4$, filtered and the solvent removed under reduced pressure to yield an orange oil. The oil was purified by column chromatography on silica gel with a solvent system of DCM/MeOH (0-3 % MeOH) to yield the product as a white solid (4.02 g,11.54 mmol, 79 %). ^{1}H-NMR (CDCl$_3$, 400 MHz): δ = 7.72 (d, 2 H, *J* = 8.25 Hz, H$_J$), 7.30 (d, 2H, *J* = 8.25 Hz, H$_K$), 6.20 (br. s, 1H, <u>NH</u>-C=O), 5.69 (s, 2H, H$_{A1}$), 5.65 (s, 1H, H$_{A2}$), 5.36 (br. s, 1H, <u>NH</u>-SO$_2$), 3.26-3.39 (m, 2H, H$_G$), 3.04 (q, 2H, *J* = 5.35 Hz, H$_H$), 2.91 (q, 1H, *J* = 7.19 Hz, H$_D$), 2.44-2.76 (m, 4H, H$_B$), 2.42 (s, 3H, H$_M$), 1.24 (d, 3H, *J* = 7.34 Hz, H$_E$) ppm; ^{13}C{^{1}H}-NMR (CDCl$_3$, 400 MHz): δ = 175.4 (1C, C$_F$), 143.6 (1C, C$_I$), 136.9 (1C, C$_L$), 134.8 (1C, C$_C$), 129.9 (2C, C$_K$), 127.1 (2C, C$_J$), 124.1 (1C, C$_{A1}$), 124.0 (1C, C$_{A1}$), 122.2 (1C, C$_{A2}$), 48.4 (1C, C$_D$), 43.5 (1C, C$_H$), 39.4 (1C, C$_G$), 26.9 (2C, C$_B$), 21.7 (1C, C$_M$), 15.1 (1C, C$_E$) ppm; HRMS (ESI$^+$) m/z found 349.1578 [M + H]$^+$; C$_{18}$H$_{25}$N$_2$O$_3$S [M + H]$^+$ requires 349.1580; **3b** (C$_{18}$H$_{24}$N$_2$O$_3$S; 348.4598 g/mol); Enantiopurity confirmed by chiral HPLC using method B.

(*S*)-*N*-(2-((2-(Cyclohexa-1,4-dien-1-yl)propyl)amino)ethyl)-4-methylbenzenesulfonamide (4b)
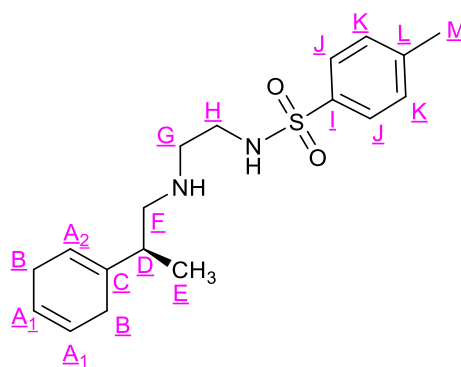
(*S*)-2-(Cyclohexa-1,4-dien-1-yl)-*N*-(2-((4-methylphenyl)sulfonamido)ethyl)propanamide (3.90 g, 11.19 mmol) was dissolved in anhydrous THF (50 mL) and added dropwise to a suspension of LiAlH$_4$ (0.95 g, 27.98 mmol, 2.50 eq.) in anhydrous THF (50 mL) under N$_2$. The reaction was heated at reflux overnight. The reaction was allowed to cool to room temperature, quenched with NaHCO$_3$ (50 mL), to give a biphasic mixture, which was then filtered. The sticky solid left behind in the flask was washed with Et$_2$O (40 mL). The combined organic phases were concentrated under reduced pressure to a volume of approximately 20 mL. Et$_2$O (40 mL) was added and the organic solution was extracted with H$_2$O (10 mL). The aqueous layer was washed with Et$_2$O (2 x 30 mL) and the organic layers combined, dried with Na$_2$SO$_4$ then filtered. The solvent was removed under reduced pressure to obtain a yellow oil. To remove any residual THF, the oil was dissolved in DCM (5 mL) then the solvent was removed under reduced pressure. This process was repeated twice. The product was dried further on a vacuum line to yield a yellow oil (3.35 g, 10.02 mmol, 89 %). ^{1}H-NMR (CDCl$_3$, 400 MHz): δ = 7.75 (d, 2H, *J* = 8.02 Hz, H$_J$), 7.30 (d, 2H, *J* = 7.79 Hz, H$_K$), 5.69 (s, 2H, H$_{A1}$), 5.44 (s, 1H, H$_{A2}$), 2.95 (t, 2H, *J* = 5.72 Hz, H$_G$), 2.65-2.69 (m, 2H, H$_H$), 2.45-2.71 (m, 4H, H$_B$), 2.40-2.43 (m, 1H, H$_F$), 2.42 (m, 3H, H$_M$), 2.27-2.32 (m, 1H, H$_F$), 2.14-2.23 (m, 1H, H$_D$), 0.95 (d, 3H, *J* = 6.88 Hz, H$_E$) ppm; ^{13}C{^{1}H}-NMR (CDCl$_3$, 400 MHz): δ = 143.4 (1C, C$_I$), 136.8 (2C, C$_C$ + C$_L$), 129.8 (2C, C$_K$), 127.3 (2C, C$_J$), 124.5 (1C, C$_{A1}$), 124.2 (1C, C$_{A1}$), 119.9 (1C, C$_{A2}$), 52.6 (1C, C$_F$), 47.7 (1C, C$_H$), 42.2 (1C, C$_G$), 41.1 (1C, C$_D$), 26.8 (1C, C$_B$), 25.6 (1C, C$_B$), 21.7 (1C, C$_M$), 17.4 (1C, C$_E$) ppm; HRMS (ESI$^+$) m/z found 335.1804 [M + H]$^+$; C$_{18}$H$_{27}$N$_2$O$_2$S [M + H]$^+$ requires 335.1788; **4b** (C$_{18}$H$_{26}$N$_2$O$_2$S; 334.4762 g/mol); Enantiopurity confirmed by chiral HPLC using method B.
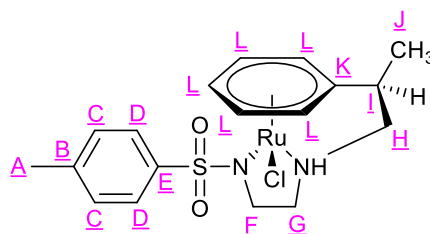
[Ru(η⁶-(*S*)-4-methyl-*N*-(2-((2-phenylpropyl)amino)ethyl)benzenesulfonamide)Cl₂]₂.2HCl (5b)
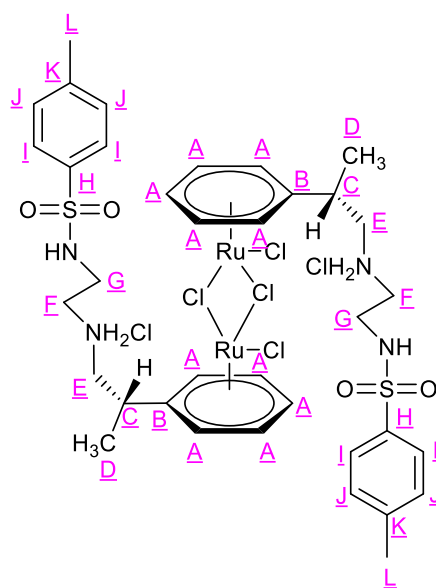
HCl$_{(aq)}$ (12 M, 0.82 mL, 9.94 mmol, 2 eq.) was added to (*S*)-*N*-(2-((2-(cyclohexa-1,4-dien-1-yl)propyl)amino)ethyl)-4-methylbenzenesulfonamide (1.66 g, 4.97 mmol) dissolved in ethanol (29 mL). The solution was stirred for 5-10 minutes then RuCl₃xH₂O (0.52 g, 2.49 mmol, 0.50 eq.) was added to the stirring solution. The reaction was heated at reflux overnight. The reaction was allowed to cool to room temperature then approximately half of the solvent was removed under reduced pressure. The solution was stored in the freezer (-18 °C) for two hours before the solid, which precipitated, was separated from the solution by centrifugation at 10,000 rpm for ten minutes. The solid was washed with Et₂O (15 mL) and separated again by centrifugation before being dried on a vacuum line to yield an orange solid (0.60 g, 0.55 mmol, 22 %). <u>Note:</u> Number of moles and % yields were calculated assuming zero equivalents of H₂O for RuCl₃xH₂O as the extent of hydration was not calculated. ¹H-NMR (DMSO, 400 MHz): δ = 9.25 (br. s, 2H, NH₂Cl), 8.83 (br. s, 2H, NH₂Cl), 8.03 (t, 2H, *J* = 5.50 Hz, 2 x NH), 7.72 (d, 4H, *J* = 8.25 Hz, H$_I$), 7.43 (d, 4H, *J* = 8.02 Hz, H$_J$), 5.97-6.03 (m, 10H, H$_A$), 3.00-3.28 (m, 12H, H$_C$ + H$_E$ + H$_F$ + H$_G$), 2.39 (s, 6H, H$_L$), 1.36 (d, 6H, *J* = 5.73 Hz, H$_D$) ppm; ¹³C{¹H}-NMR (DMSO, 400 MHz): δ = 143.1 (2C, C$_H$), 136.8 (2C, C$_K$), 129.8 (4C, C$_J$), 126.7 (4C, C$_I$), 103.6 (2C, C$_B$), 88.3 (2C, C$_A$), 87.9 (2C, C$_A$), 86.7 (2C, C$_A$), 85.7 (2C, C$_A$), 85.3 (2C, C$_A$), 51.6 (2C, C$_E$), 47.0 (2C, C$_G$), 38.5 (2C, C$_F$), 33.6 (2C, C$_C$), 21.0 (2C, C$_L$), 17.0 (2C, C$_D$) ppm; **5b** (C₃₆H₅₀Cl₆N₄O₄Ru₂S₂; 1081.7946 g/mol).

Final complex (6b)
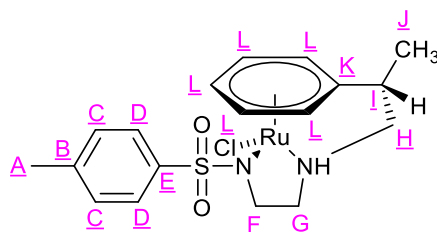
[Ru(η⁶-(*S*)-4-methyl-N-(2-((2-phenylpropyl)amino)ethyl)benzenesulfonamide)Cl₂]₂.2HCl (0.50 g, 0.46 mmol, 1 eq.) was suspended in DCM (100 mL) then DIPEA (0.32 mL, 1.84 mmol, 4 eq.) was added and the suspension was stirred under N_2. After 1.5 hours, the solution was reduced to a quarter of its volume under reduced pressure and then purified by column chromatography on silica gel with a solvent system of DCM/MeOH (0-1 % MeOH). Fractions containing the product, which were intensely yellow in colour, were combined. The solvent was removed under reduced pressure and the product was dried further on a vacuum line as an orange solid (0.41 g, 0.88 mmol, 96 %). ¹H-NMR (CDCl₃, 400 MHz): δ = 7.71-7.76 (m, 4H, H_D), 7.13-7.16 (m, 4H, H_C), 6.69 (t, 1H, *J* = 5.62 Hz, H_L), 6.49 (t, 1H, *J* = 5.62 Hz, H_L), 5.78 (t, 1H, *J* = 5.85 Hz, H_L), 5.73 (t, 1H, *J* = 5.73 Hz, H_L), 5.60 (t, 1H, *J* = 5.62 Hz, H_L), 5.46 (t, 1H, *J* = 5.62 Hz, H_L), 5.28-5.30 (m, 1H, H_L), 5.10-5.14 (m, 2H, H_L), 4.97 (d, 1H, *J* = 5.50 Hz, H_L), 4.52 (br. s, 2H, NH), 3.55-4.00 (m, 4H, H_H), 3.12-3.31 (m, 4H, H_I + $H_{F/G}$), 2.78-2.87 (m, 2H, $H_{F/G}$), 2.47-2.67 (m, 2H, $H_{F/G}$), 2.32-2.33 (m, 6H, H_A), 2.16-2.40 (m, 2H, $H_{F/G}$), 1.44-1.45 (m, 6H, H_J) ppm. Note: ¹H-NMR assigned to show the 2 diastereoisomers present in the sample, however, the signals overlap directly due to identical properties; ¹³C{¹H}-NMR (CDCl₃, 400 MHz): δ = 140.7 (1C, C_E), 140.4 (1C, C_E), 140.3 (1C, C_B), 140.2 (1C, C_B), 128.8 (1C, C_C), 128.7 (1C, C_C), 127.5 (1C, C_D), 127.4 (1C, C_D), 104.8 x 2 (2C, C_K), 95.1 (1C, C_L), 94.2 (1C, C_L), 93.6 (1C, C_L), 92.8 (1C, C_L), 78.6 (1C, C_L), 75.3 (1C, C_L), 75.1 (1C, C_L), 74.5 (1C, C_L), 72.8 (1C, C_L), 70.8 (1C, C_L), 69.8 (1C, C_H), 68.0 (1C, C_H), 56.5 (1C, $C_{F/G}$), 56.0 (1C, $C_{F/G}$), 51.1 (1C, $C_{F/G}$), 49.9 (1C, $C_{F/G}$), 44.1 (1C, C_I), 41.5 (1C, C_I), 21.5 (2C, C_A), 15.8 (1C, C_J), 15.3 (1C, C_J) ppm; HRMS (ESI⁺) m/z found 433.0540 [M - Cl]⁺; C₁₈H₂₃N₂O₂RuS [M - Cl]⁺ requires 433.0522; **6b** (C₁₈H₂₃ClN₂O₂RuS; 467.9754 g/mol); Found (%): C, 45.13; H, 5.15; N, 6.01; S, 6.63. Calculated [M + 0.25 eq DCM] (%): C, 45.20; H, 4.88; N, 5.78; S, 6.61. Expected (%): C, 46.20; H, 4.95; N, 5.99; S, 6.85; Single orange crystals were grown in EtOH (5 mL), unit cell: a = 12.3198(5) Å, b = 14.4079(8) Å, c = 20.7842(8) Å. α = 90°, β = 90°, γ = 90°.

Final complex (7)
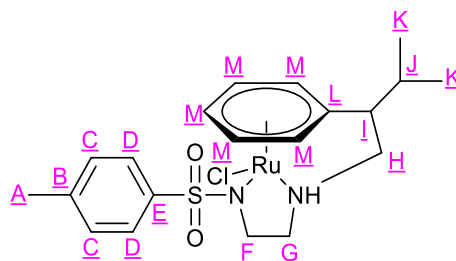
[Ru(η^6-4-methyl-*N*-(2-((3-methyl-2-phenylbutyl)amino)ethyl)benzenesulfonamide)Cl$_2$]$_2$.2HCl* (0.50 g, 0.44 mmol, 1 eq.) was suspended in DCM (15 mL) then DIPEA (0.15 mL, 0.88 mmol, 2 eq.) was added and the suspension was stirred for two hours under N$_2$. After analysis by ^{1}H-NMR, additional DIPEA (2 eq.) was added, and the suspension was stirred for 30 minutes under N$_2$. The orange solution was purified by column chromatography on silica gel with a solvent system of DCM/MeOH (0-1 % MeOH). Fractions containing the product, which were intensely yellow in colour, were combined. The solvent was removed under reduced pressure and the product was dried further on a vacuum line as an orange crystalline solid (0.41 g, 0.84 mmol, 95 %). ^{1}H-NMR (CDCl$_3$, 400 MHz): δ = 7.70-7.76 (m, 4H, H$_D$), 7.13-7.16 (m, 4H, H$_C$), 6.70 (t, 0.40H, *J* = 5.73 Hz, H$_M$), 6.44 (t, 1.60H, *J* = 5.50 Hz, H$_M$), 5.73 (t, 2H, *J* = 5.85 Hz, H$_M$), 5.63 (t, 1.60H, *J* = 5.62 Hz, H$_M$), 5.45 (t, 0.40H, *J* = 5.62 Hz, H$_M$), 5.23 (d, 0.40H, *J* = 6.19 Hz, H$_M$), 5.07 (d, 1.60H, *J* = 6.19 Hz, H$_M$), 5.00 (d, 1.60H, *J* = 5.50 Hz, H$_M$), 4.87 (d, 0.4H, *J* = 5.50 Hz, H$_M$), 4.47-4.55 (m, 2H, 2 x NH), 3.95-4.10 (m, 2H, H$_{F/G/H}$), 3.15-3.68 (m, 4H, H$_{F/G/H}$), 2.77-2.89 (m, 2H, H$_{F/G/H}$), 2.47-2.71 (m, 4H, H$_I$ + H$_{F/G/H}$), 2.32-2.33 (m, 6H, H$_A$), 2.15-2.26 (m, 2H, H$_{F/G/H}$), 1.98-2.08 (m, 2H, H$_J$), 1.10-1.13 (m, 6H, H$_K$), 1.01-1.03 (m, 6H, H$_K$) ppm. Note: ^{1}H-NMR assigned to show the two enantiomers present in the sample, however, the signals overlap directly due to identical properties. Two diastereoisomers are also present, explaining the non-integer integrals, indicating a total of four diastereosiomers; ^{13}C{^{1}H}-NMR (CDCl$_3$, 400 MHz): δ = 140.4 x 3 (3C, C$_B$ + C$_E$), 140.3 (1C, C$_B$), 128.7 (1C, C$_C$), 128.6 (1C, C$_C$), 127.5 (1C, C$_D$), 127.3 (1C, C$_D$), 104.4 (1C, C$_L$), 104.1 (1C, C$_L$), 95.1 (1C, C$_M$), 94.4 (1C, C$_M$), 93.6 (1C, C$_M$), 92.6 (1C, C$_M$), 79.0 (1C, C$_M$), 75.8 (1C, C$_M$), 74.8 (1C, C$_M$), 74.7 (1C, C$_M$), 72.8 (1C, C$_M$), 70.7 (1C, C$_M$), 67.3 (1C, C$_H$), 65.5 (1C, C$_H$), 57.0 (1C, C$_I$), 56.5 (1C, C$_{F/G}$), 56.0 (1C, C$_{F/G}$), 54.7 (1C, C$_I$), 51.0 (1C, C$_{F/G}$), 49.5 (1C, C$_{F/G}$), 30.6 (1C, C$_J$), 30.5 (1C, C$_J$), 22.3 (1C, C$_K$), 22.1 (1C, C$_K$), 21.4 (2C, C$_A$), 21.1 (1C, C$_K$), 20.8 (1C, C$_K$) ppm; HRMS (ESI$^+$) m/z found 461.0843 [M - Cl]$^+$; C$_{20}$H$_{27}$N$_2$O$_2$RuS [M - Cl]$^+$ requires 461.0836; **7**

($C_{20}H_{27}ClN_2O_2RuS$; 496.0286 g/mol); Found (%): C, 48.18; H, 5.69; N, 5.48; S, 6.23. Expected (%): C, 48.40; H, 5.49; N, 5.65; S, 6.46; Unit cell: a = 11.8781(11) Å, b = 10.8315(5) Å, c = 16.9586(12) Å. α = 90°, β = 98.221(7)°, γ = 90°.

*Orange solid previously synthesised by Dr Murray's research group.

(3,3-Dimethyl-1-nitrobutan-2-yl)benzene[294] (8)
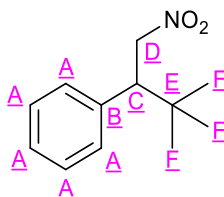
β-Nitrostyrene (3.00 g, 20.11 mmol) in anyhdrous THF (50 mL) was added dropwise to ^tBuMgCl (50.25 mL, 2 M in diethyl ether, 100.50 mol) in anyhdrous THF (150 mL) at -20 °C to afford an orange solution. Within 20 minutes, the solution was added dropwise to ice cold concentrated 5 % HCl (100 mL) and the solution was stirred for a further 30 minutes. H_2O (40 mL) was added and the biphasic mixture was extracted with DCM (3 x 75 mL). The organic layers were combined, dried with Na_2SO_4 and filtered. The solvent was removed under reduced pressur. The brown oil was purified by column chromatography on silica gel with a solvent system of EtOAc/Hexane (95/5 %) to obtain the desired product as a red/orange solid (1.51 g, 7.29 mmol, 36 %). ^1H-NMR (CDCl$_3$, 400 MHz): δ = 7.16-7.32 (m, 5H, H$_A$), 4.76-4.87 (m, 2H, H$_F$), 3.35 (dd, 1H, *J* = 11.0, 5.03 Hz, H$_E$), 0.95 (s, 9H, H$_H$) ppm; $^{13}C\{^1H\}$-NMR (CDCl$_3$, 400 MHz): δ = 137.6 (1C, C$_D$), 129.2 (2C, C$_A$), 128.3 (2C, C$_A$), 127.6 (1C, C$_A$), 77.3 (1C, C$_F$), 54.4 (1C, C$_E$), 33.8 (1C, C$_G$), 28.2 (3C, C$_H$) ppm; IR: υ$_{max}$ = 2962.52 (aliphatic C-H stretch), 2869.44 (aromatic C-H stretch), 1546.19 (aliphatic N-O stretch), 1378.44 (aliphatic C-N stretch), 745.61 (aliphatic C-H bend), 701.57 (aromatic C-H bend) cm^{-1}; LRMS (ESI$^+$): m/z found 230.1 [M + Na]$^+$ (100 %); $C_{12}H_{17}NNaO_2$ [M + Na]$^+$ requires 230.3; **8** ($C_{12}H_{17}NO_2$; 207.3 g/mol).

3,3-Dimethyl-2-phenylbutan-1-amine[295] (9)
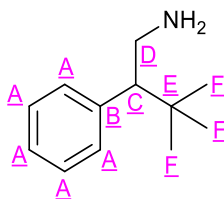
To a stirred solution of (3,3-dimethyl-1-nitrobutan-2-yl)benzene (2.62 g, 12.64 mmol) in ethanol/H_2O (200 mL, 4:1) was added Fe powder (7.05 g, 0.13 mol, 10 eq.) and solid NH_4Cl (6.76 g, 0.13 mol, 10 eq.). The mixture was stirred at 70 °C overnight and the solution turned dark brown. TLC analysis confirmed residual starting material. Additional Fe powder (0.71 g, 12.64 mmol, 1 eq.) and NH_4Cl (0.68 g, 12.64 mmol, 1 eq.) were added and stirred for 1 h at 70 °C. TLC analysis confirmed completion of the reaction. The warm reaction mixture was filtered to give an orange solution. The solvent was removed under reduced pressure to give a pale orange solid, which was dissolved in DCM (250 mL) and extracted with H_2O (3 x 200 mL) to remove residual Fe residues and salts. The organic layer was disposed of, whilst the aqueous phase was adjusted to pH 11 using $NaOH_{(aq)}$ (1 M, 150 mL). The pH adjusted aqueous phase was extracted with DCM (2 x 400 mL). The organic layers were combined, dried with Na_2SO_4 and filtered. The solvent was removed under reduced pressure to yield a pearlescent white solid (1.76 g, 9.93 mmol, 99 %). ^{1}H-NMR ($CDCl_3$, 400 MHz): δ = 7.18-7.33 (m, 5H, H_A), 3.04-3.15 (m, 2H, H_F), 2.44-2.48 (m, 1H, H_E), 1.38 (br. s, 2H, NH_2), 0.89 (s, 9H, H_H) ppm; ^{13}C{^{1}H}-NMR ($CDCl_3$, 400 MHz): δ = 141.1 (1C, C_D), 129.9 (2C, C_A), 128.1 (2C, C_A), 126.5 (1C, C_A), 60.4 (1C, C_F), 41.7 (1C, C_E), 33.5 (1C, C_G), 28.5 (3C, C_H) ppm; LRMS (ESI$^+$): m/z found 178.2 [M + H]$^+$ (100 %); $C_{12}H_{20}N$ [M + H]$^+$ requires 178.3; **9** ($C_{12}H_{19}N$; 177.3 g/mol).

(*R*)- or (*S*)-3,3-Dimethyl-2-phenylbutan-1-amine (9a/9b)
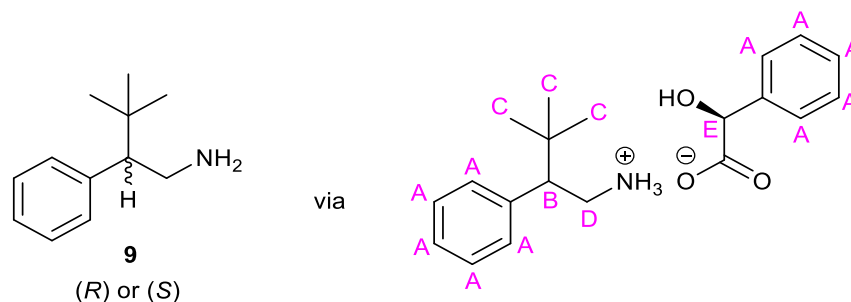
(*S*)-Mandelic acid (3.64 g, 24.00 mmol) in ethanol (10 mL) was added to 3,3-dimethyl-2-phenylbutan-1-amine (4.24 g, 24.00 mmol)[a] in ethanol (10 mL), and the solvent was removed under reduced pressure[b]. The ratio of isomers in the starting material was 47 %:53 % with retention times of 36.60 minutes and 40.20 minutes respectively (confirmed by chiral HPLC using method C). The salt was recrystallised from diethyl ether, mixtures of diethyl ether/hexane or DCM. Diethyl ether and DCM were responsible for increasing the purity of the (*R*) isomer* and (*S*) isomer* respectively, whereby the (*S*) isomer* was retained for longer on the chiral HPLC column. Hexane was utilised to encourage precipitation in the later stages as diethyl ether alone only achieved isomer ratios of ~80 %:20 %. The precipitated crystals were separated from the liquid and then separate extractions were performed on the salt (isolated crystals or solid from the filtrate once the solvent was removed under reduced pressure), in diethyl ether (5 mL) with $NaOH_{(aq)}$ (0.1 M, 2 x 5 mL) then H_2O (5 mL), were carried out to isolate the free amine. This allowed confirmation of the ratio of isomers at each stage by chiral HPLC using method C. After a total of 78 recrystallisations, 1.04 g of (*S*)-3,3-dimethyl-2-phenylbutan-1-amine (91 % ee), 0.41 g of (*S*)-3,3-dimethyl-2-phenylbutan-1-amine (80 % ee)[c] and 0.71 g of (*R*)-3,3-dimethyl-2-phenylbutan-1-amine (72 % ee) were obtained. 1.43 g (4.35 mmol, ~65 %:35 %) of the salt was removed mid-way through the recrystallisation procedure to allow for the synthesis of the racemic complex to attempt arene exchange. After the base wash and extraction using diethyl ether (100 mL) with $NaOH_{(aq)}$ (0.1 M, 2 x 100 mL) then H_2O (100 mL), the final yields of the amine were as follows: 0.36 g (91 % ee), 0.15 g (80 % ee) and 0.26 g (72 % ee). Clear single crystal needles of the salt were grown in diethyl ether (20 mL). Unit cell: a = 24.181(3) Å, b = 6.3638(7) Å, c = 25.641(3) Å. α = 90°, β =111.358(8)°, γ = 90°. The ratio of isomers for this batch were found to be 84 %:16 % by chiral HPLC using method C.

[a]The yields represent multiple batches of 3,3-dimethyl-2-phenylbutan-1-amine combined.

[b]Data for ^{1}H-NMR (DMSO, 400 MHz): δ = 7.16-7.38 (m, 10H, H_A), 4.59 (s, 1H, H_E), 3.18-3.26 (m, 2H, H_D), 2.63-2.68 (m, 1H, H_B), 0.79 (s, 9H, H_C) ppm

[c]Two batches of recrystallisations were combined: 0.23 g of 7 %: 93 % and 0.18 g of 14 %: 86 %.

*On the basis of the chiral HPLC columns selectivity, it was suspected that the isomers of **9** were retained in the order (*R*) then (*S*). This was later confirmed by the results obtained during the ATH experiments. For full explanation see section 2.4.3.2.

(*R**)-2-(Cyclohexa-1,4-dien-1-yl)-3,3-dimethylbutan-1-amine (10a)
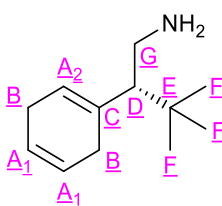
A solution of (*R**)-3,3-dimethyl-2-phenylbutan-1-amine (260 mg, 1.47 mmol) in ethanol (10 mL) was added to liquid NH_3 (50 mL) at -77 °C. Lithium wire (0.10 g, 14.70 mmol, 10 eq.) was washed in hexane before addition in 0.5 g portions until a dark blue colour persisted. The reaction was left to stand overnight to leave a white solid. H_2O (50 mL) was added whilst stirring at 0 °C and the pH was found to be ~10. The aqueous mixture was diluted with further H_2O (50 mL) then extracted with DCM (3 x 100 mL). The organic phases were combined, dried with Na_2SO_4 and filtered. The solvent was removed under reduced pressure and the product was dried further on a vacuum line as a yellow oil (0.14 g, 0.78 mmol, 53 %). ^{1}H-NMR (CDCl$_3$, 400 MHz): δ = 5.64-5.70 (m, 2H, H_{A1}), 5.45-5.50 (m, 1H, H_{A2}), 2.53-2.81 (m, 5H, H_B + H_D), 1.50-1.73 (m, 2H, H_G), 1.02-1.05 (m, 2H, NH_2), 0.86-0.89 (m, 9H, H_F) ppm; ^{13}C{^{1}H}-NMR (CDCl$_3$, 400 MHz): δ = 134.5 (1C, C_C), 124.1 (1C, C_{A1}), 123.9 (1C, C_{A1}), 122.1 (C_{A2}), 60.7 (1C, C_G), 40.1 (1C, C_D), 33.2 (1C, C_E), 28.6 (3C, C_F), 26.6 (2C, C_B) ppm; HRMS (ESI$^+$): m/z found 180.1747 [M + H]$^+$; $C_{12}H_{22}N$ [M + H]$^+$ requires 180.1750; **10a** ($C_{12}H_{21}N$; 179.3018 g/mol).

(*R**)-*N*-(2-(Cyclohexa-1,4-dien-1-yl)-3,3-dimethylbutyl)-2-((4-methylphenyl)sulfonamido)acetamide (11a)
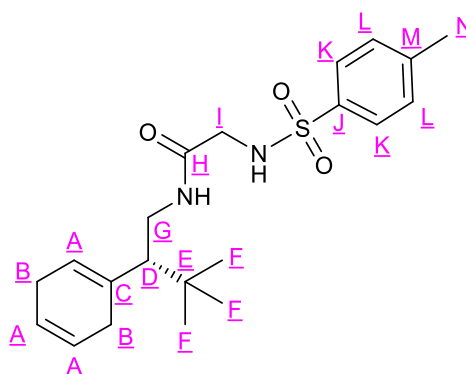
(*R**)-2-(Cyclohexa-1,4-dien-1-yl)-3,3-dimethylbutan-1-amine (0.13 g, 0.73 mmol) and TBTU (0.26 g, 0.80 mmol, 1.10 eq.) were dissolved in a mixture of DMF (2 mL), DCM (3 mL) and DIPEA (0.38 mL, 2.18 mmol, 3 eq.). The solution was left to stir for 5 minutes before (*p*-toluenesulfonyl)glycine (0.18 g, 0.80 mmol, 1.10 eq.) was added and the resulting orange suspension was left to stir overnight. Following this, the product solution was diluted with DCM (100 mL) and extracted with sat. $NH_4Cl_{(aq)}$ (3 x 50 mL). The organic layer was dried with Na_2SO_4 and filtered. The solvent was removed under reduced pressure to give an orange oil with a white precipitate. The product was purified by column chromatography on silica gel with a solvent system of DCM/MeOH (0-1 %) to obtain the desired product as a white solid (0.19 g, 0.49 mmol, 67 %). ^{1}H-NMR (CDCl$_3$, 400 MHz): δ = 7.69-7.73 (m, 2H, H$_K$), 7.30 (d, 2H, *J* = 8.00 Hz, H$_L$), 6.15-6.20 (m, 1H, NH), 5.49-5.72 (m, 3H, H$_A$), 5.38 (br. s, 1H, NH), 3.50-3.60 (m, 3H, H$_I$ + H$_G$), 3.03-3.12 (m, 1H, H$_D$), 2.55-2.78 (m, 3H, H$_B$), 2.42 (s, 3H, H$_N$), 1.77-2.12 (m, 2H, H$_B$ + H$_G$), 0.90-0.92 (m, 9H, H$_F$) ppm; ^{13}C{^{1}H}-NMR (CDCl$_3$, 400 MHz): δ = 167.9 (1C, C$_H$), 143.8 (1C, C$_J$), 136.0 (1C, C$_M$), 134.0 (1C, C$_C$), 129.8 (2C, C$_L$), 127.2 (2C, C$_K$), 124.2 + 124.1 (3C, C$_A$), 56.6 (1C, C$_G$), 45.8 (1C, C$_I$), 38.1 (1C, C$_D$), 33.0 (1C, C$_E$), 28.7 (3C, C$_F$), 26.7 (2C, C$_B$), 21.5 (1C, C$_N$) ppm; HRMS (ESI$^+$): m/z found 413.1868 [M + Na]$^+$; $C_{21}H_{30}N_2NaO_3S$ [M + Na]$^+$ requires 413.1869; **11a** ($C_{21}H_{30}N_2O_3S$; 390.5395 g/mol).

(*R**)-*N*-(2-((2-(Cyclohexa-1,4-dien-1-yl)-3,3-dimethylbutyl)amino)ethyl)-4-methylbenzenesulfonamide (12a)
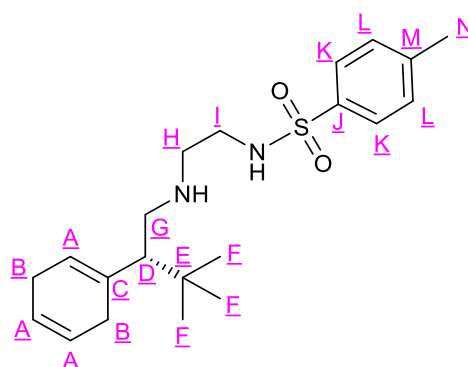
(*R**)-*N*-(2-(Cyclohexa-1,4-dien-1-yl)-3,3-dimethylbutyl)-2-(methylamino)acetamide (0.17 g, 0.44 mmol) was dissolved in anhydrous THF (25 mL) and added dropwise to a suspension of LiAlH$_4$ (0.04 g, 1.09 mmol, 2.50 eq.) in anhydrous THF (5 mL) under N$_2$. The reaction was heated at reflux overnight. The reaction was allowed to cool to room temperature, quenched with NaHCO$_3$ (20 mL), to give a biphasic mixture, which was then filtered. The sticky solid left behind in the flask was washed with Et$_2$O (40 mL). Et$_2$O (50 mL) was added and the organic solution was extracted with H$_2$O (50 mL). The aqueous layer was washed with Et$_2$O (2 x 50 mL) and the organic layers combined, dried with Na$_2$SO$_4$, then filtered. The solvent was removed under reduced pressure and the product was dried further on a vacuum line to yield an orange oil (0.12 g, 0.32 mmol, 73 %). ^{1}H-NMR (CDCl$_3$, 400 MHz): δ = 7.69-7.79 (m, 2H, H$_J$), 7.27-7.29 (m, 2H, H$_K$), 5.38-5.70 (m, 3H, H$_A$), 2.91-2.95 (m, 1H, H$_{G/H/I}$), 2.40 (s, 3H, H$_N$), 2.38-2.86 (m, 7H, H$_B$ + H$_G$ + H$_H$ + H$_I$), 1.47-2.07 (m, 3H, H$_B$ + H$_D$), 0.81-0.90 (m, 9H, H$_F$); ^{13}C{^{1}H}-NMR (CDCl$_3$, 400 MHz): δ = 143.3 (1C, C$_M$), 136.8 (1C, C$_J$), 134.9 (1C, C$_C$), 129.7 (2C, C$_L$), 127.2 (2C, C$_K$), 124.4 x 2 (3C, C$_A$), 47.8 (1C, C$_{G/H/I}$), 47.2 (1C, C$_{G/H/I}$), 42.2 (1C, C$_{G/H/I}$), 33.0 (1C, C$_E$), 30.4 (1C, C$_D$), 28.8 (3C, C$_F$), 26.8 (2C, C$_B$), 21.6 (1C, C$_N$) ppm; HRMS (ESI$^+$): m/z found 377.2265 [M + H]$^+$; C$_{21}$H$_{33}$N$_2$O$_2$S [M + H]$^+$ requires 377.2257; **12a** (C$_{21}$H$_{32}$N$_2$O$_2$S; 376.5560 g/mol).

[Ru(η⁶-(*R)-*N*-(2-((2-(Cyclohexa-1,4-dien-1-yl)-3,3-dimethylbutyl)amino)ethyl)-4-methylbenzenesulfonamide)Cl₂]₂.2HCl (13a)**

RuCl₃xH₂O (16.59 mg, 0.08 mmol, 0.25 eq.) in ethanol (4 mL) was heated at reflux for three hours. Separately, HCl$_{(aq)}$ (12 M, 50.41 μL, 0.61 mmol, 2 eq.) was added to the (*R**)-*N*-(2-((2-(cyclohexa-1,4-dien-1-yl)-3,3-dimethylbutyl)amino)ethyl)-4-methylbenzenesulfonamide (0.12 g, 0.31 mmol, 1 eq.) dissolved in ethanol (2 mL). The solution was stirred for 5-10 minutes, then added to the RuCl₃xH₂O in ethanol. The reaction was heated at reflux overnight to give a brown solution. Analysis by ¹H-NMR confirmed that excess diene remained, therefore additional RuCl₃xH₂O (16.59 mg, 0.08 mmol, 0.25 eq.) was added. The reaction was heated at reflux for six hours, then allowed to cool to room temperature. The solution was concentrated to a volume of ~2 mL and left in the fridge (5 °C) overnight to precipitate. The brown solid was separated from the supernatant by centrifugation (10,000 rpm for 5 minutes) to isolate the product (35.00 mg, 0.03 mmol, 39 %). Note: Number of moles and % yields were calculated assuming zero equivalents of H₂O for RuCl₃xH₂O as the extent of hydration was not calculated. Due to the low quantity of solid obtained, and the difficulty in separating the product from excess ligand used in the reaction, the product was taken forward and used directly in the next step of the synthesis without further purification or full characterisation. **13a** (C₄₂H₆₂Cl₆N₄O₄Ru₂S₂; 1165.95 g/mol).

Final complex (14a)
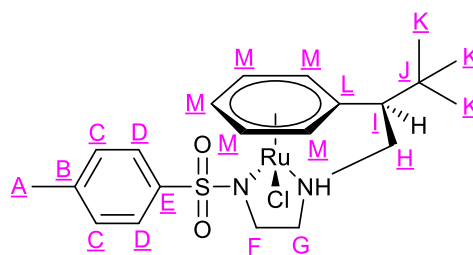
[Ru(η^6-(R^*)-N-(2-((2-(Cyclohexa-1,4-dien-1-yl)-3,3-dimethylbutyl)amino)ethyl)-4-methylbenzenesulfonamide)Cl$_2$]$_2$.2HCl (0.03 g, 0.03 mmol, 1 eq.) was suspended in DCM (5 mL) then DIPEA (0.04 mmol, 6.72 µL, 1.50 eq.) was added and the suspension was stirred under N$_2$. After one hour, the solution was purified through a pipette column containing silica gel using a solvent system of DCM/MeOH (0-1 % MeOH). The solvent was removed under reduced pressure and the product was dried further on a vacuum line as a brown oil (6.10 mg, 0.01 mmol, 17 %). ^{1}H-NMR (CDCl$_3$, 400 MHz): δ = 7.71-7.75 (m, 4H, H$_D$), 7.14-7.16 (m, 4H, H$_C$), 6.67 (t, 1.50H, J = 5.61 Hz, H$_M$), 6.38 (t, 1H, J = 5.49 Hz, H$_M$), 5.65-5.73 (m, 3.50H, H$_M$), 5.32-5.43 (m, 1H, H$_M$), 5.15 (t, 1.50H, J = 5.49 Hz, H$_M$), 5.00-5.01 (m, 1H, H$_M$), 4.93 (d, 0.5H, J = 5.49 Hz, H$_M$), 3.97-4.01 (m, 2H, 2 x NH), 2.60-3.67 (m, 14H, H$_F$ + H$_G$ + H$_H$ + H$_I$), 2.33 (s, 6H, H$_A$), 1.15 (s, 18H, H$_K$) ppm. <u>Note:</u> ^{1}H-NMR assigned to show the 2 diastereoisomers present in the sample, however, the signals overlap directly due to identical properties. DIPEA was heavily contaminating the catalyst, therefore poor spectra were acquired. Broad peaks made the spectrum challenging to determine. Only some distinct environments were observed with vague integration obtained, therefore the assignments were made based on the other catalysts within this family (especially by comparison to the opposite catalyst enantiomer and racemic analogue); ^{13}C{^{1}H}-NMR (CDCl$_3$, 400 MHz): δ = 129.8 (C$_C$), 127.6 (C$_D$), 92.4 (C$_M$), 81.4 (C$_M$), 77.6 (C$_M$), 77.5 (C$_M$), 77.2 (C$_M$), 76.0 (C$_M$), 72.8 (C$_M$), 68.3 (C$_M$), 57.3 (C$_{F/G/H/I}$), 51.7 (C$_{F/G/H/I}$), 42.3 (C$_{F/G/H/I}$), 41.9 (C$_{F/G/H/I}$), 30.0 (C$_{F/G/H/I}$), 28.1 (C$_K$), 21.7 (C$_A$) ppm. Note: Assignments obtained from DEPTq experiment, hence no quaternary carbons observed. Only one diastereoisomer observed, however this could have been due to the dilute concentration; HRMS (ESI$^+$) m/z found 475.0998 [M - Cl]$^+$; C$_{21}$H$_{29}$N$_2$O$_2$RuS [M - Cl]$^+$ requires 475.0993; **14a** (C$_{21}$H$_{29}$ClN$_2$O$_2$RuS; 510.0552 g/mol).

(*S**)-2-(Cyclohexa-1,4-dien-1-yl)-3,3-dimethylbutan-1-amine (10b)
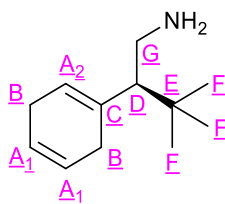
A solution of (*S**)-3,3-dimethyl-2-phenylbutan-1-amine (360 mg, 2.03 mmol) in ethanol (10 mL) was added to liquid NH_3 (50 mL) at -77 °C. Lithium wire (0.10 g, 14.70 mmol, 10 eq.) was washed in hexane before addition in 0.5 g portions until a dark blue colour persisted. The reaction was left to stand overnight to leave a white solid. H_2O (50 mL) was added whilst stirring at 0 °C and the pH was found to be ~10. The aqueous mixture was diluted with further H_2O (50 mL) then extracted with DCM (3 x 100 mL). The organic phases were combined, dried with Na_2SO_4 and filtered. The solvent was removed under reduced pressure and the product was dried further on a vacuum line to yield the amine as a yellow oil (0.17 g, 0.95 mmol, 47 %). ^{1}H-NMR (CDCl$_3$, 400 MHz): δ = 5.65-5.71 (m, 2H, H$_{A1}$), 5.46-5.50 (m, 1H, H$_{A2}$), 2.54-2.82 (m, 5H, H$_B$ + H$_D$), 1.50-1.74 (m, 2H, H$_G$), 1.08 (br. s, 2H, NH$_2$), 0.87-0.90 (m, 9H, H$_F$) ppm; ^{13}C{^{1}H}-NMR (CDCl$_3$, 400 MHz): δ = 134.6 (1C, C$_C$), 124.2-124.5 (3C, C$_A$), 60.6 (1C, C$_G$), 40.2 (1C, C$_D$), 33.2 (1C, C$_E$), 28.9 (3C, C$_F$), 26.9 (2C, C$_B$) ppm; HRMS (ESI$^+$): m/z found 180.1747 [M + H]$^+$; C$_{12}$H$_{22}$N [M + H]$^+$ requires 180.1742; **10b** (C$_{12}$H$_{21}$N; 179.3018 g/mol).

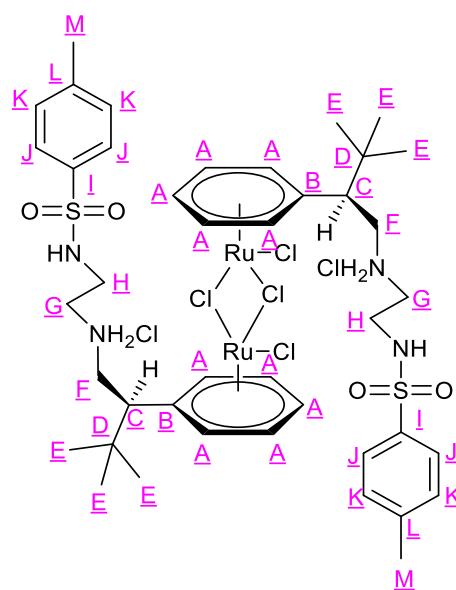### (*S**)-*N*-(2-(Cyclohexa-1,4-dien-1-yl)-3,3-dimethylbutyl)-2-((4-methylphenyl)sulfonamido)acetamide (11b)
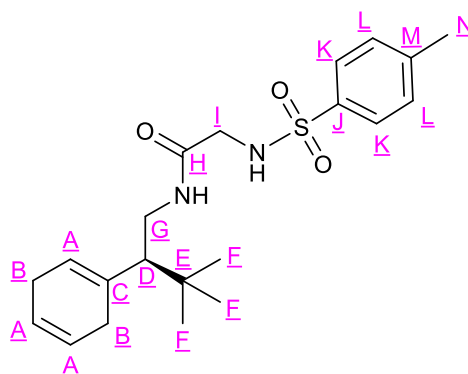
(*S**)-2-(Cyclohexa-1,4-dien-1-yl)-3,3-dimethylbutan-1-amine (0.16 g, 0.89 mmol) and TBTU (0.32 g, 0.98 mmol, 1.10 eq.) were dissolved in a mixture of DMF (2 mL), DCM (3 mL) and

DIPEA (0.47 mL, 2.68 mmol, 3 eq.). The solution was left to stir for five minutes before (*p*-toluenesulfonyl)glycine (0.23 g, 0.98 mmol, 1.10 eq.) was added and the resulting orange suspension was left to stir overnight. Following this, the product solution was diluted with DCM (100 mL) and extracted with sat. $NH_4Cl_{(aq)}$ (3 x 50 mL). The organic layer was dried with Na_2SO_4 and filtered. The solvent was removed under reduced pressure to give a yellow oil with a white precipitate. The product was purified by column chromatography on silica gel with a solvent system of DCM/MeOH (0-1 %) to obtain the desired product as a white solid (0.22 g, 0.56 mmol, 63 %). ^{1}H-NMR (CDCl$_3$, 400 MHz): δ = 7.68-7.71 (m, 2H, H$_K$), 7.28 (d, 2H, *J* = 8.02 Hz, H$_L$), 6.24-6.29 (m, 1H, <u>NH</u>-CO), 5.47-5.69 (m, 3H, H$_A$), 3.48-3.57 (m, 3H, H$_G$ + H$_I$), 3.02-3.11 (m, 1H, H$_D$), 2.54-2.75 (m, 3H, H$_B$), 2.40 (s, 3H, H$_N$), 1.76-2.08 (m, 2H, H$_B$ + H$_G$), 0.89-0.91 (m, 9H, H$_F$) ppm; ^{13}C{^{1}H}-NMR (CDCl$_3$, 400 MHz): δ = 167.8 (1C, C$_H$), 144.0 (1C, C$_J$), 135.9 (1C, C$_M$), 134.1 (1C, C$_C$), 129.9 (2C, C$_L$), 127.3 (2C, C$_K$), 124.1 + 124.3 (3C, C$_A$), 56.7 (1C, C$_G$), 45.8 (1C, C$_I$), 38.1 (1C, C$_D$), 33.1 (1C, C$_E$), 28.7 (3C, C$_F$), 26.8 (2C, C$_B$), 21.6 (1C, C$_N$) ppm; HRMS (ESI$^+$): m/z found 391.2053 [M + H]$^+$; $C_{21}H_{31}N_2O_3S$ [M + H]$^+$ requires 391.2050; **11b** ($C_{21}H_{30}N_2O_3S$; 390.5395 g/mol).

(*S**)-*N*-(2-((2-(Cyclohexa-1,4-dien-1-yl)-3,3-dimethylbutyl)amino)ethyl)-4-methylbenzenesulfonamide (12b)
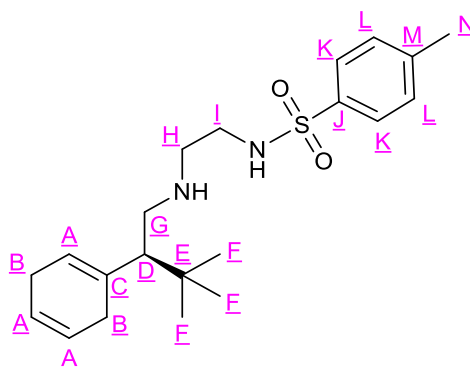
(*S**)-*N*-(2-(Cyclohexa-1,4-dien-1-yl)-3,3-dimethylbutyl)-2-(methylamino)acetamide (0.22 g, 0.56 mmol) was dissolved in anhydrous THF (15 mL) and added dropwise to a suspension of LiAlH$_4$ (0.05 g, 1.41 mmol, 2.50 eq.) in anhydrous THF (5 mL) under N$_2$. The reaction was heated at relux overnight. The reaction was allowed to cool to room temperature, quenched with NaHCO$_3$ (20 mL), to give a biphasic mixture, which was then filtered. The sticky solid was washed with Et$_2$O (200 mL). Et$_2$O (200 mL) was added and the organic solution was extracted with H$_2$O (50 mL). The aqueous layer was washed with Et$_2$O (2 x 30 mL) and the organic layers combined, dried with Na$_2$SO$_4$, then filtered. The solvent was removed under

reduced pressure and the product was dried further on a vacuum line to yield a yellow oil (0.20 g, 0.53 mmol, 95 %). ^{1}H-NMR (CDCl$_3$, 400 MHz): δ = 7.67-7.78 (m, 2H, H$_J$), 7.24-7.28 (m, 2H, H$_K$), 5.39-5.69 (m, 3H, H$_A$), 2.91-2.94 (m, 1H, H$_{G/H/I}$), 2.43 (s, 3H, H$_N$), 2.39-3.12 (m, 7H, H$_B$ + H$_G$ + H$_H$ + H$_I$), 1.47-2.01 (m, 3H, H$_B$ + H$_D$), 0.80-0.91 (m, 9H, H$_F$); ^{13}C{^{1}H}-NMR (CDCl$_3$, 400 MHz): δ = 143.3 (1C, C$_M$), 136.8 (1C, C$_J$), 134.8 (1C, C$_C$), 129.7 (2C, C$_L$), 127.1 (2C, C$_K$), 124.3 + 124.4 (3C, C$_A$), 47.8 (1C, C$_{G/H/I}$), 47.2 (1C, C$_{G/H/I}$), 42.2 (1C, C$_{G/H/I}$), 33.0 (1C, C$_E$), 30.4 (1C, C$_D$), 28.8 (3C, C$_F$), 26.8 (2C, C$_B$), 21.5 (1C, C$_N$) ppm; HRMS (ESI$^+$): m/z found 377.2260 [M + H]$^+$; C$_{21}$H$_{33}$N$_2$O$_2$S [M + H]$^+$ requires 377.2257; **12b** (C$_{21}$H$_{32}$N$_2$O$_2$S; 376.5560 g/mol).

[Ru(η^6-(*S**)-*N*-(2-((2-(Cyclohexa-1,4-dien-1-yl)-3,3-dimethylbutyl)amino)ethyl)-4-methylbenzenesulfonamide)Cl$_2$]$_2$.2HCl (13b)
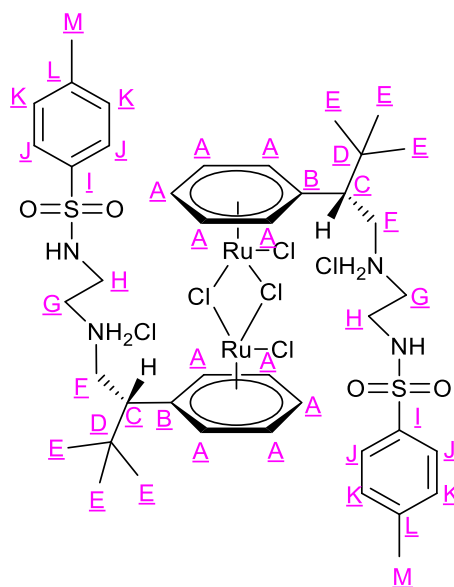

RuCl$_3$xH$_2$O (26.97 mg, 0.13 mmol, 0.25 eq.), HCl$_{(aq)}$ (12 M, 84.30 μL, 1.02 mmol, 2 eq.) and ethanol (1 mL) were added to the (*S**)-*N*-(2-((2-(cyclohexa-1,4-dien-1-yl)-3,3-dimethylbutyl)amino)ethyl)-4-methylbenzenesulfonamide (0.20 g, 0.51 mmol, 1 eq.). The reaction was heated at reflux overnight. The solution was pipetted into Et$_2$O (10 mL) and left in the fridge (5 °C) for two hours to precipitate. The light brown solid was separated from the supernatant by centrifugation (10,000 rpm for 5 minutes). Analysis by ^{1}H-NMR confirmed excess diene remained, therefore additional RuCl$_3$xH$_2$O (26.97 mg, 0.13 mmol, 0.25 eq.) was added. The reaction was heated at 70 °C overnight, then allowed to cool to room temperature. The solution was pipetted into Et$_2$O (10 mL) and left in the fridge (5 °C) for two hours to precipitate. The brown solid was separated from the supernatant by centrifugation

(10,000 rpm for five minutes) and combined with the earlier crop (24.10 mg, 0.02 mmol, 16 %). Note: Number of moles and % yields were calculated assuming zero equivalents of H_2O for $RuCl_3xH_2O$ as the extent of hydration was not calculated. Due to the low quantity of solid obtained, and the difficulty in separating the product from excess ligand used in the reaction, the product was taken forward and used directly in the next step of the synthesis without further purification or full characterisation. **13b** ($C_{42}H_{62}Cl_6N_4O_4Ru_2S_2$; 1165.95 g/mol).

Final complex (14b)

[Ru(η^6-(S^*)-N-(2-((2-(cyclohexa-1,4-dien-1-yl)-3,3-dimethylbutyl)amino)ethyl)-4-methylbenzenesulfonamide)Cl$_2$]$_2$.2HCl (24.10 mg, 0.02 mmol, 1 eq.) was suspended in DCM (5 mL) then DIPEA (0.04 mmol, 7.19 µL, 2 eq.) was added and the suspension was stirred under N_2. After 20 minutes, the solution was purified through a pipette column containing silica gel using a solvent system of DCM/MeOH (0-1 % MeOH). The solvent was removed under reduced pressure and the product was dried further on a vacuum line as a brown oil (15.60 mg, 0.03 mmol, 76 %). ^{1}H-NMR (CDCl$_3$, 400 MHz): δ = 7.71-7.76 (m, 4H, H$_D$), 7.15-7.16 (m, 4H, H$_C$), 6.67 (br. s, 1H, H$_M$), 6.38 (br. s, 1H, H$_M$), 5.67-5.88 (m, 1H, H$_M$), 5.37-5.41 (m, 1.50H, H$_M$), 5.14 (br. s, 1H, H$_M$), 4.92-5.01 (m, 1.50H, H$_M$), 3.97-4.00 (m, 2H, 2 x NH), 2.40-3.55 (m, 14H, H$_F$ + H$_G$ + H$_H$ + H$_I$), 2.33 (s, 6H, H$_A$), 1.14 (s, 18H, H$_K$) ppm. Note: ^{1}H-NMR assigned to show the two diastereoisomers present in the sample, however, the signals overlap directly due to identical properties. Broad peaks made the spectrum challenging to determine, therefore the assignments were made based on the other catalysts within this family; ^{13}C{^{1}H}-NMR (CDCl$_3$, 400 MHz): δ = 140.8 (1C, C$_E$), 140.7 (1C, C$_E$), 140.4 (1C, C$_B$), 140.3 (1C, C$_B$), 128.9 (2C, C$_C$), 128.8 (2C, C$_C$), 127.5 (2C, C$_D$), 127.4 (2C, C$_D$), 102.0 (1C, C$_L$), 101.5 (1C, C$_L$), 94.6 (1C, C$_M$), 94.5 (1C, C$_M$), 93.1 (1C, C$_M$), 92.2 (1C, C$_M$), 81.1 (1C, C$_M$), 77.4 (1C, C$_M$), 77.2 (1C, C$_M$), 75.8 (1C, C$_M$), 73.4 (1C, C$_M$), 72.7 (1C, C$_M$), 63.3 (1C, C$_H$), 61.4 (1C, C$_I$), 61.2 (1C, C$_H$), 58.4 (1C, C$_I$), 57.0 (1C, C$_I$), 56.0 (1C, C$_{F/G}$), 51.5 (1C, C$_{F/G}$), 49.7 (1C, C$_{F/G}$), 33.3 (2C, C$_J$), 28.9 (2C, C$_K$), 28.7 (2C, C$_K$), 28.2 (2C, C$_K$), 21.7 (1C, C$_A$), 21.5 (1C, C$_A$) ppm. Note: ^{13}C-NMR showed two diastereoisomers were present, plus excess

ligand was observed in the spectrum; HRMS (ESI+) m/z found 475.1001 [M - Cl]+; $C_{21}H_{29}N_2O_2RuS$ [M - Cl]+ requires 475.0993; **14b** ($C_{21}H_{29}ClN_2O_2RuS$; 510.0552 g/mol).

Final complex (14)
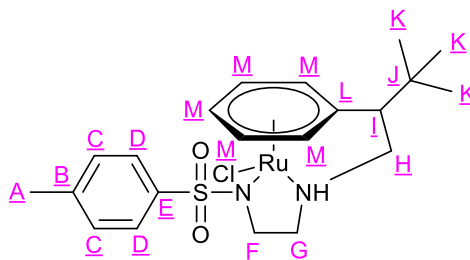
Brown oil (5 mg, 9.80 x 10^{-3} mmol) synthesised by Dr Murray's research group. ^{1}H-NMR (CDCl$_3$, 400 MHz): δ = 7.71-7.76 (m, 4H, H$_D$), 7.14-7.16 (m, 4H, H$_C$), 6.67 (t, 1H, J = 5.61 Hz, H$_M$), 6.38 (t, 1H, J = 5.15 Hz, H$_M$), 5.66-5.74 (m, 4H, H$_M$), 5.35-5.43 (m, 1.50H, H$_M$), 4.92-5.15 (m, 3.50H, H$_M$), 2.25-4.36 (m, 12H*, H$_F$ + H$_G$ + H$_H$ + H$_I$), 2.33 (s, 6H, H$_A$), 1.14 (s, 18H, H$_K$) ppm. <u>Note:</u> ^{1}H-NMR assigned to show the 2 diastereoisomers present in the sample, however, the signals overlap directly due to identical properties. Broad peaks made the spectrum challenging to determine, therefore the assignments were made based on the other catalysts within this family; ^{13}C{^{1}H}-NMR (CDCl$_3$, 400 MHz): δ = 140.8 (2C, C$_E$), 140.3 (2C, C$_B$), 129.0 (4C, C$_C$), 127.3 (4C, C$_D$), 101.2 (2C, C$_L$), 94.7 (1C, C$_M$), 94.5 (1C, C$_M$), 93.0 (1C, C$_M$), 92.2 (1C, C$_M$), 81.2 (1C, C$_M$), 77.4 (1C, C$_M$), 77.3 (1C, C$_M$), 75.8 (1C, C$_M$), 73.4 (1C, C$_M$), 72.7 (1C, C$_M$), 63.2 (2C, C$_H$), 61.5 (2C, C$_I$), 57.1 (2C, C$_{F/G}$), 51.5 (2C, C$_{F/G}$), 33.4 (2C, C$_J$), 28.6 (6C, C$_K$), 21.6 (2C, C$_A$) ppm. <u>Note:</u> peaks found based on previous assignments by other catalysts within this family that had provided more concentrated samples with cleaner spectra. Only one diastereoisomer observed, however this could have been due to the dilute concentration; HRMS (ESI+) m/z found 475.0992 [M - Cl]+; $C_{21}H_{29}N_2O_2RuS$ [M - Cl]+ requires 475.0993; **14** ($C_{21}H_{29}ClN_2O_2RuS$; 510.0552 g/mol).

*Should integrate to 14H.

3-(Cyclohexa-1,4-dien-1-yl)butanoic acid (15)
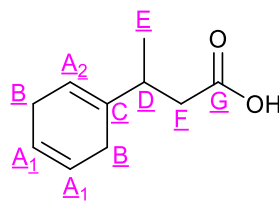
A solution of 3-phenylbutyric acid (5.00 g, 30.45 mmol, 1 eq.) in ethanol (200 mL) was added to liquid NH_3 (400 mL) at -77 °C. Lithium wire (4.10 g, 0.59 mol, 19 eq.) was washed in hexane before addition in 0.50 g portions until a dark blue colour persisted. The reaction was left to stand overnight to leave a white solid. H_2O (500 mL) was added whilst stirring at 0 °C, followed by addition of $HCl_{(aq)}$ (12 M, 100 mL) to acidify the solution. The cloudy suspension was extracted with Et_2O (3 x 100 mL) and the organic layers combined. After drying with Na_2SO_4, the solution was filtered and the solvent removed under reduced pressure to yield the acid as a colourless oil (4.28 g, 25.75 mmol, 84 %). ^{1}H-NMR (CDCl$_3$, 400 MHz): δ = 5.65-5.75 (m, 2H, H$_{A1}$), 5.50-5.50 (m, 1H, H$_{A2}$), 2.55-2.71 (m, 5H, H$_B$ + H$_D$), 2.48-2.54 (m, 1H, H$_F$), 2.28-2.34 (m, 1H, H$_F$), 1.10 (d, 3H, *J* = 6.88 Hz, H$_E$) ppm; ^{13}C{^{1}H}-NMR (CDCl$_3$, 400 MHz): δ = 179.4 (1C, C$_G$), 137.8 (1C, C$_C$), 124.3 (1C, C$_{A1}$), 124.3 (1C, C$_{A1}$), 118.3 (1C, C$_{A2}$), 40.5 (1C, C$_F$), 37.4 (1C, C$_D$), 26.8 (1C, C$_B$), 26.5 (1C, C$_B$), 19.2 (1C, C$_E$) ppm; HRMS (ESI$^-$) m/z found 163.0769 [M - 3H]$^-$; C$_{10}$H$_{11}$O$_2$ [M - 3H]$^-$ requires 163.0765; **15** (C$_{10}$H$_{14}$O$_2$; 166.2170 g/mol). This piece of MS data was unexpected and not in agreement with other data found for the compound. The data suggests re-aromatisation of the ring but this piece of evidence was an outlier as the Birch reduced ring was confirmed in the subsequent steps of this reaction pathway.

3-(Cyclohexa-1,4-dien-1-yl)-*N*-(2-((4-methylphenyl)sulfonamido)ethyl)butanamide (16)
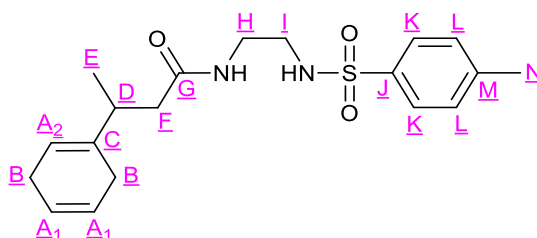
3-(Cyclohexa-1,4-dien-1-yl)butanoic acid (2.00 g, 12.03 mmol, 1 eq.), HOBt.xH$_2$O (1.62 g, 12.03 mmol, 1 eq.) and TBTU (4.62 g, 14.44 mmol, 1.20 eq.) were dissolved in DMF (20 mL), DCM (20 mL) and DIPEA (4.18 mL, 24.06 mmol, 2 eq.). The solution was left to stir for

5 minutes before N-(2-aminoethyl)-4-methylbenzenesulfonamide (2.61 g, 12.03 mmol, 1 eq.) was added and the resulting yellow solution was left to stir overnight at room temperature. The solution was pipetted into $HCl_{(aq)}$ (1 M, 100 mL) and extracted with DCM (2 x 50 mL). The organic layers were combined, dried with Na_2SO_4 and filtered. The solvent was removed under reduced pressure. The product was redissolved in Et_2O (150 mL) and the organic layer washed with H_2O (5 x 50 mL) to remove residual DMF. The organic layer was dried with Na_2SO_4 and filtered. The solvent was removed under reduced pressure to yield an orange oil and the crude product was purified by column chromatography on silica gel with a solvent system of DCM/MeOH (0-3.50 %) to obtain the desired product as a white solid (3.11 g, 8.58 mmol, 72 %). ^1H-NMR ($CDCl_3$, 400 MHz): δ = 7.68-7.74 (m, 2H, H_K), 7.27-7.32 (m, 2H, H_L), 6.27-6.39 (m, 1H, NH-C=O), 5.66-5.80 (m, 2H, H_{A1}), 5.43-5.47 (m, 1H, H_{A2}), 5.53-5.57 (m, 1H, NH-SO_2), 3.22-3.41 (m, 2H, H_H), 3.01-3.05 (m, 2H, H_I), 2.52-2.69 (m, 5H, H_B + H_D), 2.42 (s, 3H, H_N), 2.26-2.34 (m, 1H, H_F), 2.05-2.15 (m, 1H, H_F), 0.98-1.06 (m, 3H, H_E) ppm; $^{13}C\{^1H\}$-NMR ($CDCl_3$, 400 MHz): δ = 173.4 (1C, C_G), 143.6 (1C, C_J), 138.1 (1C, C_C), 136.8 (1C, C_M), 129.9 (2C, C_L), 127.0 (2C, C_K), 124.3 (2C, C_{A1}), 118.4 (1C, C_{A2}), 43.3 (1C, C_G), 42.3 (1C, C_F), 39.3 (1C, C_I), 37.8 (1C, C_D), 26.7 (1C, C_B), 26.3 (1C, C_B), 21.6 (1C, C_N), 19.0 (1C, C_E) ppm; HRMS (ESI+): m/z found 385.1556 [M + Na]+; $C_{19}H_{29}N_2NaO_2S$ [M + Na]+ requires 385.1560; **16** ($C_{19}H_{26}N_2O_3S$; 362.4863 g/mol).

N-(2-((3-(Cyclohexa-1,4-dien-1-yl)butyl)amino)ethyl)-4-methylbenzenesulfonamide (17)
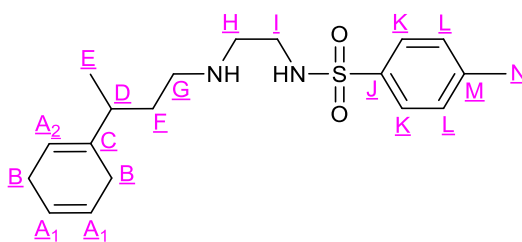
3-(Cyclohexa-1,4-dien-1-yl)-*N*-(2-((4-methylphenyl)sulfonamido)ethyl)butanamide (3.09 g, 8.52 mmol, 1 eq.) was dissolved in anhydrous THF (120 mL) and added dropwise to a suspension of $LiAlH_4$ (0.81 g, 21.31 mmol, 2.50 eq.) in anhydrous THF (30 mL) under N_2 at 0 °C. The reaction was heated at reflux overnight. The reaction was allowed to cool to room temperature, quenched with $NaHCO_{3(aq)}$ (50 mL), to give a biphasic mixture, which was filtered. The sticky residue was washed with Et_2O (100 mL). Et_2O (200 mL) was added and the organic solution was extracted with H_2O (50 mL). The aqueous layer was then washed

with Et_2O (2 x 30 mL). The organic layers were combined, dried with Na_2SO_4 and filtered. The solvent was removed under reduced pressure and the product was dried further on a vacuum line to yield a yellow oil (2.69 g, 7.72 mmol, 91 %). ^{1}H-NMR ($CDCl_3$, 400 MHz): δ = 7.74 (d, 2 H, J = 8.02 Hz, H_K), 7.29 (d, 2H, J = 8.25 Hz, H_L), 5.66-5.72 (m, 2H, H_{A1}), 5.39 (s, 1H, H_{A2}), 2.94-2.97 (m, 2H, H_I), 2.62-2.68 (m, 4H, $H_B + H_H$), 2.46-2.56 (m, 2H, H_B), 2.41 (m, 3H, H_N), 2.37-2.41 (m, 2H, H_G), 2.03-2.12 (m, 1H, H_D), 1.30-1.52 (m, 2H, H_F), 0.97 (d, 3H, J = 6.88 Hz, H_E) ppm; ^{13}C{^{1}H}-NMR ($CDCl_3$, 400 MHz): δ = 143.4 (1C, C_J), 138.7 (1C, C_C), 137.0 (1C, C_M), 129.8 (2C, C_L), 127.2 (2C, C_K), 124.5 (1C, C_{A1}), 124.4 (1C, C_{A1}), 118.3 (1C, C_{A2}), 48.1 (1C, C_H), 47.6 (1C, C_G), 42.5 (1C, C_I), 39.1 (1C, C_D), 34.9 (1C, C_F), 26.8 (1C, C_B), 25.5 (1C, C_B), 21.6 (1C, C_N), 19.7 (1C, C_E) ppm; HRMS (ESI$^+$): m/z found 349.1944 [M + H]$^+$; $C_{19}H_{29}N_2O_2S$ [M + H]$^+$ requires 349.1947; **17** ($C_{19}H_{28}N_2O_2S$; 348.5028 g/mol).

[Ru(η^6-*N*-(2-((3-(cyclohexa-1,4-dien-1-yl)butyl)amino)ethyl)-4-methylbenzenesulfonamide)Cl$_2$]$_2$.2HCl (18)
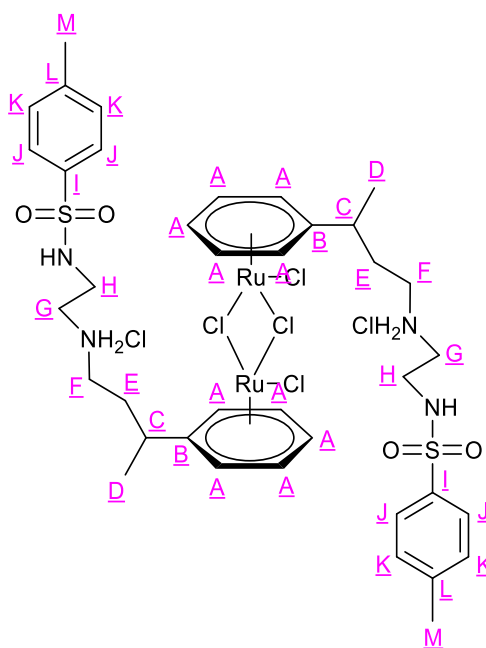
HCl$_{(aq)}$ (12 M, 1.19 mL, 14.34 mmol, 2 eq.) was added to *N*-(2-((3-(Cyclohexa-1,4-dien-1-yl)butyl)amino)ethyl)-4-methylbenzenesulfonamide (2.50 g, 7.17 mmol, 1 eq.) dissolved in ethanol (60 mL). The solution was stirred for 5-10 minutes then RuCl$_3$xH$_2$O (0.37 g, 1.79 mmol, 0.25 eq.) was added to the stirring solution. The reaction was heated at reflux overnight. Additional RuCl$_3$xH$_2$O (0.37 g, 1.79 mmol, 0.25 eq.) was added and the reaction was heated at reflux overnight again. The reaction was allowed to cool to room temperature.

Et_2O (5 mL) was added and the mixture was left in the freezer (-18 °C) for two hours to allow for precipitation. Centrifugation for 5 minutes at 10,000 rpm allowed the solid to be separated from the supernatant. The product was dried on a vacuum line as a light brown/orange solid (0.87 g, 0.79 mmol, 44 %). Note: Number of moles and % yields were calculated assuming zero equivalents of H_2O for $RuCl_3xH_2O$ as the extent of hydration was not calculated. ^{1}H-NMR (DMSO, 400 MHz): δ = 8.68 (br. s, 4H, 2 x NH_2Cl), 7.90 (m, 2H, 2 x NH), 7.68-7.72 (m, 4H, H_J), 7.42-7.44 (m, 4H, H_K), 7.14-7.33 (starting ligand), 5.19-6.45 (m, 9H*, H_A), 2.74-3.00 (m, 18H, $H_C + H_E + H_F + H_G + H_H$), 2.40 (s, 6H, H_M), 1.19-1.27 (m, 6H, H_D) ppm; ^{13}C{^{1}H}-NMR (DMSO, 400 MHz): δ = 143.2 (2C, C_I), 136.6 (2C, C_L), 129.9 (4C, C_K), 126.7 (4C, C_J), 109.0 (2C, C_B), 86.9 (2C, C_A), 86.6 (2C, C_A), 86.2 (2C, C_A), 85.4 (2C, C_A), 85.1 (2C, C_A), 46.2 (2C, C_G), 45.5 (2C, C_F), 44.9 (2C, C_H), 38.8 (2C, C_E), 33.3 (2C, C_C), 21.0 (2C, C_M), 18.6 (2C, C_D) ppm; **18** ($C_{38}H_{54}Cl_6N_4O_4Ru_2S_2$; 1109.8478 g/mol).

*Peaks only integrated to 9H but represent ten arene protons.

Final complex (19)
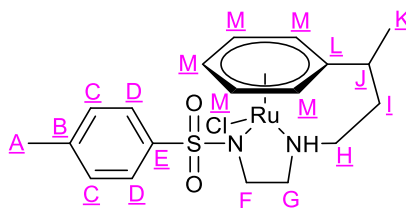
[Ru(η^6-*N*-(2-((3-(cyclohexa-1,4-dien-1-yl)butyl)amino)ethyl)-4-methylbenzenesulfonamide)Cl_2]$_2$.2HCl (0.50 g, 0.45 mmol, 1 eq.) was suspended in DCM (15 mL) then DIPEA (86.30 µL, 0.50 mmol, 1 eq.) was added and the suspension was left to stir under N_2. After 20 minutes, a sample was removed and analysed by ^{1}H-NMR to confirm an incomplete reaction. Additional DIPEA (86.30 µL, 0.50 mmol, 1 eq.) was added and left to stir for another 20 minutes. ^{1}H-NMR confirmed completion of the reaction. The product was purified by a plug of silica with a solvent system of DCM/MeOH (1 % MeOH). The product fractions, which were intensely yellow in colour, were combined. The solvent was removed under reduced pressure and the product was dried on a vacuum line as a light brown solid (0.27 g, 0.56 mmol, 62 %). ^{1}H-NMR (CDCl$_3$, 400 MHz): δ = 7.73 (t, 4H, *J* = 7.68 Hz, H_D), 7.14-7.17 (m, 4H, H_C), 6.58 (t, 1H, *J* = 5.62 Hz, H_M), 6.27 (t, 1H, *J* = 5.39 Hz, H_M), 6.00 (t, 1H, *J* = 5.62 Hz, H_M), 5.82-5.91 (m, 3H, H_M), 5.11 (d, 1H, *J* = 5.73 Hz, H_M), 4.97 (d, 1H, *J* = 5.73 Hz, H_M), 4.92 (d, 2H, *J* = 5.73 Hz, H_M), 3.74-3.92 (m, 2H, 2 x NH), 3.16-3.41 (m,

2H, H$_H$), 3.00-3.08 (m, 3H, H$_H$ + H$_{F/G}$), 2.36-2.74 (m, 8H, H$_J$ + H$_F$ + H$_G$), 2.33-2.34 (m, 6H, H$_A$), 1.84-2.29 (m, 5H, H$_I$ + H$_F$ + H$_G$), 1.39 (dd, 6H, J = 7.11 Hz, 2.52 Hz, H$_K$) ppm. <u>Note:</u> ^{1}H-NMR assigned to show the 2 diastereoisomers present in the sample, however, the signals overlap directly due to identical properties; ^{13}C{^{1}H}-NMR (CDCl$_3$, 400 MHz): δ = 140.6 (2C, C$_E$), 140.4 (2C, C$_B$), 128.9 (1C, C$_C$), 128.8 (1C, C$_C$), 127.6 (1C, C$_D$), 127.4 (1C, C$_D$), 103.4 (1C, C$_L$), 103.3 (1C, C$_L$), 94.0 (1C, C$_M$), 93.7 (1C, C$_M$), 92.4 (1C, C$_M$), 90.1 (1C, C$_M$), 79.6 (1C, C$_M$), 77.5 (1C, C$_M$), 77.43 (1C, C$_M$), 75.1 (1C, C$_M$), 75.0 (1C, C$_M$), 68.6 (1C, C$_M$), 58.4 (1C, C$_{F/G}$), 57.1 (1C, C$_{F/G}$), 53.8 (1C, C$_H$), 51.7 (1C, C$_H$), 47.9 (1C, C$_{F/G}$), 47.7 (1C, C$_{F/G}$), 38.5 (1C, C$_I$), 36.0 (1C, C$_J$), 35.7 (1C, C$_J$), 34.7 (1C, C$_I$), 21.6 (2C, C$_A$), 20.6 (1C, C$_K$), 20.5 (1C, C$_K$) ppm; HRMS (ESI$^+$) m/z found 447.0686 [M - Cl]$^+$; C$_{19}$H$_{25}$N$_2$O$_2$RuS [M - Cl]$^+$ requires 447.0679; **19** (C$_{19}$H$_{25}$ClN$_2$O$_2$RuS; 482.0020 g/mol); Found (%): C, 46.66; H, 4.92; N, 5.68. Expected (%): C, 47.34; H, 5.23; N, 5.81 (analysis performed without the addition of V$_2$O$_5$); Unit cell: a = 10.6086(15) Å, b = 17.320(4) Å, c = 21.602(4) Å. α = 90°, β = 90°, γ = 90°.

(*S*)-3-(Cyclohexa-1,4-dien-1-yl)butan-1-amine (20)
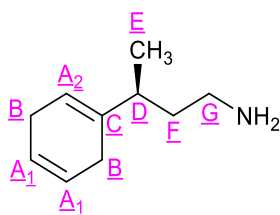
A solution of (*S*)-3-phenylbutan-1-amine (0.60 g, 4.02 mmol, 1 eq.) in ethanol (60 mL) was added to liquid NH$_3$ (170 mL) at -77 °C. Lithium wire (0.20 g, 28.00 mmol, 7 eq.) was washed in hexane before addition in 0.5 g portions until a dark blue colour persisted. The reaction was left to stand overnightto leave a white solid. H$_2$O (100 mL) was added whilst stirring at 0 °C and the pH was found to be ~10. The aqueous mixture was washed with DCM (3 x 100 mL) and the organic layers combined. After drying with Na$_2$SO$_4$, the solution was filtered and the solvent was removed under reduced pressure. The product was dried further on a vacuum line to yield the amine as a yellow oil (0.48 g, 3.17 mmol, 79 %). ^{1}H-NMR (CDCl$_3$, 400 MHz): δ = 5.63-5.72 (m, 2H, H$_{A1}$), 5.37-5.44 (m, 1H, H$_{A2}$), 2.46-2.68 (m, 6H, H$_B$ + H$_G$), 2.11-2.19 (m, 1H, H$_D$), 1.61 (br. s, 2H, NH$_2$), 1.35-1.57 (m, 4H, H$_F$), 0.97 (d, 3H, J = 6.86 Hz, H$_E$) ppm; ^{13}C{^{1}H}-NMR (CDCl$_3$, 400 MHz): δ = 138.8 (1C, C$_C$), 124.4 (2C, C$_{A1}$), 118.1 (1C, C$_{A2}$), 40.5 (1C, C$_G$), 38.8 (1C, C$_D$), 38.7 (1C, C$_F$), 26.8 (1C, C$_B$), 25.5 (1C, C$_B$), 19.6 (1C, C$_E$) ppm; HRMS (ESI$^+$): m/z found 152.1436 [M + H]$^+$; C$_{10}$H$_{18}$N [M + H]$^+$ requires 152.1434; **20** (C$_{10}$H$_{17}$N; 151.2487 g/mol).

(S)-N-(3-(Cyclohexa-1,4-dien-1-yl)butyl)-2-((4-methylphenyl)sulfonamido)acetamide (21)
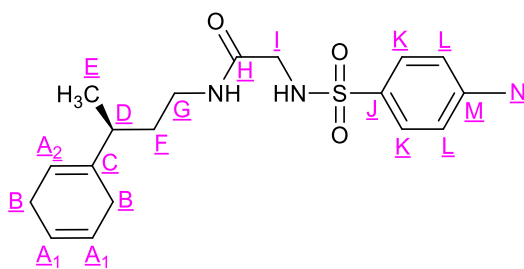
To a solution of (p-Toluenesulfonyl)glycine (0.44 g, 1.91 mmol, 1 eq.) in DMF (4 mL) was added TBTU (0.61 g, 1.91 mmol, 1 eq.) and DIPEA (1.00 mL, 5.73 mmol, 3 eq.). The solution was left to stir for 5 minutes before (S)-3-(cyclohexa-1,4-dien-1-yl)butan-1-amine (0.29 g, 1.91 mmol, 1 eq.) as a solution in DCM (6 mL) was added. The resulting orange suspension was left to stir overnight. Following this, the product solution was diluted with DCM (100 mL) and extracted with sat. $NH_4Cl_{(aq)}$ (3 x 50 mL). The organic layer was dried with Na_2SO_4 and filtered. The solvent was removed under reduced pressure. The product was purified by column chromatography on silica gel with a solvent system of DCM/MeOH (0-1 %) to obtain the product as a yellow oil (0.45 g, 1.24 mmol, 65 %). ^{1}H-NMR (CDCl$_3$, 400 MHz): δ = 7.69-7.73 (m, 2H, H$_K$), 7.28-7.31 (m, 2H, H$_L$), 6.52 (t, 1H, J = 5.72 Hz, NH), 5.66-5.72 (m, 2H, H$_{A1}$), 5.44-5.46 (m, 1H, H$_{A2}$), 3.52 (s, 2H, H$_I$), 3.04-3.21 (m, 2H, H$_G$), 2.40-2.73 (m, 4H, H$_B$), 2.41 (s, 3H, H$_N$), 2.07-2.16 (m, 1H, H$_D$), 1.38-1.61 (m, 2H, H$_F$), 0.99 (d, 3H, J = 6.86 Hz, H$_E$) ppm; ^{13}C{^{1}H}-NMR (CDCl$_3$, 400 MHz): δ = 167.9 (1C, C$_H$), 144.2 (1C, C$_J$), 138.2 (1C, C$_C$), 135.8 (1C, C$_M$), 130.1 (2C, C$_L$), 127.3 (2C, C$_K$), 124.7 (1C, C$_{A1}$), 124.4 (1C, C$_{A1}$), 118.9 (1C, C$_{A2}$), 46.0 (1C, C$_I$), 39.3 (1C, C$_D$), 38.4 (1C, C$_G$), 33.8 (1C, C$_F$), 26.8 (1C, C$_B$), 25.3 (1C, C$_B$), 21.7 (1C, C$_N$), 19.6 (1C, C$_E$) ppm; HRMS (ESI$^+$): m/z found 363.1732 [M + H]$^+$; $C_{19}H_{27}N_2O_3S$ [M + H]$^+$ requires 363.1737; **21** ($C_{19}H_{26}N_2O_3S$; 362.4863 g/mol).

(*S*)-*N*-(2-((3-(Cyclohexa-1,4-dien-1-yl)butyl)amino)ethyl)-4-methylbenzenesulfonamide (17a)
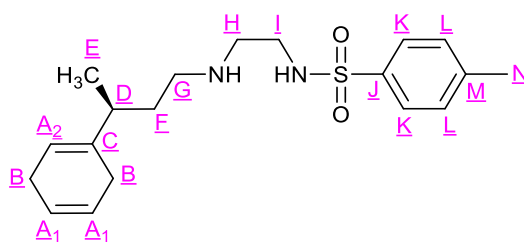
(*S*)-*N*-(3-(Cyclohexa-1,4-dien-1-yl)butyl)-2-((4-methylphenyl)sulfonamido)acetamide (0.45 g, 1.24 mmol, 1 eq.) was dissolved in anhydrous THF (25 mL) and added dropwise to a suspension of $LiAlH_4$ (0.12 g, 3.10 mmol, 2.50 eq.) in anhydrous THF (5 mL) under N_2. The reaction was stirred at room temperature for 96 hours. The reaction was cooled to 0 °C and quenched with $NaHCO_{3(aq)}$ (50 mL), to give a biphasic mixture, which was filtered. The sticky grey solid was washed with Et_2O (50 mL). Et_2O (50 mL) was added and the organic solution was extracted with H_2O (50 mL). The aqueous layer was washed with Et_2O (2 x 30 mL). The organic layers were combined, dried with Na_2SO_4 and filtered. The solvent was removed under reduced pressure. The crude product was purified by column chromatography on silica gel, eluting with DCM to obtain the product as a yellow oil (0.08 g, 0.23 mmol, 19 %). ^{1}H-NMR (CDCl$_3$, 400 MHz): δ = 7.64-7.68 (m, 2H, H$_K$), 7.18-7.23 (m, 2H, H$_L$), 5.59-5.65 (m, 2H, H$_{A1}$), 5.28-5.37 (m, 1H, H$_{A2}$), 2.84-2.92 (s, 2H, H$_I$), 2.52-2.64 (m, 4H, H$_B$ + H$_G$), 2.38-2.51 (m, 2H, H$_B$), 2.34 (s, 3H, H$_N$), 2.22-2.35 (m, 2H, H$_H$), 1.88-2.05 (m, 1H, H$_D$), 1.18-1.52 (m, 2H, H$_F$), 0.90 (d, 3H, *J* = 7.09 Hz, H$_E$) ppm; ^{13}C{^{1}H}-NMR (CDCl$_3$, 400 MHz): δ = 143.3 (1C, C$_J$), 138.5 (1C, C$_C$), 136.9 (1C, C$_M$), 129.7 (2C, C$_L$), 127.2 (2C, C$_K$), 124.4 (1C, C$_{A1}$), 124.3 (1C, C$_{A1}$), 118.2 (1C, C$_{A2}$), 48.0 (1C, C$_H$), 47.5 (1C, C$_G$), 42.3 (1C, C$_I$), 39.1 (1C, C$_D$), 34.6 (1C, C$_F$), 26.7 (1C, C$_B$), 25.4 (1C, C$_B$), 21.6 (1C, C$_N$), 19.6 (1C, C$_E$) ppm; HRMS (ESI$^+$): m/z found 349.1952 [M + H]$^+$; C$_{19}$H$_{29}$N$_2$O$_2$S [M + H]$^+$ requires 349.1944; **17a** (C$_{19}$H$_{28}$N$_2$O$_2$S; 348.5028 g/mol).

[Ru(η6-(*S*)-*N*-(2-((3-(cyclohexa-1,4-dien-1-yl)butyl)amino)ethyl)-4-methylbenzenesulfonamide)Cl2]2.2HCl (18a)
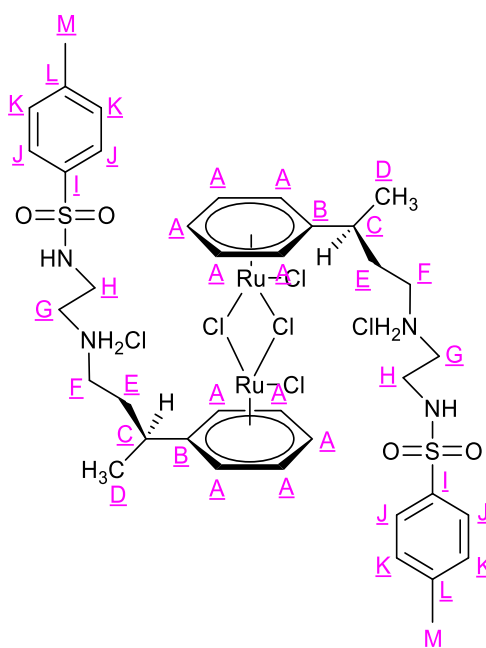
RuCl3xH2O (12.45 mg, 0.06 mmol, 0.25 eq.) in ethanol (1 mL) was refluxed for three hours. HCl(aq) (12 M, 38.02 µL, 0.46 mmol, 2 eq.) was added to (*S*)-*N*-(2-((3-(Cyclohexa-1,4-dien-1-yl)butyl)amino)ethyl)-4-methylbenzenesulfonamide (0.08 g, 0.23 mmol, 1 eq.) dissolved in ethanol (2 mL). The solution was stirred for 5-10 minutes and then was added to the RuCl3xH2O in ethanol. The reaction was heated at reflux overnight. The reaction was allowed to cool to room temperature. The solution was added to Et2O (8 mL) and left in the fridge (5 °C) to precipitate. The dark brown solid was separated from the liquid by centrifugation at 10,000 rpm for five minutes. The solid was confirmed by ^{1}H-NMR to not be the product. The solvent of the liquid phase was removed under reduced pressure and then the product was redissolved in ethanol (1 mL). RuCl3xH2O (12.45 mg, 0.06 mmol, 0.25 eq.) was added and the solution was heated at reflux overnight. The reaction was allowed to cool to room temperature. The solution was added to Et2O (8 mL) and left in the fridge (5 °C) to precipitate. The light brown solid was separated from the liquid by centrifugation at 10,000 rpm for five minutes. The product was dried on a vacuum line to give the product as a light brown solid (0.03 g, 0.03 mmol, 52 %). Note: Number of moles and % yields were calculated assuming zero equivalents of H2O for RuCl3xH2O as the extent of hydration was not calculated. Due to the low quantity of solid obtained, and the difficulty in separating the product from excess ligand used in the reaction, the product was taken forward and used directly in the next step

of the synthesis without further purification or full characterisation. **18a** ($C_{38}H_{54}Cl_6N_4O_4Ru_2S_2$; 1109.8478 g/mol).

Final complex (19a)
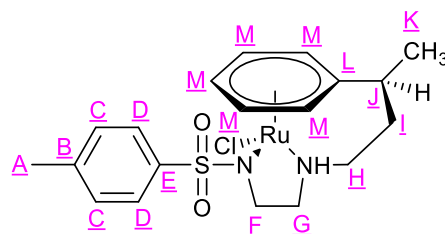
[Ru(η^6-(*S*)-*N*-(2-((3-(cyclohexa-1,4-dien-1-yl)butyl)amino)ethyl)-4-methylbenzenesulfonamide)Cl$_2$]$_2$.2HCl (0.03 g, 0.03 mmol, 1 eq.) was suspended in DCM (5 mL) then DIPEA (10.45 µL, 0.06 mmol, 2 eq.) was added and the suspension was stirred under N_2. After one hour, a colour change to yellow/orange was seen and the suspension became a solution. ^{1}H-NMR confirmed completion of the reaction. The product was purified through a pipette column containing silica gel using a solvent system of DCM/MeOH (0-5 % MeOH). The solvent was removed under reduced pressure and the product was dried further on a vacuum line as a brown oil (7.50 mg, 0.02 mmol, 33 %). ^{1}H-NMR (CDCl$_3$, 400 MHz): δ = 7.73 (t, 4H, *J* = 6.63 Hz, H$_D$), 7.15-7.16 (m, 4H, H$_C$), 6.54-6.58 (m, 1H, H$_M$), 6.24-6.28 (m, 1H, H$_M$), 5.97-6.01 (m, 1H, H$_M$), 5.83-5.89 (m, 3H, H$_M$), 5.11-5.13 (m, 1H, H$_M$), 4.92-4.98 (m, 3H, H$_M$), not observed (br. s, 2H, 2 x NH), 3.34-3.41 (m, 2H, H$_H$), not observed (3H, H$_H$ + H$_{F/G}$), 2.67-2.74 (m, 2H, H$_{F/G/J}$), not observed (6H, H$_{F/G/J}$), 2.33 (s, 6H, H$_A$), 1.84-2.29 (m, 5H, H$_I$ + H$_F$ + H$_G$), not observed (6H, H$_K$) ppm. <u>Note:</u> ^{1}H-NMR assigned to show the two diastereoisomers present in the sample, however, the signals overlap directly due to identical properties. Integrals of aliphatic protons did not perfectly match arene protons (or simply were not observed) due to contaminating DIPEA, however, ppm shifts match that of the racemic analogue; ^{13}C{^{1}H}-NMR (CDCl$_3$, 400 MHz): δ = 140.7, 140.4, 128.9, 128.8, 127.6, 127.4, 103.4, 103.3, 94.0, 93.7, 92.4, 90.1, 79.6, 77.5, 77.3, 75.2, 75.0, 68.6, 58.6, 57.1, 53.9, 51.7, 47.9, 47.7, 38.5, 36.0, 35.7, 34.7, 21.6, 20.6, 20.5 ppm. <u>Note:</u> ppm shifts were identified by comparison to the racemic analogue, some peaks were very small in size. Assignments can be assumed to match that assigned for the racemic analogue but cannot be unambiguously assigned based on the NMR data (including 2D-NMR) collected for this compound; HRMS (ESI$^+$) m/z found 447.0688 [M - Cl]$^+$; $C_{19}H_{25}N_2O_2RuS$ [M - Cl]$^+$ requires 447.0679; **19a** ($C_{19}H_{25}ClN_2O_2RuS$; 482.0020 g/mol).

(*R*)-2-(Cyclohexa-1,4-dien-1-yl)propan-1-amine (22)
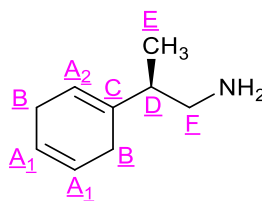
A solution of (*R*)-2-phenylpropan-1-amine (5.00 g, 36.98 mmol, 1 eq.) in ethanol (100 mL) was added to liquid NH_3 (500 mL) at -77 °C. Lithium wire (0.92 g, 0.13 mol, 3.60 eq.) was washed in hexane before addition in 0.5 g portions until a dark blue colour persisted. The reaction was left to stand overnight to leave a white solid. H_2O (200 mL) was added whilst stirring at 0 °C and the pH was found to be ~10. The aqueous mixture was extracted with DCM (3 x 100 mL) and the organic layers were combined. After drying with Na_2SO_4, the solution was filtered and the solvent was removed under reduced pressure. The product was dried further on a vacuum line as a yellow oil (4.45 g, 32.43 mmol, 88 %). ^{1}H-NMR (CDCl$_3$, 400 MHz): δ = 5.65-5.72 (m, 2H, H$_{A1}$), 5.47 (s, 1H, H$_{A2}$), 2.45-2.72 (m, 6H, H$_B$ + H$_B$ + H$_F$), 2.05-2.13 (m, 1H, H$_D$), 0.98 (d, 3H, *J* = 7.09 Hz H$_F$) ppm; ^{13}C{^{1}H}-NMR (CDCl$_3$, 400 MHz): δ = 136.7 (1C, C$_C$), 124.4 (1C, C$_{A1}$), 124.3 (1C, C$_{A1}$), 119.8 (1C, C$_{A2}$), 45.9 (1C, C$_F$), 44.6 (1C, C$_D$), 26.8 (1C, C$_B$), 25.9 (1C, C$_B$), 16.8 (1C, C$_E$) ppm; HRMS (ESI$^+$): m/z found 138.1277 [M + H]$^+$; C$_9$H$_{16}$N [M + H]$^+$ requires 138.1276; **22** (C$_9$H$_{15}$N; 137.2221 g/mol).

[Ru(η^6-(*R*)-2-(cyclohexa-1,4-dien-1-yl)propan-1-amine)Cl$_2$]$_2$.2HCl (23)
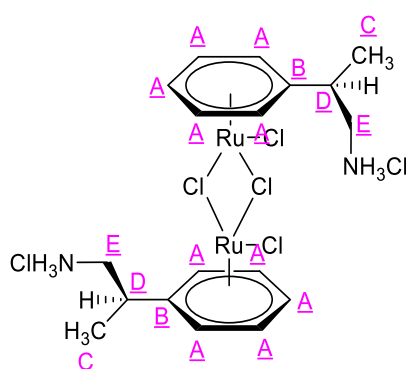
HCl$_{(aq)}$ (12 M, 2.41 mL, 29.20 mmol, 2 eq.) was added to (*R*)-2-(cyclohexa-1,4-dien-1-yl)propan-1-amine (2.00 g, 14.60 mmol) dissolved in ethanol (30 mL). The solution was stirred for 5-10 minutes then RuCl$_3$xH$_2$O (1.65 g, 7.30 mmol, 0.50 eq.) was added to the stirring solution. The reaction was heated at reflux overnight. The reaction was allowed to cool to room temperature. The sample was put in the freezer (-18 °C) for two hours. The

precipitate was isolated by centrifugation at 8,000 rpm for five minutes. The product was dried on a vacuum line as an orange solid (0.45 g, 0.65 mmol, 9 %). <u>Note:</u> Number of moles and % yields were calculated assuming zero equivalents of H_2O for $RuCl_3xH_2O$ as the extent of hydration was not calculated. ^{1}H-NMR (DMSO, 400 MHz): δ = 8.12 (s, 5H, NH$_3$Cl), 7.81-7.94 (m, 1H, NH$_3$Cl), 5.97-6.02 (m, 10H, H$_A$), 3.21-3.29 (m, 2H, H$_D$), 2.96-3.07 (m, 4H, H$_E$), 1.33 (d, 6H, J = 6.17 Hz H$_C$) ppm; ^{13}C{^{1}H}-NMR (DMSO, 400 MHz): δ = 104.0 (1C, C$_B$), 87.9 (2C, C$_A$), 86.4 (1C, C$_A$), 85.8 (1C, C$_A$), 85.6 (1C, C$_A$), 43.3 (1C, C$_E$), 34.6 (1C, C$_D$), 16.9 (1C, C$_C$) ppm; **23** ($C_{18}H_{28}Cl_6N_2Ru_2$; 687.2863 g/mol).

Final complex (24)
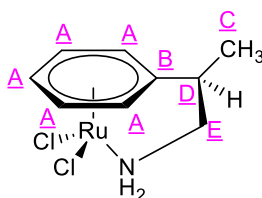
[Ru(η^6-(*R*)-2-(cyclohexa-1,4-dien-1-yl)propan-1-amine)Cl$_2$]$_2$.2HCl (0.20 g, 0.29 mmol, 1 eq.) was suspended in DCM (20 mL) then DIPEA (0.20 mL, 1.17 mmol, 4 eq.) was added and the suspension was left to stir under N$_2$ for 10 minutes. The reaction was purified on a plug of silica gel with a solvent system of DCM/MeOH (0-1 %). The product fractions, which were pale yellow coloured, were combined. The solvent was removed under reduced pressure and the product was dried further on a vacuum line to yield an orange solid (0.17 g, 0.55 mmol, 95 %). To remove residual DIPEA, the solid was dissolved in ethanol (~10 mL) and then the solution was concentrated to a volume of ~5 mL. The solution was left in the fridge (5 °C) to yield orange crystals, which were dried on a vacuum line (7.10 mg, 0.02 mmol, 3 %). ^{1}H-NMR (CDCl$_3$, 400 MHz): δ = 5.94 (t, 1H, J = 5.61 Hz, H$_A$), 5.83 (t, 1H, J = 5.61 Hz, H$_A$), 5.48 (t, 1H, J = 5.72 Hz, H$_A$), 5.34 (d, 1H, J = 5.49 Hz, H$_A$), 5.25 (d, 1H, J = 5.95 Hz, H$_A$), 3.33-4.03 (m, 4H, H$_E$ + NH$_2$), 3.15-3.24 (m, 1H, H$_D$), 1.45 (d, 3H, J = 6.86 Hz, H$_C$) ppm; ^{13}C{^{1}H}-NMR (CDCl$_3$, 400 MHz): δ = 108.2 (1C, C$_B$), 93.2 (1C, C$_A$), 92.4 (1C, C$_A$), 77.3 (1C, C$_A$), 72.8 (1C, C$_A$), 72.7 (1C, C$_A$), 62.8 (1C, C$_E$), 43.0 (1C, C$_D$), 15.2 (1C, C$_C$) ppm; HRMS (ESI$^+$) m/z found 271.9781 [M - Cl]$^+$; C_9H_{13}ClNRu [M - Cl]$^+$ requires 271.9774; **24** ($C_9H_{13}Cl_2NRu$; 307.1822 g/mol); Found (%): C, 34.66; H, 3.77; N, 4.22. Expected (%): C, 35.19; H, 4.27; N, 4.56 (analysis performed without the addition of V_2O_5, therefore we believe the difference in the theoretical and obtained results may be due to the incomplete

combustion of the sample); Unit cell: a = 7.9073(8) Å, b = 9.8097(11) Å, c = 14.1690(17) Å. α = 76.958(9)°, β = 81.930(9)°, γ = 89.229(8)°.

Arene exchange[122]

The ligand* was added to [Ru(C$_6$H$_5$CO$_2$Et)Cl$_2$]$_2$ in chlorobenzene. The red reaction mixture was heated to 90 °C for twenty-seven hours. After five hours the reaction turned black. The product was purified by column chromatography on silica gel with a solvent system of pure DCM. The different products observed by TLC were separated and the ^{1}H-NMR run, showing either no product or starting ligand.

Alternatively, the ligand* was added to [Ru(C$_6$H$_5$CO$_2$Et)Cl$_2$]$_2$ in chlorobenzene. The red reaction mixture was heated to 140 °C in a microwave for three consecutive runs; thirty minutes, thirty minutes and one hour. Although TLC analysis proved promising with the appearance of a new product spot, decomposition occurred, and ^{1}H-NMR confirmed the expected product was not present.

*Ligands investigated were the aromatic analogues of compounds **12** and **17**, i.e., the ring was not Birch reduced.

General procedure for the ATH reactions[150]
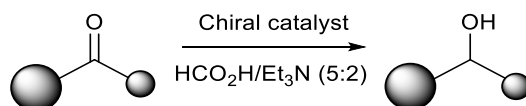
Scheme 90. Generic scheme showing the asymmetric transfer hydrogenation of ketones by a chiral catalyst. The larger ball signifies a group comprising of high electron density, for example an aryl or alkyne moiety, and the smaller ball signifies a group comprising of low electron density, for example an alkyl moiety.[111]

A solution of ruthenium complex (0.0150 mmol - **6a**, **6b**, **7**, **14a**, **14b**, **19a**, **24**) in an azeotropic mixture of formic acid/triethylamine (5:2, 1.50 mL) was stirred for 30 minutes at 40 °C under an inert atmosphere. The ketone substrate (3.00 mmol) was then added and the reaction mixture was stirred at 40 °C for 24 hours. The reaction mixture was diluted with DCM (20 mL) and then washed with NaHCO$_{3(aq)}$ (3 x 15 mL). The organic phase was dried with Na$_2$SO$_4$ and filtered. The solvent was removed under reduced pressure prior to analysis by ^{1}H-NMR. Residual metal-containing residues were removed from the resulting oil by purification through a plug of silica in a pipette eluting with a solvent system of EtOAc/Hexane

(1:1). The solvent was removed under reduced pressure and then the sample was analysed by chiral GC. GC chiral column: Restek RT-βDEXsm, 30 m x 0.25 mm x 0.25 μm. Method D: flow rate = 2.0 mL/min, start temperature = 60 °C, end temperature = 177 °C, rate of temperature ramp = 5 °C/min. Method E: flow rate = 2.0 mL/min, start temperature = 100 °C, end temperature = 100 °C, rate of temperature ramp = 0 °C/min.

Reduction products

1-Phenylethanol (25)
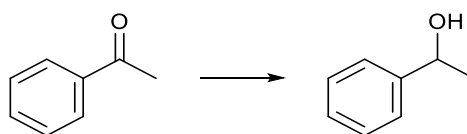
Prepared using general ATH procedure described above. Beige oil. Conversion determined by ^{1}H-NMR (CDCl$_3$, 400 MHz): δ = 7.96-7.99 (m, 2H, ketone Ph H), 7.56-7.60 (m, 4H, alcohol Ph H), 7.46-7.50 (m, 2H, ketone Ph H), 7.34-7.41 (m, 1H, ketone Ph H), 7.26-7.30 (m, 1H, alcohol Ph H), 4.92 (q, 1H, J = 11.6, 6.54 Hz, alcohol CHOH), 2.62 (s, 3H, ketone CH$_3$), 2.28 (br. s, 1H, OH), 1.52 (d, 3H, J = 6.42 Hz, alcohol CH$_3$) ppm. Enantioselectivity determined by chiral GC: METHOD D, ketone = 16.09 minutes, (*R*)-isomer = 18.72 minutes, (*S*)-isomer = 18.93 minutes.

1-Phenylpropanol (26)
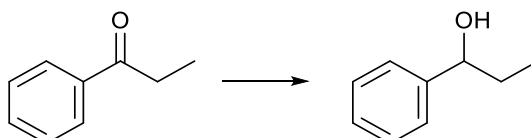
Prepared using general ATH procedure described above. Beige oil. Conversion determined by ^{1}H-NMR (CDCl$_3$, 400 MHz): δ = 7.94-8.03 (m, 2H, ketone Ph H), 7.55-7.58 (m, 1H, ketone Ph H), 7.43-7.53 (m, 2H, ketone Ph H), 7.35-7.41 (m, 4H, alcohol Ph H), 7.26-7.34 (m, 1H, alcohol Ph H), 4.60-4.64 (m, 1H, alcohol CHOH), 2.95-3.08 (m, 2H, ketone CH$_2$), 2.14 (br. s, 1H, OH), 1.72-1.90 (m, 2H, alcohol CH$_2$), 1.19-1.30 (m, 3H, ketone CH$_3$), 0.90-0.98 (m, 3H, alcohol CH$_3$) ppm. Enantioselectivity determined by chiral GC: METHOD E, ketone = 36.16 minutes, (*R*)-isomer = 81.58 minutes, (*S*)-isomer = 84.91 minutes.

2-Methyl-1-phenylpropanol (27)

Prepared using general ATH procedure described above. Colourless oil. Conversion determined by ^{1}H-NMR (CDCl$_3$, 400 MHz): δ = 7.93-8.02 (m, 2H, ketone Ph H), 7.54-7.58 (m, 1H, ketone Ph H), 7.46-7.49 (m, 2H, ketone Ph H), 7.33-7.35 (m, 1H, alcohol Ph H), 7.27-7.29 (m, 4H, alcohol Ph H), 4.39 (br. d, 1H, *J* = 6.19 Hz, alcohol CHOH), 3.50-3.65 (m, 1H, ketone CH), 1.95-2.00 (m, 1H, alcohol CH), 1.85 (br. s, 1H, OH), 1.19-1.28 (m, 6H, ketone CH$_3$), 1.02 (d, 3H, *J* = 6.65 Hz, alcohol CH$_3$), 0.82 (d, 3H, *J* = 6.65 Hz, alcohol CH$_3$) ppm. Low conversion did not allow for the enantioselectivity to be determined by chiral GC.

1-(4-Chlorophenyl)-ethanol (28)

Prepared using general ATH procedure described above. Beige oil. Conversion determined by ^{1}H-NMR (CDCl$_3$, 400 MHz): δ = 7.84-7.94 (m, 2H, ketone Ph H), 7.39-7.52 (m, 2H, ketone Ph H), 7.31 (s, 4H, alcohol Ph H), 4.84-4.93 (m, 1H, alcohol CHOH), 2.59 (s, 3H, ketone CH$_3$), 1.47 (d, 3H, *J* = 6.42 Hz, alcohol CH$_3$) ppm. Enantioselectivity determined by chiral GC: METHOD D, ketone = 24.31 minutes, t$_{R1}$ = 28.23 minutes, t$_{R2}$ =28.41 minutes.

1-(4-Methylphenyl)-ethanol (29)

Prepared using general ATH procedure described above. Colourless oil. Conversion determined by ^{1}H-NMR (CDCl$_3$, 400 MHz): δ =7.87 (d, 2H, *J* = 8.23 Hz, ketone Ph H), 7.30 (2H, alcohol Ph H hidden under ketone Ph H peak), 7.27 (d, 2H, *J* = 8.00 Hz, ketone Ph H), 7.16-7.18 (m, 2H, alcohol Ph H), 4.89 (q, 1H, *J* = 12.8, 6.4 Hz, alcohol CHOH), 2.59 (s, 3H, ketone CH$_3$), 2.42 (s, 3H, ketone CH$_3$), 2.35 (s, 3H, alcohol CH$_3$), 1.50 (d, 3H, *J* = 6.63 Hz,

alcohol CH$_3$) ppm. Enantioselectivity determined by chiral GC: METHOD D, ketone = 22.85 minutes, t_{R1} = 23.96 minutes, t_{R2} = 24.21 minutes.

1-(Pyridin-2-yl)ethanol (30)

Prepared using general ATH procedure described above. Colourless oil. Conversion determined by ^{1}H-NMR (CDCl$_3$, 400 MHz): δ = 8.68-8.69 (m, 1H, ketone Ph H), 8.03-8.04 (m, 1H, ketone Ph H), 7.83 (td, 1H, J = 7.72, 1.68 Hz, ketone Ph H), 7.46-7.49 (m, 1H, ketone Ph H), 2.72 (s, 3H, ketone CH$_3$) ppm. No conversion therefore enantioselectivity not determined by chiral GC.

1-Cyclohexylethanol (31)
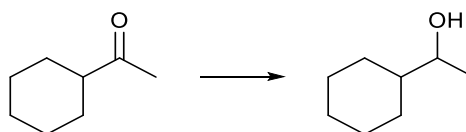
Prepared using general ATH procedure described above. Colourless oil. Conversion determined by ^{1}H-NMR (CDCl$_3$, 400 MHz): δ = 3.50-3.57 (m, 1H, ketone CHOH), 2.27-2.36 (m, 3H, alcohol cyclohexyl + CH$_3$), 2.12 (s, 3H, ketone CH$_3$), 1.64-1.87 (m, 5H, ketone cyclohexyl), 1.14-1.36 (m, 5H, ketone cyclohexyl) ppm. Enantioselectivity determined by chiral GC: METHOD E, ketone = 18.45 minutes, t_{R1} = 30.52 minutes, t_{R2} = 31.01 minutes.
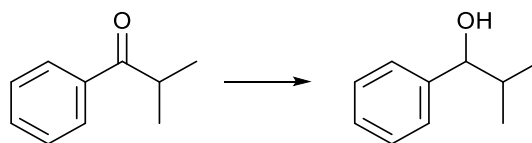
1-Phenyl-2,2,2-trifluoroethanol (32)
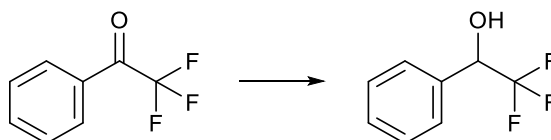
Prepared using general ATH procedure described above. Orange oil. Conversion determined by ^{1}H-NMR (CDCl$_3$, 400 MHz): δ = 8.10 (d, 2H, J = 7.78 Hz, ketone Ph H), 7.73 (t, 1H, J = 7.44 Hz, ketone Ph H), 7.57 (t, 2H, J = 7.89 Hz, ketone Ph H), 7.47-7.50 (m, 2H, alcohol Ph H), 7.42-7.44 (m, 3H, alcohol Ph H), 4.99-5.05 (m, 1H, alcohol CHOH) ppm.

Enantioselectivity determined by chiral GC: METHOD D, ketone = 9.09 minutes, t_{R1} = 20.63 minutes, t_{R2} = 20.73 minutes.
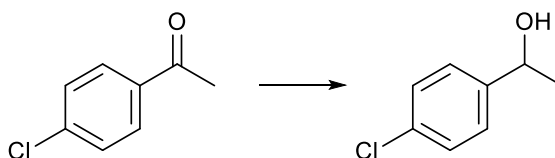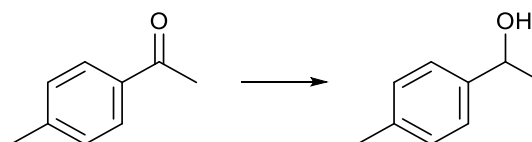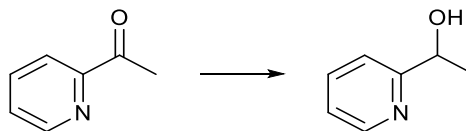
3,3-dimethylbutan-2-ol (33)

Prepared using general ATH procedure described above. Colourless oil. Conversion determined by ^{1}H-NMR (CDCl$_3$, 400 MHz): δ = 3.47 (q, 1H, J = 12.8, 6.40 Hz, alcohol CHOH), 2.13 (s, 3H, ketone CH$_3$), 1.14 (s, 3H, ketone CH$_3$), 1.11 (d, 9H, J = 6.40 Hz, alcohol CH$_3$ hidden under ketone CH$_3$ peak), 0.88 (s, 9H, alcohol CH$_3$) ppm. Low conversion did not allow for the enantioselectivity to be determined by chiral GC.

Cytotoxicity MTT assay

The cytotoxicity of the complexes **6a** and **6b** were determined using the Human Colorectal Adenocarcinoma cell line HT-29 grown in McCoy's 5A modified medium + 10% fœtal bovine serum. 100 µL of an initial concentration of 3x10^4 cells/mL was added to wells of a 96-well plate and left to attach for 24 hours. After this period, 100 µL of medium was carefully removed and replaced by the same amount of the complexes (solubilised in DMSO then diluted in medium as above) at various concentrations and left to incubate for 72 hours. The cell viability was determined using an MTT colorimetric assay as follows: 10 µL of a 12 mM MTT solution was added to each well and returned to incubate at 37 ˚C. Once the colour had developed sufficiently (1 to 2 hours), 150 µL of an acid-alcohol mixture (0.04 M HCl in isopropanol) was added to each well and the contents triturated to release the colour. The absorbance was read at 570 nm using a Biotek ELX800 Universal Microplate Reader. The results were expressed with respect to control values (i.e. cells only wells = 100% cell survival). (*R*)-catalyst (compound **6a**) IC$_{50}$ = 106.00 µM. (*S*)-catalyst (compound **6b**) IC$_{50}$ = 114.80 µM. IC$_{50}$ values were calculated by dose response curves using non-linear regression of log(agonist) vs. response, where the agonist was the concentration of the catalyst, and the response represented the cell survival/viability (%).

(*R*)-2-amino-1-phenylethan-1-ol hydrochloride (34)
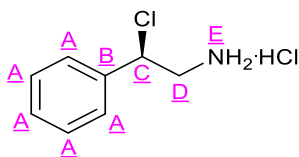
To a solution of (*R*)-2-amino-1-phenylethan-1-ol (3.63 g, 0.03 mol, 1 eq.) in anhydrous toluene (40 mL), $SOCl_2$ (4.00 g, 0.03 mol, 1.26 eq.) was slowly added and the reaction mixture stirred at 60 °C for six hours. The reaction mixture was left to cool to room temperature and the product started to precipitate. The solid was collected by filtration, washed with toluene (60 mL) and dried on the vacuum line to afford the crude product as a brown solid (2.52 g, 13.12 mmol, 90 %). ^{1}H-NMR (DMSO, 400 MHz): δ = 8.62 (br. s, 2H, H_E), 7.34-7.52 (m, 5H, H_A), 5.45-5.48 (m, 1H, H_C), 3.41 (s, 2H, H_D) ppm; ^{13}C{^{1}H}-NMR (DMSO, 400 MHz): δ = 137.7 (1C, C_B), 129.3 (2C, C_A), 129.0 (2C, C_A), 127.5 (1C, C_A), 59.7 (1C, $C_{C/D}$), 45.3 (1C, $C_{C/D}$) ppm; LRMS (ES$^+$): m/z found 156.9 [M - ^{35}Cl]$^+$ (17 %), 155.9 [M - H^{35}Cl]$^+$ (100 %), 154.9 [M - ^{37}Cl]$^+$ (10 %); C_8H_{10}ClN [M - Cl]$^+$ requires 155.6 m/z; **34** ($C_8H_{11}Cl_2N$; 192.1 g/mol).

Organolithium derivatised cymantrene intermediate (35)
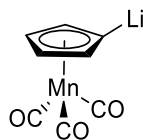
A solution of *n*-BuLi (0.34 mL of 1.6 M solution in hexanes, 0.54 mol, 1.10 eq.) was added dropwise to a solution of cymantrene (0.10 g, 0.49 mmol) in anhydrous THF (20 mL) at −80 °C. The reaction mixture was further stirred at −80 °C for 1.5 hours. The lithium intermediate was carried forwards to the next step without isolation and characterisation. **35** ($C_8H_4LiMnO_3$; 209.9946 g/mol).

[(η⁵-C₅H₄CH(C₆H₆)CH₂NH₂)Mn(CO)₃] (36)
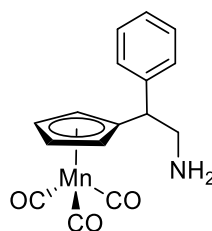
34 (0.05 g, 0.25 mmol, 0.50 eq.) was added in situ to **35** to produce a yellow solution. After two hours the reaction mixture changed colour to orange and was quenched with a couple of drops of MeOH/H₂O. ¹H-NMR and ¹³C{¹H}-NMR (DMSO, 400 MHz): inconclusive, reaction determined unsuccessful; **36** (C₁₆H₁₄MnNO₃; 323.2253 g/mol).

Acetylcymantrene[321] **(37)**
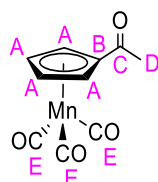
A mixture of cymantrene (0.77 g, 3.79 mmol, 1 eq.) and AlCl₃ (1.00 g, 7.57 mmol, 2 eq.) in anhydrous benzene (8 mL) was cooled at 5 °C, then a solution of acetyl chloride (0.27 g, 3.79 mmol, 1 eq.) in anhydrous benzene (4 mL) was added dropwise over 30 minutes causing a colour change from yellow to orange to red. The solution was stirred at room temperature for three hours. The solution was quenched with H₂O (50 mL), neutralised with 1M NaOH solution (50 mL) from pH 2 and extracted with EtOAc (2 x 200 mL). The organic phases were combined, dried with Na₂SO₄ and filtered. The solvent was removed under reduced pressure and the product was purified by column chromatography on silica gel with a solvent system of Et₂O/Hexane (5-50 % Et₂O) to obtain the pure product as an orange oil (0.52 g, 2.11 mmol, 56 %). Though only one spot was observed on the TLC plate, the product was highly contaminated with solvent, hence the % yield being over that expected from the ratios collected during the crude ¹H-NMR analysis (0.30:1.70:1.00 for cymantrene, acetophenone and **37** respectively). ¹H-NMR (DMSO, 400 MHz): δ = 5.79 (s, 2H, H$_A$), 5.21 (s, 2H, H$_A$), 2.29 (s, 3H, H$_D$) ppm; ¹³C{¹H}-NMR (DMSO, 400 MHz): δ = 223.8 (3C, C$_E$), 195.4 (1C, C$_C$), 92.3 (1C, C$_B$), 87.9 (2C, C$_A$), 85.3 (2C, C$_A$), 26.8 (1C, C$_D$) ppm; HRMS (ES⁺) m/z found 268.9612 [M + Na]⁺; C₁₀H₉MnNaO₄ [M + Na]⁺ requires 268.9617; **37** (C₁₀H₇MnO₄; 246.0982 g/mol).

[(η⁵-C₅H₄C(CH₃)NCH₂CH₂NHTs)Mn(CO)₃] (38)
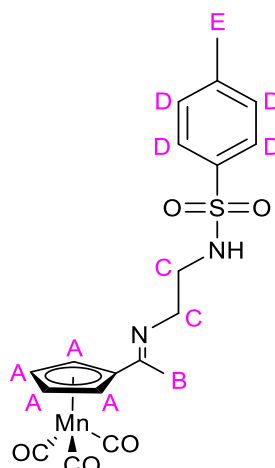
A few drops of acetic acid were added to a stirred solution of **37** (0.10 g, 4.07 mmol, 1 eq.) and **1** (0.06 g, 4.07 mmol, 1 eq.) in MeOH (5 mL) at room temperature. The mixture was stirred overnight and analysed by TLC the following morning. Another equivalent of **1** was added and the solution was left to stir overnight at 50 °C. The solvent was removed under reduced pressure and the product re-dissolved in MeOH (2 mL) with an additional one equivalent of **1**. The reaction was left to stir overnight at 50 °C. An additional one equivalent of **1** was added with stirring overnight at 50 °C. The solvent was removed under reduced pressure and the brown solid dried on a vacuum line as a crude product. ¹H-NMR (DMSO, 400 MHz): δ = 7.59-7.69 (m, 2H, H_D), 7.37-7.40 (s, 2H, H_D), 5.55 (s, 0.30H*, H_A), 5.06 (s, 0.30H*, H_A), 3.17 (s, 2H, H_C), 2.67-2.99 (m, 2H, H_C), 2.38 (m, 3H, tosyl H_E), 1.87 (s, 0.40H**, H_B) ppm; **38** (C₁₉H₁₉MnN₂O₅S; 442.3676 g/mol). Route terminated; full analysis not collected.

*Should integrate to 2H.
**Should integrate to 3H.

1-cymantrenylethanol[309,322] **(40)**
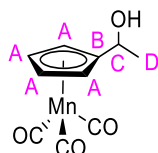
To a solution of **37** (0.84 g, 3.41 mmol) in MeOH (20 mL) cooled to 0 °C, NaBH₄ (0.26 g, 6.82 mmol, 2 eq.) in MeOH (10 mL) was added dropwise. The mixture was stirred for two hours. The solvent was removed under reduced pressure. The product was dissolved in

EtOAc (70 mL), extracted with 1M HCl (2 x 50 mL) then $NaHCO_3$ (50 mL). The aqueous phase was washed again with EtOAc (50 mL). The organic layers were combined, dried over Na_2SO_4 and filtered. The solvent was removed under reduced pressure and the product was dried on a vacuum line as a yellow oil (0.76 g, 3.06 mmol, 90 %). ^{1}H-NMR (DMSO, 400 MHz): δ = 5.26 (d, 1 H, J = 5.03 Hz, OH), 5.04-5.07 (m, 2H, H_A), 4.85-4.92 (m, 2H, H_A), 4.36-4.42 (m, 1H, H_C), 1.26 (d, 3H, J = 6.40 Hz, H_D) ppm; D_2O shake confirmed assignment of peak at δ = 5.26 ppm to be the OH group due to disappearance of the peak; ^{13}C{^{1}H}-NMR (DMSO, 400 MHz): δ = 112.3 (1C, C_B), 83.0 (1C, C_A), 82.0 (1C, C_A), 81.9 (1C, C_A), 81.2 (1C, C_A), 61.9 (1C, C_C), 24.4 (1C, C_D) ppm. Carbonyl ligands not observed as ppm window was not large enough for the ^{1}H-NMR spectrum collected; HRMS (ES$^+$) m/z found 270.9770 [M + Na]$^+$; $C_{10}H_9MnNaO_4$ [M + Na]$^+$ requires 270.9773; LRMS (ES$^+$) m/z found 287.1 [M + K]$^+$ (100 %); $C_{10}H_9KMnO_4$ [M + K]$^+$ requires 287.2; **40** ($C_{10}H_9MnO_4$; 248.1141 g/mol).

[(η^5-C$_5$H$_4$CH(CH$_3$)Br)Mn(CO)$_3$][322] (41)
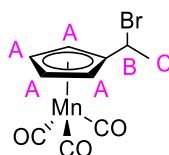
To a solution of **40** (0.79 g, 3.16 mmol) in anhydrous benzene (40 mL) cooled to 0 °C, PBr$_3$ (1.58 mL, 16.8 mmol, 5 eq.) in anhydrous benzene (40 mL) was added dropwise. The mixture was stirred for two hours. Additional PBr$_3$ (4 eq.) was added over the course of one hour with stirring. The mixture was poured onto ice and left to stand for one hour. The mixture was extracted with Et$_2$O (3 x 100 mL), followed by NaHCO$_3$ (100 mL), H$_2$O (100 mL) and then brine (100 mL). The organic layers were combined, dried over Na$_2$SO$_4$ and filtered. The solvent was removed under reduced pressure and the crude product was dried further on a vacuum line as a yellow oil (0.80 g), which comprised of starting material **40** and anticipated product **41** in a 1:1 mixture. Unfortunately we were unable to separate **41** from the starting material. ^{1}H-NMR (DMSO, 400 MHz): δ = 5.49-5.50 (m, 1H, H_A), 5.28-5.29 (m, 1H, H_A), 5.13-5.20 (m, 1H, H_B), 5.04-5.07 (m, 1H, H_A), 4.93-4.94 (m, 1H, H_A), 1.85 (d, 3H, J = 6.86 Hz, H_C) ppm; ^{13}C{^{1}H}-NMR (DMSO, 400 MHz): inconclusive; **41** ($C_{10}H_8BrMnO_3$; 311.0107 g/mol).

$[(\eta^5\text{-}C_5H_4CH(CH_3)CN)Mn(CO)_3]$ (42)

Anticipated: Actual:
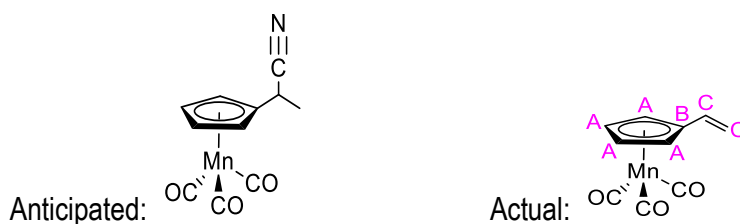
Crude **41** (0.80 g, 2.58 mmol, 1 eq.) was dissolved in anhydrous DMF (10 mL) and added dropwise to KCN (0.19 g, 2.83 mmol, 1.10 eq.). After stirring at 80 °C overnight, the reaction was left to cool to room temperature and H_2O (20 mL) was added slowly. The mixture was pipetted into Et_2O (50 mL) and extracted. The aqueous layer was washed with Et_2O (2 x 50 mL). The organic layers were combined and washed again with H_2O (50 mL). The resulting organic layer was dried with Na_2SO_4, filtered and the solvent was removed under reduced pressure. The crude product was dried on the vacuum line as a brown oil (0.28 g, 1.22 mmol). ^{1}H-NMR (DMSO, 400 MHz): δ = 6.26-6.33 (m, 1H, H_C), 5.61-5.66 (m, 1H, H_C), 5.36 (t, 2H, J = 2.00 Hz, H_A), 5.17-5.20 (m, 1H, H_C), 5.03 (t, 2H, J = 2.06 Hz, H_A) ppm; ^{13}C{^{1}H}-NMR (DMSO, 400 MHz): δ = 129.1 (1C, C_C), 115.8 (2C, C_C), 101.0 (1C, C_B), 83.1 (2C, C_A), 82.0 (2C, C_A) ppm. Carbonyl ligands not observed as ppm window was not large enough for the ^{1}H-NMR spectrum collected; HRMS (ES$^+$) m/z found 230.9851 [M + H]$^+$; $C_{10}H_8MnO_3$ [M + H]$^+$ requires 230.9848; **42** (anticipated: $C_{11}H_8MnNO_3$; 257.1241 g/mol, actual: $C_{10}H_7MnNO_3$; 230.0988 g/mol).

1-Mesitylimidazole[323] (43)
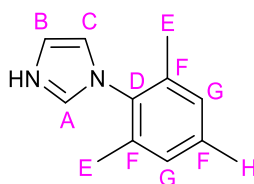
Glacial acetic acid (10 mL), aqueous formaldehyde (3 mL, 37 wt %, 0.04 mol), and aqueous glyoxal (4.60 mL, 40 wt %, 0.04 mol, 1 eq.) were combined and heated at 70 °C. A solution of glacial acetic acid (10 mL), ammonium acetate (3.08 g in 2 mL of H_2O, 0.04 mol, 1 eq.), and mesitylamine (5.60 mL, 0.04 mol, 1 eq.) was added dropwise to the reaction mixture. The resulting solution was continuously stirred and heated overnight, resulting in a dark brown solution. The reaction mixture was left to cool to room temperature and then added

dropwise to a stirred solution of $NaHCO_3$ (29.4 g in 300 mL of H_2O). The product formed a precipitate, which was filtered off and washed with H_2O before being allowed to air-dry. The product was purified by flash column chromatography on silica gel with a solvent system of DCM/MeOH (0-50 % MeOH) to obtain a purer product as a brown solid (3.67 g, 19.59 mmol, 50 %). ^{1}H-NMR (DMSO, 400 MHz): δ = 7.63 (s, 1H, H_A), 7.18 (s, 1H, $H_{B/C}$), 7.11 (s, 1H, $H_{B/C}$), 7.03 (s, 2H, H_G), 2.29 (s, 3H, H_H), 1.92 (s, 6H, H_E); ^{1}H-NMR ($CDCl_3$, 400 MHz): δ = 7.43 (s, 1H, H_A), 7.23 (s, 1H, $H_{B/C}$), 6.96 (s, 2H, H_G), 6.89 (s, 1H, $H_{B/C}$), 2.33 (s, 3H, H_H), 1.98 (s, 6H, H_E); ^{13}C{^{1}H}-NMR ($CDCl_3$, 400 MHz): δ = 138.9 (1C, C_D), 137.6 (1C, C_A), 135.5 (2C, C_F), 133.5 (1C, C_F), 129.7 (1C, $C_{B/C}$), 129.1 (2C, C_G), 120.2 (1C, $C_{B/C}$), 21.1 (1C, C_H), 17.4 (2C, C_E) ppm; HRMS (ES$^+$) m/z found 187.1240 [M]$^+$; $C_{12}H_{15}N_2$ [M]$^+$ requires 187.1230; LRMS (ES$^+$) m/z found 187.1 [M]$^+$ (100 %); **43** ($C_{12}H_{15}N_2$; 187.2609 g/mol); unit cell: a = 10.38 Å, b = 9.25 Å, c = 10.82 Å. α = 90°, β = 90°, γ = 90°.

[($η^5$-$C_5H_4CH(CH_3)NHC^{Mes}$)$Mn(CO)_3$]Br [(44)Br]
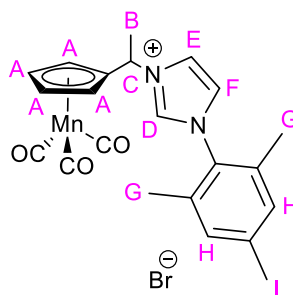
NaH (60% dispersion in mineral oil, 32.40 mg, 0.81 mmol, 1 eq.) was added slowly to **43** (66.42 mg, 0.35 mmol, 0.40 eq.*) in anhydrous DMF (0.6 mL) at 0 °C and the mixture was kept stirring at this temperature for 15 minutes. **41** (0.25 g, 0.81 mmol, 1 eq.) in anhydrous DMF (0.8 mL) was added dropwise. The mixture was heated to room temperature and stirred over the weekend. H_2O was added slowly to the reaction mixture on ice and the reaction mixture was extracted with DCM (3 × 75 mL). The organic extracts were dried over Na_2SO_4 and the solvent was removed under reduced pressure to give a brown oil (0.26 g) as a crude product. ^{1}H-NMR ($CDCl_3$, 400 MHz): δ = 7.95 (s, 1H, H_D), 7.63 (s, 1H, $H_{E/F}$), 7.11-7.19 (m, 1H, $H_{E/F}$), 7.03 (s, 2H, H_H), 4.86-5.36** (m, 4H, H_A), 4.36-4.42 (m, 1H, H_C), 2.29 (s, 3H, H_I), 1.92 (s, 6H, H_G), 1.26 (d, 3H, *J* = 6.40 Hz, H_B) ppm; **[(44)Br]** ($C_{22}H_{22}BrMnN_2O_3$; 497.2637 g/mol); Route terminated; full analysis not collected.

*Should have added 1 eq. but calculations in the lab were carried out incorrectly.

**Full region stated integrated to 13H; unclear which environments corresponded to anticipated product's Cp ring.

1-cymantrenylethyl methanesulfonate (45)
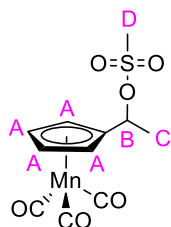
MsCl (0.04 mL, 0.56 mmol) in anhydrous DCM (7 mL) was added dropwise to a stirring solution of **40** (0.14 g, 0.56 mmol, 1 eq.), TEA (0.08 mL, 0.56 mmol, 1 eq.) and DMAP (0.07 g, 0.56 mmol, 1 eq.) in anhydrous DCM (7 ml) at 0 °C. The mixture was left to stir at room temperature for three hours until the solution turned orange. ^{1}H-NMR (CDCl$_3$, 400 MHz): δ = 4.92-4.96 (m, 2H, H$_A$), 4.78 (q, 1H, J = 13.53, 6.88 Hz, H$_B$), 4.64-4.72 (m, 2H, H$_A$), 1.75 (d, 3H, J = 6.88 Hz, H$_C$), 1.25 (s, 3H, H$_D$); **45** (C$_{11}$H$_{11}$MnSO$_6$; 326.2045 g/mol). The mesylate was carried forwards as an intermediate to the next step without isolation and full characterisation.

[(η^5-C$_5$H$_4$CH(CH$_3$)NHC^{Mes})Mn(CO)$_3$]OMs [(46)OMs]
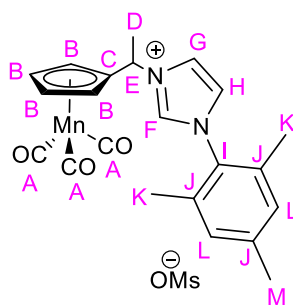
Crude **45** was centrifuged to remove a white coloured solid. The solvent was removed under reduced pressure from the liquid phase. **43** (0.57 g, 3.06 mmol, 1 eq.) was added and the combined solids were dissolved in anhydrous toluene (10 mL). The mixture was heated to 110 °C and stirred overnight. The reaction mixture was left to cool to room temperature and the solvent was removed under reduced pressure to obtain a brown sticky oil. The oil was dissolved in DCM and filtered through celite until the washings were colourless. The organic extracts were combined and the solvent was evaporated under reduced pressure. Et$_2$O (30 mL) was added dropwise whilst stirring to induce precipitation of impurities. This step was repeated twice more. The solution was filtered and the solvent was removed under reduced

pressure to obtain the product. The brown solid was dried on a vacuum line. The crude product was purified through a silica plug in a sintered fritt under vacuum with a solvent system of toluene/hexane (50 %) then DCM/MeOH (50 %). The fractions were combined to obtain a purer product as a brown oil (0.18 g). ^{1}H-NMR (CDCl$_3$, 400 MHz): δ = 6.98 (s, 2H, H$_L$), 6.18-6.25 (m, 1H, H$_F$), 5.45-5.49 (m, 1H, H$_{G/H}$), 5.16-5.18 (m, 1H, H$_{G/H}$), 4.90 (t, 2H, J = 2.18 Hz, H$_B$), 4.70 (t, 2H, J = 2.18 Hz, H$_B$), 3.14 (q, 1H, J = 14.67, 7.34 Hz, H$_E$), 2.34 (s, 3H, H$_M$), 1.99 (s, 6H, H$_K$), 1.37 (t, 3H, J = 7.34 Hz, H$_D$). Mesylate CH$_3$ not observed, assignments in agreement with Lugan et al.[236]; ^{13}C{^{1}H}-NMR (CDCl$_3$, 400 MHz): δ = 224.7 (3C, C$_A$), 138.9 (1C, C$_I$), 136.3 (1C, C$_F$), 129.4 (3C, C$_J$), 129.1 (2C, C$_L$), 115.9 (2C, C$_G$ + C$_H$), 100.5 (1C, C$_C$), 82.3 (2C, C$_B$), 81.1 (2C, C$_B$), 46.2 (1C, C$_E$), 21.1 (1C, C$_M$), 17.4 (2C, C$_K$), 8.7 (1C, C$_D$) ppm. Mesylate CH$_3$ not observed, shifts assignments based on those made by Lugan et al.[236] as no 2D NMR experiments were run; HRMS (ES$^+$) m/z found 417.1013 [M - OMs]$^+$; C$_{22}$H$_{22}$MnN$_2$O$_3$ [M - OMs]$^+$ requires 417.1005; **[(46)OMs]** (C$_{23}$H$_{25}$MnN$_2$O$_6$S; 512.4574 g/mol).

1-cymantrenylethyl acetate (47)
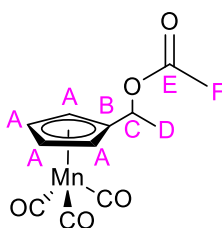
Acetic anhydride (5 mL) was added to **40** (0.42 g, 1.70 mmol) and the yellow solution was heated at 40 ^{o}C for one hour. The reaction mixture was left to cool to room temperature but no precipitate was observed. The solvent was removed on the rotary evaporator slowly in intervals over three weeks with the flask residing in the fridge (5 °C) between each removal of solvent. Unfortunately, no product precipitated out. Instead, the yellow solution was diluted with acetic anhydride (2 mL) and anhydrous pyridine (2 drops) was added, then the reaction mixture was heated at 40 ^{o}C overnight. The solvent was removed under reduced pressure and the crude product dried further on a vacuum line as a yellow oil (0.24 g, 0.83 mmol, 49 %). ^{1}H-NMR (400 MHz, DMSO): δ = 5.55 (q, 1H, J = 12.95, 6.54 Hz, H$_C$), 5.26-5.26 (m, 1H, H$_A$), 5.20-5.20 (m, 1H, H$_A$), 4.93-4.94 (m, 2H, H$_A$), 2.03 (s, 3H, H$_F$), 1.38 (d, 3H, J = 6.65 Hz, H$_D$) ppm; ^{13}C{^{1}H}-NMR (400 MHz, DMSO): δ = 169.5 (1C, C$_E$), 104.6 (1C, C$_B$), 84.6 (1C, C$_A$), 84.2 (1C, C$_A$), 82.2 (1C, C$_A$), 82.0 (1C, C$_A$), 65.3 (1C, C$_C$), 20.9 (1C, C$_{D/F}$), 20.7 (1C,

$C_{D/F}$) ppm. Carbonyl ligands not observed as ppm window in the ^{13}C-NMR spectrum was not large enough for the carbonyl ligands to be observed; **47** ($C_{12}H_{11}MnO_5$; 290.1508 g/mol).

[(η⁵-C₅H₄CH(CH₃)CH₃C₃H₃N₂)Mn(CO)₃]OAc [(48)OAc]

Anticipated: Actual:
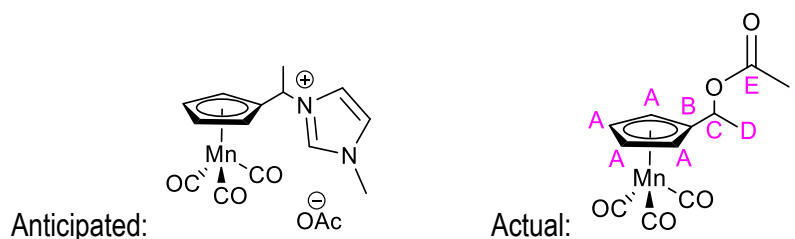
47 (90 mg, 0.31 mmol) was stirred in acetic acid (3 mL) with 1-methylimidazole (0.03 mL, 0.37 mmol) at 60 ᵒC overnight under N_2. The solvent was removed under reduced pressure to give an orange oil. NaI (0.23 g, 1.55 mmol) in ethanol (10 mL) was added and the resulting mixture was stirred at room temperature for one hour. The solvent was removed under reduced pressure to give a yellow solid. DCM (12 mL) was added and the sample was centrifuged at 10,000 rpm for five mins. The intense yellow liquid was pipetted off and the solvent removed under reduced pressure to yield a yellow solid (0.16 g). The crude product was purified through a plug of silica (~3 cm) with a solvent system of DCM/MeOH (1-25 %). The product eluted at 1 % MeOH, but analysis confirmed it to be the starting material **47** (20 mg). This reduction in yield indicates that a majority of the starting material was consumed and either decomposed on the column or reacted to form a product that couldn't be isolated. Excess **43** was also found in the ^{1}H-NMR. The reaction was therefore unsuccessful. ^{1}H-NMR (400 MHz, DMSO): δ = 8.64 (s, 4H, imidazole - should be 1H but excess), 7.45-7.54 (m, 8H, imidazole - should be 2H but excess), 5.54 (q, 1H, *J* = 12.92, 6.54 Hz, H_C), 5.27 (q, 1H, *J* = 4.00, 1.95 Hz, H_A), 5.21 (q, 1H, *J* = 3.89, 1.83 Hz, H_A), 4.95 (t, 2H, *J* = 2.06 Hz, H_A), 2.03 (s, 3H, H_F), 1.91 (s, 8H, imidazole CH₃ - should be 3H but excess), 1.38 (d, 3H, *J* = 6.63 Hz, H_D) ppm; **[(48)OAc]** (anticipated: $C_{16}H_{17}MnN_2O_5$; 372.2546 g/mol, actual: $C_{12}H_{11}MnO_5$; 290.1508 g/mol). Route terminated; full analysis not obtained.

Alternatively, **47** (50 mg, 0.17 mmol) was stirred in a mixture of MeCN (1.90 mL) and H_2O (0.96 mL) with 1-methylimidazole (0.02 mL, 0.21 mmol) at 60 ᵒC overnight under N_2. The solvent was removed under reduced pressure to give a brown oil. NaI (0.23 g, 1.55 mmol) in ethanol (10 mL) was added and the resulting mixture stirred at room temperature for one hour. The solvent was removed under reduced pressure to give a yellow solid, which was dissolved in DCM (12 mL). The solution was centrifuged at 10,000 rpm for five mins. The

intense yellow liquid was pipetted off and the solvent removed under reduced pressure to yield a yellow solid (0.04 g). The crude product was purified through a plug of silica (~3 cm) with a solvent system of DCM/MeOH (1-25 %). The product eluted at 1 % MeOH, but analysis confirmed it to be the starting material **47** (20 mg). This reduction in yield indicates that a majority of the starting material was consumed and either decomposed on the column or reacted to form a product that couldn't be isolated. The reaction was therefore unsuccessful. ^{1}H-NMR (400 MHz, DMSO): δ = 5.54 (q, 1H, J = 12.92, 6.52 Hz, H$_C$), 5.27 (m, 1H, J = 4.12, 1.83 Hz, H$_A$), 5.21 (m, 1H, J = 4.12, 1.83 Hz, H$_A$), 4.95 (t, 2H, J = 2.06 Hz, H$_A$), 2.03 (s, 3H, H$_F$), 1.38 (d, 3H, J = 6.65 Hz, H$_D$) ppm; **[(48)OAc]** (anticipated: $C_{14}H_{17}MnNO_5$; 334.2265 g/mol, actual: $C_{12}H_{11}MnO_5$; 290.1508 g/mol). Route terminated; full analysis not obtained.

[(η^5-C$_5$H$_4$CH(N(CH$_3$)$_2$)CH$_3$)Mn(CO)$_3$]OAc [(49)OAc]

Anticipated: Actual:
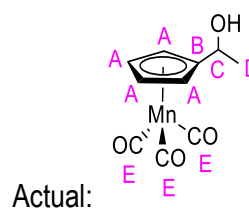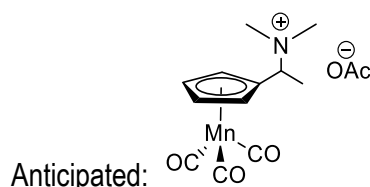
47 (20.00 mg, 0.069 mmol) was dissolved in MeOH (0.6 mL) and dimethylamine (40 % in H$_2$O, 8.73 µL, 0.069 mmol) was added. The reaction mixture was left to stir under N$_2$ at room temperature overnight. Analysis by ^{1}H-NMR confirmed conversion to the product by 16 %*. The reaction mixture was left to stir for another five hours at room temperature. Analysis by ^{1}H-NMR confirmed no change to conversion to the product*. Additional dimethylamine (4 eq.) and MeOH (0.6 mL) was added and the reaction mixture was left to stir overnight. Analysis by ^{1}H-NMR confirmed conversion to the product by 74 %*. The reaction mixture was left to stir for another seven hours at room temperature. Analysis by ^{1}H-NMR confirmed conversion to the product by 87 %*. Additional dimethylamine (1 eq.) was added and the reaction mixture was left to stir under N$_2$ at room temperature overnight. Analysis by ^{1}H-NMR showed full conversion to the product* but upon full analysis, it was confirmed that the product formed was in fact compound **40**[309,322]. ^{1}H-NMR (400 MHz, DMSO): δ = 5.24-5.25 (m, 1H, OH), 5.04-5.06 (m, 2H, H$_A$), 4.85-4.92 (m, 2H, H$_A$), 4.36-4.42 (m, 1H, H$_C$), 1.26 (d, 3H, J = 6.40 Hz, H$_D$) ppm; D$_2$O shake confirmed assignment of peak at δ = 5.24-5.25 ppm to be the OH group due to disappearance of the peak; **[(49)OAc]** (anticipated: $C_{14}H_{17}MnNO_5$; 334.2265 g/mol, actual: $C_{10}H_9MnO_4$; 248.1141 g/mol). Reaction unsuccessful.

*Calculated by integrating the two CH_3 groups correlating to starting material and product, and ratioing the integrals against each other.

Chloropropionylcymantrene[326] (50)
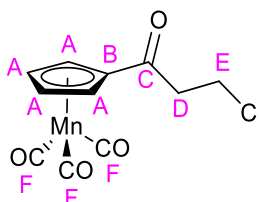
Cymantrene (500 mg, 2.45 mmol) in dichloromethane (25 mL) was treated with 3-chloropropionyl chloride (234 µL, 2.45 mmol) and $AlCl_3$ (327 mg, 2.45 mmol). After stirring for five hours at room temperature, the reaction mixture was poured into 3 % $HCl_{(aq)}$. The organic phase was dried with Na_2SO_4, filtered, and the solvent was removed under reduced pressure. The product was dried on a vacuum line as a yellow solid (0.62 g, 2.10 mmol, 86 %). The crude product was purified by column chromatography on silica with a solvent system of hexane/EtOAc (0-20 % EtOAc) to obtain a purer product as a yellow oil (0.17 g, 0.58 mmol, 24 %). ^1H-NMR (400 MHz, DMSO): δ = 5.87-5.88 (m, 2H, H_A), 5.22-5.23 (m, 2H, H_A), 3.84 (m, 2H, J = 5.95 Hz, $H_{D/E}$), 3.16 (m, 2H, J = 5.95 Hz, $H_{D/E}$) ppm; $^{13}C\{^1H\}$-NMR (400 MHz, DMSO): δ = 222.8 (3C, C_F), 193.6 (1C, C_C), 90.9 (1C, C_B), 87.2 (2C, C_A), 84.5 (2C, C_A), 40.3 (1C, $C_{D/E}$), 38.3 (1C, $C_{D/E}$) ppm; HRMS (ES⁺) m/z found 316.9391 [M + Na]⁺; $C_{11}H_8ClMnNaO_4$ [M + Na]⁺ requires 316.9384; **50** ($C_{11}H_8ClMnO_4$; 294.5700 g/mol).

[(η⁵-C₅H₄COCH₂CH₂(NHC-CH₃))Mn(CO)₃]Cl [(51)Cl]
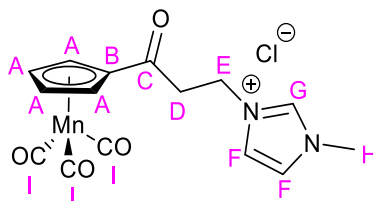
Triethylamine (0.15 mL, 1.09 mmol, 2 eq.) was added to **50** (0.16 g, 0.54 mmol) in DMF (15 mL) and stirred for 20 minutes at room temperature. 1-methylimidazole (43.2 µL, 0.54 mmol, 1 eq.) was added and the reaction heated to 75 °C for five hours. The reaction was left to cool to room temperature and then the solvent was removed under reduced pressure. The resulting dark brown oil was dissolved in DCM (3 mL) and then Et_2O (7 mL) was added to precipitate the product. The product was separated from the supernatant by centrifugation

(10,000 rpm for 5 minutes) and the crude product was dried further on a vacuum line as a dark brown solid (0.20 g, 0.53 mmol, 97 %). ^{1}H-NMR (400 MHz, DMSO): δ = 9.12 (s, 1H, H_G), 7.69-7.74 (m, 2H, H_F), 5.80 (t, 2H, J = 2.29 Hz, H_A), 5.25 (t, 2H, J = 2.29 Hz, H_A), 4.46 (t, 2H, J = 6.17 Hz, $H_{D/E}$), 3.82 (s, 3H, H_H), under H_2O peak in range of 3.14-3.52 (s, 2H, $H_{D/E}$) ppm; ^{13}C{^{1}H}-NMR (400 MHz, DMSO): δ = 222.4 (3C, C_I), 194.4 (1C, C_C), 136.6 (1C, C_G), 123.2 (1C, C_F), 122.1 (1C, C_F), 90.4 (1C, C_B), 87.3 (1C, C_A), 84.8 (1C, C_A), 44.8 (1C, $C_{D/E}$), 43.6 (1C, $C_{D/E}$), 36.0 (1C, C_H) ppm; HRMS (ES$^+$) m/z found 341.0331 [M - Cl]$^+$; $C_{15}H_{14}MnN_2O_4$ [M - Cl]$^+$ requires 341.0329; **[(51)Cl]** ($C_{15}H_{14}ClMnN_2O_4$; 376.6737 g/mol).

(η^5-C$_5$H$_4$COCH$_2$CH$_2$(NHC-CH$_3$))Mn(CO)$_2$ (52)
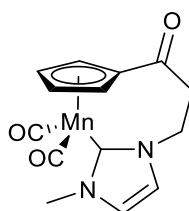
To a stirring suspension of **[(51)Cl]** (5.26 mg, 0.014 mmol) in THF-d^8 (5 mL) was slowly added a solution of KO*t*Bu (0.30 eq. in 0.3 mL THF-d^{8*}) at room temperature. The reaction mixture was stirred for 15 minutes, the volume was reduced to ~0.5 mL and the reaction mixture was transferred to an NMR tube made of borosilicate glass. ^{1}H-NMR confirmed successful deprotonation of the NHC. The sample was set up ~1-2 cm from the light source and irradiated with UV light on the long wavelength setting (315 nm, 6W) with N_2 bubbling through the solvent. The irradiation was carried out at room temperature with no cooling required as the vessels did not get hot. Results were inconclusive, therefore the route was terminated; full analysis not collected.

*A stock solution (x20) was made up i.e. 0.0314 g of KO*t*Bu in 20 mL THF-d^8.

(*R*)-2-Amino-2-(cyclohexa-1,4-dien-1-yl)acetic acid (53)
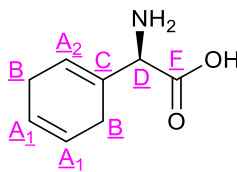
A solution of (*R*)-2-amino-2-phenylacetic acid hydrochloride (5.00 g, 26.60 mmol, 1 eq.) in ethanol (120 mL) was added to liquid NH_3 (300 mL) at -77 °C. Lithium wire (1.22 g, 0.18 mol, 6.60 eq.) was washed in hexane before addition in 0.50 g portions until a dark blue colour persisted. The reaction was left to stand overnight to leave a white solid. H_2O (100 mL) was added whilst stirring at 0 °C and the pH was found to be ~10. The solvent was removed under reduced pressure. Acetic acid (~ 5 mL) was added to acidify the solution to pH 7. A white solid precipitated, which was filtered under vacuum and washed with H_2O. The crude product was dried further on a vacuum line to yield the product as a pearlescent white solid (3.18 g, 20.76 mmol, 78 %). ^{1}H-NMR (D_2O + 3 drops of DCl, 400 MHz): δ = 6.01 (s, 1H, H_{A2}), 5.69 (s, 2H, H_{A1}), 4.53 (s, 1H, H_D), 2.50-2.74 (m, 4H, H_B) ppm; ^{13}C{^{1}H}-NMR (D_2O + 3 drops of DCl, 400 MHz): δ = 170.5 (1C, C_F), 130.4 (1C, C_C), 126.0 (1C, C_{A2}), 123.7 (1C, C_{A1}), 122.8 (1C, C_{A1}), 58.2 (1C, C_D), 26.2 (1C, C_B), 24.6 (1C, C_B) ppm; HRMS (ES$^-$): m/z found 152.0717 [M - H]$^-$; $C_8H_{10}NO_2$ [M - H]$^-$ requires 152.0719; **53** ($C_8H_{11}NO_2$; 153.1784 g/mol).

(*R*)-2-((*Tert*-butoxycarbonyl)amino)-2-(cyclohexa-1,4-dien-1-yl)acetic acid[332] (54)
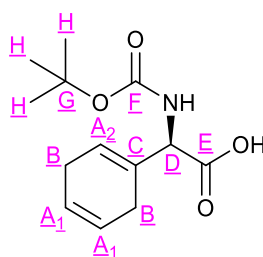
Di-*tert*-butyl dicarbonate (2.14 g, 9.80 mmol, 1 eq.) suspended in a mixture of H_2O (15 mL) and MeOH (3.75 mL) was added dropwise to a stirred mixture of **53** (1.50 g, 9.80 mmol, 1 eq.) and K_2CO_3 (1.35 g, 11.76 mmol, 1.20 eq.) in H_2O (15 mL) and MeOH (3.75 mL) at 0 °C. The cloudy white suspension was left to stir overnight at room temperature. After 24 hours, 1M HCl (~ 20 mL) was added slowly to acidify the reaction mixture from pH 9 to pH 4.95. The reaction mixture was extracted with EtOAc (100 mL) and H_2O (100 mL). The aqueous layer was washed with EtOAc (2 x 50 mL). The organic layers were combined and washed

with brine (50 mL). The organic layer was dried over Na_2SO_4, filtered and the solvent was removed under reduced pressure. The crude product was dried further under vacuum to yield the product as a white honeycomb solid. The product was purified through a plug of silica using DCM/MeOH (3 % MeOH) and the solvent was removed under reduced pressure. The purified product was dried further on a vacuum line as a white honeycomb solid (1.36 g, 5.37 mmol, 55 %). ^{1}H-NMR (CDCl$_3$, 400 MHz): δ = 5.84 (s, 1H, H$_A$), 5.65-5.73 (m, 2H, H$_A$), 4.52-4.75 (m, 1H, H$_D$), 2.60-2.75 (m, 4H, H$_B$), 1.42-1.44 (m, 9H, H$_H$) ppm; ^{13}C{^{1}H}-NMR (CDCl$_3$, 400 MHz): δ = 173.7 (1C, C$_E$), 157.2 (1C, C$_F$), 131.5 (1C, C$_C$), 124.0 (1C, C$_A$), 123.8 (1C, C$_A$), 123.7 (1C, C$_A$), 81.6 (1C, C$_G$), 60.3 (1C, C$_D$), 28.3 (3C, C$_H$), 26.8 (1C, C$_B$), 26.0 (1C, C$_B$) ppm; LRMS (ES$^+$): m/z found 276.1 [M + Na]$^+$ (100 %); $C_{13}H_{19}NNaO_4$ [M + Na]$^+$ requires 276.3; **54** ($C_{13}H_{19}NO_4$; 253.2943 g/mol).

(*R*)-*Tert*-butyl (1-(cyclohexa-1,4-dien-1-yl)-2-((2-((4-methylphenyl)sulfonamido)ethyl)amino)-2-oxoethyl)carbamate (55)
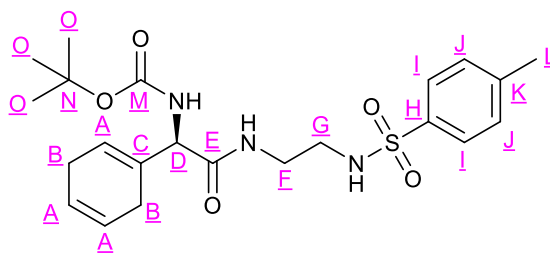
54 (1.30 g, 5.13 mmol, 1 eq.), DIPEA (2.68 mL, 15.39 mmol, 3 eq.) and TBTU (1.98 g, 4.28 mmol, 1.20 eq.) were dissolved in a mixture of DMF (10 mL) and DCM (10 mL). The solution was stirred for five minutes then N-(2-aminoethyl)-4-methylbenzenesulfonamide (1.12 g, 5.13 mmol, 1 eq.) was added and left to stir at room temperature overnight. The reaction was pipetted into 1M HCl (100 mL) and extracted with DCM (3 x 100 mL). The organic layers were combined and extracted with H_2O (3 x 100 mL). The solvent of the organic layer was removed under reduced pressure. The yellow oil was redissolved in Et_2O (100 mL) and extracted with H_2O (5 x 100 mL). The organic layer was dried with Na_2SO_4, filtered and the solvent was removed under reduced pressure. The product was dried further on a vacuum line as a yellow honeycomb solid. The crude product was purified by column chromatography on silica gel using a solvent system of DCM/Methanol (0-1 % MeOH). The solvent was removed under reduced pressure and the purified product was dried further on a vacuum line as a white honeycomb solid (1.61 g, 3.58 mmol, 70 %). ^{1}H-NMR (CDCl$_3$, 400 MHz): δ = 7.69 (d, 2H, J = 8.23 Hz, H$_I$), 7.26 (d, 2H, J = 8.00 Hz, H$_J$), 6.86-6.89 (m, 1H, NH), 5.90-5.94

(m, 1H, NH), 5.58-5.79 (m, 3H, H_A), 4.54-4.56 (m, 1H, H_D), 3.23-3.42 (m, 2H, $H_{F/G}$), 2.98-3.02 (m, 2H, $H_{F/G}$), 2.42-2.71 (m, 4H, H_B), 2.38 (s, 3H, H_L), 1.39 (s, 9H, H_O), ppm; $^{13}C\{^1H\}$-NMR (CDCl$_3$, 400 MHz): δ = 170.9 (1C, C_E), 155.5 (1C, C_M), 143.5 (1C, C_H), 136.7 (1C, C_K), 131.7 (1C, C_C), 129.8 (2C, C_J), 127.0 (2C, C_I), 124.5 (1C, C_A), 123.7 (1C, C_A), 123.6 (1C, C_A), 80.0 (1C, C_N), 60.3 (1C, C_D), 42.8 (1C, $C_{F/G}$), 39.7 (1C, $C_{F/G}$), 28.4 (3C, C_O), 26.7 (1C, C_B), 25.3 (1C, C_B), 21.6 (1C, C_L) ppm; HRMS (ES$^+$): m/z found 472.1879 [M + Na]$^+$; $C_{22}H_{31}N_3NaO_5S$ [M + Na]$^+$ requires 472.1877; **55** ($C_{22}H_{31}N_3O_5S$; 449.5636 g/mol).

(*R*)-2-Amino-2-(cyclohexa-1,4-dien-1-yl)-*N*-(2-((4-methylphenyl)sulfonamido)ethyl)acetamide (56)
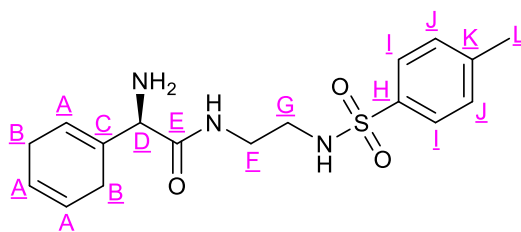
55 (1.61 g, 3.58 mmol) was dissolved in anhydrous DCM (6.5 mL). TFA (5.5 mL) was added slowly and the reaction mixture was stirred at room temperature under N$_2$ for one hour. The solvent was removed under reduced pressure and then the product was redissolved in DCM (10 mL). The solvent was removed under reduced pressure and the process was repeated five times to yield a yellow/orange oil. The sample was dissolved in DCM (200 mL) and washed with NaHCO$_3$ (3 x 100 mL). A white solid precipitated. The organic layer was dried over Na$_2$SO$_4$, filtered and the solvent was removed under reduced pressure. The crude product was dried further on a vacuum line as a yellow honeycomb solid (0.96 g, 2.75 mmol, 77 %). ^{1}H-NMR (CDCl$_3$, 400 MHz): δ = 7.72 (d, 2H, *J* = 8.46 Hz, H_I), 7.29 (d, 2H, *J* = 7.78 Hz, H_J), 5.64-5.77 (m, 3H, H_A), 3.89 (s, 1H, H_D), 3.32-3.42 (m, 2H, $H_{F/G}$), 3.05-3.11 (m, 2H, $H_{F/G}$), 2.45-2.81 (m, 4H, H_B), 2.41 (s, 3H, H_L), 1.68 (br. s, 2H, NH$_2$) ppm; $^{13}C\{^1H\}$-NMR (CDCl$_3$, 400 MHz): δ = 174.1 (1C, C_E), 143.5 (1C, C_H), 137.0 (1C, C_K), 134.5 (1C, C_C), 129.8 (2C, C_J), 127.1 (2C, C_I), 123.9 (1C, C_A), 123.8 (1C, C_A), 123.1 (1C, C_A), 61.4 (1C, C_D), 43.2 (1C, $C_{F/G}$), 39.2 (1C, $C_{F/G}$), 26.8 (1C, C_B), 25.3 (1C, C_B), 21.6 (1C, C_L) ppm; HRMS (ES$^+$): m/z found 350.1533 [M + H]$^+$; $C_{17}H_{24}N_3O_3S$ [M + H]$^+$ requires 350.1535; **56** ($C_{17}H_{23}N_3O_3S$; 349.4478 g/mol).

(*R*)-*N*-(2-((2-Amino-2-(cyclohexa-1,4-dien-1-yl)ethyl)amino)ethyl)-4-methylbenzenesulfonamide (57)
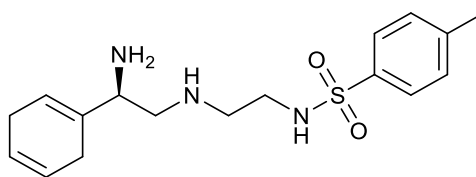
56 (0.83 g, 2.38 mmol, 1 eq.) was dissolved in anhydrous THF (20 mL) and added dropwise to the stirring solution of solid LiAlH$_4$ (0.23 g, 5.94 mmol, 2.50 eq.) in anhydrous THF (5 mL) under N$_2$. The reaction was stirred at room temperature for three days. The reaction was cooled to 0 °C and effervescence was observed whilst NaHCO$_3$ (50 mL) was added, to give a biphasic mixture, which was filtered. The sticky grey solid was washed with Et$_2$O (40 mL). The organic solvent was removed under reduced pressure. Et$_2$O (50 mL) was added to redissolve the product, which was extracted with H$_2$O (50 mL). The aqueous layer was washed with Et$_2$O (2 x 50 mL) and the organic layers were combined, dried over Na$_2$SO$_4$ and filtered. The solvent was removed under reduced pressure and the crude product dried further on a vacuum line to yield a yellow oil (0.25 g).The product was found to be impure starting material. Route terminated; full analysis not collected.

(*R*)-2-Amino-2-phenylethan-1-ol[333] (58)
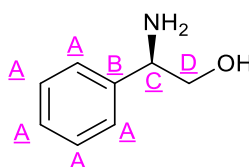
LiAlH$_4$ (1.82 g, 48.00 mmol, 2 eq.) was suspended in anyhdrous THF (100 mL) under N$_2$ at 0 °C. Solid (*R*)-2-amino-2-phenylacetic acid hydrochloride (4.50 g, 24.00 mmol, 1 eq.) was added in small portions. The mixture was stirred at 0 °C for one hour, then slowly heated to reflux and left to stir with heat overnight under N$_2$. The reaction was allowed to cool to room temperature and then was cooled further to 0 °C. THF (50 mL) was added and a saturated K$_2$CO$_3$ solution (50 mL) was added very slowly to the mixture. The mixture was filtered and the sticky grey solid was washed with THF (50 mL). The organic solvent was removed under reduced pressure. The orange oil was purified through a plug of silica. DCM was used to flush off the impurities and the pure product was eluted with DCM/MeOH (10 % MeOH). The solvent was removed under reduced pressure and the purified product was dried further on

a vacuum line as an orange solid (2.33 g, 17.11 mmol, 71 %). ^{1}H-NMR (CDCl$_3$, 400 MHz): δ = 7.26-7.37 (m, 5H, H$_A$), 4.03-4.06 (m, 1H, H$_C$), 3.72-3.75 (m, 1H, H$_D$), 3.54-3.58 (m, 1H, H$_D$), 2.49 (s, 2H, NH$_2$) ppm; ^{13}C{^{1}H}-NMR (CDCl$_3$, 400 MHz): δ = 142.6 (1C, C$_B$), 128.7 (2C, C$_A$), 127.6 (1C, C$_A$), 126.6 (2C, C$_A$), 68.0 (1C, C$_D$), 57.5 (1C, C$_C$) ppm; LRMS (ES$^+$): m/z found 138.1 [M + H]$^+$ (100 %); C$_8$H$_{12}$NO [M + H]$^+$ requires 138.2; **58** (C$_8$H$_{11}$NO; 137.2 g/mol).

(*R*)-*Tert*-butyl (2-hydroxy-1-phenylethyl)carbamate[334] (59)
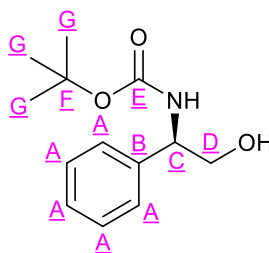
Di-*tert*-butyl dicarbonate (2.92 g, 13.40 mmol, 1 eq.) suspended in a mixture of H$_2$O (22.50 mL) and MeOH (5.50 mL) was added dropwise to a stirred mixture of **58** (2.33 g, 13.40 mmol, 1 eq.) and K$_2$CO$_3$ (2.23 g, 16.08 mmol, 1.20 eq.) in H$_2$O (22.50 mL) and MeOH (5.50 mL) at 0 °C. The cloudy yellow suspension with orange clumps was left to vigorously stir overnight at room temperature under N$_2$. A light yellow precipitate was observed in place of the orange clumps. The solvent was removed under reduced pressure and the product was extracted with H$_2$O (50 mL) and DCM (3 x 100 mL). The organic layers were combined, dried over Na$_2$SO$_4$ and filtered. The solvent was removed under reduced pressure and the crude product was dried further on a vacuum line as a yellow solid (3.23 g, 13.60 mmol, 101 %). The yield can be explained by the excess DCM observed in the ^{1}H-NMR. ^{1}H-NMR (CDCl$_3$, 400 MHz): δ = 7.27-7.38 (m, 5H, H$_A$), 4.78 (s, 1H, H$_C$), 3.84 (s, 2H, H$_D$), 2.37 (s, 1H, NH), 1.44 (s, 9H, H$_G$) ppm; ^{13}C{^{1}H}-NMR (CDCl$_3$, 400 MHz): δ = 156.3 (1C, C$_E$), 139.7 (1C, C$_B$), 128.7 (2C, C$_A$), 127.7 (1C, C$_A$), 126.6 (2C, C$_A$), 80.0 (1C, C$_F$), 66.6 (1C, C$_D$), 56.8 (1C, C$_C$), 28.4 (3C, C$_G$) ppm; LRMS (ES$^+$): m/z found 260.1 [M + Na]$^+$ (100 %); C$_{13}$H$_{19}$NNaO$_3$ [M + Na]$^+$ requires 260.3; **59** (C$_{13}$H$_{19}$NO$_3$; 237.3 g/mol).

(*R*)-2-((*Tert*-butoxycarbonyl)amino)-2-phenylethyl methanesulfonate[335] **(60)**
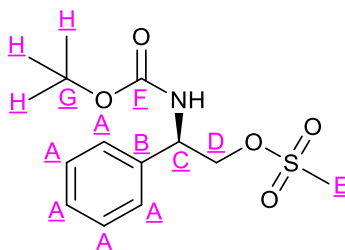
A solution of **59** (3.23 g, 13.60 mmol, 1 eq.) in DCM (100 mL) was cooled to 0 °C, followed by the addition of TEA (3.79 mL, 27.20 mmol, 2 eq.). The solution was stirred for ten minutes before methanesulfonyl chloride (1.16 mL, 15.00 mmol, 1.10 eq.) was added dropwise. The solution was stirred for 1.5 hours at 0 °C under N_2 and then washed with brine (3 x 50 mL). The organic phase was dried over Na_2SO_4, filtered and the solvent was removed under reduced pressure. Hexane (100 mL) was added to the resulting yellow solid and the product was collected by filtration. The crude product was dried further on a vacuum line to yield a beige solid (3.75 g, 11.89 mmol, 87 %). ^{1}H-NMR (CDCl$_3$, 400 MHz): δ = 7.29-7.39 (m, 5H, H$_A$), 5.25-5.27 (m, 1H, NH), 5.01 (s, 1H, H$_C$), 4.37-4.47 (m, 2H, H$_D$), 2.86 (s, 3H, C$_E$), 1.43 (s, 9H, H$_H$) ppm; ^{13}C{^{1}H}-NMR (CDCl$_3$, 400 MHz): δ = 155.2 (1C, C$_F$), 137.8 (1C, C$_B$), 129.0 (1C, C$_A$), 128.4 (2C, C$_A$), 126.8 (2C, C$_A$), 80.4 (1C, C$_G$), 71.4 (1C, C$_D$), 53.7 (1C, C$_C$), 37.5 (1C, C$_E$), 28.4 (3C, C$_H$) ppm; LRMS (ES$^+$): m/z found 338.1 [M + Na]$^+$ (100 %); C$_{14}$H$_{21}$NNaO$_5$S [M + Na]$^+$ requires 338.4; **60** (C$_{14}$H$_{21}$NO$_5$S; 315.4 g/mol).

(*R*)-*Tert*-butyl-(2-((2-aminoethyl)amino)-1-phenylethyl)carbamate (61)
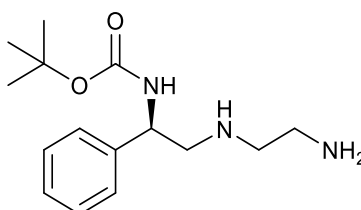
60 (3.75 g, 11.89 mmol, 1 eq.) and ethylenediamine (16 mL, 0.24 mol, 20 eq.) were dissolved in anhydrous THF (75 mL). The solution was heated at 60 °C overnight. The reaction mixture was allowed to cool to room temperature, then the solvent was removed under reduced pressure. The product was redissolved in DCM (200 mL) and extracted with H_2O (3 x 100 mL). The organic phase was dried with Na_2SO_4, filtered and the solvent removed under reduced pressure. The crude product was dried further on a vacuum line to yield an orange

oil (3.00 g). Purification on 60 Å alumina using DCM/MeOH (0-5 %) decomposed the product. Route terminated; full analysis not collected.

(*R*)-2-Amino-2-(cyclohexa-1,4-dien-1-yl)ethan-1-ol[336] (62)
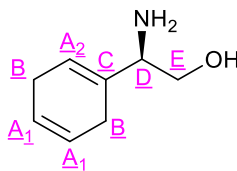
A solution of **58** (2.75 g, 20.20 mmol, 1 eq.) in ethanol (80 mL) was added to liquid NH_3 (300 mL) at -77 °C. Lithium wire (0.93 g, 0.13 mol, 6.60 eq.) was washed in hexane before addition in 0.50 g portions until a dark blue colour persisted. The reaction was left to stand overnight, followed by addition of H_2O (400 mL) and extraction with Et_2O (3 x 100 mL). The organic layers were combined, dried with Na_2SO_4 and filtered. The solvent was removed under reduced pressure. The aqueous phase was re-extracted with DCM (5 x 100 mL). The organic layers were combined, dried with Na_2SO_4 and filtered. The solvent was removed under reduced pressure. The crude product was dried further on a vacuum line as an orange oil (2.07 g, 15.00 mmol, 74 %). ^{1}H-NMR ($CDCl_3$, 400 MHz): δ = 5.68-5.74 (m, 3H, H_{A1} + H_{A2}), 3.60-3.66 (m, 1H, H_E), 3.40-3.46 (m, 1H, H_E), 3.32-3.35 (m, 1H, H_D), 2.53-2.75 (m, 4H, H_B), 2.34 (s, 2H, NH_2) ppm; ^{13}C{^{1}H}-NMR ($CDCl_3$, 400 MHz): δ = 135.8 (1C, C_C), 124.3 (1C, C_{A1}), 124.0 (1C, C_{A1}), 120.1 (1C, C_{A2}), 65.1 (1C, C_E), 58.4 (1C, C_D), 26.6 (1C, C_B), 26.4 (1C, C_B) ppm; LRMS (ES$^+$): m/z found 140.1 [M + H]$^+$ (100 %); $C_8H_{14}NO$ [M + H]$^+$ requires 140.2; **62** ($C_8H_{13}NO$; 139.2 g/mol).

(*R*)-*Tert*-butyl (1-(cyclohexa-1,4-dien-1-yl)-2-hydroxyethyl)carbamate (63)
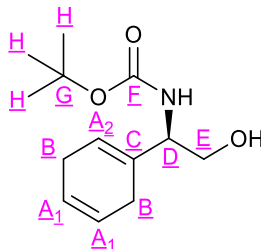
Di-*tert*-butyl dicarbonate (3.27 g, 15.00 mmol, 1 eq.) suspended in MeOH (10 mL) was added dropwise to a stirred mixture of **62** (2.07 g, 15.00 mmol, 1 eq.) and K_2CO_3 (2.48 g, 18.00 mmol, 1.20 eq.) in MeOH (20 mL) at 0 °C. The yellow suspension was left to stir overnight at room temperature under N_2. Analysis by ^{1}H-NMR proved the reaction to be incomplete,

therefore MeOH (30 mL) was added and the yellow suspension was left to stir for one hour at room temperature under N_2. The solvent was removed under reduced pressure and the product was extracted with H_2O (100 mL) and DCM (3 x 100 mL). The organic layers were combined, dried with Na_2SO_4 and filtered. The solvent was removed under reduced pressure and the product was dried further on a vacuum line as an orange solid. Hexane was used to triturate the product. The solid was collected by filtration and washed further with hexane. The crude product was dried further on a vacuum line to yield a beige solid (1.68 g, 7.05 mmol, 47 %). ^{1}H-NMR (CDCl$_3$, 400 MHz): δ = 5.68-5.73 (m, 3H, H$_{A1}$ + H$_{A2}$), 4.97-4.99 (m, 1H, OH), 4.06 (s, 1H, H$_D$), 3.69-3.70 (m, 2H, H$_E$), 2.63-2.73 (m, 4H, H$_B$), 1.45 (s, 9H, H$_H$) ppm; ^{13}C{^{1}H}-NMR (CDCl$_3$, 400 MHz): δ = 156.3 (1C, C$_F$), 132.6 (1C, C$_C$), 124.2 (1C, C$_{A1}$), 123.8 (1C, C$_{A1}$), 121.2 (1C, C$_{A2}$), 79.9 (1C, C$_G$), 64.2 (1C, C$_E$), 57.4 (1C, C$_D$), 28.5 (3C, C$_H$), 27.1 (1C, C$_B$), 26.6 (1C, C$_B$) ppm; HRMS (ES$^+$): m/z found 262.1414 [M + Na]$^+$; C$_{13}$H$_{21}$NNaO$_3$ [M + Na]$^+$ requires 262.1421; **63** (C$_{13}$H$_{21}$NO$_3$; 239.3107 g/mol).

(*R*)-2-((*Tert*-butoxycarbonyl)amino)-2-(cyclohexa-1,4-dien-1-yl)ethyl methanesulfonate (64)
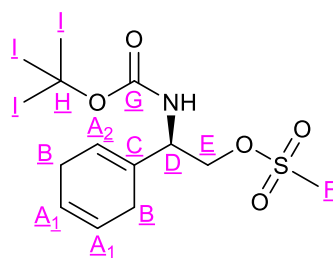
A solution of **63** (1.66 g, 6.97 mmol, 1 eq.) in DCM (50 mL) was cooled to 0 °C, followed by the addition of TEA (1.94 mL, 13.90 mmol, 2 eq.). The solution was stirred for ten minutes before methanesulfonyl chloride (0.59 mL, 7.67 mmol, 1.10 eq.) was added dropwise. The solution was stirred for 1.5 hours at 0 °C under N_2, diluted with DCM (50 mL) and then washed with brine (3 x 50 mL). The organic phase was dried with Na_2SO_4, filtered and the solvent was removed under reduced pressure. The crude product was dried further on a vacuum line to yield an orange solid (2.15 g, 6.77 mmol, 97 %). ^{1}H-NMR (CDCl$_3$, 400 MHz): δ = 5.65-5.71 (m, 3H, H$_{A1}$ + H$_{A2}$), 4.88 (s, 1H, H$_D$), 4.29-4.31 (m, 2H, H$_E$), 2.99-3.03 (m, 3H, C$_F$), 2.62-2.76 (m, 4H, H$_B$), 1.43 (s, 9H, H$_I$) ppm; ^{13}C{^{1}H}-NMR (CDCl$_3$, 400 MHz): δ = 155.3 (1C, C$_G$), 131.1 (1C, C$_C$), 124.0 (1C, C$_{A1}$), 123.5 (1C, C$_{A1}$), 122.4 (1C, C$_{A2}$), 80.2 (1C, C$_H$), 69.6 (1C, C$_E$), 54.2 (1C, C$_D$), 37.7 (1C, C$_F$), 28.4 (3C, C$_I$), 26.8 (1C, C$_B$), 26.6 (1C, C$_B$) ppm;

HRMS (ES$^+$): m/z found 340.1192 [M + Na]$^+$; C$_{14}$H$_{23}$NNaO$_5$S [M + Na]$^+$ requires 340.1189; **64** (C$_{14}$H$_{23}$NO$_5$S; 317.4011 g/mol).

(*R*)-*Tert*-butyl (1-(cyclohexa-1,4-dien-1-yl)-2-((2-((4-methylphenyl)sulfonamido)ethyl)amino)ethyl)carbamate (65)

Anticipated:
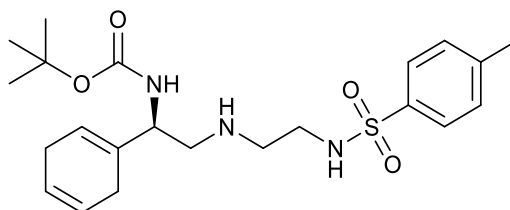
Actual:
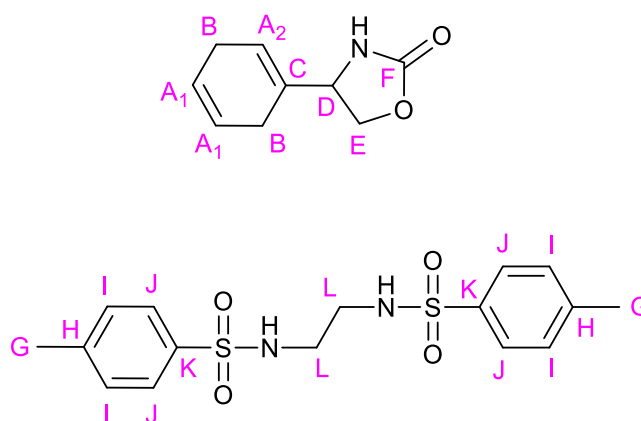

64 (20 mg, 0.064 mmol, 1 eq.) and **1** (0.14 g, 0.64 mmol, 10 eq.) were dissolved in ethanol (4 mL). The solution was heated to 100 ˚C overnight. The reaction was allowed to cool to room temperature, then DCM (100 mL) was added and the reaction mixture was extracted with H$_2$O (3 x 100 mL). The organic phase was dried with Na$_2$SO$_4$, filtered and the solvent was removed under reduced pressure. The product was dried further on a vacuum line to yield yellow solid. The crude product was purified by column chromatography with a solvent system of DCM/MeOH (0-13 % MeOH) to obtain the purer product as a pale yellow solid. The yield has not been included as the actual products obtained were not those that were anticipated. ^{1}H-NMR (CDCl$_3$, 400 MHz): δ = 7.70 (d, 4H, *J* = 8.23 Hz, H$_I$), 7.29 (d, 4H, *J* = 8.00 Hz, H$_J$), 5.67-5.76 (m, 6H, H$_{A1}$ + H$_{A2}$), 5.35-5.42 (m, 2H, linker NH), 4.49-4.53 (m, 2H, H$_E$), 4.34-4.38 (m, 2H, H$_D$), 4.11-4.14 (m, 2H, H$_E$), 3.03-3.04 (m, 4H, H$_L$), 2.61-2.75 (m, 8H, H$_B$), 2.42 (s, 6H, H$_G$), 1.70 (br. s, 2H, cyclic carbamate NH) ppm. Spectrum assigned to show

the correct number of protons for the ditosylated linker**, indicating that there were then two cyclic carbamate* molecules for every ditosylated linker molecule; $^{13}C\{^1H\}$-NMR (CDCl$_3$, 400 MHz): δ = 160.0*** (2C, C$_F$), 143.7 (2C, C$_H$), 136.6 (2C, C$_K$), 132.4 (2C, C$_C$), 129.2 (4C, C$_J$), 127.2 (4C, C$_I$), 124.2 (2C, C$_{A2}$), 123.3 (2C, C$_{A1}$), 123.2 (2C, C$_{A1}$), 69.1 (2C, C$_E$), 58.0 (2C, C$_D$), 43.0 (4C, C$_L$), 26.6 (2C, C$_B$), 24.1 (2C, C$_B$), 21.7 (2C, C$_G$) ppm. Spectrum assigned to show the correct number of carbons for the ditosylated linker, indicating that there were then two cyclic carbamate* molecules for every ditosylated linker** molecule; LRMS (ES$^+$) m/z found 391.1 [M + Na]$^+$ (100 %), C$_{16}$H$_{20}$N$_2$NaO$_4$S$_2$ requires 391.5 m/z; found 188.1 [M + Na]$^+$ (33 %), C$_9$H$_{11}$NNaO$_2$ requires 188.2 m/z; **65** (anticipated: C$_{22}$H$_{33}$N$_3$O$_4$S; 435.5801 g/mol, actual: C$_{16}$H$_{20}$N$_2$O$_4$S$_2$ and C$_9$H$_{11}$NO$_2$; 368.4710 g/mol and 165.1891).

*Cyclic carbamate ^{1}H-NMR and ^{13}C-NMR in close agreement with the literature.[338]

**Linker ^{1}H-NMR and ^{13}C-NMR in close agreement with the literature.[337]

***Baseline level peak, picked out based on literature.[338]

(*R*)-*Tert*-butyl (2-azido-1-(cyclohexa-1,4-dien-1-yl)ethyl)carbamate (66)
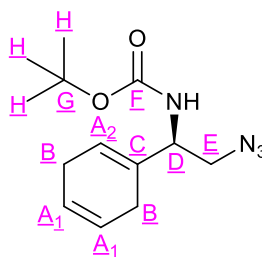
64 (50 mg, 0.16 mmol, 1 eq.) was dissolved in DMF (1 mL), followed by addition of sodium azide (51 mg, 0.79 mmol, 5 eq.), which was insoluble in the DMF reaction mixture. The reaction was heated to 80 °C under N$_2$ for four hours, which was coupled with a colour change from yellow to orange after heating. The reaction was quenched with H$_2$O (10 mL), followed by extraction with Et$_2$O (3 x 10 mL). The organic layers were dried with Na$_2$SO$_4$, filtered and the solvent was removed under reduced pressure. The crude product was dried further on a vacuum line to yield a yellow oil. The yield of the pure product was not calculated as the route was preliminary. ^{1}H-NMR (CDCl$_3$, 400 MHz): δ = 5.66-5.76 (m, 3H, H$_{A1}$ + H$_{A2}$), 4.11-5.11 (m, 2H, H$_{D/E}$), 3.42-3.51 (m, 1H, H$_{D/E}$), 2.58-2.76 (m, 4H, H$_B$), 1.45 (s, 7H, H$_H$) ppm; $^{13}C\{^1H\}$-NMR (CDCl$_3$, 400 MHz): δ = 155.3 (1C, C$_F$), 132.3 (1C, C$_C$), 124.1 (1C, C$_{A1}$), 123.5 (1C, C$_{A1}$), 121.8 (1C, C$_{A2}$), 80.1 (1C, C$_G$), 57.9 (1C, C$_D$), 53.2 (1C, C$_E$), 28.5 (3C, C$_H$), 26.8 (1C, C$_B$), 26.7 (1C, C$_B$) ppm; IR: υ$_{max}$ = 2099.02 (aliphatic C-N stretch) cm^{-1}; HRMS (ES$^+$)

m/z found 287.1481 [M + Na]$^+$; $C_{13}H_{20}N_4NaO_2$ [M + Na]$^+$ requires 287.1478; LRMS (ES$^+$) m/z found 287.1 [M + Na]$^+$ (100 %), 188.1 [(M – C_4H_9O*) + Na]$^+$ (26 %); **66** ($C_{13}H_{20}N_4O_2$; 264.3235 g/mol).

*Loss of Boc group only occurred during MS analysis.

(*R*)-*Tert*-butyl (2-amino-1-(cyclohexa-1,4-dien-1-yl)ethyl)carbamate (67)
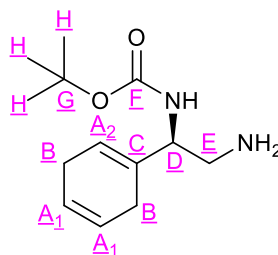
66 (50 mg, 0.19 mmol, 1 eq.) was dissolved in anhydrous THF (1 mL) and cooled to -41 ^{o}C, using a dry ice and acetonitrile cooling bath, followed by addition of LiAlH$_4$ (7.17 mg, 0.38 mmol, 2 eq.). The reaction mixture was left to stir under N$_2$ for seven hours, then a 0.5M solution of NaHSO$_4$ (5 mL) was added dropwise with fizzing observed. EtOAc (5 mL) was added and the mixture was filtered through celite under vacuum. The organic layer was dried with Na$_2$SO$_4$, filtered and the solvent was removed under reduced pressure. The product was dried further on a vacuum line to yield a yellow oil. The crude product was purified through silica under vacuum, using EtOAc/Hexane (10 % EtOAc) to flush the impurities off, followed by DCM/MeOH (20 % MeOH). The yield of the pure product was not calculated as the route was preliminary. ^{1}H-NMR (CDCl$_3$, 400 MHz): δ = 5.54-5.75 (m, 3H, H$_{A1}$ + H$_{A2}$), 4.05-5.05 (m, 3H, H$_D$ + H$_E$), 3.78 (br. s, 1H, NH$_2$), 3.63 (br. s, 1H, NH$_2$), 2.55-2.77 (m, 4H, H$_B$), 1.36-1.51 (m, 2H, H$_H$*) ppm; ^{13}C{^{1}H}-NMR (CDCl$_3$, 400 MHz): δ = 132.5 (1C, C$_C$), 126.2 (1C, C$_{A2}$), 124.2 (1C, C$_{A1}$), 123.3 (1C, C$_{A1}$), 69.0 (1C, C$_E$), 58.0 (1C, C$_D$), 26.6 (1C, C$_B$), 24.1 (1C, C$_B$) ppm; HRMS (ES$^+$) m/z found 239.1753 [M + H]$^+$; $C_{13}H_{25}N_2O_2$ [M + H]$^+$ requires 239.1754; LRMS (ES$^+$): m/z found 239.2 [M + H]$^+$ (32 %), 188.1 [(M – C_4H_9O*) + Na]$^+$ (100 %); **67** ($C_{13}H_{22}N_2O_2$; 238.3 g/mol).

*Unconfirmed if Boc or just an impurity. More likely to be an impurity as Boc was not observed in the ^{13}C-NMR. However, loss of part of the Boc fragment (C_4H_9O) was observed during MS analysis, though this technique is much more sensitive and hence the amount of Boc protected product could have been too small to observe by NMR.

(*R*)-*Tert*-butyl-(1-(cyclohexa-1,4-dien-1-yl)-2-(1,3-dioxoisoindolin-2-yl)ethyl)carbamate (68)

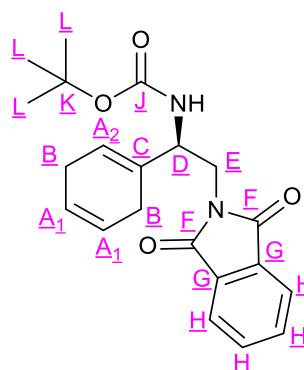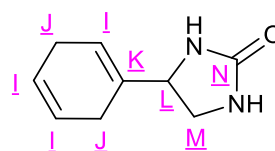
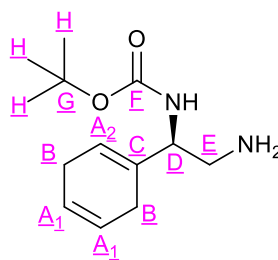Target product (successfully obtained):

Side product:

64 (100 mg, 0.32 mmol, 1 eq.) was dissolved in DMF (1 mL), followed by addition of potassium phthalimide (64.60 mg, 0.35 mmol, 1.10 eq.) and the reaction was heated to 100 °C overnight under N_2. The reaction was allowed to cool to room temperature before DCM (50 mL) and H_2O (50 mL) were added. The mixture was extracted and the aqueous layer was washed with DCM (2 x 50 mL). The organic layers were combined and washed with 0.2M NaOH solution (100 mL). The organic layer was dried with Na_2SO_4, filtered and the solvent was removed under reduced pressure. The crude product was dried further on a vacuum line to yield a yellow solid. The yield of the pure product was not calculated as the route was preliminary. ^{1}H-NMR (CDCl$_3$, 400 MHz): δ = 7.71-7.86 (m, 3H*, H_H), 5.65-5.74 (m, 3H, H_{A1} + H_{A2}), 3.70-4.53 (m, 3H, H_D + H_E), 2.61-2.74 (m, 4H, H_B), 1.24 (s, 5H**, H_L) ppm; ^{13}C{^{1}H}-NMR (CDCl$_3$, 400 MHz): δ = 168.7 (2C, C_F), 134.2 (2C, C_G), 134.1 (2C, C_H), 124.0 (1C, C_{A1}), 123.7 (1C, C_{A1}), 123.5 (2C, C_H), 121.3 (1C, C_{A2}), 77.8 (1C, C_K), 69.0 (1C, C_E), 57.9 (1C, C_D), 28.2 (3C, C_L), 26.7 (1C, C_B), 26.6 (1C, C_B) ppm; HRMS (ES$^+$) m/z found 391.1633 [M + Na]$^+$; $C_{21}H_{24}N_2NaO_4$ [M + Na]$^+$ requires 391.1628; LRMS (ES$^+$): m/z found 391.2 [M + Na]$^+$ (100 %), 185.1 [side product + Na]$^+$ (50 %); $C_9H_{10}N_2NaO$ [side product + Na]$^+$ requires 185.2; **68** ($C_{21}H_{24}N_2O_4$; 368.4262 g/mol), side product ($C_9H_{10}N_2NaO$; 162.1885 g/mol).

*Should integrate to 4H.

**Should integrate to 7H.

Note: The side product was not observed in the NMR spectra. It is suspected that this cyclisation occurs due to easy loss of the Boc group, however, it has not been concluded as to the conditions allowing for the mechanism to happen since we can't determine whether the cyclisation is occurring during the reaction or just analysis.

(*R*)-*Tert*-butyl (2-amino-1-(cyclohexa-1,4-dien-1-yl)ethyl)carbamate (67)

Target product (successfully obtained):
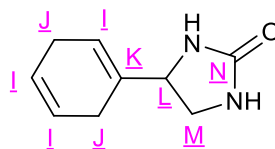
Side product:

68 (0.14 g, 0.38 mmol, 1 eq.) was dissolved in ethanol (4 mL), followed by addition of hydrazine hydrate (42.50 µL, 2.66 mmol, 7 eq.) and the reaction was heated at reflux for five hours under N_2. The reaction was allowed to cool to room temperature and a white solid precipitated. The solvent was removed under reduced pressure before H_2O (50 mL) was added. The aqueous layer was washed with DCM (4 x 20 mL). The organic layers were combined, dried with Na_2SO_4 and filtered. The solvent was removed under reduced pressure and the crude product was dried further on a vacuum line to yield a yellow oil. The yield of the pure product was not calculated as the route was preliminary. ^{1}H-NMR (CDCl$_3$, 400 MHz): δ = 5.52-5.72 (m, 3H, H$_{A1}$ + H$_{A2}$), 3.88-5.07 (m, 3H, H$_D$ + H$_E$), 2.55-2.78 (m, 4H, H$_B$), 1.41 (m, 12H, H$_H$*) ppm; ^{13}C{^{1}H}-NMR (CDCl$_3$, 400 MHz): δ = 160.1 (1C, C$_N$), 155.8 (1C, C$_F$), 135.1 (1C, C$_C$), 132.5 (1C, C$_K$), 125.7 (1C, C$_{A2}$), 124.2 (1C, C$_{A1}$), 124.1 (1C, C$_I$), 123.8 (1C, C$_I$), 123.3 (1C, C$_{A1}$), 122.9 (1C, C$_I$), 79.4 (1C, C$_G$), 69.3 (1C, C$_E$), 69.0 (1C, C$_M$), 58.2 (1C, C$_D$), 57.9 (1C, C$_L$), 28.5 (3C, C$_H$), 26.6 (1C, C$_J$), 25.8 (1C, C$_J$), 25.0 (1C, C$_B$), 25.0 (1C, C$_B$) ppm; HRMS (ES$^+$) m/z found 239.1758 [M + H]$^+$; C$_{13}$H$_{25}$N$_2$O$_2$ [M + H]$^+$ requires 239.1754; LRMS (ES$^+$): m/z found 239.2 [M + H]$^+$ (100 %), 185.1 [side product + Na]$^+$ (56 %); C$_9$H$_{10}$N$_2$NaO [side product + Na]$^+$ requires 185.2; **67** (C$_{13}$H$_{22}$N$_2$O$_2$; 238.3260 g/mol), side product (C$_9$H$_{10}$N$_2$NaO; 162.1885 g/mol).

*Should integrate to 9H.

Note: The side product was not observed in the ^{1}H-NMR spectra, likely due to overlapping signals with the desired product. It is suspected that this cyclisation occurs due to easy loss of the Boc group, however, it has not been concluded as to the conditions allowing for the mechanism to happen since we can't determine whether the cyclisation is occurring during the reaction or just analysis.

Chapter 6

References

1   S. P. Mulcahy and E. Meggers, *Top. Organomet. Chem.*, 2010, **32**, 141–153.
2   H. Bregman, P. J. Carroll and E. Meggers, *J. Am. Chem. Soc.*, 2006, **128**, 877–884.
3   S. S. David and E. Meggers, *Curr. Opin. Chem. Biol.*, 2008, **12**, 194–196.
4   G. E. Atilla-Gokcumen, N. Pagano, C. Streu, J. Maksimoska, P. Filippakopoulos, S. Knapp and E. Meggers, *ChemBioChem*, 2008, **9**, 2933–2936.
5   J. Maksimoska, L. Feng, K. Harms, C. Yi, J. Kissil, R. Marmorstein and E. Meggers, *J. Am. Chem. Soc.*, 2008, **130**, 15764–15765.
6   G. E. Atilla-Gokcumen, L. Di Costanzo and E. Meggers, *J. Biol. Inorg. Chem.*, 2011, **16**, 45–50.
7   E. Meggers, G. E. Atilla-Gokcumen, K. Gründler, C. Frias and A. Prokop, *Dalt. Trans.*, 2009, 10882–10888.
8   R. Anand, J. Maksimoska, N. Pagano, E. Y. Wong, P. A. Gimotty, S. L. Diamond, E. Meggers and R. Marmorstein, *J. Med. Chem.*, 2009, **52**, 1602–1611.
9   C. Streu, L. Feng, P. J. Carroll, J. Maksimoska, R. Marmorstein and E. Meggers, *Inorganica Chim. Acta*, 2011, **377**, 34–41.
10 E. Meggers, *Angew. Chemie Int. Ed.*, 2011, **50**, 2442–2448.
11 S. Blanck, J. Maksimoska, J. Baumeister, K. Harms, R. Marmorstein and E. Meggers, *Angew. Chemie Int. Ed.*, 2012, **51**, 5244–5246.
12 L. Gong, L.-A. Chen and E. Meggers, *Angew. Chemie Int. Ed.*, 2014, **53**, 10868–10874.
13 H. Bregman, D. S. Williams, E. Atilla, P. J. Carroll and E. Meggers, *J. Am. Chem. Soc.*, 2004, **126**, 13594–13595.
14 E. K. Martin, N. Pagano, M. E. Sherlock, K. Harms and E. Meggers, *Inorganica Chim. Acta*, 2014, **423**, 530–539.
15 J. Ma, X. Ding, Y. Hu, Y. Huang, L. Gong and E. Meggers, *Nat. Commun.*, 2014, **5**, 4531.
16 M. Dörr and E. Meggers, *Curr. Opin. Chem. Biol.*, 2014, **19**, 76–81.
17 E. Meggers, *Curr. Opin. Chem. Biol.*, 2007, **11**, 287–292.
18 E. Meggers, *Chem. Commun.*, 2009, 1001–1010.
19 L. Zhang, P. J. Carroll and E. Meggers, *Org. Lett.*, 2004, **6**, 521–523.
20 D. S. Williams, E. Atilla, H. Bregman, A. Arzoumanian, P. S. Klein and E. Meggers, *Angew. Chemie Int. Ed.*, 2005, **44**, 1984–1987.
21 G. E. Atilla-Gokcumen, D. S. Williams, H. Bregman, N. Pagano and E. Meggers, *ChemBioChem*, 2006, **7**, 1443–1450.
22 J. É. Debreczeni, A. N. Bullock, G. E. Atilla, D. S. Williams, H. Bregman, S. Knapp and E. Meggers, *Angew. Chemie Int. Ed.*, 2006, **45**, 1580–1585.
23 T. Cui, J. Qin, K. Harms and E. Meggers, *Eur. J. Inorg. Chem.*, 2019, **2019**, 195–198.
24 H. Bregman and E. Meggers, *Org. Lett.*, 2006, **8**, 5465–5468.
25 N. Pagano, J. Maksimoska, H. Bregman, D. S. Williams, R. D. Webster, F. Xue and E. Meggers, *Org. Biomol. Chem.*, 2007, **5**, 1218–1227.
26 S. H. van Rijt and P. J. Sadler, *Drug Discov. Today*, 2009, **14**, 1089–97.
27 M. Wills, *Top. Curr. Chem.*, 2016, **374**, 14.
28 E. B. Bauer, *Chem. Soc. Rev.*, 2012, **41**, 3153–3167.

29   P. Kumar, R. K. Guptaa and D. S. Pandey, *Chem. Soc. Rev.*, 2014, **43**, 707–733.

30   G. Consiglio, *Chem. Rev.*, 1987, **87**, 761–778.

31   Y. Hong, L. Jarrige, K. Harms and E. Meggers, *J. Am. Chem. Soc.*, 2019, **141**, 4569–4572.

32   Y. Zheng, Y. Tan, K. Harms, M. Marsch, R. Riedel, L. Zhang and E. Meggers, *J. Am. Chem. Soc.*, 2017, **139**, 4322–4325.

33   J. Ma, X. Zhang, X. Huang, S. Luo and E. Meggers, *Nat. Protoc.*, 2018, **13**, 605–632.

34   E. Winterling, S. Ivlev and E. Meggers, *Organometallics*, 2021, **40**, 1148–1155.

35   J. Wei, B. Cao, C. W. Tse, X. Y. Chang, C. Y. Zhou and C. M. Che, *Chem. Sci.*, 2020, **11**, 684–693.

36   H. Huo, C. Fu, K. Harms and E. Meggers, *J. Am. Chem. Soc.*, 2014, **136**, 2990–2993.

37   L. Zhang and E. Meggers, *Chem. - An Asian J.*, 2017, **12**, 2335–2342.

38   Z. Lin, M. A. Celik, C. Fu, K. Harms, G. Frenking and E. Meggers, *Chem. - A Eur. J.*, 2011, **17**, 12602–12605.

39   A. M. R. Hall, D. B. G. Berry, J. N. Crossley, A. Codina, I. Clegg, J. P. Lowe, A. Buchard and U. Hintermair, *ACS Catal.*, 2021, **11**, 13649–13659.

40   B. Zhang, H. Wang, G. Q. Lin and M. H. Xu, *European J. Org. Chem.*, 2011, 4205–4211.

41   O. Matuška, M. Kindl and P. Kačer, *New Adv. Hydrog. Process. - Fundam. Appl.*, 2017, DOI: 10.5772/65311.

42   A. E. Cotman, *Chem. – A Eur. J.*, 2020, DOI: 10.1002/chem.202002779.

43   N. Haraguchi, K. Tsuru, Y. Arakawa and S. Itsuno, *Org. Biomol. Chem.*, 2009, **7**, 69–75.

44   A. Pavlova and E. J. Meijer, *ChemPhysChem*, 2012, **13**, 3492–3496.

45   A. J. Blacker, in *The Handbook of Homogeneous Hydrogenation*, 2008, pp. 1215–1240.

46   S. Gladiali and E. Alberico, *Chem. Soc. Rev.*, 2006, **35**, 226–236.

47   A. N. Kim and B. M. Stoltz, *ACS Catal.*, 2020, **10**, 13834–13851.

48   D. Šterk, M. S. Stephan and B. Mohar, *Tetrahedron Asymmetry*, 2002, **13**, 2605–2608.

49   R. Guo, C. Elpelt, X. Chen, D. Song and R. H. Morris, *Chem. Commun.*, 2005, 3050–3052.

50   X. Wu, D. Vinci, T. Ikariya and J. Xiao, *Chem. Commun.*, 2005, 4447–4449.

51   E. Alza, A. Bastero, S. Jansat and M. A. Pericàs, *Tetrahedron Asymmetry*, 2008, **19**, 374–378.

52   B. Pugin and H. U. Blaser, *Top. Catal.*, 2010, **53**, 953–962.

53   X. Wu, J. Liu, D. Di Tommaso, J. A. Iggo, C. R. A. Catlow, J. Bacsa and J. Xiao, *Chem. - A Eur. J.*, 2008, **14**, 7699–7715.

54   S. E. Clapham, A. Hadzovic and R. H. Morris, *Coord. Chem. Rev.*, 2004, **248**, 2201–2237.

55   K. B. Hansen, J. R. Chilenski, R. Desmond, P. N. Devine, E. J. J. Grabowski, R. Heid, M. Kubryk, D. J. Mathre and R. Varsolona, *Tetrahedron Asymmetry*, 2003, **14**, 3581–3587.

56   D. G. I. Petra, J. N. H. Reek, J. W. Handgraaf, E. J. Meijer, P. Dierkes, P. C. J. Kamer, J. Brussee, H. E. Schoemaker and P. W. N. M. Van Leeuwen, *Chem. - A Eur. J.*, 2000, **6**, 2818–2829.

57   T. Touge, T. Hakamata, H. Nara, T. Kobayashi, N. Sayo, T. Saito, Y. Kayaki and T. Ikariya, *J. Am. Chem. Soc.*, 2011, **133**, 14960–14963.

58   J. Václavík, P. Šot, B. Vilhanová, J. Pecháček, M. Kuzma and P. Kačer, *Molecules*, 2013, **18**, 6804–6828.

59   R. Noyori, M. Yamakawa and S. Hashiguchi, *J. Org. Chem.*, 2001, **66**, 7931–7942.

60   X. Wu and J. Xiao, *Chem. Commun.*, 2007, 2449–2466.

61   R. M. Bullock, *Chem. - A Eur. J.*, 2004, **10**, 2366–2374.

62   A. J. Sandee, D. G. I. Petra, J. N. H. Reek, P. C. J. Kamer and P. W. N. M. van Leeuwen, *Chemistry (Easton).*, 2001, **7**, 1202–1208.

63   S. Elias, K. Goren and A. Vigalok, *Synlett*, 2012, **23**, 2619–2622.

64   A. Barrón-Jaime, O. F. Narvaez-Garayzar, J. González, V. Ibarra-Galván, G. Aguirre, M. Parra-Hake, D. Chávez and R. Somanathan, *Chirality*, 2011, **23**, 178–184.

65   Y.-M. He, F.-T. Song and Q.-H. Fan, in *Top Curr Chem*, 2014, pp. 145–190.

66   P. Oswal, A. Arora, S. Singh, D. Nautiyal, S. Kumar, G. K. Rao and A. Kumar, *Dalt. Trans.*, 2020, **49**, 12503–12529.

67   J. Václavík, P. Kačer, M. Kuzma and L. Červený, *Molecules*, 2011, **16**, 5460–5495.

68   A. J. Hutt and J. O'Grady, *J. Antimicrob. Chemother.*, 1996, **37**, 7–32.

69   P. Jeschke, *Pest Manag. Sci.*, 2018, **74**, 2389–2404.

70   R. Noyori, *Angew. Chemie - Int. Ed.*, 2002, **41**, 2008–2022.

71   J. Goswami, R. L. Bezbaruah, A. Goswami and N. Borthakur, *Tetrahedron Asymmetry*, 2001, **12**, 3343–3348.

72   L. A. Nguyen, H. He and C. Pham-Huy, *Int. J. Biomed. Sci.*, 2006, **2**, 85–100.

73   American Chemical Society, *Mol. Week*, 2014, https://www.acs.org/content/acs/en/molecule-of-the.

74   L. Huang, J. Liu, W. Shan, B. Liu, A. Shi and X. Li, *Chirality*, 2010, **22**, 206–211.

75   H. S. Wilkinson, G. J. Tanoury, S. A. Wald and C. H. Senanayake, *Org. Process Res. Dev.*, 2002, **6**, 146–148.

76   Y. Zheng, L. Zhang and E. Meggers, *Org. Process Res. Dev.*, 2018, **22**, 101–107.

77   P. O. Carvalho, Q. B. Cass, S. A. Calafatti, F. J. Contesini and R. Bizaco, *Brazilian J. Chem. Eng.*, 2006, **23**, 291–300.

78   M. E. Tiritan, C. Fernandes, A. S. Maia, M. Pinto and Q. B. Cass, *J. Chromatogr. A*, 2018, **1569**, 1–7.

79   E. Meggers, *Chem. - A Eur. J.*, 2010, **16**, 752–758.

80   V. K. Aggarwal, A. Lerchen, N. Gandhamsetty, E. Farrar, N. Winter, J. Platzek and M. Grayson, *Angew. Chemie Int. Ed.*, 2020, doi: 10.1002/anie.202011256.

81   H. G. Nedden, A. Zanotti-Gerosa and M. Wills, *Chem. Rec.*, 2016, **16**, 2623–2643.

82   R. Noyori and T. Ohkuma, *Angew. Chemie - Int. Ed.*, 2001, **40**, 40–73.

83   M. J. Palmer and M. Wills, *Tetrahedron Asymmetry*, 1999, **10**, 2045–2061.

84   H. Y. Rhyoo, Y. A. Yoon, H. J. Park and Y. K. Chung, *Tetrahedron Lett.*, 2001, **42**, 5045–5048.

85   L. Li, J. Wu, F. Wang, J. Liao, H. Zhang, C. Lian, J. Zhu and J. Deng, *Green Chem.*, 2007, **9**, 23–25.

86   F. Chen, D. He, L. Chen, X. Chang, D. Z. Wang, C. Xu and X. Xing, *ACS Catal.*, 2019, **9**, 5562–5566.

87   R. Soni, T. H. Hall, B. P. Mitchell, M. R. Owen and M. Wills, *J. Org. Chem.*, 2015, **80**, 6784–6793.

88   T. Ikariya and A. J. Blacker, *Acc. Chem. Res.*, 2007, **40**, 1300–1308.

89   M. Aitali, S. Allaoud, A. Karim, C. Meliet and A. Mortreux, *Tetrahedron Asymmetry*, 2000, **11**, 1367–1374.

90   C. Wang, X. Wu and J. Xiao, *Chem. - An Asian J.*, 2008, **3**, 1750–1770.

91   Q. H. Fan, Y. M. Li and A. S. C. Chan, *Chem. Rev.*, 2002, **102**, 3385–3466.

92   V. K. Vyas, G. J. Clarkson and M. Wills, *Angew. Chemie - Int. Ed.*, 2020, **59**, 14265–14269.

93   P. A. Dub, A. Matsunami, S. Kuwata and Y. Kayaki, *J. Am. Chem. Soc.*, 2019, **141**, 2661–2677.

94   H. Y. Rhyoo, H. J. Park and Y. K. Chung, *Chem. Commun.*, 2001, 2064–2065.

95   P. T. Anastas, M. M. Kirchhoff and T. C. Williamson, *Appl. Catal. A Gen.*, 2001, **221**, 3–13.

96   F. Chen, J. J. Soldevila-Barreda, I. Romero-Canelón, J. P. C. Coverdale, J.-I. Song, G. J. Clarkson, J. Kasparkova, A. Habtemariam, V. Brabec, J. A. Wolny, V. Schünemann and P. J. Sadler, *Dalt. Trans.*, 2018, **47**, 7178–7189.

97   P. A. Dub, N. V. Tkachenko, V. K. Vyas, M. Wills, J. S. Smith and S. Tretiak, *Organometallics*, 2021, **40**, 1402–1410.

98   M. Wills, M. Palmer, A. Smith, J. Kenny and T. Walsgrove, *Molecules*, 2000, **5**, 4–18.

99   K. E. Jolley, G. J. Clarkson and M. Wills, *J. Organomet. Chem.*, 2015, **776**, 157–162.

100   V. Parekh, J. A. Ramsden and M. Wills, *Catal. Sci. Technol.*, 2012, **2**, 406–414.

101   P. E. Sues, K. Z. Demmans and R. H. Morris, *Dalt. Trans.*, 2014, **43**, 7650–7667.

102   J. E. D. Martins, G. J. Clarkson and M. Wills, *Org. Lett.*, 2009, **11**, 847–850.

103   J. E. D. Martins, M. A. Contreras Redondo and M. Wills, *Tetrahedron Asymmetry*, 2010, **21**, 2258–2264.

104   J. Barrios-Rivera, Y. Xu, M. Wills and V. K. Vyas, *Org. Chem. Front.*, 2020, **7**, 3312–3342.

105   T. Ikariya, K. Murata and R. Noyori, *Org. Biomol. Chem.*, 2006, **4**, 393–406.

106   K. Everacre, A. Mortreux and J. F. Carpentier, *Adv. Synth. Catal.*, 2003, **345**, 67–77.

107   K. C. Fung, A. M. Hayes, J. Hannedouche, A. S. Y. Yim and M. Wills, *J. Org. Chem.*, 2005, **70**, 3188–3197.

108   J. Barrios-Rivera, Y. Xu and M. Wills, *Org. Lett.*, 2020, **22**, 6283–6287.

109   R. Hodgkinson, V. Jurčík, H. Nedden, A. Blackaby and M. Wills, *Tetrahedron Lett.*, 2018, **59**, 930–933.

110   A. M. R. Hall, P. Dong, A. Codina, J. P. Lowe and U. Hintermair, *ACS Catal.*, 2019, **9**, 2079–2090.

111   R. J. Chew and M. Wills, *J. Catal.*, 2018, **361**, 40–44.

112   D. S. Matharu, D. J. Morris, G. J. Clarkson and M. Wills, *Chem. Commun.*, 2006, 3232–3234.

113   J. Ansell and M. Wills, *Chem. Soc. Rev.*, 2002, **31**, 259–268.

114   F. Chen, I. Romero-Canelón, J. J. Soldevila-Barreda, J. I. Song, J. P. C. Coverdale, G. J. Clarkson, J. Kasparkova, A. Habtemariam, M. Wills, V. Brabec and P. J. Sadler, *Organometallics*, 2018, **37**, 1555–1566.

115   Z. Zuo, L. Zhang, X. Leng and Z. Huang, *Chem. Commun.*, 2015, **51**, 5073–5076.

116   R. H. Morris, *Chem. Soc. Rev.*, 2009, **38**, 2282–2291.

117   S. Gaillard and J. L. Renaud, *ChemSusChem*, 2008, **1**, 505–509.

118   M. Zhang and A. Zhang, *Appl. Organomet. Chem.*, 2010, **24**, 751–757.

119   A. M. Thayer, *Chem. Eng. News*, 2013, **91**, 68.

120   D. Wang and D. Astruc, *Chem. Rev.*, 2015, **115**, 6621–6686.

121   S. Hashiguchi, A. Fujii, J. Takehara, T. Ikariya and R. Noyori, *J. Am. Chem. Soc.*, 1995, **117**, 7562–7563.

122   R. Soni, K. E. Jolley, G. J. Clarkson and M. Wills, *Org. Lett.*, 2013, **15**, 5110–5113.

123   A. M. Hayes, D. J. Morris, G. J. Clarkson and M. Wills, *J. Am. Chem. Soc.*, 2005,

127, 7318–7319.

124 N. A. Cortez, G. Aguirre, M. Parra-Hake and R. Somanathan, *Tetrahedron Asymmetry*, 2008, **19**, 1304–1309.

125 R. C. Knighton, V. K. Vyas, L. H. Mailey, B. M. Bhanage and M. Wills, *J. Organomet. Chem.*, 2018, **875**, 72–79.

126 B. Mohar, A. Valleix, J. R. Desmurs, M. Felemez, A. Wagner and C. Mioskowski, *Chem. Commun.*, 2001, 2572–2573.

127 M. Yamakawa, H. Ito and R. Noyori, *J. Am. Chem. Soc.*, 2000, **122**, 1466–1478.

128 R. Noyori and S. Hashiguchi, *Acc. Chem. Res.*, 1997, **30**, 97–102.

129 D. J. Cross, I. Houson, A. M. Kawamoto and M. Wills, *Tetrahedron Lett.*, 2004, **45**, 843–846.

130 J. S. M. Samec, J. E. Bäckvall, P. G. Andersson and P. Brandt, *Chem. Soc. Rev.*, 2006, **35**, 237–248.

131 K. C. Fung, M. A. Graham, F. Minissi and M. Wills, *Organometallics*, 2007, **26**, 5346–5351.

132 J. E. D. Martins, D. J. Morris, B. Tripathi and M. Wills, *J. Organomet. Chem.*, 2008, **693**, 3527–3532.

133 A. Hayes, G. Clarkson and M. Wills, *Tetrahedron Asymmetry*, 2004, **15**, 2079–2084.

134 N. J. Alcock, I. Mann, P. Peach and M. Wills, *Tetrahedron Asymmetry*, 2002, **13**, 2485–2490.

135 I. Yamada and R. Noyori, *Org. Lett.*, 2000, **2**, 3425–3427.

136 P. N. Liu, P. M. Gu, F. Wang and Y. Q. Tu, *Org. Lett.*, 2004, **6**, 169–172.

137 K. Ahlford, J. Lind, L. Mäler and H. Adolfsson, *Green Chem.*, 2008, **10**, 832–835.

138 K. Abdur-Rashid, M. Faatz, A. J. Lough and R. H. Morris, *J. Am. Chem. Soc.*, 2001, **123**, 7473–7474.

139 Nobel Media AB 2018, Ryoji Noyori - Nobel Lecture: Asymmetric Catalysis: Science and Technology, https://www.nobelprize.org/prizes/chemistry/2001/noyori/lecture/, (accessed 20 August 2018).

140 C. A. Sandoval, T. Ohkuma, K. Muñiz and R. Noyori, *J. Am. Chem. Soc.*, 2003, **125**, 13490–13503.

141 B. Zhao, Z. Han and K. Ding, *Angew. Chemie - Int. Ed.*, 2013, **52**, 4744–4788.

142 Y. (Andy) Xu, G. C. Clarkson, G. Docherty, C. L. North, G. Woodward and M. Wills, *J. Org. Chem.*, 2005, **70**, 8079–8087.

143 M. A. Amin, M. A. Camerino, S. J. Mountford, X. Ma, D. T. Manallack, D. K. Chalmers, M. Wills and P. E. Thompson, *Tetrahedron*, 2019, **75**, 130591.

144 D. J. Morris, A. M. Hayes and M. Wills, *J. Org. Chem.*, 2006, **71**, 7035–7044.

145 A. Kišic, M. Stephan and B. Mohar, *Adv. Synth. Catal.*, 2015, **357**, 2540–2546.

146 J. Hannedouche, G. J. Clarkson and M. Wills, *J. Am. Chem. Soc.*, 2004, **126**, 986–987.

147 T. Touge, H. Nara, M. Fujiwhara, Y. Kayaki and T. Ikariya, *J. Am. Chem. Soc.*, 2016, **138**, 10084–10087.

148 A. Kišić, M. Stephan and B. Mohar, *Adv. Synth. Catal.*, 2014, **356**, 3193–3198.

149 A. Fujii, S. Hashiguchi, N. Uematsu, T. Ikariya and R. Noyori, *J. Am. Chem. Soc.*, 1996, **118**, 2521–2522.

150 F. K. Cheung, C. Lin, F. Minissi, A. L. Crivillé, M. A. Graham, D. J. Fox and M. Wills, *Org. Lett.*, 2007, **9**, 4659–4662.

151 R. Hodgkinson, V. Jurčík, A. Zanotti-Gerosa, H. G. Nedden, A. Blackaby, G. J. Clarkson and M. Wills, *Organometallics*, 2014, **33**, 5517–5524.

152 C. Dean, S. Rajkumar, S. Roesner, N. Carson, G. J. Clarkson, M. Wills, M. Jones

and M. Shipman, *Chem. Sci.*, 2020, **11**, 1636–1642.

153   T. Hamada, T. Torii, K. Izawa, R. Noyori and T. Ikariya, *Org. Lett.*, 2002, **4**, 4373–4376.

154   T. Hamada, T. Torii, K. Izawa and T. Ikariya, *Tetrahedron*, 2004, **60**, 7411–7417.

155   Y. Ma, H. Liu, L. Chen, X. Cui, J. Zhu and J. Deng, *Org. Lett.*, 2003, **5**, 2103–2106.

156   *World Intellect. Prop. Organ.*, 2009, WO2009130056A1.

157   *Process asymmetric Transf. Hydrog. ketones (Archimica GMBH)*, 2011, WO2011131315A.

158   *World Intellect. Prop. Organ.*, 2012, WO2012156693A1.

159   The University of Warwick Impact Case Study (REF3b), *Wills Catalysts: commercialised systems for enantioselective production of pharmaceutical intermediates*, 2014.

160   *New CCR2 Antagon. (Boehringer Ingelheim Int. GMBH)*, 2010, US20130217728.

161   *Synth. route Prep. substituted 2-phenyl-1,2,3,4-tetrahydronaphthalene-1-ols (LEK Pharm. d.d.)*, 2012, EP2644603A1.

162   N. Uematsu, A. Fujii, S. Hashiguchi, T. Ikariya and R. Noyori, *J. Am. Chem. Soc.*, 1996, **118**, 4916–4917.

163   J. Takehara, S. Hashiguchi, A. Fujii, S. I. Inoue, T. Ikariya and R. Noyori, *Chem. Commun.*, 1996, 233–234.

164   I. Kawasaki, K. Tsunoda, T. Tsuji, T. Yamaguchi, H. Shibuta, N. Uchida, M. Yamashita and S. Ohta, *Chem. Commun.*, 2005, 2134–2136.

165   D. A. Alonso, P. Brandt, S. J. M. Nordin and P. G. Andersson, *J. Am. Chem. Soc.*, 1999, **121**, 9580–9588.

166   R. Aznar, A. Grabulosa, A. Mannu, G. Muller, D. Sainz, V. Moreno, M. Font-Bardia, T. Calvet and J. Lorenzo, *Organometallics*, 2013, **32**, 2344–2362.

167   K. E. Jolley, A. Zanotti-Gerosa, F. Hancock, A. Dyke, D. M. Grainger, J. A. Medlock, H. G. Nedden, J. J. M. Le Paih, S. J. Roseblade, A. Seger, V. Sivakumar, I. Prokes, D. J. Morris and M. Wills, *Adv. Synth. Catal.*, 2012, **354**, 2545–2555.

168   Y. Zheng, J. A. Martinez-Acosta, M. Khimji, L. C. A. Barbosa, G. J. Clarkson and M. Wills, *Eur. Soc. Journal Catal.*, 2021, **13**, 4384–4391.

169   K. C. Fung, A. M. Hayes, D. J. Morris and M. Wills, *Org. Biomol. Chem.*, 2007, **5**, 1093–1103.

170   F. K. (Kathy) Cheung, A. K. Clarke, G. J. Clarkson, D. J. Fox, M. A. Graham, C. Lin, A. L. Crivillé and M. Wills, *Dalt. Trans.*, 2010, **39**, 1395–1402.

171   X. Zhou, X. Wu, B. Yang and J. Xiao, *J. Mol. Catal. A Chem.*, 2012, **357**, 133–140.

172   R. Soni, J.-M. Collinson, G. C. Clarkson and M. Wills, *Org. Lett.*, 2011, **13**, 4304–4307.

173   C. Hedberg, *Modern Reduction Methods*, 2008.

174   K. Murata, T. Ikariya and R. Noyori, *J. Org. Chem.*, 1999, **64**, 2186–2187.

175   R. Soni, F. K. Cheung, G. C. Clarkson, J. E. D. Martins, M. A. Graham and M. Wills, *Org. Biomol. Chem.*, 2011, **9**, 3290–3294.

176   J. Barrios-Rivera, Y. Xu and M. Wills, *Org. Biomol. Chem.*, 2019, **17**, 1301–1321.

177   T. Koike and T. Ikariya, *Adv. Synth. Catal.*, 2004, **346**, 37–41.

178   M. Yamakawa, I. Yamada and R. Noyori, *Angew. Chemie - Int. Ed.*, 2001, **40**, 2818–2821.

179   K. Y. Wan, A. J. Lough and R. H. Morris, *Organometallics*, 2016, **35**, 1604–1612.

180   K. Y. Wan, F. Roelfes, A. J. Lough, F. E. Hahn and R. H. Morris, *Organometallics*, 2018, **37**, 491–504.

181   R. Noyori, C. A. Sandoval, K. Muñiz and T. Ohkuma, *Source Philos. Trans. Math. Phys. Eng. Sci.*, 2005, **363**, 901–912.

182   A. S. Y. Yim and M. Wills, *Tetrahedron*, 2005, **61**, 7994–8004.

183   K. J. Haack, S. Hashiguchi, A. Fujii, T. Ikariya and R. Noyori, *Angew. Chemie (International Ed. English)*, 1997, **36**, 285–288.

184   P. Brandt, P. Roth and P. G. Andersson, *J. Org. Chem.*, 2004, **69**, 4885–4890.

185   J. Canivet and G. Süss-Fink, *Green Chem.*, 2007, **9**, 391–397.

186   R. Soni, K. E. Jolley, S. Gosiewska, G. J. Clarkson, Z. Fang, T. H. Hall, B. N. Treloar, R. C. Knighton and M. Wills, *Organometallics*, 2018, **37**, 48–64.

187   T. Ohkuma, N. Utsumi, K. Tsutsumi, K. Murata, C. Sandoval and R. Noyori, *J. Am. Chem. Soc.*, 2006, **128**, 8724–8725.

188   A. E. Cotman, D. Cahard and B. Mohar, *Angew. Chemie - Int. Ed.*, 2016, **55**, 5294–5298.

189   Y. Zheng, G. J. Clarkson and M. Wills, *Org. Lett.*, 2020, **22**, 3717–3721.

190   K. Matsumura, S. Hashiguchi, T. Ikariya and R. Noyori, *J. Am. Chem. Soc.*, 1997, **119**, 8738–8739.

191   K. Murata, K. Okano, M. Miyagi, H. Iwane, R. Noyori and T. Ikariya, *Org. Lett.*, 1999, **1**, 1119–1121.

192   S. Forshaw, A. J. Matthews, T. J. Brown, L. J. Diorazio, L. Williams and M. Wills, *Org. Lett.*, 2017, **19**, 2789–2792.

193   Z. Fang and M. Wills, *Org. Lett.*, 2014, **16**, 374–377.

194   V. K. Vyas, R. C. Knighton, B. M. Bhanage and M. Wills, *Org. Lett.*, 2018, **20**, 975–978.

195   F. Eustache, P. I. Dalko and J. Cossy, *Org. Lett.*, 2002, **4**, 1263–1265.

196   J. A. Marshall and M. P. Bourbeau, *Org. Lett.*, 2003, **5**, 3197–3199.

197   J. Cossy, F. Eustache and P. I. Dalko, *Tetrahedron Lett.*, 2001, **42**, 5005–5007.

198   P. Peach, D. J. Cross, J. A. Kenny, I. Mann, I. Houson, L. Campbell, T. Walsgrove and M. Wills, *Tetrahedron*, 2006, **62**, 1864–1876.

199   S. K. Gediya, V. K. Vyas, G. J. Clarkson and M. Wills, *Org. Lett.*, 2021, **23**, 7803–7807.

200   T. H. Hall, H. Adams, V. K. Vyas, K. L. M. Chu and M. Wills, *Tetrahedron*, 2021, **77**, 131771.

201   A. A. Bisset, A. Dishington, T. Jones, G. J. Clarkson and M. Wills, *Tetrahedron*, 2014, **70**, 7207–7220.

202   Z. Fang and M. Wills, *J. Org. Chem.*, 2013, **78**, 8594–8605.

203   T. Ohkuma, H. Ooka, S. Hashiguchi, T. Ikariya and R. Noyori, *J. Am. Chem. Soc.*, 1995, **117**, 2675–2676.

204   A. Kišić, M. Stephan and B. Mohar, *Org. Lett.*, 2013, **15**, 1614–1617.

205   Y. K. Yan, M. Melchart, A. Habtemariam and P. J. Sadler, *Chem. Commun.*, 2005, 4764–4776.

206   E. J. Anthony, E. M. Bolitho, H. E. Bridgewater, O. W. L. Carter, J. M. Donnelly, C. Imberti, E. C. Lant, F. Lermyte, R. J. Needham, M. Palau, P. J. Sadler, H. Shi, F.-X. Wang, W.-Y. Zhang and Z. Zhang, *Chem. Sci.*, 2020, DOI: 10.1039/D0SC04082G.

207   S. J. Dougan, A. Habtermariam, S. E. McHale, S. Parsons and P. J. Sadler, *PNAS*, 2008, **105**, 11628–11633.

208   A. M. Pizarro, A. Habtemariam and P. J. Sadler, *Top. Organomet. Chem.*, 2010, **32**, 21–56.

209   R. Soni, T. H. Hall, D. J. Morris, G. J. Clarkson, M. R. Owen and M. Wills, *Tetrahedron Lett.*, 2015, **56**, 6397–6401.

210   2015, US20150094468.

211   J. Barrios-Rivera, Y. Xu and M. Wills, *Org. Lett.*, 2019, **21**, 7223–7227.

212   T. J. Prior, H. Savoie, R. W. Boyle and B. S. Murray, *Organometallics*, 2018, **37**,

294–297.

213   Y. Wang, J. Jin, L. Shu, T. Li, S. Lu, M. K. M. Subarkhan, C. Chen and H. Wang, *Chem. – A Eur. J.*, 2020, 1-30 doi: 10.1002/chem.202002970.

214   S. P. Mulcahy, K. Gründler, C. Frias, L. Wagner, A. Prokop and E. Meggers, *Dalt. Trans.*, 2010, **39**, 8177–8182.

215   S. M. Meier-Menches, C. Gerner, W. Berger, C. G. Hartinger and B. K. Keppler, *Chem. Soc. Rev.*, 2018, **47**, 909–928.

216   W. M. Motswainyana and P. A. Ajibade, *Adv. Chem.*, 2015, **2015**, 859730.

217   Y. Fu, C. Sanchez-Cano, R. Soni, I. Romero-Canelon, J. M. Hearn, Z. Liu, M. Wills and P. J. Sadler, *Dalt. Trans.*, 2016, **45**, 8367–8378.

218   J. J. Soldevila-Barreda, I. Romero-Canelón, A. Habtemariam and P. J. Sadler, *Nat. Commun.*, 2015, **6**, 6582.

219   J. P. C. Coverdale, I. Romero-Canelón, C. Sanchez-Cano, G. J. Clarkson, A. Habtemariam, M. Wills and P. J. Sadler, *Nat. Chem.*, 2018, **10**, 347–354.

220   J. J. Soldevila-Barreda, P. C. A. Bruijnincx, A. Habtemariam, G. J. Clarkson, R. J. Deeth and P. J. Sadler, *Organometallics*, 2012, **31**, 5958–5967.

221   Y. K. Yan, M. Melchart, A. Habtemariam, A. F. A. Peacock and P. J. Sadler, *J. Biol. Inorg. Chem.*, 2006, **11**, 483–488.

222   P. Zhang and P. J. Sadler, *J. Organomet. Chem.*, 2017, **839**, 5–14.

223   R. Van Putten, G. A. Filonenko, A. Gonzalez De Castro, C. Liu, M. Weber, C. Müller, L. Lefort and E. Pidko, *Organometallics*, 2019, **38**, 3187–3196.

224   H. Nishiyama and A. Furuta, *Chem. Commun.*, 2007, 760–762.

225   R. M. Bullock, *Science (80-.).*, 2013, **342**, 1054–1055.

226   K. Riener, M. P. Högerl, P. Gigler and F. E. Kühn, *ACS Catal.*, 2012, **2**, 613–621.

227   R. Lopes, J. M. S. Cardoso, L. Postigo and B. Royo, *Catal. Letters*, 2013, **143**, 1061–1066.

228   F. Jiang, D. Bézier, J. B. Sortais and C. Darcel, *Adv. Synth. Catal.*, 2011, **353**, 239–244.

229   K. Riener, S. Haslinger, A. Raba, M. P. Högerl, M. Cokoja, W. A. Herrmann and F. E. Kühn, *Chem. Rev.*, 2014, **114**, 5215–5272.

230   V. V. K. M. Kandepi, J. M. S. Cardoso, E. Peris and B. Royo, *Organometallics*, 2010, **29**, 2777–2782.

231   V. César, L. C. Misal Castro, T. Dombray, J. B. Sortais, C. Darcel, S. Labat, K. Miqueu, J. M. Sotiropoulos, R. Brousses, N. Lugan and G. Lavigne, *Organometallics*, 2013, **32**, 4643–4655.

232   J. M. S. Cardoso and B. Royo, *Chem. Commun.*, 2012, **48**, 4944–4946.

233   L. C. M. Castro, J. B. Sortais and C. Darcel, *Chem. Commun.*, 2012, **48**, 151–153.

234   P. Buchgraber, L. Toupet and V. Guerchais, *Organometallics*, 2003, **22**, 5144–5147.

235   S. Demir, Y. Gökçe, N. Kaloğlu, J. B. Sortais, C. Darcel and I. Özdemir, *Appl. Organomet. Chem.*, 2013, **27**, 459–464.

236   D. A. Valyaev, D. Wei, S. Elangovan, M. Cavailles, V. Dorcet, J. B. Sortais, C. Darcel and N. Lugan, *Organometallics*, 2016, **35**, 4090–4098.

237   J. Zheng, S. Elangovan, D. A. Valyaev, R. Brousses, V. César, J. B. Sortais, C. Darcel, N. Lugan and G. Lavigne, *Adv. Synth. Catal.*, 2014, **356**, 1093–1097.

238   S. Sulieman, D. Can, J. Mertens, H. W. P. N'Dongo, Y. Liu, P. Schmutz, M. Bauwens, B. Spingler and R. Alberto, *Organometallics*, 2012, **31**, 6880–6886.

239   D. Bézier, F. Jiang, T. Roisnel, J. B. Sortais and C. Darcel, *Eur. J. Inorg. Chem.*, 2012, 1333–1337.

240   D. J. Bayston, C. B. Travers and M. E. C. Polywka, *Tetrahedron Asymmetry*, 1998,

9, 2015–2018.

241   Y. Li, Z. Li, F. Li, Q. Wang and F. Tao, *Org. Biomol. Chem.*, 2005, **3**, 2513–2518.

242   G. Liu, M. Yao, F. Zhang, Y. Gao and H. Li, *Chem. Commun.*, 2008, 347–349.

243   J. Wu, F. Wang, Y. Ma, X. Cui, L. Cun, J. Zhu, J. Deng and B. Yu, *Chem. Commun.*, 2006, 1766–1768.

244   S. B. Wendicke, E. Burri, R. Scopelliti and K. Severin, *Organometallics*, 2003, **22**, 1894–1897.

245   C. Maillet, T. Praveen, P. Janvier, S. Minguet, M. Evain, C. Saluzzo, M. L. Tommasino and B. Bujoli, *J. Org. Chem.*, 2002, **67**, 8191–8196.

246   X. Li, W. Chen, W. Hems, F. King and J. Xiao, *Org. Lett.*, 2003, **5**, 4559–4561.

247   H. Y. Rhyoo, H. J. Park, W. H. Suh and Y. K. Chung, *Tetrahedron Lett.*, 2002, **43**, 269–272.

248   M. T. Zarka, O. Nuyken and R. Weberskirch, *Chem. - A Eur. J.*, 2003, **9**, 3228–3234.

249   S. Bastin, R. J. Eaves, C. W. Edwards, O. Ichihara, M. Whittaker and M. Wills, *J. Org. Chem.*, 2004, **69**, 5405–5412.

250   Y. C. Chen, T. F. Wu, J. G. Deng, H. Liu, X. Cui, J. Zhu, Y. Z. Jiang, M. C. K. Choi and A. S. C. Chan, *J. Org. Chem.*, 2002, **67**, 5301–5306.

251   Y. C. Chen, T. F. Wu, L. Jiang, J. G. Deng, H. Liu, J. Zhu and Y. Z. Jiang, *J. Org. Chem.*, 2005, **70**, 1006–1010.

252   S. Itsuno, A. Tsuji and M. Takahashi, *Tetrahedron Lett.*, 2003, **44**, 3825–3828.

253   X. Li, W. Chen, W. Hems, F. King and J. Xiao, *Tetrahedron Lett.*, 2004, **45**, 951–953.

254   X. Li, X. Wu, W. Chen, F. E. Hancock, F. King and J. Xiao, *Org. Lett.*, 2004, **6**, 3321–3324.

255   Y. Arakawa, A. Chiba, N. Haraguchi and S. Itsuno, *Adv. Synth. Catal.*, 2008, **350**, 2295–2304.

256   Y. Arakawa, N. Haraguchi and S. Itsuno, *Tetrahedron Lett.*, 2006, **47**, 3239–3243.

257   J. Dimroth, J. Keilitz, U. Schedler, R. Schomäcker and R. Haag, *Adv. Synth. Catal.*, 2010, **352**, 2497–2506.

258   R. ter Halle, E. Schulz and M. Lemaire, *Synlett*, 1997, **11**, 1257–1018.

259   J. Liu, Y. Zhou, Y. Wu, X. Li and A. S. C. Chan, *Tetrahedron Asymmetry*, 2008, **19**, 832–837.

260   W. Shan, F. Meng, Y. Wu, F. Mao and X. Li, *J. Organomet. Chem.*, 2011, **696**, 1687–1690.

261   H. F. Zhou, Q. H. Fan, Y. Y. Huang, L. Wu, Y. M. He, W. J. Tang, L. Q. Gu and A. S. C. Chan, *J. Mol. Catal. A Chem.*, 2007, **275**, 47–53.

262   C. M. Zammit and M. Wills, *Tetrahedron Asymmetry*, 2013, **24**, 844–852.

263   R. Wang, J. Wan, X. Ma, X. Xu and L. Liu, *Dalt. Trans.*, 2013, **42**, 6513–6522.

264   P. N. Liu, P. M. Gu, J. G. Deng, Y. Q. Tu and Y. P. Ma, *European J. Org. Chem.*, 2005, **15**, 3221–3227.

265   P. N. Liu, J. G. Deng, Y. Q. Tu and S. H. Wang, *Chem. Commun.*, 2004, **18**, 2070–2071.

266   C. F. Nie and J. S. Suo, *Chinese J. Chem.*, 2005, **23**, 315–320.

267   W. Xiao, R. Jin, T. Cheng, D. Xia, H. Yao, F. Gao, B. Deng and G. Liu, *Chem. Commun.*, 2012, **48**, 11898–11900.

268   J. Li, Y. Zhang, D. Han, Q. Gao and C. Li, *J. Mol. Catal. A Chem.*, 2009, **298**, 31–35.

269   H. Yang, J. Li, J. Yang, Z. Liu, Q. Yang and C. Li, *Chem. Commun.*, 2007, 1086–1088.

270   S. Bai, H. Yang, P. Wang, J. Gao, B. Li, Q. Yang and C. Li, *Chem. Commun.*, 2010, **46**, 8145–8147.

271   C. Bubert, J. Blacker, S. M. Brown, J. Crosby, S. Fitzjohn, J. P. Muxworthy, T. Thorpe and J. M. J. Williams, *Tetrahedron Lett.*, 2001, **42**, 4037–4039.

272   X. Wu, X. Li, F. King and J. Xiao, *Angew. Chemie - Int. Ed.*, 2005, **44**, 3407–3411.

273   F. Wang, H. Liu, L. Cun, J. Zhu, J. Deng and Y. Jiang, *J. Org. Chem.*, 2005, **70**, 9424–9429.

274   J. Li, Y. Tang, Q. Wang, X. Li, L. Cun, X. Zhang, J. Zhu, L. Li and J. Deng, *J. Am. Chem. Soc.*, 2012, **134**, 18522–18525.

275   M. A. N. Virboul and R. J. M. K. Gebbink, *Organometallics*, 2012, **31**, 85–91.

276   X. Wu, X. Li, W. Hems, F. King and J. Xiao, *Org. Biomol. Chem.*, 2004, **2**, 1818–1821.

277   N. A. Cortez, G. Aguirre, M. Parra-Hake and R. Somanathan, *Tetrahedron Lett.*, 2007, **48**, 4335–4338.

278   T. K. Olszewski, M. Bieniek and K. Skowerski, *Org. Process Res. Dev.*, 2020, **24**, 125–145.

279   A. Matsunami and Y. Kayaki, *Tetrahedron Lett.*, 2018, **59**, 504–513.

280   R. J. Lundgren, M. A. Rankin, R. McDonald, G. Schatte and M. Stradiotto, *Angew. Chemie - Int. Ed.*, 2007, **46**, 4732–4735.

281   R. B. Nasir Baig, M. N. Nadagouda and R. S. Varma, *Coord. Chem. Rev.*, 2015, **287**, 137–156.

282   A. Zanotti-Gerosa, W. Hems, M. Groarke and F. Hancock, *Platin. Met. Rev.*, 2005, **49**, 158–165.

283   T. K. Jones, J. J. Mohan, L. C. Xavier, T. J. Blacklock, D. J. Mathre, P. Sohar, E. T. T. Jones, R. A. Reamer, F. E. Roberts and E. J. J. Grabowski, *J. Org. Chem.*, 1991, **56**, 763–769.

284   A. O. King, E. G. Corley, R. K. Anderson, R. D. Larsen, T. R. Verhoeven and P. J. Reider, *J. Org. Chem.*, 1993, **58**, 3731–3735.

285   N. Meriç, C. Kayan, N. Gürbüz, M. Karakaplan, N. E. Binbay and M. Aydemir, *Tetrahedron Asymmetry*, 2017, **28**, 1739–1749.

286   K. O. Miwa Miyagi, Jun Takehara, Sylvain Collet, *Org. Process Res. Dev.*, 2000, **4**, 346–348.

287   P. J. Dyson, *Chimia (Aarau).*, 2019, **73**, 332–333.

288   R. Pedrosa, J. María Andrés, R. Manzano and C. Pérez-López, *Tetrahedron Lett.*, 2013, **54**, 3101–3104.

289   J. Wu, X. L. Hou and L. X. Dai, *J. Org. Chem.*, 2000, **65**, 1344–1348.

290   L. Andna and L. Miesch, *Org. Lett.*, 2018, **20**, 3430–3433.

291   J. C. Spetzler, M. Meldal, J. Felding, P. Vedsø and M. Begtrup, *J. Chem. Soc. - Perkin Trans. 1*, 1998, **1**, 1727–1732.

292   M. M. Joullié and K. M. Lassen, *Arkivoc*, 2010, **2010**, 189–250.

293   P. Reddy and R. Bandichhor, *Tetrahedron Lett.*, 2013, **54**, 3911–3915.

294   M. Dell'Aera, F. M. Perna, P. Vitale, A. Altomare, A. Palmieri, L. C. H. Maddock, L. J. Bole, A. R. Kennedy, E. Hevia and V. Capriati, *Chem. - A Eur. J.*, 2020, **26**, 8742–8748.

295   D. R. J. Hose, M. F. Mahon, K. C. Molloy, T. Raynham and M. Wills, *J. Chem. Soc. - Perkin Trans. 1*, 1996, 691–703.

296   K. Stanley and M. C. Baird, *J. Am. Chem. Soc.*, 1975, **97**, 6598–6599.

297   X. Wu, C. Wang and J. Xiao, *Platin. Met. Rev.*, 2010, **54**, 3–19.

298   C. Thoumazet, M. Melaimi, L. Ricard, F. Mathey and P. Le Floch, *Organometallics*, 2003, **22**, 1580–1581.

299   L. Biancalana, L. K. Batchelor, G. Ciancaleoni, S. Zacchini, G. Pampaloni, P. J. Dyson and F. Marchetti, *Dalt. Trans.*, 2018, **47**, 9367–9384.

300   S. Dayan, N. K. Ozpozan, N. Özdemir and O. Dayan, *J. Organomet. Chem.*, 2014, **770**, 21–28.

301   R. Pettinari, F. Marchetti, C. Di Nicola, C. Pettinari, A. Galindo, R. Petrelli, L. Cappellacci, M. Cuccioloni, L. Bonfili, A. M. Eleuteri, M. F. C. Guedes Da Silva and A. J. L. Pombeiro, *Inorg. Chem.*, 2018, **57**, 14123–14133.

302   H. Ohara, W. N. O. Wylie, A. J. Lough and R. H. Morris, *Dalt. Trans.*, 2012, **41**, 8797–8808.

303   X. Ma, S. G. Guillet, M. Peng, K. Van Hecke and S. P. Nolan, *Dalt. Trans.*, 2021, **50**, 3959–3965.

304   J. M. Zimbron, M. Dauphinais and A. B. Charette, *Green Chem.*, 2015, **00**, 1–3.

305   A. P. Da Costa, R. Lopes, J. M. S. Cardoso, J. A. Mata, E. Peris and B. Royo, *Organometallics*, 2011, **30**, 4437–4442.

306   D. Wang, A. Bruneau-Voisine and J.-B. Sortais, *Catal. Commun.*, 2018, **105**, 31–36.

307   B. Royo and E. Peris, *Eur. J. Inorg. Chem.*, 2012, 1309–1318.

308   Y. Zhou, Y. Chen and C. He, *Dalt. Trans.*, 2021, **50**, 4231–4236.

309   V. I. Potkin, S. K. Petkevich, A. V. Kletskov, I. A. Kolesnik, E. A. Dikusar, I. B. Rozentsveig, G. G. Levkovskaya, D. K. Nasirova, K. K. Borisova and F. I. Zubkov, *Russ. J. Org. Chem.*, 2018, **54**, 452–462.

310   K. Y. Wan, M. M. H. Sung, A. J. Lough and R. H. Morris, *ACS Catal.*, 2017, **7**, 6827–6842.

311   L. Mercs, G. Labat, A. Neels, A. Ehlers and M. Albrecht, *Organometallics*, 2006, **25**, 5648–5656.

312   V. V. K. M. Kandepi, A. P. Da Costa, E. Peris and B. Royo, *Organometallics*, 2009, **28**, 4544–4549.

313   A. P. Da Costa, M. Viciano, M. Sanaú, S. Merino, J. Tejeda, E. Peris and B. Royo, *Organometallics*, 2008, **27**, 1305–1309.

314   O. Baslé, J. Thongpaen and R. Manguin, *Angew. Chemie Int. Ed. Engl.*, , DOI:10.1002/anie.201911898.

315   J. Bohnenberger and I. Krossing, *Angew. Chemie - Int. Ed.*, 2020, **59**, 5581–5585.

316   C. Ayya Swamy P, A. Varenikov and G. de Ruiter, *Chem. - A Eur. J.*, 2020, **26**, 2333–2337.

317   N. Ségaud, C. Johnson, A. Farrea and M. Albrecht, *Chem. Commun.*, 2021, DOI:10.1039/D1CC02740A.

318   K. Lubitz and U. Radius, *Organometallics*, 2019, **38**, 2558–2572.

319   A. P. Da Costa, J. A. Mata, B. Royo and E. Peris, *Organometallics*, 2010, **29**, 1832–1838.

320   L. N. Telegina, E. S. Kelbysheva, T. V. Strelkova, M. G. Ezernitskaya, A. F. Smol'yakov, Y. A. Borisov, B. V. Lokshin and N. M. Loim, *J. Organomet. Chem.*, 2018, **867**, 71–78.

321   S. S. Jones, M. D. Rausch and T. E. Bitterwolf, *J. Organomet. Chem.*, 1990, **396**, 279–287.

322   E. S. Kelbysheva, L. N. Telegina, E. A. Ershova, T. V. Strelkova, M. G. Ezernitskaya, E. V. Nosova, A. F. Smol'yakov, F. M. Dolgushin and N. M. Loim, *Russ. Chem. Bull.*, 2017, **66**, 327–335.

323   A. J. Ruddlesden, R. E. Mewis, G. G. R. Green, A. C. Whitwood and S. B. Duckett, *Organometallics*, 2015, **34**, 2997–3006.

324   S. C. E. S. Jacob Brannon, Beverly E. Stretch, *CCDC 1875908: Experimental*

Crystal Structure Determination, 2018.

325   H. Seo, H. Park, B. Y. Kim, J. H. Lee, S. U. Son and Y. K. Chung, *Organometallics*, 2003, **22**, 618–620.

326   K. Kowalski, Ł. Szczupak, S. Saloman, D. Steverding, A. J.́ski, V. Vrc̆ek, A. Hildebrandt, H. Lang and A. Rybarczyk-Pirek, *Chempluschem*, 2017, **82**, 303–314.

327   E. A. Martynova, N. V. Tzouras, G. Pisanò, C. S. J. Cazin and S. P. Nolan, *Chem. Commun.*, 2021, **57**, 3836–3856.

328   T. J. Dickerson, N. N. Reed and K. D. Janda, *Chem. Rev.*, 2002, **102**, 3325–3344.

329   J. Liu, D. Zhou, X. Jia, L. Huang, X. Li and A. S. C. Chan, *Tetrahedron Asymmetry*, 2008, **19**, 1824–1828.

330   V. A. Larionov, T. Cruchter, T. Mietke and E. Meggers, *Organometallics*, 2017, **36**, 1457–1460.

331   J. Chaussard, C. Combellas and A. Thiebault, *Tetrahedron Lett.*, 1987, **28**, 1173–1174.

332   A. C. C. Velho and J. E. D. Martins, *J. Braz. Chem. Soc.*, 2020, **31**, 2462–2469.

333   P. Mendonça Matos, W. Lewis, S. P. Argent, J. C. Moore and R. A. Stockman, *Org. Lett.*, 2020, **22**, 2776–2780.

334   A. Del Vecchio, F. Caillé, A. Chevalier, O. Loreau, K. Horkka, C. Halldin, M. Schou, N. Camus, P. Kessler, B. Kuhnast, F. Taran and D. Audisio, *Angew. Chemie - Int. Ed.*, 2018, **57**, 9744–9748.

335   F. Zhang, Y. Wang, Y. Wang and Y. Pan, *Org. Lett.*, 2021, **23**, 7524–7528.

336   S. Chavda, E. Coulbeck, M. Dingjan, J. Eames, A. Flinn and J. Northen, *Tetrahedron Asymmetry*, 2018, **19**, 1536–1548.

337   M. Sarmaa and B. Mondal, *Dalt. Trans.*, 2012, **41**, 2927–2934.

338   G. Wang, Z. Zhou, X. Shen, S. Ivleva and E. Meggers, *Chem. Commun.*, 2020, **56**, 7714–7717.

339   Y. L. Tnay and P. S. Chiba, *Chem. - An Asian J.*, 2015, **10**, 873–877.

340   Y. Kobayashi, D. Tanaka, H. Danjo and Y. Uozumi, *Adv. Synth. Catal.*, 2006, **348**, 1561–1566.

341   S. Shahsavari, C. McNamara, M. Sylvester, E. Bromley, S. Joslin, B.-Y. Lu and S. Fang, *J. Org. Chem.*, 2018, **14**, 1750–1757.

342   R. Pedrosa, J. M. Andrés, R. Manzano and C. Pérez-López, *Tetrahedron Lett.*, 2013, **54**, 3101–3104.

Chapter 7

Appendix
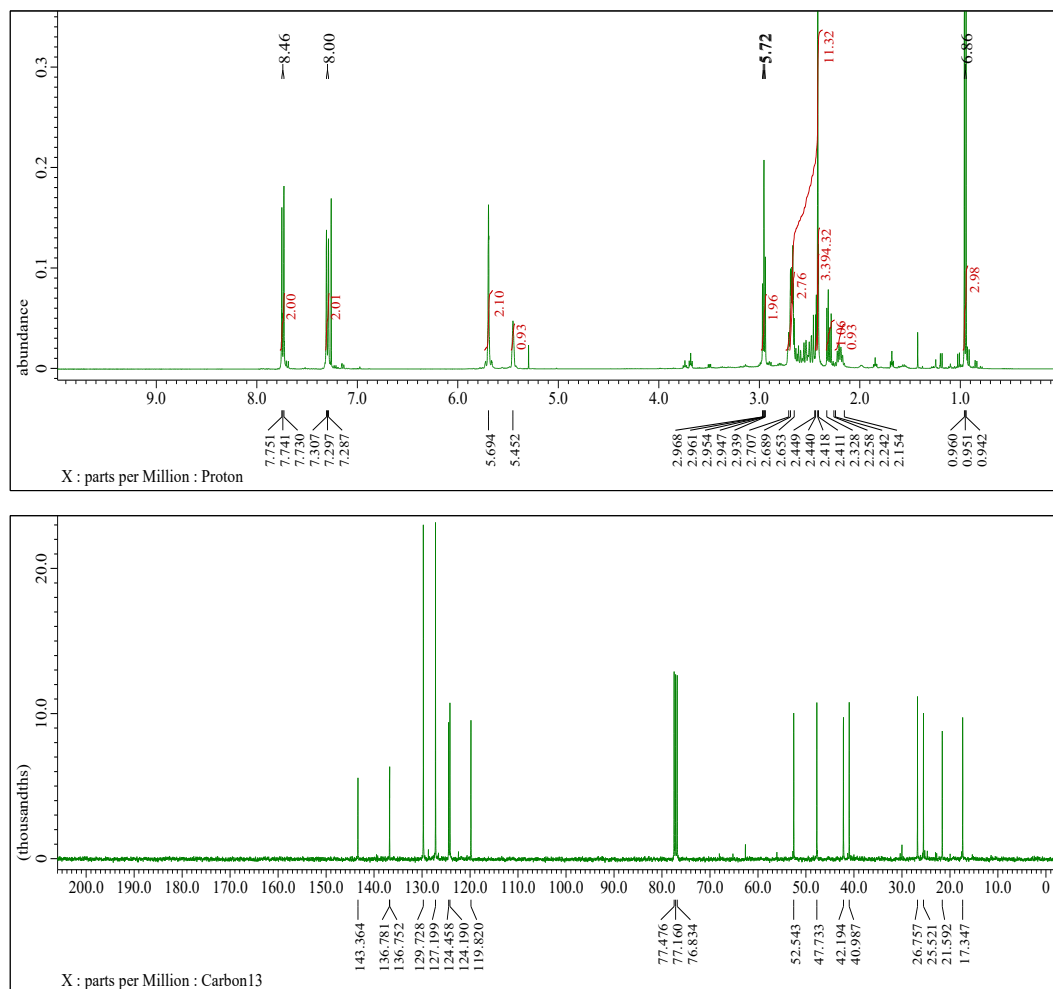
Figure 141. ^{1}H (top) and ^{13}C{^{1}H} (bottom) NMR spectra (recorded in CDCl$_3$) of **4a**
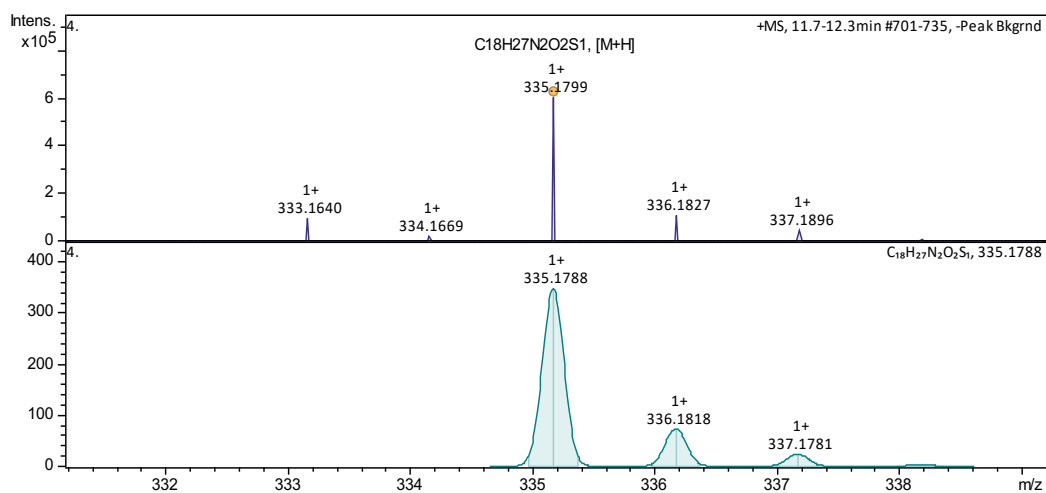
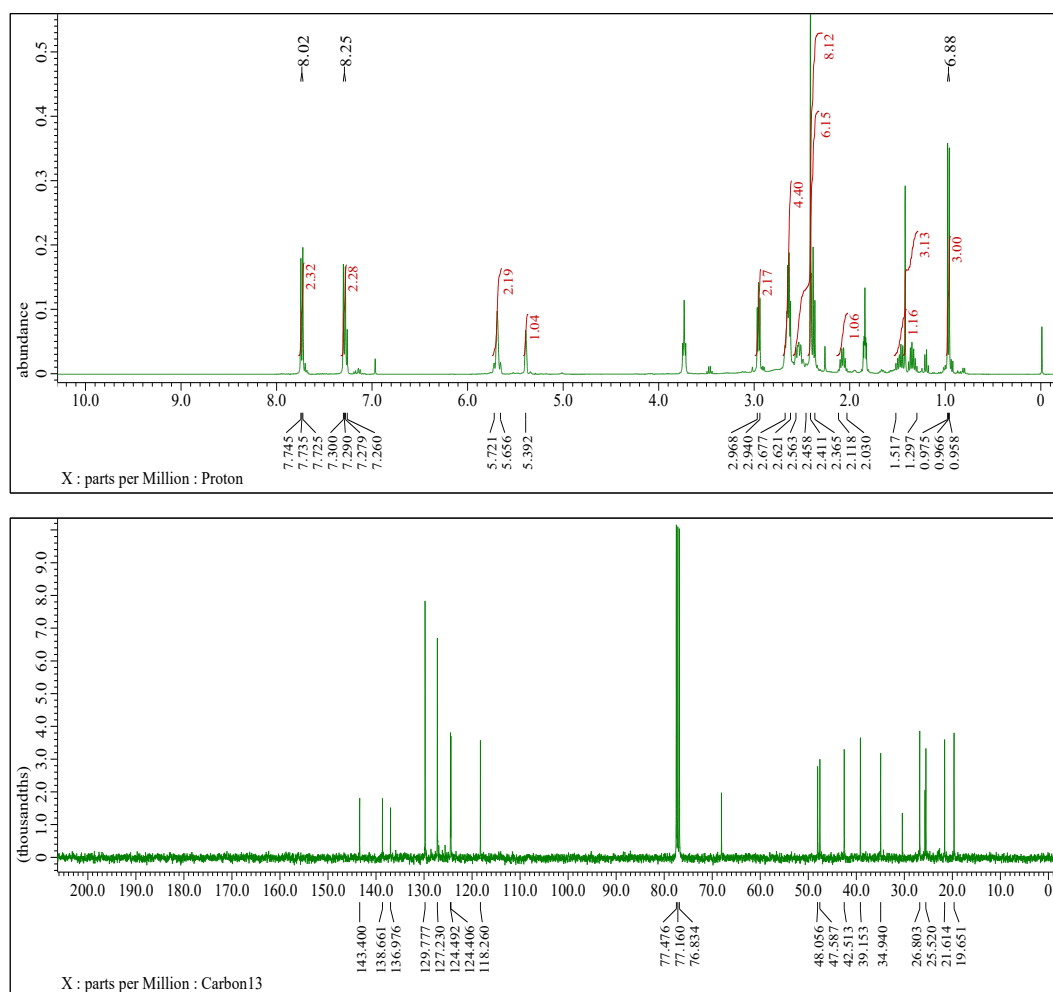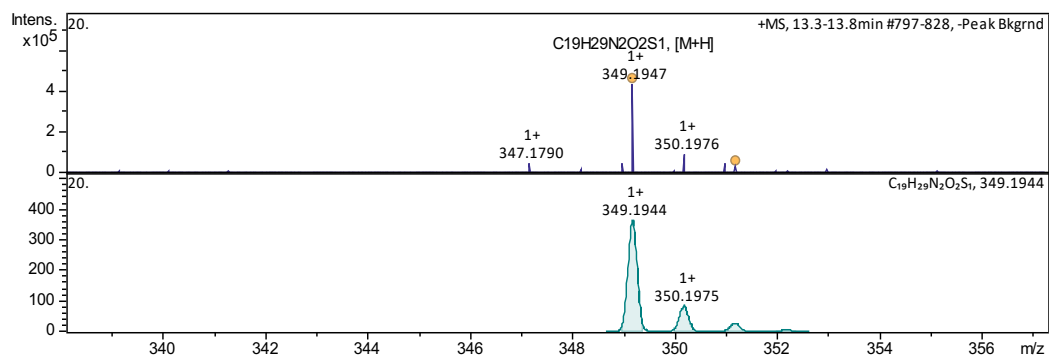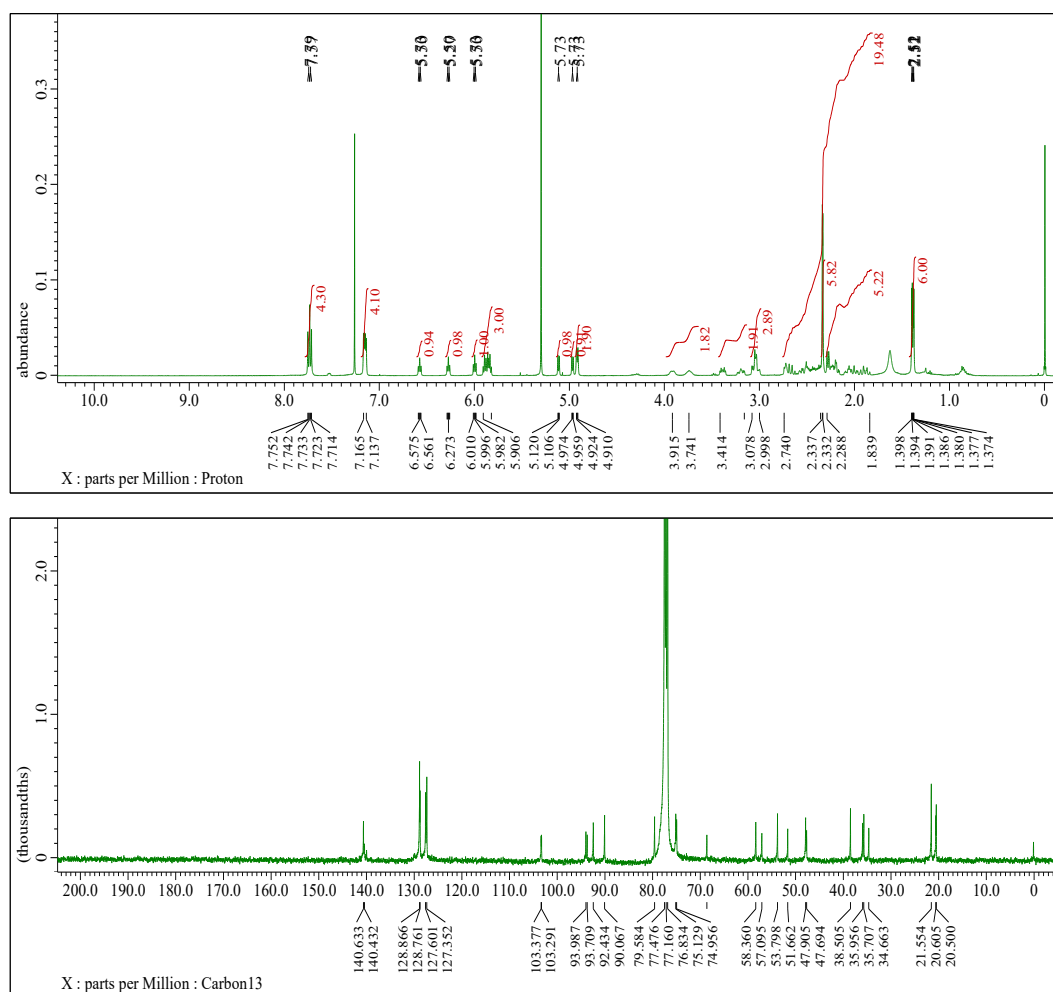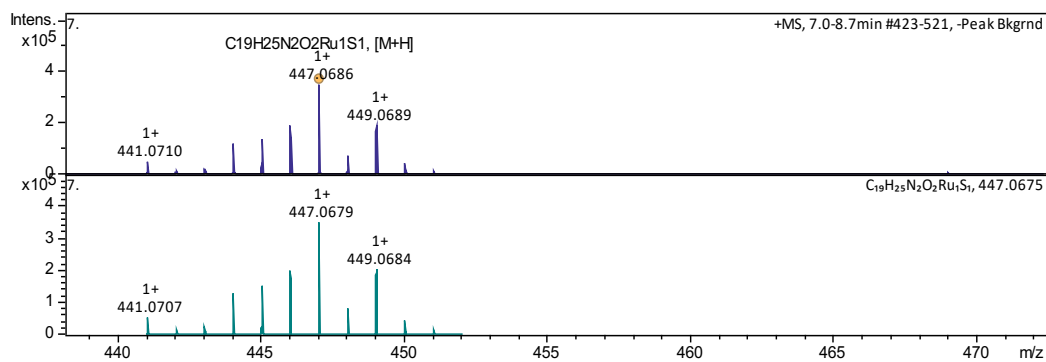Figure 142. High resolution ESI$^+$ spectra of **4a**
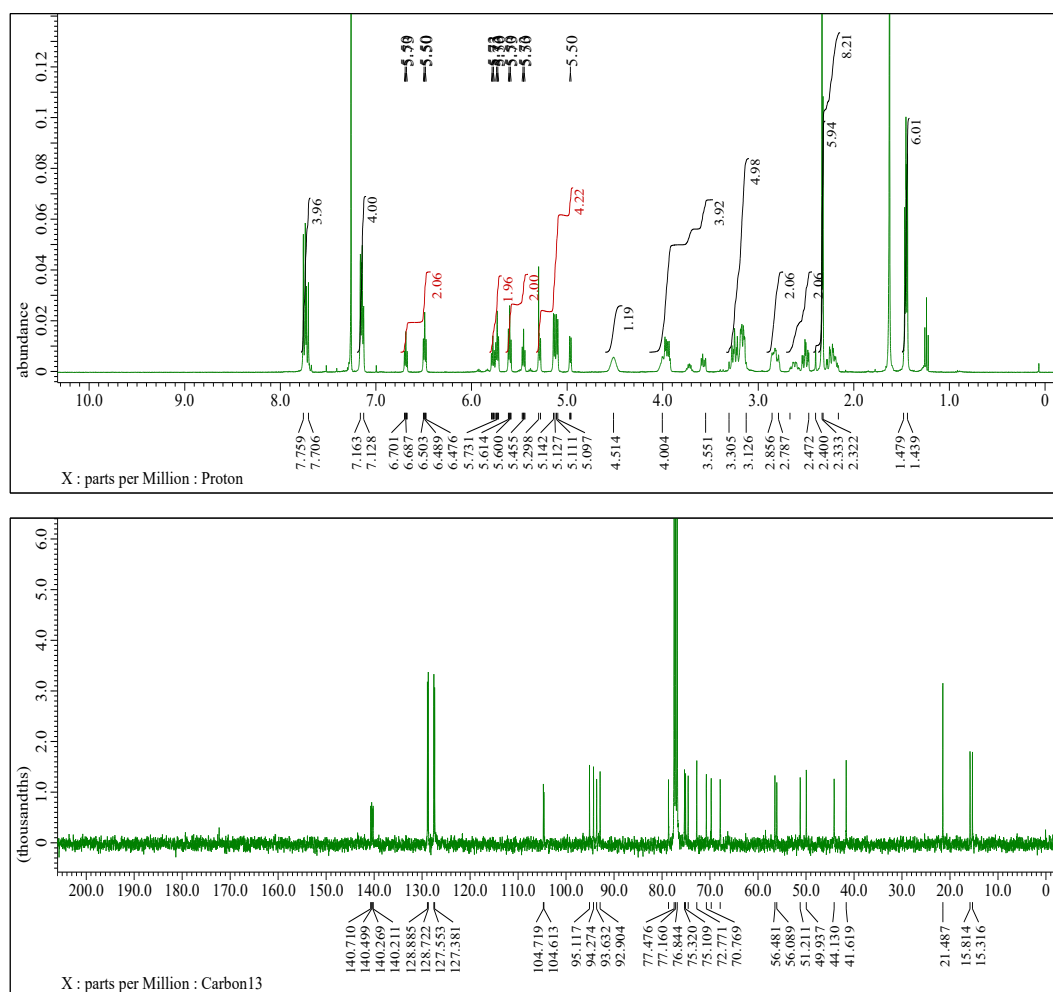
Figure 143. ¹H (top) and ¹³C{¹H} (bottom) NMR spectra (recorded in CDCl₃) of **6a**
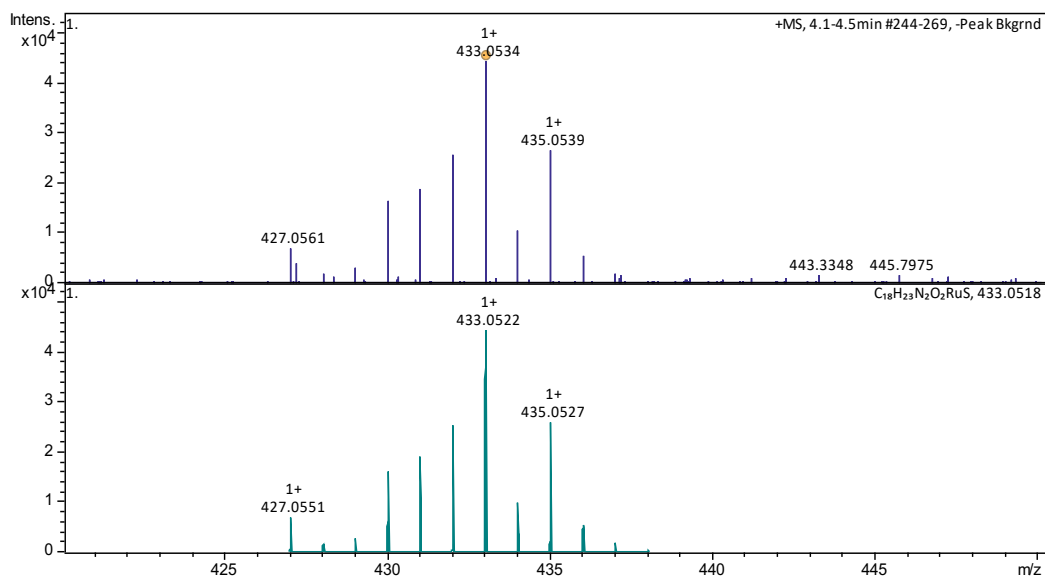
Figure 144. High resolution ESI⁺ spectra of **6a**
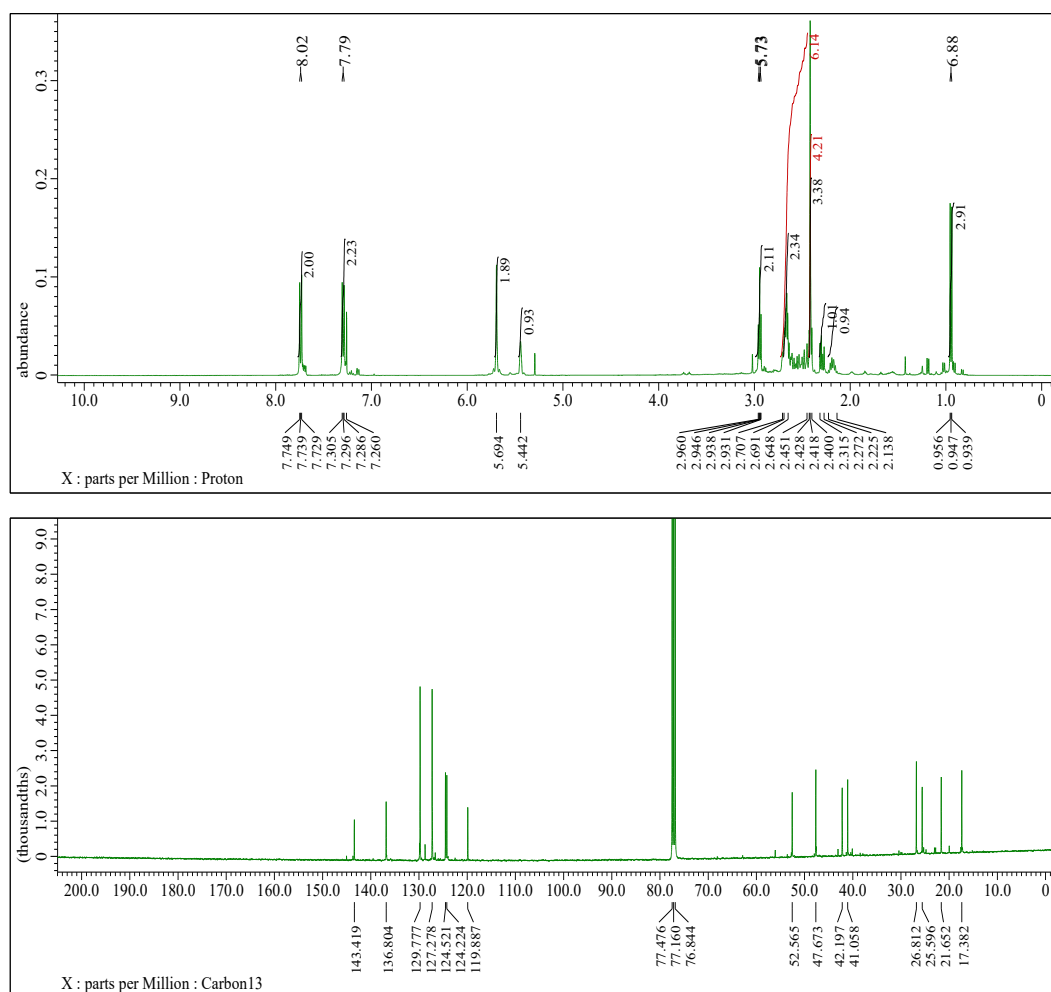
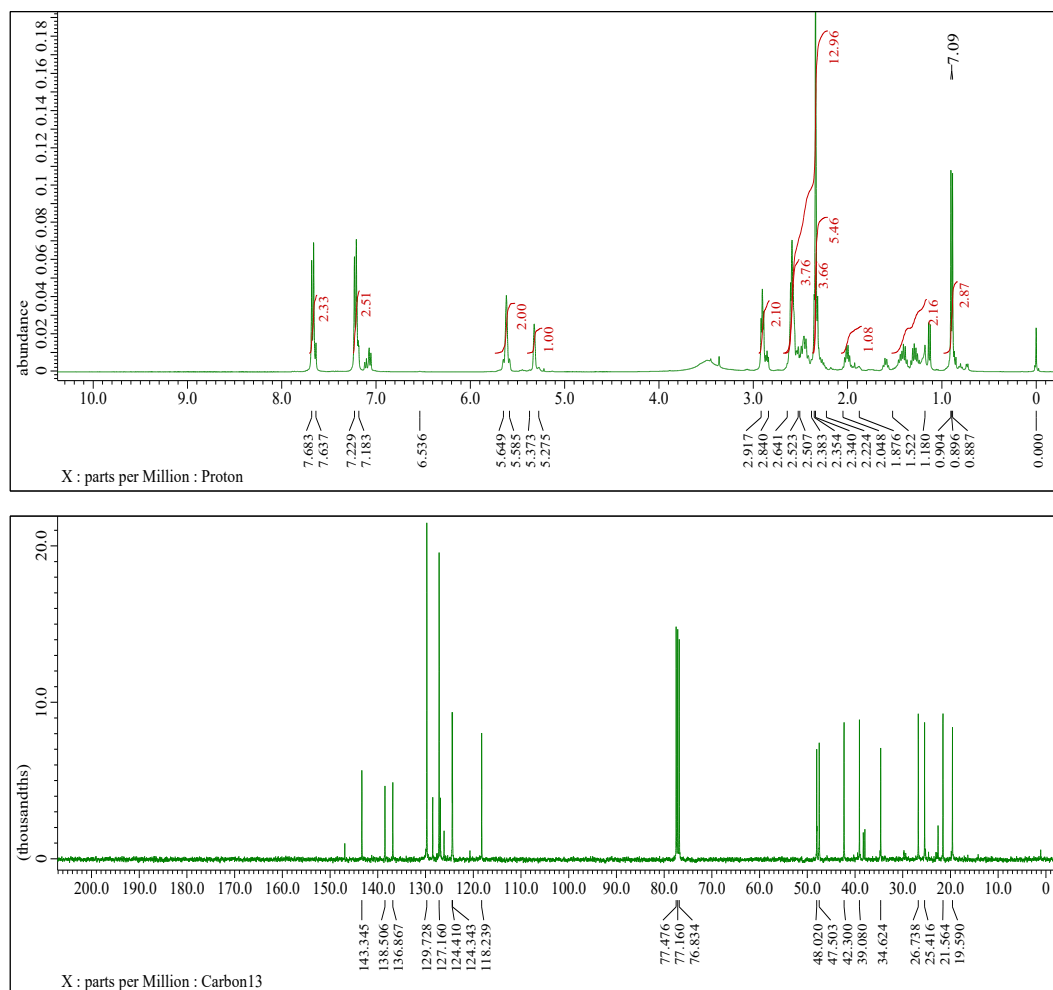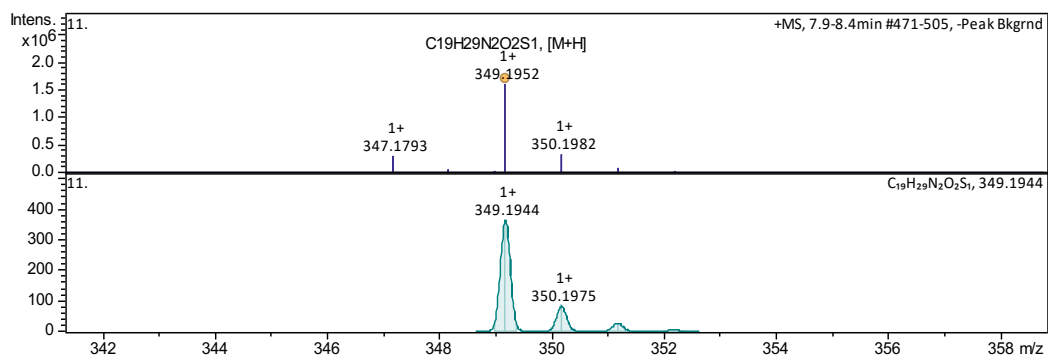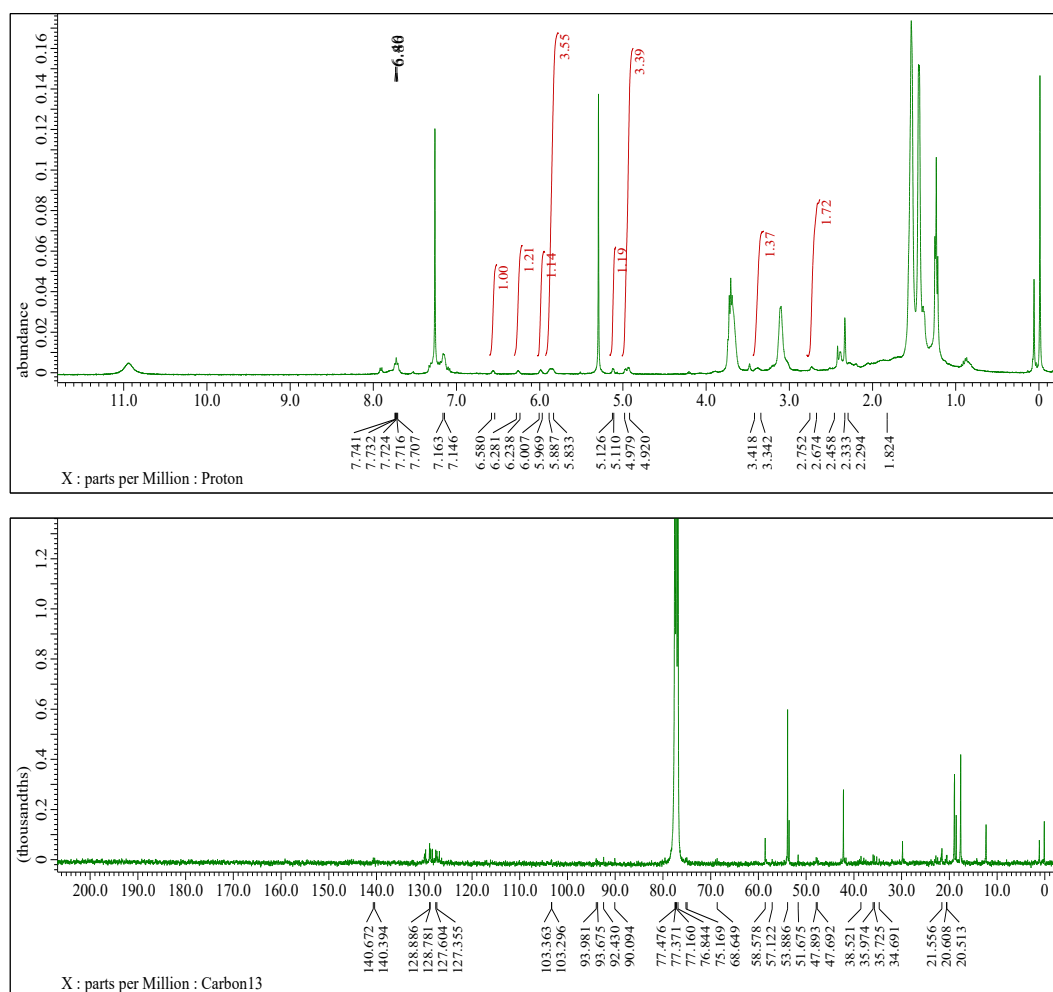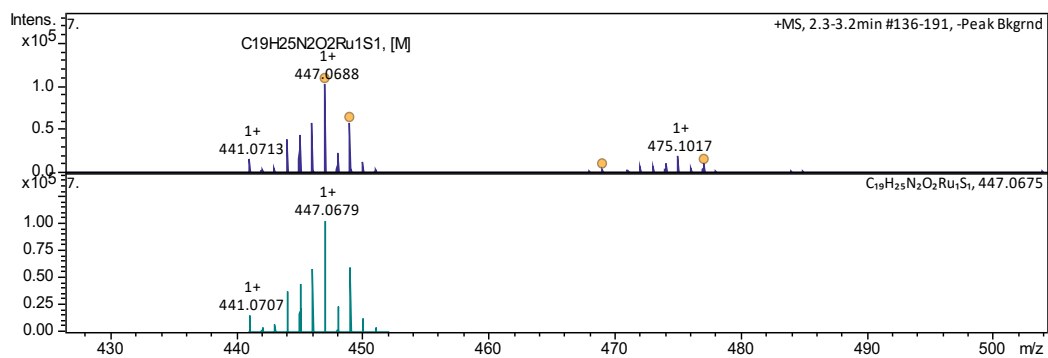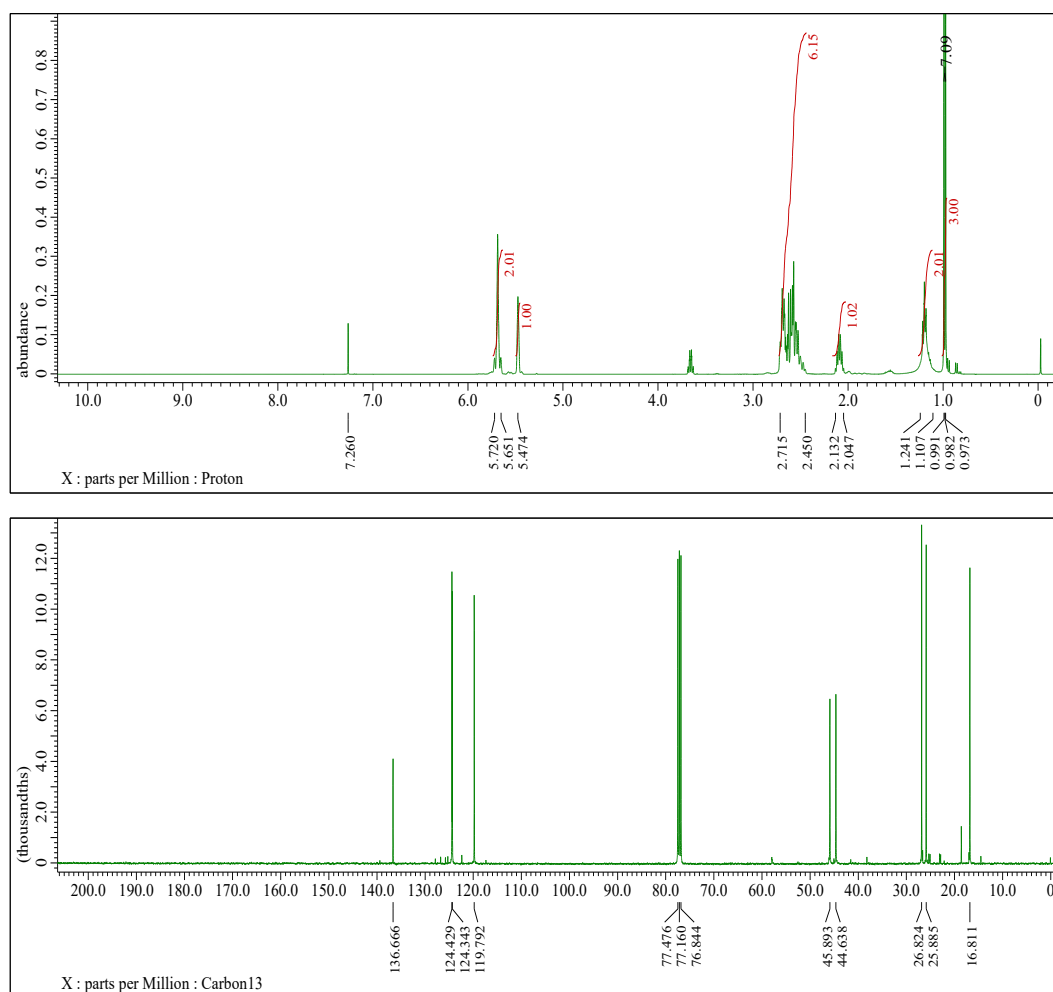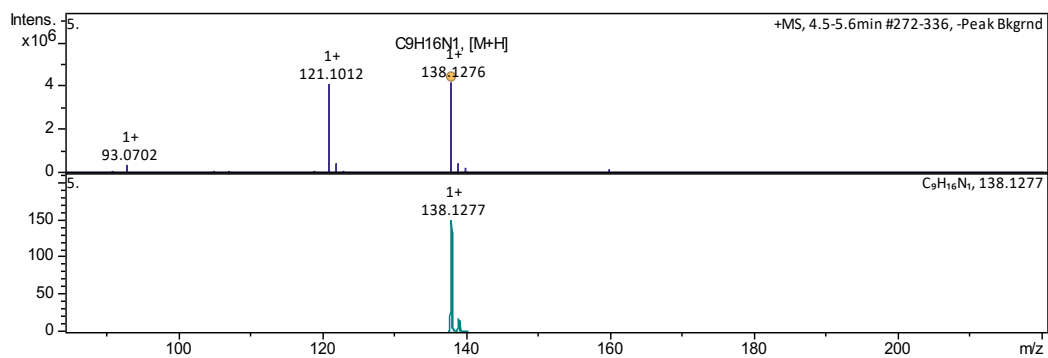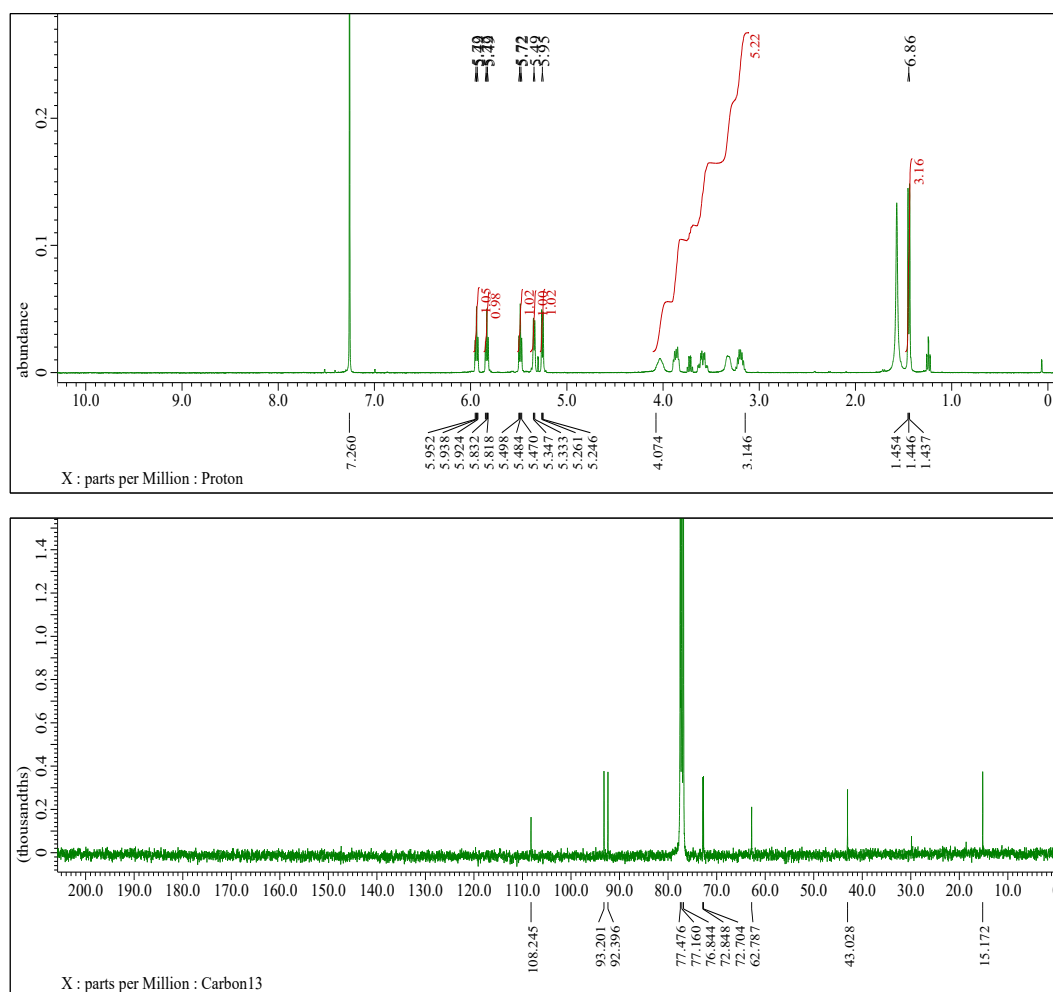Figure 145. ^{1}H (top) and ^{13}C{^{1}H} (bottom) NMR spectra (recorded in CDCl$_3$) of **4b**
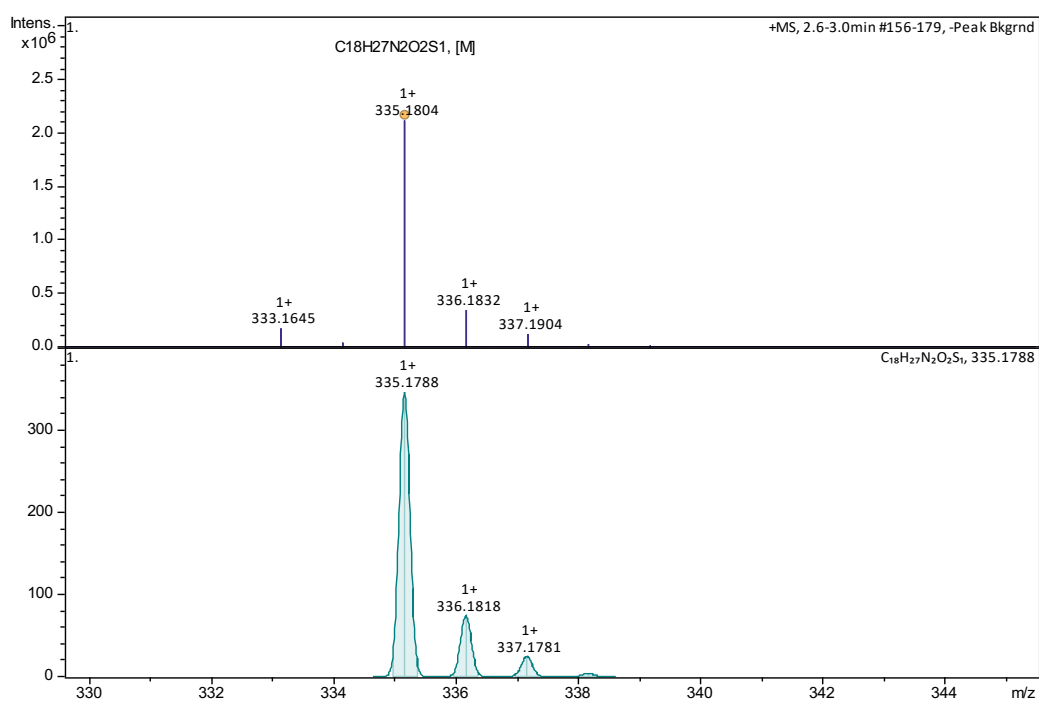
Figure 146. High resolution ESI$^+$ spectra of **4b**
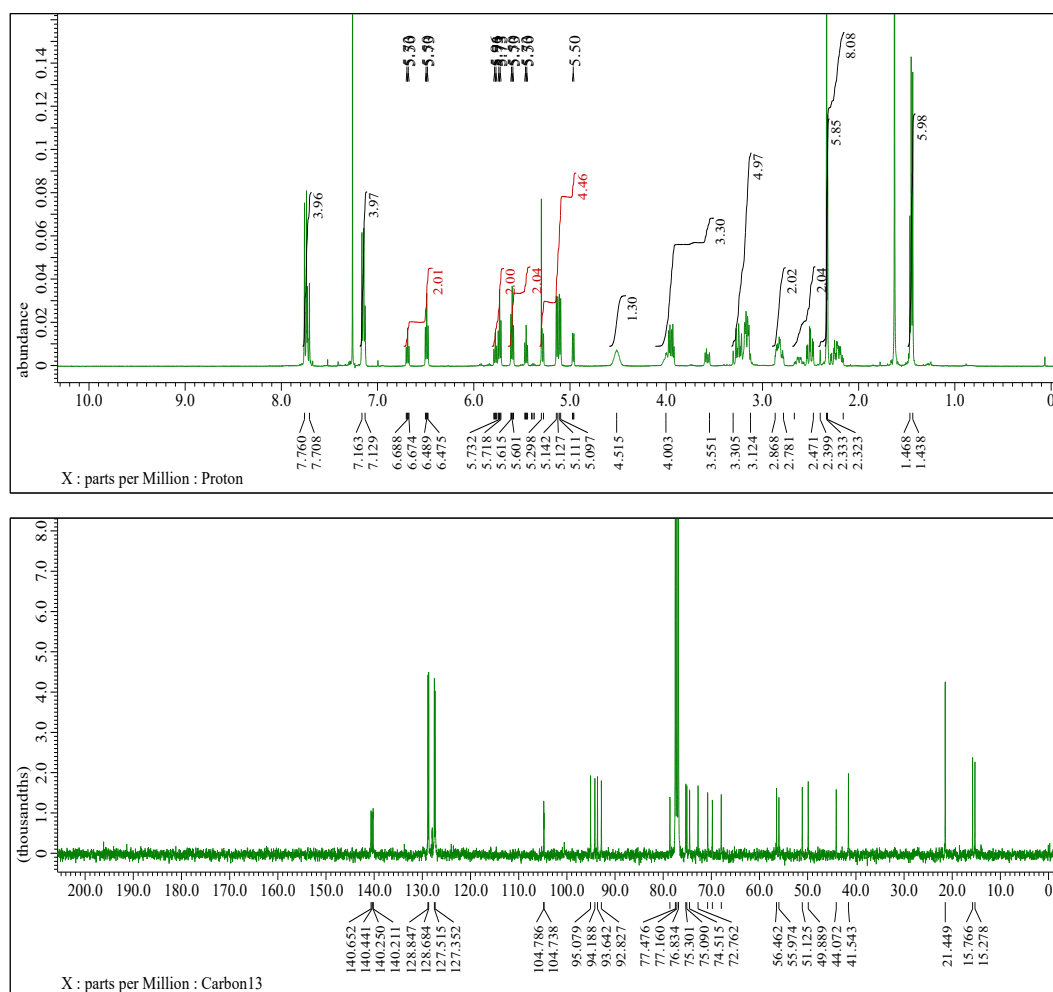
Figure 147. ^{1}H (top) and ^{13}C{^{1}H} (bottom) NMR spectra (recorded in CDCl$_3$) of **6b**
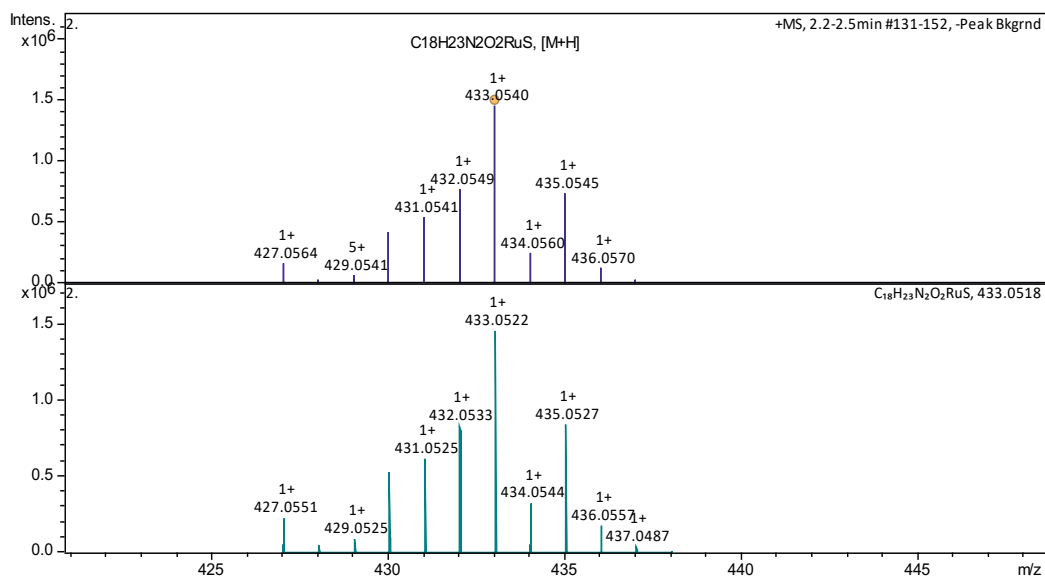
Figure 148. High resolution ESI$^+$ spectra of **6b**
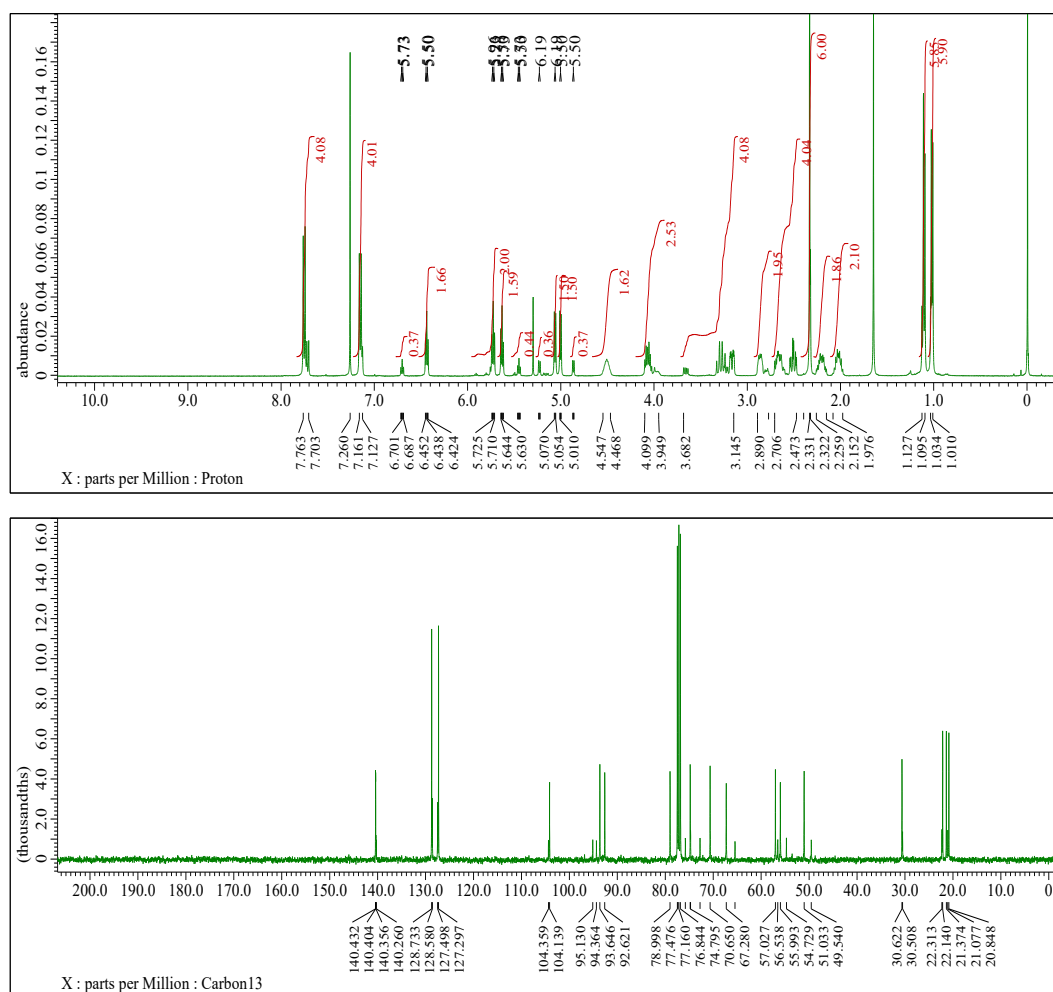
Figure 149. ^{1}H (top) and ^{13}C{^{1}H} (bottom) NMR spectra (recorded in CDCl$_3$) of **7**
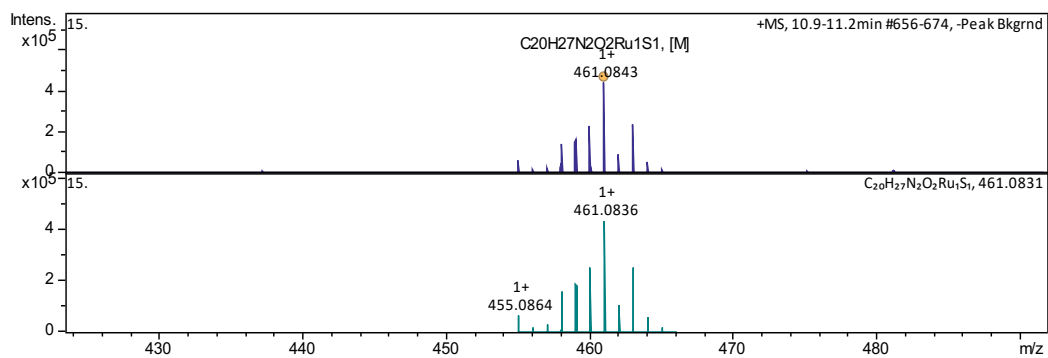
Figure 150. High resolution ESI$^+$ spectra of **7**

Figure 151. ^{1}H (top) and ^{13}C{^{1}H} (bottom) NMR spectra (recorded in CDCl$_3$) of **12a**

Figure 152. High resolution ESI$^+$ spectra of **12a**
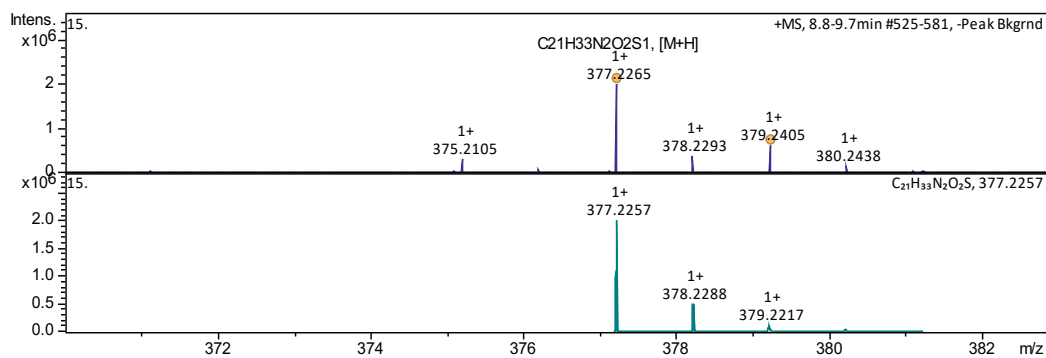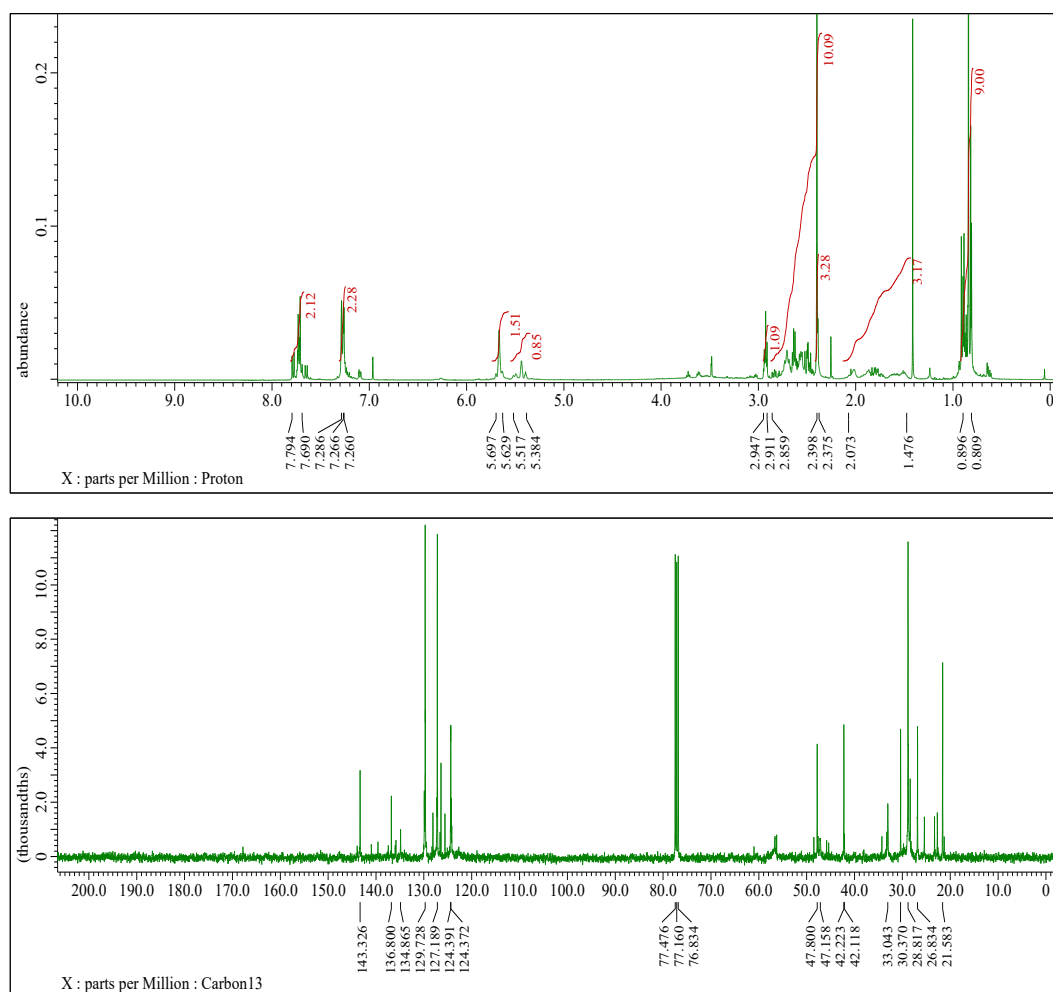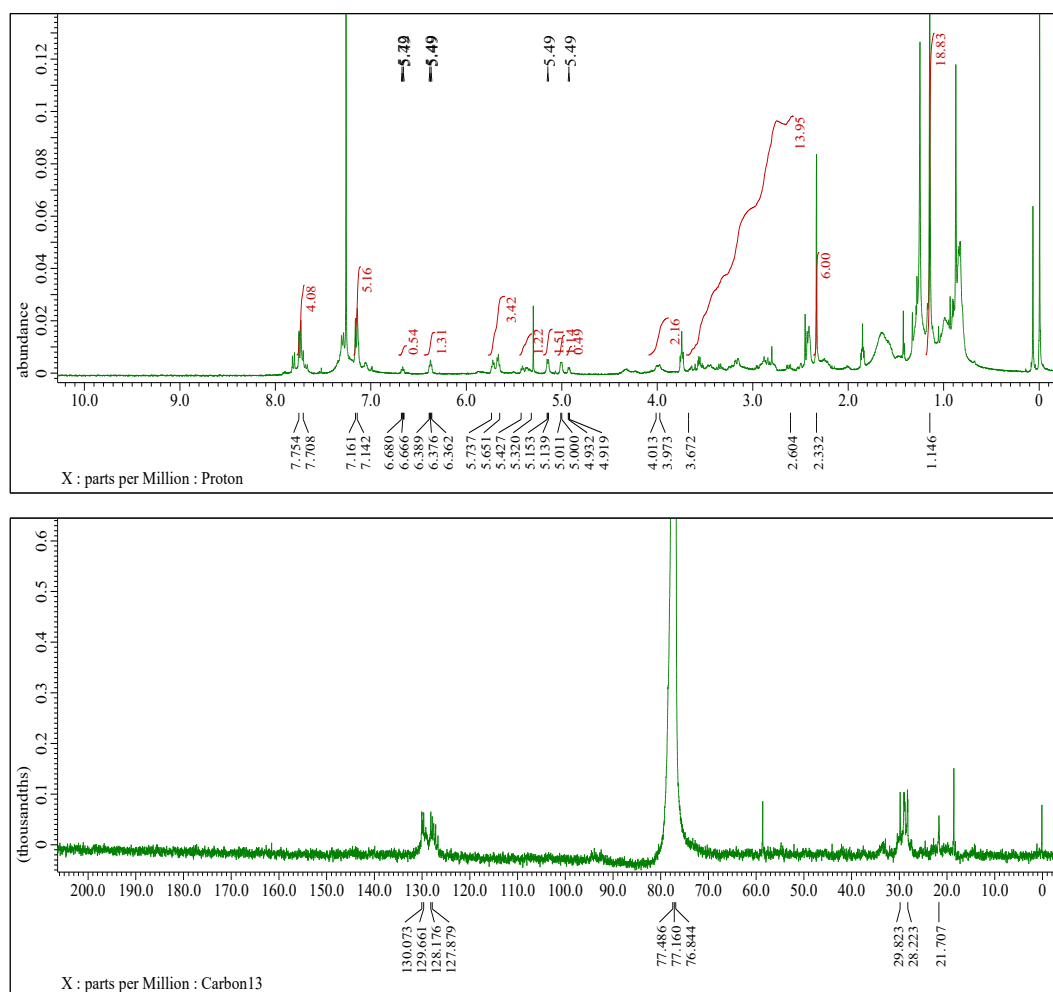
Figure 153. ^{1}H (top) and ^{13}C{^{1}H} (bottom) NMR spectra (recorded in CDCl$_3$) of **14a**
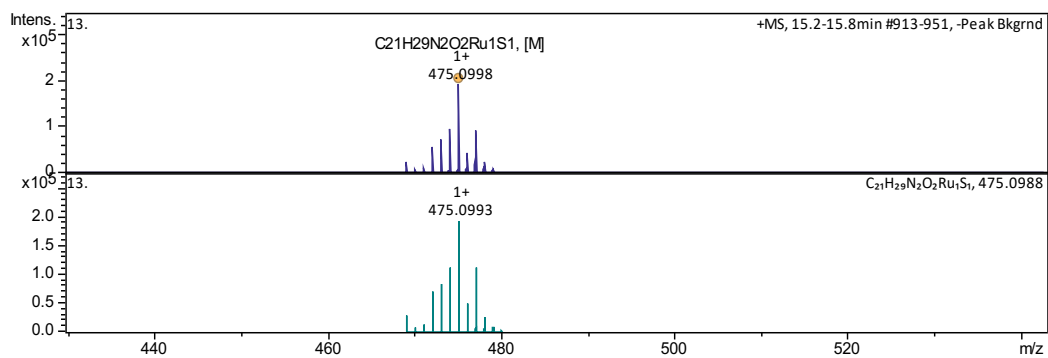
Figure 154. High resolution ESI$^+$ spectra of **14a**
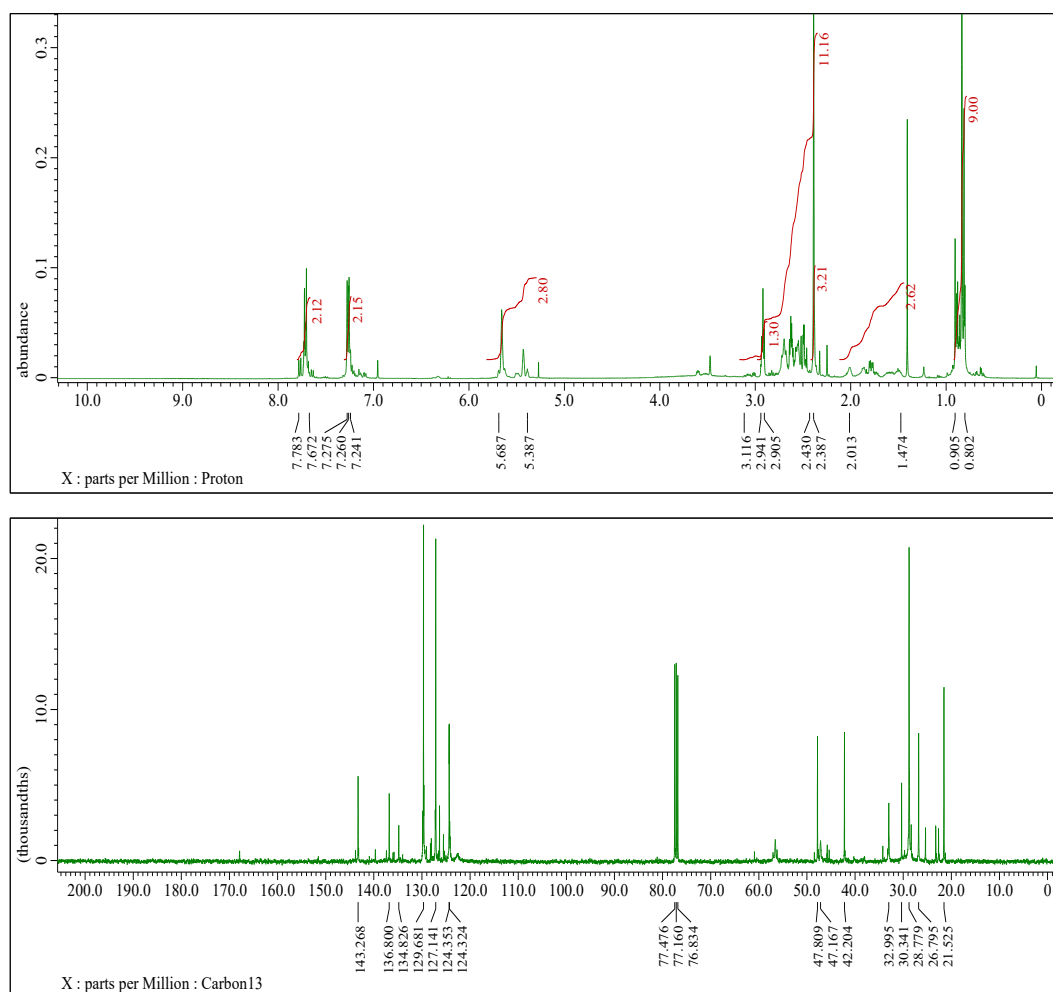
Figure 155. ^{1}H (top) and ^{13}C{^{1}H} (bottom) NMR spectra (recorded in CDCl$_3$) of **12b**
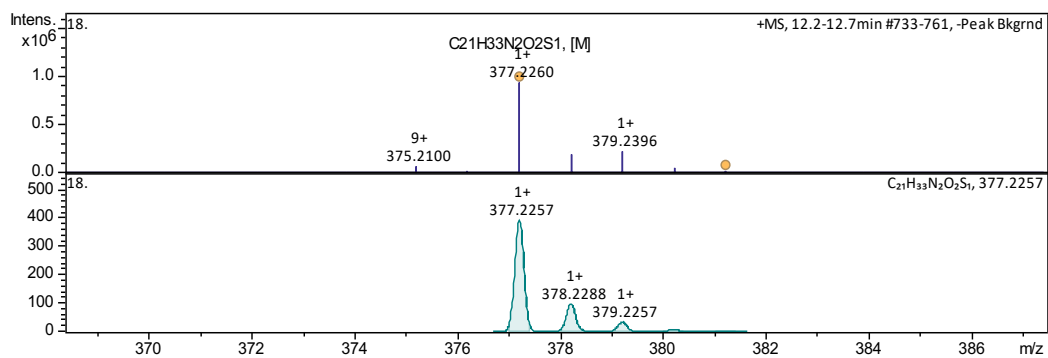
Figure 156. High resolution ESI$^+$ spectra of **12b**
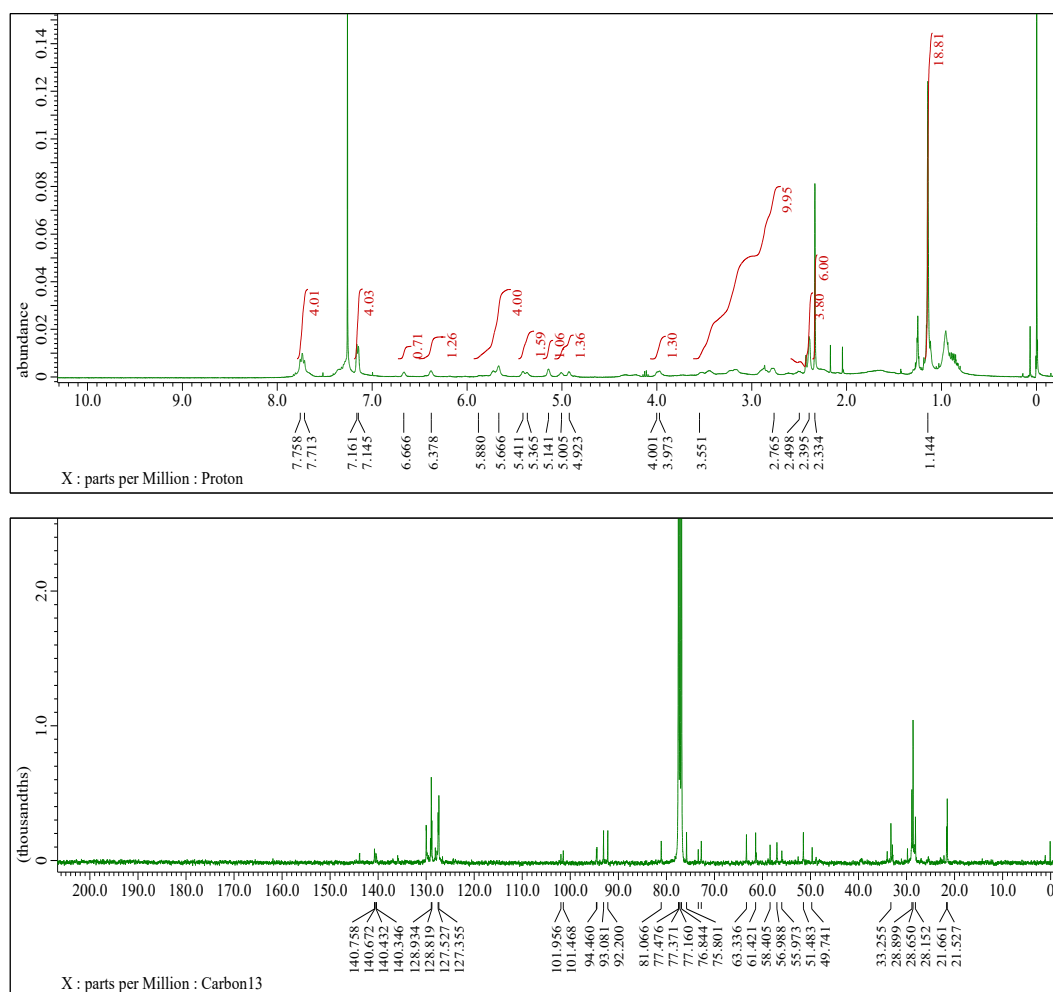
Figure 157. ^{1}H (top) and ^{13}C{^{1}H} (bottom) NMR spectra (recorded in CDCl$_3$) of **14b**
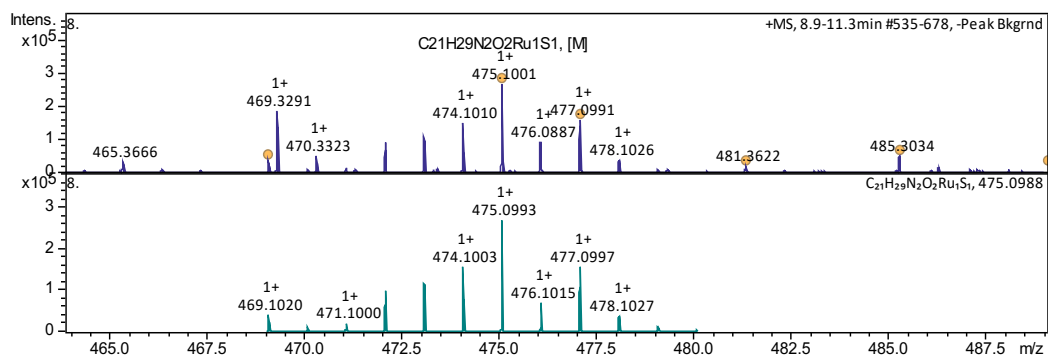
Figure 158. High resolution ESI$^+$ spectra of **14b**
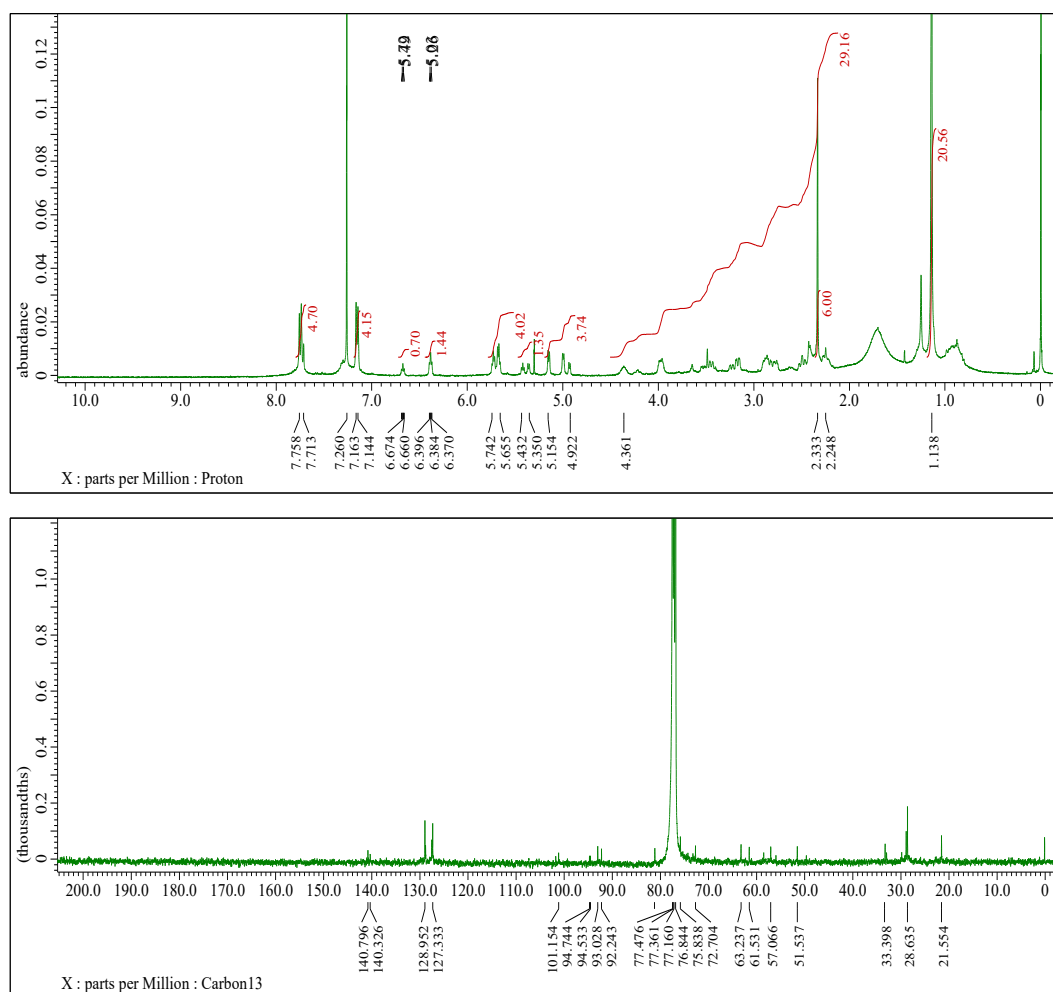
Figure 159. ^{1}H (top) and ^{13}C{^{1}H} (bottom) NMR spectra (recorded in CDCl$_3$) of **14**
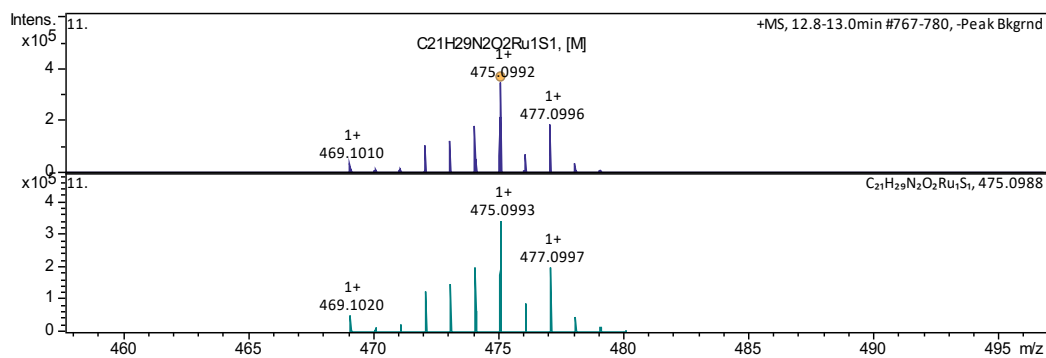
Figure 160. High resolution ESI$^+$ spectra of **14**

Figure 161. ¹H (top) and ¹³C{¹H} (bottom) NMR spectra (recorded in CDCl₃) of **17**

Figure 162. High resolution ESI⁺ spectra of **17**

Figure 163. ^{1}H (top) and ^{13}C{^{1}H} (bottom) NMR spectra (recorded in CDCl$_3$) of **19**

Figure 164. High resolution ESI$^+$ spectra of **19**

Figure 165. ¹H (top) and ¹³C{¹H} (bottom) NMR spectra (recorded in CDCl₃) of **17a**

Figure 166. High resolution ESI⁺ spectra of **17a**

Figure 167. ^{1}H (top) and ^{13}C{^{1}H} (bottom) NMR spectra (recorded in CDCl$_3$) of **19a**

Figure 168. High resolution ESI$^+$ spectra of **19a**

Figure 169. ¹H (top) and ¹³C{¹H} (bottom) NMR spectra (recorded in CDCl₃) of **22**

Figure 170. High resolution ESI⁺ spectra of **22**

Figure 171. ¹H (top) and ¹³C{¹H} (bottom) NMR spectra (recorded in CDCl₃) of **24**
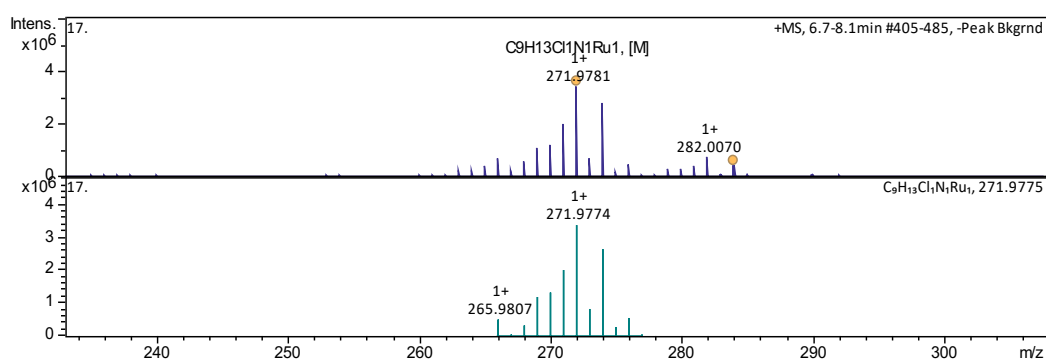
Figure 172. High resolution ESI⁺ spectra of **24**
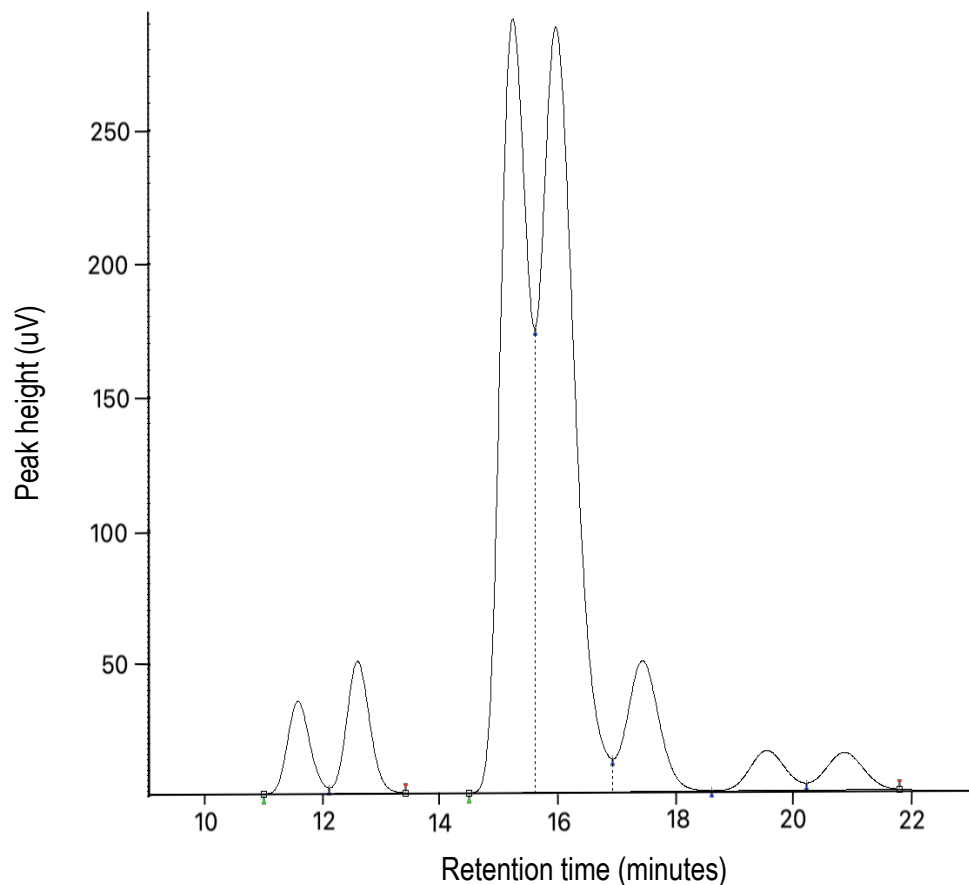
Figure 173. Chromatogram of (*R*)- and (*S*)-2-(cyclohexa-1,4-dien-1-yl)-N-(2-((4-methylphenyl)sulfonamido)ethyl)propenamide obtained using chiral HPLC, whereby the two peaks overlayed relate to the two isomers of **3a** and **3b**. The peak at 15 minutes corresponds to **3a** and the peak at 16 minutes corresponds to **3b**.
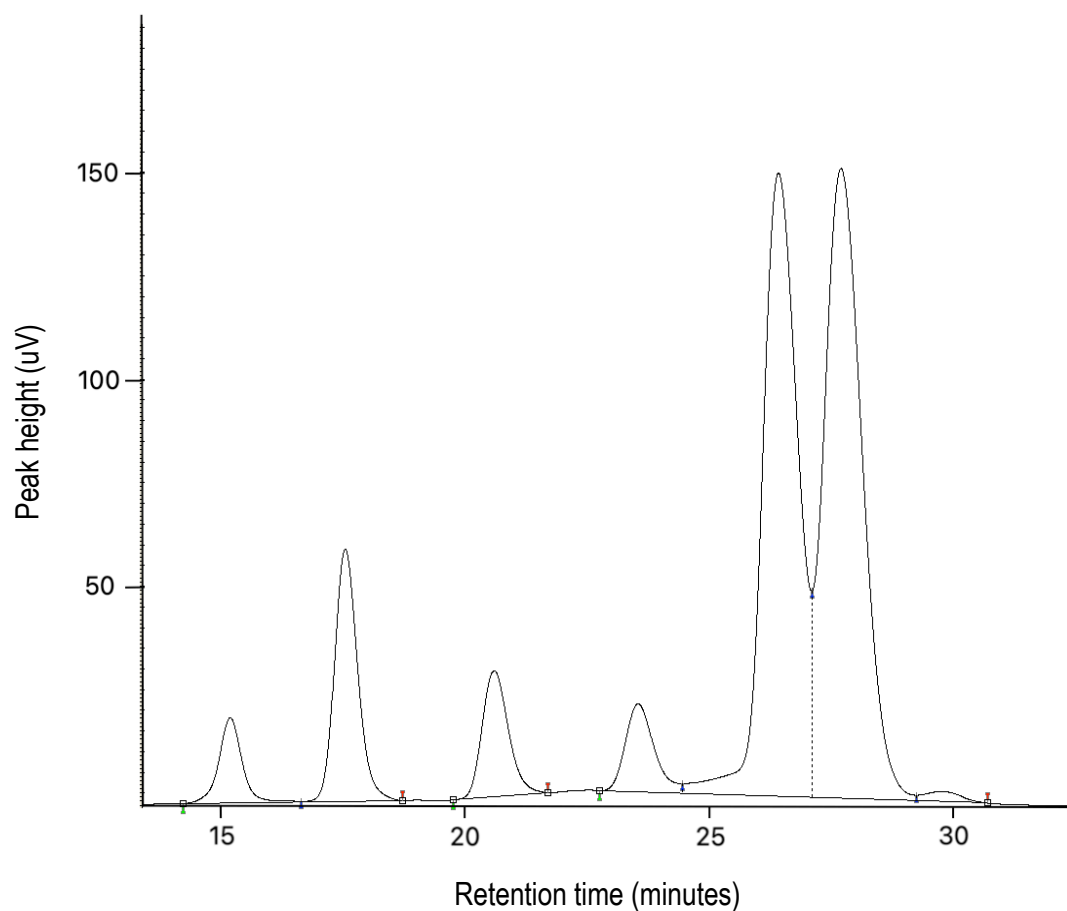
Figure 174. Chromatogram of (*R*)- and (*S*)-*N*-(2-((2-(cyclohexa-1,4-dien-1-yl)propyl)amino)ethyl)-4-methylbenzenesulfonamide obtained using chiral HPLC, whereby the two peaks overlayed relate to the two isomers of **4a** and **4b**. The peak at 26 minutes corresponds to **4a** and the peak at 28 minutes corresponds to **4b**.
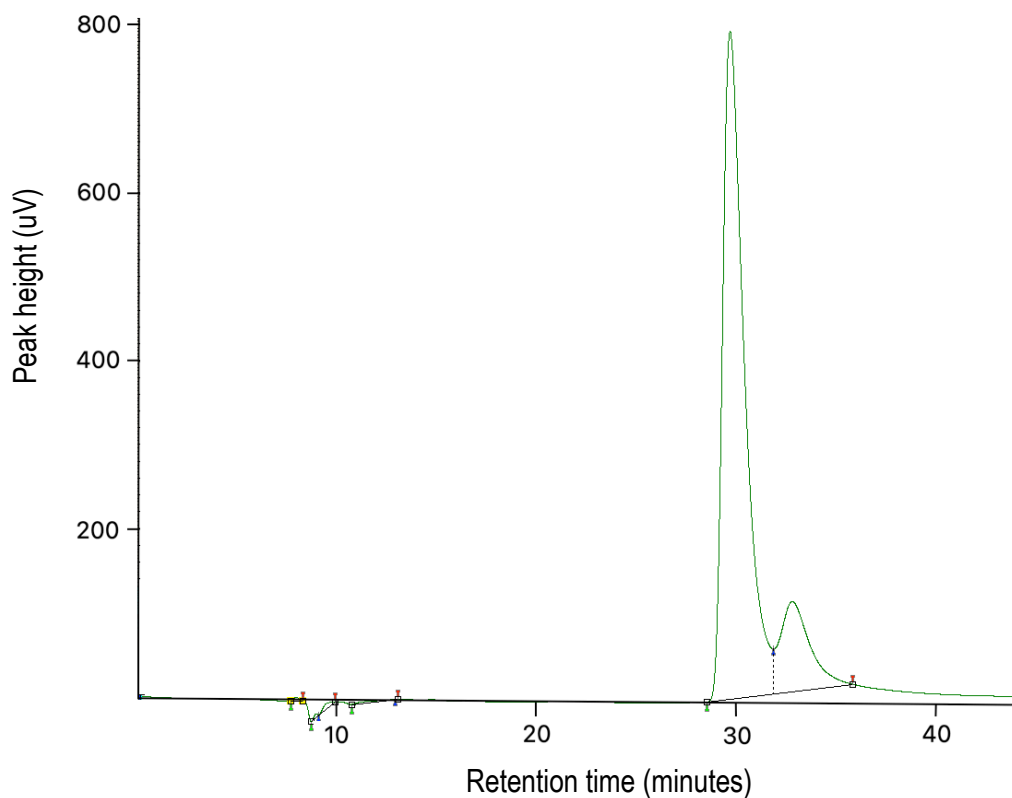
Figure 175. Chromatogram of **9** (crystals analysed by x-ray diffraction - see section 2.4.2) obtained using chiral HPLC, whereby the ratio of peaks gave the percentage of isomers in the amine to be 84 %:16 % (68 % ee).
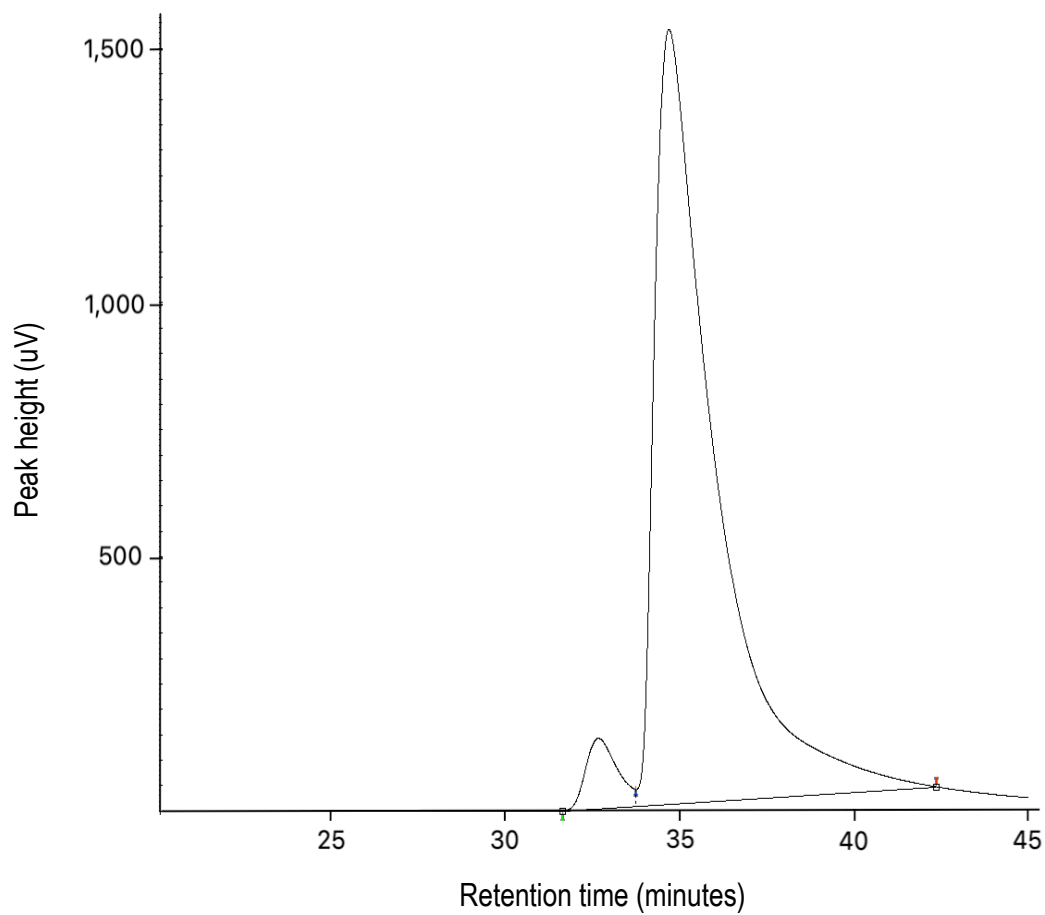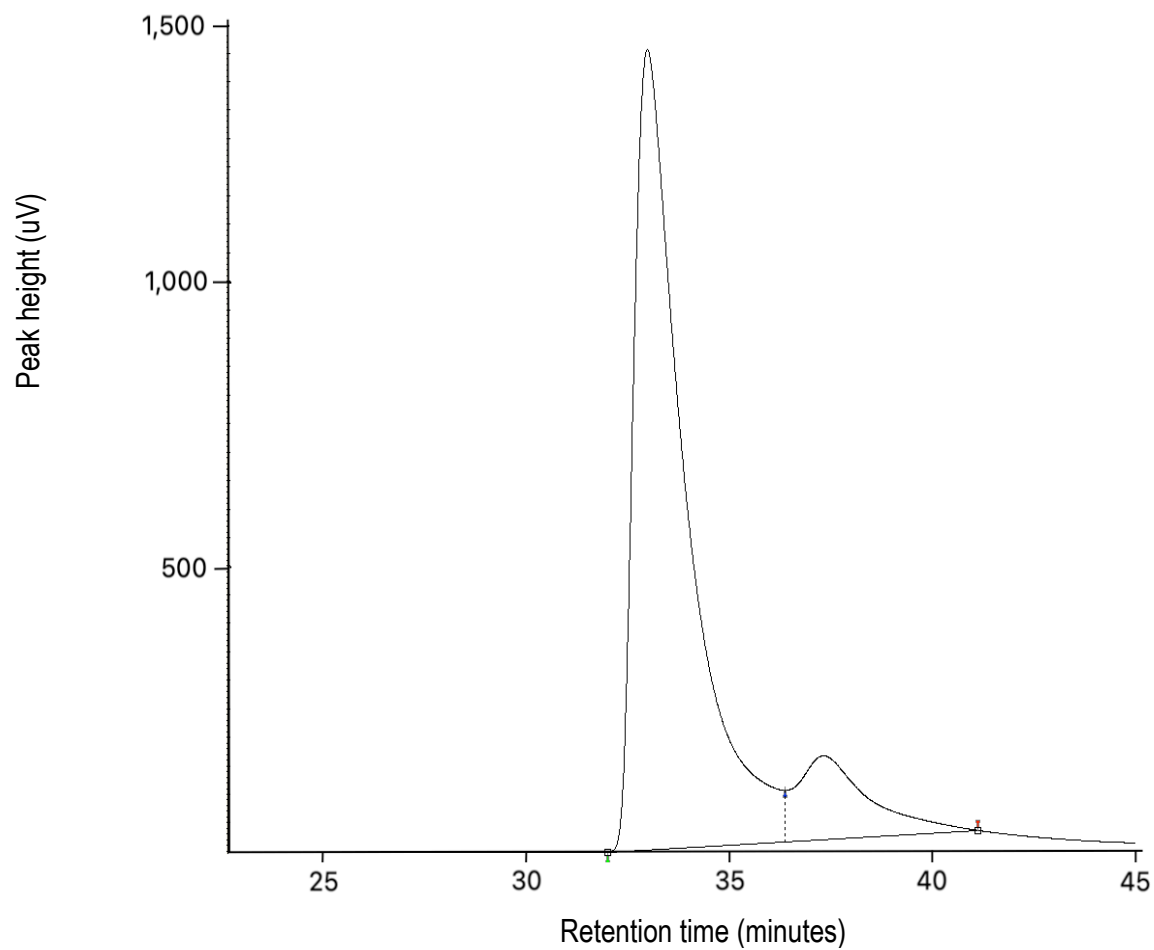
Figure 176. Chromatogram of **9** obtained using chiral HPLC, whereby the ratio of peaks gave the percentage of isomers in the amine to be 4.5 %:95.5 % (91 % ee).
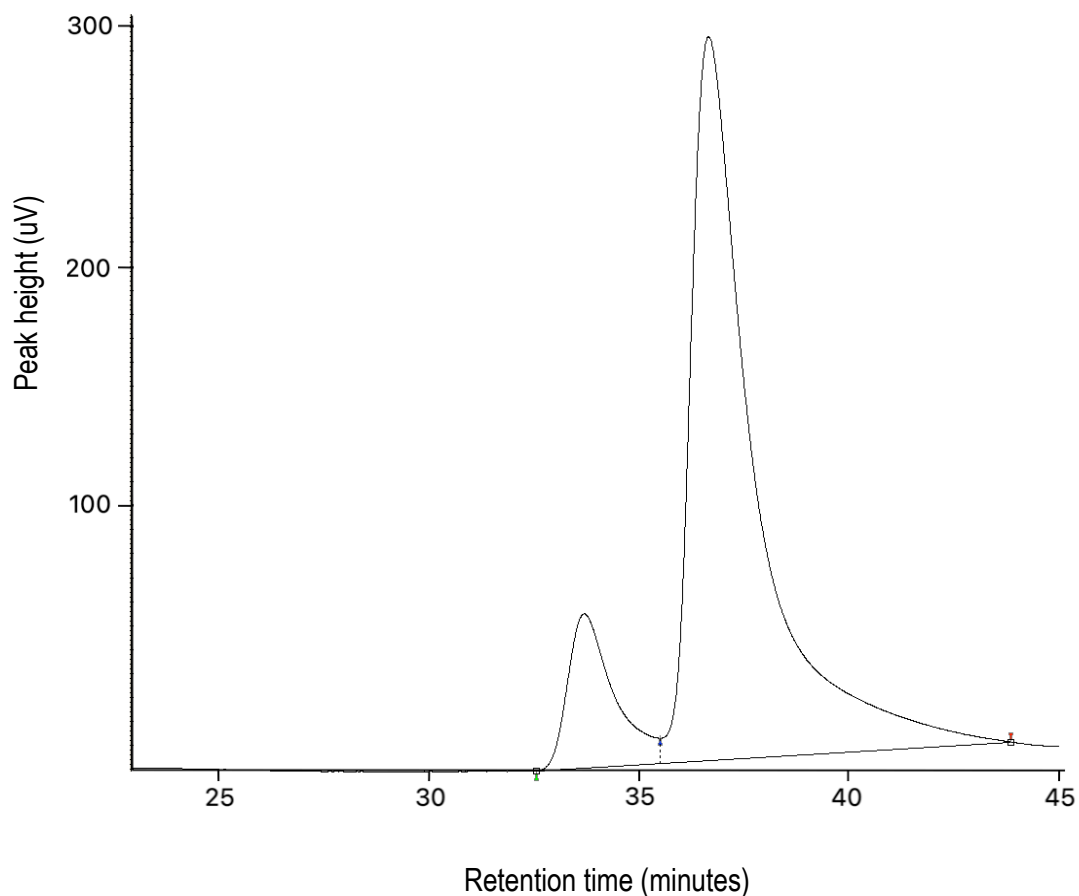
Figure 177. Chromatogram of **9** obtained using chiral HPLC, whereby the ratio of peaks gave the percentage of isomers in the amine to be ~10 %:90 % (80 % ee). Two batches of recrystallisations were combined: 0.23 g of 7 %: 93 % and 0.18 g of 14 %: 86 %. Note: this chromatogram represents the isomers in the ratio of 13 %:87 %.
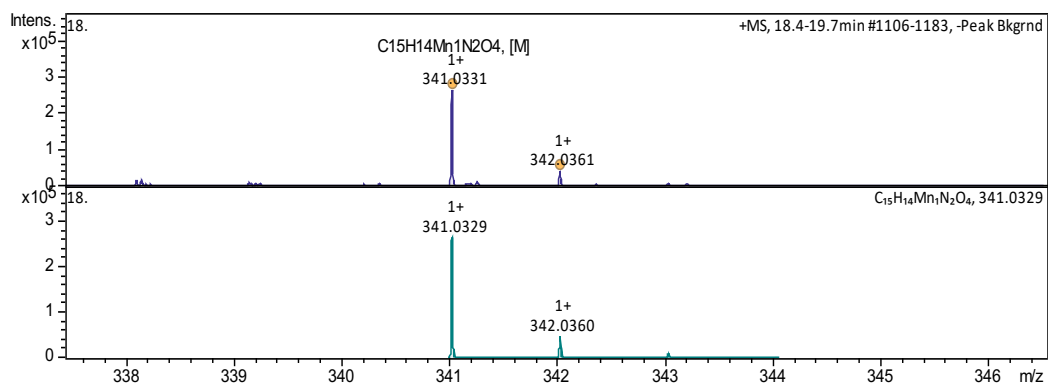
Figure 178. Chromatogram of **9** obtained using chiral HPLC, whereby the ratio of peaks gave the percentage of isomers in the amine to be 86 %:14 % (72 % ee).
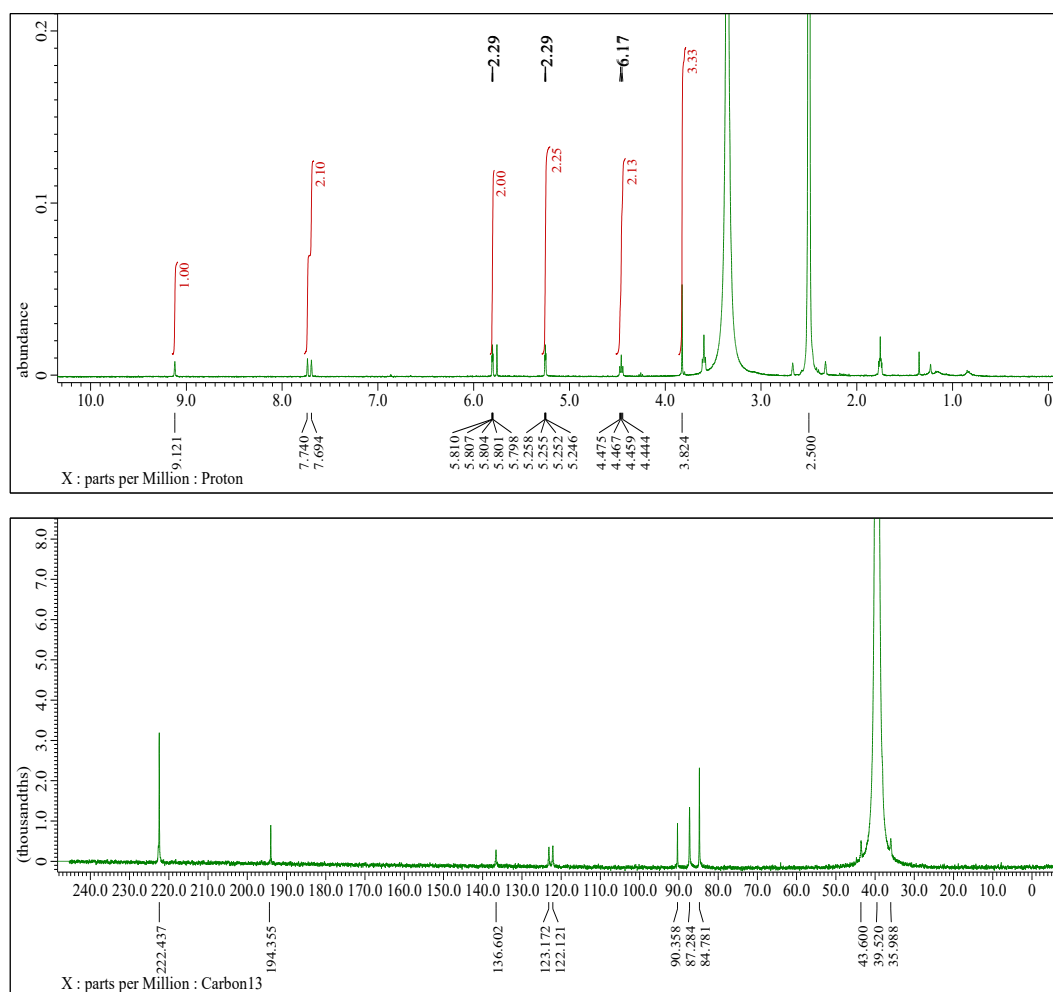
Figure 179. ¹H (top) and ¹³C{¹H} (bottom) NMR spectra (recorded in DMSO) of **[(51)Cl]**
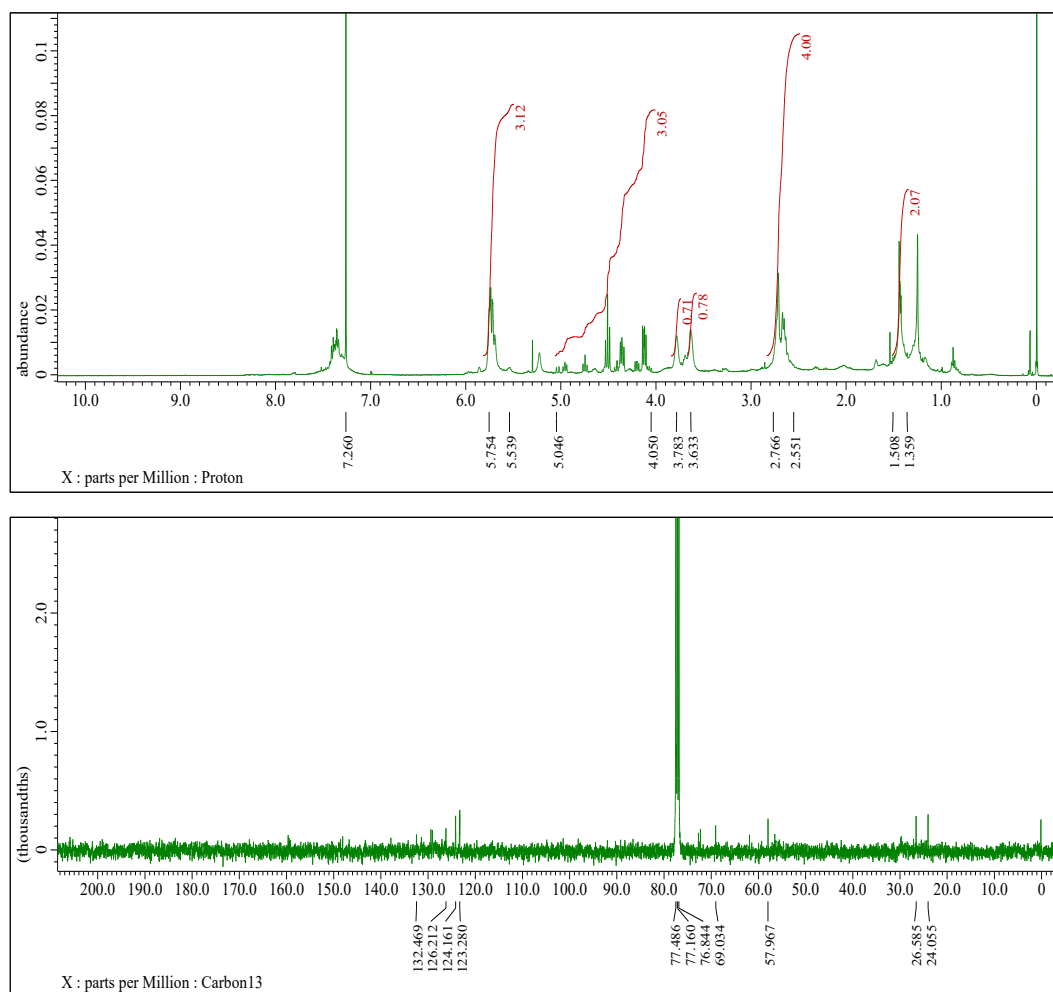

Figure 180. High resolution ESI⁺ spectra of **[(51)Cl]**

Figure 181. ^{1}H (top) and ^{13}C{^{1}H} (bottom) NMR spectra (recorded in CDCl$_3$) of **67** (via the azide route)
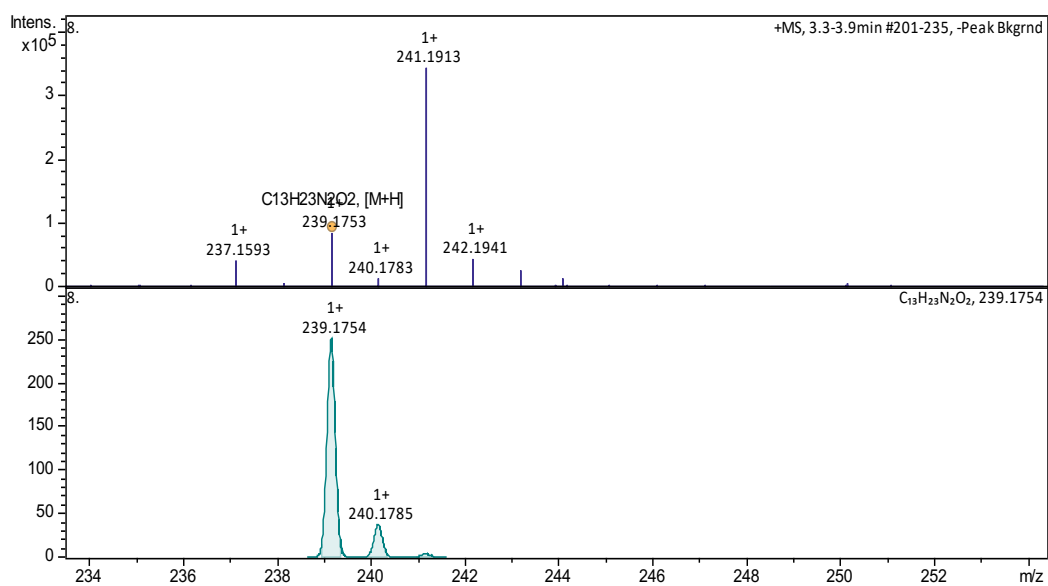

Figure 182. High resolution ESI$^+$ spectra of **67** (via the azide route)
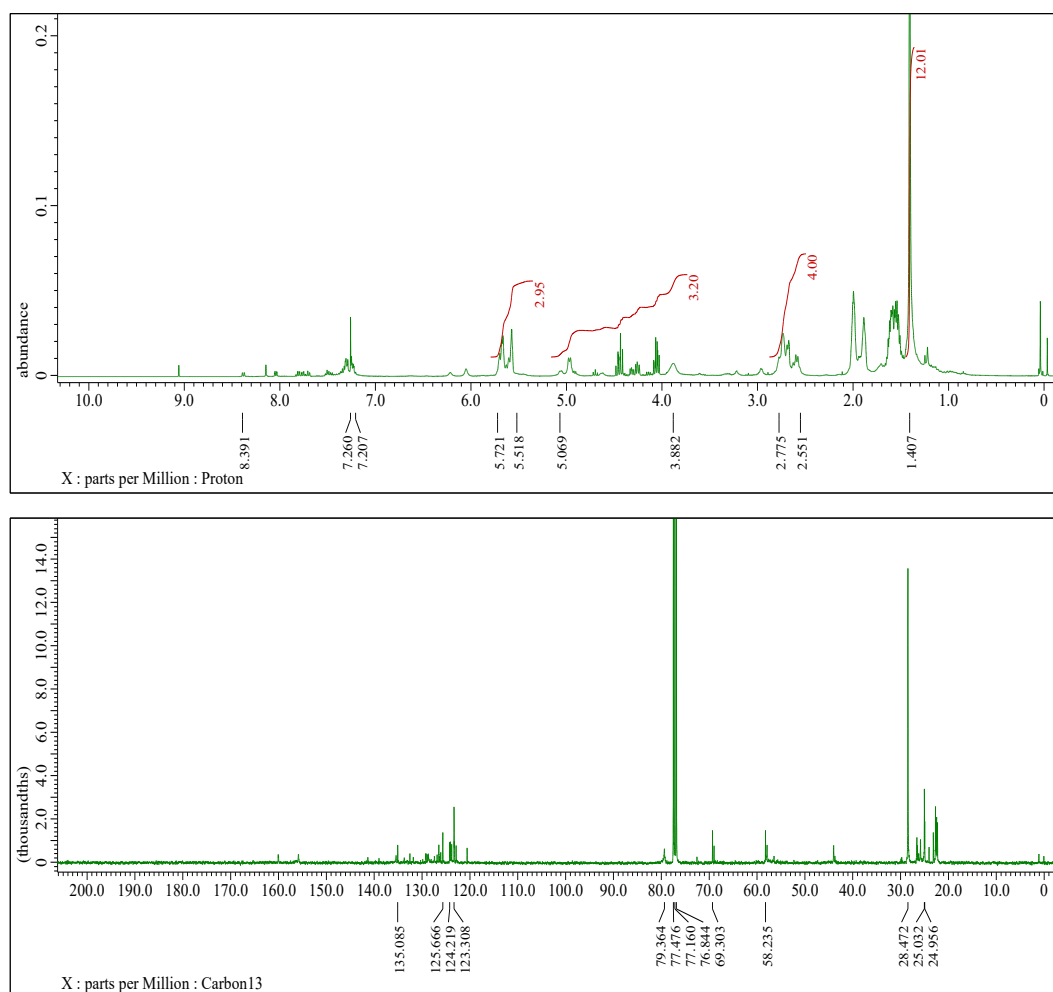
Figure 183. ¹H (top) and ¹³C{¹H} (bottom) NMR spectra (recorded in CDCl₃) of **67** (via the phthalimide route)
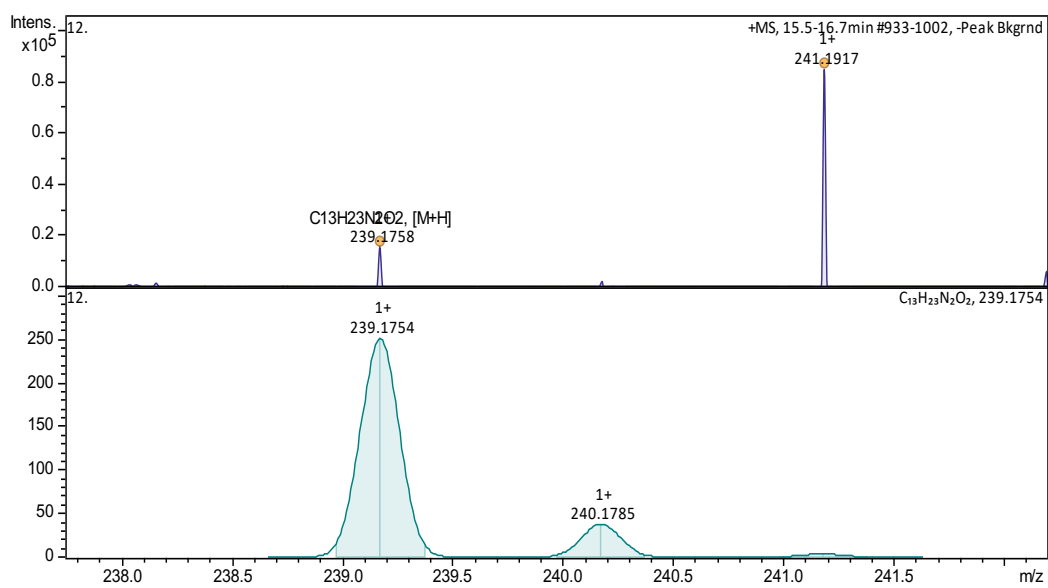

Figure 184. High resolution ESI⁺ spectra of **67** (via the phthalimide route)